N6310219

NTIS®
Information is our business.

# LINEARIZED THEORY OF WIND-TUNNEL JET-BOUNDARY CORRECTIONS AND GROUND EFFECT FOR VTOL-STOL AIRCRAFT

LANGLEY RESEARCH CENTER
LANGLEY AIR FORCE BASE, VA

1962

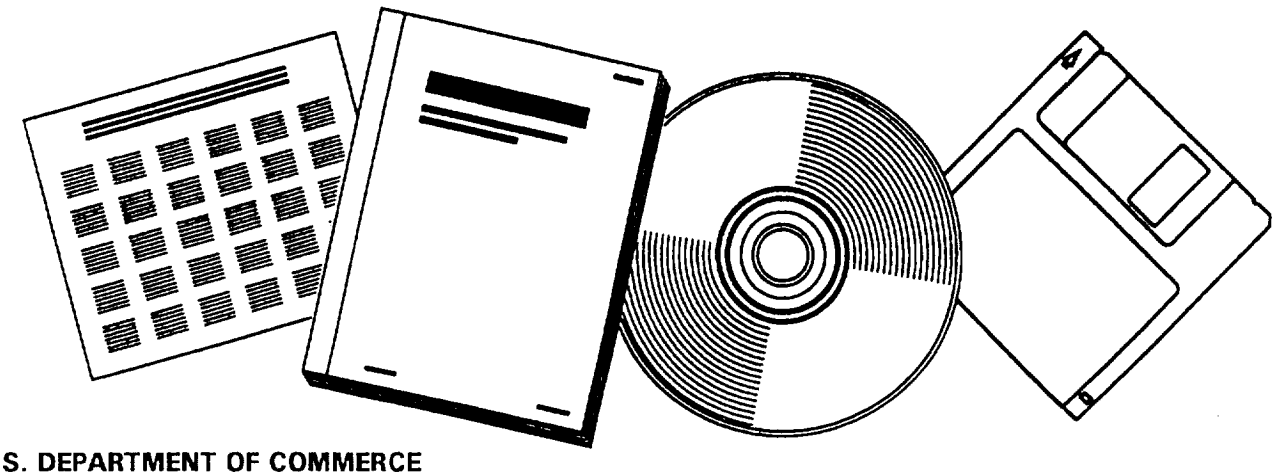

U.S. DEPARTMENT OF COMMERCE
National Technical Information Service

N63-10219

NASA TR R-124

NASA TR R-124

# NATIONAL AERONAUTICS AND SPACE ADMINISTRATION

TECHNICAL REPORT
R-124

# LINEARIZED THEORY OF WIND-TUNNEL JET-BOUNDARY CORRECTIONS AND GROUND EFFECT FOR VTOL-STOL AIRCRAFT

By HARRY H. HEYSON

1962

REPRODUCED BY
NATIONAL TECHNICAL
INFORMATION SERVICE
U. S. DEPARTMENT OF COMMERCE
SPRINGFIELD, VA. 22161

# TECHNICAL REPORT R-124

## LINEARIZED THEORY OF WIND-TUNNEL JET-BOUNDARY CORRECTIONS AND GROUND EFFECT FOR VTOL-STOL AIRCRAFT

By HARRY H. HEYSON

Langley Research Center
Langley Air Force Base, Va.

# CONTENTS


| | Page |
|---|---|
| SUMMARY | 1 |
| INTRODUCTION | 1 |
| SYMBOLS | 3 |
| THEORY | 5 |
| General Plan | 5 |
| Wake in Free Air | 5 |
| Wake of vertical doublets | 5 |
| Wake of longitudinal doublets | 7 |
| Wake and Image Near Wind-Tunnel Floor | 8 |
| Wake of vertical doublets | 8 |
| Wake of longitudinal doublets | 9 |
| Wake and Image Near Open Lower Boundary | 10 |
| Wake of vertical doublets | 10 |
| Wake of longitudinal doublets | 10 |
| Wind-Tunnel Jet-Boundary Corrections | 11 |
| Ground Effect | 13 |
| Application of Results | 14 |
| Finding $u_0$, $w_0$, and $\chi$ | 14 |
| Alternate form for interference velocities | 18 |
| Interference at model | 18 |
| Corrections to data | 18 |
| Open Boundaries at Low Speeds | 19 |
| NUMERICAL CALCULATIONS | 19 |
| RESULTS AND DISCUSSION | 21 |
| Interference at the Model | 21 |
| Corrections at $\chi=90°$ | 21 |
| Effect of $\chi$ and $\zeta$ | 21 |
| Effect of $\gamma$ | 22 |
| Minimizing Corrections | 22 |
| Correction to ground effect | 22 |
| Selection of vertical height in tunnel | 22 |
| Choice of Wind-Tunnel Configuration | 22 |
| Longitudinal Distribution of Interference | 23 |
| Corrections to free air | 23 |
| Ground effect | 24 |
| Corrections to ground effect | 24 |
| Measurement of forward velocity | 24 |
| Lateral Distribution of Interference | 24 |
| Closed wind tunnels | 24 |
| Wind tunnels closed on the bottom only | 25 |
| Ground effect | 25 |
| Corrections to ground effect | 25 |
| Laterally offset models | 25 |
| Vertical Distribution of Interference | 25 |
| Closed wind tunnels | 25 |
| Wind tunnels closed on the bottom only | 26 |
| Ground effect | 26 |
| More Complex Models | 26 |
| Tandem system | 26 |
| Side-by-side model | 27 |
| Vertically arranged model | 28 |

RESULTS AND DISCUSSION—Continued Page
Extension to Finite-Size Models 28
Wings 28
Rotors and propellers 28
Effect of Finite Size for Wings 28
Interference at center of span 28
Distribution of interference over span 28
Effect of Finite Size for Rotors 29
Wake of rotor 29
Approximate calculation of wind-tunnel interference 29
Effect of finite size on $\delta_{w,L}$ at rotor center 29
Effect of finite size on distribution of $\delta_{w,L}$ 29
Maximum Allowable Size of Model 30
Experimental Verification 30
Jet flap 31
Jet flap in ground effect 31
Propeller-driven configurations 32
Ducted fan 32
Rotors 32
Extent of verification 33
CONCLUSIONS 33
APPENDIX A—DERIVATION OF CLOSED-FORM EXPRESSIONS FOR THE INTERFERENCE VELOCITIES AT THE MODEL IN GROUND EFFECT 34
Vertical Interference Due to Lift 34
Longitudinal Interference Due to Lift 35
Vertical Interference Due to Drag 35
Longitudinal Interference Due to Drag 36
APPENDIX B—DERIVATION OF CLOSED-FORM EXPRESSIONS FOR THE INTERFERENCE VELOCITIES AT THE MODEL FOR ONLY AN OPEN LOWER BOUNDARY 38
Vertical Interference Due to Lift 38
Longitudinal Interference Due to Lift 39
Vertical Interference Due to Drag 40
Longitudinal Interference Due to Drag 41
APPENDIX C—SAMPLE CASE OF APPLICATION OF CORRECTIONS TO TEST DATA 43
APPENDIX D—SAMPLE CALCULATION OF INTERFERENCE FACTOR FOR FINITE WING 45
REFERENCES 46

# TECHNICAL REPORT R-124

## LINEARIZED THEORY OF WIND-TUNNEL JET-BOUNDARY CORRECTIONS AND GROUND EFFECT FOR VTOL-STOL AIRCRAFT

By Harry H. Heyson


### SUMMARY

*A linearized theory is developed to obtain interference factors for wind tunnels and ground effect. The calculated results, presented in tabular form in NASA Technical Notes D-933, D-934, D-935, and D-936, indicate that the degree to which the wake is deflected downward has a primary effect on the magnitude of the interference. When the wake is undeflected the corrections are essentially the same as those of classical theory. When the wake is deflected severely downward, the corrections are primarily determined by the floor of the wind tunnel. Under these conditions, the corrections are, in general, much larger than those given by previously available results. Because of deformations at the lower boundary of the jet, the corrections for an open wind tunnel are uncertain. Testing at low speeds and high lift coefficients in open wind tunnels, therefore, is not recommended.*

*Although the theory is developed expressly for single-element, vanishingly small models, methods, with sample calculations, are given for extending the results to multielement and finite-span models.*

*The theory is at least partially verified by available test data; however, complete verification would require a substantially more detailed experimental study.*


### INTRODUCTION

Attempts to combine the hovering or low-speed capability of the helicopter with the high-speed potential of conventional aircraft have led to a wide variety of proposed VTOL-STOL configurations. Almost every conceivable combination of wings, rotors, fans, and jets has been considered. Unfortunately the mutual interference between the various elements of the complete aircraft is usually of such a magnitude that, in general, it is not possible to predict the performance of a given VTOL-STOL aircraft by completely analytical means. Thus, a reasonably accurate evaluation of the merits of a VTOL-STOL configuration will generally require wind-tunnel tests.

Wind-tunnel data, unless corrected for the effects introduced by the presence of the walls, do not necessarily correspond with the results which would be obtained in flight. This fact has been recognized for many years and the appropriate corrections for wings are well known as the result of theoretical and experimental studies (refs. 1 to 6, for example). In the present case, however, experiments (ref. 7) have already shown that the required corrections for low-speed VTOL-STOL tests are much larger than those usually applied to wings.

There are, of course, several possible ways of circumventing the problems of either large or unknown wind-tunnel corrections. One way is to test only very small models in very large wind tunnels. This procedure, when carried to extremes, may result in either an impossibly small model or in the requirement for a very large wind tunnel which may not be available. In the latter case, it may be possible to conduct the tests in the return passage of the wind tunnel, thus effectively obtaining a larger, but lower speed, test section. Unfortunately, wind tunnels are constructed and adjusted so as to maintain steady uniform flow only in the test section itself; consequently, the flow in the return passage may be found quite unsuitable for test purposes. At best, return-passage testing presents the problem of an expensive and time-consuming calibration of the return-passage flow.

The ability to correct the wind-tunnel data to free-air conditions greatly relaxes the requirement for a relatively large wind tunnel. Previous attempts to correct data from low-speed VTOL-STOL wind-tunnel tests have not shown the degree of correlation necessary for acceptance of the present correction methods (ref. 7). These attempts at correction, however, used only the usual wind-tunnel wall corrections for wings. Furthermore, only the lift contribution of the wing was considered in the corrections on the assumption that the corrections depend only on the so-called "circulation" lift of the system. These assumptions are untenable on both counts. First, the representation of the wake, which is assumed to pass directly downstream in the classical corrections (refs. 1 to 6), is entirely inadequate for VTOL-STOL models where the wake may be deflected downward by as much as 90°. Second, since the entire lifting system deflects air against the walls of the wind tunnel, the entire lift of the system must be considered.

The fundamental requirement in developing corrections for VTOL-STOL wind-tunnel tests is to treat a wake which may be deflected substantially downward from the horizontal. A recent paper (ref. 8) treats precisely this problem in computing corrections for a lifting rotor. One portion of reference 8 is of particular interest in the present problem; that is, the portion which treats the case where the rotor is assumed to be vanishingly small. This assumption, while simplifying the mathematical treatment, retains the essential characteristic of the wake; that is, its large deflection from the horizontal. When the assumption of small size is made, the rotor wake is reduced to a semi-infinite string of point doublets, which, when the wake is undeflected, corresponds exactly to the customary representation of a small wing in a wind tunnel (refs. 1 and 8).

The present analysis proceeds from this point to consider the wake of any generalized lifting system to be represented by a semi-infinite string of point doublets whose axes are tilted by some angle related to the lift and drag of the model. The results obtained in this manner are directly applicable, regardless of the physical configuration of the model, provided that the model is reasonably small with respect to the wind-tunnel dimensions. In the course of the analysis, it develops that there may be a significant longitudinal component of jet-boundary interference as well as the usual vertical interference. Both components are treated throughout the analysis.

Sufficient theoretical (ref. 8) and experimental (ref. 7) evidence has been accumulated to indicate that the floor of the wind tunnel assumes an increased importance when the wake is greatly deflected. Thus, large changes in the correction factors may be expected when the model is moved either closer to or farther from the wind-tunnel floor. Consequently, the effect of the vertical placement of the model in the wind tunnel is examined in some detail. Such considerations lead naturally into a study of ground effect as the degenerate case of a wind-tunnel correction. Therefore, ground-effect corrections, as well as corrections directly from the wind tunnel to ground effect, are treated.

The distribution of wind-tunnel interference along all three axes is also studied. Such information is obviously needed for the longitudinal axis if it is desired to correct the pitching moments measured in the wind tunnel. These interference distributions will also be required merely to correct the performance data for cases of complex models. Such cases are those in which discrete lifting elements are disposed predominantly along one or more axes. Perhaps the simplest examples are: tandem rotors, which require a knowledge of the longitudinal interference distribution; side-by-side rotors, which require a knowledge of the lateral distribution; and unloaded rotor systems, which require a knowledge of the vertical distribution.

It will be observed that these distributions of interference, in combination with suitably displaced lifting-point positions, may be used to determine, by superposition, the corrections for models of finite size. A system for such a treatment is indicated herein and it is illustrated by two sample cases. Aside from these cases, the effect of size is also treated by studying the distribution of interference over uniformly loaded lifting rotors. The latter results have been obtained from the equations of reference 8.

The data of reference 7, which were obtained for identical models in two different wind-tunnel test sections, have been corrected by means of the present theory in an effort to determine its validity. The degree of improvement in correlation is

shown by comparison of the corrected and uncorrected data for the two test sections.

Correction factors have been computed for a vast variety of wind-tunnel configurations, proportions, and mounting positions. Although a substantial number of these factors are presented graphically herein, the number of cases is such as to preclude a complete presentation in this form. Consequently, references 9 to 12 have been prepared in order to present the complete set of calculated results in tabular form.

A preliminary account of the present study has been presented in reference 13.

## SYMBOLS

| | |
|---|---|
| $A$ | area, sq ft |
| $A_G$ | tunnel-equivalent flow area in ground effect, $4h^2$, sq ft |
| $A_m$ | momentum area of lifting system, sq ft |
| $A_R$ | rotor-disk area, sq ft |
| $A_T$ | cross-sectional area of wind-tunnel test section, $4BH$, sq ft |
| $b$ | lateral distance from center of model to right-hand side of wind tunnel (viewed from behind), ft |
| $B$ | semiwidth of wind-tunnel test section, ft |
| $\bar{c}$ | mean aerodynamic chord, ft |
| $C_D$ | drag coefficient, $\frac{D}{qS}$ |
| $C_{D,c}$ | corrected value of drag coefficient |
| $C_L$ | lift coefficient, $\frac{L}{qS}$ |
| $C_{L,c}$ | corrected value of lift coefficient |
| $C_T$ | thrust coefficient, $\frac{\text{Thrust}}{qS}$ |
| $C_{T,c}$ | corrected value of thrust coefficient |
| $C_\mu$ | jet-momentum coefficient, $\frac{(\text{Jet mass flow})v_j}{qS}$ |
| $C_{\mu,c}$ | corrected value of jet-momentum coefficient |
| $d$ | exit diameter of ducted fan, ft |
| $D$ | total drag, lb; also diameter of rotor or propeller, ft |
| $D_c$ | corrected value of total drag |
| $D_i$ | induced drag, positive rearward, ft/sec (note that a forward-directed longitudinal thrust is considered in this context as a negative induced drag) |
| $h$ | height of center of model above wind-tunnel floor or above ground, ft |
| $H$ | semiheight of wind tunnel, ft |
| $K$ | function related to induced velocities of model |
| $l$ | distance along model wake, measured from model, ft |
| $L$ | lift, lb |
| $L_c$ | corrected value of lift, lb |
| $m^*$ | strength of a doublet, ft$^4$/sec |
| $M_T$ | mass flow through wind tunnel, $\rho A_T V$, slugs/sec |
| $M_u$ | longitudinal mass flow due to induced drag, $\rho A_m u_O$, slugs/sec |
| $M_w$ | vertical mass flow due to lift, $\rho A_m w_O$, slugs/sec |
| $m, n, p, q, r, s, t$ | integers (see eq. (23)) |
| $n$ | ratio of final induced velocities in far wake to initial induced velocities at model |
| $q$ | dynamic pressure, $\frac{1}{2}\rho V^2$, lb/sq ft |
| $q_c$ | corrected value of dynamic pressure, lb/sq ft |
| $R$ | rotor radius, ft |
| $s$ | semispan of wing, ft |
| $S$ | wing, propeller, or fan-exit area, sq ft |
| $u$ | longitudinal induced velocity, positive rearward, ft/sec |
| $u_D$ | longitudinal induced velocity due to drag, positive rearward, ft/sec |
| $u_L$ | longitudinal induced velocity due to lift, positive rearward, ft/sec |
| $u_O$ | mean or momentum-theory value of longitudinal induced velocity at model, positive rearward, ft/sec |

$u_\infty$ longitudinal induced velocity for a semi-infinite wake, positive rearward, ft/sec

$\Delta u$ total longitudinal interference velocity, positive rearward, ft/sec

$\Delta u_D$ longitudinal interference velocity due to induced drag, positive rearward, ft/sec

$\Delta u_L$ longitudinal interference velocity due to lift, positive rearward, ft/sec

$v_j$ axial velocity at exit of jet, ft/sec

$V$ wind-tunnel velocity, ft/sec

$V_c$ corrected forward velocity, ft/sec

$w$ vertical induced velocity, positive upward, ft/sec

$w_D$ vertical induced velocity due to induced drag, positive upward, ft/sec

$w_h$ reference velocity, positive upward, $-\sqrt{\frac{L}{n\rho A_m}}$, ft/sec

$w_L$ vertical induced velocity due to lift, positive upward, ft/sec

$w_O$ mean or momentum-theory value of vertical induced velocity, positive upward, ft/sec

$w_\infty$ vertical induced velocity for a semi-infinite wake, positive upward, ft/sec

$\Delta w$ total vertical interference velocity, positive upward, ft/sec

$\Delta w_D$ vertical interference velocity due to induced drag, positive upward, ft/sec

$\Delta w_L$ vertical interference velocity due to lift, positive upward, ft/sec

$x,y,z$ location of a point with respect to $X$-, $Y$-, and $Z$-axes, respectively ($x$ measured positive rearward, $y$ measured positive to right when viewed from behind, and $z$ measured positive upward), ft

$x',y',z'$ location of a point with respect to $X'$-, $Y'$-, and $Z'$-axes, respectively ($x'$ measured positive rearward, $y'$ measured positive to right when viewed from behind, and $z'$ measured positive upward), ft

$X,Y,Z$ Cartesian axes with origin at center of model

$X',Y',Z'$ Cartesian axes centered at center of wind tunnel

$\alpha$ angle of attack, radians unless otherwise noted

$\alpha_c$ corrected angle of attack, radians unless otherwise noted

$\Delta\alpha$ change in angle of attack due to interference, radians unless otherwise noted

$\gamma$ ratio of wind-tunnel width to wind-tunnel height, $B/H$

$\Gamma$ circulation, ft²/sec

$\delta$ jet-boundary correction, or interference, factor (general)

$\delta_{u,D}$ interference factor for longitudinal interference velocity due to drag

$\delta_{u,L}$ interference factor for longitudinal interference velocity due to lift

$\delta_{w,D}$ interference factor for vertical interference velocity due to drag

$\delta_{w,L}$ interference factor for vertical interference velocity due to lift

$\zeta$ ratio of wind-tunnel semi-height to height of model above wind-tunnel floor, $H/h$

$\eta$ ratio of lateral distance between model center and right-hand side of wall (viewed from behind) to semiwidth of wind tunnel, $b/B$

$\theta_n$ net wake-deflection angle in forward flight, complement of wake skew angle, deg

$\rho$ mass density of air, slugs/cu ft

$\sigma$ ratio of rotor diameter or total wing span to total wind-tunnel width, $D/2B$, $R/B$, or $s/B$

$\phi_\infty$ potential function for a semi-infinite wake, ft²/sec

$\chi$ wake skew angle, angle between $Z$-axis (negative direction) and wake center line, positive rearward, deg

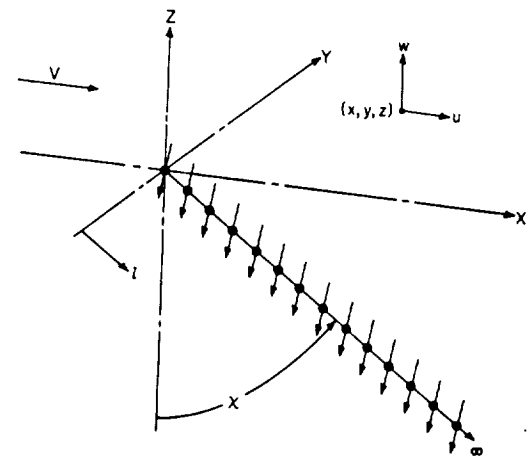


FIGURE 1.—Wake in free air.

## THEORY

### GENERAL PLAN

The general plan of this analysis is to first find the induced velocities in the space surrounding the wake in free air. Then, by superposition, the induced velocities are found for the wake and its mirror image directly below the test-section floor (the ground-effect image). Finally, superposition is used to obtain the correction factor for all the tunnel walls. Many of the equations used herein are derived in reference 8. In such cases, only the final result is stated in the present paper.

### WAKE IN FREE AIR

The wake, under the assumption that the model is small in comparison with the wind tunnel (see ref. 8), is shown in figure 1. It consists merely of a uniform distribution of point doublets along a straight line which begins at the model and extends to infinity. In general, the line is inclined to the free stream by the net wake-deflection angle $\theta_n$, which is the complement of the wake skew angle $\chi$. In conformity with reference 8, the present work is derived in terms of $\chi$ rather than $\theta_n$. Since the net deflection angle may be a more familiar quantity to VTOL-STOL designers, computed results will be presented in terms of both parameters.

The wake-doublet inclination angle will be determined primarily by the lift-drag ratio at the particular operating condition. For convenience, the present report considers the longitudinal and vertical doublet strength separately. The required velocities may then be found for each case as a linear combination of the velocities due to a wake of longitudinal doublets and those due to a wake of vertical doublets.

**Wake of vertical doublets.**—The potential function for a wake of vertical doublets of strength $-\frac{dm^*}{dl}$ is derived in reference 8 as

$$\phi_\infty=-\frac{dm^*}{dl}\left[\frac{z+\cos\chi\sqrt{x^2+y^2+z^2}}{(\sqrt{x^2+y^2+z^2}+z\cos\chi-x\sin\chi)\sqrt{x^2+y^2+z^2}}\right] \tag{1}$$

The vertical induced velocity at a point $(x,y,z)$ is given by the partial derivative of equation (1) with respect to $z$. Reference 8 shows this to be

$$w_\infty=-\frac{dm^*}{dl}\left\{\frac{x^2+y^2}{(\sqrt{x^2+y^2+z^2}+z\cos\chi-x\sin\chi)(x^2+y^2+z^2)^{3/2}}-\left[\frac{z+\cos\chi\sqrt{x^2+y^2+z^2}}{(\sqrt{x^2+y^2+z^2}+z\cos\chi-x\sin\chi)\sqrt{x^2+y^2+z^2}}\right]^2\right\} \tag{2}$$

Similarly, the longitudinal induced velocity at the point $(x,y,z)$ is the partial derivative of $\phi_\infty$ with respect to $x$, or

$$u_\infty=-\frac{dm^*}{dl}\left[\frac{-xz}{(\sqrt{x^2+y^2+z^2}+z\cos\chi-x\sin\chi)(x^2+y^2+z^2)^{3/2}}\right.$$
$$\left.-\frac{(z+\cos\chi\sqrt{x^2+y^2+z^2})(x-\sin\chi\sqrt{x^2+y^2+z^2})}{(\sqrt{x^2+y^2+z^2}+z\cos\chi-x\sin\chi)^2(x^2+y^2+z^2)}\right] \tag{3}$$

Now, if $dm^*/dl$ is taken, as in reference 8, to be

$$\frac{dm^*}{dl}=w_o\frac{R^2}{2}=w_o\frac{A_m}{2\pi} \tag{4}$$

and if equations (2) and (3) are nondimensionalized with respect to $h$, the height of the center of the model above the lower boundary of a wind tunnel, the vertical induced velocity may be expressed as (note that $1/h=\zeta/H$)

$$w_\infty=w_o\frac{A_m}{A_T}\left[-\zeta^2\frac{2\gamma}{\pi}K\left(\zeta\frac{x}{H},\zeta\frac{y}{H},\zeta\frac{z}{H}\right)\right] \tag{5a}$$

where

$$K\left(\zeta\frac{x}{H},\zeta\frac{y}{H},\zeta\frac{z}{H}\right)=\frac{\left(\zeta\frac{x}{H}\right)^2+\left(\zeta\frac{y}{H}\right)^2}{\left[\sqrt{\left(\zeta\frac{x}{H}\right)^2+\left(\zeta\frac{y}{H}\right)^2+\left(\zeta\frac{z}{H}\right)^2}+\zeta\frac{z}{H}\cos\chi-\zeta\frac{x}{H}\sin\chi\right]\left[\left(\zeta\frac{x}{H}\right)^2+\left(\zeta\frac{y}{H}\right)^2+\left(\zeta\frac{z}{H}\right)^2\right]^{3/2}}$$
$$-\left\{\frac{\zeta\frac{z}{H}+\cos\chi\sqrt{\left(\zeta\frac{x}{H}\right)^2+\left(\zeta\frac{y}{H}\right)^2+\left(\zeta\frac{z}{H}\right)^2}}{\left[\sqrt{\left(\zeta\frac{x}{H}\right)^2+\left(\zeta\frac{y}{H}\right)^2+\left(\zeta\frac{z}{H}\right)^2}+\zeta\frac{z}{H}\cos\chi-\zeta\frac{x}{H}\sin\chi\right]\sqrt{\left(\zeta\frac{x}{H}\right)^2+\left(\zeta\frac{y}{H}\right)^2+\left(\zeta\frac{z}{H}\right)^2}}\right\}^2 \tag{5b}$$

and, as a special case, when $\chi=90°$

$$K|_{\chi=90°}\left(\zeta\frac{x}{H},\zeta\frac{y}{H},\zeta\frac{z}{H}\right)=\frac{\left(\zeta\frac{x}{H}\right)^2+\left(\zeta\frac{y}{H}\right)^2}{\left[\sqrt{\left(\zeta\frac{x}{H}\right)^2+\left(\zeta\frac{y}{H}\right)^2+\left(\zeta\frac{z}{H}\right)^2}-\zeta\frac{x}{H}\right]\left[\left(\zeta\frac{x}{H}\right)^2+\left(\zeta\frac{y}{H}\right)^2+\left(\zeta\frac{z}{H}\right)^2\right]^{3/2}}$$
$$-\left\{\frac{\zeta\frac{z}{H}}{\left[\sqrt{\left(\zeta\frac{x}{H}\right)^2+\left(\zeta\frac{y}{H}\right)^2+\left(\zeta\frac{z}{H}\right)^2}-\zeta\frac{x}{H}\right]\sqrt{\left(\zeta\frac{x}{H}\right)^2+\left(\zeta\frac{y}{H}\right)^2+\left(\zeta\frac{z}{H}\right)^2}}\right\}^2 \tag{5c}$$

Note that in reference 8, $\zeta=1.0$.

Similarly, the longitudinal induced velocity may be expressed as

$$u_\infty=w_o\frac{A_m}{A_T}\left[-\zeta^2\frac{2\gamma}{\pi}K\left(\zeta\frac{x}{H},\zeta\frac{y}{H},\zeta\frac{z}{H}\right)\right] \tag{6a}$$

where

$$K\left(\zeta\frac{x}{H},\zeta\frac{y}{H},\zeta\frac{z}{H}\right)=\frac{-\left(\zeta\frac{x}{H}\right)\left(\zeta\frac{z}{H}\right)}{\left[\sqrt{\left(\zeta\frac{x}{H}\right)^2+\left(\zeta\frac{y}{H}\right)^2+\left(\zeta\frac{z}{H}\right)^2}+\zeta\frac{z}{H}\cos\chi-\zeta\frac{x}{H}\sin\chi\right]\left[\left(\zeta\frac{x}{H}\right)^2+\left(\zeta\frac{y}{H}\right)^2+\left(\zeta\frac{z}{H}\right)^2\right]^{3/2}}$$

$$-\frac{\left[\zeta\frac{z}{H}+\cos\chi\sqrt{\left(\zeta\frac{x}{H}\right)^2+\left(\zeta\frac{y}{H}\right)^2+\left(\zeta\frac{z}{H}\right)^2}\right]\left[\zeta\frac{x}{H}-\sin\chi\sqrt{\left(\zeta\frac{x}{H}\right)^2+\left(\zeta\frac{y}{H}\right)^2+\left(\zeta\frac{z}{H}\right)^2}\right]}{\left[\sqrt{\left(\zeta\frac{x}{H}\right)^2+\left(\zeta\frac{y}{H}\right)^2+\left(\zeta\frac{z}{H}\right)^2}+\zeta\frac{z}{H}\cos\chi-\zeta\frac{x}{H}\sin\chi\right]^2\left[\left(\zeta\frac{x}{H}\right)^2+\left(\zeta\frac{y}{H}\right)^2+\left(\zeta\frac{z}{H}\right)^2\right]} \tag{6b}$$

and, as a special case, when $\chi=90°$

$$K|_{\chi=90°}\left(\zeta\frac{x}{H},\zeta\frac{y}{H},\zeta\frac{z}{H}\right)=\frac{\zeta\frac{z}{H}}{\left[\left(\zeta\frac{x}{H}\right)^2+\left(\zeta\frac{y}{H}\right)^2+\left(\zeta\frac{z}{H}\right)^2\right]^{3/2}} \tag{6c}$$

It will be observed that the effective momentum area $A_m$ of the lifting system has been substituted for the rotor-disk area $A_R$ of reference 8. It is clear from the derivation in that paper that this is indeed the proper meaning to assign to this area. Notice that, for a rotor or for a propeller, $A_R=A_m$.

**Wake of longitudinal doublets.**—Reference 8 gives the potential function for a wake of longitudinal *forward*-directed doublets as (note that the forward direction of the doublets corresponds to a drag or a negative thrust)

$$\phi_\infty=-\frac{dm^*}{dl}\frac{x-\sin\chi\sqrt{x^2+y^2+z^2}}{(\sqrt{x^2+y^2+z^2}+z\cos\chi-x\sin\chi)\sqrt{x^2+y^2+z^2}} \tag{7}$$

From reference 8, the corresponding vertical velocity is

$$w_\infty=-\frac{dm^*}{dl}\left[\frac{-xz}{(\sqrt{x^2+y^2+z^2}+z\cos\chi-x\sin\chi)(x^2+y^2+z^2)^{3/2}}-\frac{(z+\cos\chi\sqrt{x^2+y^2+z^2})(x-\sin\chi\sqrt{x^2+y^2+z^2})}{(\sqrt{x^2+y^2+z^2}+z\cos\chi-x\sin\chi)^2(x^2+y^2+z^2)}\right] \tag{8}$$

The correspondence between equations (3) and (8) can be noted immediately. As shown subsequently, however, this correspondence does not imply an equivalent correspondence between the final correction factors.

The longitudinal induced velocity is then the partial derivative of $\phi_\infty$ with respect to $x$ or

$$u_\infty=-\frac{dm^*}{dl}\left\{\frac{y^2+z^2}{(\sqrt{x^2+y^2+z^2}+z\cos\chi-x\sin\chi)(x^2+y^2+z^2)^{3/2}}-\left[\frac{x-\sin\chi\sqrt{x^2+y^2+z^2}}{(\sqrt{x^2+y^2+z^2}+z\cos\chi-x\sin\chi)\sqrt{x^2+y^2+z^2}}\right]^2\right\} \tag{9}$$

For the wake of longitudinal doublets, $dm^*/dl$ depends upon the mean longitudinal induced velocity $u_O$ rather than upon $w_O$. Thus, take

$$\frac{dm^*}{dl}=u_O\frac{A_m}{2\pi} \tag{10}$$

Then, after nondimensionalizing equations (8) and (9) with respect to $h$ (again, note that $1/h=\zeta/H$),

the following results are obtained

$$w_\infty = u_0 \frac{A_m}{A_T}\left[-\zeta^2 \frac{2\gamma}{\pi} K\left(\zeta\frac{x}{H}, \zeta\frac{y}{H}, \zeta\frac{z}{H}\right)\right] \tag{11a}$$

where

$$K\left(\zeta\frac{x}{H}, \zeta\frac{y}{H}, \zeta\frac{z}{H}\right) = \frac{-\left(\zeta\frac{x}{H}\right)\left(\zeta\frac{z}{H}\right)}{\left[\sqrt{\left(\zeta\frac{x}{H}\right)^2+\left(\zeta\frac{y}{H}\right)^2+\left(\zeta\frac{z}{H}\right)^2}+\zeta\frac{z}{H}\cos\chi-\zeta\frac{x}{H}\sin\chi\right]\left[\left(\zeta\frac{x}{H}\right)^2+\left(\zeta\frac{y}{H}\right)^2+\left(\zeta\frac{z}{H}\right)^2\right]^{3/2}}$$

$$-\frac{\left[\zeta\frac{z}{H}+\cos\chi\sqrt{\left(\zeta\frac{x}{H}\right)^2+\left(\zeta\frac{y}{H}\right)^2+\left(\zeta\frac{z}{H}\right)^2}\right]\left[\zeta\frac{x}{H}-\sin\chi\sqrt{\left(\zeta\frac{x}{H}\right)^2+\left(\zeta\frac{y}{H}\right)^2+\left(\zeta\frac{z}{H}\right)^2}\right]}{\left[\sqrt{\left(\zeta\frac{x}{H}\right)^2+\left(\zeta\frac{y}{H}\right)^2+\left(\zeta\frac{z}{H}\right)^2}+\zeta\frac{z}{H}\cos\chi-\zeta\frac{x}{H}\sin\chi\right]^2\left[\left(\zeta\frac{x}{H}\right)^2+\left(\zeta\frac{y}{H}\right)^2+\left(\zeta\frac{z}{H}\right)^2\right]} \tag{11b}$$

and, as a special case, when $\chi=90°$

$$K|_{\chi=90°}\left(\zeta\frac{x}{H}, \zeta\frac{y}{H}, \zeta\frac{z}{H}\right) = \frac{\zeta\frac{z}{H}}{\left[\left(\zeta\frac{x}{H}\right)^2+\left(\zeta\frac{y}{H}\right)^2+\left(\zeta\frac{z}{H}\right)^2\right]^{3/2}} \tag{11c}$$

Also, the longitudinal induced velocity may be expressed as

$$u_\infty = u_0 \frac{A_m}{A_T}\left[-\zeta^2 \frac{2\gamma}{\pi} K\left(\zeta\frac{x}{H}, \zeta\frac{y}{H}, \zeta\frac{z}{H}\right)\right] \tag{12a}$$

where

$$K\left(\zeta\frac{x}{H}, \zeta\frac{y}{H}, \zeta\frac{z}{H}\right) = \frac{\left(\zeta\frac{y}{H}\right)^2+\left(\zeta\frac{z}{H}\right)^2}{\left[\sqrt{\left(\zeta\frac{x}{H}\right)^2+\left(\zeta\frac{y}{H}\right)^2+\left(\zeta\frac{z}{H}\right)^2}+\zeta\frac{z}{H}\cos\chi-\zeta\frac{x}{H}\sin\chi\right]\left[\left(\zeta\frac{x}{H}\right)^2+\left(\zeta\frac{y}{H}\right)^2+\left(\zeta\frac{z}{H}\right)^2\right]^{3/2}}$$

$$-\left\{\frac{\zeta\frac{x}{H}-\sin\chi\sqrt{\left(\zeta\frac{x}{H}\right)^2+\left(\zeta\frac{y}{H}\right)^2+\left(\zeta\frac{z}{H}\right)^2}}{\left[\sqrt{\left(\zeta\frac{x}{H}\right)^2+\left(\zeta\frac{y}{H}\right)^2+\left(\zeta\frac{z}{H}\right)^2}+\zeta\frac{z}{H}\cos\chi-\zeta\frac{x}{H}\sin\chi\right]\sqrt{\left(\zeta\frac{x}{H}\right)^2+\left(\zeta\frac{y}{H}\right)^2+\left(\zeta\frac{z}{H}\right)^2}}\right\}^2 \tag{12b}$$

and, as a special case, when $\chi=90°$

$$K|_{\chi=90°}\left(\zeta\frac{x}{H}, \zeta\frac{y}{H}, \zeta\frac{z}{H}\right) = \frac{\zeta\frac{x}{H}}{\left[\left(\zeta\frac{x}{H}\right)^2+\left(\zeta\frac{y}{H}\right)^2+\left(\zeta\frac{z}{H}\right)^2\right]^{3/2}} \tag{12c}$$

### WAKE AND IMAGE NEAR WIND-TUNNEL FLOOR

**Wake of vertical doublets.**—In the present analysis the wake is assumed to pass downward and rearward in a straight line. In general, the wake then intersects the floor at some point behind the model. From this point rearward, the wake flows along the floor. In order to maintain zero flow through the floor, it is necessary to assume the existence of a mirror-image wake

directly below the floor. Figure 2(a) shows the real and mirror-image wake for a wake of vertical doublets. It will be observed that the portions of the real and image wakes along the floor merely cancel each other. Noting this fact, the vertical induced velocity due to lift for the entire wake system may be written, by superposition, as

$$w_L=w_O\frac{A_m}{A_T}\left\{-\zeta^2\frac{2\gamma}{\pi}\left[K\left(\zeta\frac{x}{H},\zeta\frac{y}{H},\zeta\frac{z}{H}\right)\right.\right.$$
$$-K\left(\zeta\frac{x}{H}-\tan\chi,\zeta\frac{y}{H},\zeta\frac{z}{H}+1\right)$$
$$-K\left(\zeta\frac{x}{H},\zeta\frac{y}{H},-\zeta\frac{z}{H}-2\right)$$
$$\left.\left.+K\left(\zeta\frac{x}{H}-\tan\chi,\zeta\frac{y}{H},-\zeta\frac{z}{H}-1\right)\right]\right\} \quad (13)$$

where $K$ is given by equation (5b), and the longitudinal induced velocity may be written as

$$u_L=w_O\frac{A_m}{A_T}\left\{-\zeta^2\frac{2\gamma}{\pi}\left[K\left(\zeta\frac{x}{H},\zeta\frac{y}{H},\zeta\frac{z}{H}\right)\right.\right.$$
$$-K\left(\zeta\frac{x}{H}-\tan\chi,\zeta\frac{y}{H},\zeta\frac{z}{H}+1\right)$$
$$+K\left(\zeta\frac{x}{H},\zeta\frac{y}{H},-\zeta\frac{z}{H}-2\right)$$
$$\left.\left.-K\left(\zeta\frac{x}{H}-\tan\chi,\zeta\frac{y}{H},-\zeta\frac{z}{H}-1\right)\right]\right\} \quad (14)$$

where $K$ is given by equation (6b).

**Wake of longitudinal doublets.**—The wake and its mirror image are shown in figure 2(b) for a wake of longitudinal doublets. Note that, when the doublets are longitudinal, the wake and its image along the floor add rather than subtract. The contribution of this portion of the wake may be found by first setting $\chi=90°$ in equations (11) and (12) and then making the substitution

$$\left.\begin{aligned}\zeta\frac{x}{H}&=\zeta\frac{x}{H}-\tan\chi\\ \zeta\frac{y}{H}&=\zeta\frac{y}{H}\\ \zeta\frac{z}{H}&=\zeta\frac{z}{H}+1\end{aligned}\right\} \quad (15)$$

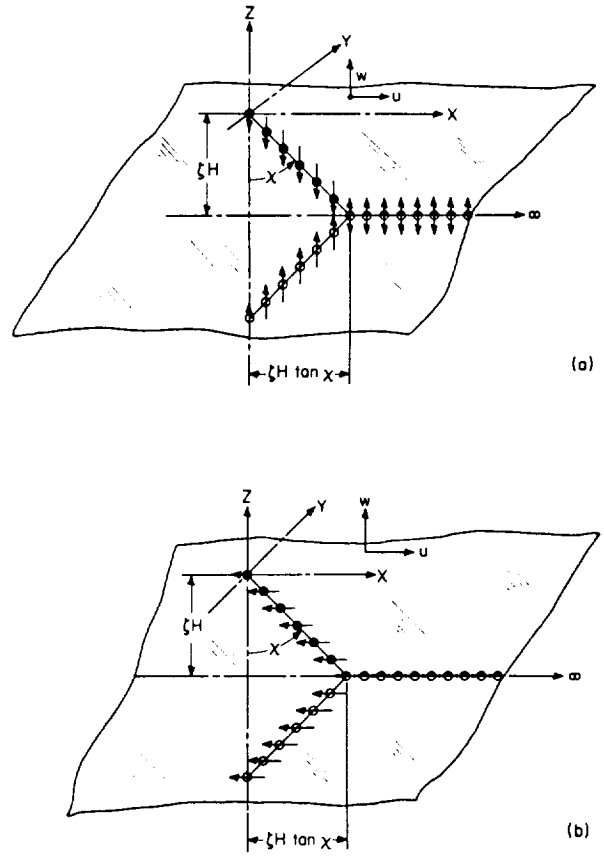


(a) Wake of vertical doublets.
(b) Wake of longitudinal doublets.

FIGURE 2.—Wake and image system for only the closed wind-tunnel floor.

Thus, for a wake of longitudinal doublets near the wind-tunnel floor, the vertical induced velocity due to drag may be written as

$$w_D=u_O\frac{A_m}{A_T}\left\{-\zeta^2\frac{2\gamma}{\pi}\left[K\left(\zeta\frac{x}{H},\zeta\frac{y}{H},\zeta\frac{z}{H}\right)\right.\right.$$
$$-K\left(\zeta\frac{x}{H}-\tan\chi,\zeta\frac{y}{H},\zeta\frac{z}{H}+1\right)$$
$$-K\left(\zeta\frac{x}{H},\zeta\frac{y}{H},-\zeta\frac{z}{H}-2\right)$$
$$+K\left(\zeta\frac{x}{H}-\tan\chi,\zeta\frac{y}{H},-\zeta\frac{z}{H}-1\right)$$
$$\left.\left.+2K|_{\chi=90°}\left(\zeta\frac{x}{H}-\tan\chi,\zeta\frac{y}{H},\zeta\frac{z}{H}+1\right)\right]\right\} \quad (16)$$

where $K$ is given by equation (11b), and the

longitudinal induced velocity due to drag may be written as

$$u_D=u_O\frac{A_m}{A_T}\left\{-\zeta^2\frac{2\gamma}{\pi}\left[K\left(\zeta\frac{x}{H},\zeta\frac{y}{H},\zeta\frac{z}{H}\right)\right.\right.$$
$$-K\left(\zeta\frac{x}{H}-\tan\chi,\zeta\frac{y}{H},\zeta\frac{z}{H}+1\right)$$
$$+K\left(\zeta\frac{x}{H},\zeta\frac{y}{H},-\zeta\frac{z}{H}-2\right)$$
$$-K\left(\zeta\frac{x}{H}-\tan\chi,\zeta\frac{y}{H},-\zeta\frac{z}{H}-1\right)$$
$$\left.\left.+2K|_{\chi=90^\circ}\left(\zeta\frac{x}{H}-\tan\chi,\zeta\frac{y}{H},\zeta\frac{z}{H}+1\right)\right]\right\} \quad (17)$$

where $K$ is given by equation (12b).

#### WAKE AND IMAGE NEAR OPEN LOWER BOUNDARY

If the lower boundary of the wind tunnel is open, the induced velocities will differ from those given in the preceding section because the image below the boundary will be of the opposite sign. This change is required in order to obtain a boundary condition of a continuous pressure gradient across the boundary.

**Wake of vertical doublets.**—The wake and image system for a wake of vertical doublets near an open lower boundary is shown in figure 3(a). It will be observed that the effect of the portion of the wake which trails along the floor does not cancel the effect of the similar portion of the image wake. Thus, the vertical induced velocity due to lift is

$$w_L=w_O\frac{A_m}{A_T}\left\{-\zeta^2\frac{2\gamma}{\pi}\left[K\left(\zeta\frac{x}{H},\zeta\frac{y}{H},\zeta\frac{z}{H}\right)\right.\right.$$
$$-K\left(\zeta\frac{x}{H}-\tan\chi,\zeta\frac{y}{H},\zeta\frac{z}{H}+1\right)$$
$$+K\left(\zeta\frac{x}{H},\zeta\frac{y}{H},-\zeta\frac{z}{H}-2\right)$$
$$-K\left(\zeta\frac{x}{H}-\tan\chi,\zeta\frac{y}{H},-\zeta\frac{z}{H}-1\right)$$
$$\left.\left.+2K|_{\chi=90^\circ}\left(\zeta\frac{x}{H}-\tan\chi,\zeta\frac{y}{H},\zeta\frac{z}{H}+1\right)\right]\right\} \quad (18)$$

where $K$ is given by equation (5b), and the longitudinal induced velocity due to lift is

$$u_L=w_O\frac{A_m}{A_T}\left\{-\zeta^2\frac{2\gamma}{\pi}\left[K\left(\zeta\frac{x}{H},\zeta\frac{y}{H},\zeta\frac{z}{H}\right)\right.\right.$$
$$-K\left(\zeta\frac{x}{H}-\tan\chi,\zeta\frac{y}{H},\zeta\frac{z}{H}+1\right)$$
$$-K\left(\zeta\frac{x}{H},\zeta\frac{y}{H},-\zeta\frac{z}{H}-2\right)$$
$$+K\left(\zeta\frac{x}{H}-\tan\chi,\zeta\frac{y}{H},-\zeta\frac{z}{H}-1\right)$$
$$\left.\left.+2K|_{\chi=90^\circ}\left(\zeta\frac{x}{H}-\tan\chi,\zeta\frac{y}{H},\zeta\frac{z}{H}+1\right)\right]\right\} \quad (19)$$

where $K$ is given by equation (6b).

**Wake of longitudinal doublets.**—The corresponding wake and image pattern for longitudinal doublets is shown in figure 3(b). Note that for this case the effect of the wake along the boundary does cancel the effect of the corresponding part of

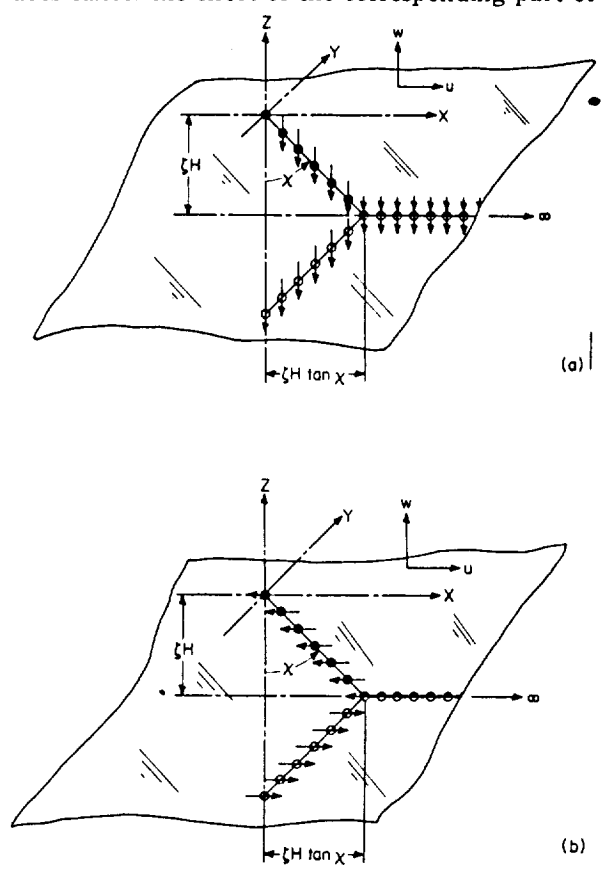


(a) Wake of vertical doublets.
(b) Wake of longitudinal doublets.

FIGURE 3.—Wake and image system for only the open wind-tunnel floor.

the image wake. Thus, the induced velocities will be

$$w_D=u_O\frac{A_m}{A_T}\left\{-\zeta^2\frac{2\gamma}{\pi}\left[K\left(\zeta\frac{x}{H},\zeta\frac{y}{H},\zeta\frac{z}{H}\right)\right.\right.$$
$$-K\left(\zeta\frac{x}{H}-\tan\chi,\zeta\frac{y}{H},\zeta\frac{z}{H}+1\right)$$
$$+K\left(\zeta\frac{x}{H},\zeta\frac{y}{H},-\zeta\frac{z}{H}-2\right)$$
$$\left.\left.-K\left(\zeta\frac{x}{H}-\tan\chi,\zeta\frac{y}{H},-\zeta\frac{z}{H}-1\right)\right]\right\} \quad (20)$$

where $K$ is given by equation (11b), and the longitudinal induced velocity due to drag is

$$u_D=u_O\frac{A_m}{A_T}\left\{-\zeta^2\frac{2\gamma}{\pi}\left[K\left(\zeta\frac{x}{H},\zeta\frac{y}{H},\zeta\frac{z}{H}\right)\right.\right.$$
$$-K\left(\zeta\frac{x}{H}-\tan\chi,\zeta\frac{y}{H},\zeta\frac{z}{H}+1\right)$$
$$-K\left(\zeta\frac{x}{H},\zeta\frac{y}{H},-\zeta\frac{z}{H}-2\right)$$
$$\left.\left.+K\left(\zeta\frac{x}{H}-\tan\chi,\zeta\frac{y}{H},-\zeta\frac{z}{H}-1\right)\right]\right\} \quad (21)$$

where $K$ is given by equation (12b).

### WIND-TUNNEL JET-BOUNDARY CORRECTIONS

Three different wind-tunnel boundary configurations, representative of almost all rectangular wind tunnels now in operation, are considered in this report. These are a completely closed wind tunnel, a wind tunnel closed on the bottom only, and a completely open wind tunnel. The image systems required to represent these wind tunnels are shown in figure 4. It may be seen that these image systems are similar to those for wings in the classical theory (refs. 1 to 6). Images are reflected across solid boundaries with opposite sign so as to meet the requirement of zero normal velocity at the boundaries, and images are reflected across free boundaries with like sign so as to meet the requirement of a continuous pressure gradient across the boundaries.

Notice that the vertical distance from any image to the origin is $-4nH$ and that the corresponding lateral distance is $\gamma H(1-\eta)[1-(-1)^m]-2m\gamma H$. Therefore, by superposition, from equations (18) and (19) $\left(\text{with the substitutions } \frac{x}{H}=\frac{x}{H},\ \frac{y}{H}=\frac{y}{H}-2m\gamma+\gamma(1-\eta)\,[1-(-1)^m],\text{ and } \frac{z}{H}=\frac{z}{H}-4n\right)$, the

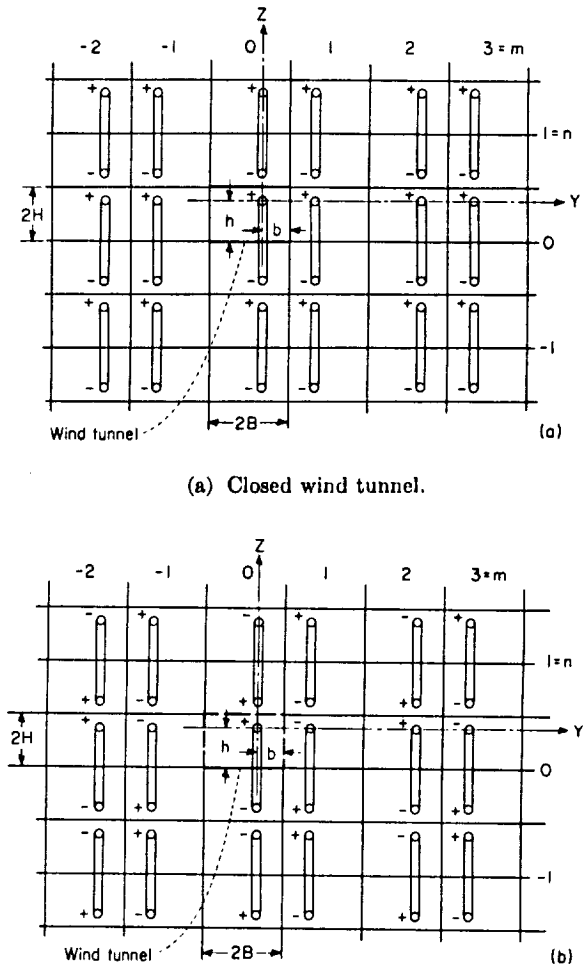


(a) Closed wind tunnel.

(b) Wind tunnel closed on bottom only.

FIGURE 4.—Central portion of image system representing effect of wind-tunnel boundaries. Plus signs indicate same direction of vertical doublets as wake in wind tunnel.

interference velocities in the wind tunnel are found as

$$\Delta w_L=\delta_{w,L}\frac{A_m}{A_T}w_O \quad (22a)$$

$$\Delta u_L=\delta_{u,L}\frac{A_m}{A_T}w_O \quad (22b)$$

$$\Delta w_D=\delta_{w,D}\frac{A_m}{A_T}u_O \quad (22c)$$

$$\Delta u_D=\delta_{u,D}\frac{A_m}{A_T}u_O \quad (22d)$$

where $\delta$ is given by

$$
\begin{aligned}
\delta=-\frac{2\gamma}{\pi}\zeta^2\Bigg\{&\sum_{\substack{n=-\infty\\ m=m\neq 0}}^{\infty}\sum_{m=-\infty}^{\infty}(-1)^p r\Bigg\{K\left[\zeta\frac{x}{H},\zeta\left\{\frac{y}{H}-2m\gamma+\gamma(1-\eta)[1-(-1)^m]\right\},\zeta\left(\frac{z}{H}-4n\right)\right]\\
&-K\left[\left(\zeta\frac{x}{H}-\tan\chi\right),\zeta\left\{\frac{y}{H}-2m\gamma+\gamma(1-\eta)[1-(-1)^m]\right\},\zeta\left(\frac{z}{H}-4n\right)+1\right]\\
&-(-1)^q K\left[\zeta\frac{x}{H},\zeta\left\{\frac{y}{H}-2m\gamma+\gamma(1-\eta)[1-(-1)^m]\right\},-\zeta\left(\frac{z}{H}-4n\right)-2\right]\\
&+(-1)^q K\left[\left(\zeta\frac{x}{H}-\tan\chi\right),\zeta\left\{\frac{y}{H}-2m\gamma+\gamma(1-\eta)[1-(-1)^m]\right\},-\zeta\left(\frac{z}{H}-4n\right)-1\right]\\
&+2sK|_{\chi=90^\circ}\left[\left(\zeta\frac{x}{H}-\tan\chi\right),\zeta\left\{\frac{y}{H}-2m\gamma+\gamma(1-\eta)[1-(-1)^m]\right\},\zeta\left(\frac{z}{H}-4n\right)+1\right]\Bigg\}\\
&+t\Bigg\{-K\left[\left(\zeta\frac{x}{H}-\tan\chi\right),\zeta\frac{y}{H},\zeta\frac{z}{H}+1\right]-(-1)^q K\left[\zeta\frac{x}{H},\zeta\frac{y}{H},-\zeta\frac{z}{H}-2\right]\\
&+(-1)^q K\left[\left(\zeta\frac{x}{H}-\tan\chi\right),\zeta\frac{y}{H},-\zeta\frac{z}{H}-1\right]+2sK|_{\chi=90^\circ}\left[\left(\zeta\frac{x}{H}-\tan\chi\right),\zeta\frac{y}{H},\zeta\frac{z}{H}+1\right]\Bigg\}\Bigg\}
\end{aligned}
\tag{23}
$$

The correct combination of $K$, $p$, $q$, $r$, $s$, and $t$ for $\delta_{w,L}$, $\delta_{u,L}$, $\delta_{w,D}$, and $\delta_{u,D}$ is given in the following table for the various wind-tunnel configurations:

| Wind-tunnel configuration | Correction to | Correction factor | $K$ from equations | $p$ | $q$ | $r$ | $s$ | $t$ |
|---|---|---|---|---|---|---|---|---|
| Closed | Free air | $\delta_{w,L}$ | (5) | 0 | 0 | 1 | 0 | 1 |
| | | $\delta_{u,L}$ | (6) | 0 | 1 | 1 | 0 | 1 |
| | | $\delta_{w,D}$ | (11) | 0 | 0 | 1 | 1 | 1 |
| | | $\delta_{u,D}$ | (12) | 0 | 1 | 1 | 1 | 1 |
| Closed on bottom only | Free air | $\delta_{w,L}$ | (5) | $m+n$ | 0 | 1 | 0 | 1 |
| | | $\delta_{u,L}$ | (6) | $m+n$ | 1 | 1 | 0 | 1 |
| | | $\delta_{w,D}$ | (11) | $m+n$ | 0 | 1 | 1 | 1 |
| | | $\delta_{u,D}$ | (12) | $m+n$ | 1 | 1 | 1 | 1 |
| Open | Free air | $\delta_{w,L}$ | (5) | $m$ | 1 | 1 | 1 | 1 |
| | | $\delta_{u,L}$ | (6) | $m$ | 0 | 1 | 1 | 1 |
| | | $\delta_{w,D}$ | (11) | $m$ | 1 | 1 | 0 | 1 |
| | | $\delta_{u,D}$ | (12) | $m$ | 0 | 1 | 0 | 1 |
| Closed floor only (ground effect) | Free air | $\delta_{w,L}$ | (5) | -------- | 0 | 0 | 0 | 1 |
| | | $\delta_{u,L}$ | (6) | -------- | 1 | 0 | 0 | 1 |
| | | $\delta_{w,D}$ | (11) | -------- | 0 | 0 | 1 | 1 |
| | | $\delta_{u,D}$ | (12) | -------- | 1 | 0 | 1 | 1 |
| Open floor only | Free air | $\delta_{w,L}$ | (5) | -------- | 1 | 0 | 1 | 1 |
| | | $\delta_{u,L}$ | (6) | -------- | 0 | 0 | 1 | 1 |
| | | $\delta_{w,D}$ | (11) | -------- | 1 | 0 | 0 | 1 |
| | | $\delta_{u,D}$ | (12) | -------- | 0 | 0 | 0 | 1 |
| Closed | Ground effect | $\delta_{w,L}$ | (5) | 0 | 0 | 1 | 0 | 0 |
| | | $\delta_{u,L}$ | (6) | 0 | 1 | 1 | 0 | 0 |
| | | $\delta_{w,D}$ | (11) | 0 | 0 | 1 | 1 | 0 |
| | | $\delta_{u,D}$ | (12) | 0 | 1 | 1 | 1 | 0 |
| Closed on bottom only | Ground effect | $\delta_{w,L}$ | (5) | $m+n$ | 0 | 1 | 0 | 0 |
| | | $\delta_{u,L}$ | (6) | $m+n$ | 1 | 1 | 0 | 0 |
| | | $\delta_{w,D}$ | (11) | $m+n$ | 0 | 1 | 1 | 0 |
| | | $\delta_{u,D}$ | (12) | $m+n$ | 1 | 1 | 1 | 0 |

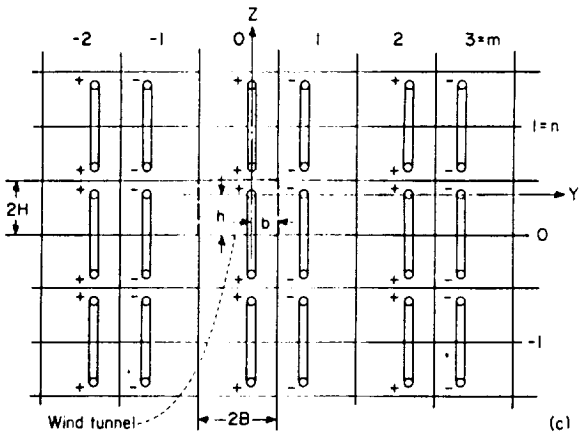


(c) Open wind tunnel.

FIGURE 4.—Concluded.

For $\chi=90°$, the wake never intersects the floor. Thus, for this case, the second, fourth, fifth, sixth, eighth, and ninth terms on the right-hand side of equation (23) are zero and may be ignored.

It will be observed that the terms corresponding to the wind tunnel and the image immediately below it ($m=n=0$) are omitted from the summation and treated separately at the end of equation (23). The term corresponding to the free-air wake itself is omitted entirely since it is *only* the *interference* velocities which are of interest herein.

The terms outside the summation of equation (23) are precisely those necessary to represent the interference velocities in ground effect. Thus, if ground effect is to be computed, the summation is set equal to zero for any wind-tunnel configuration with a solid floor. The case of an open lower boundary, or floor, has no analogy in free flight. It is only used herein in discussing the results obtained for the open wind tunnels.

It is occasionally desired to obtain wind-tunnel data for conditions in ground effect. The proper corrections are then those in which all terms after the summation (those existing in ground effect) are omitted. Alternatively, these correction factors may be obtained as the difference between the corresponding correction factors for the wind tunnel and for the wind-tunnel floor only.

## GROUND EFFECT

It has been noted previously that the case of the closed wind-tunnel floor only is identical to ground effect. Inspection of equations (5), (6), (11), (12), and (23), however, shows that for this case the $\delta$ factors are all functions of the wind-tunnel dimensions, which, for all practical purposes, do not exist. However, it will also be observed that the parameter $\delta/\zeta^2\gamma$ is only a function of height above the floor (or ground). Thus, for ground effect, set, for example,

$$\Delta w_L=\zeta^2\gamma\frac{\delta_{w,L}}{\zeta^2\gamma}\frac{A_m}{A_T}w_O \tag{24}$$

Now note that

$$\frac{A_T}{\zeta^2\gamma}=\frac{4BH}{\left(\frac{H}{h}\right)^2\frac{B}{H}}=4h^2=A_G \tag{25}$$

Therefore, equation (24) reduces to

$$\Delta w_L=\left(\frac{\delta_{w,L}}{\zeta^2\gamma}\right)\frac{A_m}{A_G}w_O \tag{26}$$

Similarly, for the other three interference velocities

$$\Delta u_L=\left(\frac{\delta_{u,L}}{\zeta^2\gamma}\right)\frac{A_m}{A_G}w_O \tag{27}$$

$$\Delta w_D=\left(\frac{\delta_{w,D}}{\zeta^2\gamma}\right)\frac{A_m}{A_G}u_O \tag{28}$$

$$\Delta u_D=\left(\frac{\delta_{u,D}}{\zeta^2\gamma}\right)\frac{A_m}{A_G}u_O \tag{29}$$

Equations (26) to (29), of course, refer to the interference velocities at the center of lift ($x=y=z=0$) when the model is a distance $h$ above the ground. The interference at other points near the model may be obtained from the tables of references 9 to 12 by noting that

$$\frac{x}{h}=\frac{H}{h}\frac{x}{H}=\zeta\frac{x}{H} \tag{30a}$$

$$\frac{y}{h}=\zeta\frac{y}{H} \tag{30b}$$

$$\frac{z}{h}=\zeta\frac{z}{H} \tag{30c}$$

The coefficients $\delta/\zeta^2\gamma$ may be obtained in closed form for the center of lift. The derivation of the closed-form expressions for the interference velocities at the model in ground effect is presented in

appendix A. The results are then as follows:

$$\Delta w_L=-\frac{1}{\pi}\left(3\cos^4\chi+\frac{1}{2}\right)\frac{A_m}{A_G}w_O \tag{31}$$

$$\Delta u_L=\frac{1}{\pi}\left(3\sin\chi\cos^3\chi+\sin\chi\cos\chi+\frac{1}{2}\tan\frac{\chi}{2}\right)\frac{A_m}{A_G}w_O \tag{32}$$

$$\Delta w_D=\frac{1}{\pi}\left(2\sin\chi\cos^3\chi-\sin^3\chi\cos\chi-4\cos^3\chi-\frac{1}{2}\tan\frac{\chi}{2}\right)\frac{A_m}{A_G}u_O \tag{33}$$

$$\Delta u_D=\frac{1}{\pi}\left(4\sin\chi\cos^2\chi-3\sin^2\chi\cos^2\chi+\frac{1}{2}\frac{\cos\chi}{1+\cos\chi}\right)\frac{A_m}{A_G}u_O \tag{34}$$

These interference factors are shown in figure 5(a) for ground effect.

Since the model was assumed to be vanishingly small in the analysis, it is necessary that the height above the ground be reasonably large with respect to the model dimensions. Reference 14, which treats a similar case for lifting rotors, indicates that severe changes in the interference velocities may be encountered if this condition is not met. A subsequent section of this paper will indicate a method of extending this analysis to include cases in which the height above the ground may be small.

The case of an open floor does not have a practical significance such as ground effect, but it will be used in discussing the results obtained for open wind tunnels. The equations for the corresponding interference factors are derived in closed form for the center of lift in appendix B. These interference factors are shown in figure 5(b).

## APPLICATION OF RESULTS

**Finding $u_O$, $w_O$, and $\chi$.**—It will be observed from equations (5), (6), (11), (12), and (22) that it is necessary to know $u_O$, $w_O$, and $\chi$ for any given operating condition in the wind tunnel in order to solve for the interference velocities. Reference 15 presents a simple nomographic solution for these quantities. The pertinent charts are presented herein as figures 6 and 7. In order to use these charts it is only necessary to know the

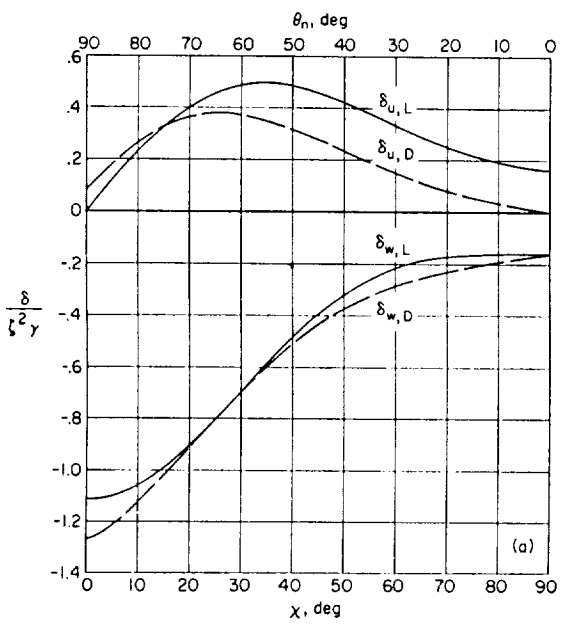


(a) Closed boundary (ground effect).

FIGURE 5.—Boundary interference factors for only lower wind-tunnel boundary.

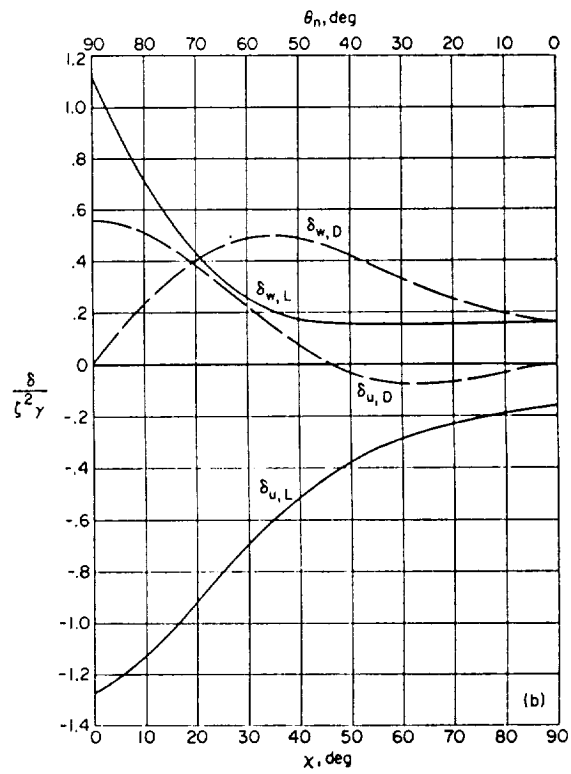


(b) Open boundary.

FIGURE 5.—Concluded.

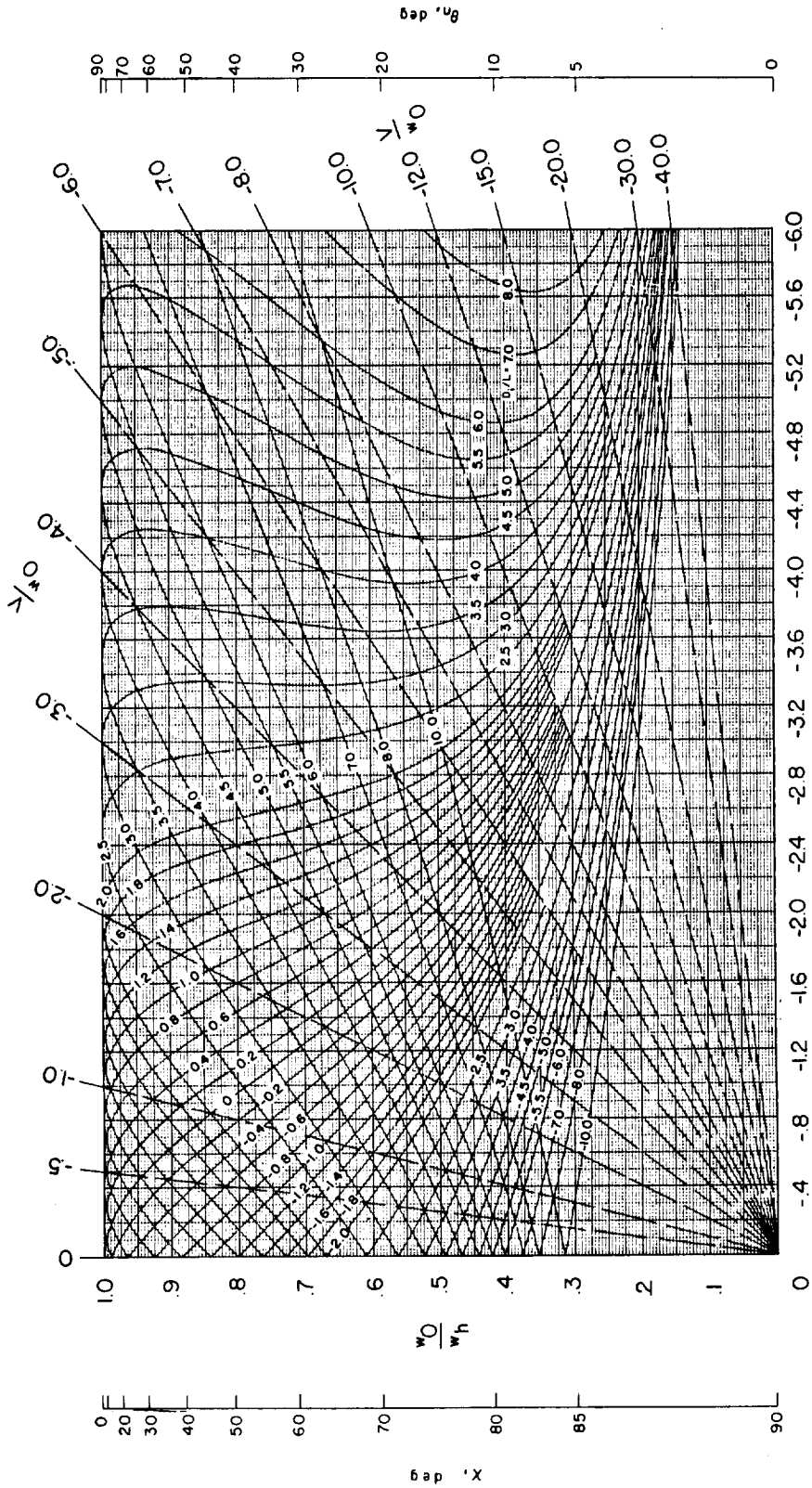


(a) $0 \geq \frac{V}{w_h} \geq -6.0$.

Figure 6.- Nondimensional values of the vertical induced velocity for various values of $D_i/L$ as a function of forward velocity.

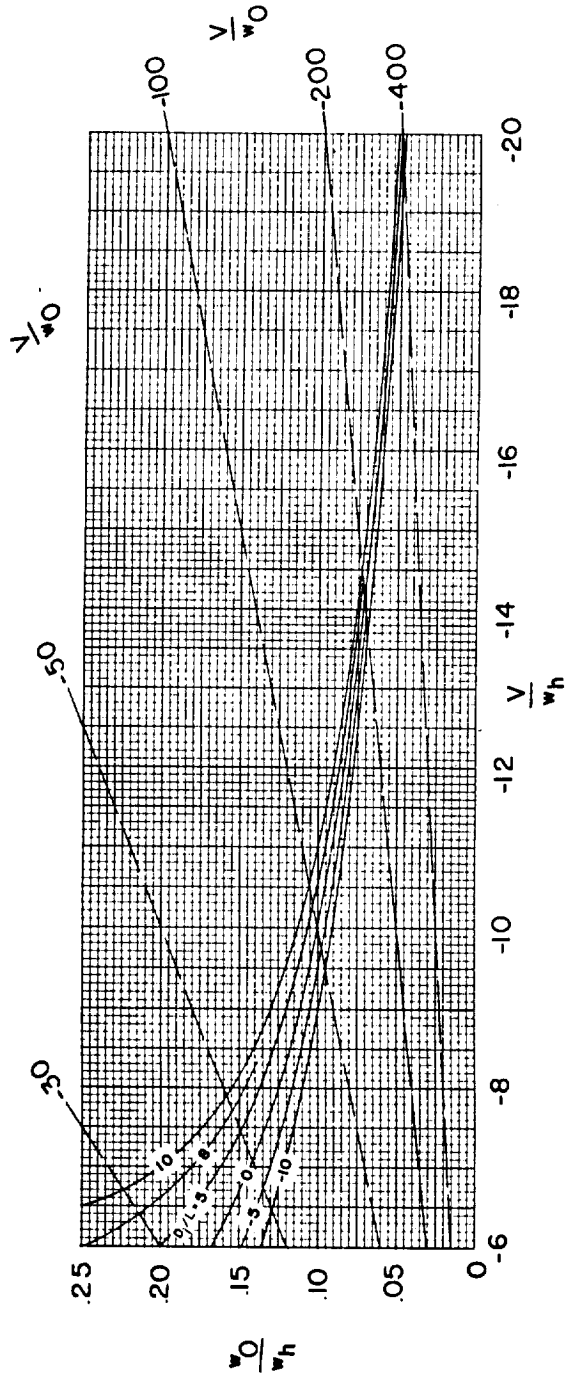


(b) $-6 \geq \frac{V}{w_h} \geq -20$.

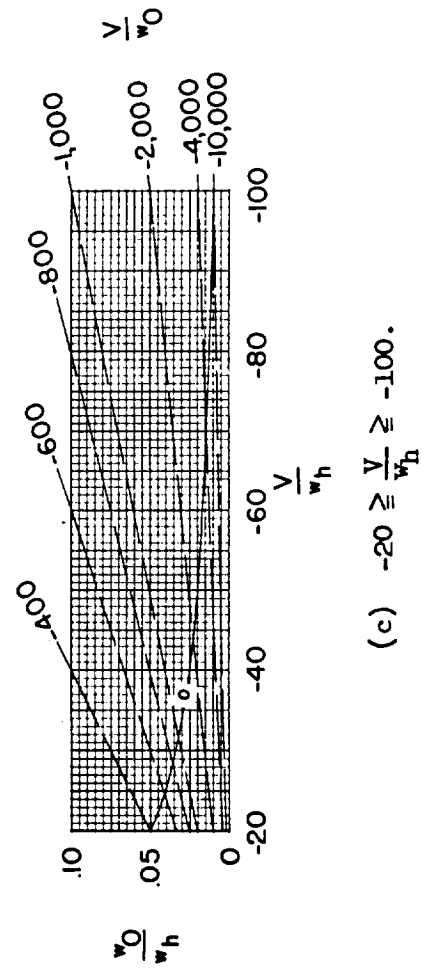


(c) $-20 \geq \frac{V}{w_h} \geq -100$.

Figure 6.- Concluded.

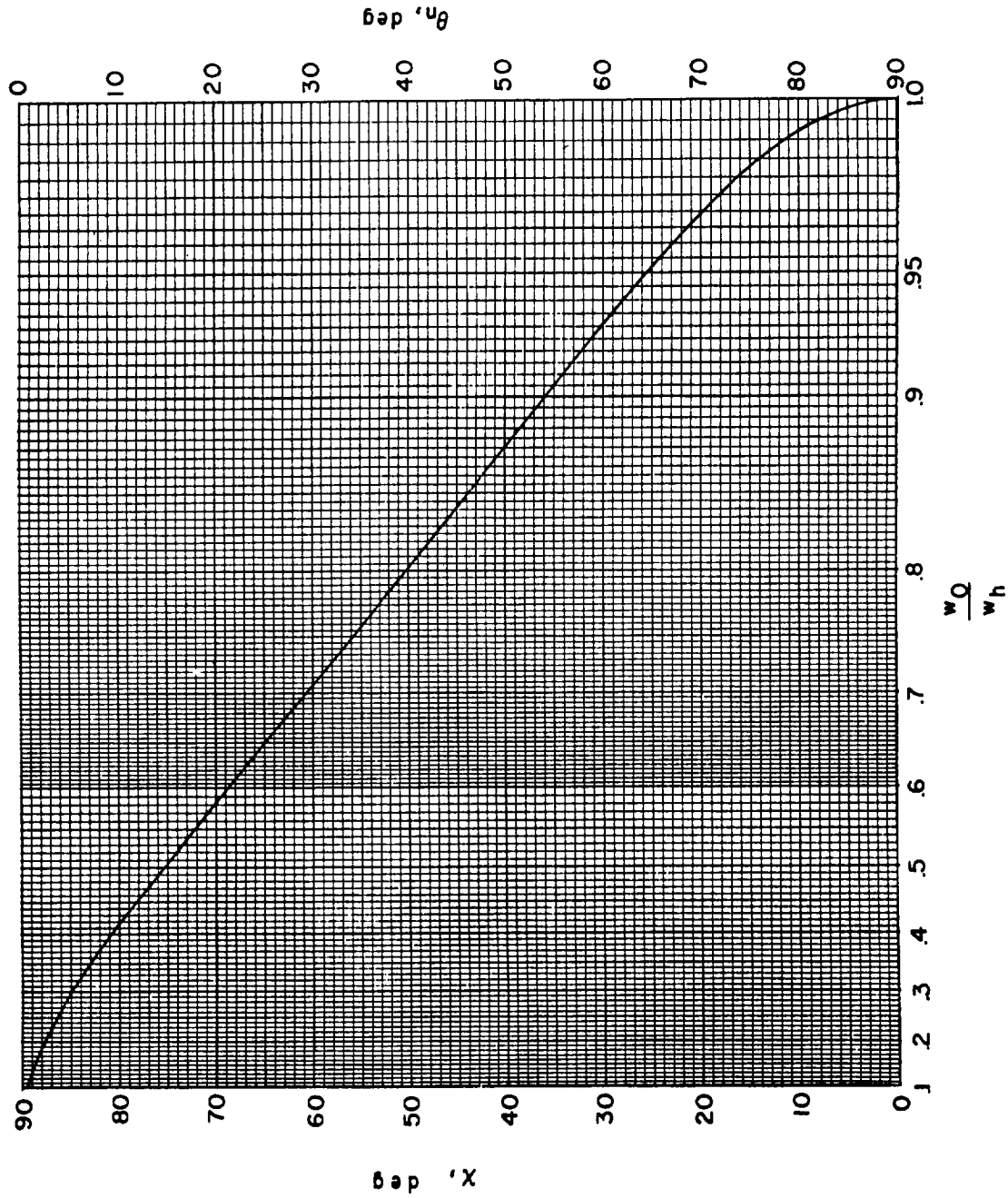


Figure 7.- Skew angle and wake deflection angle as functions of $w_0/w_h$.

forward (or wind-tunnel) velocity, the induced drag-lift ratio, and a reference velocity $w_h$ defined as

$$w_h=-\sqrt{\frac{L}{n\rho A_m}} \tag{35}$$

where $n$ is the ratio of the final induced velocities in the far wake to the initial induced velocities $u_O$ and $w_O$ at the model. If the corrections are applied by machine data-reduction processes, these charts amount to the simultaneous iterative solution of the equations

$$\left(\frac{w_O}{w_h}\right)^4=\frac{1}{1+\left(\frac{V}{w_O}+\frac{D_i}{L}\right)^2} \tag{36}$$

and

$$\frac{V}{w_h}=\frac{V}{w_O}\frac{w_O}{w_h} \tag{37}$$

Then, the mean value of the longitudinal induced velocity is obtained as

$$u_O=\frac{D_i}{L}w_O \tag{38}$$

and the wake skew angle is obtained as

$$|\chi|=\cos^{-1}\left(\frac{w_O}{w_h}\right)^2 \tag{39}$$

where $\chi$ is positive if $\frac{V}{-w_O}>\frac{D_i}{L}$ and negative if $\frac{V}{-w_O}<\frac{D_i}{L}$.

**Alternate form for interference velocities.**—If the forward velocity is not actually zero, the equations for the interference velocities may be rewritten in a form more convenient for computational purposes. Note, for example, that equations (22) may be rewritten as

$$\frac{\Delta w_L}{V}=\delta_{w,L}\frac{\rho A_m w_O}{\rho A_T V}=\delta_{w,L}\frac{M_w}{M_T} \tag{40}$$

$$\frac{\Delta u_L}{V}=\delta_{u,L}\frac{\rho A_m w_O}{\rho A_T V}=\delta_{u,L}\frac{M_w}{M_T} \tag{41}$$

$$\frac{\Delta w_D}{V}=\delta_{w,D}\frac{\rho A_m u_O}{\rho A_T V}=\delta_{w,D}\frac{M_u}{M_T} \tag{42}$$

$$\frac{\Delta u_D}{V}=\delta_{w,D}\frac{\rho A_m u_O}{\rho A_T V}=\delta_{u,D}\frac{M_u}{M_T} \tag{43}$$

where $M_w$ is the *vertical* mass flow required to obtain the given lift, $M_u$ is the *longitudinal* mass flow required to obtain the given drag, and $M_T$ is the mass flow through the wind tunnel. The advantage of using equations (40) to (43) is that it is only necessary to deal with simple and easily found ratios rather than the actual physical quantities; for example,

$$\frac{M_w}{M_T}=\frac{A_m/A_T}{V/w_O} \tag{44}$$

and, with the use of equation (38),

$$\frac{M_u}{M_T}=\frac{M_w}{M_T}\frac{D_i}{L} \tag{45}$$

If the forward velocity is actually zero, it will, of course, be necessary to use the more basic forms given earlier.

**Interference at model.**—Having found the four interference velocity ratios defined in equations (40) to (43), it is evident that the total interference at the model is given by

$$\frac{\Delta w}{V}=\frac{\Delta w_L}{V}+\frac{\Delta w_D}{V} \tag{46}$$

and

$$\frac{\Delta u}{V}=\frac{\Delta u_L}{V}+\frac{\Delta u_D}{V} \tag{47}$$

The solution to the problem could now be stated in terms of a similarity viewpoint; that is, the performance of the model in the wind tunnel is equivalent to the performance in free air with an increased rate of sink given by $\Delta w$ and an increased velocity given by $\Delta u$.

**Corrections to data.**—Unfortunately, the data from a usual wind-tunnel test are generally required for a level flight condition and not for a rate of sink which cannot be predetermined. From figure 8, it may be seen that, with respect to the effective relative velocity in the wind tunnel, the model is now operating at an angle of attack given by

$$\alpha_c=\alpha+\Delta\alpha \tag{48a}$$

where

$$\Delta\alpha=\tan^{-1}\frac{\Delta w}{V+\Delta u}=\tan^{-1}\frac{\Delta w/V}{1+\frac{\Delta u}{V}} \tag{48b}$$

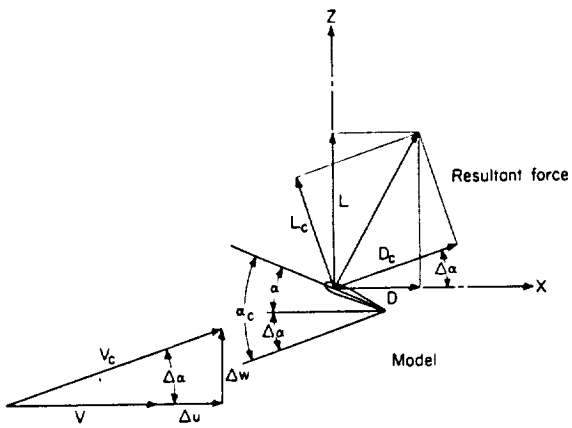


FIGURE 8.—Sketch illustrating correction of forces, velocities, and angles at model.

and at a new forward velocity given by

$$V_c=\sqrt{(V+\Delta u)^2+(\Delta w)^2} \tag{49a}$$

or in terms of dynamic pressure

$$\frac{q_c}{q}=\left(1+\frac{\Delta u}{V}\right)^2+\left(\frac{\Delta w}{V}\right)^2 \tag{49b}$$

Since lift and drag are always defined as being perpendicular and parallel, respectively, to the relative wind, it will then be necessary to resolve these components with respect to the new effective velocity; that is,

$$L_c=L\cos\Delta\alpha-D\sin\Delta\alpha \tag{50a}$$

$$D_c=L\sin\Delta\alpha+D\cos\Delta\alpha \tag{50b}$$

Finally, the lift and drag coefficients may be formed from the corrected lift and drag forces by using the dynamic pressure given by equation (49b). Notice that any other coefficients based on dynamic pressure must also be formed using the corrected dynamic pressure. For example,

$$C_{T,c}=\frac{C_T}{q_c/q} \tag{51a}$$

and

$$C_{\mu,c}=\frac{C_\mu}{q_c/q} \tag{51b}$$

A sample case of application of corrections to test data is worked out, step by step, in appendix C.

### OPEN BOUNDARIES AT LOW SPEEDS

It will be observed that the boundary condition employed for the free boundaries in this analysis depends upon the induced velocities being small in comparison with the wind-tunnel velocity; that is, the shape of the free edges of the jet is unaltered by the presence of the model. For very low speeds, which correspond to low skew angles, this condition is severely violated since the induced effects may be large even when the model is very small. This is particularly true when the free boundary is the floor of the wind tunnel. (See fig. 9.)

In the limiting case of hovering, the wind-tunnel jet does not even exist and the open boundaries will have no effect whatever. (Note that the presence of the test-chamber walls exterior to the jet is ignored.) Under such hovering conditions there will be no correction whatever to the data obtained in a completely open wind tunnel. Provided that the floor of a wind tunnel closed on the bottom only can be assumed infinite in breadth, the corrections at zero skew angle will correspond to those obtained herein for the closed floor only (with none of the free boundaries considered).

At low forward speeds other than hovering, it is assumed herein that the interference velocities for the open wind tunnel will lie somewhere between zero and those calculated for the completely open wind tunnel. Similarly, at low forward speeds, it is assumed that the interference velocities for the wind tunnel closed on the bottom only will lie between those calculated for the complete wind tunnel (closed bottom and three open boundaries) and those calculated for only the closed floor of the wind tunnel (without consideration of the three open boundaries). The consequences of these assumptions are discussed more completely in a subsequent section of this paper.

It should also be noted that the present analysis treats all wind tunnels on the assumption that the wind-tunnel boundaries extend to infinity both in front of and behind the model. Reference 6 treats the case of wind tunnels of finite test-section length and shows that large effects may exist when the test section is at least partly open. Such effects exist in the present case as well; however, inclusion of these effects is substantially beyond the scope of the present study.

## NUMERICAL CALCULATIONS

Numerical values of the correction factors were

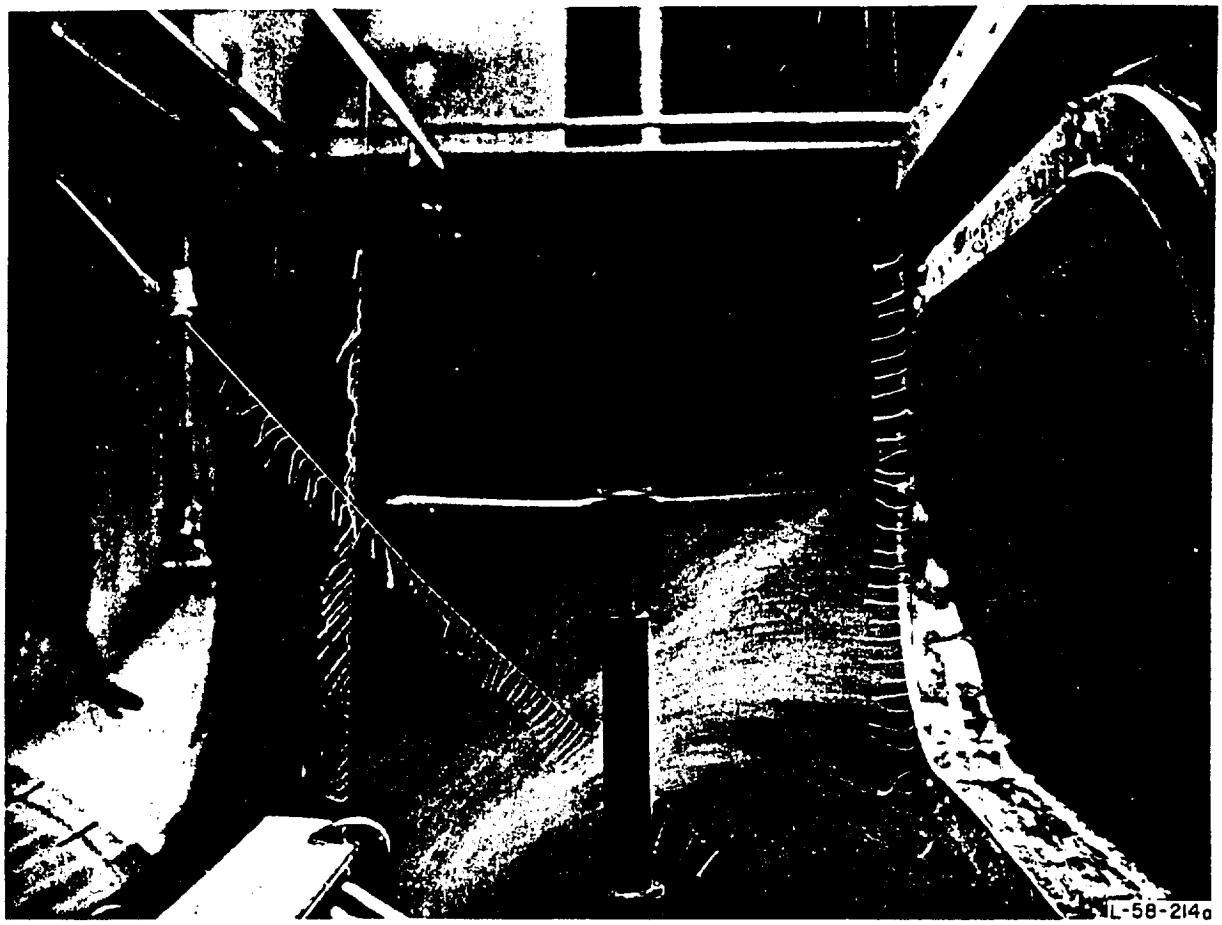


FIGURE 9.—Photograph of flow through bottom of an open wind tunnel caused by a rotor at low forward speed.

obtained by evaluating equation (23) on the digital computers at the Langley Reaserch Center (IBM 704 and IBM 7090 electronic data processing systems). With each computer, the capacity was such that it was possible to compute all four correction factors for all seven cases treated by equation (23) (28 answers in all) simultaneously. In all cases, it was assumed that all images having both $n$ and $m$ greater than 3 provided negligible contributions. On the IBM 704 computer approximately 45 seconds were required for each case, and on the IBM 7090 computer approximately 6 seconds were required for each case. The IBM 7090 computer, as installed at the Langley Research Center, is somewhat less complete than many commercial installations. It is estimated that additional time savings on the order of 20 percent could be obtained with the complete computer.

The entire numerical results are presented in tabular form in references 9 to 12. (A major portion of these results is presented graphically in subsequent sections of this paper in order that the general trends may be discussed.) The wind-tunnel configurations treated in these tables are completely closed, closed on the bottom only, and completely open. The closed-floor-only (ground effect) and open-floor-only cases are also treated. For those wind tunnels which are completely closed and those which are closed on the bottom only, corrections to ground effect are given. In all cases, wind-tunnel width-height ratios $\gamma$ of 0.5, 1.0, 1.5, and 2.0 are considered. For laterally centered models ($\eta=1.0$), the longitudinal, lateral, and vertical distributions of the interference factors are given for ratios of semiheight to height of model above floor $\zeta$ of 0.6, 0.7, 0.8, 1.0, 1.5, 2.0, 4.0, and 10.0. The lateral distribution of the

interference factors is given for models laterally offset so that $\eta$ is 0.25, 0.50, and 0.75 and simultaneously $\zeta$ is 0.7, 1.0, 2.0, and 4.0. When interference factors for other locations are required, they may be computed from the equations derived earlier in this report.

## RESULTS AND DISCUSSION

### INTERFERENCE AT THE MODEL

The interference factors at the model for use in correcting data to free-air conditions are presented in figures 10 to 21. The correction factors for correcting directly to a ground-effect condition are presented in figures 22 to 29.

**Corrections at $\chi=90°$.**—Examine first the completely symmetrical cases treated herein; that is, those cases where the model is centered ($\zeta=1.0$, $\eta=1.0$) in a completely symmetrical (either completely open or completely closed) wind tunnel. For these cases, at $\chi=90°$, symmetry can be used to show that $\delta_{u,L}$, $\delta_{w,D}$, and $\delta_{u,D}$ must all be identically zero. (Actually, the tables of refs. 9 to 12 show small values which are indicative of the accuracy of the calculation.)

Now examine the remaining factor $\delta_{w,L}$. The correction resulting from this factor is (from eq. (40))

$$\frac{\Delta w_L}{V}=\delta_{w,L}\frac{A_m w_O}{A_T V} \tag{52}$$

For a simple wing, of semispan $s$, the momentum area is

$$A_m=\pi s^2 \tag{53}$$

Furthermore, from momentum considerations, the lift is

$$L=\rho\pi s^2 V(-2w_O) \tag{54}$$

so that

$$w_O=\frac{-L}{2\rho\pi s^2 V}=\frac{-C_L S V}{4\pi s^2} \tag{55}$$

Substitute equations (53) and (55) into equation (52), and then assume that $\Delta w_L$ is small in comparison with $V$, to obtain

$$\Delta\alpha\approx\tan\Delta\alpha=\frac{\Delta w_L}{V}=\frac{-\delta_{w,L}}{4}\frac{S}{A_T}C_L \tag{56}$$

Equation (56) may be compared with the classical wind-tunnel corrections where the wake is always at $\chi=90°$. The correction from classical theory is

$$\Delta\alpha=\delta\frac{S}{A_T}C_L \tag{57}$$

It is evident from the comparison of equations (56) and (57) that, under these conditions, $\delta_{w,L}$ when divided by $-4$ coincides exactly with the classical wind-tunnel correction factor. (See ref. 8.) Thus, for these cases, the present theory contains exactly the older theory as a limiting case.

When the model is not mounted in the center of the tunnel ($\zeta\neq1.0$) or when the tunnel boundaries are not completely symmetrical (for example, the wind tunnel which is closed on the bottom only), equations (52) to (57) still hold and $-\delta_{w,L}/4$ still corresponds to $\delta$. On the other hand, the other three correction factors are no longer always zero at a skew angle of 90°. However, if the speed is high enough, and if the lift coefficient is low enough, to achieve skew angles near 90°, then $u_O$ and $w_O$ will both be small. Under such conditions, the contributions of $\delta_{w,D}$, $\delta_{u,L}$, and $\delta_{u,D}$ to the total interference at the model will be small for the usual model mounting heights. Thus, in general, the previously available correction factors may be considered as nearly, although not exactly, representing a limiting case of the present analysis.

**Effect of $\chi$ and $\zeta$.**—Figures 10 to 21 illustrate the large dependence of the correction factors upon skew angle. In general, for model locations at or below the center of the wind tunnel, the correction factors approach those calculated for only the wind-tunnel floor as the skew angle approaches zero. (This result may be noted directly in figs. 14 to 17 for the wind tunnel closed on the bottom only; in figs. 18 to 21 for the open wind tunnel; and in figs. 22 to 25, where the differences between the factors for the complete tunnel and those for the tunnel floor only are shown for the closed wind tunnel.) This trend is not as marked if the model is mounted above the center of the tunnel since the upper boundary, because of its closer proximity, then has an increased effect.

The effect of the height at which the model is mounted is extremely pronounced. Figures 10 to 21, in particular, show large differences in the correction factors even when the vertical model height is changed by as little as ⅛ of the total height of the wind tunnel. (Compare $\zeta=0.8$ with

$\zeta=1.0$.) Thus the choice of model location offers a powerful means of controlling the magnitude of the corrections required in any specific test. This point is discussed in a subsequent section of this paper.

**Effect of $\gamma$.**—It is evident from figures 10 to 29 that the correction factors become smaller as $\gamma$, the ratio of wind-tunnel width to height, becomes smaller. At very low wake skew angles, where the corrections are almost the same as those for the floor only, the correction factors vary almost in direct proportion to $\gamma$. It is generally physically possible to mount a larger model in the wider wind tunnels; however, some consideration must be given to the magnitude of the corrections that may be encountered if this is done.

Classical jet-boundary correction theory (for example, ref. 1) has pointed out several combinations of wind-tunnel configuration and proportion which lead to zero corrections for a small model. It is notable that no combination of configuration and proportions treated herein leads to a zero-correction tunnel for the entire range of skew angles.

### MINIMIZING CORRECTIONS

In selecting a model size and a wind tunnel for any test, it should be borne in mind that there is no real substitute for a very small model in a very large wind tunnel. This procedure is, of course, not always possible, particularly when the choice is restricted to models which may already be on hand, or to wind tunnels in which testing time is available. When model size and wind tunnel are fixed by such considerations, at least two alternative means of reducing the corrections are still available. These are discussed in the following paragraphs.

**Correction to ground effect.**—The first means of reducing the magnitude of the boundary corrections is to correct the data to the equivalent ground-effect condition rather than to the free-air condition. A comparison between figures 10 to 17 and figures 22 to 29 indicates that this procedure leads to substantially smaller corrections at low skew angles. This procedure is objectionable, however, in at least one regard—namely, that ground-effect data may not be desirable. On the other hand, these corrections are obtained by omitting the closest and therefore least accurate image of the reflection system. Thus, when the corrections are large, the corrections to ground effect are probably more accurate than the corrections to free air.

If corrections to ground effect are only employed at the lowest speeds, which correspond to transition from hovering to forward flight, correction to the ground-effect condition becomes less objectionable since in practice such flight conditions will usually be encountered near the ground.

**Selection of vertical height in tunnel.**—The large effect of vertical height on the correction factors affords an additional control over the magnitude of the correction factors. This is illustrated in figure 30 for the case of a closed wind tunnel with $\gamma=2.0$. The difference in vertical height in figure 30 is only ⅛ of the total wind-tunnel height, which illustrates the powerful nature of this means of control. For maximum effectiveness, the range of skew angles under which the tests will be conducted should be known in advance so that the model height can be chosen so as to minimize the corrections in this range of skew angles.

### CHOICE OF WIND-TUNNEL CONFIGURATION

It has been noted previously that as the skew angle approaches zero, the correction factors, for models at or below the wind-tunnel centerline, approach those for only the floor of the wind tunnel. As a consequence, there is little difference between the calculated correction factors for the closed and for the closed-on-the-bottom-only configurations. Both approach nearly the same corrections, namely, those of the physically realizable ground-effect condition, as the forward speed and skew angle approach zero.

In contrast, the correction factors for an open wind tunnel approach those for an open floor at low skew angles. Unfortunately, an open floor has no physical counterpart in practice. Furthermore, the correction factors for the open floor are, in general, substantially different from those for ground effect. Consequently, correction to a ground-effect condition leads to impossibly large correction factors.

Correction to ground effect is not in itself a vital matter; however, the effect of the free boundaries at low speed is vital. As discussed previously, the effect of the free boundaries vanishes as the forward speed vanishes. Thus, at low speeds, the actual corrections for a wind

tunnel closed on the bottom only are probably between those for the complete wind tunnel and those for ground effect. Since the differences between these two sets of correction factors are small, there will only be a small uncertainty (figs. 14 to 17) in the proper values to use. For a completely open wind tunnel at low speeds and high lift coefficients, the proper correction factors probably lie between zero and those computed for the complete wind tunnel. Figures 18 and 21 show these differences to be very large, and, consequently, there will be a large uncertainty in the proper values of the correction factors.

As pointed out previously, reference 6 indicates large effects of jet length on the corrections, even at $\chi=90°$. For other skew angles these jet-length effects may be even greater since they would probably exhibit a dependence upon whether the assumed wake intersects the free lower boundary or whether it intersects the closed lower boundary of the exit cone. In view of the foregoing considerations, low-speed tests of VTOL-STOL models in open wind tunnels are not recommended.

If only an open wind tunnel is available, it should be preferable to install a ground board or reflection plane along the lower edge of the jet in order to simulate a tunnel with a closed floor. This solution has proved feasible even in wind tunnels as large as the Langley full-scale tunnel which has a test section 30 feet high and 60 feet wide (fig. 31). In this case, an available reflection plane designed for semispan wing tests was modified to accept the normal tunnel mounting struts. Calibrations of the tunnel jet with the reflection plane in place were thus already available. Many open wind tunnels already have such semispan reflection planes and can be simply modified to accept a complete model. Even in those cases where a reflection plane does not already exist, construction and calibration of a reflection plane may be preferable to testing in the uneven flow often found in the return passages.

### LONGITUDINAL DISTRIBUTION OF INTERFERENCE

While a knowledge of the interference at the model itself will often be adequate if the model is sufficiently small, there are many cases in which it is necessary to know much more about the distribution of the interference over the region occupied by the model. The most obvious case in which this is true is that of tests in which pitching moments are measured. Here there will be a correction to the moments which will, in general, depend upon the difference in the interference at the center of lift and the interference at the tail location. Evaluating this correction requires a knowledge of the longitudinal distribution of the interference behind the model. This information is given in the tables of references 9 to 12. For certain cases, the interferences are displayed graphically herein in order to assist the discussion of the nature of these effects.

**Corrections to free air.**—The interference factors for correcting to free air from a closed tunnel are presented in figures 32 to 35 for a model centered in wind tunnels having width-height ratios of 2.0, 1.5, 1.0, and 0.5. The corresponding interference factors for wind tunnels closed on the bottom only are presented in figures 36 to 39.

It will be observed that the corrections for both wind tunnels are roughly similar in trend. This is particularly true at low skew angles. This result might be expected since it has already been remarked that at low skew angles the corrections are almost entirely due to the floor which is identical for either configuration. For wind tunnels with $\gamma \geqq 1.0$, the main effect of decreasing $\gamma$ is to decrease the magnitude of the correction factors. This does not hold, in general, for the narrow, deep wind tunnels ($\gamma=0.5$) where the side boundaries, because of their relatively closer proximity, can have pronounced effects upon the distribution of the interference factors.

The effect of skew angle upon the longitudinal distribution is very pronounced. Notice that the interference factors giving $\Delta w$ behave in roughly the same manner. For $\chi=0°$, the maximum value of these correction factors is found at the model location and they decrease both in front of, and behind, this point. As the skew angle increases, the point of maximum interference shifts rearward and is usually found nearly directly above the point at which the assumed wake intersects the floor. For $\chi=90°$, of course, the final value of $\delta_{w,L}$ well downstream will be twice that at the model. This is in accordance with previous work on wings.

The factors giving the horizontal interference velocities all vary in the same manner, but the trends are rather different from those discussed previously. It will be seen that, in general, the

horizontal interference velocities reverse sign at some point at or behind the model location. Thus, if the walls induce a horizontal velocity opposing the forward velocity in front of the model, then, for the same condition, but well behind the model, the walls will induce a horizontal velocity which adds to the forward velocity. Notice too that, even for cases in which the corrections are zero at the model, there may be substantial corrections required at points ahead of or behind the model (fig. 35, for example).

**Ground effect.**—The longitudinal distribution of interference in ground effect (for only the closed floor of a wind tunnel) is shown in figure 40. The trends with skew angle will not be discussed in detail since they are essentially as given in the preceding section. Note that figure 40 is presented in terms of $x/h$, which is more appropriate here. The quantity $x/h$ is given by

$$\frac{x}{h}=\zeta\frac{x}{H} \tag{58}$$

**Corrections to ground effect.**—The longitudinal distributions of interference factors for correcting directly to ground effect from a closed wind tunnel with $\gamma=1.0$ are given in figures 41 to 44. The corresponding interference factors for a wind tunnel which is closed on the bottom only are given in figures 45 to 48.

The corrections to ground effect, of course, do not include the effect of the image system directly below the wind-tunnel floor. Consequently, the effects of the upper boundary and the sides of the test chamber assume a relatively greater importance in determining the interference. These three walls are all completely closed for the closed tunnel and completely open for the wind tunnel which is closed on the bottom only. Consequently, it is found that the corresponding factors for the two wind tunnels are generally of opposite sign and that they are usually of the same order of magnitude in absolute value.

It will be seen that $\delta_{w,L}$, $\delta_{u,L}$, and $\delta_{w,D}$ all approach zero rather rapidly as the model is brought closer to the floor. In the case of $\delta_{u,L}$ and $\delta_{w,D}$ this decrease is so rapid that these correction factors are usually completely negligible for models mounted at, or below, the wind-tunnel centerline. The same result is found for low skew angles in the case of $\delta_{w,L}$; however, the reduction is somewhat less rapid at high skew angles. Even so, the corrections are small by comparison with corrections to the free-air condition. The factor $\delta_{u,D}$, however, displays a somewhat different behavior. In this case, the reduction in magnitude as the model is lowered is much slower, and a substantial correction factor exists even at $\zeta=10.0$ where the model is virtually buried in the floor. It will be noted that in this case the effect of skew angle diminishes markedly as the model is lowered. Thus, at these low model heights, a correction to the horizontal velocity at the tail may still be required; however, it may be possible to apply this correction without actually having to find the skew angle first.

**Measurement of forward velocity.**—The distribution of horizontal interference through the test chamber has important consequences with regard to the measurement of the wind-tunnel velocity itself. Notice that if the forward velocity is measured within the test section by means of a pitot tube or similar device, the walls, because of the presence of the model, will induce a horizontal velocity in the presence of the measuring device. The proper correction factor to apply in such a case will be equal to the difference between the correction factor at the model and the correction factor at the measuring device. The measurement can become even more difficult if the velocity measuring device is sensitive to small changes in pitch angle, since it will then be found necessary to correct the measuring device for the vertical interference velocity as well. Systems which measure forward velocity by sensing static pressure in the settling chamber should be much less sensitive to such effects.

### LATERAL DISTRIBUTION OF INTERFERENCE

A knowledge of the lateral distribution of interference is of importance in assessing the degree of nonuniformity of the interference over the span of a model. As will be shown in subsequent sections of this paper, the lateral distribution of interference is also of importance in estimating the interference effects on models having elements arranged in side-by-side configurations as well as in extending the analysis to models of finite span.

**Closed wind tunnels.**—The lateral distribution of the interference factors for closed wind tunnels is shown in figures 49 to 52. The interference factors are plotted against $y/B$ which may be

obtained by noting that

$$\frac{y}{B}=\frac{1}{\gamma}\frac{y}{H} \tag{59}$$

It will be seen that the interference factors which determine the vertical interference velocity are substantially less near the sides of the wind tunnel when the width-height ratio $\gamma$ is large and the skew angle $\chi$ is small. This effect is much less marked for small values of $\gamma$ and large values of $\chi$. Indeed, for $\gamma=0.5$ (fig. 49(d)) the trend is actually reversed throughout the entire range of skew angles. The lateral variation in the interference factors $\delta_{u,L}$ and $\delta_{u,D}$ is not as great as the variation in the factors $\delta_{w,L}$ and $\delta_{w,D}$. In general, the longitudinal interference factors are found to be most positive at the model and least positive near the walls.

**Wind tunnels closed on the bottom only.**—The lateral distribution of the interference factors for wind tunnels closed on the bottom only is shown in figures 53 to 56. These figures are also presented in terms of $y/B$.

It is observed in figures 53 and 55 that the interference factors giving the vertical interference velocities are uniformly most negative at the model and become less negative toward the walls. The opposite trend is shown in figures 54 and 56 for the interference factors yielding the horizontal interference velocities when the width-height ratio is large. For small width-height ratio, however, there is a tendency for this trend to reverse, yielding the most negative factors at the model.

**Ground effect.**—The lateral distribution of interference factors in ground effect is shown in figure 57. Here the interference factors are presented plotted against the appropriate nondimensional length $y/h$ where

$$\frac{y}{h}=\zeta\frac{y}{H} \tag{60}$$

In all cases, in ground effect, the maximum interference is found at the model, and as would be expected, the interference factors decrease rapidly with distance from the model.

**Corrections to ground effect.**—The lateral distribution of interference for correcting from a closed wind tunnel to ground effect is shown in figures 58 to 61 for a square wind tunnel ($\gamma=1.0$). The corresponding factors for a wind tunnel which is closed on the bottom only are shown in figures 62 to 65. It will be observed, in general, that these factors are much smaller and much less variable across the tunnel width than the corresponding factors for corrections to the free-air condition. (Note the change in scale.)

**Laterally offset models.**—The lateral distribution of interference when the model is laterally offset is shown in figures 66 to 69 for a closed wind tunnel with $\gamma=2.0$. The corresponding factors for a wind tunnel which is closed on the bottom only are shown in figures 70 to 73. These factors are plotted against the lateral location as measured from the center of the wind tunnel rather than the location as measured from the model; that is, the factors are plotted against $y'/B$ which is defined as follows:

$$\frac{y'}{B}=1-\eta+\frac{1}{\gamma}\frac{y}{H} \tag{61}$$

The location of the model for each curve is indicated by the symbol on each curve.

As expected, the distribution of interference is no longer symmetrical about the model location when the model is not mounted in the center of the wind tunnel. The differences in interference at a given distance from the model are small when the model is still near the center of the wind tunnel ($\eta=0.75$) but become increasingly larger as the model is mounted nearer the wind-tunnel wall ($\eta=0.25$).

Interference factors have only been calculated for model locations approaching one wall of the wind tunnel. There is an obvious symmetry with respect to model location. This symmetry may be stated by specifying that the correction factors for a position given by $y/H$ and $\eta$ are the same as those for $-y/H$ and $(2-\eta)$.

### VERTICAL DISTRIBUTION OF INTERFERENCE

A knowledge of the distribution of interference above and below a model becomes of importance when assessing the interference for models which consist of lifting elements arranged in a vertical array. The simplest such case is probably that of the unloaded rotor or "Rotodyne" configuration.

**Closed wind tunnels.**—The vertical distribution of the interference factors for a closed wind tunnel with a width-height ratio of 2.0 is shown in figures 74 to 77. These interference factors are plotted against the location in the wind tunnel

as given by

$$\frac{z'}{H}=\frac{z}{H}+\frac{1}{\zeta}-1 \tag{62}$$

The location of the model corresponding to each curve is shown by the symbol on the curve.

In general, the minimum rate of change of the interference factors with vertical position is found to correspond with model locations at or slightly above the center of the wind tunnel. The actual model location for minimum rate of change is, however, a function of skew angle.

For a closed wind tunnel, $\delta_{w,L}$ is a minimum at approximately the same model location as that for minimum rate of change (fig. 74). For models mounted above this point, $\delta_{w,L}$ is greater above the model than below the model. For models mounted below the point for minimum interference, $\delta_{w,L}$ is always larger below the model than above it.

The remaining three correction factors, $\delta_{u,L}$, $\delta_{w,D}$, and $\delta_{u,D}$, display an entirely different behavior. Figures 75 to 77 show that $\delta_{u,L}$ and $\delta_{u,D}$ always increase in the positive direction and that $\delta_{w,D}$ increases in the negative direction as the model is lowered.

**Wind tunnels closed on the bottom only.**—The corresponding correction factors for a wind tunnel closed on the bottom only (with $\gamma=2$) are shown in figures 78 to 81. It may be seen in figure 78 that, for this tunnel, $\delta_{w,L}$ is always greater in the positive sense above the model for all vertical locations of the model. The other three correction factors, in general, display minimum values for model locations near the center of the wind tunnel. The opposing character of the trends between this and the preceding case may be explained by the fact that in the previous case the model was positioned between two similar boundaries whereas in the present case the model was positioned between two dissimilar boundaries.

**Ground effect.**—The vertical distribution of the interference factors above and below a model in ground effect is shown in figure 82. It may be seen that all four interference factors always increase below the model and near the ground. The increase toward the ground is always greatest at low skew angles for those factors which give the vertical interference velocities. For the factors giving the horizontal interference velocities, the maximum increase is noted for skew angles near 30°.

## MORE COMPLEX MODELS

The foregoing considerations apply to models consisting either of a single lifting element or of several elements which are very closely spaced with respect to the wind-tunnel dimensions. When these conditions are met, the interference factors presented previously may be used directly. When the model consists of several lifting elements which are widely spaced in comparison with the wind-tunnel dimensions, such a simple treatment is not, in general, adequate. In such cases, it is necessary to consider the various elements of the model independently and to consider additional interference at each lifting element caused by the presence of the other elements within the wind tunnel as well as the interference at each element due to its own presence in the wind tunnel. These considerations are illustrated herein by examining three cases of equally loaded two-element lifting systems with the elements arranged in tandem, side by side, and vertically. In all cases, the discussion as well as the figures presented refer to a closed wind tunnel with a width-height ratio of 2.0.

**Tandem system.**—Consider a lifting system of two individual equally loaded elements arranged one behind the other, separated by a distance $H$ equal to the semiheight of the wind tunnel, and centered in the wind tunnel. Since effects of finite test-section length are neglected in this analysis, the longitudinal distribution of interference factors shown in part (a) of figures 32 to 35 applies to either element, provided that the origin is always assumed to be at the location of the appropriate element.

Each element of the lifting system, because of its own presence in the wind tunnel, experiences interferences at its own location which are found at $x/H=0$ in figures 32 to 35 (or alternatively, as given in figs. 10(a), 11(a), 12(a), and 13(a) for $\zeta=1.0$). This interference is shown in figure 83 as the curves labeled "Isolated element." In addition, because of the presence of the rear element, there is an additional interference at the front element. This interference may be found (in figs. 32 to 35) at the position of the front element ($x/H=-1.0$) with respect to the rear element. The total interference at the front element

is the sum of the interference caused by its own presence and the interference caused by the presence of the rear element. This sum is shown in figure 83 as the curves labeled "Front element of pair." Similarly, the rear element of the pair experiences an additional interference due solely to the presence of the front element in the wind tunnel. Thus, the total interference at the rear element is the sum of the interference caused by its own presence and the interference caused by the presence of the front rotor (found at $x/H=1.0$ in figs. 32 to 35). This sum is shown in figure 83 by the curves labeled "Rear element of pair."

It will be seen in figure 83 that the interference factors are quite different for the front and rear elements of the system. Thus, if the model is large, or if the lift is great, each element of the system will operate at substantially different effective rates of sink and effective forward velocities. Under such conditions, the actual test data may be of dubious value. It is imperative, therefore, that models incorporating tandem lifting systems be kept quite small in order to minimize such effects.

The interference factors obtained in the preceding manner are based upon only the momentum area of a single element. If it is desired to correct only the overall lift and drag of the tandem system, it is preferable to base the coefficient upon the total momentum area of the entire system. Since this momentum area is twice that of a single unit, the correction factors in this system will be one-half of those computed by the foregoing procedure. Such interference factors, giving the average interference of both elements, are presented as the curves labeled "Overall correction" in figure 83. The correction factors obtained in this manner are markedly less at low skew angles than the isolated element corrections. As will be shown in a subsequent portion of this paper, similar effects are obtained as a result of finite size of a single element.

The preceding example is relatively simple in that the lifts of the two elements have been considered to be in a fixed relation to each other; that is, the lifts were assumed to be always equal. When the lifts of the two elements are assumed to vary according to the operating condition, it is no longer permissible to add together the effects of the lifting system on itself and the effect due to the presence of the other rotor. This ensues from the fact that these two effects are caused by different systems which may have different lifts, drags, and momentum areas. In such cases, it is necessary to maintain the identity of the source of interference by finding four, rather than two, sets of interference factors. These are as follows: The interference at the front element due to its own presence, the interference at the rear element due to the presence of the front element, the interference at the rear element due to its own presence, and the interference at the front element due to the presence of the rear element. Then the interference velocities at both elements may be determined by using $A_m$, $u_o$, and $w_o$ of the front element to find the first two interferences, and $A_m$, $u_o$, and $w_o$ of the rear element to find the second two interferences. Finally, the appropriate interference *velocities* at each element may be added to obtain the total interference velocities. It is implied, of course, that the *individual* lift and drag of each element must be known in order to carry out this procedure.

**Side-by-side model.**—Consider now a side-by-side model consisting of two lifting elements separated by a distance $H$ equal to the semi-height of the wind tunnel. Assume, further, that the entire system is centered in the wind tunnel such that the two elements assume the positions described by $\eta=0.75$ and $\eta=1.25$. Because of the symmetry of the system it is necessary to consider only one element, say the element at $\eta=0.75$.

Because of its own presence in the wind tunnel, each element of the pair incurs interference velocities corresponding to the interference factors for $\eta=0.75$ at $x/H=y/H=z/H=0$. These factors are shown as a function of skew angle in figure 84, where it may be seen that they differ only slightly from those for $\eta=1.00$.

Because of the presence of the second element in the wind tunnel there is an additional interference which may be found (from the symmetry considerations previously discussed) as the interference for $\eta=0.75$ at $x/H=z/H=0$, $y/H=-1.0$. The total interference is the sum of these two terms and this sum is shown in figure 84 as the curves labeled "Either element of pair."

It may be seen in figure 84 that the total interference at either element is substantially increased over that of a single isolated element.

However, if as before, an overall correction based on the total momentum area within the wind tunnel is used, the net result is a decrease in the interference factors. The decrease is greatest at low skew angles and again is similar to the trends with finite size that will be discussed subsequently.

**Vertically arranged model.**—Finally, consider a model consisting of two equally loaded elements arranged one above the other and separated by a distance equal to $0.2H$, where $H$ is the semiheight of the wind tunnel. Assume that the upper element is centered ($\zeta=1.00$) in the wind tunnel; the lower element is then situated at $\zeta=1.25$. The interference for isolated elements in these positions is shown in figure 85. In addition to this interference, each element experiences an interference due to the presence of the other element. The total interference for each element is as shown in figure 85. The overall correction, however, when based on total momentum area, is approximately that for a single isolated element located midway between the two elements of the pair.

### EXTENSION TO FINITE-SIZE MODELS

The theory developed herein expressly applies only to models which are vanishingly small with respect to the wind-tunnel dimensions. In general, most wind-tunnel tests are conducted with models of a comparatively large size. It is well known that classic wind-tunnel interference theory (for example, ref. 2) predicts substantial effects of model size on the wind-tunnel interference. Similar work for rotors (ref. 8) predicts similar effects.

Actually, it is possible to use the present results, together with superpositions thereof, to obtain equivalent results for finite-size models. In essence, the procedure is to consider the wake originating from the model as broken into segments, each representing the wake of only a portion of the model. The effect of each partial wake as well as the interferences of all the other partial wakes in the wind tunnel can then be added at each point on the model in order to obtain an overall correction for the finite-size model.

**Wings.**—For a wing, the system of partial wakes just described would superficially resemble the wakes of several vanishingly small models flying side by side. For a wing with a ratio of span to wind-tunnel width $\sigma=0.625$ centered in a closed wind tunnel of width-height ratio $\gamma=2.0$, this system of partial wakes would appear as shown schematically in figure 86. At any point on the wing span, the interference factors will be given a a summation of the form

$$\delta=\frac{\sum_{\eta}\delta\frac{\Delta L}{\Delta s}\Delta s}{\sum_{\eta}\frac{\Delta L}{\Delta s}\Delta s} \tag{63}$$

A sample case is worked in tabular form in appendix D.

**Rotors and propellers.**—Equation (63) should be adequate for systems where the wake is planar as a result of originating essentially along a line representing the trailing edge. For a rotor or a propeller, however, the wake originates from an area, and thus describes a solid cylinder rather than a plane. In such cases, the following alternate form may be used to obtain the effect of finite size:

$$\delta=\frac{\sum_{A}\delta\frac{\Delta L}{\Delta A}\Delta A}{\sum_{A}\frac{\Delta L}{\Delta A}\Delta A} \tag{64}$$

### EFFECT OF FINITE SIZE FOR WINGS

**Interference at center of span.**—Calculations according to equation (63) have been made for wings of varying span-to-tunnel-width ratio $\sigma$ in a closed wind tunnel having a width-height ratio of 2.0. The computed interference factors at the center of the centrally located wing are shown as a function of skew angle in figure 87. It may be seen that, in this case, an increase in span always results in a significant decrease in the magnitude of all four interference factors. This does not necessarily mean, however, that the interference velocities themselves decrease, because the momentum area of the wing increases rapidly with the span of the wing. Note that, in general, for wings,

$$\frac{A_m}{A_T}=\frac{\pi s^2}{4BH}=\frac{\pi}{4}\sigma^2\gamma \tag{65}$$

Thus, as $\sigma$ increases, the interference velocities increase although not as rapidly as the momentum area increases.

**Distribution of interference over span.**—The distribution of the interference velocities over the

span of a series of finite-size wings is shown in figures 88 to 91 for the same cases treated above. In general, although not without exception (fig. 91(a)), an increase in span-width ratio leads to reduced interference factors in the central portion of the wind tunnel and increased interference factors near the walls of the wind tunnel. These interference distributions are of most importance in determining the distortion of flow over the model as a result of wind-tunnel interference. The significant item to be obtained for any individual case is the maximum difference in the interference velocities between any two points on the span. Thus, not only is it necessary to account for the increase in momentum area with span, but it is also necessary to account for the varying span itself in determining the pertinent difference. Note, for example, that because of its zero span, a wing having $\sigma=0$ has no distortion whatever, despite the fact that such a wing produces the most nonlinear distribution of the interference factors on the lateral axis of the tunnel. This point will be discussed more fully with respect to rotors in another section of this paper.

### EFFECT OF FINITE SIZE FOR ROTORS

**Wake of rotor.**—For rotors (or, equally well, for propellers near $\alpha=90°$), the wake may be represented as a continuous distribution of vortex rings, parallel to the rotor disk and carried away, under the mutual influence of the downwash and forward velocity, along an axis inclined to the rotor axis by the skew angle $\chi$ (ref. 16). For the case of uniform disk-load distribution, this wake resolves itself into a single skewed cylinder, the surface of which consists of continuous, uniformly distributed, vorticity.

**Approximate calculation of wind-tunnel interference.**—For the approximate calculation of wind-tunnel interference, that is, by using the present results to obtain interference factors for a rotor, the disk area of the rotor is broken into five equal portions as indicated schematically in figure 92. The wake of each portion of the rotor is then represented by a doublet wake, as shown, and furthermore, under the assumption of uniform disk-load distribution, the strengths of the five doublet wakes are all equal. Then the interference factors at the center of the rotor for $\sigma=0.333$ in a closed tunnel with $\gamma=2.0$ are computed by the use of equation (64).

632643 O—62——3

The interference factors, computed as outlined above, for $\sigma=0.333$ are shown in figure 93. In each case, the equivalent factors for $\sigma=0$ are also shown. In addition, for $\delta_{w,L}$, the interference factors for $\sigma=0.3$ and 0.4, as obtained by direct integration of the cylindrical vortex wake in reference 8, are shown for comparison. It may be seen, first, that the results obtained by the present method are entirely equivalent to those obtained by the method of reference 8. Second, it may be seen that, in this case, as well as for the wings treated previously, the effect of finite size is to decrease the correction factors. Although the trends are the same, however, a closer comparison of figures 87 and 93 will show differences which are ascribable to the differences in model configuration.

**Effect of finite size on $\delta_{w,L}$ at rotor center.**—More complete calculations for a rotor could be carried out according to the approximate method outlined above. On the other hand, if the discussion is restricted to $\delta_{w,L}$ only, the equations of reference 8 provide a more rapid means of obtaining this factor entirely on the digital computer. It will be noted that the equations of reference 8 are essentially equivalent to equation (23) in the present report with the sole exception that the $K$ functions are replaced by expressions more appropriate to the basic cylindrical wake and image system shown in figure 94.

Figure 95 presents $\delta_{w,L}$ as a function of wake skew angle for several size rotors in a closed wind tunnel and in a wind tunnel closed on the bottom only. Also shown in figure 95(b) is the interference for only the closed floor of either tunnel. In all cases, the rotor is centered in the wind tunnel and $\gamma$ is 2.0. It may be seen that, regardless of wind-tunnel configuration, an increase of rotor size generally decreases the interference factor. Furthermore, the magnitude of the decrease is essentially the same in all cases. In particular, figure 95(b) indicates that even when finite size is considered, the interference at low skew angles is still primarily due to only the floor of the wind tunnel.

**Effect of finite size on distribution of $\delta_{w,L}$.**—The longitudinal distribution of $\delta_{w,L}$ for various values of $\sigma$ is presented in figures 96 to 98 for the three cases treated in the preceding section. The equivalent lateral distributions are presented in figures 99 to 101. It may be seen that, in

general, an increase in $\sigma$ does not alter the general trends indicated by calculations for $\sigma=0$. However, an increase in rotor size does distinctly affect the maximum values of the interference factors found along the axes. In general, the maximum interference factor decreases with an increase in rotor size. As before, however, this decrease in the factor is not sufficient to overcome the effect of increased momentum area so that the actual interference velocities still increase with rotor size.

### MAXIMUM ALLOWABLE SIZE OF MODEL

In any test, there is a maximum size of model which can be satisfactorily employed without the necessity for excessively detailed correction procedures. For normal tests of conventional models, this size is sometimes stated in terms of a maximum allowable correction. For example, reference 17 states that the model size should be chosen so that the maximum angle-of-attack correction due to wall interference shall be less than 2°. Such limitations as those of reference 17 actually contain within themselves two features. The first is that the theoretical corrections are only approximations and a limit to the maximum size of correction also limits the approximation errors in the theory. The second feature is that if the overall correction is small, then the accompanying distortion of interference over the model will also be small. Thus it will not be necessary to provide corrections for such effects as induced camber due to nonuniform interference.

As pointed out in reference 13, the aforementioned criterion for maximum correction angle should be relaxed to some degree when the results of the present analysis are used to correct data. The basis for this statement is the fact that the 2° limitation is set on the basis of a theory which absorbs all effects of wake skew angle as an approximating error. In the present case, this problem is taken into account.

The actual size limitation for models will be set, in general, by the degree of nonuniformity of the interference over the region occupied by the model. Reference 13, by using the distributions of interference similar to those given in figures 96 to 101, develops a criterion for rotors on this basis. Note that for rotors, where the momentum area is $\pi R^2$, the vertical interference due to lift can be written as

$$\frac{\Delta w}{w_O}=\delta_{w,L}\frac{\pi R^2}{4BH}=\frac{\pi}{4}\sigma^2\gamma\delta_{w,L} \tag{66}$$

In consequence of equation (66), the vertical interference velocity is now expressed explicitly in terms of the mean vertical induced velocity of the rotor itself. If, now, the maximum difference in vertical interference velocity along the axes of the rotor is obtained from figures 96, 97, 99, and 100, it is possible, after some cross plotting, to obtain charts such as those given in figure 102. This figure shows the size of rotor which incurs a given maximum difference in interference velocity along its principal axes. This maximum difference is stated as a fraction of the mean induced velocity of the rotor itself.

Figure 102 may be used as a guide in selecting a rotor size for a given test. It would appear that for tests in which only crude qualitative data are expected, interference nonuniformities of as much as 50 percent of the rotor induced velocity might be tolerated with a maximum nonuniformity of 25 percent of the rotor induced velocity being desirable. For general-purpose quantitative test work, the corresponding percentages would be nearer 25 percent and 10 percent. If, however, it is desired to do very detailed work, such as measuring the pressure distribution on the blades for loads work, it may be necessary to restrict the maximum nonuniformity of interference velocity to the order of 5 percent or even 2 percent. Thus, once the purpose of a planned test is firmly in mind, and once the range of wake skew angles in which the test will be conducted is known, it is possible to use figure 102 to obtain the maximum allowable rotor size that is permissible.

Figure 102, of course, only applies to centrally located rotors in wind tunnels having width-height ratios of 2.0. For other mounting positions, wind-tunnel proportions, and model configurations, similar charts can be prepared by using the considerations discussed in the earlier sections of this paper.

### EXPERIMENTAL VERIFICATION

The utility of the computed corrections, of course, depends upon the degree to which they can be verified by experiment. Unfortunately,

the existence of more than one correction factor, as well as the dependence of the correction factors upon skew angle, makes direct experimental determination of the correction factors extremely difficult. Thus, in the present case, the alternative approach of attempting to correct comparative data from different wind-tunnel test sections will be used.

One source of such comparative data is reference 7 which presents the results of tests of a number of different VTOL configurations in both a 7- by 10-foot test section (fig. 103) and a 17-foot-square test section (fig. 104). The data of reference 7 have all been partially corrected by the use of standard wing corrections applied to only that portion of lift not provided by direct thrust, that is, the so-called "circulation" lift. Such corrections provide no correlation at low speeds and they have been removed from the data before presentation herein as uncorrected data.

In all cases, the interference factors for a vanishingly small model have been used in correcting the data.

**Jet flap.**—As the first example, consider the swept wing with a jet flap deflected 60°. The data for this configuration are presented in figure 105(a) (obtained from fig. 9(a) of ref. 7). The uncorrected data for the 7- by 10-foot and 17-foot sections are shown to be quite similar except for the angle of stall which is substantially less in the 7- by 10-foot test section. The corrections presented in this paper alter the two sets of data so that they appear as shown in figure 105(b). The disparity in stall angle has now essentially disappeared; but, at first glance, it would appear that the agreement between the two sets of data has been worsened in all other respects by the corrections. It should be noted, however, that the alteration in dynamic pressure has altered $C_\mu$ as well as both $C_L$ and $C_D$. Thus each point on each curve represents the performance at a different value of $C_\mu$ as well as a different value of $\alpha$. The peak values of both $C_{\mu,c}$ and $\Delta\alpha$ are noted for each case. It will be observed that the peak values are substantially different for the data from the two test sections.

In order to obtain a more graphic picture of the validity of the theory, the data have also been corrected to a common value of $C_\mu$ by the use of the experimental data for jet flaps as presented in reference 18. After this additional correction, the data appear as in figure 105(c). It may be seen that the data from the two test sections now agree within the probable experimental accuracy of the tests.

**Jet flap in ground effect.**—A similar comparison may be obtained from the ground-effect tests run on the same model in the 17-foot test section. Neglecting the finite extent of the ground board, these tests would be roughly equivalent to operating the model in a position lower than the centerline in a tunnel of width-height ratio greater than 2.0. The correction factors for such tunnels have not been computed; however, as pointed out elsewhere in this paper, the correction factors for such cases should be almost identical to those for simple ground effect. Consequently, an attempt has been made to correct these data to the free-air condition by applying the correction factors for ground effect. The uncorrected data are shown in figure 106(a). After correction, the data appear as in figure 106(b) where the peak values of $C_{\mu,c}$ and $\Delta\alpha$ are shown in each case. Finally, after correction to a common value of $C_\mu$, the data appear as in figure 106(c).

It will be observed in figure 106(c) that reasonable agreement is obtained between the data for the two highest heights; but that the agreement becomes substantially poorer at the two lower ground heights. There are several reasons for this disagreement. Note, in particular, that there is a variation of the wind-tunnel-wall induced interference along the chord of the model. This variation is relatively moderate with the model in the two highest positions but becomes increasingly severe as the model is progressively lowered. This gradient of interference is, in fact, aerodynamically equivalent to camber. The percentage of camber, computed by assuming a circular-arc camber line between the one-quarter-chord and the three-quarter-chord points of the mean aerodynamic chord of the airfoil, is noted in figure 106(c). (It should be noted that the effective camber and dihedral will also vary along the span because of sweepback as well as because of lateral gradients of interference. These features are neglected herein.) The differences between the fully corrected curves are of the nature and magnitude that might be expected as a result of the large induced inverse camber. The main point of figure 106(c) is that the model size and tunnel

size should be chosen so as to avoid pronounced variations in interference along the chord. This, rather than the absolute size of the correction factor, probably determines the maximum size of model that can be tested successfully in a given wind tunnel. In this regard, there is no real substitute for a very small model in a very large wind tunnel.

Several other reasons exist for poor agreement in this case. These include: The fact that the system used to correct the data to a common value of $C_\mu$ is only valid before stall; the finite extent of the ground board; the small differences between the corrections for ground effect and those for the appropriate wide wind tunnel; and, finally, the representation of the model as a point source of lift, a representation that becomes difficult to justify when applied to a model of over 7-foot full span operating only 1½ feet above the ground.

**Propeller-driven configurations.**—Reference 7 also presents data for a series of propeller-driven VTOL models in both test sections. Since no systematic means exist for correcting the operating variable $C_T$ to a common basis, it is not possible to use these data to obtain a clear-cut indication of the validity of the theory. The data of reference 7 have, however, been corrected by the present theory in order to provide an indication of the magnitude of the corrections and their effect upon the data. The data, uncorrected and corrected, are presented for the same model tested as a tilt-wing VTOL aircraft, a tilt-wing-with-flap VTOL aircraft, and a deflected-slipstream VTOL aircraft in figures 107, 108, and 109, respectively.

The degree of agreement or disagreement between the data for the two wind tunnels is not the main item to be gained from these figures because the degree of improved agreement will be dependent upon the sensitivity of the model performance to changes of velocity in the velocity range through which it is tested. The magnitude of the corrections is, however, important. The main difference (neglecting small changes in skew angle and wind-tunnel width-height ratio) between the data obtained in the 7- by 10-foot and 17-foot test sections is a reduction of area ratio by a factor of 4. The effect of the walls should therefore be reduced by approximately the same factor of 4; that is, the 17-foot tunnel data should still require correction by an amount approximately equal to one-third of the difference between the two sets of data. In general, this is the magnitude of the correction predicted by the present theory.

The impact of corrections upon the conclusions to be drawn from the data is illustrated by the data from the deflected-slipstream model tests presented in figure 109. Here the extent to which the aircraft may decelerate in unstalled flight is indicated by the portion of the drag polar on the right (positive drag) side of the ordinate. On this basis, the uncorrected 17-foot tunnel data would indicate that this aircraft would have to accelerate to avoid stall at $C_T=14$, and the 7- by 10-foot tunnel data would indicate that level flight without stall could just barely be maintained at $C_T=14$. On the other hand, the corrected 17-foot tunnel data indicate that the aircraft could maintain steady unaccelerated level flight at a $C_T$ of 15.1, and the corrected 7- by 10-foot tunnel data indicate an ability to maintain decelerations of 0.2g in level flight without stall at a $C_T$ of 17.0. The effect of the corrections is, therefore, of extreme importance in determining the limiting conditions of flight for this configuration.

**Ducted fan.**—The ducted-fan data of reference 7 are of particular interest since comparative tests in the 7- by 10-foot and 17-foot test sections indicated that a wall correction exists even though the fan area was less than 2 percent of the 7- by 10-foot tunnel area. The corrected and uncorrected data are shown in figure 110. For this case, the correction to $C_T$ is small percentagewise, and, as a consequence, the corrected curves nearly coincide.

**Rotors.**—Reference 19 gives data for rotor tests in an 8- by 12-foot tunnel and in 3- by 4.5-foot and 2.4- by 3.6-foot inserts within the wind tunnel. For high speeds and reasonably small lift coefficients, it is shown that the use of standard wing corrections brings the data from the various test sections into satisfactory agreement. This is as shown by the work presented herein. At the lowest speed and at lift coefficients greater than unity, the wing corrections failed to bring the data into satisfactory agreement. Unfortunately, the complete report (ref. 20), of which reference 19 is a summary, indicates that the presence of a 2-foot leading-edge extension on

the wind-tunnel inserts caused a change in the data at the lowest speed which was of the same magnitude as that observed by placing the rotor within the insert. In view of this result, it appears that the test inserts of references 19 and 20 were too short to simulate completely the smaller tunnel at this speed. Therefore, no attempt is made herein to correct these data.

**Extent of verification.**—The foregoing material indicates that there is at least partial experimental verification of the theory available. A more complete verification would require tests in different wind tunnels at very closely spaced increments of velocity in order that a uniform value of the operating conditions could be obtained by interpolation between the corrected data. Such complete comparative wind-tunnel tests are not presently available.

## CONCLUSIONS

A linearized theory of wind-tunnel jet-boundary corrections and ground effect for VTOL–STOL aircraft is presented. Numerical values of the interference factors for a wide variety of rectangular wind-tunnel configurations are presented in tabular form in NASA Technical Notes D–933, D–934, D–935, and D–936. A study of these numerical values indicates the following conclusions:

1. Wind-tunnel interference and ground effect are functions of the degree to which the wake is deflected from the horizontal. When undeflected, the present results correspond almost exactly with the results of classical jet-boundary-correction theory. When the wake is directed substantially downward, the correction factors are much increased in size. Furthermore, with substantial wake deflections, the longitudinal as well as the vertical interference velocities must be accounted for.

2. When the wake is deflected to nearly vertical angles, the wind-tunnel interference is primarily determined by the wind-tunnel floor. Therefore, under these conditions, tests in a wind tunnel with a closed floor closely correspond to tests in simple ground effect. Under similar conditions in a wind tunnel with an open floor, large distortions of the lower boundary will occur so that, in practice, the corrections will be indeterminate. For this reason, the use of completely open wind tunnels for low-speed and high-lift-coefficient testing is not recommended.

3. The theoretical results, as presented herein, strictly apply to single-element, vanishingly small models. However, methods of extending the present results to multielement systems and to finite-span models are indicated, and sample results are presented for a number of cases.

4. The theory is at least partially verified by available wind-tunnel test data. Complete verification, however, would entail substantially more meticulous tests than those for which data are presented available.

Langley Research Center,
National Aeronautics and Space Administration,
Langley Air Force Base, Va., *July 18, 1961.*

# APPENDIX A

## DERIVATION OF CLOSED-FORM EXPRESSIONS FOR THE INTERFERENCE VELOCITIES AT THE MODEL IN GROUND EFFECT

### VERTICAL INTERFERENCE DUE TO LIFT

The vertical interference velocity due to lift (wake of vertical doublets) is given by equation (26) as

$$\Delta w_L=\left(\frac{\delta_{w,L}}{\zeta^2\gamma}\right)\frac{A_m}{A_G}w_O \tag{A1a}$$

where, from equation (23) (with the double summation set equal to zero),

$$\frac{\delta_{w,L}}{\zeta^2\gamma}=-\frac{2}{\pi}\left[-K\left(\frac{x}{h}-\tan\chi,\frac{y}{h},\frac{z}{h}+1\right)-K\left(\frac{x}{h},\frac{y}{h},-\frac{z}{h}-2\right)+K\left(\frac{x}{h}-\tan\chi,\frac{y}{h},\frac{z}{h}+1\right)\right] \tag{A1b}$$

where, in turn, from equation (5b),

$$K\left(\frac{x}{h},\frac{y}{h},\frac{z}{h}\right)=\frac{\left(\frac{x}{h}\right)^2+\left(\frac{y}{h}\right)^2}{\left[\sqrt{\left(\frac{x}{h}\right)^2+\left(\frac{y}{h}\right)^2+\left(\frac{z}{h}\right)^2}+\frac{z}{h}\cos\chi-\frac{x}{h}\sin\chi\right]\left[\left(\frac{x}{h}\right)^2+\left(\frac{y}{h}\right)^2+\left(\frac{z}{h}\right)^2\right]^{3/2}}$$
$$-\left\{\frac{\frac{z}{h}+\cos\chi\sqrt{\left(\frac{x}{h}\right)^2+\left(\frac{y}{h}\right)^2+\left(\frac{z}{h}\right)^2}}{\left[\sqrt{\left(\frac{x}{h}\right)^2+\left(\frac{y}{h}\right)^2+\left(\frac{z}{h}\right)^2}+\frac{z}{h}\cos\chi-\frac{x}{h}\sin\chi\right]\sqrt{\left(\frac{x}{h}\right)^2+\left(\frac{y}{h}\right)^2+\left(\frac{z}{h}\right)^2}}\right\}^2 \tag{A1c}$$

Since it is the interference velocity at the model itself which is of interest herein, $x=y=z=0$ in equations (A1). Then, substituting equation (A1c) into equation (A1b) yields

$$\frac{\delta_{w,L}}{\zeta^2\gamma}=-\frac{2}{\pi}\left\{\frac{-\tan^2\chi}{(\sqrt{1+\tan^2\chi}+\cos\chi+\tan\chi\sin\chi)(1+\tan^2\chi)^{3/2}}+\left[\frac{1+\cos\chi\sqrt{1+\tan^2\chi}}{(\sqrt{1+\tan^2\chi}+\cos\chi+\tan\chi\sin\chi)\sqrt{1+\tan^2\chi}}\right]^2\right.$$
$$+\left[\frac{-2+2\cos\chi}{(2-2\cos\chi)(2)}\right]^2+\frac{\tan^2\chi}{(\sqrt{1+\tan^2\chi}-\cos\chi+\tan\chi\sin\chi)(1+\tan^2\chi)^{3/2}}$$
$$\left.-\left[\frac{-1+\cos\chi\sqrt{1+\tan^2\chi}}{(\sqrt{1+\tan^2\chi}-\cos\chi+\tan\chi\sin\chi)\sqrt{1+\tan^2\chi}}\right]^2\right\} \tag{A2}$$

Equation (A2) may be considerably simplified and yields

$$\frac{\delta_{w,L}}{\zeta^2\gamma}=-\frac{2}{\pi}\left(-\frac{1}{2}\sin^2\chi\cos^2\chi+\cos^4\chi+\frac{1}{4}+\frac{1}{2}\cos^2\chi\right) \tag{A3}$$

or

$$\frac{\delta_{w,L}}{\zeta^2\gamma}=-\frac{2}{\pi}\left(\frac{3}{2}\cos^4\chi+\frac{1}{4}\right) \tag{A4}$$

Finally, substituting equation (A4) into equation (A1a) yields

$$\Delta w_L=-\frac{1}{\pi}\left(3\cos^4\chi+\frac{1}{2}\right)\frac{A_m}{A_G}w_o \tag{A5}$$

LONGITUDINAL INTERFERENCE DUE TO LIFT

The longitudinal interference velocity due to lift (wake of vertical doublets) is given by equation (27):

$$\Delta u_L=\left(\frac{\delta_{u,L}}{\zeta^2\gamma}\right)\frac{A_m}{A_G}w_o \tag{A6a}$$

where, from equation (23) (with the double summation set equal to zero),

$$\frac{\delta_{u,L}}{\zeta^2\gamma}=-\frac{2}{\pi}\left[-K\left(\frac{x}{h}-\tan\chi,\frac{y}{h},\frac{z}{h}+1\right)+K\left(\frac{x}{h},\frac{y}{h},-\frac{z}{h}-2\right)-K\left(\frac{x}{h}-\tan\chi,\frac{y}{h},-\frac{z}{h}-1\right)\right] \tag{A6b}$$

where, in turn, from equation (6b),

$$K\left(\frac{x}{h},\frac{y}{h},\frac{z}{h}\right)=\frac{-\frac{x}{h}\frac{z}{h}}{\left[\sqrt{\left(\frac{x}{h}\right)^2+\left(\frac{y}{h}\right)^2+\left(\frac{z}{h}\right)^2}+\frac{z}{h}\cos\chi-\frac{x}{h}\sin\chi\right]\left[\left(\frac{x}{h}\right)^2+\left(\frac{y}{h}\right)^2+\left(\frac{z}{h}\right)^2\right]^{3/2}}$$

$$-\frac{\left[\frac{z}{h}+\cos\chi\sqrt{\left(\frac{x}{h}\right)^2+\left(\frac{y}{h}\right)^2+\left(\frac{z}{h}\right)^2}\right]\left[\frac{x}{h}-\sin\chi\sqrt{\left(\frac{x}{h}\right)^2+\left(\frac{y}{h}\right)^2+\left(\frac{z}{h}\right)^2}\right]}{\left[\sqrt{\left(\frac{x}{h}\right)^2+\left(\frac{y}{h}\right)^2+\left(\frac{z}{h}\right)^2}+\frac{z}{h}\cos\chi-\frac{x}{h}\sin\chi\right]^2\left[\left(\frac{x}{h}\right)^2+\left(\frac{y}{h}\right)^2+\left(\frac{z}{h}\right)^2\right]} \tag{A6c}$$

Substituting equation (A6c) into equation (A6b), with $x=y=z=0$, yields

$$\frac{\delta_{u,L}}{\zeta^2\gamma}=-\frac{2}{\pi}\left[\frac{-\tan\chi}{(\sqrt{1+\tan^2\chi}+\cos\chi+\tan\chi\sin\chi)(1+\tan^2\chi)^{3/2}}+\frac{(1+\cos\chi\sqrt{1+\tan^2\chi})(-\tan\chi-\sin\chi\sqrt{1+\tan^2\chi})}{(\sqrt{1+\tan^2\chi}+\cos\chi+\tan\chi\sin\chi)^2(1+\tan^2\chi)}\right.$$

$$-\frac{(-2+2\cos\chi)(-2\sin\chi)}{(2-2\cos\chi)^2(4)}+\frac{\tan\chi}{(\sqrt{1+\tan^2\chi}-\cos\chi+\tan\chi\sin\chi)(1+\tan^2\chi)^{3/2}}$$

$$\left.+\frac{(-1+\cos\chi\sqrt{1+\tan^2\chi})(-\tan\chi-\sin\chi\sqrt{1+\tan^2\chi})}{(\sqrt{1+\tan^2\chi}-\cos\chi+\tan\chi\sin\chi)^2(1+\tan^2\chi)}\right] \tag{A7}$$

which, after simplification, reduces to

$$\frac{\delta_{u,L}}{\zeta^2\gamma}=\frac{1}{\pi}\left(3\sin\chi\cos^3\chi+\sin\chi\cos\chi+\frac{1}{2}\tan\frac{\chi}{2}\right) \tag{A8}$$

Substituting equation (A8) into equation (A6a) yields

$$\Delta u_L=\frac{1}{\pi}\left(3\sin\chi\cos^3\chi+\sin\chi\cos\chi+\frac{1}{2}\tan\frac{\chi}{2}\right)\frac{A_m}{A_G}w_o \tag{A9}$$

VERTICAL INTERFERENCE DUE TO DRAG

The vertical interference velocity due to drag (wake of longitudinal doublets) is given by

equation (28) as

$$\Delta w_D=\left(\frac{\delta_{w,D}}{\zeta^2\gamma}\right)\frac{A_m}{A_G}u_O \tag{A10a}$$

where, from equation (23) (with the double summation set equal to zero),

$$\frac{\delta_{w,D}}{\zeta^2\gamma}=-\frac{2}{\pi}\left[-K\left(\frac{x}{h}-\tan\chi,\frac{y}{h},\frac{z}{h}+1\right)-K\left(\frac{x}{h},\frac{y}{h},-\frac{z}{h}-2\right)+K\left(\frac{x}{h}-\tan\chi,\frac{y}{h},-\frac{z}{h}-1\right)\right.$$
$$\left.+2K|_{\chi=90^\circ}\left(\frac{x}{h}-\tan\chi,\frac{y}{h},\frac{z}{h}+1\right)\right] \tag{A10b}$$

where, in turn, from equation (11b),

$$K\left(\frac{x}{h},\frac{y}{h},\frac{z}{h}\right)=\frac{-\frac{x}{h}\frac{z}{h}}{\left[\sqrt{\left(\frac{x}{h}\right)^2+\left(\frac{y}{h}\right)^2+\left(\frac{z}{h}\right)^2}+\frac{z}{h}\cos\chi-\frac{x}{h}\sin\chi\right]\left[\left(\frac{x}{h}\right)^2+\left(\frac{y}{h}\right)^2+\left(\frac{z}{h}\right)^2\right]^{3/2}}$$
$$-\frac{\left[\frac{z}{h}+\cos\chi\sqrt{\left(\frac{x}{h}\right)^2+\left(\frac{y}{h}\right)^2+\left(\frac{z}{h}\right)^2}\right]\left[\frac{x}{h}-\sin\chi\sqrt{\left(\frac{x}{h}\right)^2+\left(\frac{y}{h}\right)^2+\left(\frac{z}{h}\right)^2}\right]}{\left[\sqrt{\left(\frac{x}{h}\right)^2+\left(\frac{y}{h}\right)^2+\left(\frac{z}{h}\right)^2}+\frac{z}{h}\cos\chi-\frac{x}{h}\sin\chi\right]^2\left[\left(\frac{x}{h}\right)^2+\left(\frac{y}{h}\right)^2+\left(\frac{z}{h}\right)^2\right]} \tag{A10c}$$

and from equation (11c)

$$K|_{\chi=90^\circ}\left(\frac{x}{h},\frac{y}{h},\frac{z}{h}\right)=\frac{z/h}{\left[\left(\frac{x}{h}\right)^2+\left(\frac{y}{h}\right)^2+\left(\frac{z}{h}\right)^2\right]^{3/2}} \tag{A10d}$$

Substituting equations (A10c) and (A10d) into equation (A10b), with $x=y=z=0$, yields

$$\frac{\delta_{w,D}}{\zeta^2\gamma}=-\frac{2}{\pi}\left[\frac{-\tan\chi}{(\sqrt{1+\tan^2\chi}+\cos\chi+\tan\chi\sin\chi)(1+\tan^2\chi)^{3/2}}-\frac{(1+\cos\chi\sqrt{1+\tan^2\chi})(\tan\chi+\sin\chi\sqrt{1+\tan^2\chi})}{(\sqrt{1+\tan^2\chi}+\cos\chi+\tan\chi\sin\chi)^2(1+\tan^2\chi)}\right.$$
$$\left.-\frac{(-2+2\cos\chi)(2\sin\chi)}{(2-2\cos\chi)^2(4)}-\frac{\tan\chi}{(\sqrt{1+\tan^2\chi}-\cos\chi+\tan\chi\sin\chi)(1+\tan^2\chi)^{3/2}}+\frac{2}{(1+\tan^2\chi)^{3/2}}\right] \tag{A11}$$

which, after simplification, reduces to

$$\frac{\delta_{w,D}}{\zeta^2\gamma}=\frac{1}{\pi}\left(2\sin\chi\cos^3\chi-\sin^3\chi\cos\chi-4\cos^3\chi-\frac{1}{2}\tan\frac{\chi}{2}\right) \tag{A12}$$

Finally, substituting equation (A12) into equation (A10a) yields

$$\Delta w_D=\frac{1}{\pi}\left(2\sin\chi\cos^3\chi-\sin^3\chi\cos\chi-4\cos^3\chi-\frac{1}{2}\tan\frac{\chi}{2}\right)\frac{A_m}{A_G}u_O \tag{A13}$$

### LONGITUDINAL INTERFERENCE DUE TO DRAG

The longitudinal interference due to drag (wake of longitudinal doublets) is given by equation (29) as

$$\Delta u_D=\left(\frac{\delta_{u,D}}{\zeta^2\gamma}\right)\frac{A_m}{A_G}u_O \tag{A14a}$$

where, from equation (23) (with the double summation set equal to zero),

$$\frac{\delta_{u,D}}{\zeta^2\gamma}=-\frac{2}{\pi}\left[-K\left(\frac{x}{h}-\tan\chi,\frac{y}{h},\frac{z}{h}+1\right)+K\left(\frac{x}{h},\frac{y}{h},-\frac{z}{h}-2\right)\right.$$
$$\left.-K\left(\frac{x}{h}-\tan\chi,\frac{y}{h},-\frac{z}{h}-1\right)+2K|_{\chi=90^\circ}\left(\frac{x}{h}-\tan\chi,\frac{y}{h},\frac{z}{h}+1\right)\right] \quad \text{(A14b)}$$

where, in turn, from equation (12b),

$$K\left(\frac{x}{h},\frac{y}{h},\frac{z}{h}\right)=\frac{\left(\frac{y}{h}\right)^2+\left(\frac{z}{h}\right)^2}{\left[\sqrt{\left(\frac{x}{h}\right)^2+\left(\frac{y}{h}\right)^2+\left(\frac{z}{h}\right)^2}+\frac{z}{h}\cos\chi-\frac{x}{h}\sin\chi\right]\left[\left(\frac{x}{h}\right)^2+\left(\frac{y}{h}\right)^2+\left(\frac{z}{h}\right)^2\right]^{3/2}}$$
$$-\left\{\frac{\frac{x}{h}-\sin\chi\sqrt{\left(\frac{x}{h}\right)^2+\left(\frac{y}{h}\right)^2+\left(\frac{z}{h}\right)^2}}{\left[\sqrt{\left(\frac{x}{h}\right)^2+\left(\frac{y}{h}\right)^2+\left(\frac{z}{h}\right)^2}+\frac{z}{h}\cos\chi-\frac{x}{h}\sin\chi\right]\sqrt{\left(\frac{x}{h}\right)^2+\left(\frac{y}{h}\right)^2+\left(\frac{z}{h}\right)^2}}\right\}^2 \quad \text{(A14c)}$$

and, from equation (12c),

$$K|_{\chi=90^\circ}\left(\frac{x}{h},\frac{y}{h},\frac{z}{h}\right)=\frac{x/h}{\left[\left(\frac{x}{h}\right)^2+\left(\frac{y}{h}\right)^2+\left(\frac{z}{h}\right)^2\right]} \quad \text{(A14d)}$$

Substituting equations (A14c) and (A14d) into equation (A14b), with $x=y=z=0$, yields

$$\frac{\delta_{u,D}}{\zeta^2\gamma}=-\frac{2}{\pi}\left\{\frac{-1}{(\sqrt{1+\tan^2\chi}+\cos\chi+\tan\chi\sin\chi)(1+\tan^2\chi)^{3/2}}+\left[\frac{-\tan\chi-\sin\chi\sqrt{1+\tan^2\chi}}{(\sqrt{1+\tan^2\chi}+\cos\chi+\tan\chi\sin\chi)\sqrt{1+\tan^2\chi}}\right]^2\right.$$
$$+\frac{(-2)^2}{(2-2\cos\chi)(4)^{3/2}}-\left[\frac{-2\sin\chi}{(2-2\cos\chi)\sqrt{4}}\right]^2-\frac{1}{(\sqrt{1+\tan^2\chi}-\cos\chi+\tan\chi\sin\chi)(1+\tan^2\chi)^{3/2}}$$
$$\left.+\left[\frac{-\tan\chi-\sin\chi\sqrt{1+\tan^2\chi}}{(\sqrt{1+\tan^2\chi}-\cos\chi+\tan\chi\sin\chi)\sqrt{1+\tan^2\chi}}\right]^2-\frac{2\tan\chi}{(1+\tan^2\chi)^{3/2}}\right\} \quad \text{(A15)}$$

which becomes, after simplification,

$$\frac{\delta_{u,D}}{\zeta^2\gamma}=\frac{1}{\pi}\left(4\sin\chi\cos^2\chi-3\sin^2\chi\cos^2\chi+\frac{1}{2}\frac{\cos\chi}{1+\cos\chi}\right) \quad \text{(A16)}$$

Finally, substitution of equation (A16) into equation (A14a) yields

$$\Delta u_D=\frac{1}{\pi}\left(4\sin\chi\cos^2\chi-3\sin^2\chi\cos^2\chi+\frac{1}{2}\frac{\cos\chi}{1+\cos\chi}\right)\frac{A_m}{A_a}u_o \quad \text{(A17)}$$

# APPENDIX B

## DERIVATION OF CLOSED-FORM EXPRESSIONS FOR THE INTERFERENCE VELOCITIES AT THE MODEL FOR ONLY AN OPEN LOWER BOUNDARY

### VERTICAL INTERFERENCE DUE TO LIFT

The vertical interference velocity due to lift (wake of vertical doublets) is given by equation (26) as

$$\Delta w_L=\left(\frac{\delta_{w,L}}{\zeta^2\gamma}\right)\frac{A_m}{A_G}w_O \tag{B1a}$$

where, from equation (23) (with the double summation set equal to zero),

$$\frac{\delta_{w,L}}{\zeta^2\gamma}=-\frac{2}{\pi}\left[-K\left(\frac{x}{h}-\tan\chi,\frac{y}{h},\frac{z}{h}+1\right)+K\left(\frac{x}{h},\frac{y}{h},-\frac{z}{h}-2\right)\right.$$
$$\left.-K\left(\frac{x}{h}-\tan\chi,\frac{y}{h},-\frac{z}{h}-1\right)+2K|_{\chi=90^\circ}\left(\frac{x}{h}-\tan\chi,\frac{y}{h},\frac{z}{h}+1\right)\right] \tag{B1b}$$

where, in turn, from equation (5b),

$$K\left(\frac{x}{h},\frac{y}{h},\frac{z}{h}\right)=\frac{\left(\frac{x}{h}\right)^2+\left(\frac{y}{h}\right)^2}{\left[\sqrt{\left(\frac{x}{h}\right)^2+\left(\frac{y}{h}\right)^2+\left(\frac{z}{h}\right)^2}+\frac{z}{h}\cos\chi-\frac{x}{h}\sin\chi\right]\left[\left(\frac{x}{h}\right)^2+\left(\frac{y}{h}\right)^2+\left(\frac{z}{h}\right)^2\right]^{3/2}}$$
$$-\left\{\frac{\frac{z}{h}+\cos\chi\sqrt{\left(\frac{x}{h}\right)^2+\left(\frac{y}{h}\right)^2+\left(\frac{z}{h}\right)^2}}{\left[\sqrt{\left(\frac{x}{h}\right)^2+\left(\frac{y}{h}\right)^2+\left(\frac{z}{h}\right)^2}+\frac{z}{h}\cos\chi-\frac{x}{h}\sin\chi\right]\sqrt{\left(\frac{x}{h}\right)^2+\left(\frac{y}{h}\right)^2+\left(\frac{z}{h}\right)^2}}\right\}^2 \tag{B1c}$$

and, from equation (5c),

$$K|_{\chi=90^\circ}\left(\frac{x}{h},\frac{y}{h},\frac{z}{h}\right)=\frac{\left(\frac{x}{h}\right)^2+\left(\frac{y}{h}\right)^2}{\left[\sqrt{\left(\frac{x}{h}\right)^2+\left(\frac{y}{h}\right)^2+\left(\frac{z}{h}\right)^2}-\frac{x}{h}\right]\left[\left(\frac{x}{h}\right)^2+\left(\frac{y}{h}\right)^2+\left(\frac{z}{h}\right)^2\right]^{3/2}}$$
$$-\left\{\frac{z/h}{\left[\sqrt{\left(\frac{x}{h}\right)^2+\left(\frac{y}{h}\right)^2+\left(\frac{z}{h}\right)^2}-\frac{x}{h}\right]\sqrt{\left(\frac{x}{h}\right)^2+\left(\frac{y}{h}\right)^2+\left(\frac{z}{h}\right)^2}}\right\}^2 \tag{B1d}$$

Since it is the interference velocity at the model itself which is of interest herein, $x=y=z=0$ in

equations (B1). Then substituting equations (B1c) and (B1d) into equation (B1b) yields

$$\frac{\delta_{w,L}}{\zeta^2\gamma}=-\frac{2}{\pi}\left\{\frac{-\tan^2\chi}{(\sqrt{1+\tan^2\chi}+\cos\chi+\tan\chi\sin\chi)(1+\tan^2\chi)^{3/2}}\right.$$
$$+\left[\frac{1+\cos\chi\sqrt{1+\tan^2\chi}}{(\sqrt{1+\tan^2\chi}+\cos\chi+\tan\chi\sin\chi)\sqrt{1+\tan^2\chi}}\right]^2$$
$$-\left[\frac{-2+2\cos\chi}{(2-2\cos\chi)(2)}\right]^2-\frac{\tan^2\chi}{(\sqrt{1+\tan^2\chi}-\cos\chi+\tan\chi\sin\chi)(1+\tan^2\chi)^{3/2}}$$
$$\left.+\frac{2\tan^2\chi}{(\sqrt{1+\tan^2\chi}+\tan\chi)(1+\tan^2\chi)^{3/2}}-2\left[\frac{1}{(\sqrt{1+\tan^2\chi}+\tan\chi)\sqrt{1+\tan^2\chi}}\right]^2\right\} \quad \text{(B2)}$$

Equation (B2) may be considerably simplified, to yield

$$\frac{\delta_{w,L}}{\zeta^2\gamma}=\frac{1}{\pi}\left(\frac{7}{2}-8\sin\chi+4\sin^2\chi+4\sin^3\chi-3\sin^4\chi\right) \quad \text{(B3)}$$

Finally, substitute equation (B3) into equation (B1a) to obtain the vertical interference velocity at the model for an open lower boundary:

$$\Delta w_L=\frac{1}{\pi}\left(\frac{7}{2}-8\sin\chi+4\sin^2\chi+4\sin^3\chi-3\sin^4\chi\right)\frac{A_m}{A_G}w_o \quad \text{(B4)}$$

### LONGITUDINAL INTERFERENCE DUE TO LIFT

The longitudinal interference velocity due to lift (wake of vertical doublets) is given by equation (27) as

$$\Delta u_L=\left(\frac{\delta_{u,L}}{\zeta^2\gamma}\right)\frac{A_m}{A_G}w_o \quad \text{(B5a)}$$

where, from equation (23) (with the double summation set equal to zero),

$$\frac{\delta_{u,L}}{\zeta^2\gamma}=-\frac{2}{\pi}\left[-K\left(\frac{x}{h}-\tan\chi,\frac{y}{h},\frac{z}{h}+1\right)-K\left(\frac{x}{h},\frac{y}{h},-\frac{z}{h}-2\right)+K\left(\frac{x}{h}-\tan\chi,\frac{y}{h},-\frac{z}{h}-1\right)\right.$$
$$\left.+2K|_{\chi=90^\circ}\left(\frac{x}{h}-\tan\chi,\frac{y}{h},\frac{z}{h}+1\right)\right] \quad \text{(B5b)}$$

where, in turn, from equation (6b),

$$K\left(\frac{x}{h},\frac{y}{h},\frac{z}{h}\right)=\frac{-\frac{x}{h}\frac{z}{h}}{\left[\sqrt{\left(\frac{x}{h}\right)^2+\left(\frac{y}{h}\right)^2+\left(\frac{z}{h}\right)^2}+\frac{z}{h}\cos\chi-\frac{x}{h}\sin\chi\right]\left[\left(\frac{x}{h}\right)^2+\left(\frac{y}{h}\right)^2+\left(\frac{z}{h}\right)^2\right]^{3/2}}$$
$$-\frac{\left[\frac{z}{h}+\cos\chi\sqrt{\left(\frac{x}{h}\right)^2+\left(\frac{y}{h}\right)^2+\left(\frac{z}{h}\right)^2}\right]\left[\frac{x}{h}-\sin\chi\sqrt{\left(\frac{x}{h}\right)^2+\left(\frac{y}{h}\right)^2+\left(\frac{z}{h}\right)^2}\right]}{\left[\sqrt{\left(\frac{x}{h}\right)^2+\left(\frac{y}{h}\right)^2+\left(\frac{z}{h}\right)^2}+\frac{z}{h}\cos\chi-\frac{x}{h}\sin\chi\right]^2\left[\left(\frac{x}{h}\right)^2+\left(\frac{y}{h}\right)^2+\left(\frac{z}{h}\right)^2\right]} \quad \text{(B5c)}$$

and, from equation (6c),

$$K|_{\chi=90^\circ}\left(\frac{x}{h},\frac{y}{h},\frac{z}{h}\right)=\frac{z/h}{\left[\left(\frac{x}{h}\right)^2+\left(\frac{y}{h}\right)^2+\left(\frac{z}{h}\right)^2\right]^{3/2}} \tag{B5d}$$

Since it is the interference velocity at the model itself which is of interest herein, $x=y=z=0$ in equation (B5b). Then substituting equations (B5c) and (B5d) into equation (B5b) yields

$$\begin{aligned}\frac{\delta_{u,L}}{\zeta^2\gamma}=-\frac{2}{\pi}\Bigg[&\frac{-\tan\chi}{(\sqrt{1+\tan^2\chi}+\cos\chi+\tan\chi\sin\chi)(1+\tan^2\chi)^{3/2}}\\&+\frac{(1+\cos\chi\sqrt{1+\tan^2\chi})(-\tan\chi-\sin\chi\sqrt{1+\tan^2\chi})}{(\sqrt{1+\tan^2\chi}+\cos\chi+\tan\chi\sin\chi)^2(1+\tan^2\chi)}+\frac{(-2+2\cos\chi)(-2\sin\chi)}{(2-2\cos\chi)^2(4)}\\&+\frac{-\tan\chi}{(\sqrt{1+\tan^2\chi}-\cos\chi+\tan\chi\sin\chi)(1+\tan^2\chi)^{3/2}}+\frac{2}{(1+\tan^2\chi)^{3/2}}\Bigg]\end{aligned} \tag{B6}$$

which may be simplified to yield

$$\frac{\delta_{u,L}}{\zeta^2\gamma}=\frac{1}{\pi}\left(3\sin\chi\cos^3\chi-\frac{1}{2}\tan\frac{\chi}{2}-\sin\chi\cos\chi-4\cos^3\chi\right) \tag{B7}$$

Finally, substitute equation (B7) into equation (B5a) to obtain

$$\Delta u_L=\frac{1}{\pi}\left(3\sin\chi\cos^3\chi-\frac{1}{2}\tan\frac{\chi}{2}-\sin\chi\cos\chi-4\cos^3\chi\right)\frac{A_m}{A_G}w_O \tag{B8}$$

### VERTICAL INTERFERENCE DUE TO DRAG

The vertical interference velocity due to drag (wake of longitudinal doublets) is given by equation (28) as

$$\Delta w_D=\left(\frac{\delta_{w,D}}{\zeta^2\gamma}\right)\frac{A_m}{A_G}u_O \tag{B9a}$$

where, from equation (23) (with the double summation set equal to zero),

$$\frac{\delta_{w,D}}{\zeta^2\gamma}=-\frac{2}{\pi}\left[-K\left(\frac{x}{h}-\tan\chi,\frac{y}{h},\frac{z}{h}+1\right)+K\left(\frac{x}{h},\frac{y}{h},-\frac{z}{h}-2\right)-K\left(\frac{x}{h}-\tan\chi,\frac{y}{h},-\frac{z}{h}-1\right)\right] \tag{B9b}$$

where, in turn, from equation (11b),

$$\begin{aligned}K\left(\frac{x}{h},\frac{y}{h},\frac{z}{h}\right)=&\frac{-\frac{x}{h}\frac{z}{h}}{\left[\sqrt{\left(\frac{x}{h}\right)^2+\left(\frac{y}{h}\right)^2+\left(\frac{z}{h}\right)^2}+\frac{z}{h}\cos\chi-\frac{x}{h}\sin\chi\right]\left[\left(\frac{x}{h}\right)^2+\left(\frac{y}{h}\right)^2+\left(\frac{z}{h}\right)^2\right]^{3/2}}\\&-\frac{\left[\frac{z}{h}+\cos\chi\sqrt{\left(\frac{x}{h}\right)^2+\left(\frac{y}{h}\right)^2+\left(\frac{z}{h}\right)^2}\right]\left[\frac{x}{h}-\sin\chi\sqrt{\left(\frac{x}{h}\right)^2+\left(\frac{y}{h}\right)^2+\left(\frac{z}{h}\right)^2}\right]}{\left[\sqrt{\left(\frac{x}{h}\right)^2+\left(\frac{y}{h}\right)^2+\left(\frac{z}{h}\right)^2}+\frac{z}{h}\cos\chi-\frac{x}{h}\sin\chi\right]^2\left[\left(\frac{x}{h}\right)^2+\left(\frac{y}{h}\right)^2+\left(\frac{z}{h}\right)^2\right]}\end{aligned} \tag{B9c}$$

Substitution of equation (B9c) into equation (B9b), with $x=y=z=0$, yields

$$\frac{\delta_{w,D}}{\zeta^2\gamma}=-\frac{2}{\pi}\left[\frac{-\tan\chi}{(\sqrt{1+\tan^2\chi}+\cos\chi+\tan\chi\sin\chi)(1+\tan^2\chi)^{3/2}}+\frac{(1+\cos\chi\sqrt{1+\tan^2\chi})(-\tan\chi-\sin\chi\sqrt{1+\tan^2\chi})}{(\sqrt{1+\tan^2\chi}+\cos\chi+\tan\chi\sin\chi)^2(1+\tan^2\chi)}\right.$$

$$-\frac{(-2+2\cos\chi)(-2\sin\chi)}{(2-2\cos\chi)^2(4)}+\frac{\tan\chi}{(\sqrt{1+\tan^2\chi}-\cos\chi+\tan\chi\sin\chi)(1+\tan^2\chi)^{3/2}}$$

$$\left.+\frac{(-1+\cos\chi\sqrt{1+\tan^2\chi})(-\tan\chi-\sin\chi\sqrt{1+\tan^2\chi})}{(\sqrt{1+\tan^2\chi}-\cos\chi+\tan\chi\sin\chi)^2(1+\tan^2\chi)}\right] \tag{B10}$$

Simplification of equation (B10) yields

$$\frac{\delta_{w,D}}{\zeta^2\gamma}=\frac{1}{\pi}\left(3\sin\chi\cos^3\chi+\sin\chi\cos\chi+\frac{1}{2}\tan\frac{\chi}{2}\right) \tag{B11}$$

Finally, substitute equation (B11) into equation (B9a) to obtain

$$\Delta w_D=\frac{1}{\pi}\left(3\sin\chi\cos^3\chi+\sin\chi\cos\chi+\frac{1}{2}\tan\frac{\chi}{2}\right)\frac{A_m}{A_G}u_O \tag{B12}$$

### LONGITUDINAL INTERFERENCE DUE TO DRAG

The longitudinal interference due to drag (wake of longitudinal doublets) is given by equation (29) as

$$\Delta u_D=\left(\frac{\delta_{u,D}}{\zeta^2\gamma}\right)\frac{A_m}{A_G}u_O \tag{B13a}$$

where, from equation (23) (with the double summation equal to zero),

$$\frac{\delta_{u,D}}{\zeta^2\gamma}=-\frac{2}{\pi}\left[-K\left(\frac{x}{h}-\tan\chi,\frac{y}{h},\frac{z}{h}+1\right)-K\left(\frac{x}{h},\frac{y}{h},-\frac{z}{h}-2\right)+K\left(\frac{x}{h}-\tan\chi,\frac{y}{h},-\frac{z}{h}-1\right)\right] \tag{B13b}$$

where, in turn, from equation (12b),

$$K\left(\frac{x}{h},\frac{y}{h},\frac{z}{h}\right)=\frac{\left(\frac{y}{h}\right)^2+\left(\frac{z}{h}\right)^2}{\left[\sqrt{\left(\frac{x}{h}\right)^2+\left(\frac{y}{h}\right)^2+\left(\frac{z}{h}\right)^2}+\frac{z}{h}\cos\chi-\frac{x}{h}\sin\chi\right]\left[\left(\frac{x}{h}\right)^2+\left(\frac{y}{h}\right)^2+\left(\frac{z}{h}\right)^2\right]^{3/2}}$$

$$-\left\{\frac{\frac{x}{h}-\sin\chi\sqrt{\left(\frac{x}{h}\right)^2+\left(\frac{y}{h}\right)^2+\left(\frac{z}{h}\right)^2}}{\left[\sqrt{\left(\frac{x}{h}\right)^2+\left(\frac{y}{h}\right)^2+\left(\frac{z}{h}\right)^2}+\frac{z}{h}\cos\chi-\frac{x}{h}\sin\chi\right]\sqrt{\left(\frac{x}{h}\right)^2+\left(\frac{y}{h}\right)^2+\left(\frac{z}{h}\right)^2}}\right\}^2 \tag{B13c}$$

Substitution of equation (B13c) into equation (B13b), with $x=y=z=0$, yields

$$\frac{\delta_{u,D}}{\zeta^2\gamma}=-\frac{2}{\pi}\left\{\frac{-1}{(\sqrt{1+\tan^2\chi}+\cos\chi+\tan\chi\sin\chi)(1+\tan^2\chi)^{3/2}}+\left[\frac{-\tan\chi-\sin\chi\sqrt{1+\tan^2\chi}}{(\sqrt{1+\tan^2\chi}+\cos\chi+\tan\chi\sin\chi)\sqrt{1+\tan^2\chi}}\right]^2\right.$$
$$-\frac{4}{(2-2\cos\chi)(8)}+\left[\frac{-2\sin\chi}{(2-2\cos\chi)(2)}\right]^2+\frac{1}{(\sqrt{1+\tan^2\chi}-\cos\chi+\tan\chi\sin\chi)(1+\tan^2\chi)^{3/2}}$$
$$\left.-\left[\frac{-\tan\chi-\sin\chi\sqrt{1+\tan^2\chi}}{(\sqrt{1+\tan^2\chi}-\cos\chi+\tan\chi\sin\chi)\sqrt{1+\tan^2\chi}}\right]^2\right\} \tag{B14}$$

Simplification of equation (B14) yields

$$\frac{\delta_{u,D}}{\zeta^2\gamma}=\frac{1}{\pi}\left(2\cos^4\chi-\sin^2\chi\cos^2\chi-\frac{1}{2}\frac{\cos\chi}{1+\cos\chi}\right) \tag{B15}$$

Finally, substitute equation (B15) into equation (B13a) to obtain

$$\Delta u_D=\frac{1}{\pi}\left(2\cos^4\chi-\sin^2\chi\cos^2\chi-\frac{1}{2}\frac{\cos\chi}{1+\cos\chi}\right)\frac{A_m}{A_G}u_O \tag{B16}$$

# APPENDIX C

## SAMPLE CASE OF APPLICATION OF CORRECTIONS TO TEST DATA

Assume the following characteristics of the small model and the closed wind tunnel:

$S=8$ sq ft
$A_m=10$ sq ft
$n=2$
$A_T=100$ sq ft; therefore, $\frac{A_m}{A_T}=\frac{10 \text{ sq ft}}{100 \text{ sq ft}}=0.100$
$\gamma=1.5$
$\zeta=1.0$
$\eta=1.0$

The test is conducted under standard atmospheric conditions with the following conditions and results:

$C_T=10$
$V=25$ ft/sec; therefore, $q=0.743$ lb/sq ft
$\alpha=30.0°$
$L=125.0$ lb
$D=-30.0$ lb for which an estimated value of $D_t=-35.0$ lb is obtained

The following steps are then followed in the computation of this sample case:

(1) $\frac{D_t}{L}=\frac{-35.0 \text{ lb}}{125.0 \text{ lb}}=-0.280$

(2) From equation (35)

$$w_h=-\sqrt{\frac{L}{n\rho A_m}}=$$
$$-\sqrt{\frac{125.0 \text{ lb}}{2(0.002378 \text{ slug/cu ft})(10 \text{ sq ft})}}$$
$$=-51.3 \text{ ft/sec}$$

(3) $\frac{V}{w_h}=\frac{25.0 \text{ ft/sec}}{-51.3 \text{ ft/sec}}=-0.487$

(4) From figure 6

$\frac{w_O}{w_h}=0.877$

(5) $\frac{V}{w_O}=\frac{V/w_h}{w_O/w_h}=\frac{-0.487}{0.877}=-0.555$

(6) From figure 7

$\chi=39.7°$

(7) From figure 10(b)

$\delta_{w,L}=-0.87$

(8) From figure 11(b)

$\delta_{u,L}=0.72$

(9) From figure 12(b)

$\delta_{w,D}=-0.66$

(10) From figure 13(b)

$\delta_{u,D}=0.28$

(11) From equation (44)

$$\frac{M_w}{M_T}=\frac{A_m/A_T}{V/w_O}=\frac{0.100}{-0.555}=-0.180$$

(12) From equation (45)

$$\frac{M_u}{M_T}=\frac{M_w}{M_T}\frac{D_t}{L}=(-0.180)(-0.280)=0.0504$$

(13) From equation (40)

$$\frac{\Delta w_L}{V}=\delta_{w,L}\frac{M_w}{M_T}=(-0.87)(-0.180)=0.157$$

(14) From equation (41)

$$\frac{\Delta u_L}{V}=\delta_{u,L}\frac{M_w}{M_T}=(0.72)(-0.180)=-0.130$$

(15) From equation (42)

$$\frac{\Delta w_D}{V}=\delta_{w,D}\frac{M_u}{M_T}=(-0.66)(0.0504)=-0.0333$$

(16) From equation (43)

$$\frac{\Delta u_D}{V}=\delta_{u,D}\frac{M_u}{M_T}=(0.28)(0.0504)=0.0141$$

(17) From equation (46)

$$\frac{\Delta w}{V}=\frac{\Delta w_L}{V}+\frac{\Delta w_D}{V}=0.157+(-0.0333)=0.124$$

(18) From equation (47)

$$\frac{\Delta u}{V}=\frac{\Delta u_L}{V}+\frac{\Delta u_D}{V}=-0.130+0.0141=-0.116$$

(19) From equation (48b)

$$\Delta\alpha=\tan^{-1}\frac{\Delta w/V}{1+\frac{\Delta u}{V}}=\tan^{-1}\frac{0.124}{1-0.116}=8.0°$$

(20) From equation (48a)

$$\alpha_c=\alpha+\Delta\alpha=30.0°+8.0°=38.0°$$

(21) From equation (49b)

$$\frac{q_c}{q}=\left(1+\frac{\Delta u}{V}\right)^2+\left(\frac{\Delta w}{V}\right)^2$$
$$=(1-0.116)^2+(0.124)^2=0.797$$

(22) $q_c=\frac{q_c}{q}q=0.797(0.743\text{ lb/sq ft})=0.592\text{ lb/sq ft}$

(23) $V_c=\sqrt{\frac{2q_c}{\rho}}=\sqrt{\frac{2(0.592\text{ lb/sq ft})}{0.002378\text{ slug/cu ft}}}=22.3\text{ ft/sec}$

(24) From equation (51a)

$$C_{T,c}=\frac{C_T}{q_c/q}=\frac{10}{0.797}=12.55$$

(25) From equation (50a)

$$L_c=L\cos\Delta\alpha-D\sin\Delta\alpha$$
$$=(125.0\text{ lb})(\cos 8.0°)-(-30.0\text{ lb})(\sin 8.0°)=128.0\text{ lb}$$

(26) From equation (50b)

$$D_c=L\sin\Delta\alpha+D\cos\Delta\alpha$$
$$=(125.0\text{ lb})(\sin 8.0°)+(-30.0\text{ lb})(\cos 8.0°)=-12.3\text{ lb}$$

(27) $C_{L,c}=\frac{L_c}{q_cS}=\frac{128.0\text{ lb}}{(0.592\text{ lb/sq ft})(8\text{ sq ft})}=27.03$

(28) $C_{D,c}=\frac{D_c}{q_cS}=\frac{-12.3\text{ lb}}{(0.592\text{ lb/sq ft})(8\text{ sq ft})}=-2.60$

# APPENDIX D

## SAMPLE CALCULATION OF INTERFERENCE FACTOR FOR A FINITE WING

In this appendix, $\delta_{w,L}$ will be computed at $y'/H=0.5$ for a wing having a span-to-tunnel-width ratio $\sigma$ of 0.625 and operating at $\chi=60°$ in a closed wind tunnel with a width-height ratio $\gamma$ of 2.0. The wing is assumed to be centered in the wind tunnel and to have a uniform span-load distribution, with a total lift of 2.50. For the purposes of this calculation the wing wake is represented by five doublet wakes as indicated in figure 86. The calculation is carried out in tabular form as follows:

| Doublet wake at $\eta=$ | $y/H$ for $y'/H=0.5$ | $\delta$ (obtained by symmetry considerations from ref. 9) for— | | $\delta_{w,L}$ for doublet wake | Relative strength of doublet wake, $\frac{\Delta L}{\Delta s}\Delta s$ | $\delta_{w,L}\frac{\Delta L}{\Delta s}\Delta s$ |
|---|---|---|---|---|---|---|
| | | $\eta$ | $y/H$ | | | |
| 0.50 | −0.5 | 0.50 | −0.50 | −0.546 | 0.50 | −0.273 |
| .75 | 0 | .75 | 0 | −.638 | .50 | −.319 |
| 1.00 | .5 | 1.00 | .50 | −.482 | .50 | −.241 |
| 1.25 | 1.0 | .75 | −1.00 | −.224 | .50 | −.112 |
| 1.50 | 1.5 | .50 | −1.50 | −.051 | .50 | −.026 |
| Summation | | | | | 2.50 | −0.971 |

Then, with the use of equation (63),

$$\delta_{w,L}=\frac{\sum_{\eta}\delta_{w,L}\frac{\Delta L}{\Delta s}\Delta s}{\sum_{\eta}\frac{\Delta L}{\Delta s}\Delta s}=\frac{-0.971}{2.50}=-0.388$$

In order to carry out the calculation for a loading other than uniform, it is only necessary to adjust the column for the relative strength of doublet wake $\frac{\Delta L}{\Delta s}\Delta s$ to correspond to the desired loading.



632643 O—62——4

## REFERENCES


1. Theodorsen, Theodore: The Theory of Wind-Tunnel Wall Interference. NACA Rep. 410, 1931.
2. Glauert, H.: The Interference on the Characteristics of an Aerofoil in a Wind Tunnel of Rectangular Section. R. & M. No. 1459, British A.R.C., 1932.
3. Rosenhead, L.: Interference Due to Walls of a Wind-Tunnel. Proc. Roy. Soc. (London), ser. A, vol. 142, Oct. 2, 1933, pp. 308-320.
4. Theodorsen, Theodore, and Silverstein, Abe: Experimental Verification of the Theory of Wind-Tunnel Boundary Interference. NACA Rep. 478, 1934.
5. Silverstein, Abe, and White, James A.: Wind-Tunnel Interference With Particular Reference to Off-Center Positions of the Wing and to the Downwash at the Tail. NACA Rep. 547, 1936.
6. Katzoff, S., Gardner, Clifford S., Diesendruck, Leo, and Eisenstadt, Bertram J.: Linear Theory of Boundary Effects in Open Wind Tunnels With Finite Jet Lengths. NACA Rep. 976, 1950. (Supersedes NACA TN 1826.)
7. Kuhn, Richard E., and Naeseth, Rodger L.: Tunnel-Wall Effects Associated with VTOL-STOL Model Testing. Presented to Wind Tunnel and Model Testing Panel of AGARD (Brussels, Belgium), Mar. 2-5, 1959.
8. Heyson, Harry H.: Jet-Boundary Corrections for Lifting Rotors Centered in Rectangular Wind Tunnels. NASA TR R-71, 1960.
9. Heyson, Harry H.: Tables of Interference Factors for Use in Wind-Tunnel and Ground-Effect Calculations for VTOL-STOL Aircraft. Part I—Wind Tunnels Having Width-Height Ratio of 2.0. NASA TN D-933, 1961.
10. Heyson, Harry H.: Tables of Interference Factors for Use in Wind-Tunnel and Ground-Effect Calculations for VTOL-STOL Aircraft. Part II—Wind Tunnels Having Width-Height Ratio of 1.5. NASA TN D-934, 1961.
11. Heyson, Harry H.: Tables of Interference Factors for Use in Wind-Tunnel and Ground-Effect Calculations for VTOL-STOL Aircraft. Part III—Wind Tunnels Having Width-Height Ratio of 1.0. NASA TN D-935, 1961.
12. Heyson, Harry H.: Tables of Interference Factors for Use in Wind-Tunnel and Ground-Effect Calculations for VTOL-STOL Aircraft. Part IV—Wind Tunnels Having Width-Height Ratio of 0.5. NASA TN D-936, 1961.
13. Heyson, Harry H.: Wind-Tunnel Wall Interference and Ground Effect for VTOL-STOL Aircraft. Jour. Am. Helicopter Soc., vol. 6, no. 1, Jan. 1961, pp. 1-9.
14. Heyson, Harry H.: Ground Effect for Lifting Rotors in Forward Flight. NASA TN D-234, 1960.
15. Heyson, Harry H.: Nomographic Solution of the Momentum Equation for VTOL-STOL Aircraft. NASA TN D-814, 1961.
16. Heyson, Harry H., and Katzoff, S.: Induced Velocities Near a Lifting Rotor With Nonuniform Disk Loading. NACA Rep. 1319, 1957. (Supersedes NACA TN 3690 by Heyson and Katzoff and TN 3691 by Heyson.)
17. Anscombe, A., and Williams, J.: Some Comments on High-Lift Testing in Wind Tunnels With Particular Reference to Jet-Blowing Models. Rep. 63, AGARD, North Atlantic Treaty Organization (Paris), Aug. 1956.
18. Lockwood, Vernard E., Turner, Thomas R., and Riebe, John M.: Wind-Tunnel Investigation of Jet-Augmented Flaps on a Rectangular Wing to High Momentum Coefficients. NACA TN 3865, 1956.
19. Ganzer, Victor M., and Rae, William H., Jr.: An Experimental Investigation of the Effect of Wind Tunnel Walls on the Aerodynamic Performance of a Helicopter Rotor. NASA TN D-415, 1960.
20. Rae, William H., Jr., and Ganzer, Victor M.: An Experimental Investigation of the Effect of Wind Tunnel Walls on a Lifting Rotor in a Closed Rectangular Test Section. Rep. 470, Univ. of Washington Aero. Lab. (Contract NAw-6442), Apr. 15, 1958.

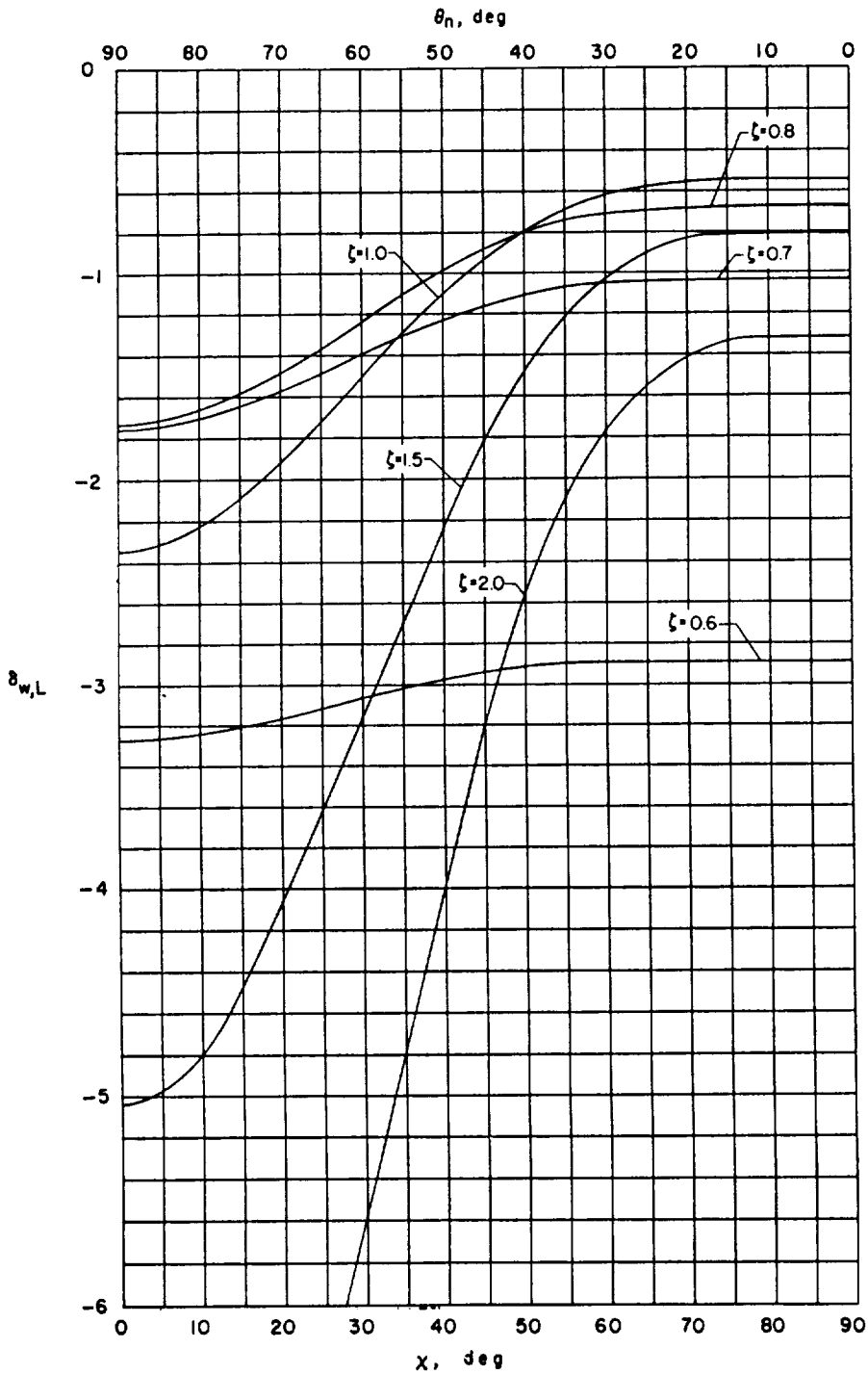


(a) $\gamma = 2.0$.

Figure 10.- Interference factors for vertical interference velocity due to lift for a small model mounted in a closed wind tunnel. $\eta = 1.0$.

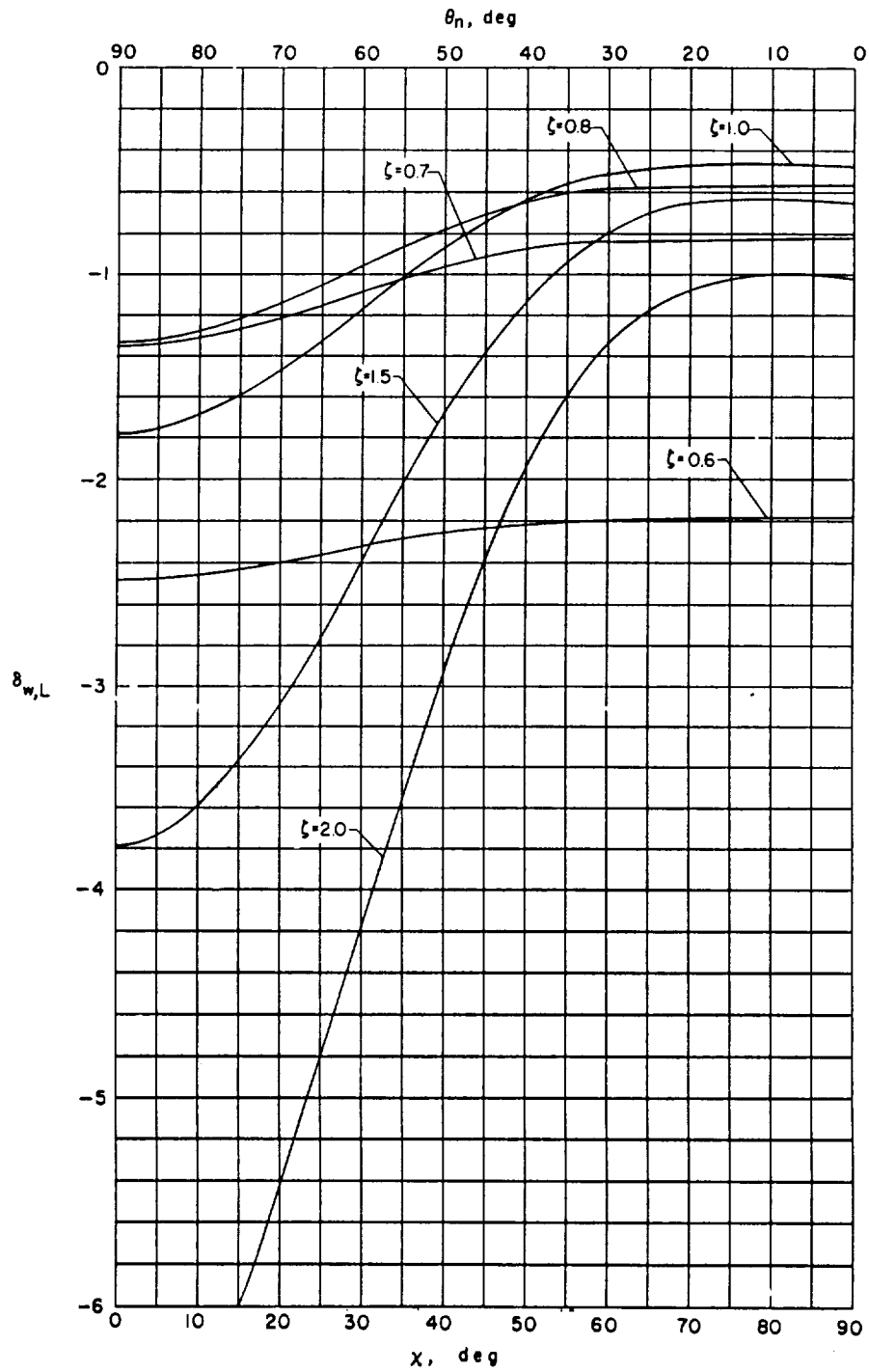


(b) $\gamma = 1.5$.

Figure 10.- Continued.

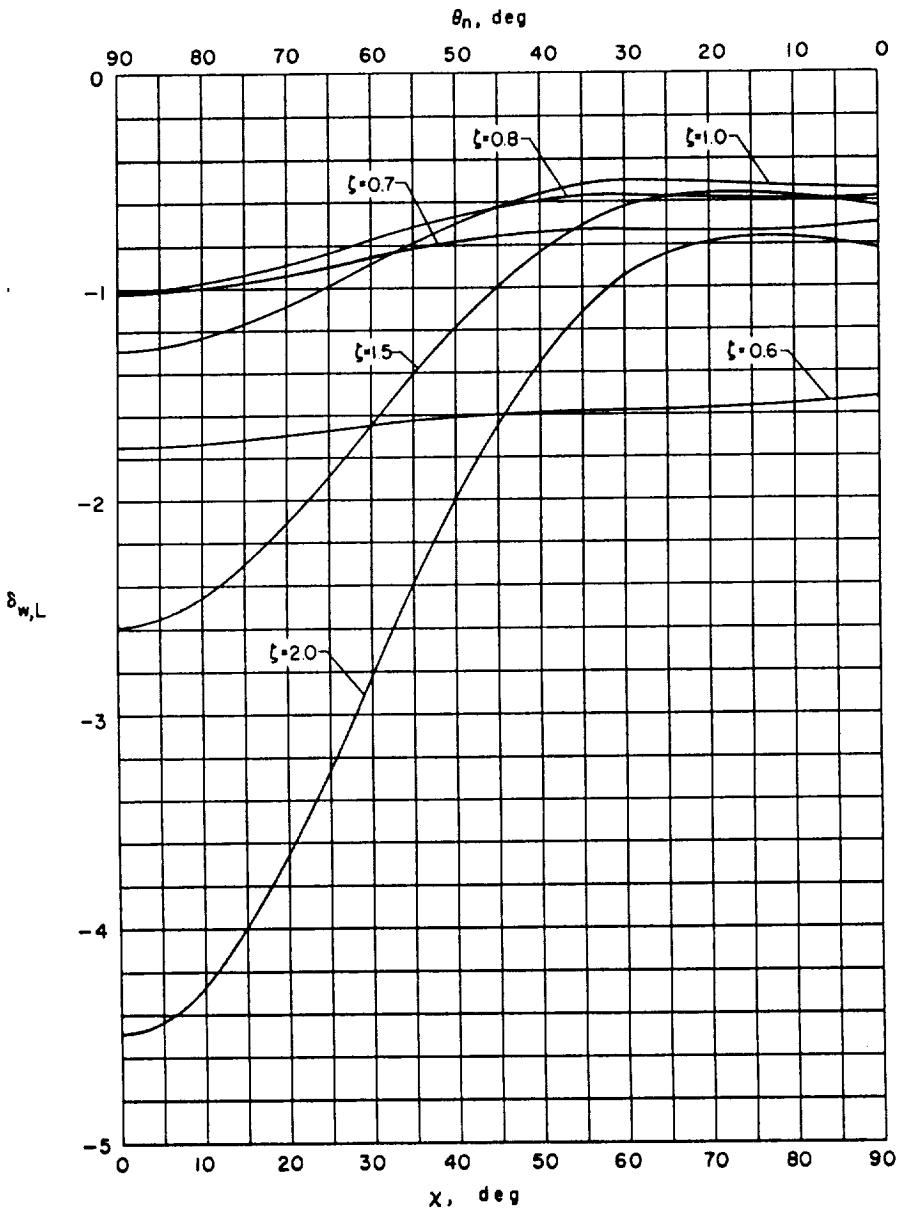


(c) $\gamma = 1.0$.

**Figure 10.- Continued.**

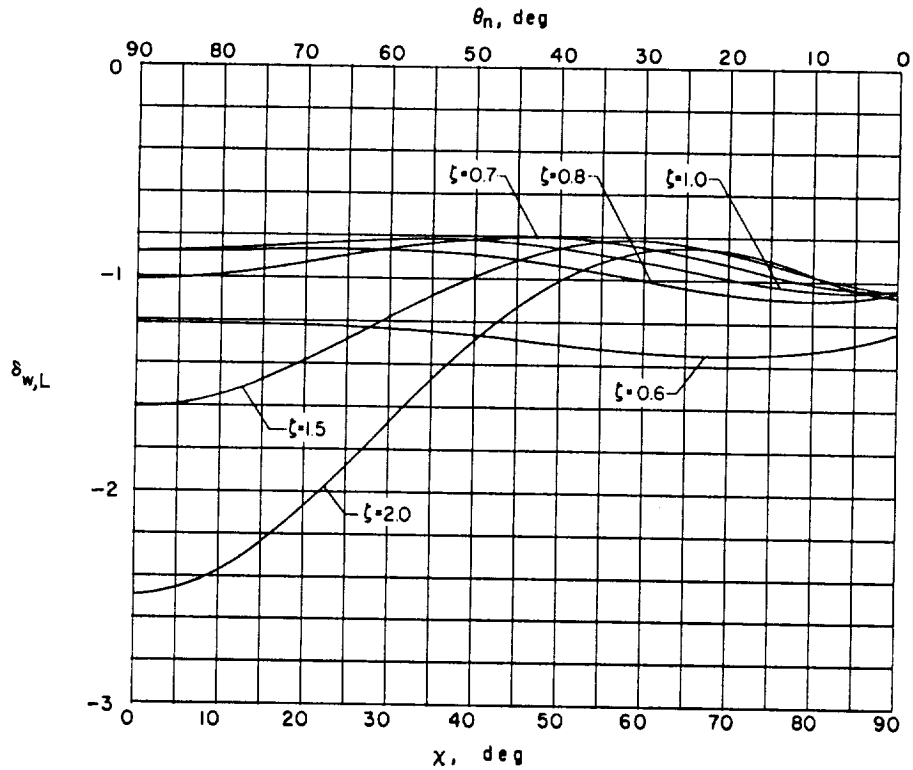


(d) $\gamma = 0.5$.

Figure 10.- Concluded.

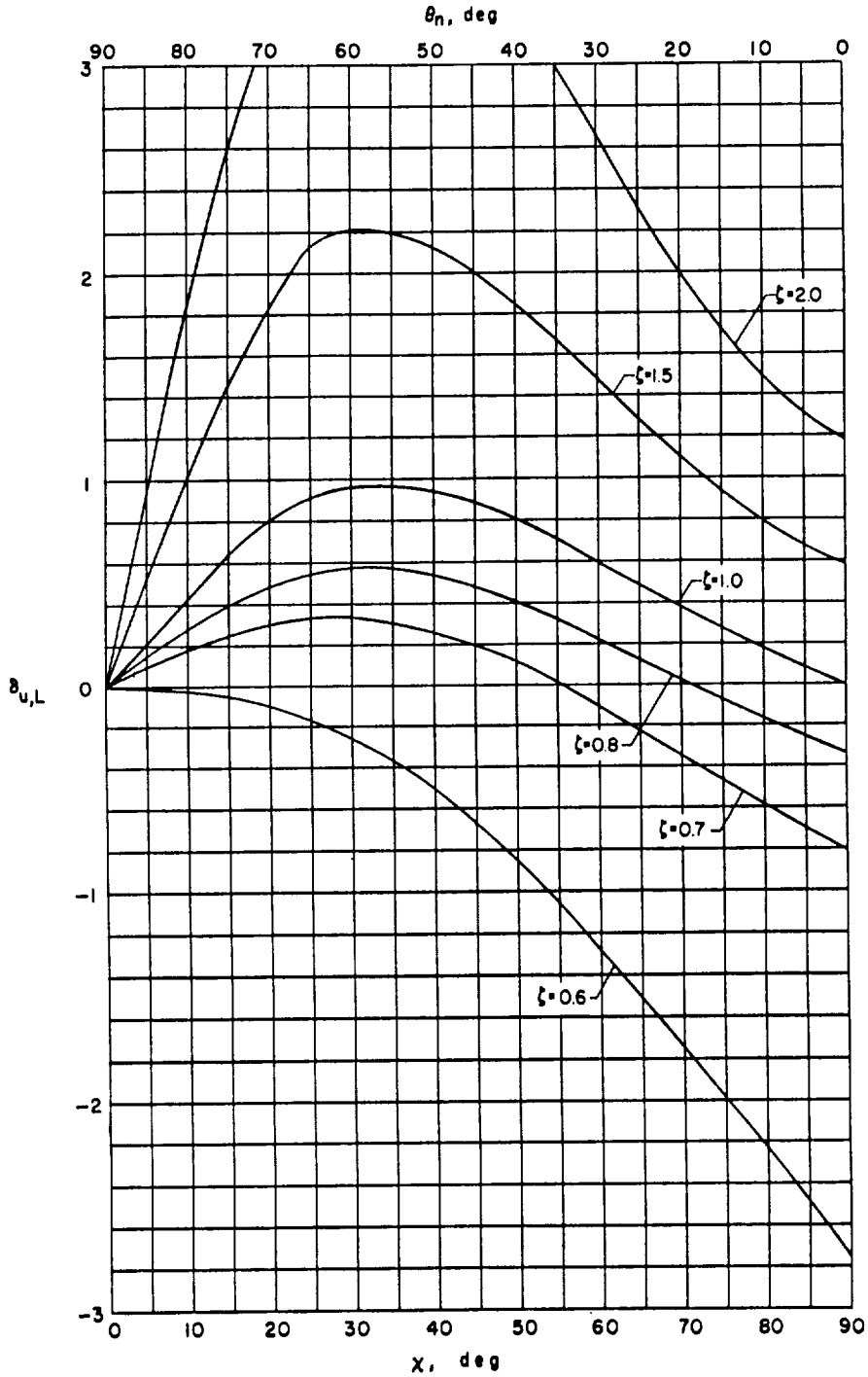


(a) $\gamma = 2.0$.

Figure 11.- Interference factors for longitudinal interference velocity due to lift for a small model mounted in a closed wind tunnel. $\eta = 1.0$.

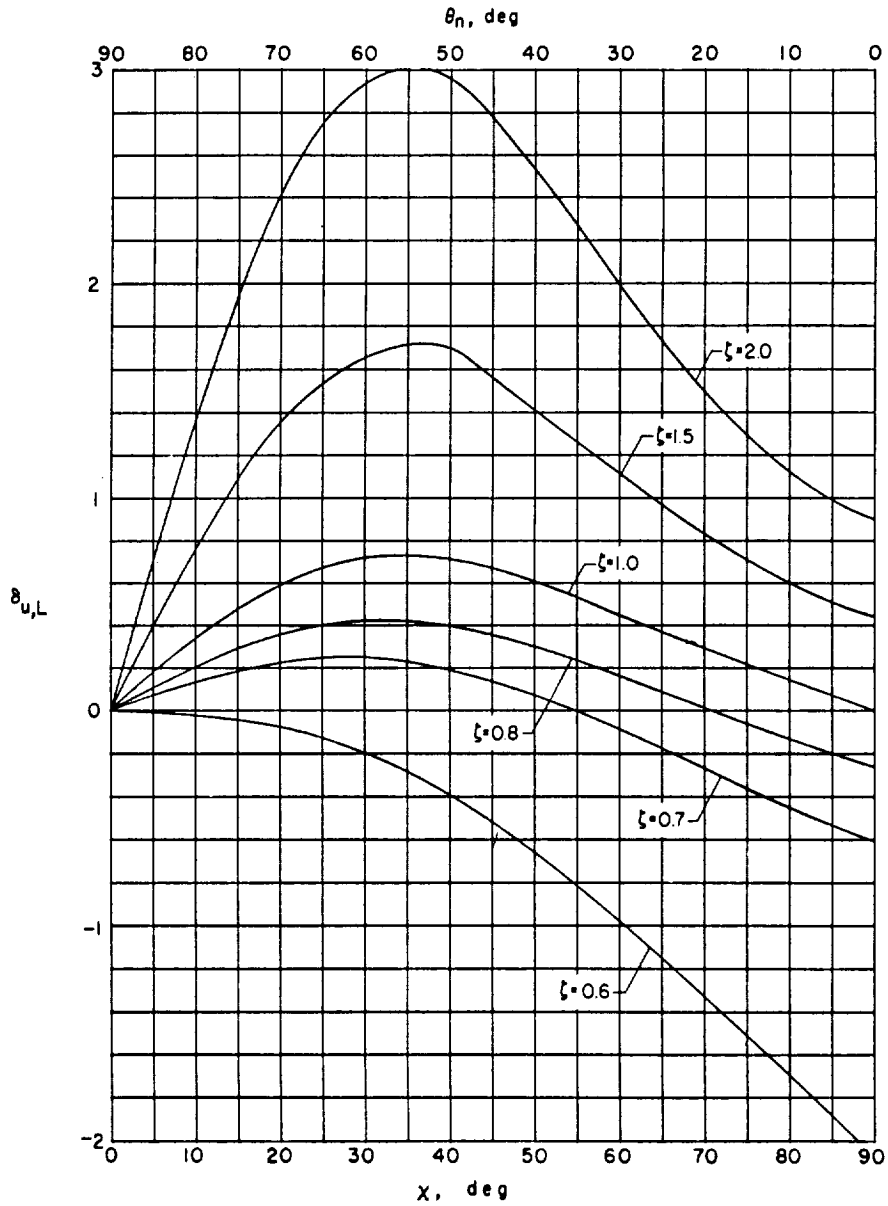


(b) $\gamma = 1.5$

**Figure 11.- Continued.**

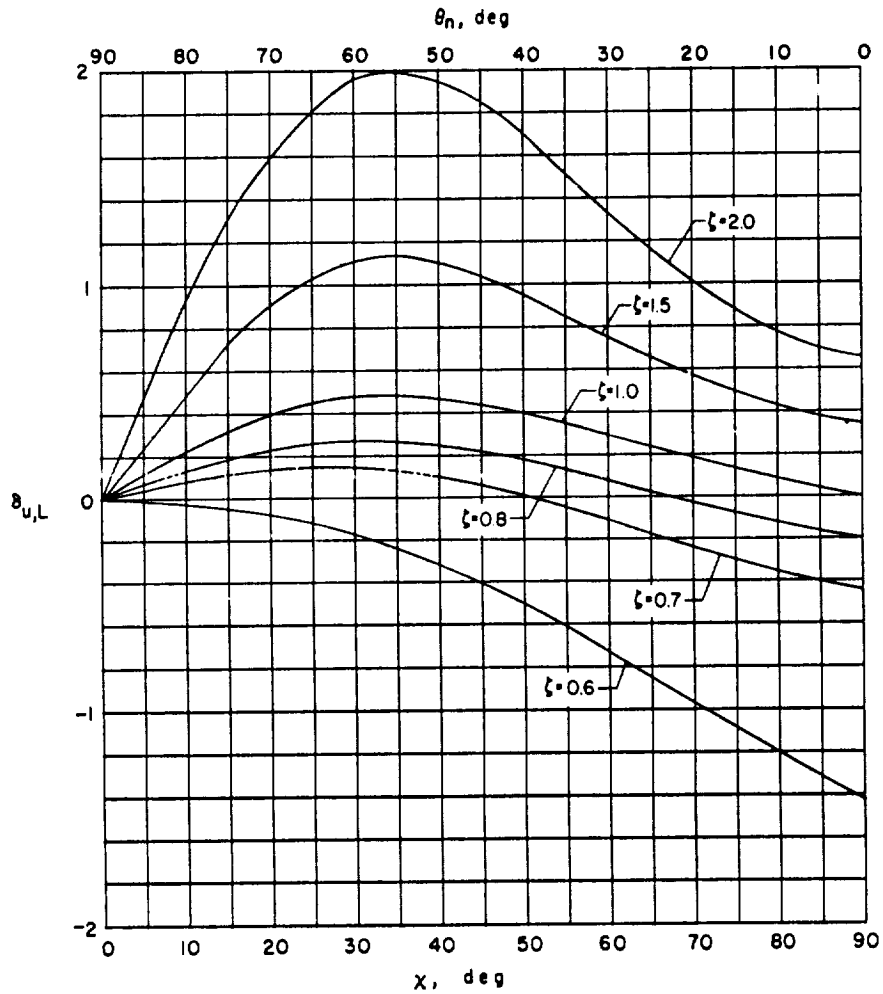


(c) $\gamma = 1.0$.

Figure 11.- Continued.

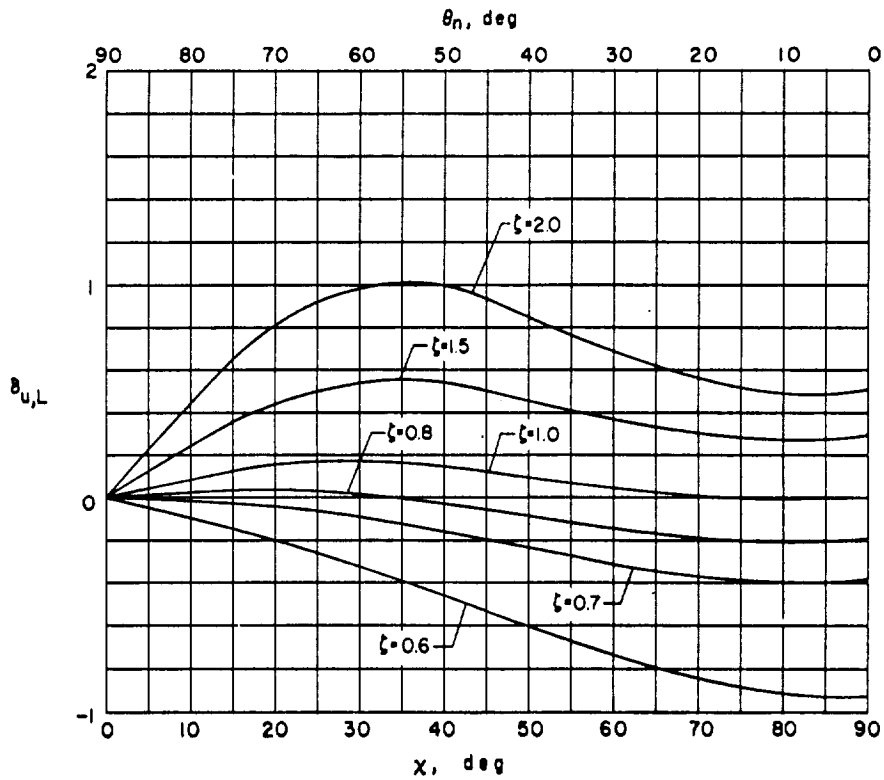


(d) $\gamma = 0.5$.

**Figure 11.- Concluded.**

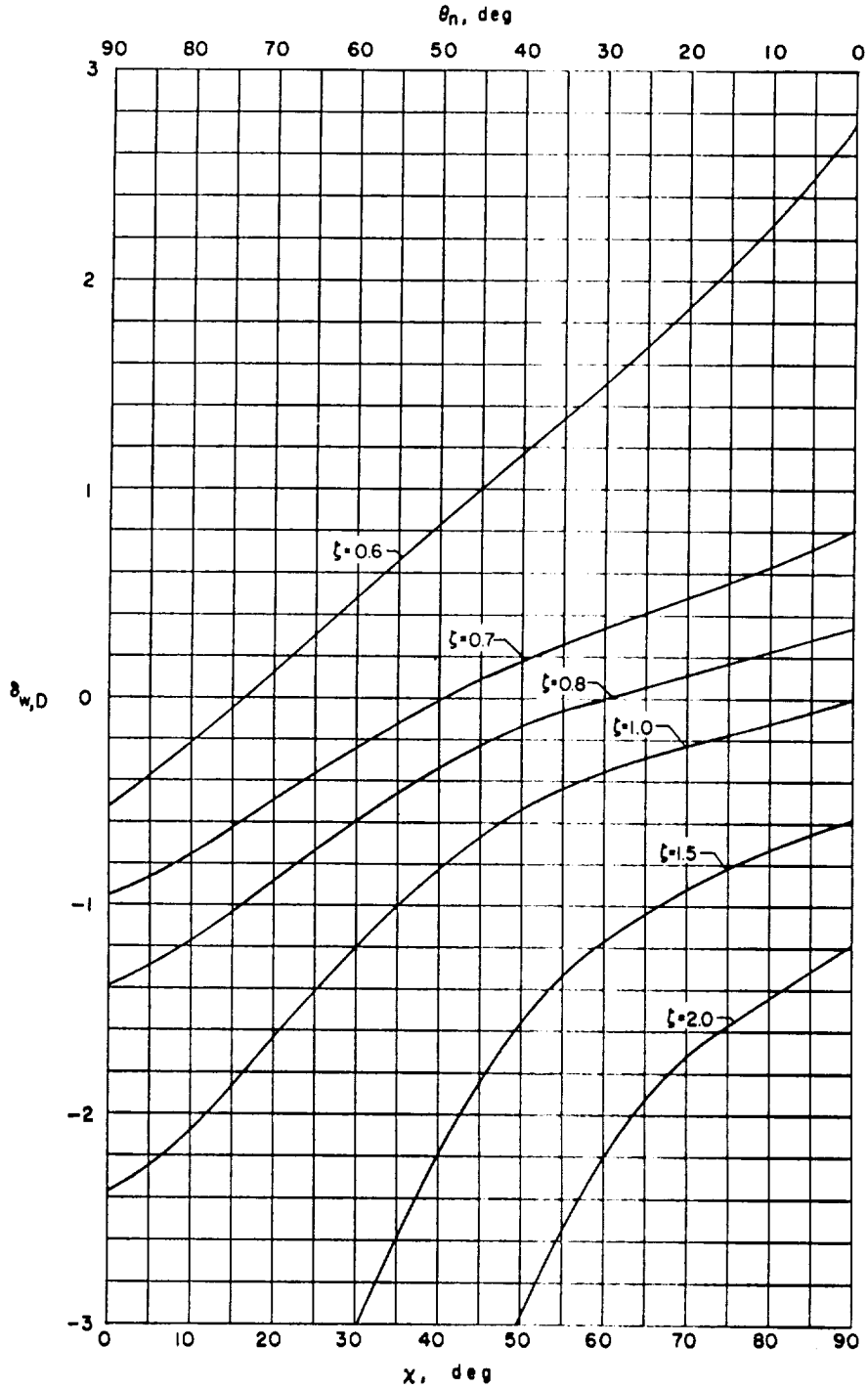


(a) $\gamma = 2.0$.

Figure 12.- Interference factors for vertical interference velocity due to drag for a small model mounted in a closed wind tunnel. $\eta = 1.0$.

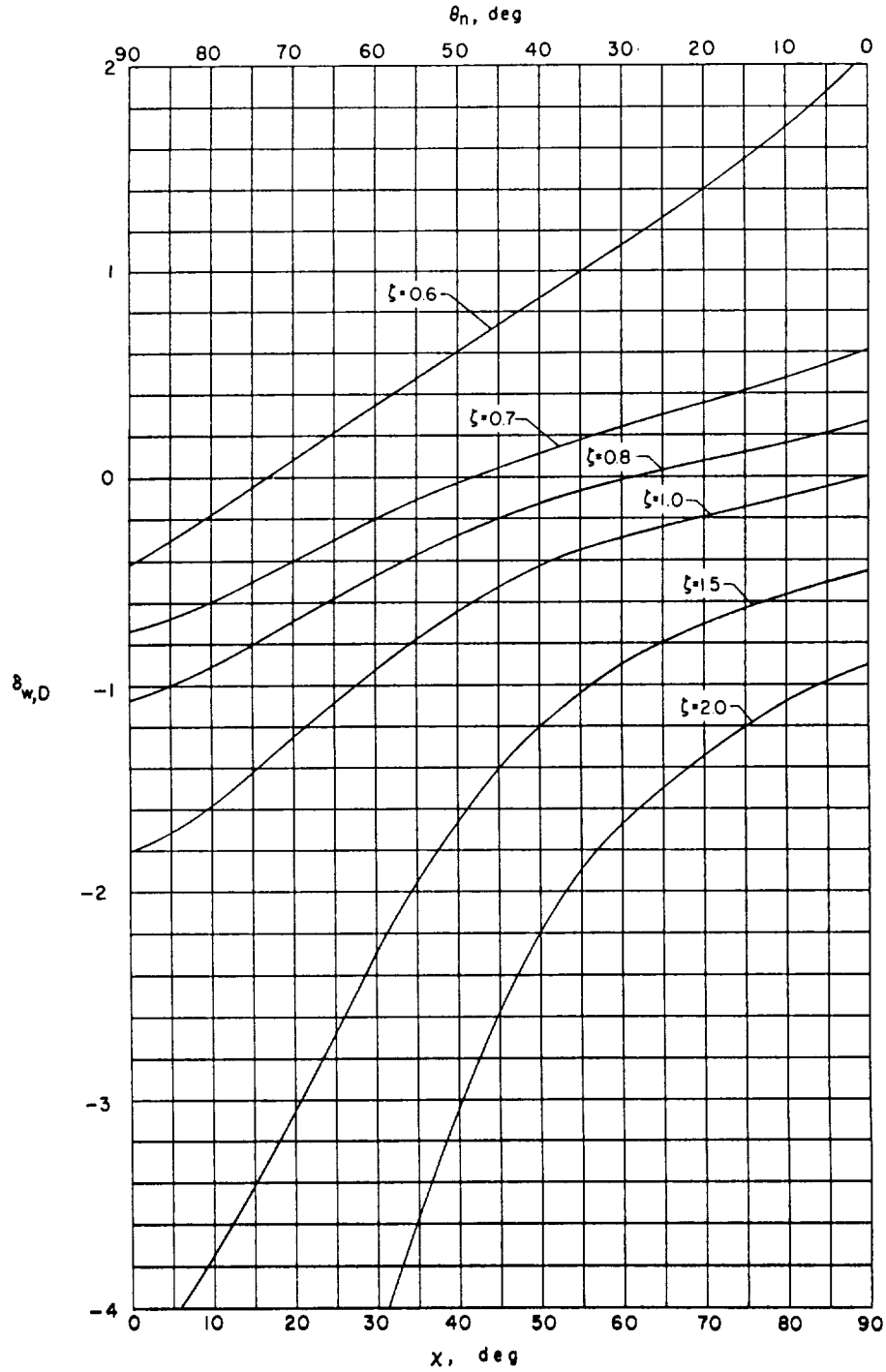


(b) $\gamma = 1.5$.

Figure 12.- Continued.

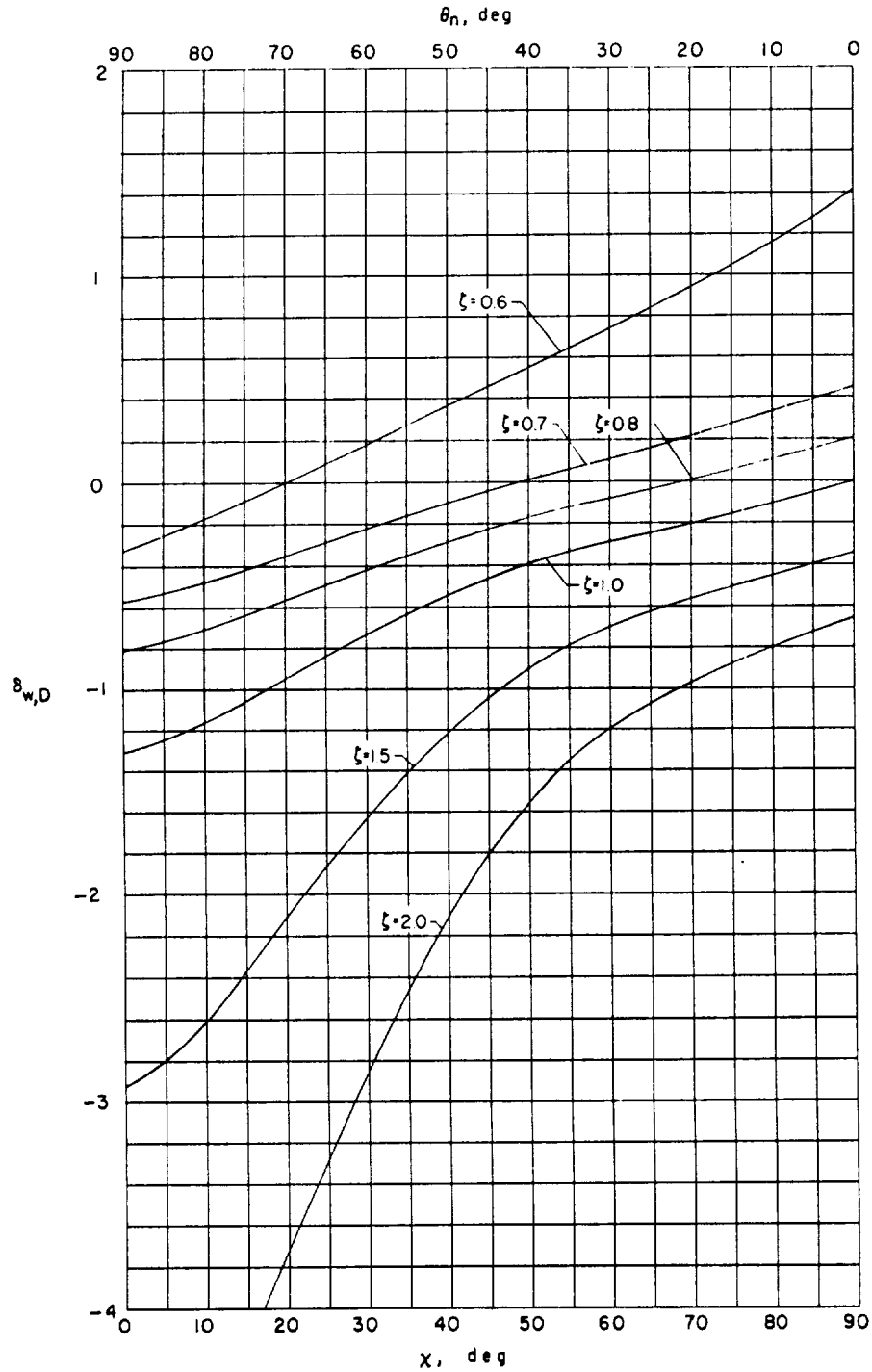


(c) $\gamma$ = 1.0.

Figure 12.- Continued.

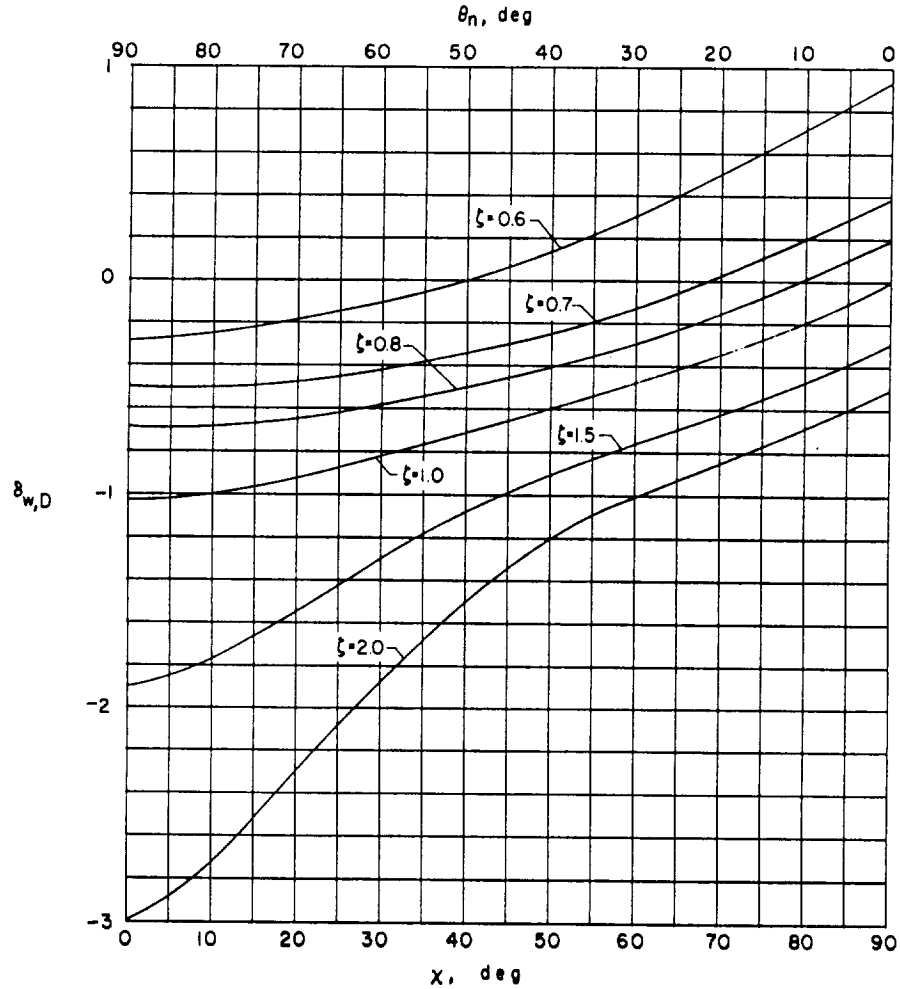


(d) $\gamma = 0.5$.

**Figure 12.- Concluded.**

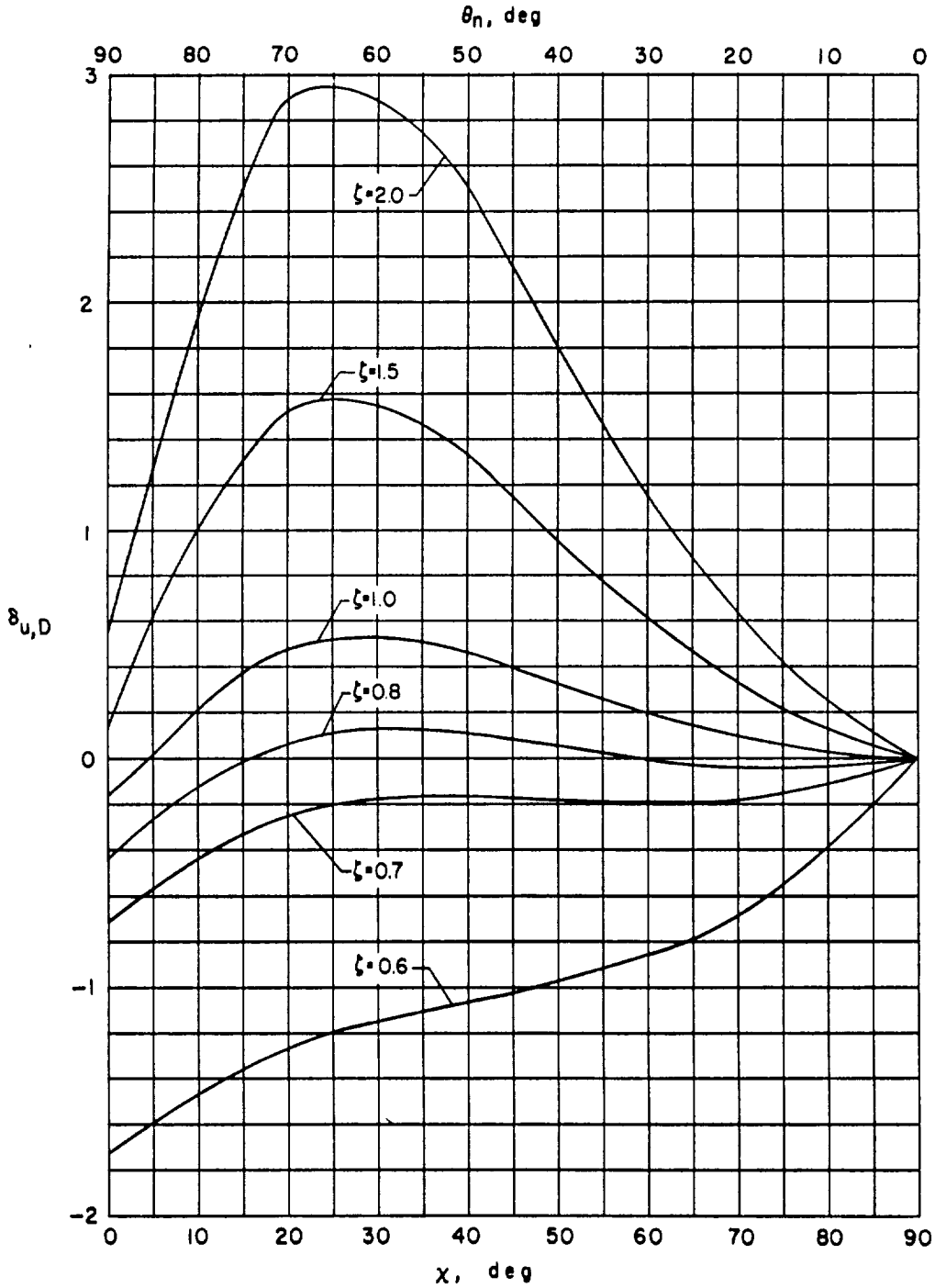


(a) $\gamma = 2.0$.

Figure 13.- Interference factors for longitudinal interference velocity due to drag for a small model mounted in a closed wind tunnel. $\eta = 1.0$.

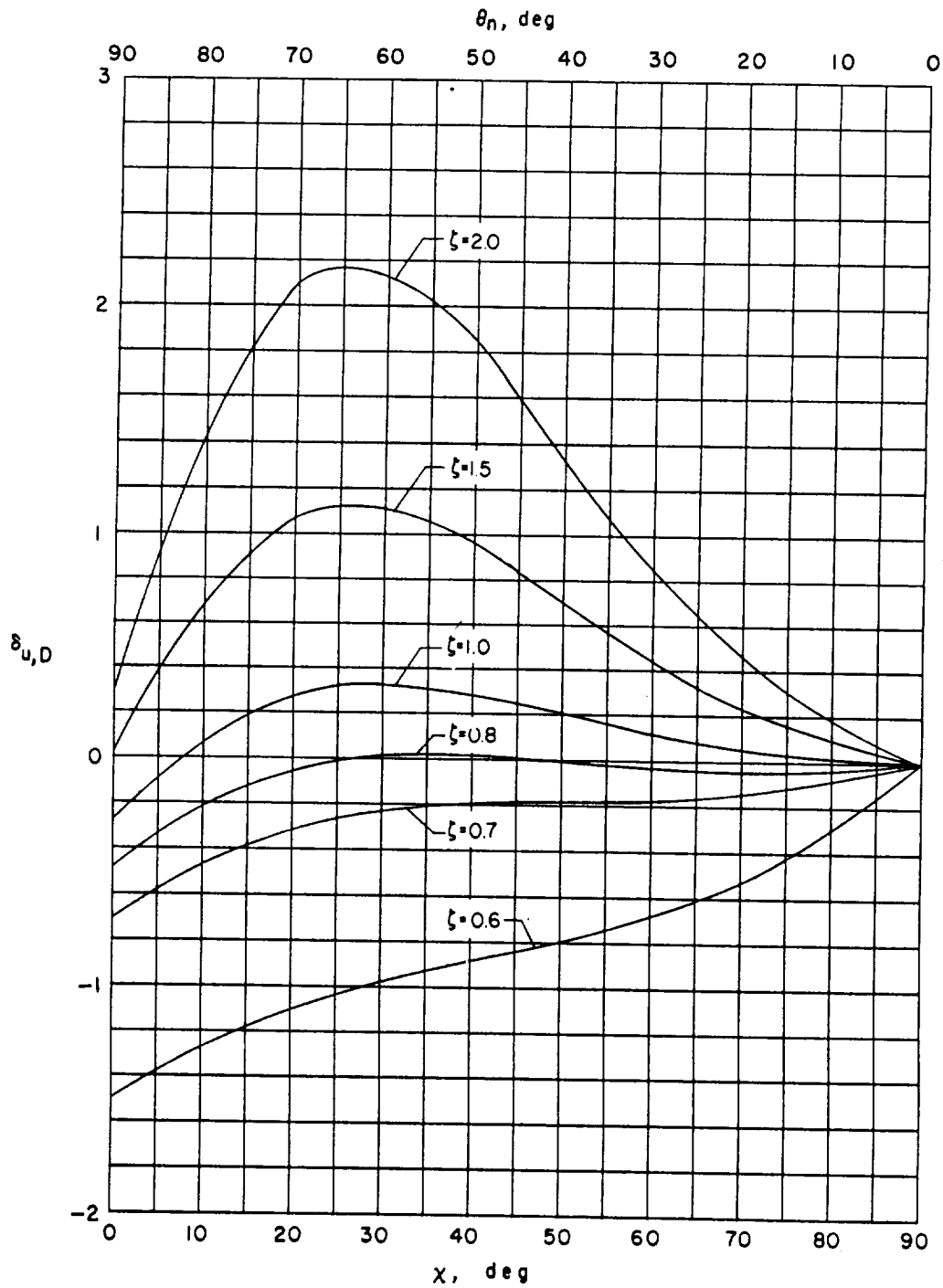


(b) $\gamma = 1.5$.

Figure 13.- Continued.

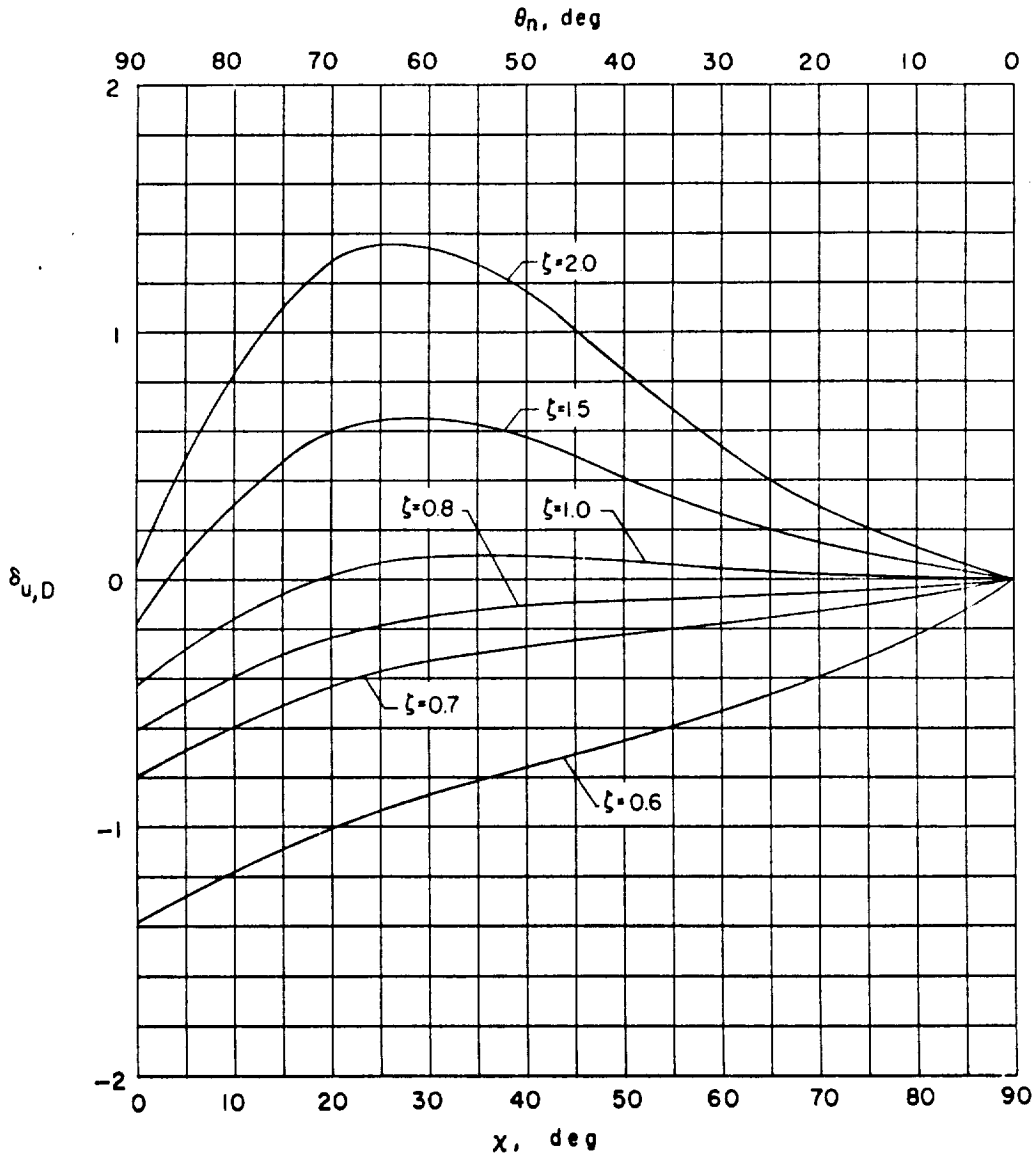


(c) $\gamma = 1.0$.

632643 O—62——5

Figure 13.- Continued.

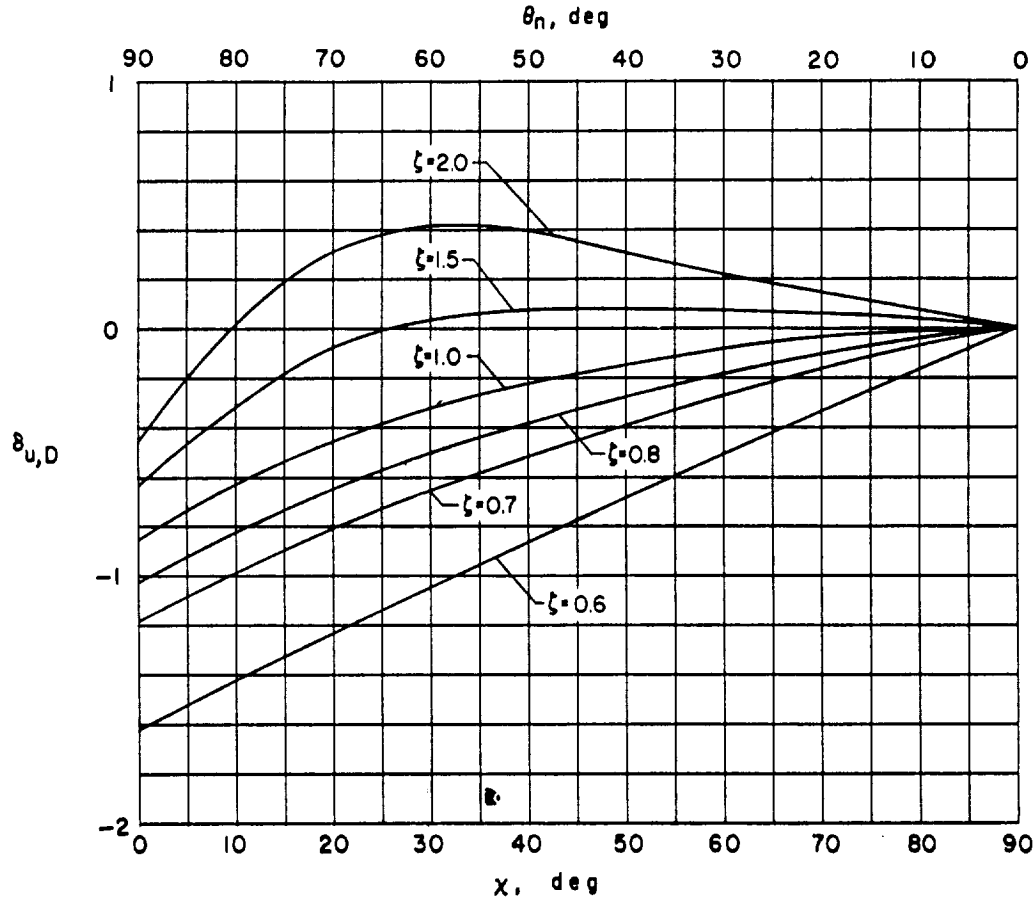


(d) $\gamma = 0.5$.

Figure 13.- Concluded.

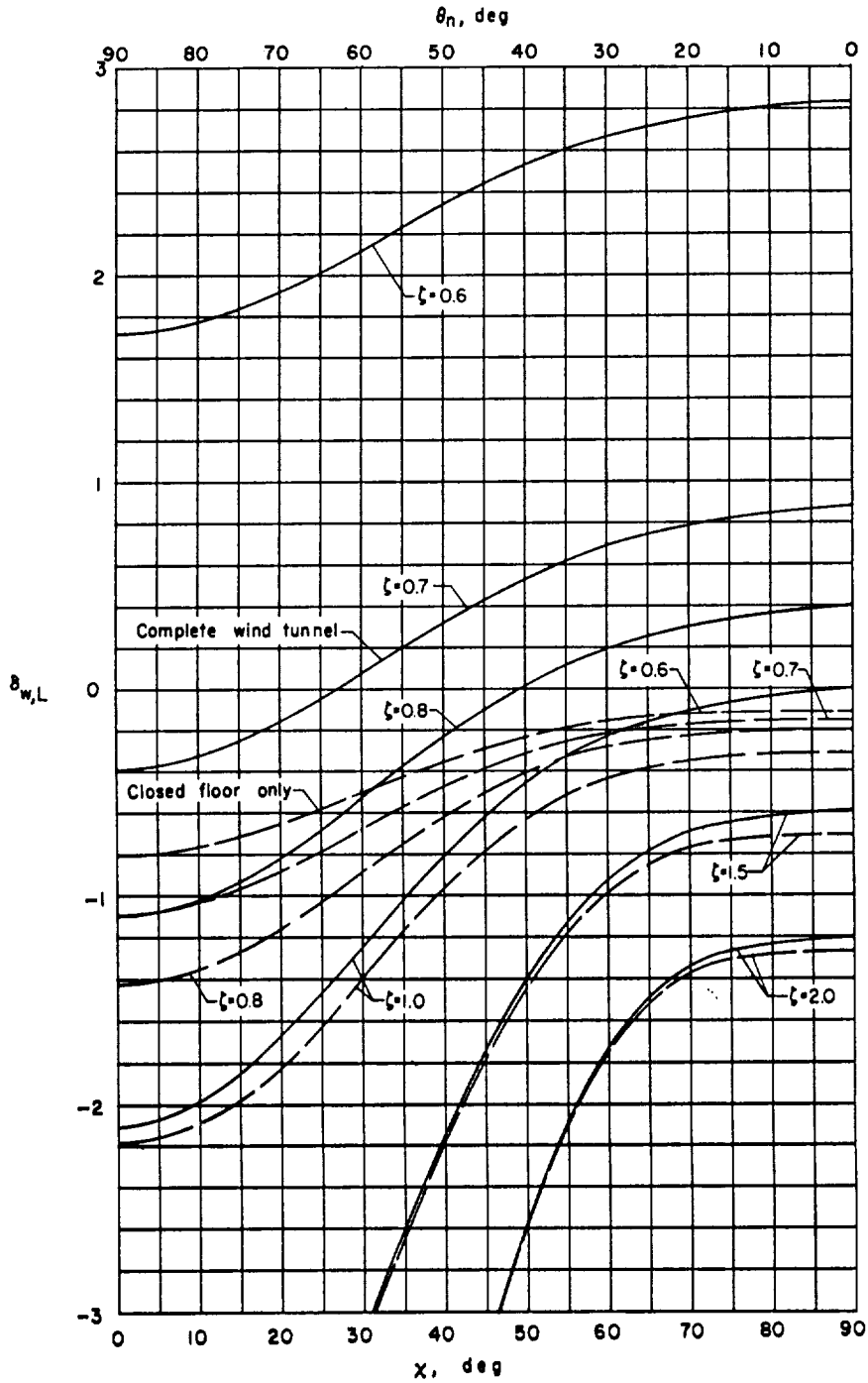


(a) $\gamma$ = 2.0.

Figure 14.- Interference factors for vertical interference velocity due to lift for a small model mounted in a wind tunnel closed on the bottom only. $\eta$ = 1.0.

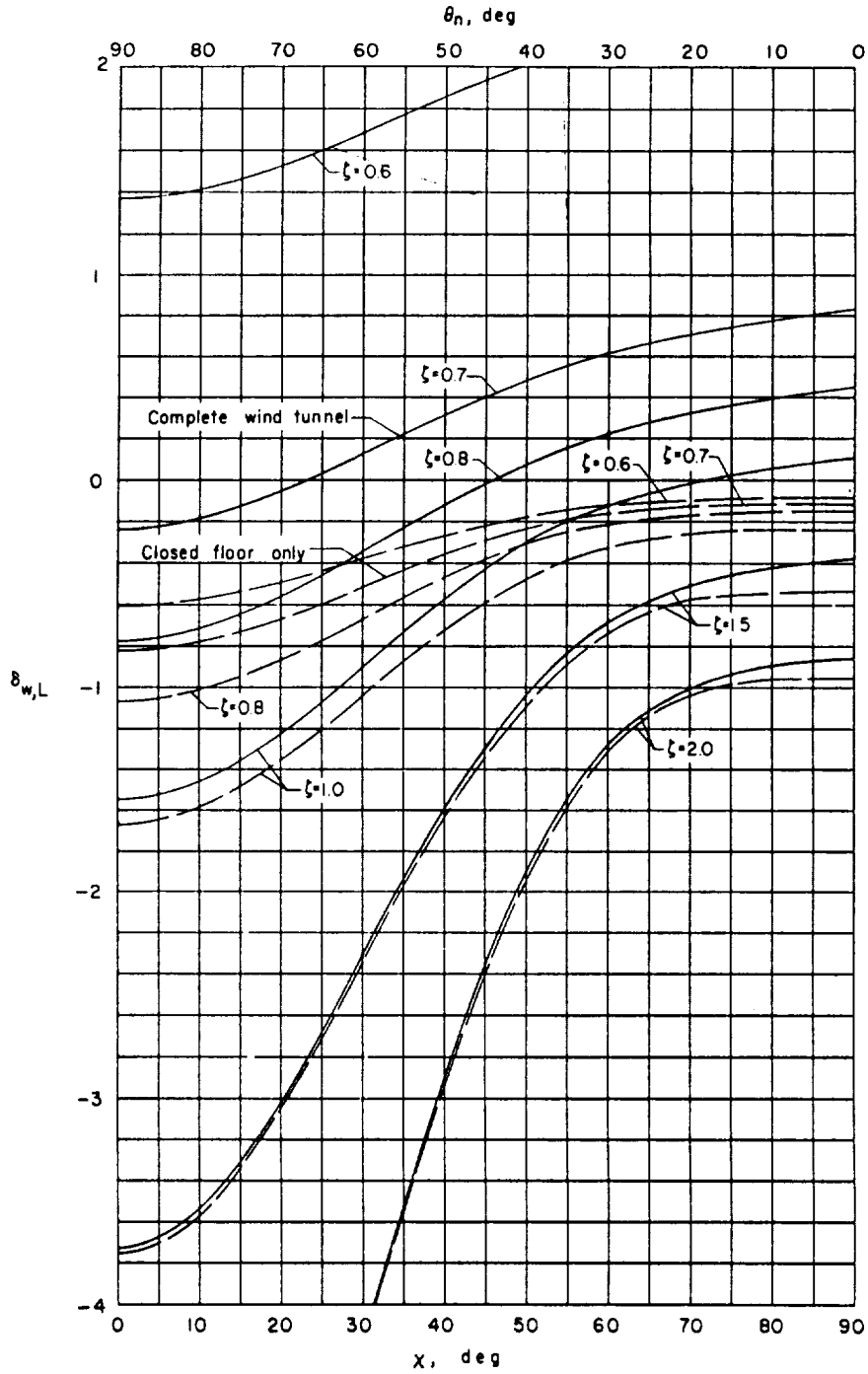


(b) $\gamma = 1.5$.

Figure 14.- Continued.

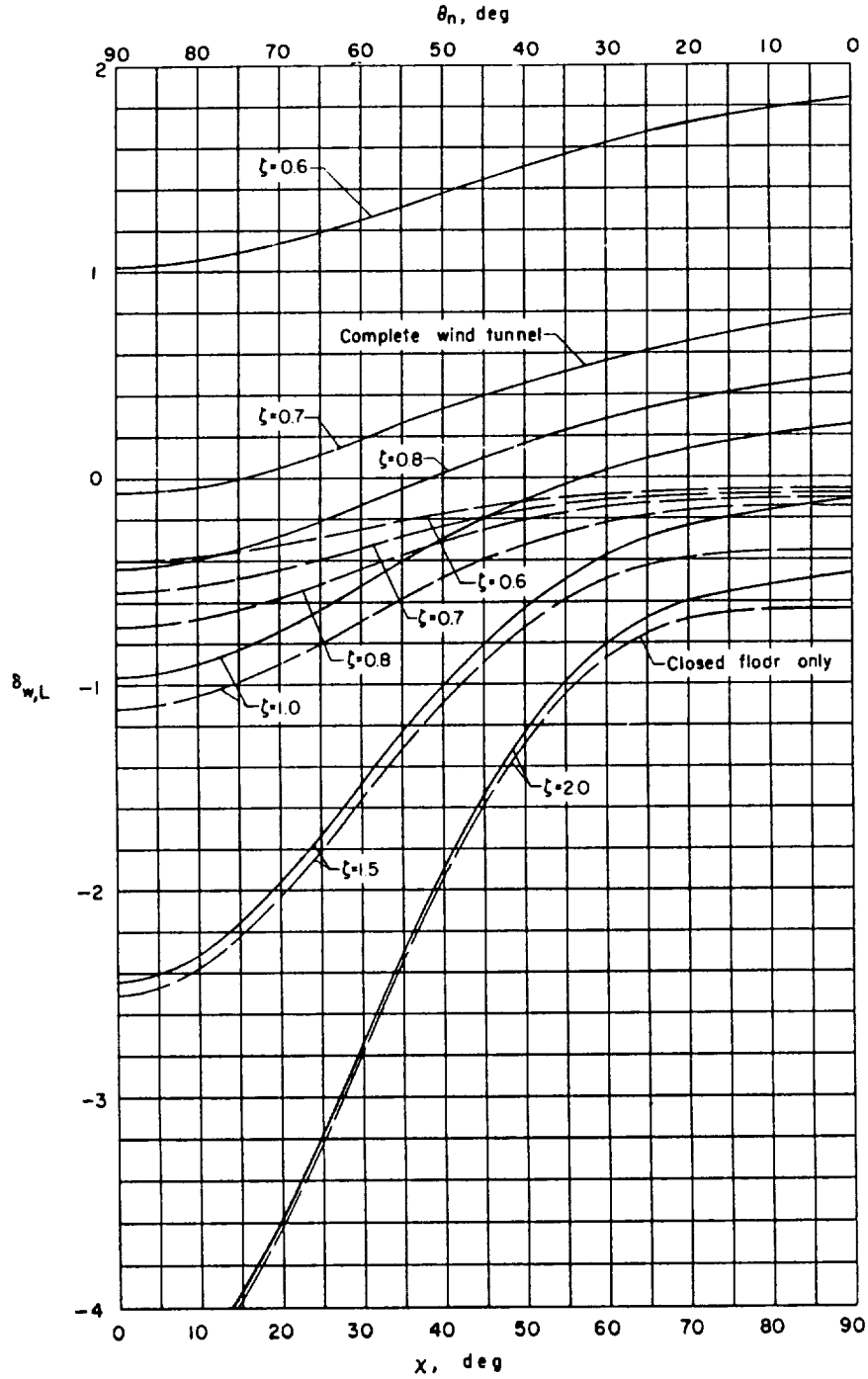


(c) $\gamma = 1.0$.

Figure 14.- Continued.

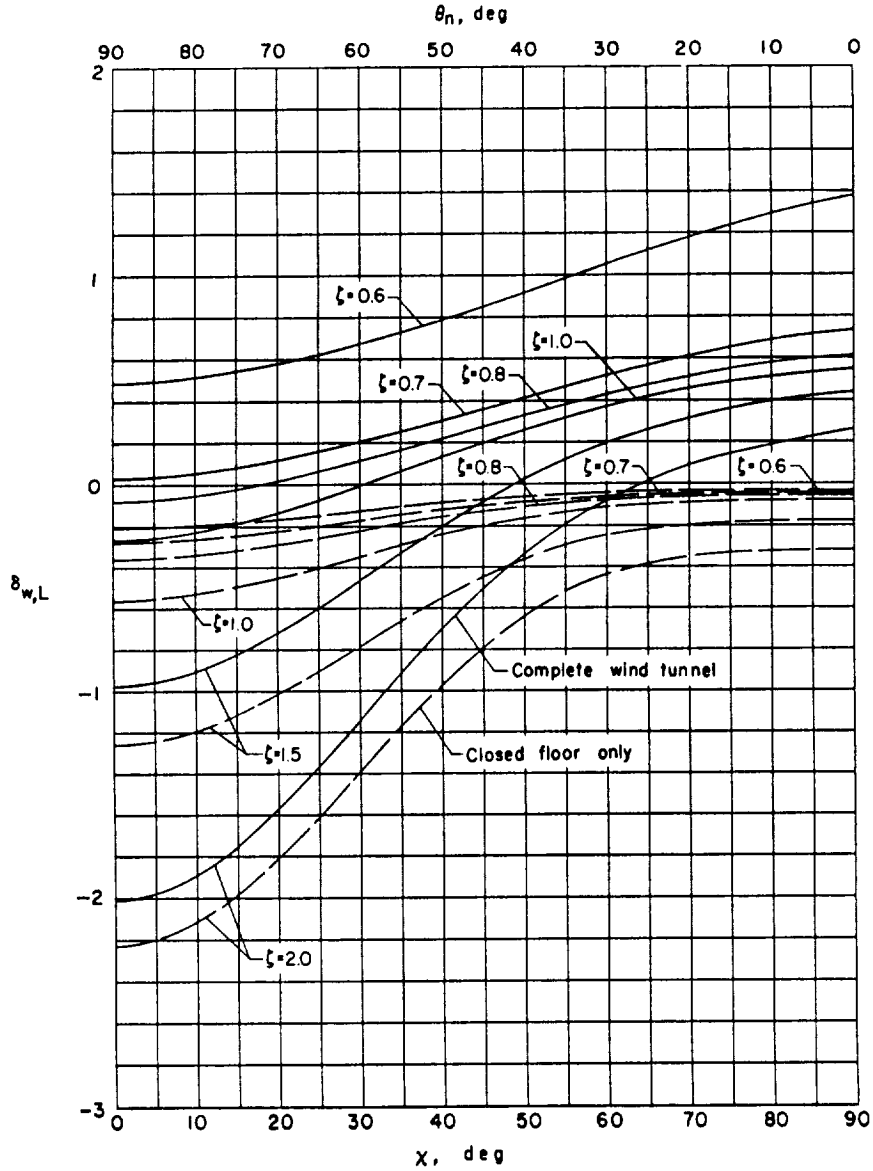


(d) $\gamma = 0.5$.

Figure 14.- Concluded.

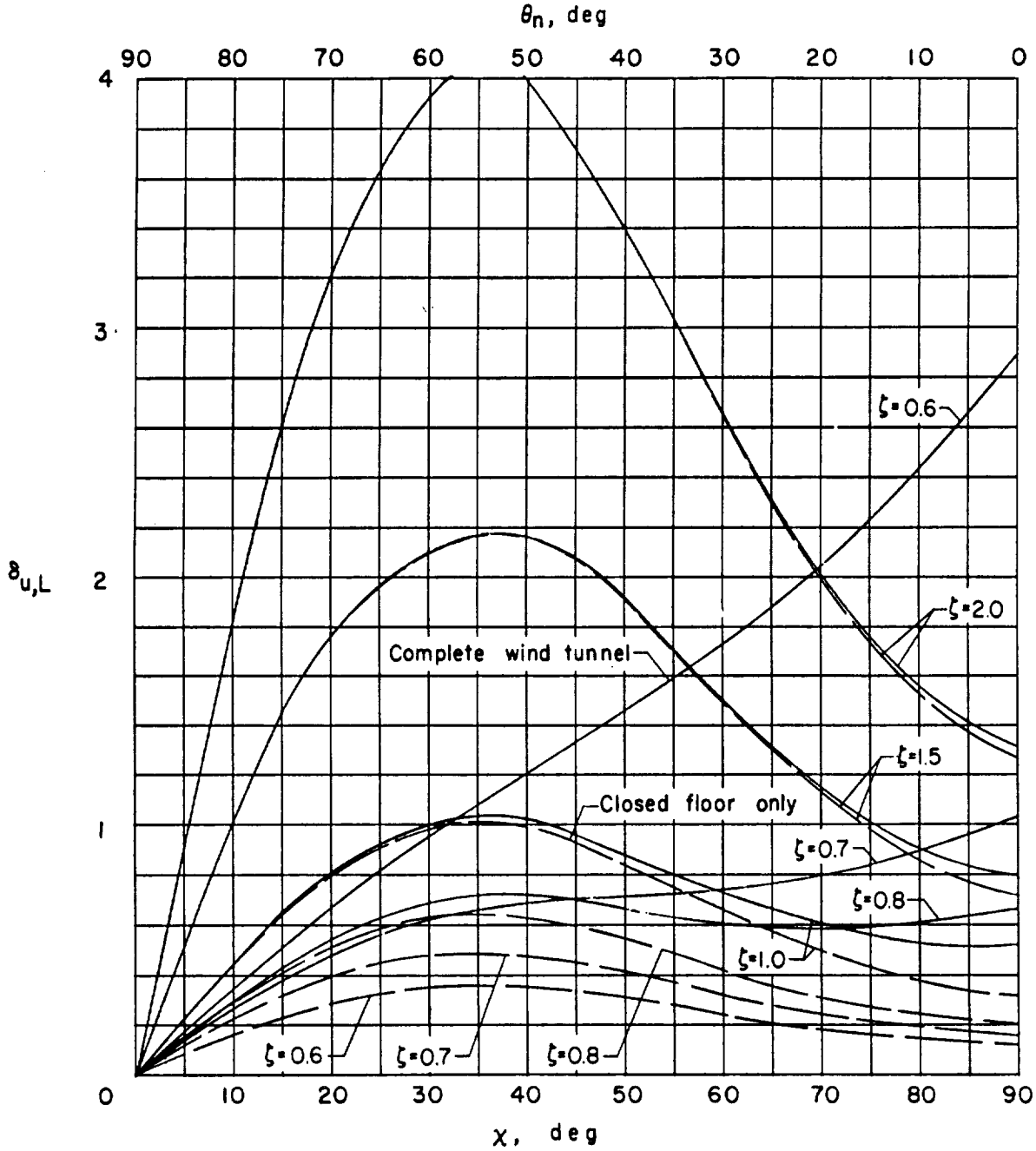


(a) $\gamma = 2.0$.

Figure 15.- Interference factors for longitudinal interference velocity due to lift for a small model mounted in a wind tunnel closed on the bottom only. $\eta = 1.0$.

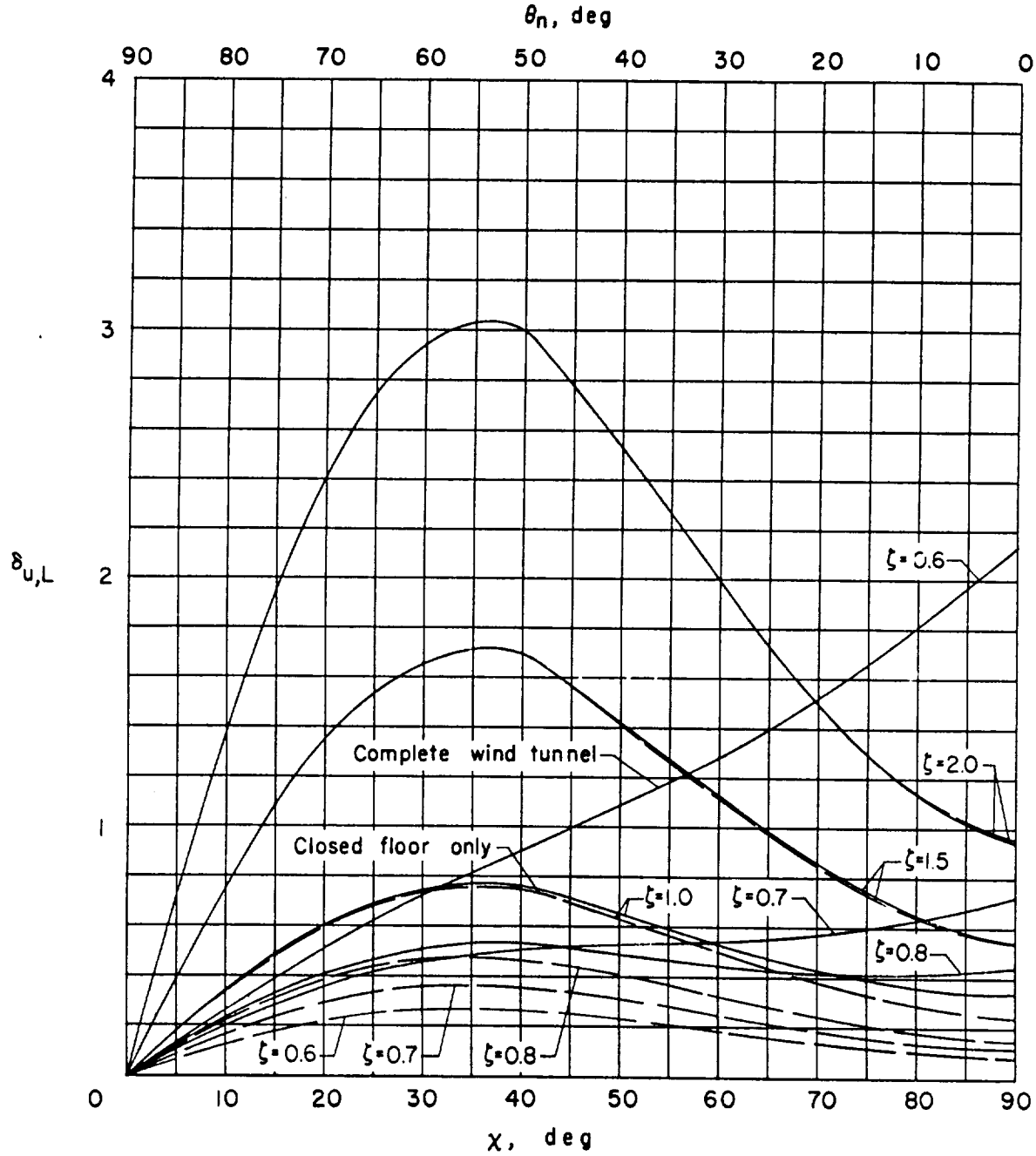


(b) $\gamma = 1.5$.

Figure 15.- Continued.

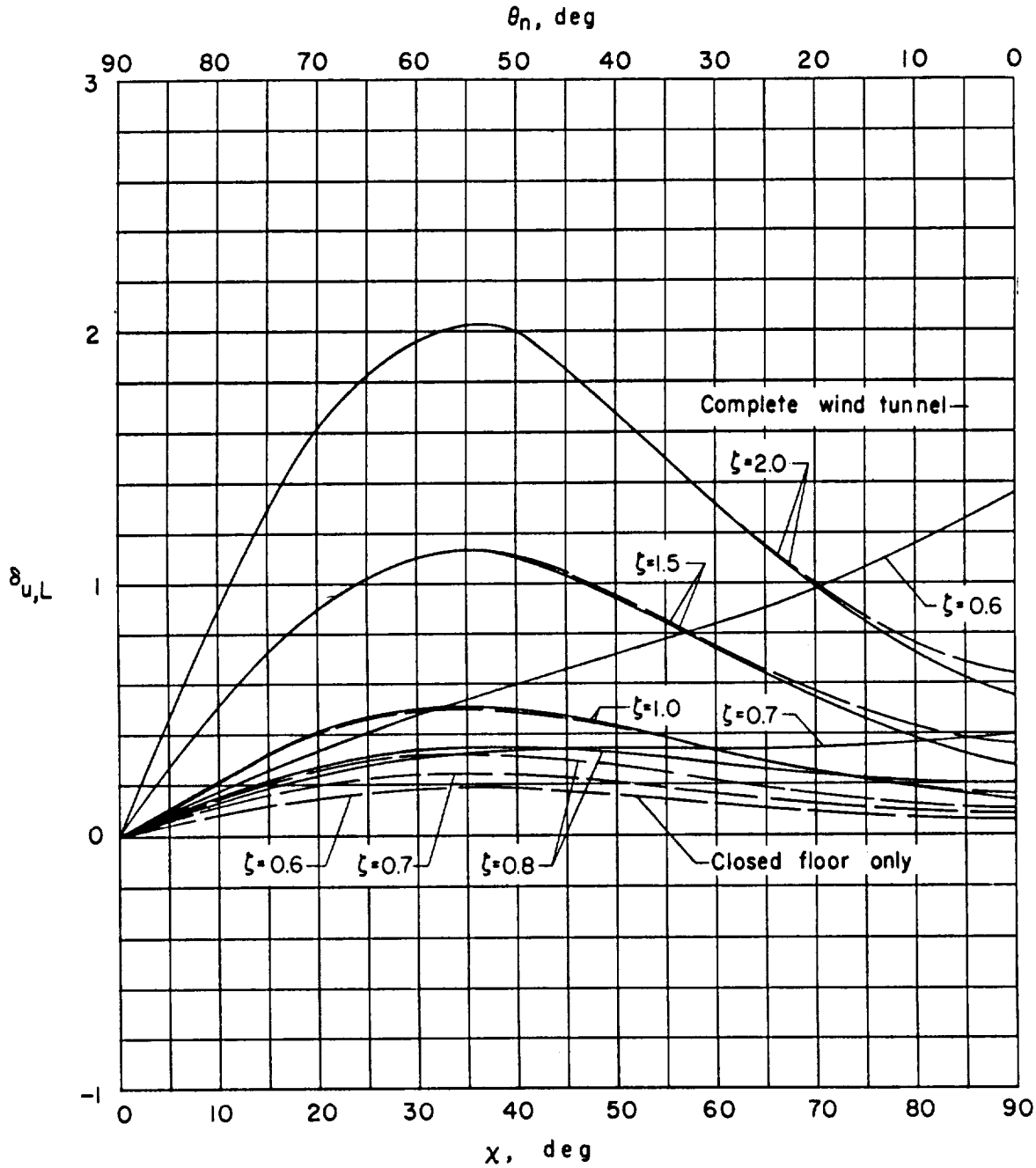


(c) $\gamma = 1.0$.

Figure 15.- Continued.

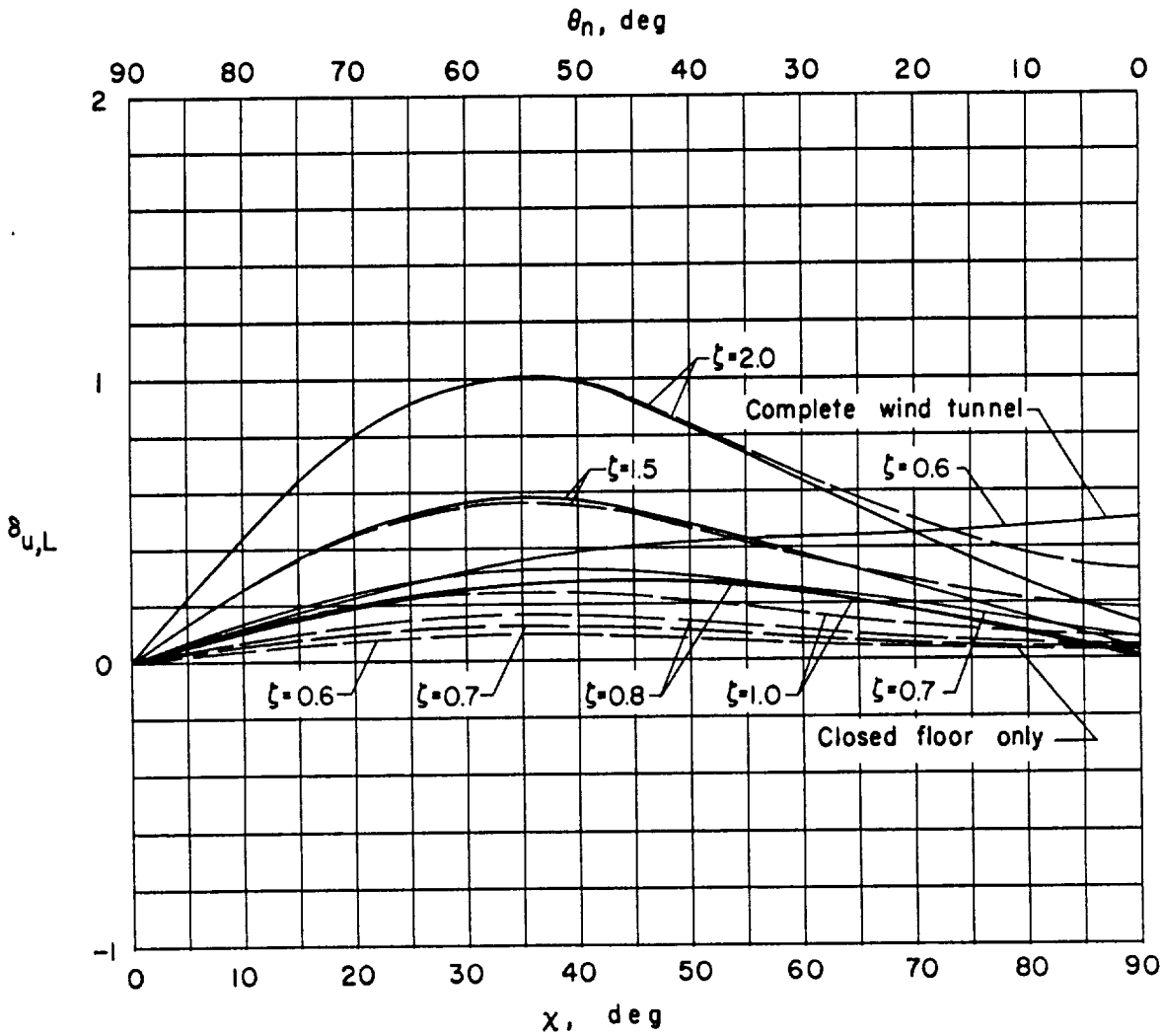


(d) $\gamma = 0.5$.

Figure 15.- Concluded.

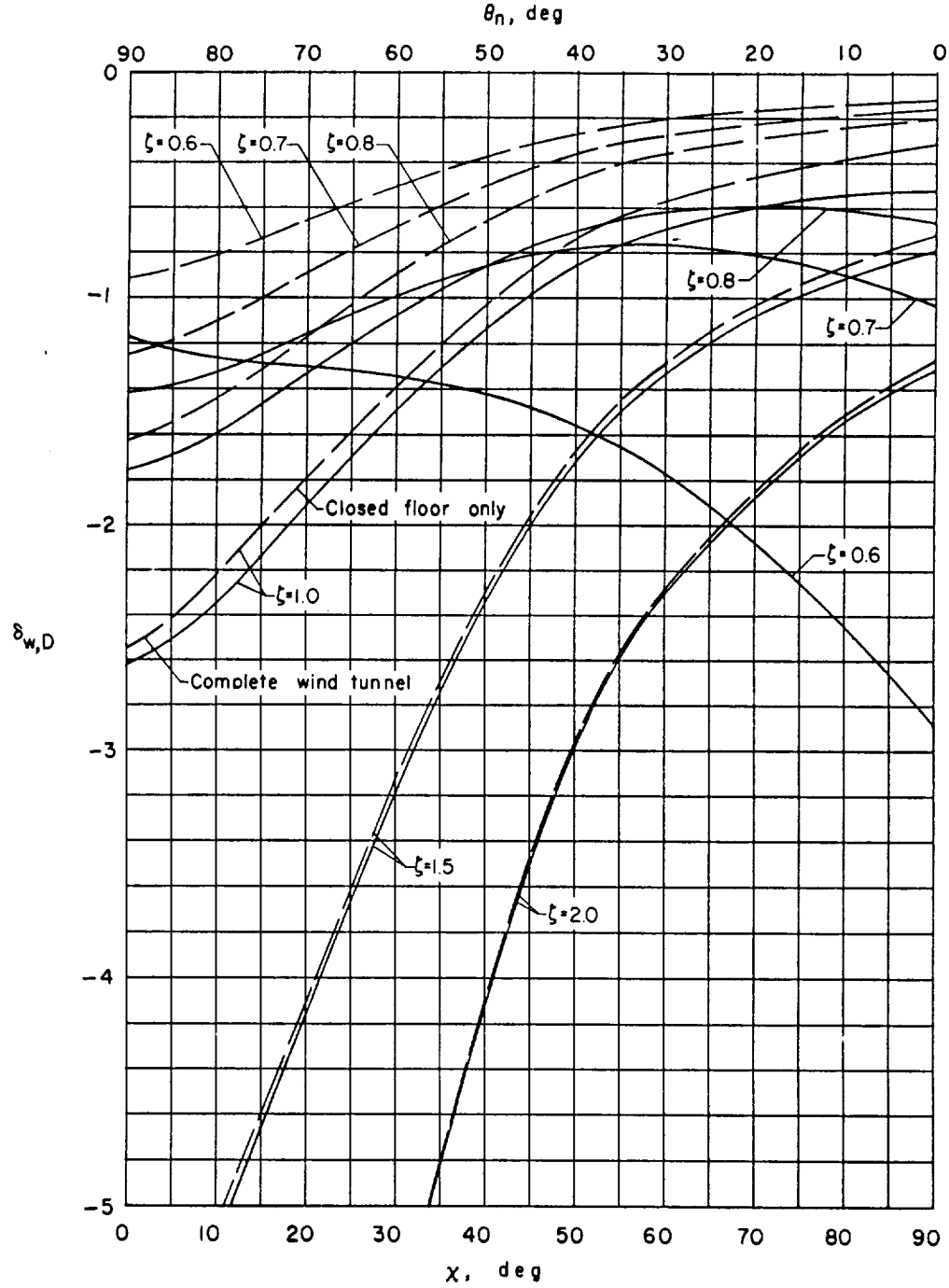


(a) $\gamma$ = 2.0.

Figure 16.- Interference factors for vertical interference velocity due to drag for a small model mounted in a wind tunnel closed on the bottom only. $\eta$ = 1.0.

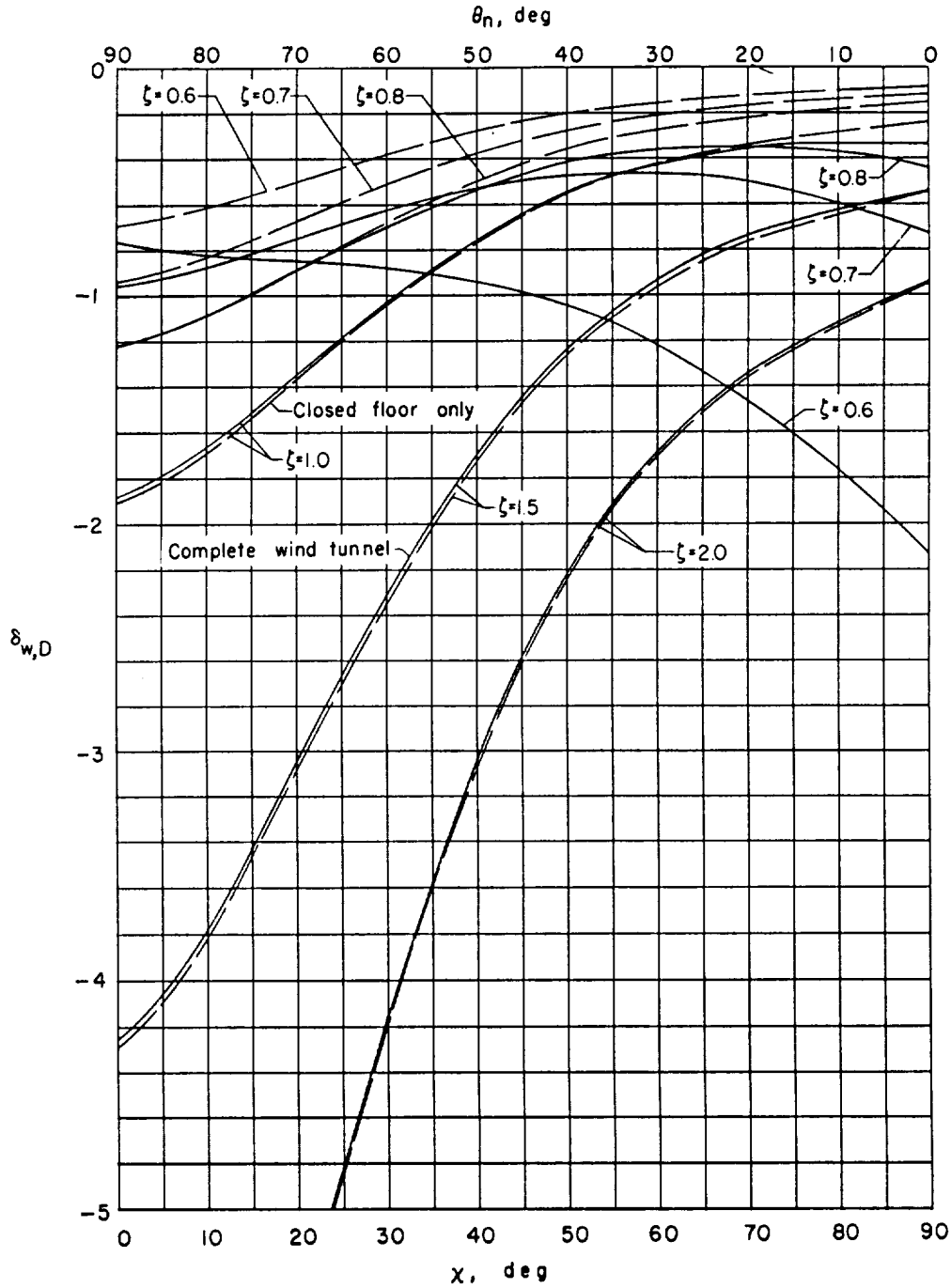


(b) $\gamma = 1.5$.

Figure 16.- Continued.

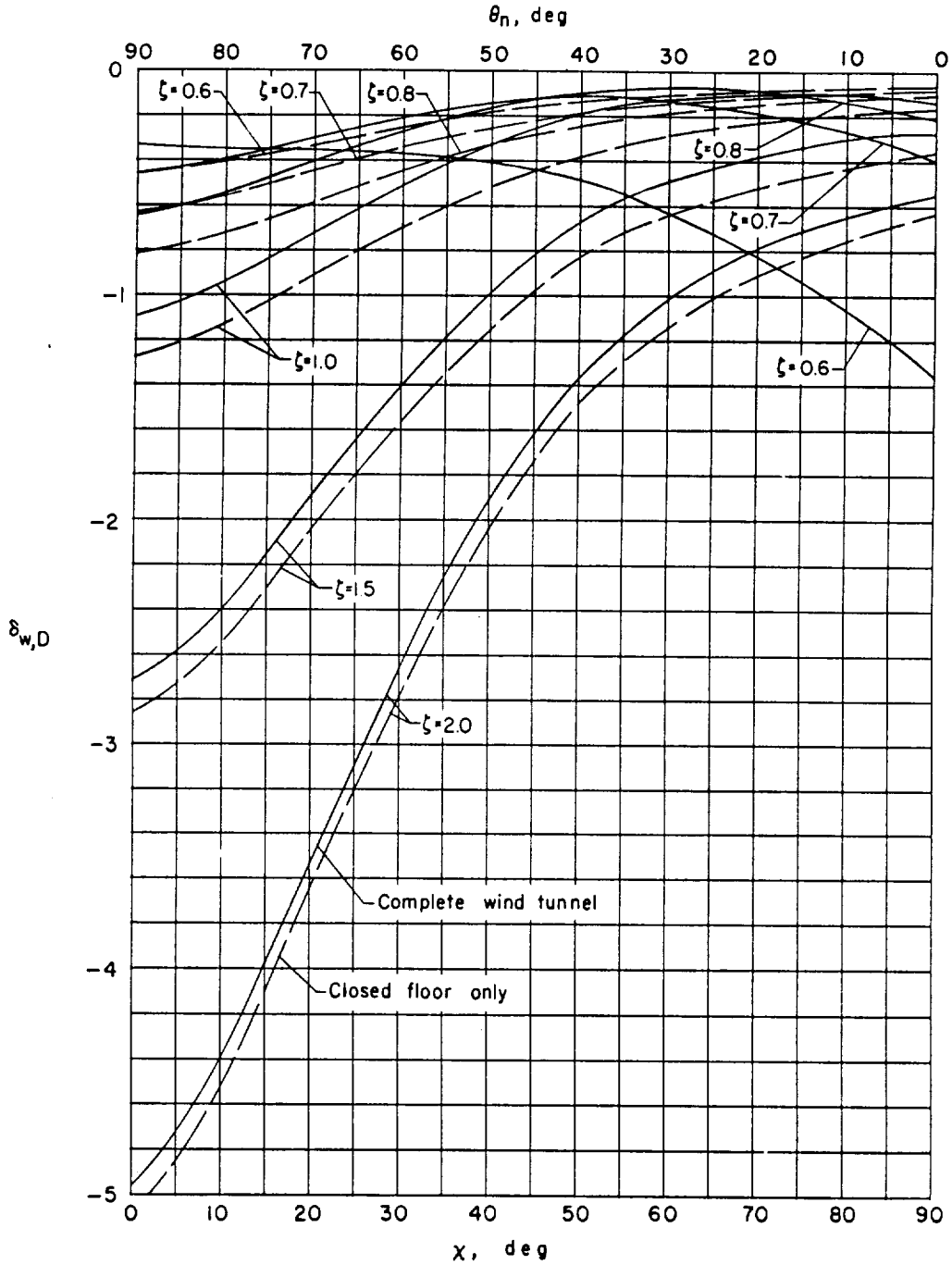


(c) $\gamma = 1.0$.

Figure 16.- Continued.

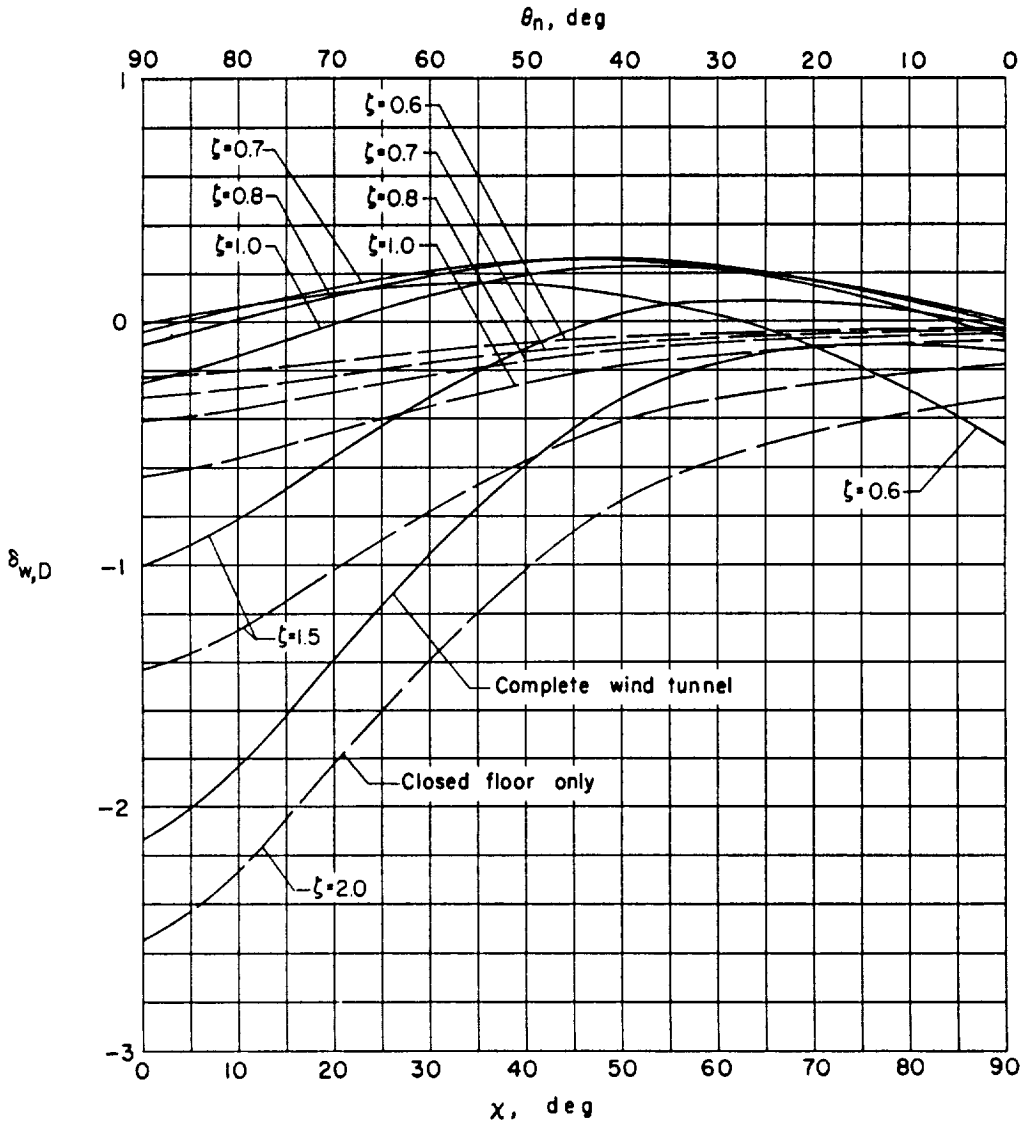


(d) $\gamma = 0.5$.

Figure 16.- Concluded.

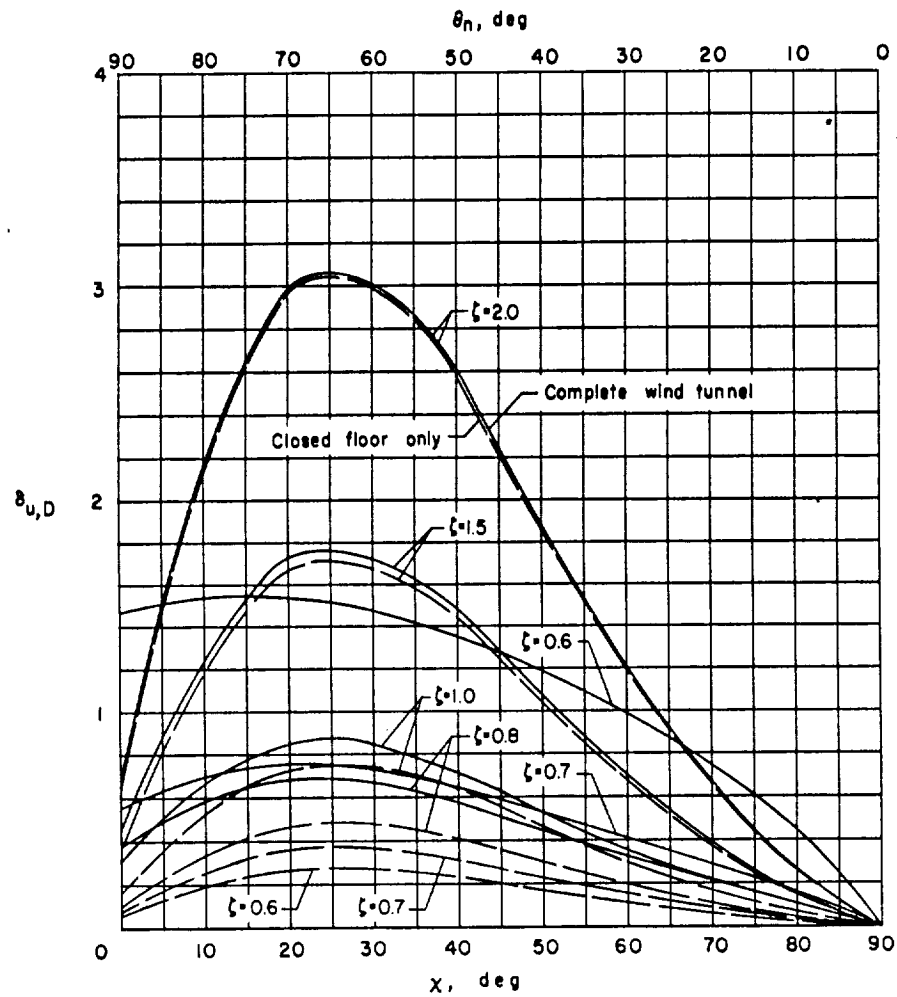


(a) $\gamma = 2.0$.

Figure 17.- Interference factors for longitudinal interference velocity due to drag for a small model mounted in a wind tunnel closed on the bottom only. $\eta = 1.0$.

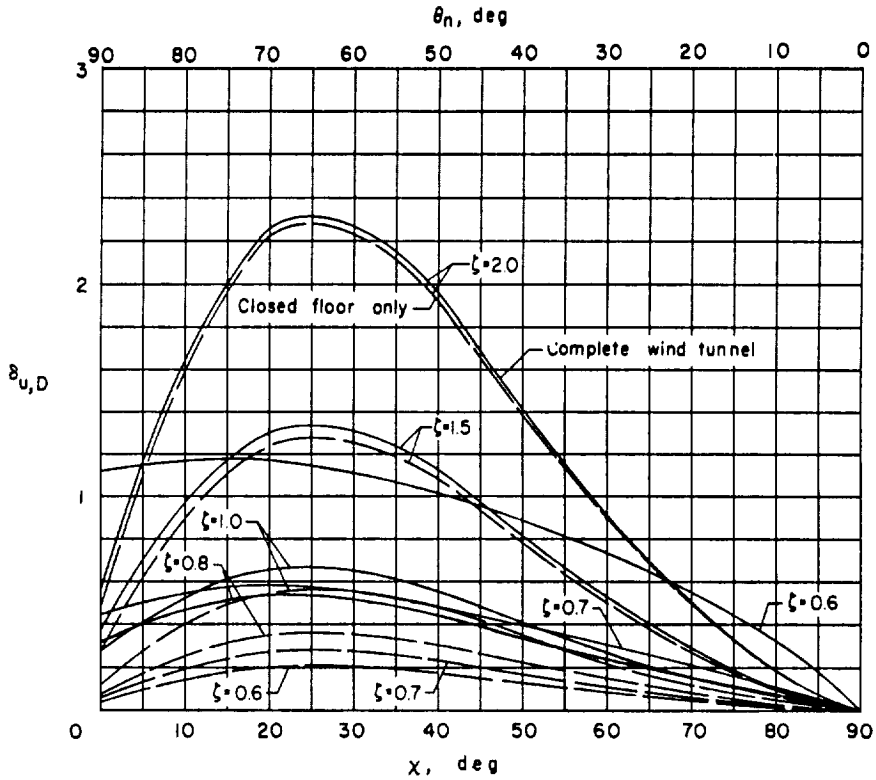


(b) $\gamma = 1.5$

Figure 17.- Continued.

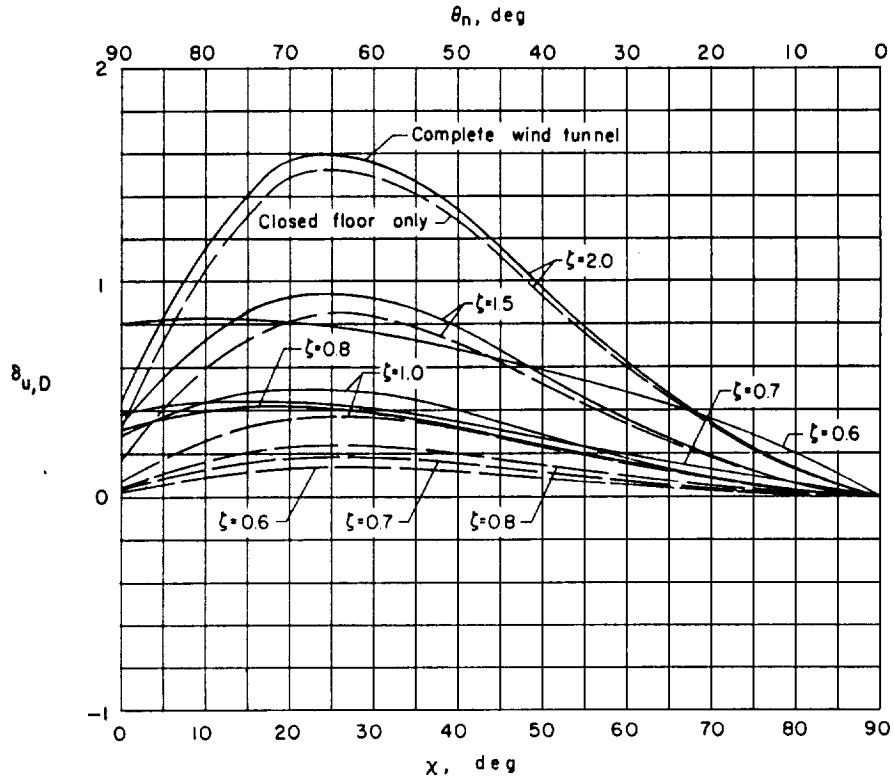


(c) $\gamma = 1.0$.

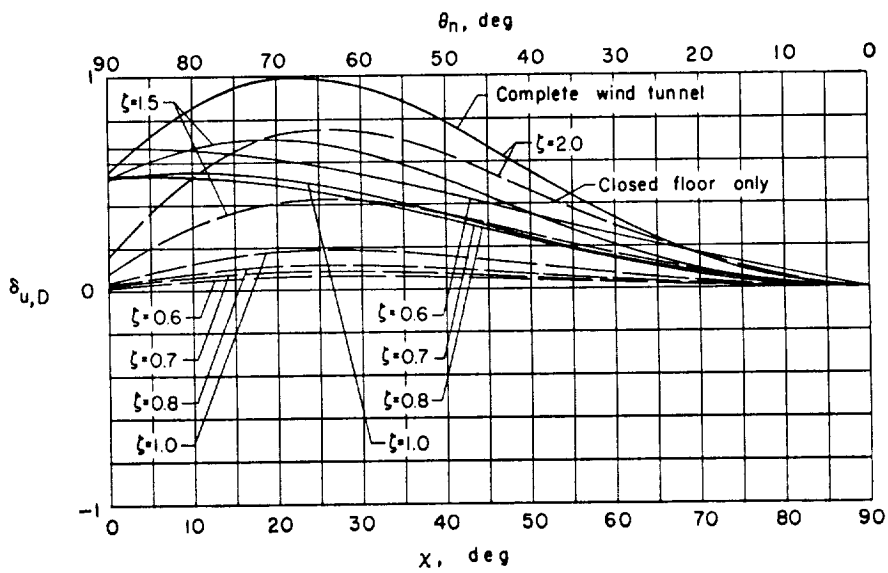


(d) $\gamma = 0.5$.

632643 O—62——6

Figure 17.- Concluded.

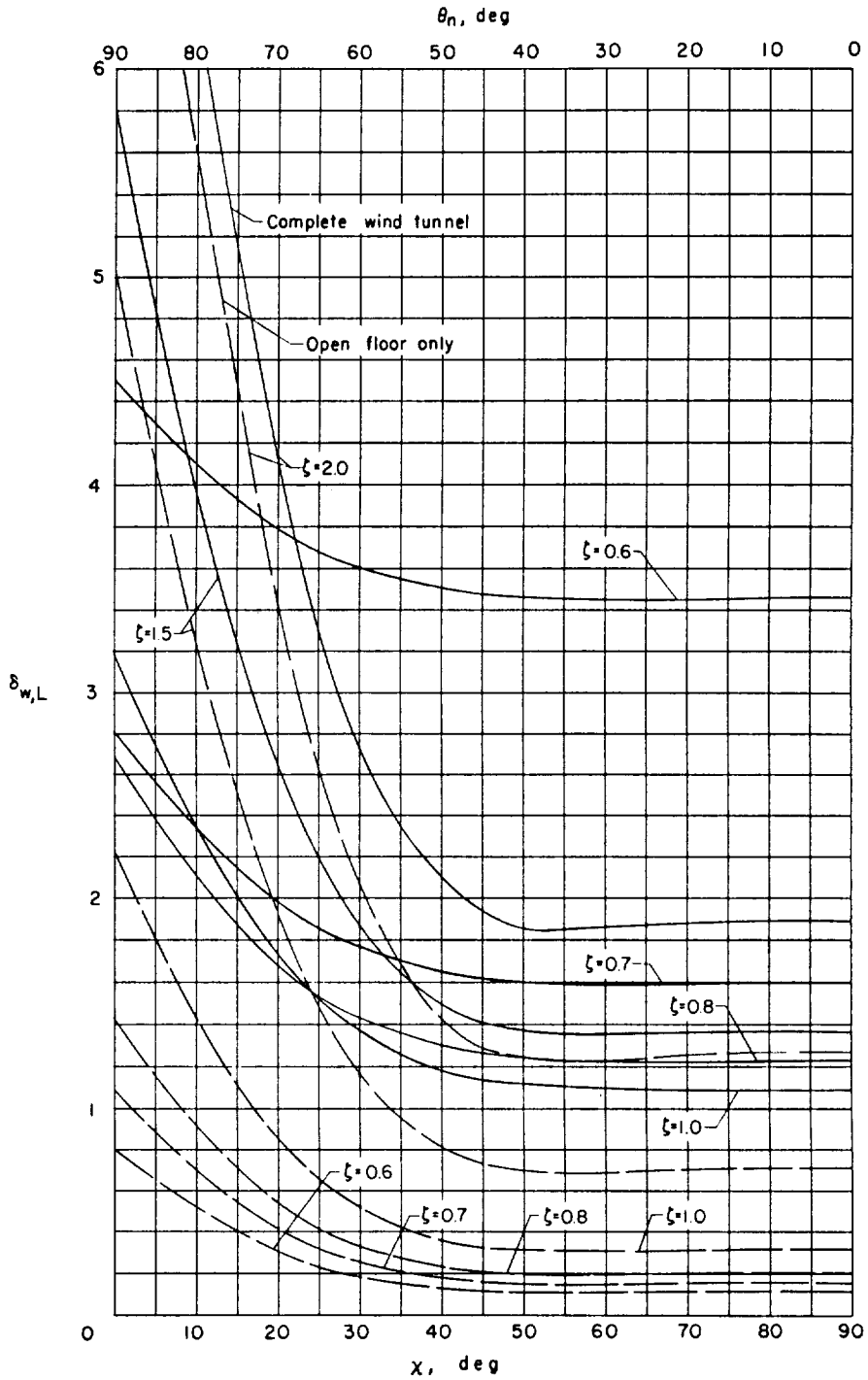


(a) $\gamma = 2.0$.

Figure 18.- Interference factors for vertical interference velocity due to lift for a small model in an open wind tunnel. $\eta = 1.0$.

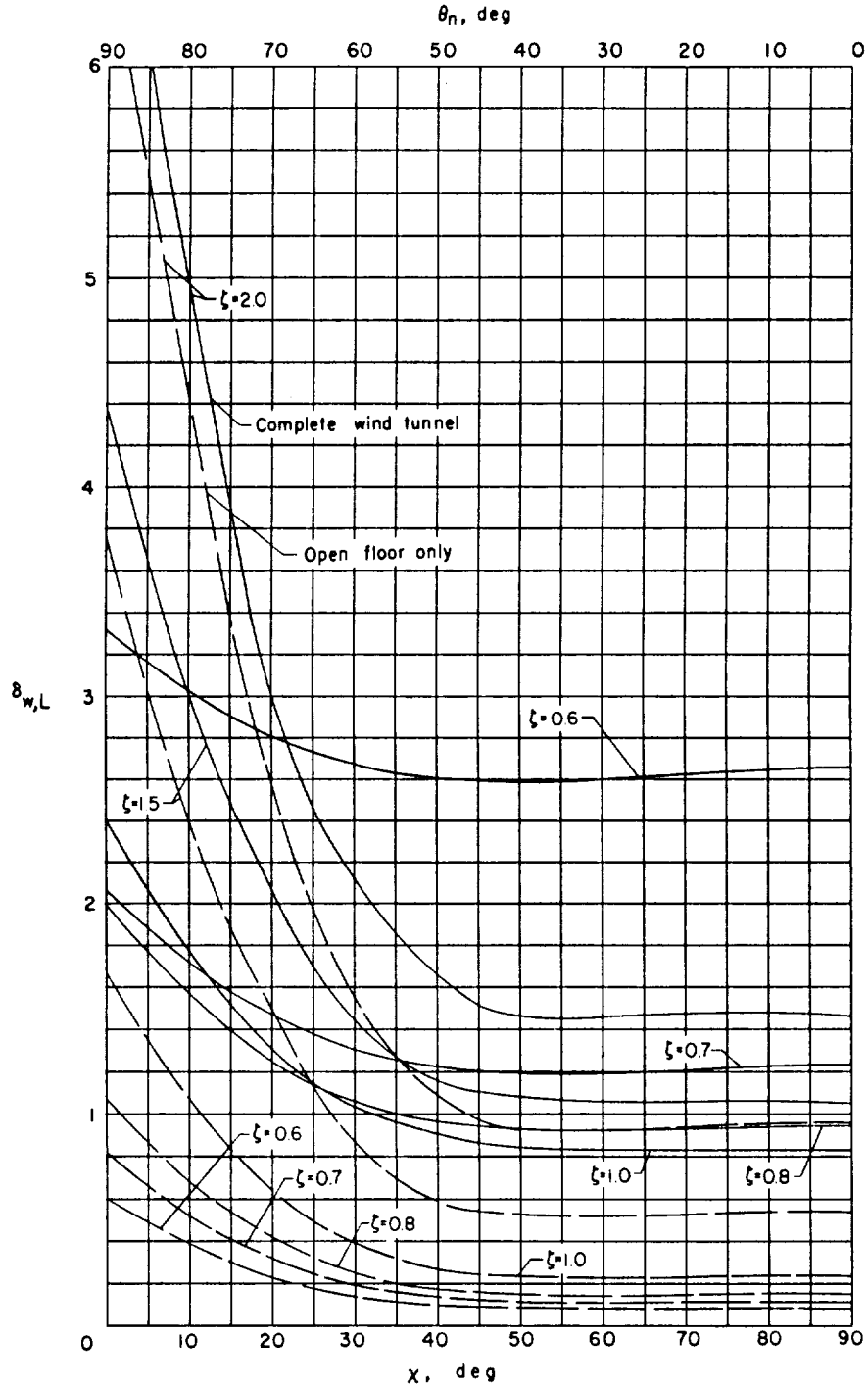


(b) $\gamma = 1.5$.

Figure 18.- Continued.

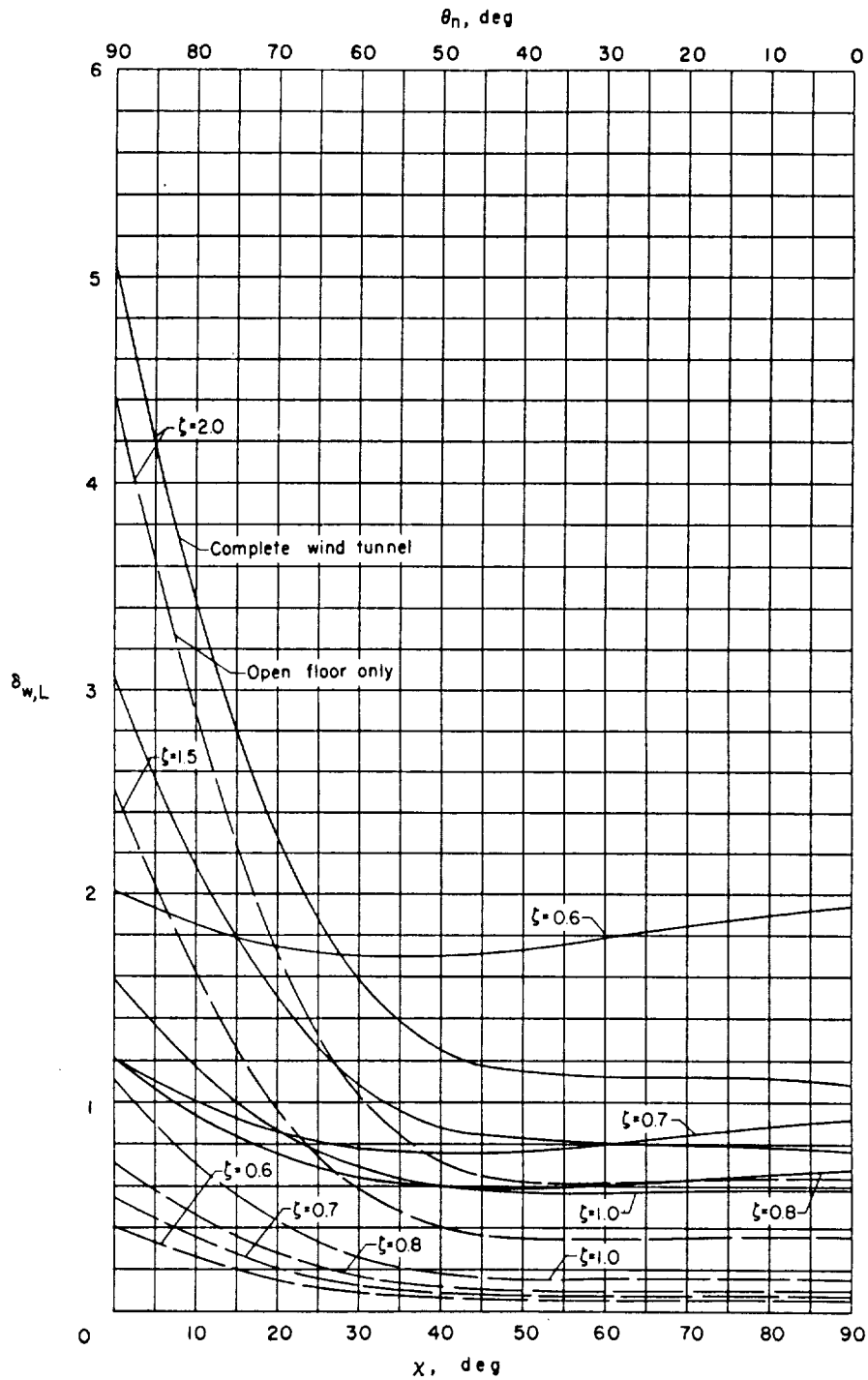


(c) $\gamma = 1.0$.

Figure 18.- Continued.

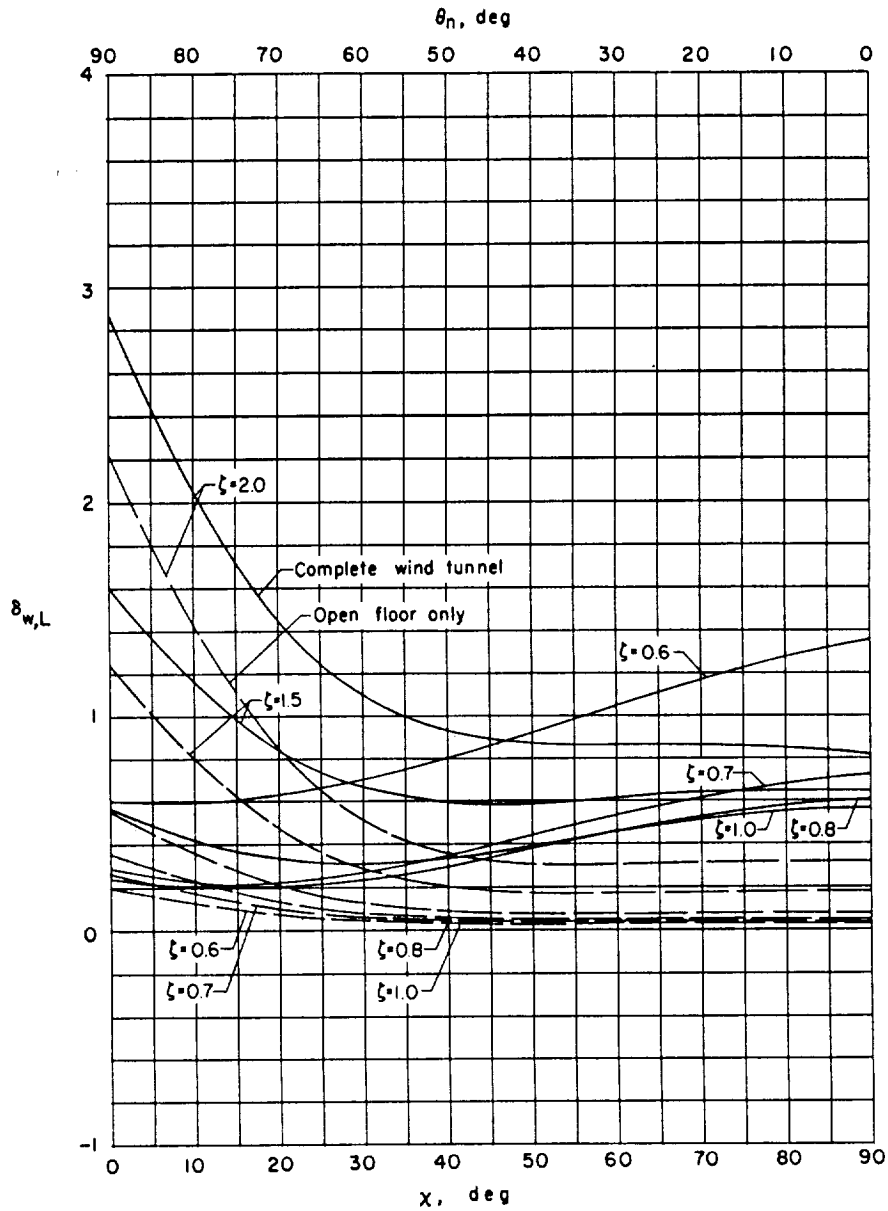


(d) $\gamma = 0.5$.

Figure 18.- Concluded.

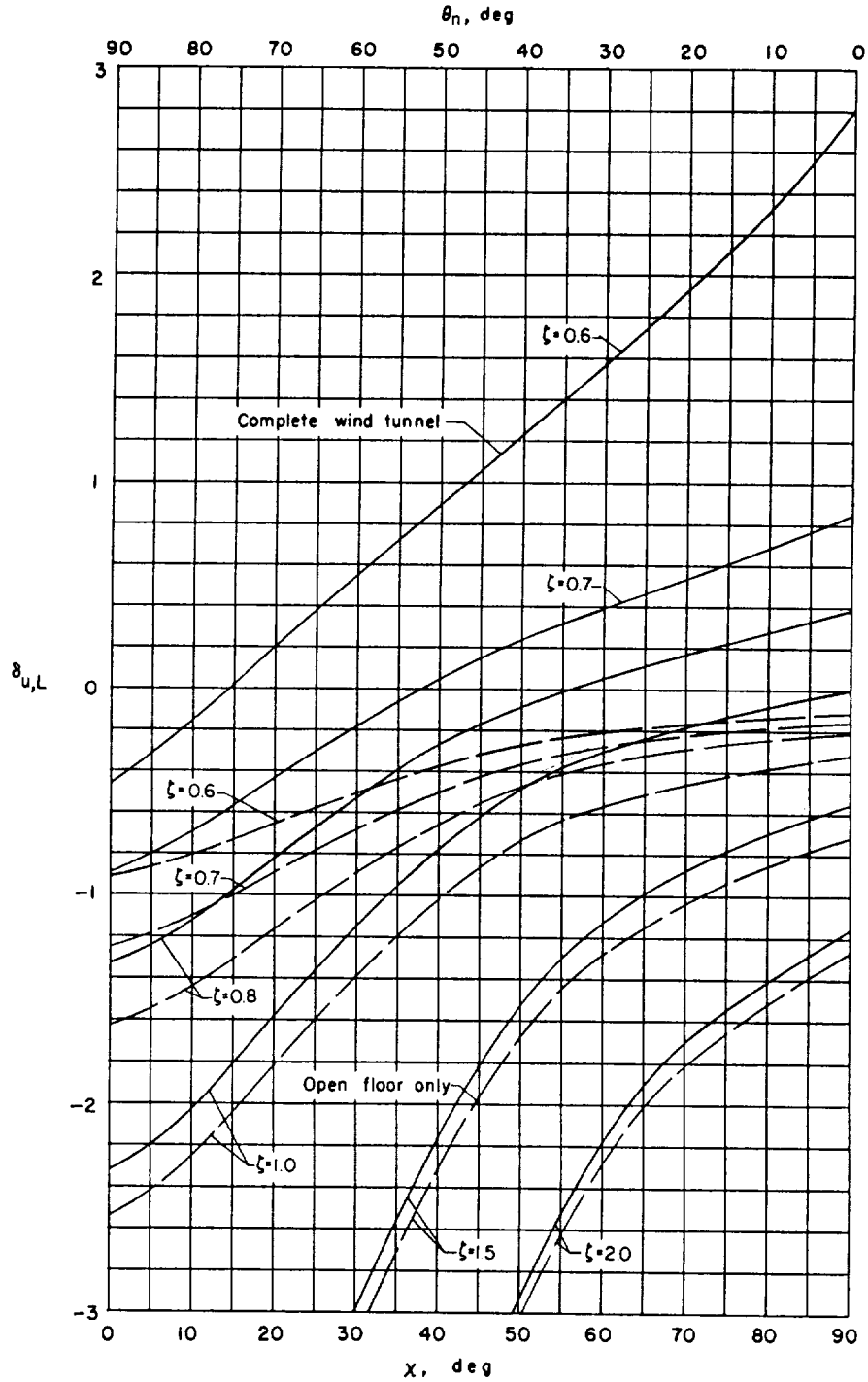


(a) $\gamma$ = 2.0.

Figure 19.- Interference factors for longitudinal interference velocity due to lift for a small model in an open wind tunnel. $\eta$ = 1.0.

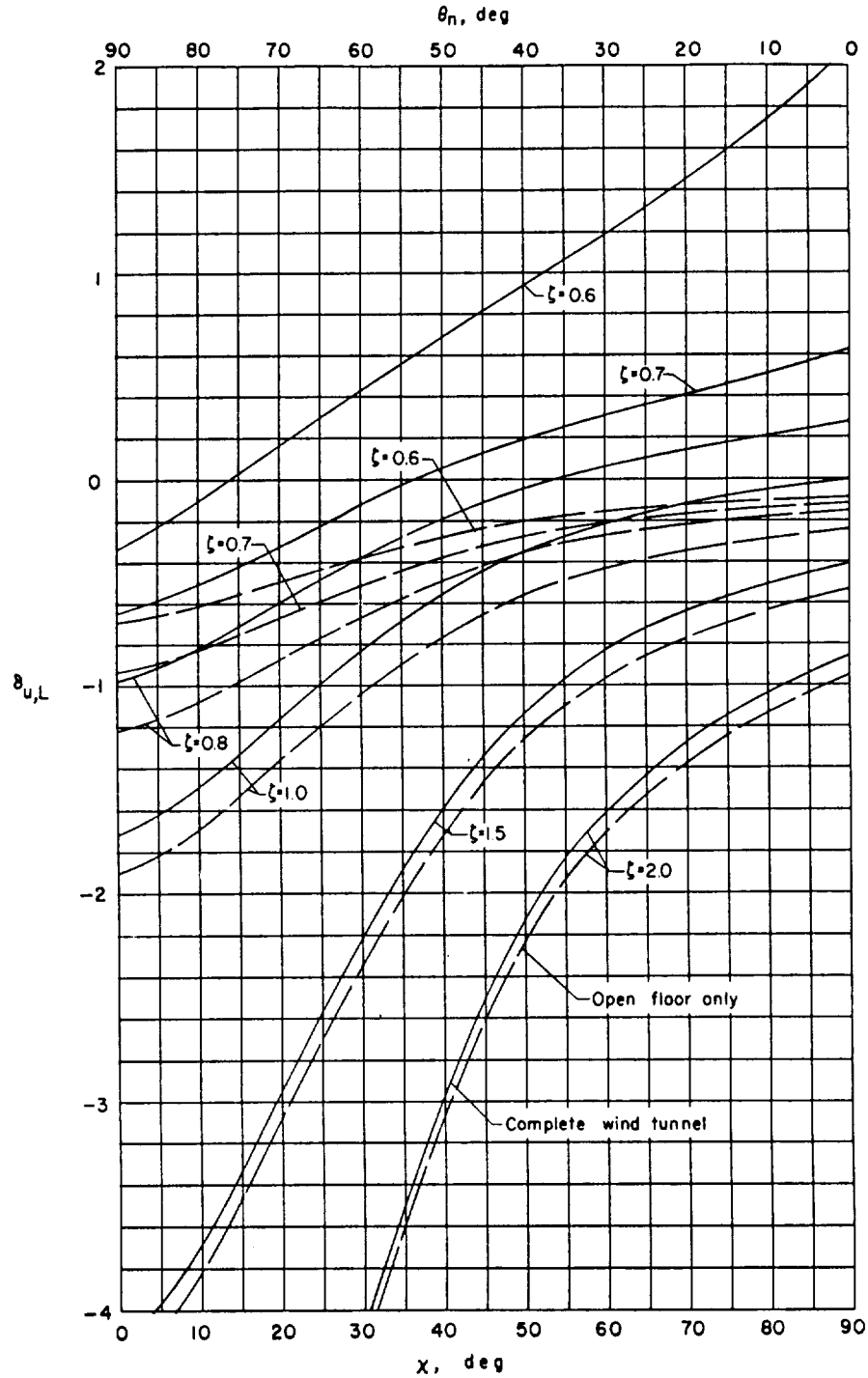


(b) $\gamma = 1.5$.

Figure 19.- Continued.

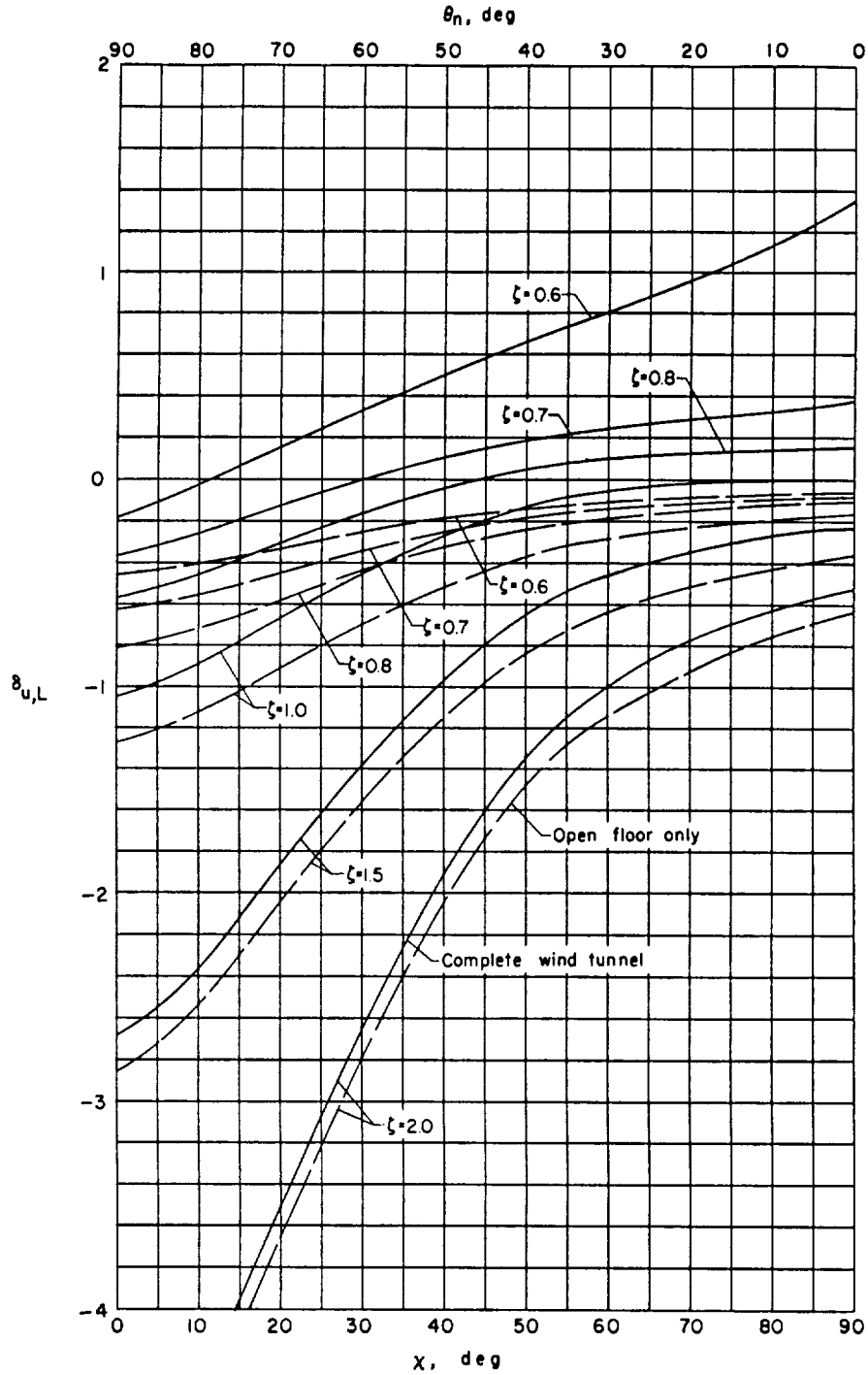


(c) $\gamma$ = 1.0.

Figure 19.- Continued.

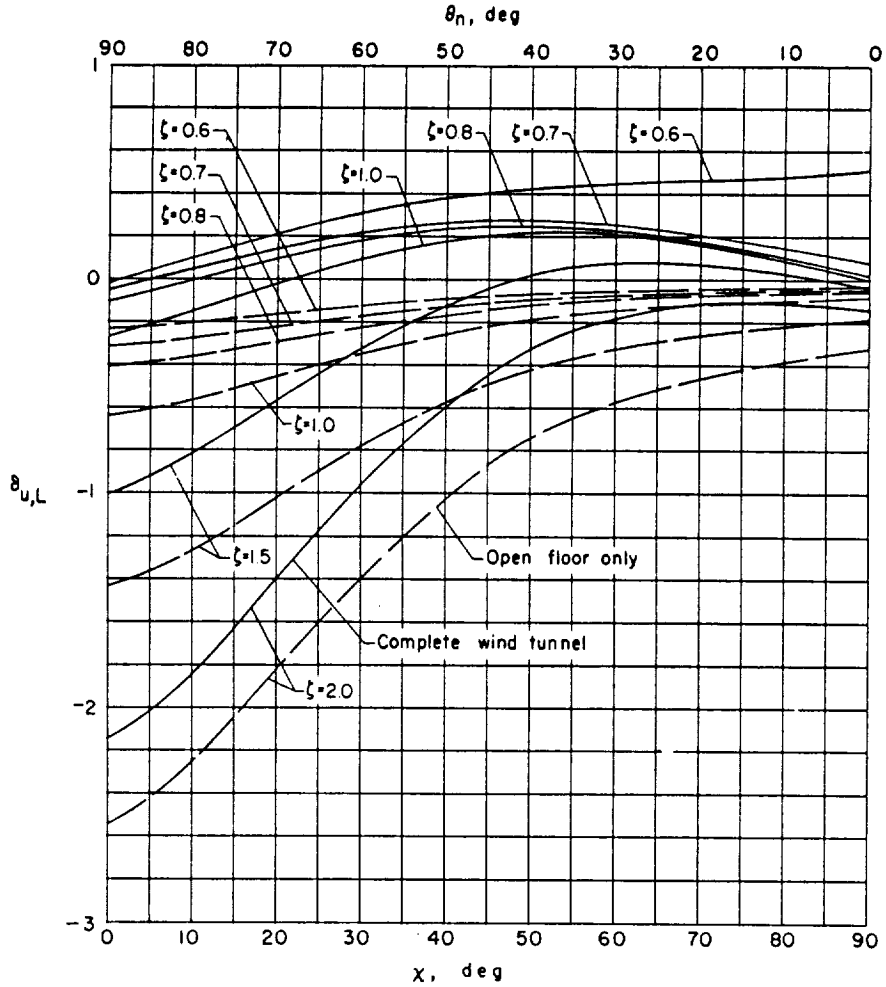


(d) $\gamma = 0.5$.

Figure 19.- Concluded.

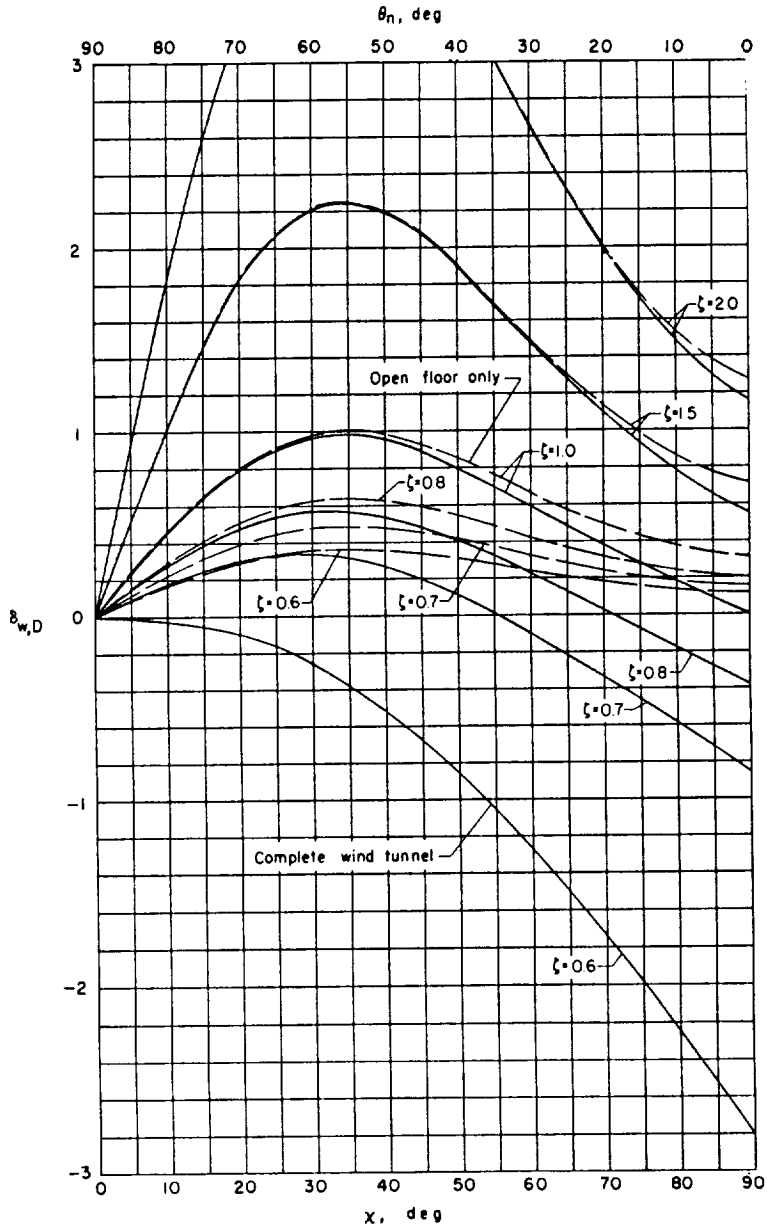


(a) $\gamma = 2.0$.

Figure 20.- Interference factors for vertical interference velocity due to drag for a small model in an open wind tunnel. $\eta = 1.0$.

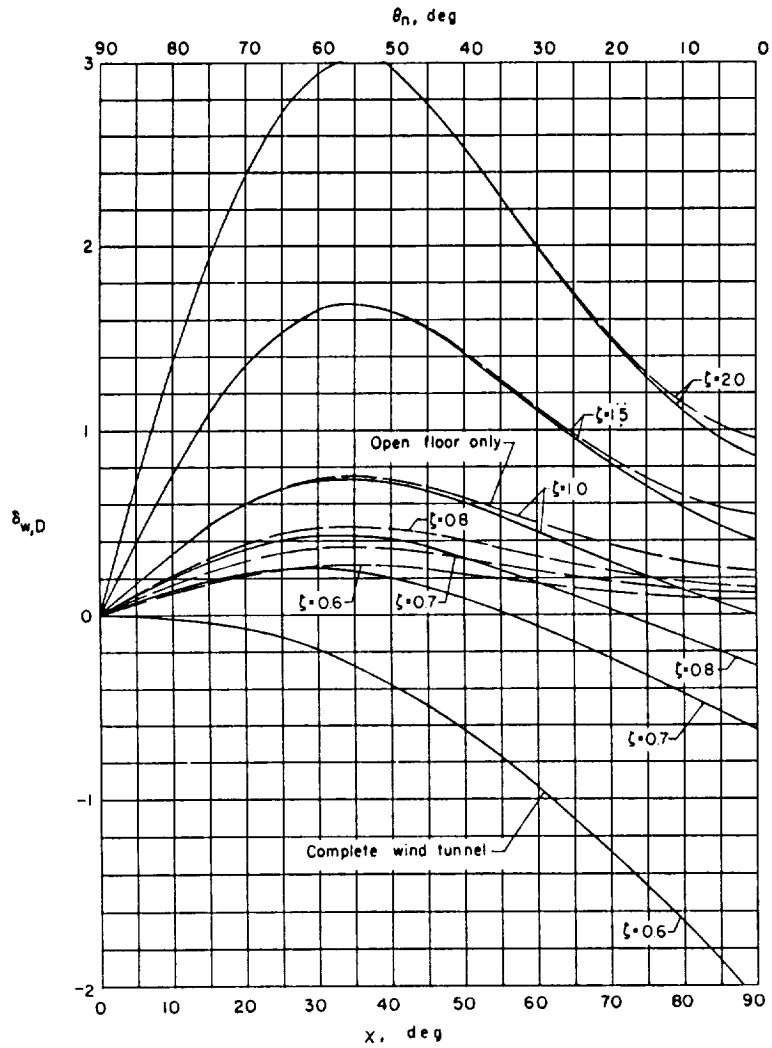


(b) $\gamma = 1.5$.

Figure 20.- Continued.

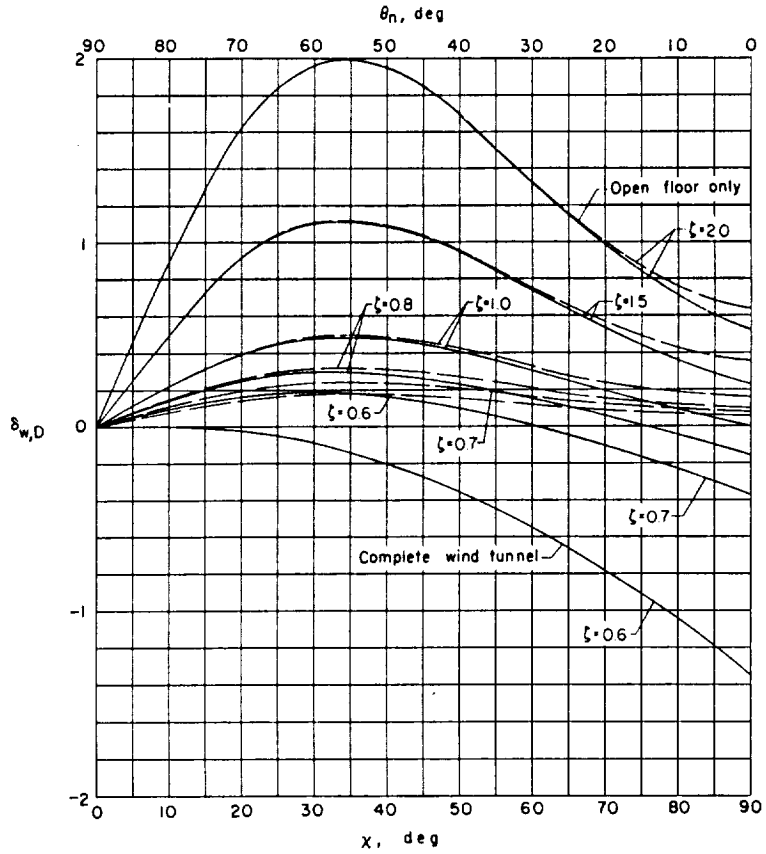


(c) $\gamma = 1.0$.

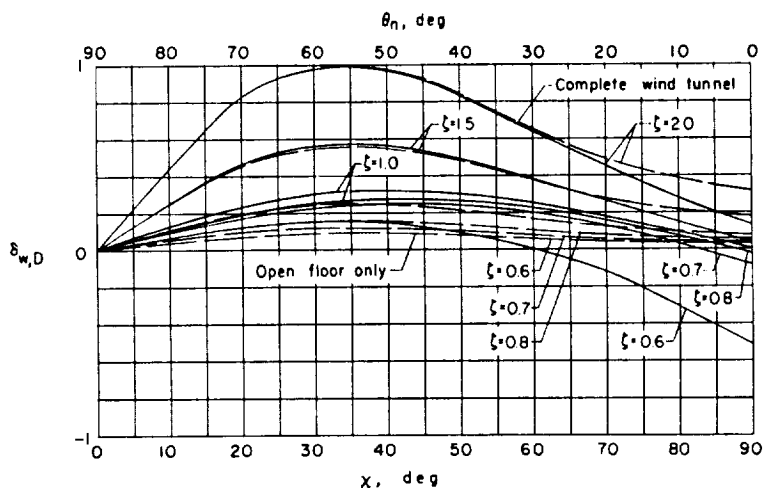


(d) $\gamma = 0.5$.

Figure 20.- Concluded.

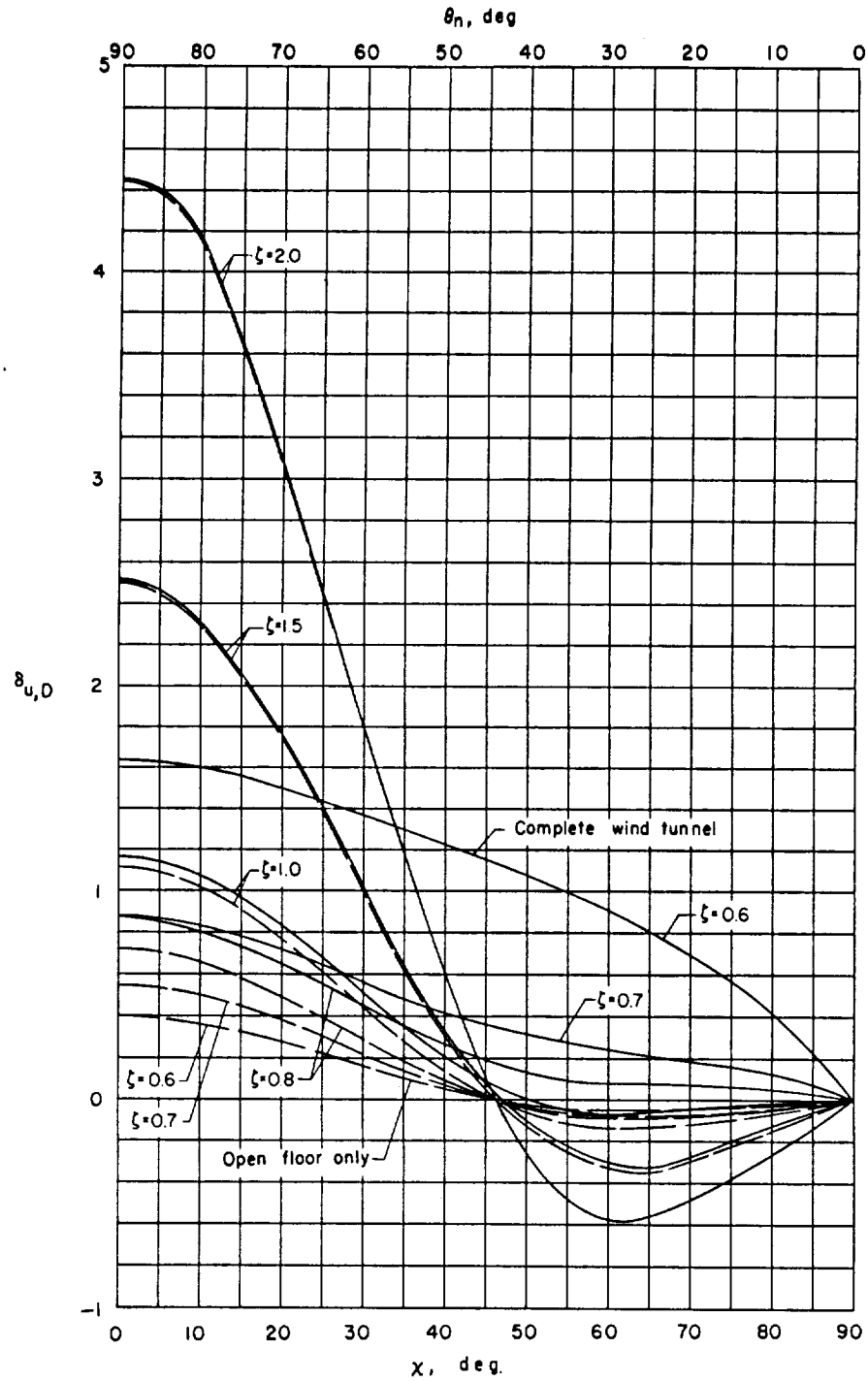


(a) $\gamma$ = 2.0.

Figure 21.- Interference factors for longitudinal interference velocity due to drag for a small model in an open wind tunnel. $\eta$ = 1.0.

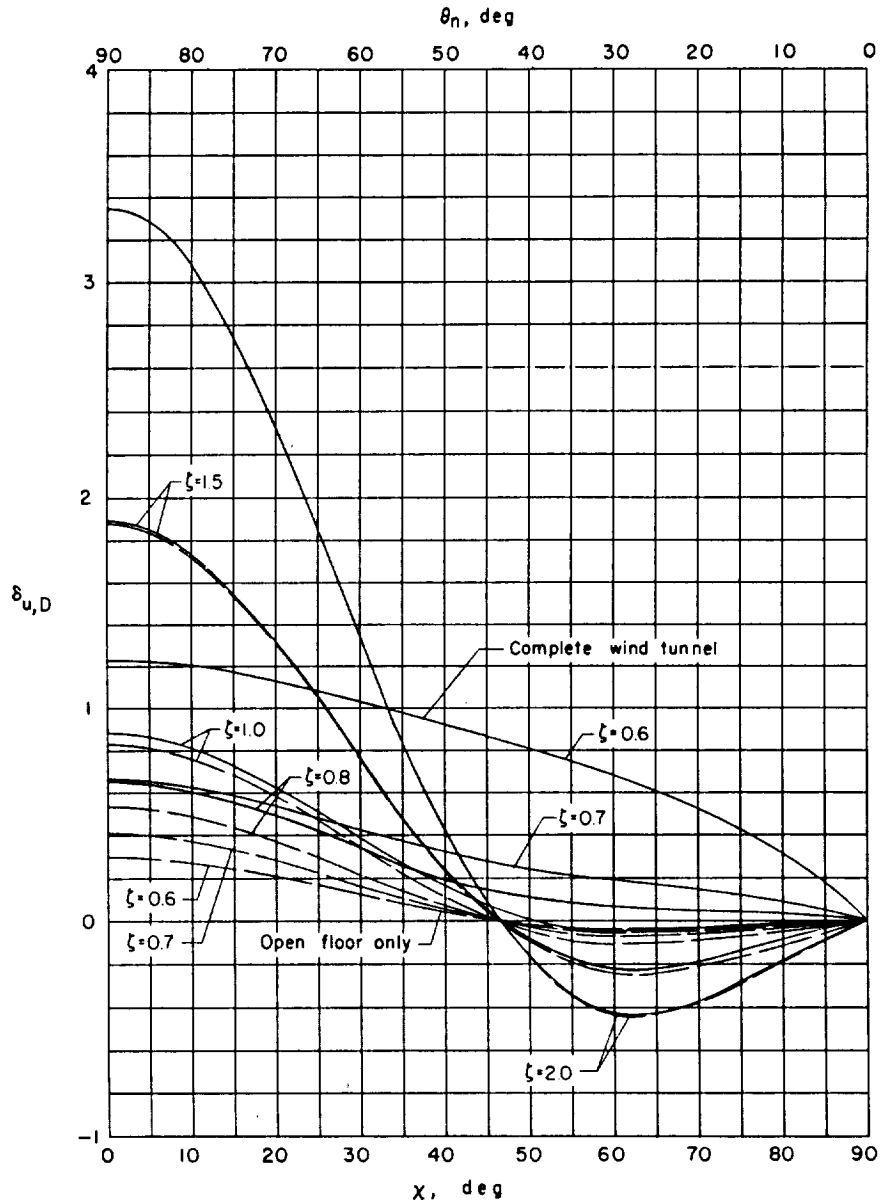


(b) $\gamma = 1.5$.

Figure 21.- Continued.

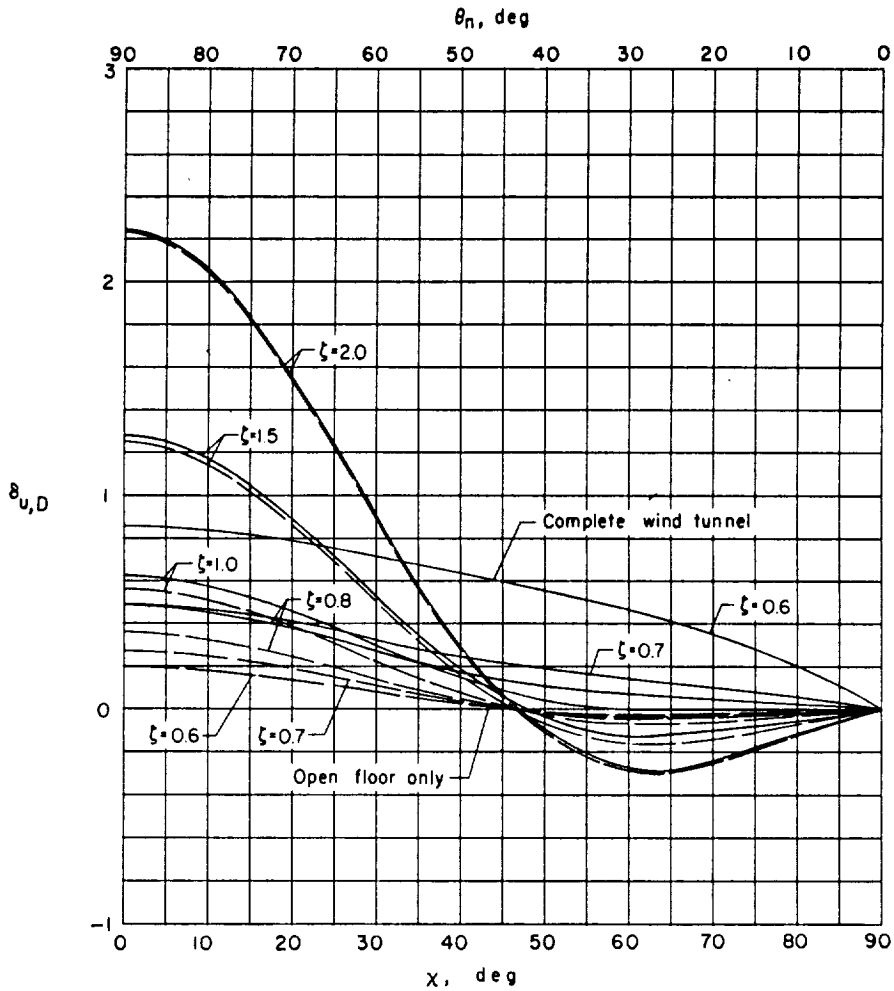


(c) $\gamma$ = 1.0.

Figure 21.- Continued.

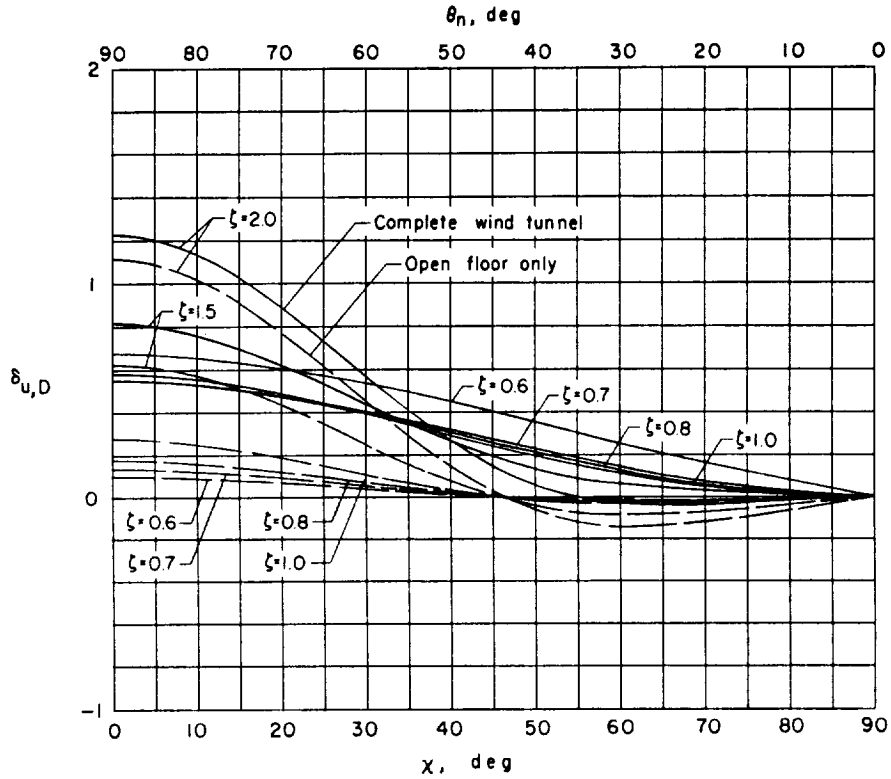


(d) $\gamma = 0.5$.

Figure 21.- Concluded.

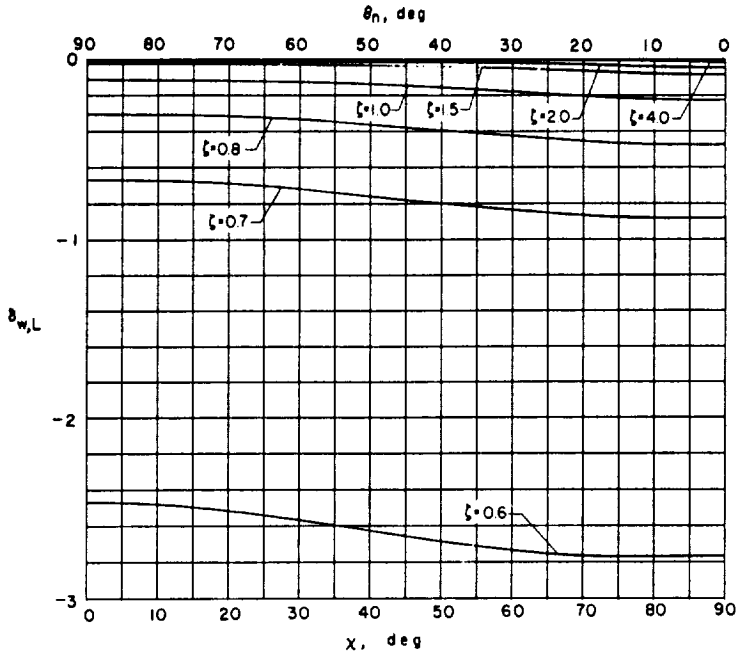


(a) $\gamma = 2.0$.

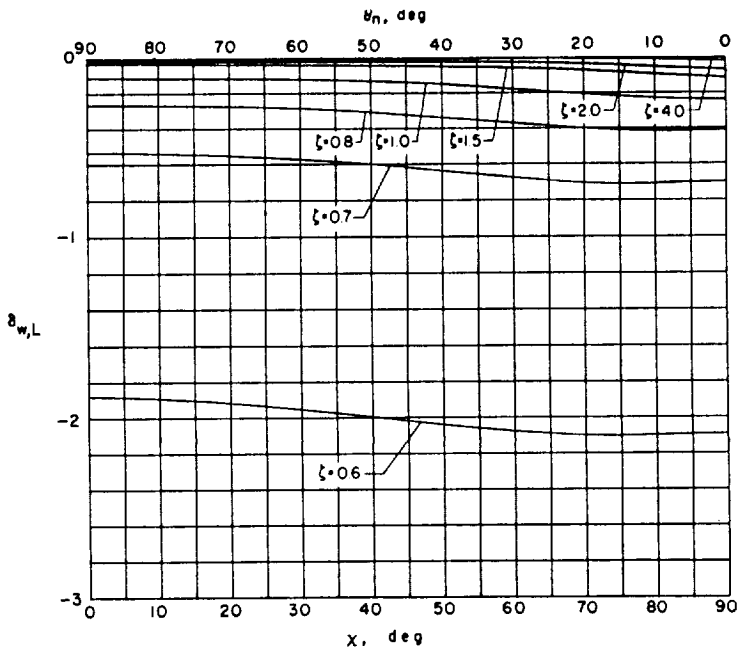


(b) $\gamma = 1.5$.

Figure 22.- Interference factors for vertical interference velocity due to lift for correcting from a closed wind tunnel to ground effect. $\eta = 1.0$.

632043 O—62——7

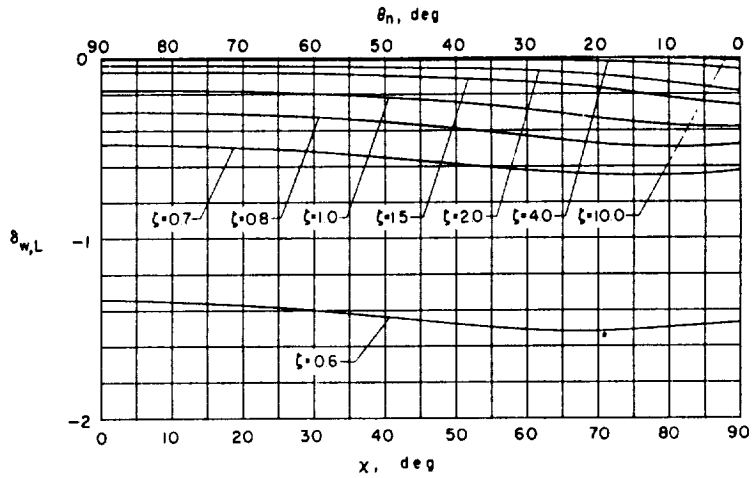


(c) $\gamma = 1.0$.

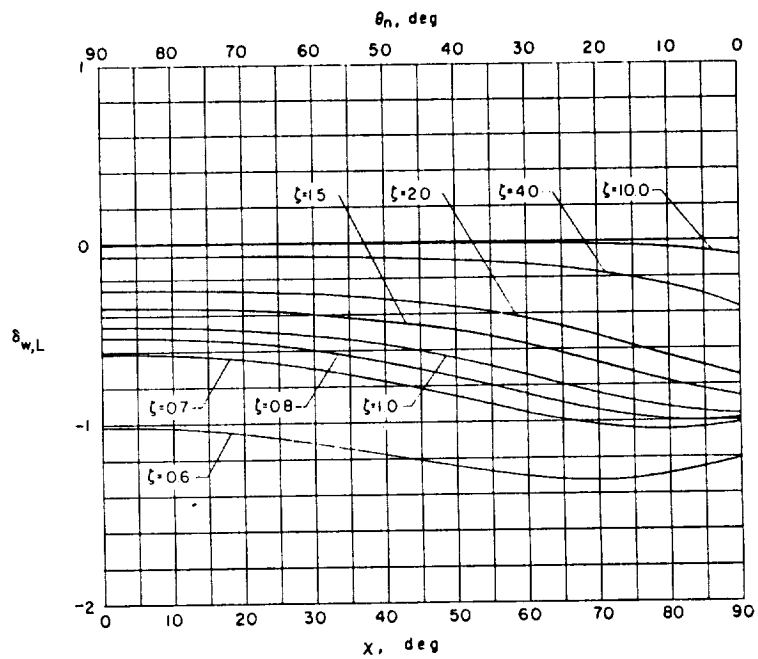


(d) $\gamma = 0.5$.

Figure 22.- Concluded.

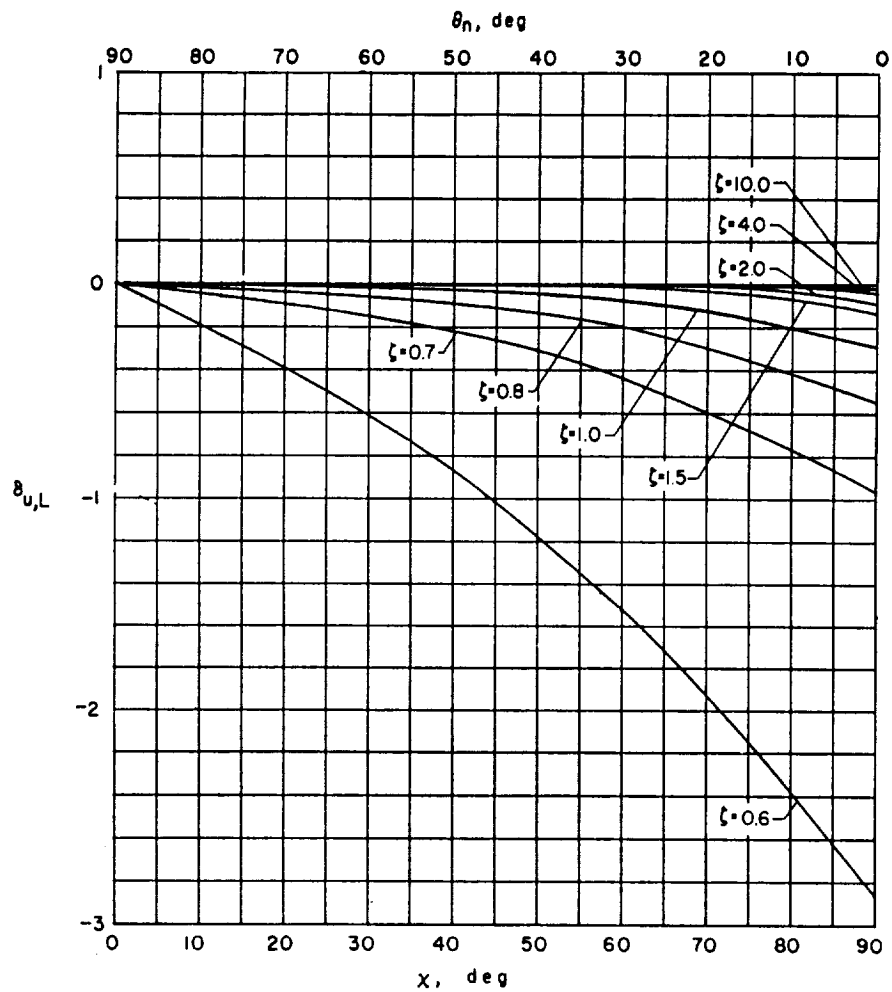


(a) $\gamma$ = 2.0.

Figure 23.- Interference factors for longitudinal interference velocity due to lift for correcting from a closed wind tunnel to ground effect. $\eta$ = 1.0.

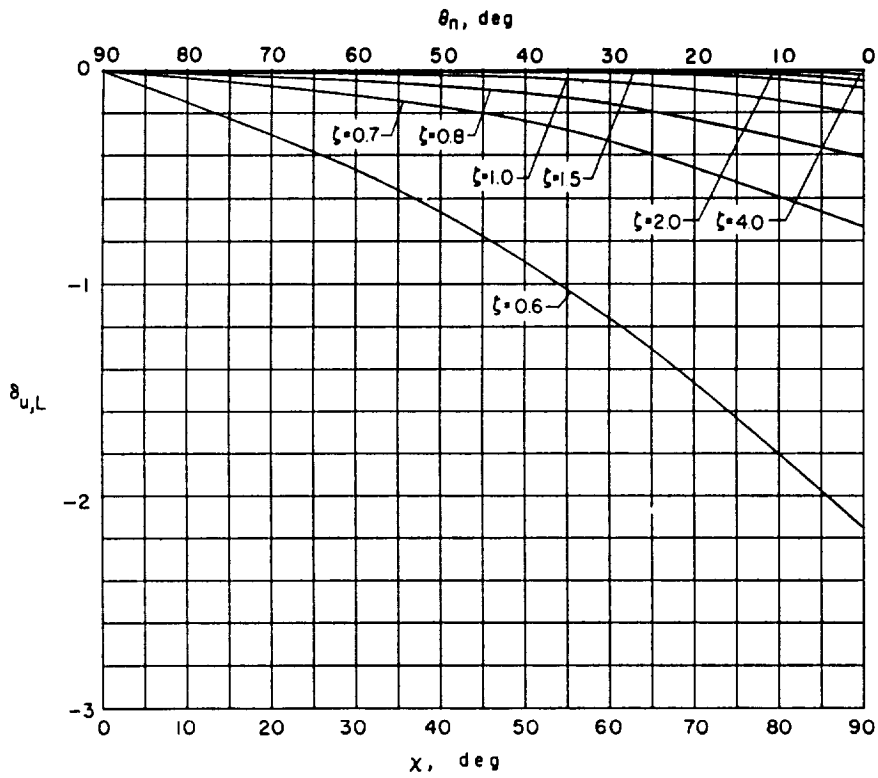


(b) $\gamma = 1.5$.

Figure 23.- Continued.

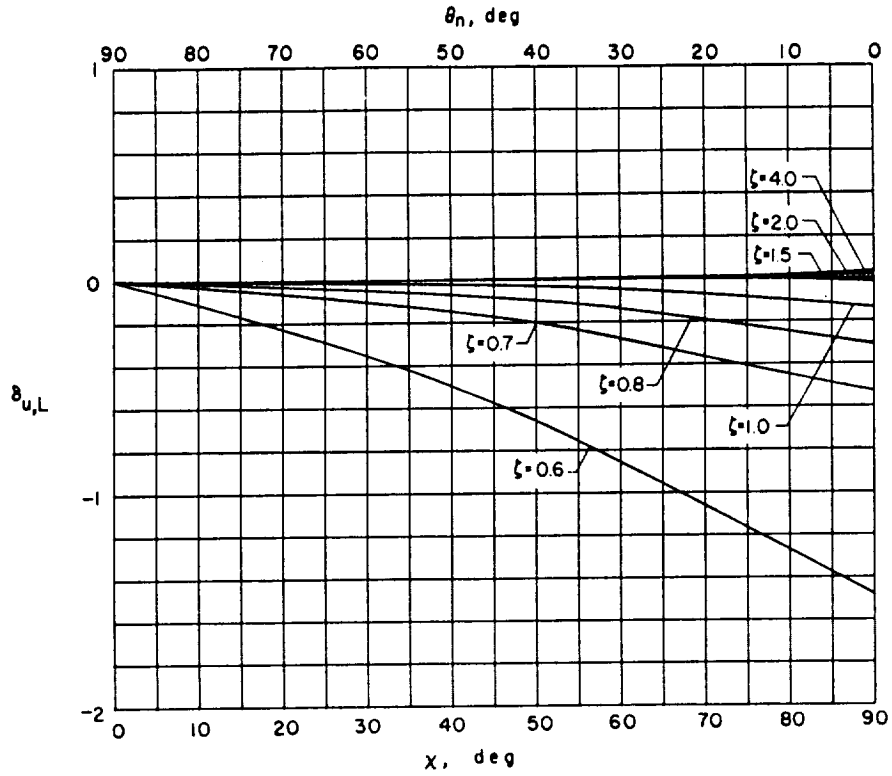


(c) $\gamma = 1.0$.

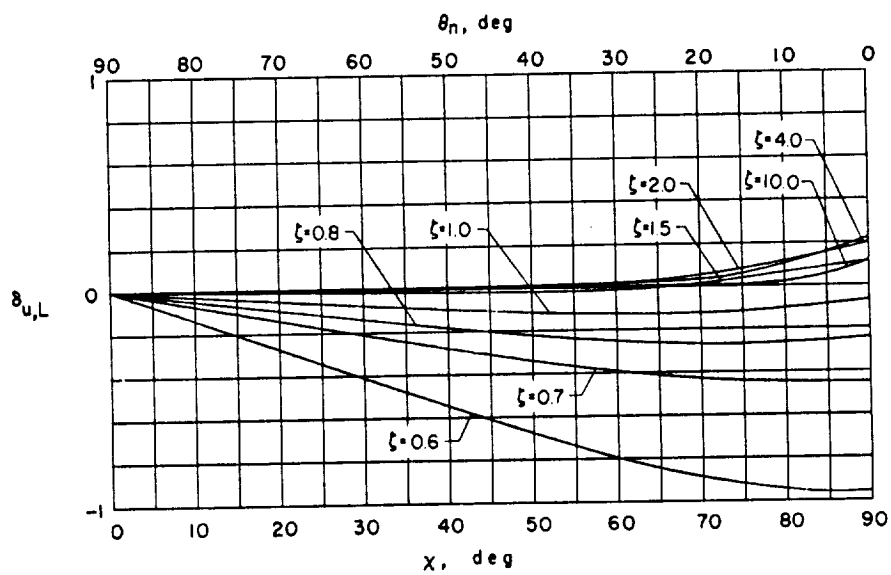


(d) $\gamma = 0.5$.

Figure 23.- Concluded.

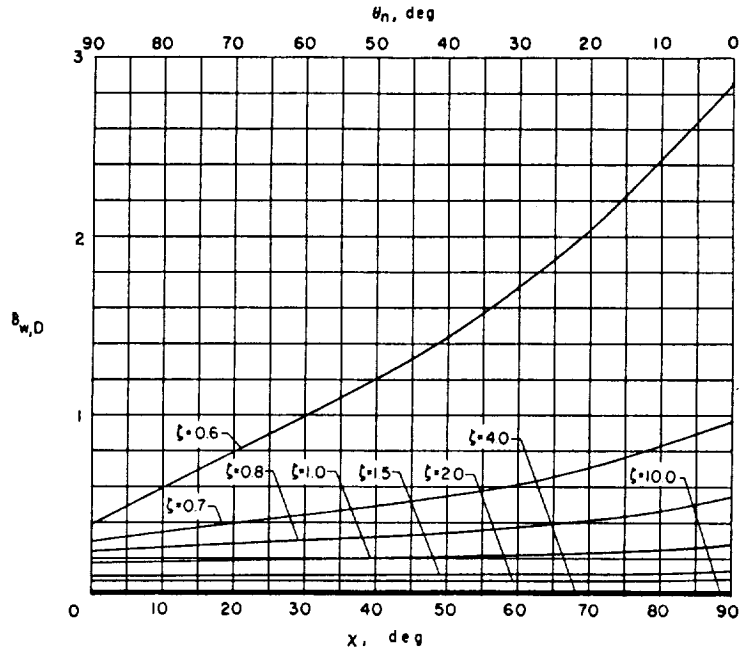


(a) $\gamma = 2.0$.

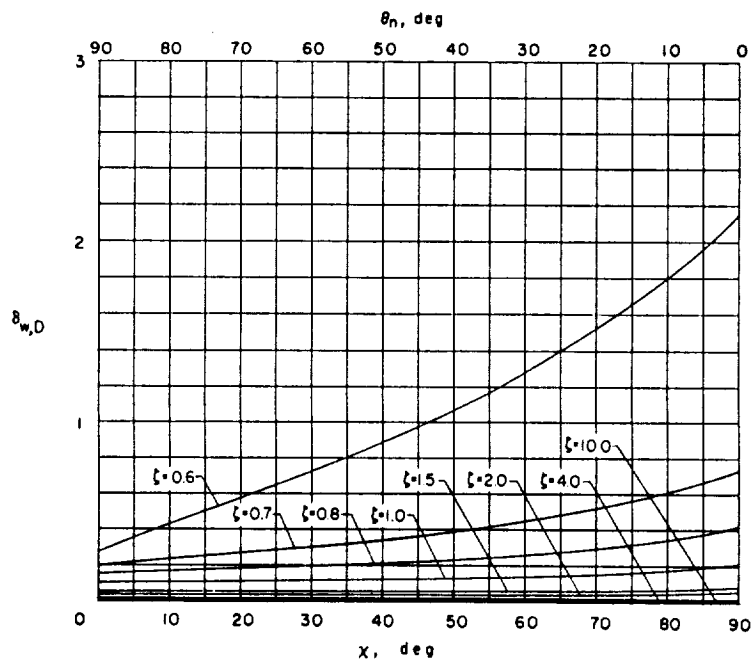


(b) $\gamma = 1.5$.

Figure 24.- Interference factors for vertical interference velocity due to drag for correcting from a closed wind tunnel to ground effect. $\eta = 1.0$.

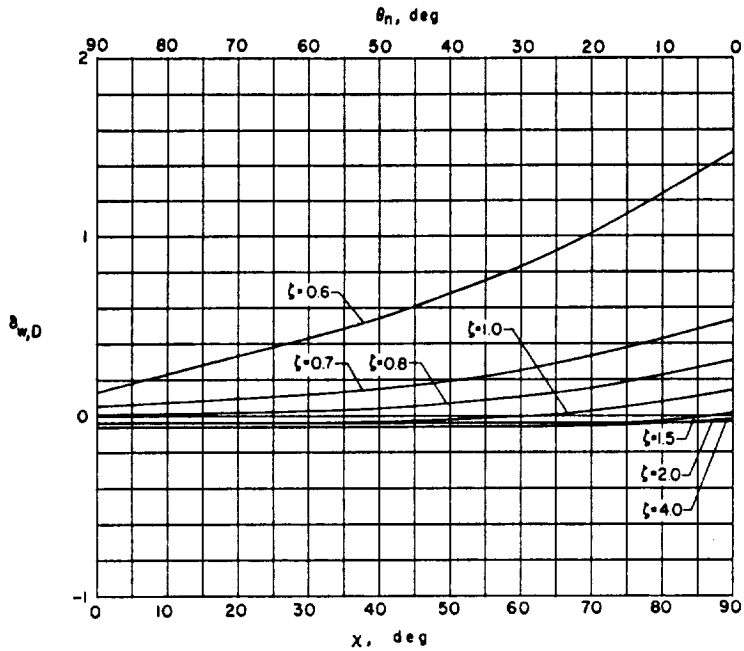


(c) $\gamma = 1.0$.

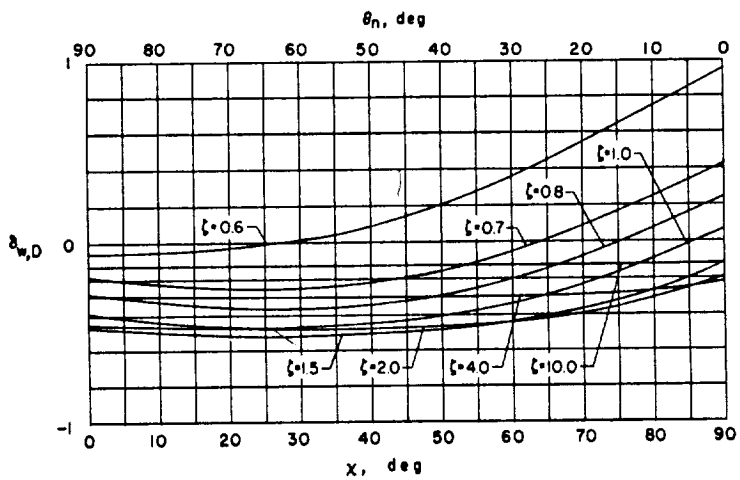


(d) $\gamma = 0.5$.

**Figure 24.- Concluded.**

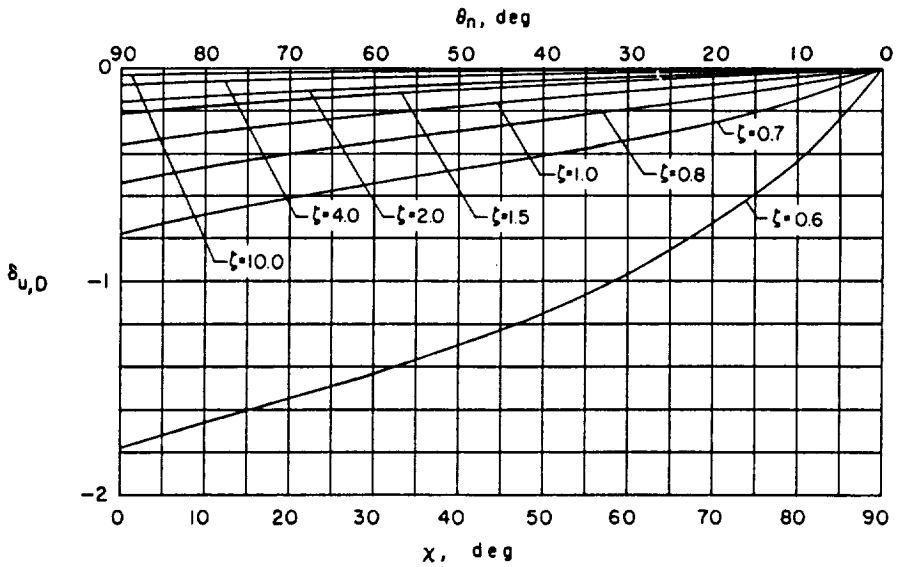


(a) $\gamma = 2.0$.

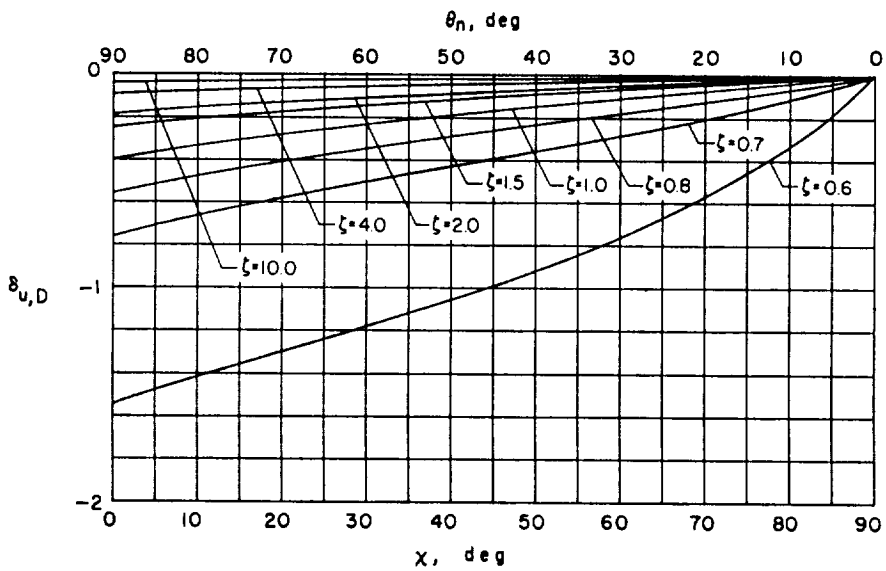


(b) $\gamma = 1.5$.

Figure 25.- Interference factors for longitudinal interference velocity due to drag for correcting from a closed wind tunnel to ground effect. $\eta = 1.0$.

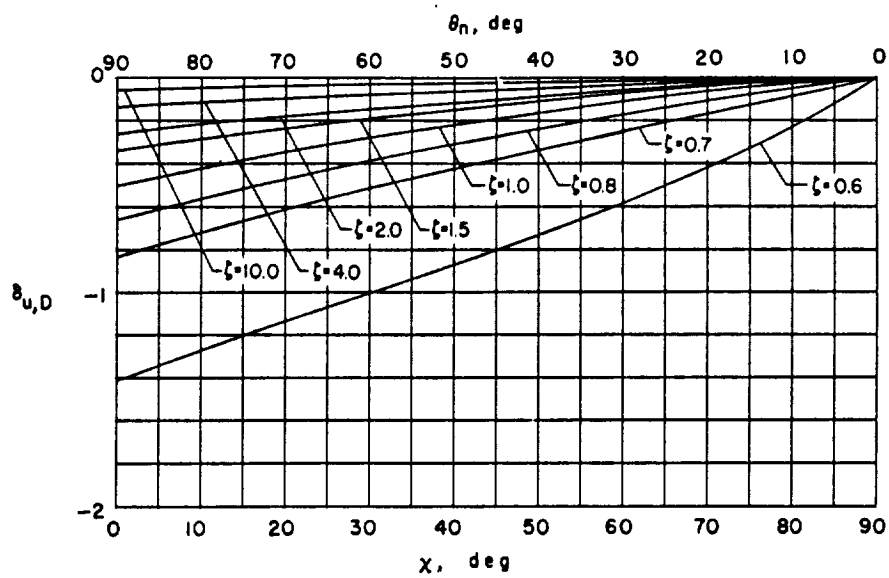


(c) $\gamma = 1.0$.

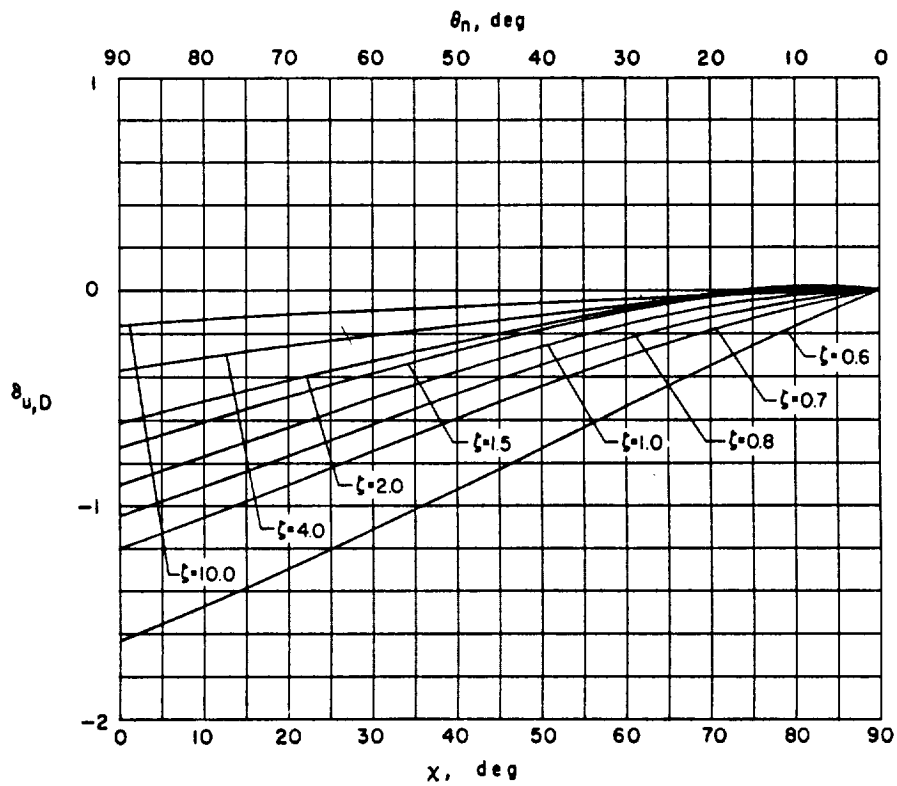


(d) $\gamma = 0.5$.

Figure 25.- Concluded.

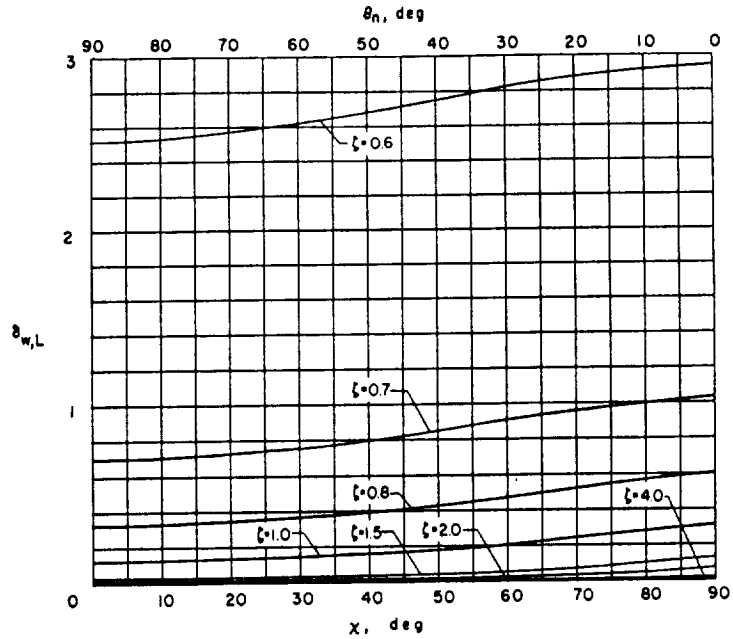


(a) $\gamma = 2.0$.

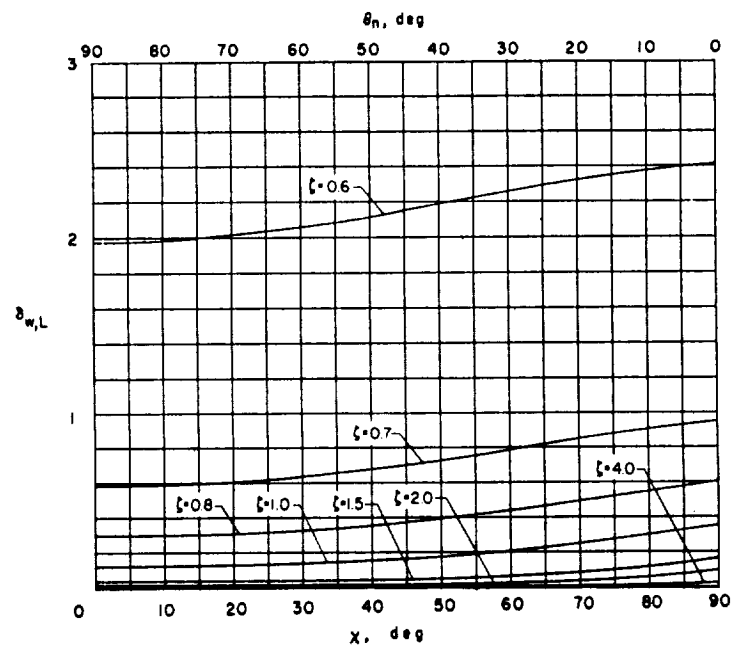


(b) $\gamma = 1.5$.

Figure 26.- Interference factors for vertical interference velocity due to lift for correcting from a wind tunnel closed on the bottom only to ground effect. $\eta = 1.0$.

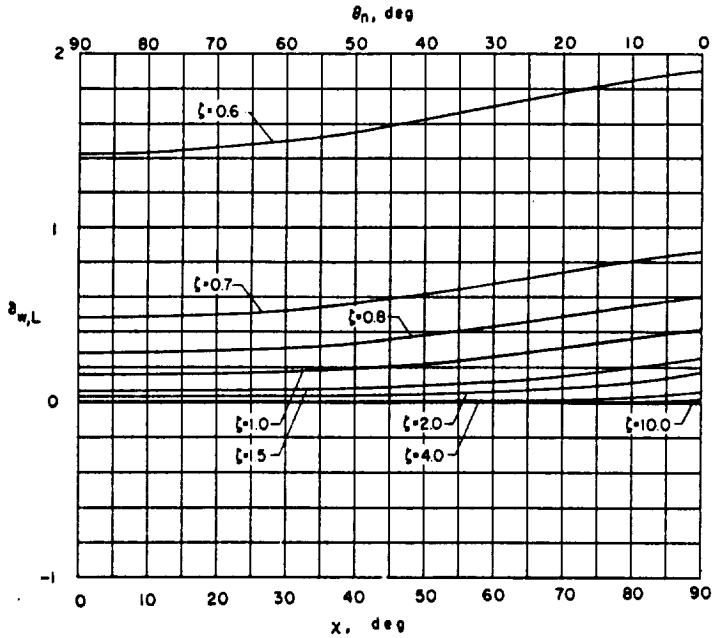


(c) $\gamma = 1.0$.

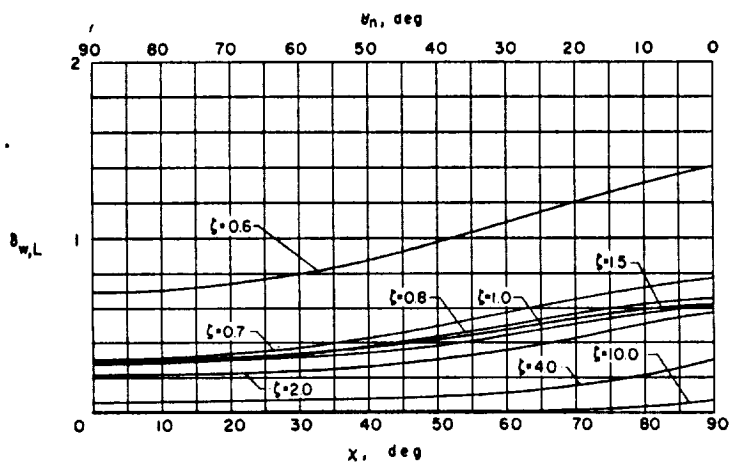


(d) $\gamma = 0.5$.

**Figure 26.- Concluded.**

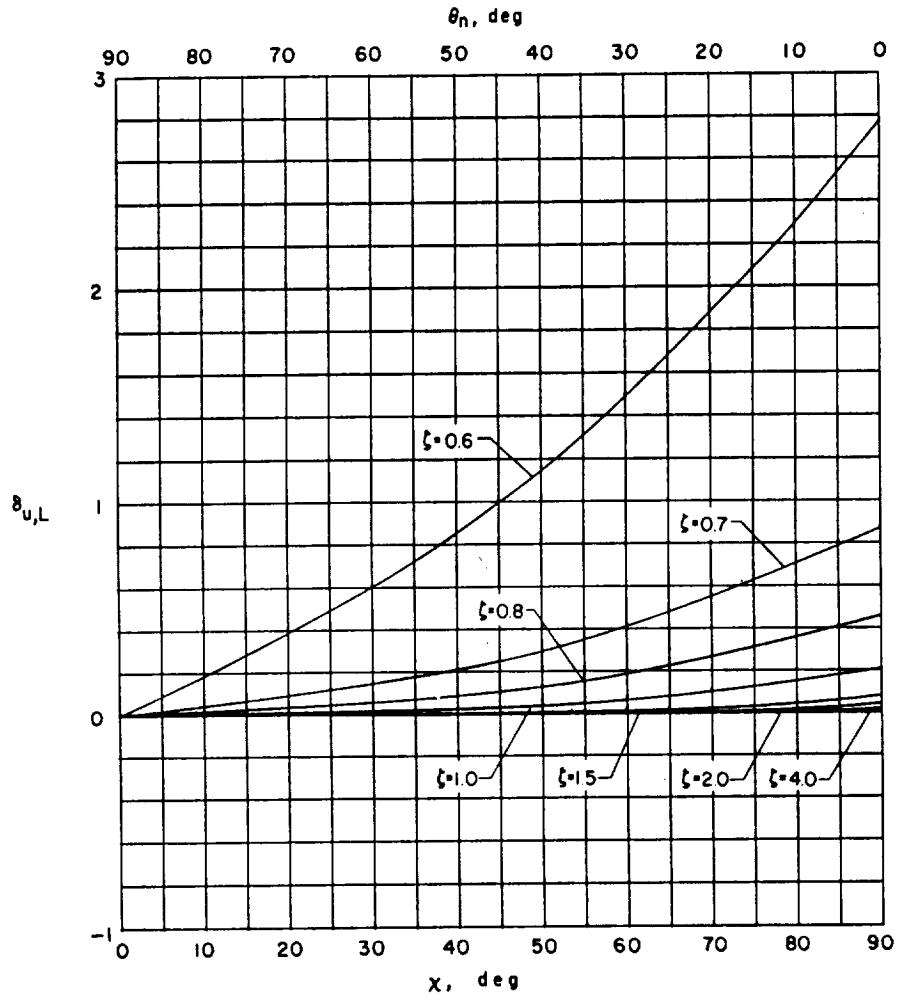


(a) $\gamma = 2.0$.

Figure 27.- Interference factors for longitudinal interference velocity due to lift for correcting from a wind tunnel closed on the bottom only to ground effect. $\eta = 1.0$.

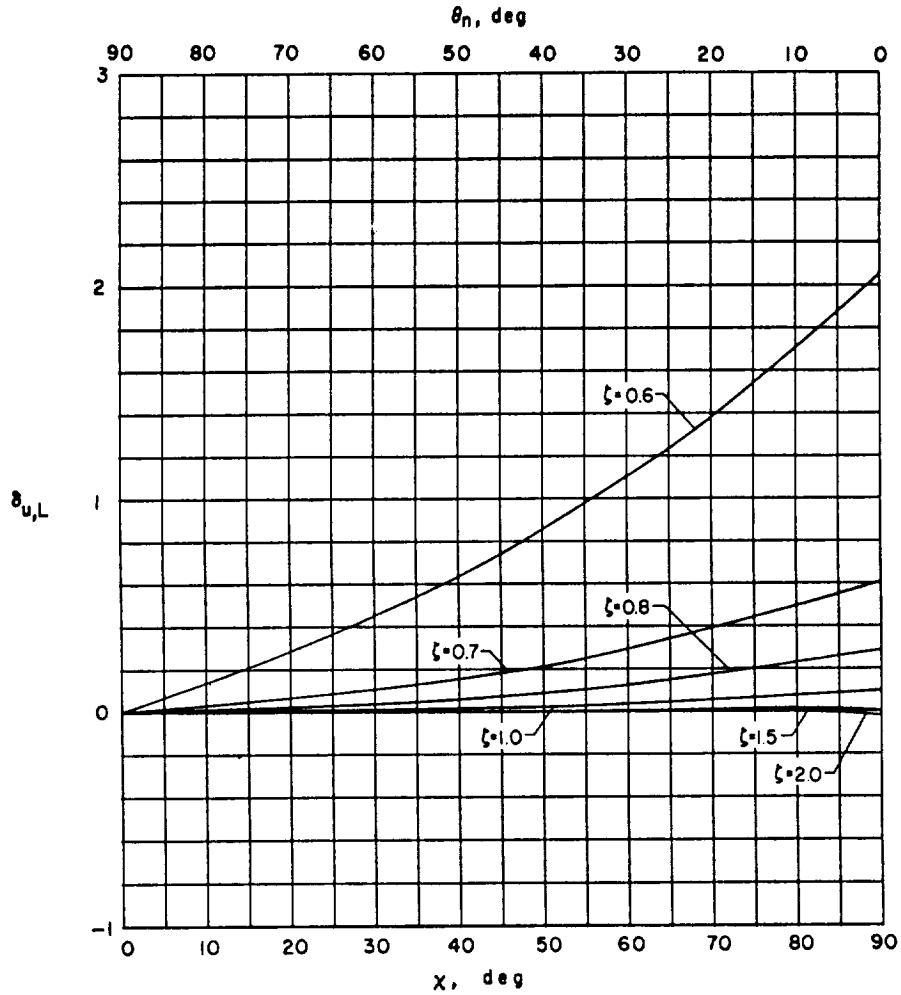


(b) $\gamma = 1.5$.

Figure 27.- Continued.

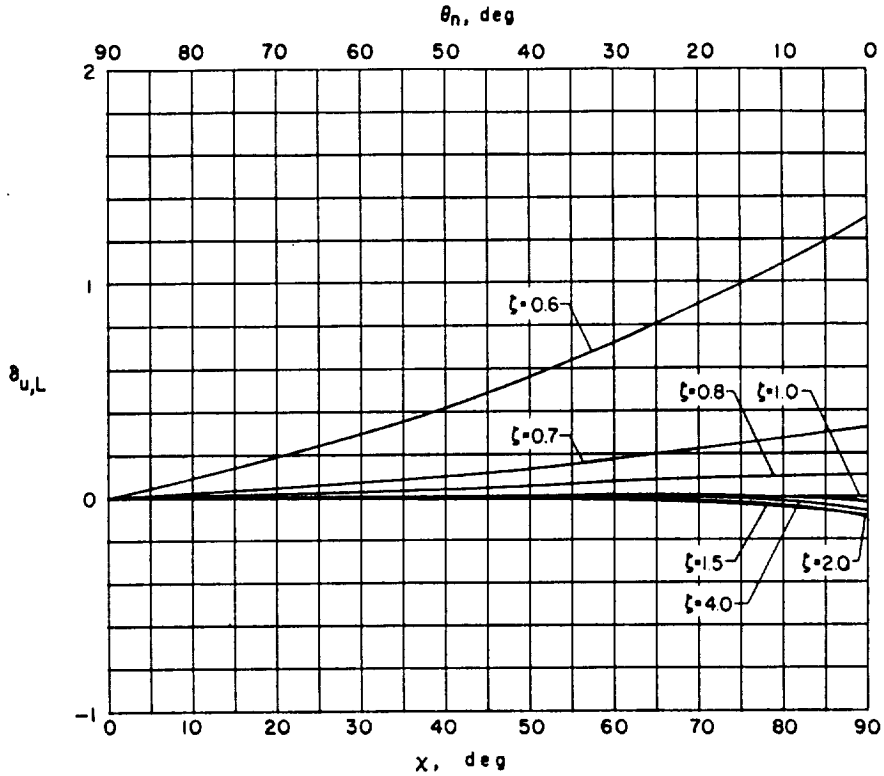


(c) $\gamma = 1.0$.

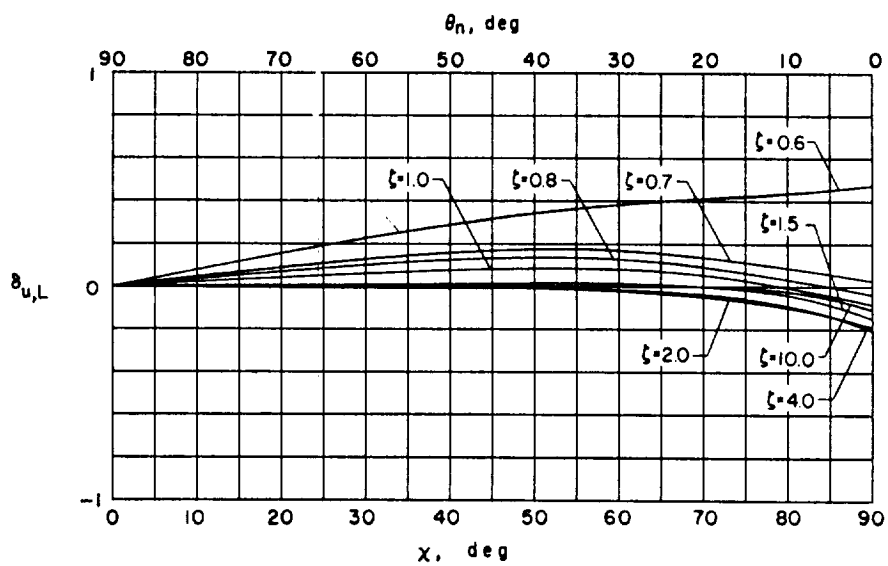


(d) $\gamma = 0.5$.

Figure 27.- Concluded.

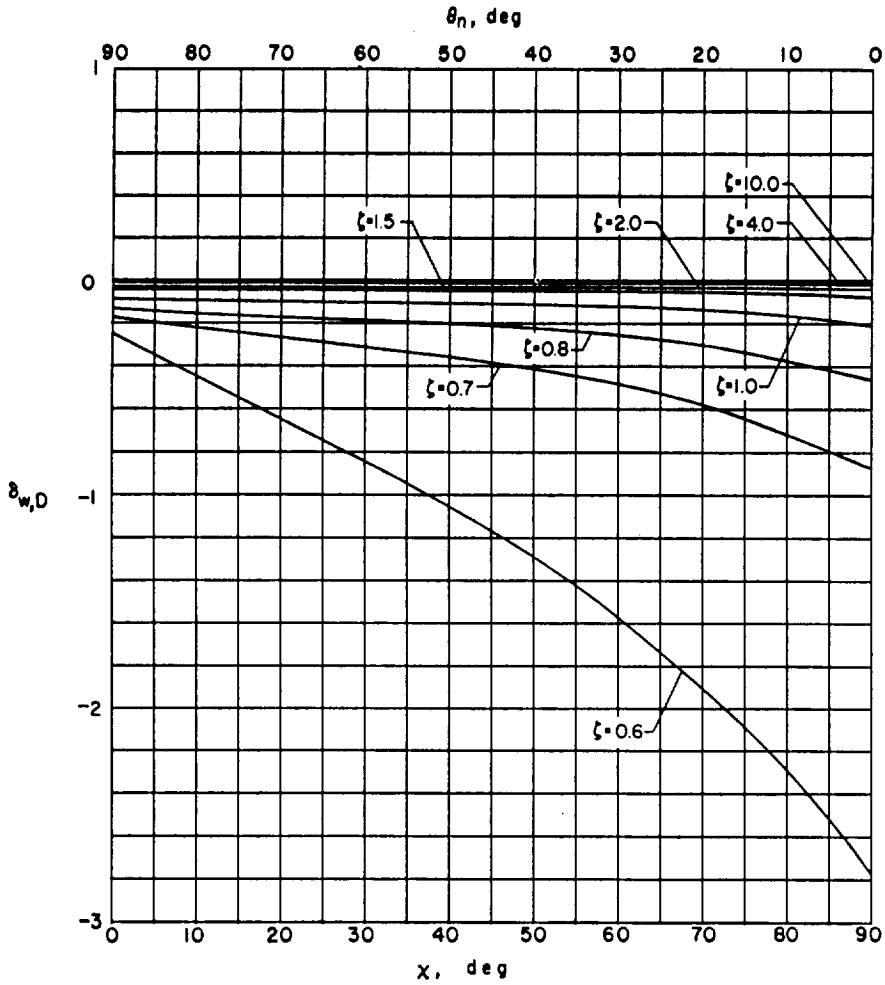


(a) $\gamma = 2.0$.

Figure 28.- Interference factors for vertical interference velocity due to drag for correcting from a wind tunnel closed on the bottom only to ground effect. $\eta = 1.0$.

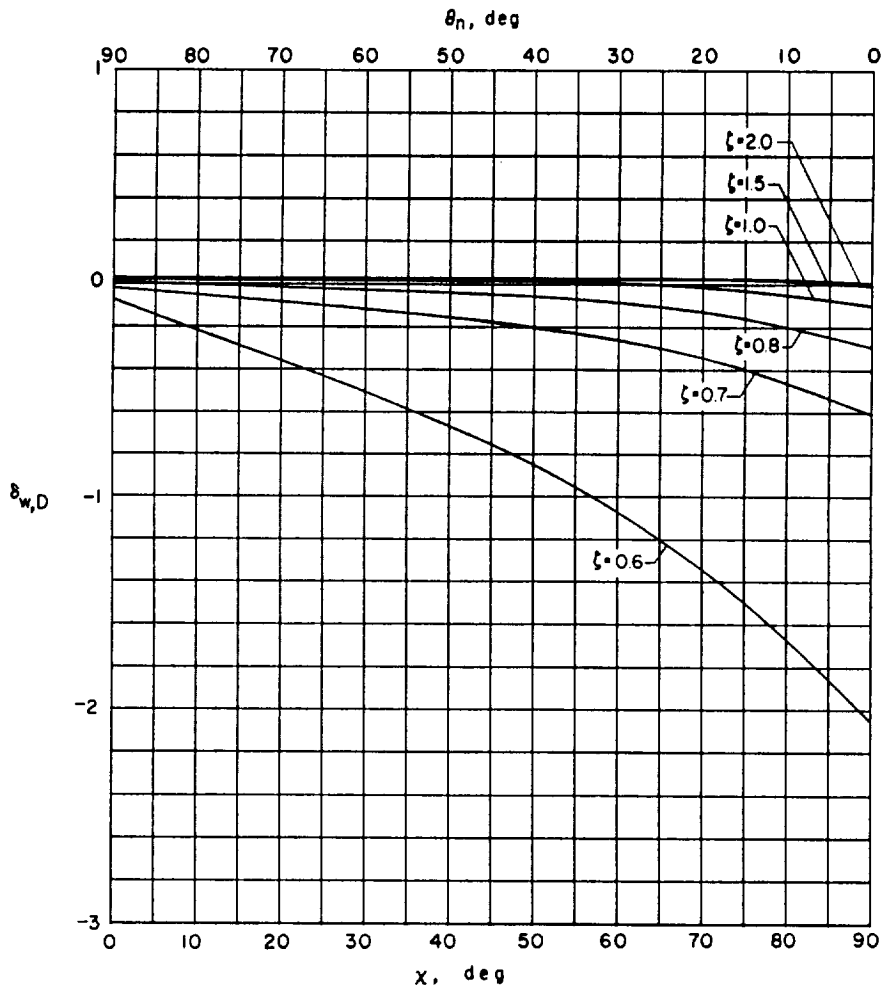


(b) $\gamma = 1.5$.

Figure 28.- Continued.

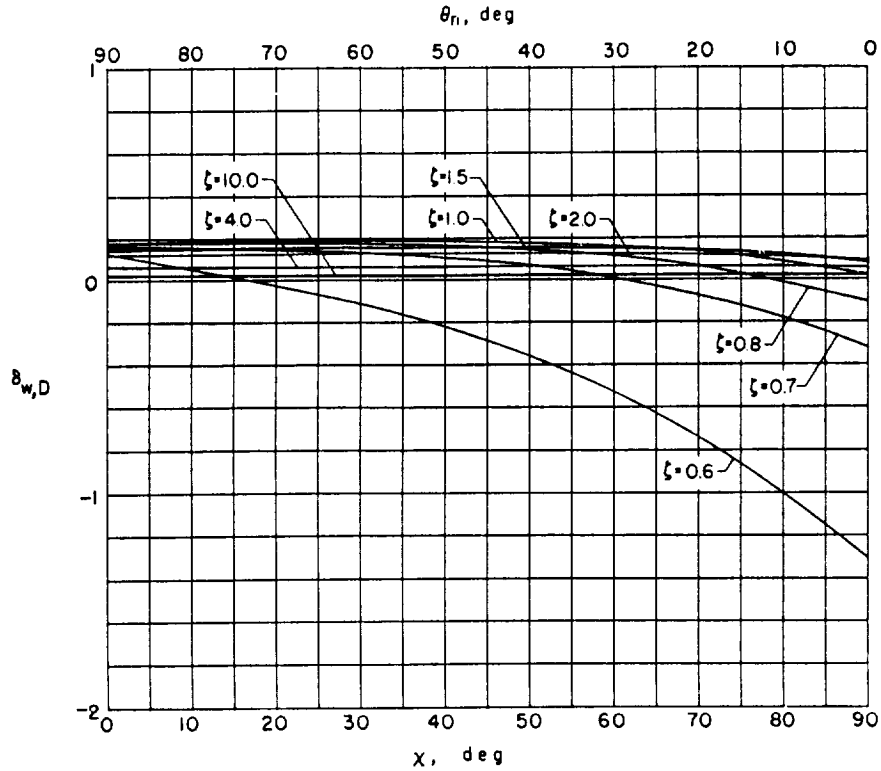


(c) $\gamma = 1.0$.

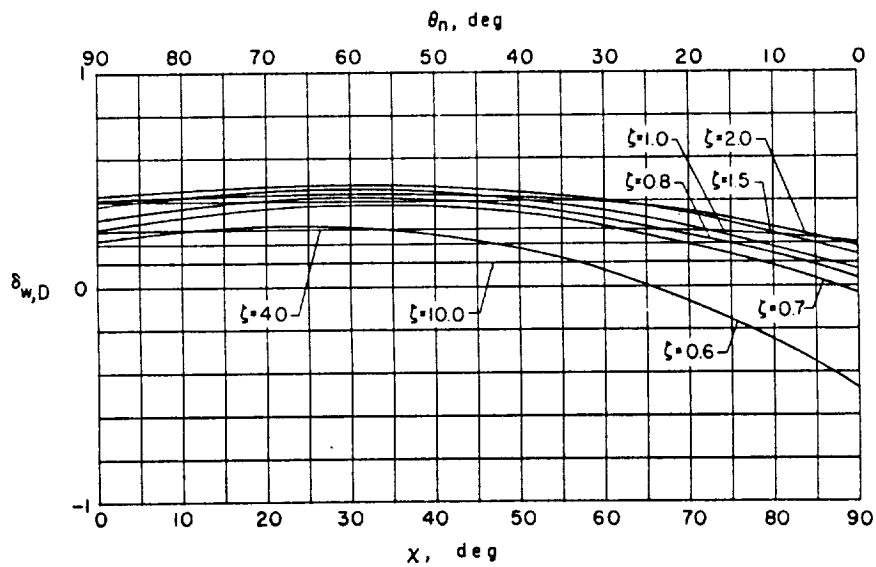


(d) $\gamma = 0.5$.

632643 O—62——8

Figure 28.- Concluded.

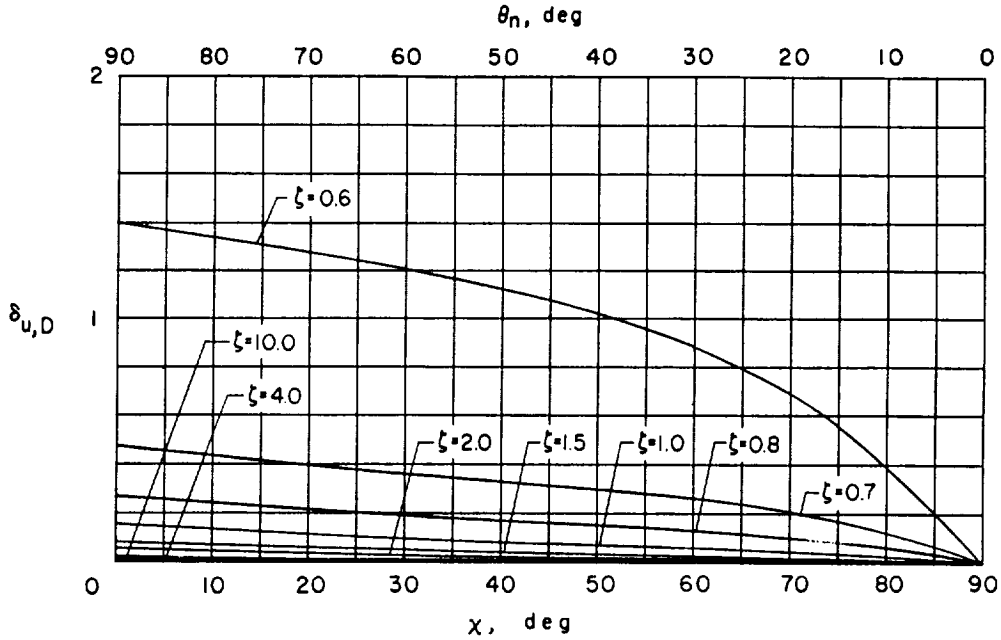


(a) $\gamma$ = 2.0.

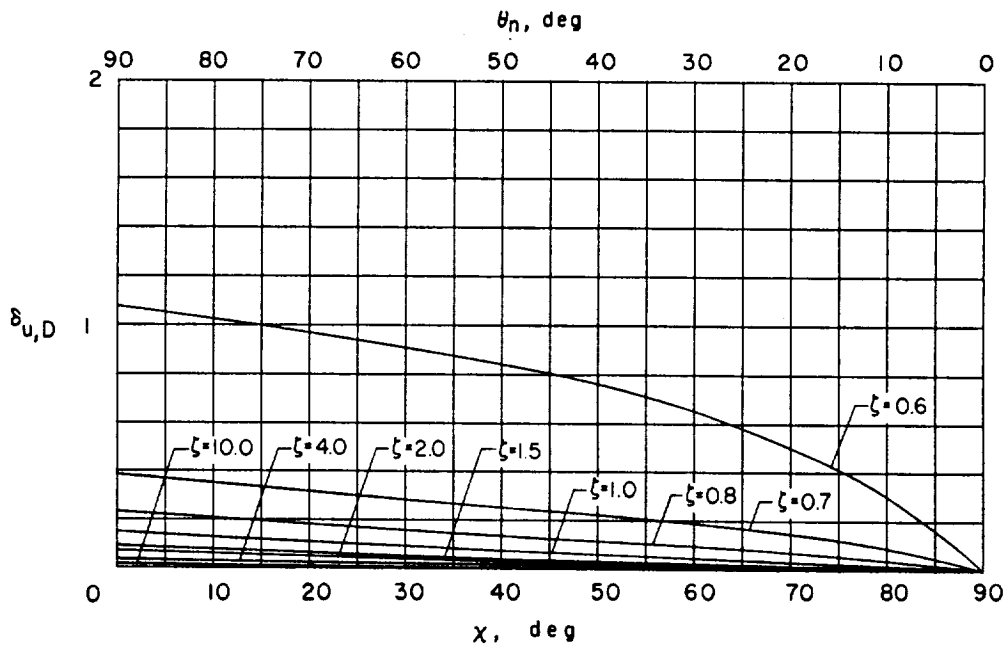


(b) $\gamma$ = 1.5.

Figure 29.- Interference factors for longitudinal interference velocity due to drag for correcting from a wind tunnel closed on the bottom only to ground effect. $\eta$ = 1.0.

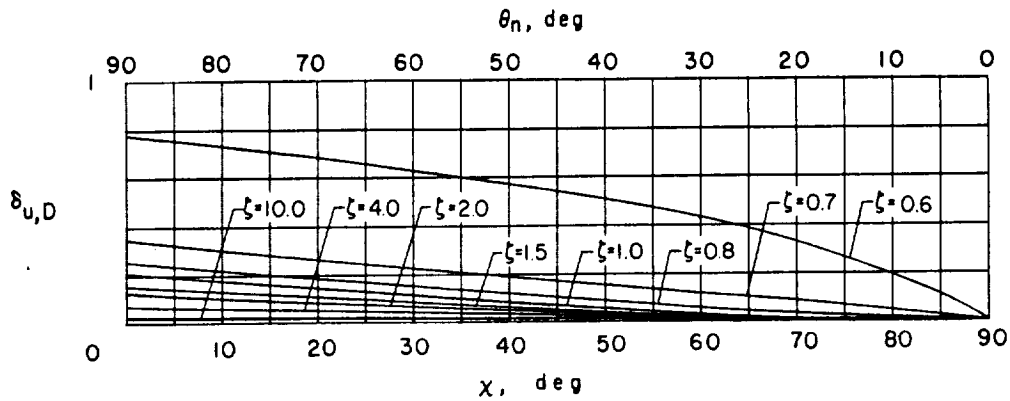


(c) $\gamma = 1.0$.

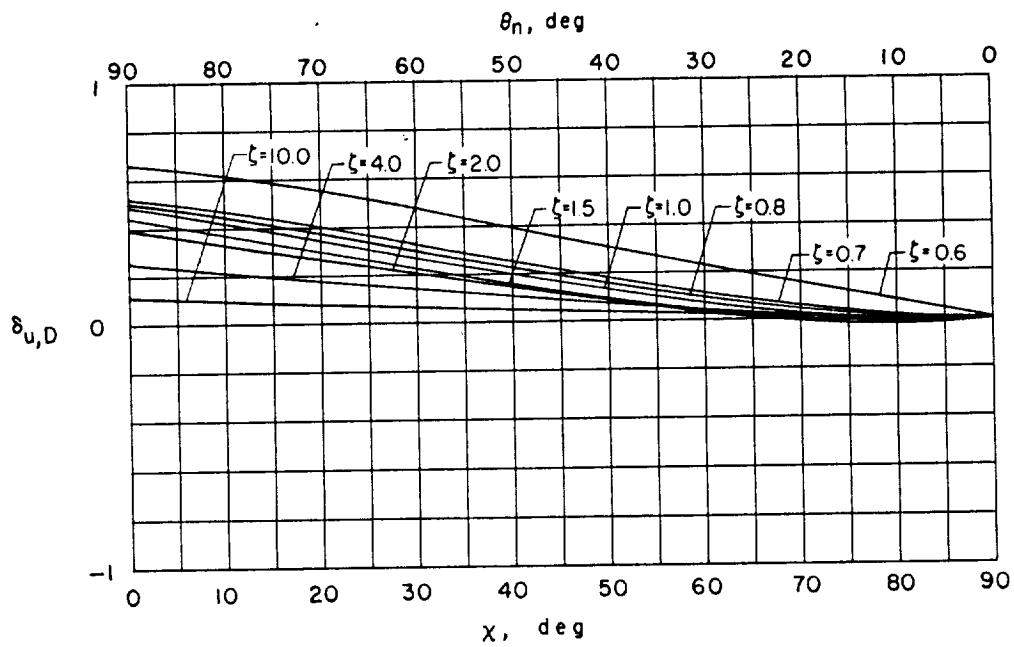


(d) $\gamma = 0.5$.

Figure 29.- Concluded.

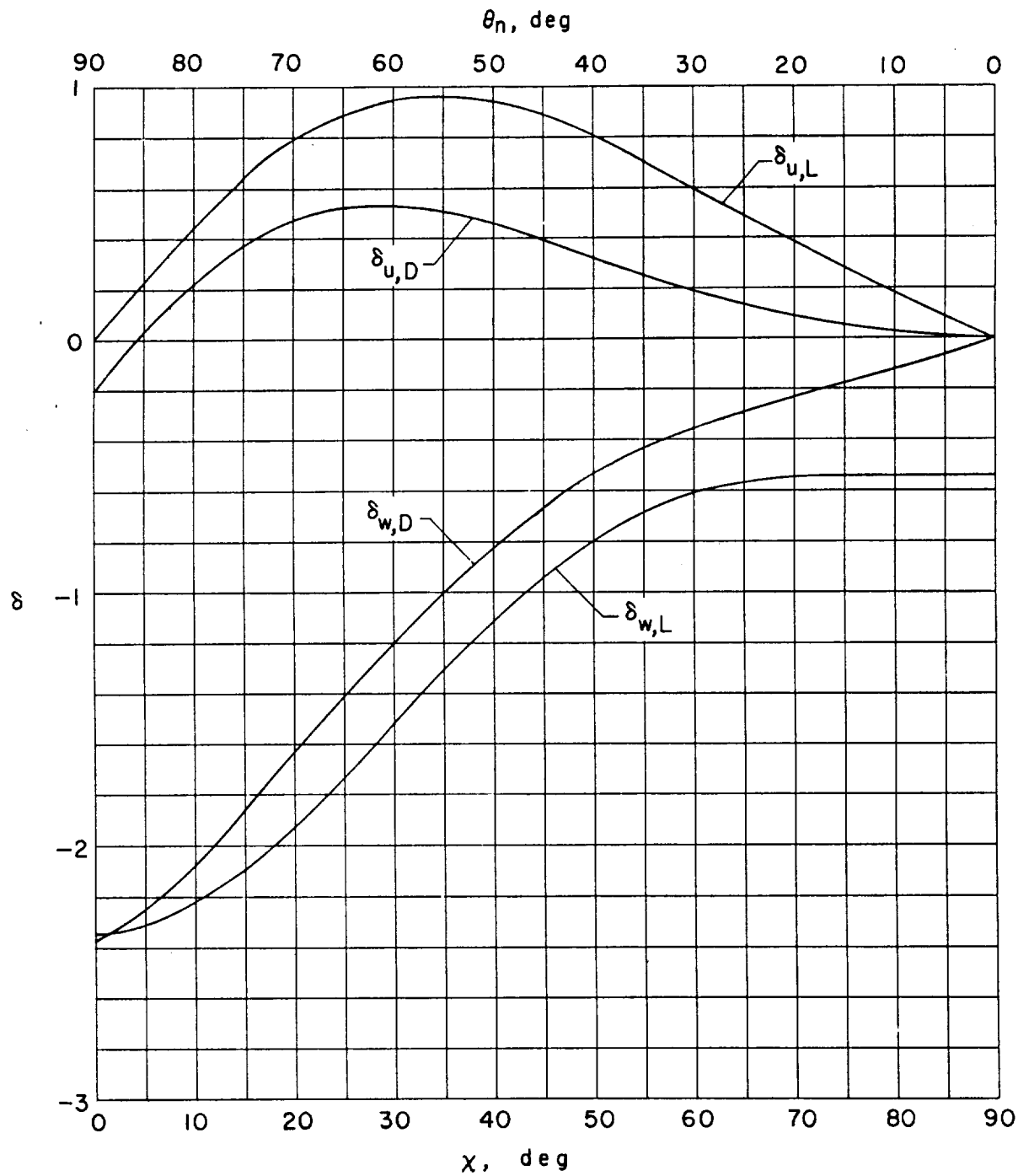


(a) $\zeta = 1.0$.

Figure 30.- Illustration of reduction of wind-tunnel interference at low speeds by above-center model mounting in closed wind tunnel. $\gamma = 2.0$; $\eta = 1.0$.

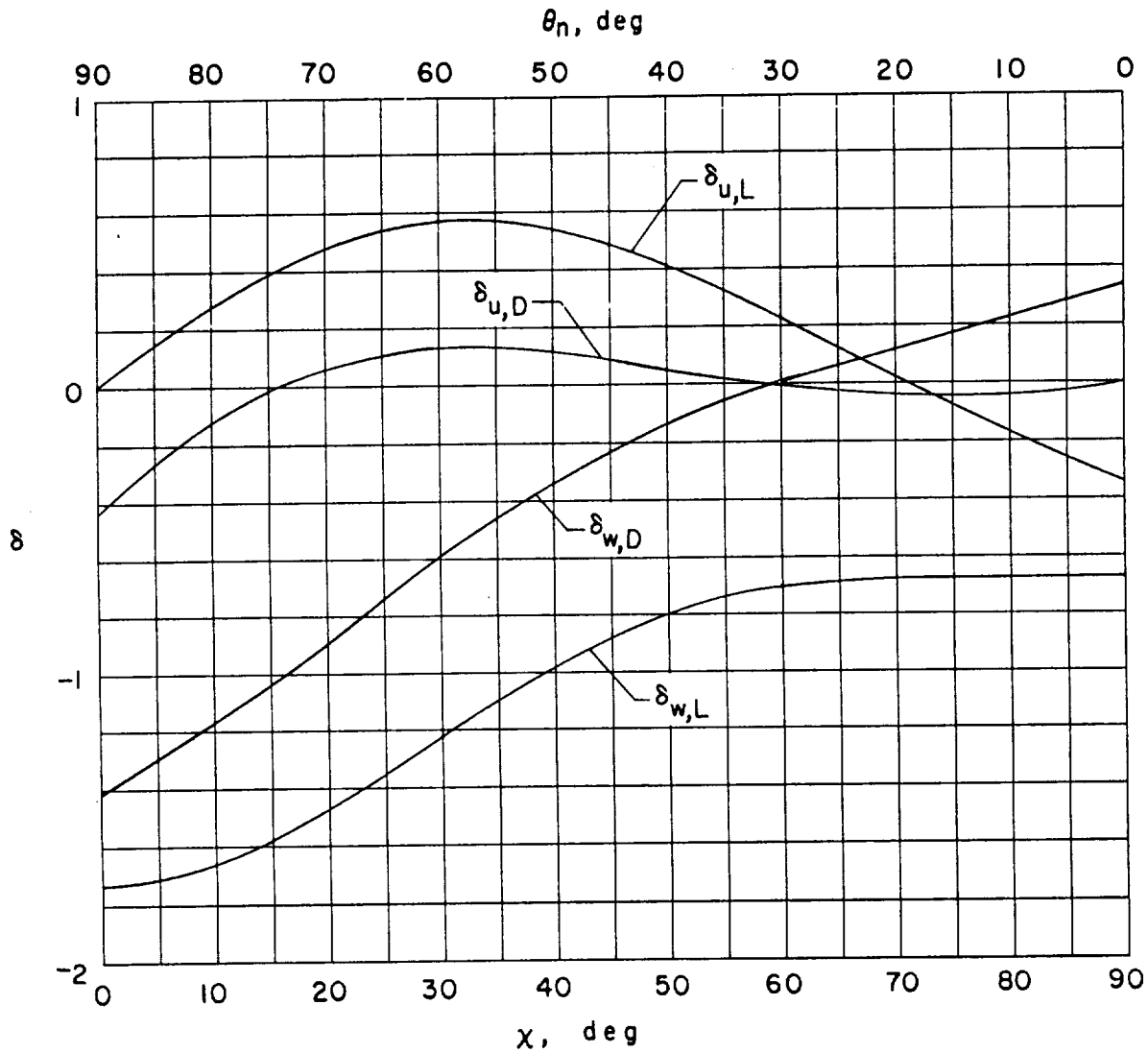


(b) $\zeta = 0.8$.

Figure 30.- Concluded.

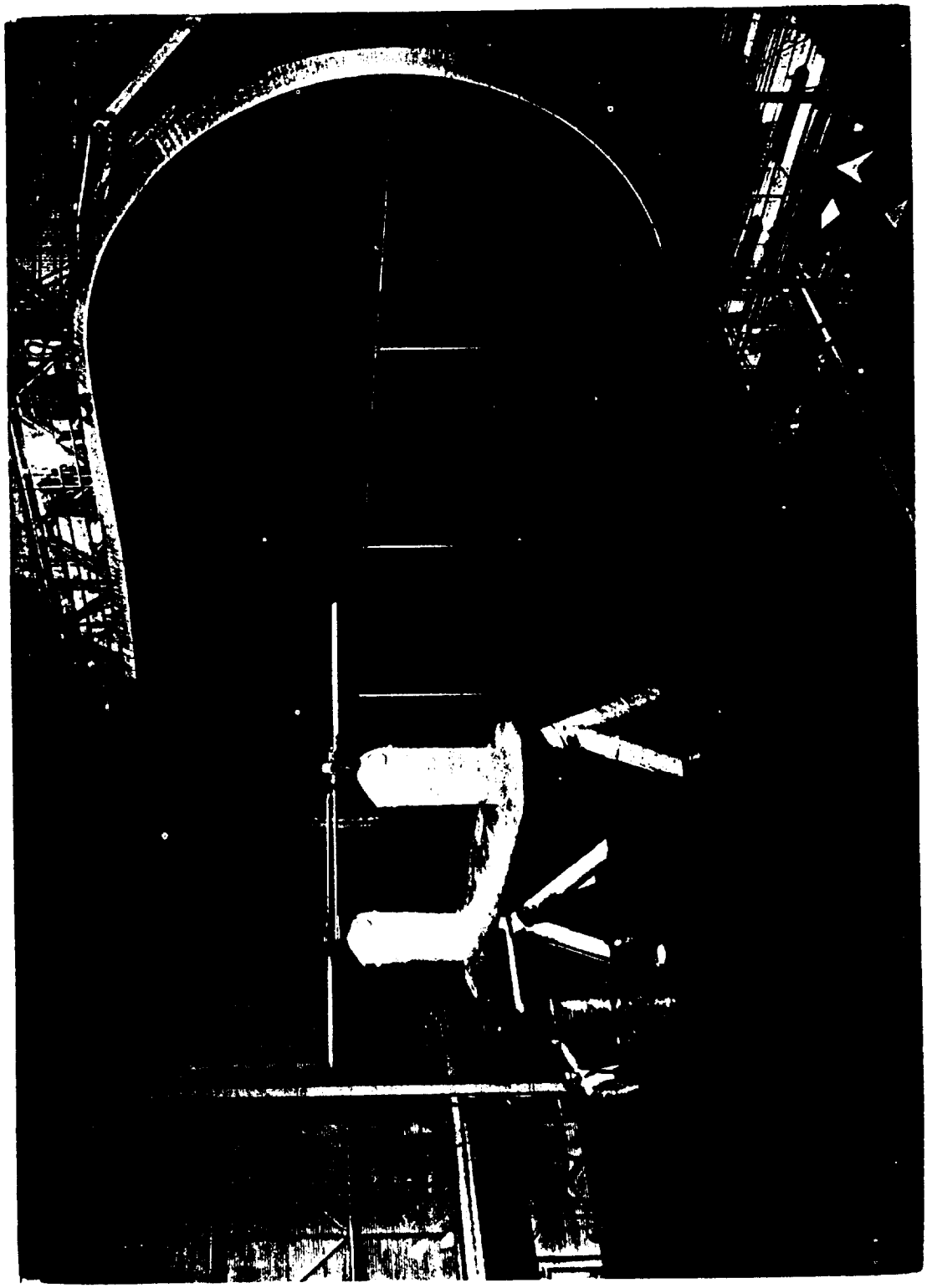

L-96046

Figure 31.- Photograph of ground-board installation in Langley full-scale tunnel. Test section is 30 feet high and 60 feet wide.

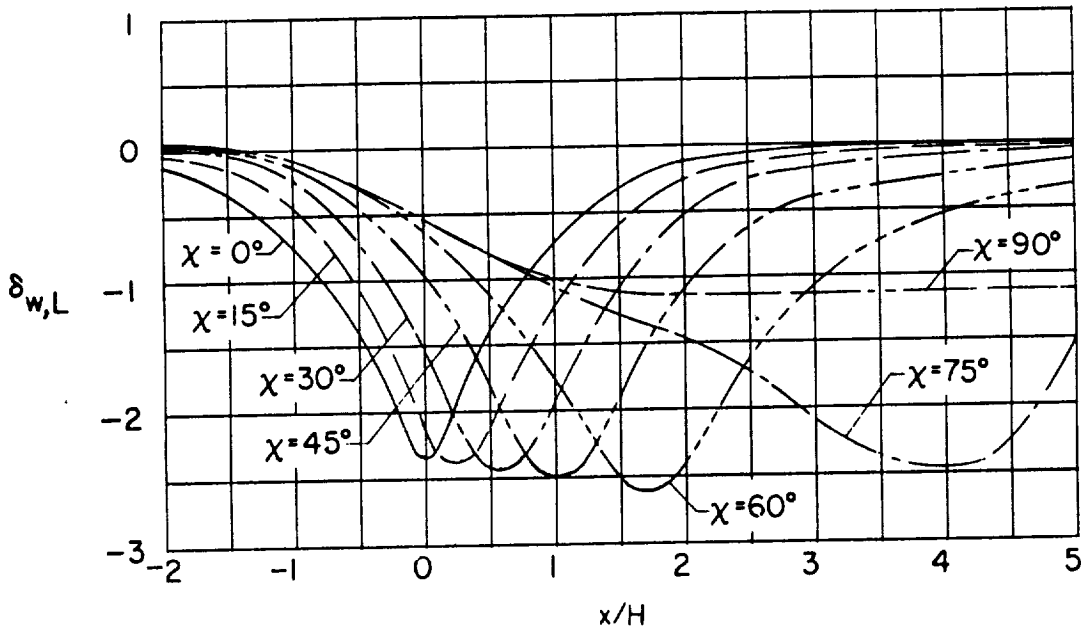


(a) $\gamma$ = 2.0.

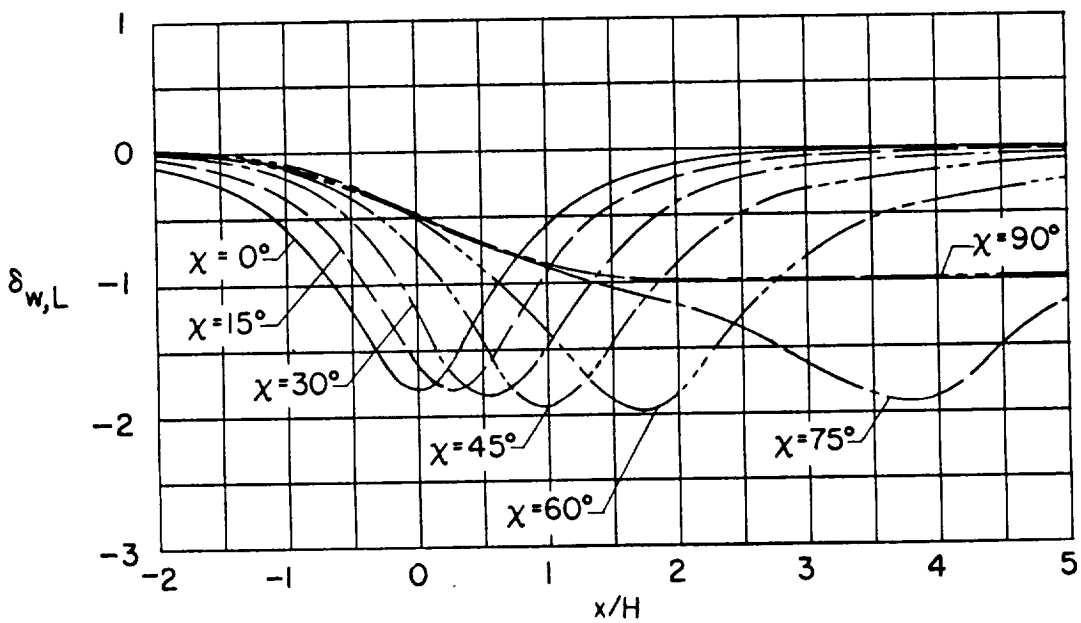


(b) $\gamma$ = 1.5.

Figure 32.- Effect of wind-tunnel width-height ratio on longitudinal distribution of vertical interference due to lift in a closed wind tunnel. $\zeta$ = 1.0; $\eta$ = 1.0.

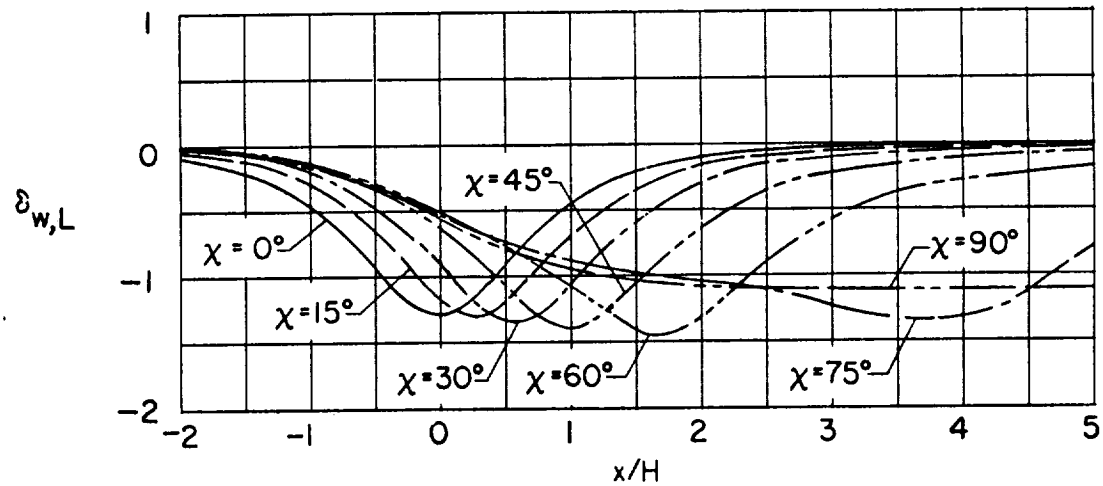


(c) $\gamma$ = 1.0.

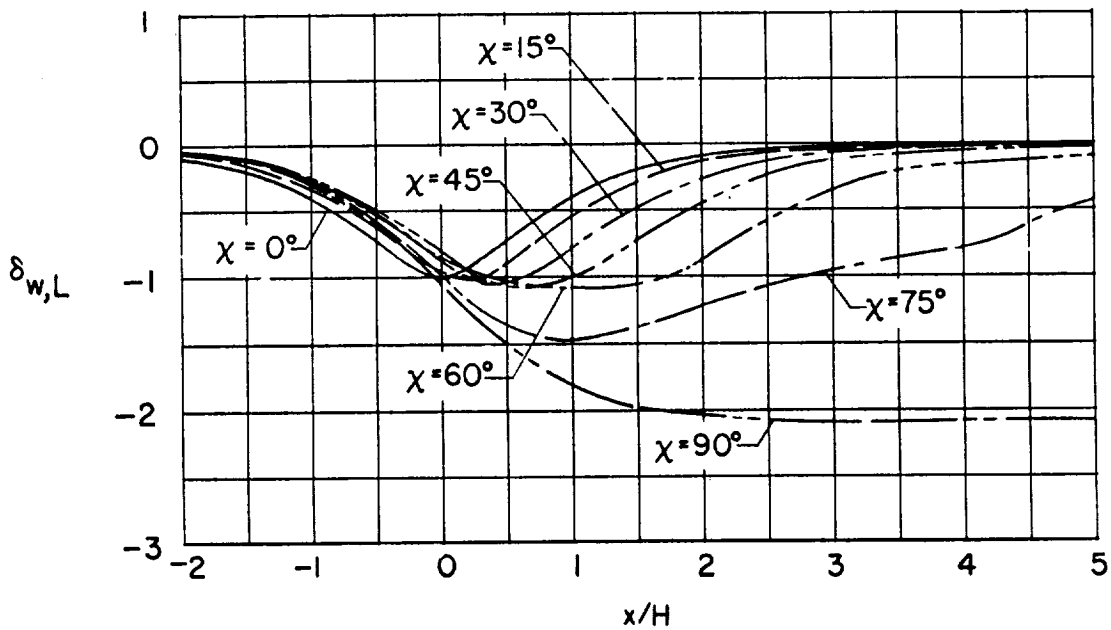


(d) $\gamma$ = 0.5.

Figure 32.- Concluded.

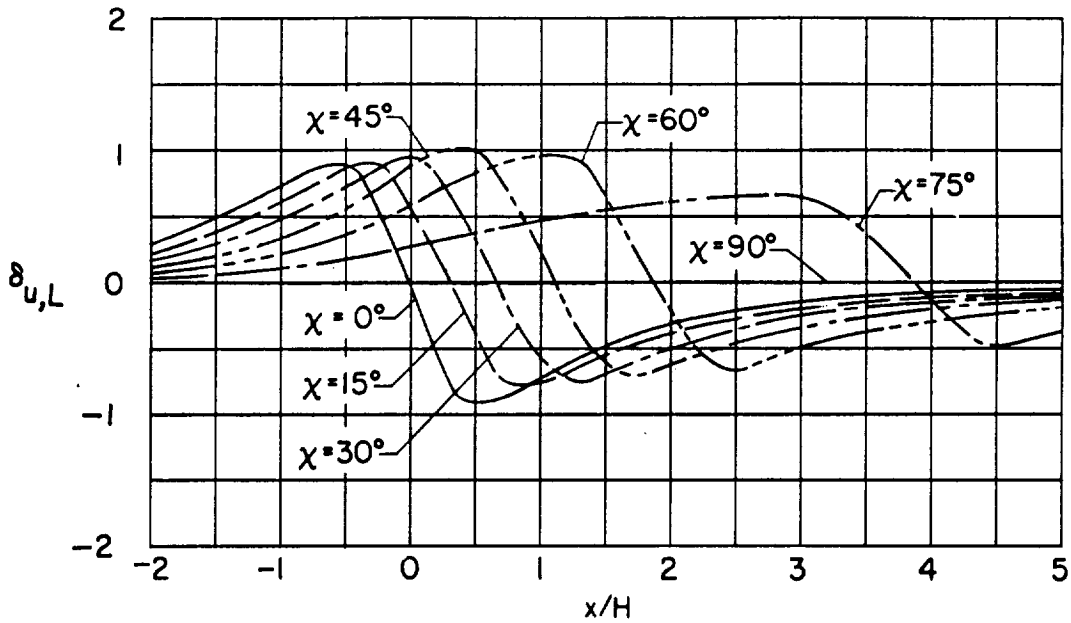


(a) $\gamma$ = 2.0.

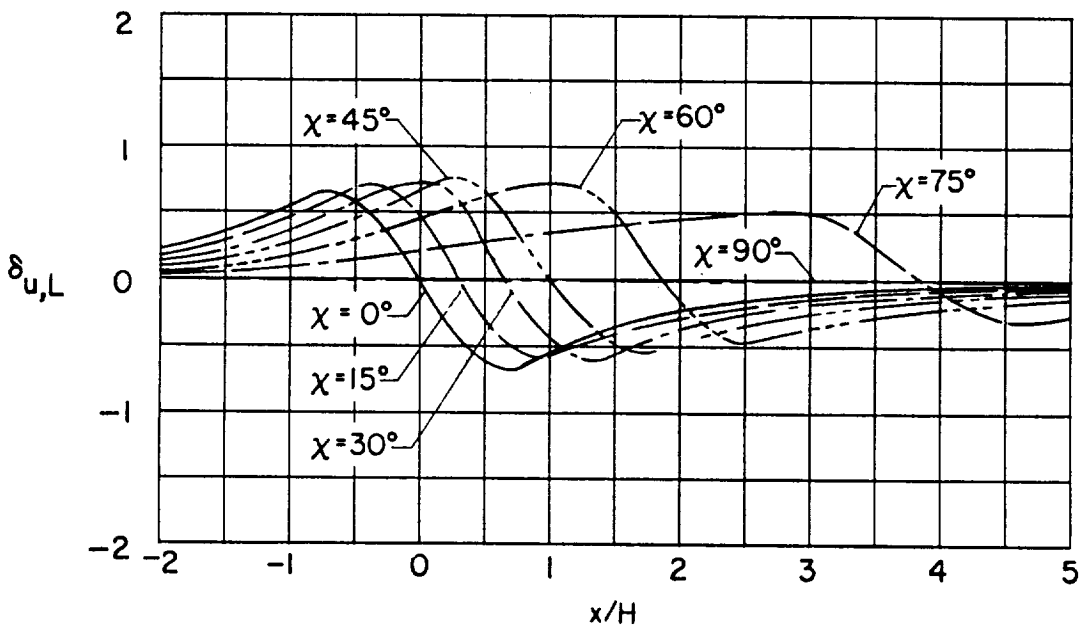


(b) $\gamma$ = 1.5.

Figure 33.- Effect of wind-tunnel width-height ratio on the longitudinal distribution of longitudinal interference due to lift in a closed wind tunnel. $\zeta$ = 1.0; $\eta$ = 1.0.

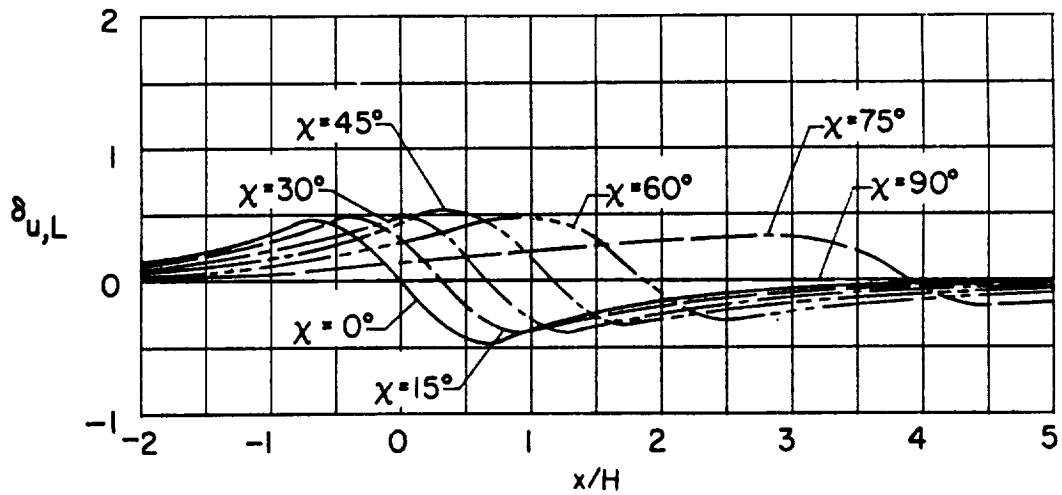


(c) $\gamma = 1.0$.

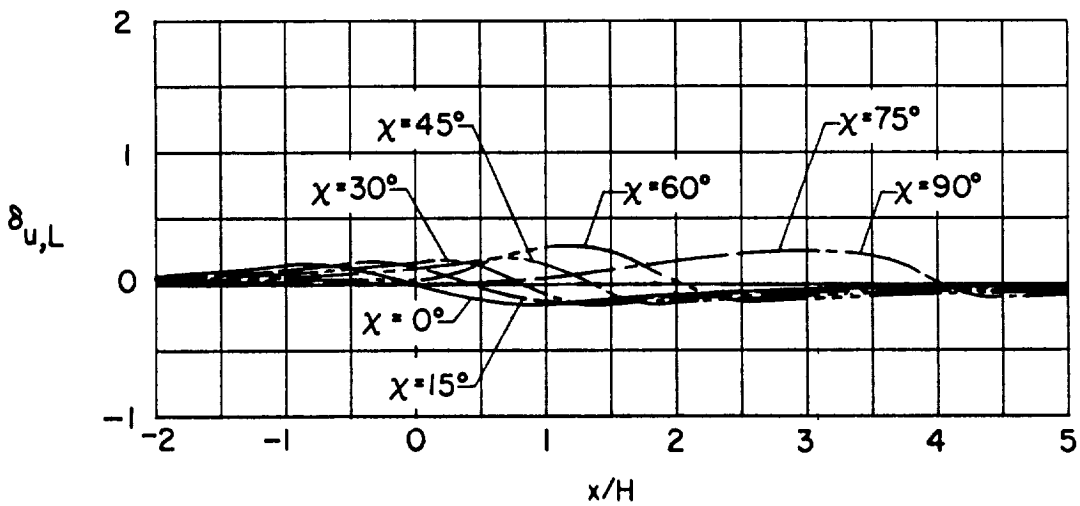


(d) $\gamma = 0.5$.

Figure 33.- Concluded.

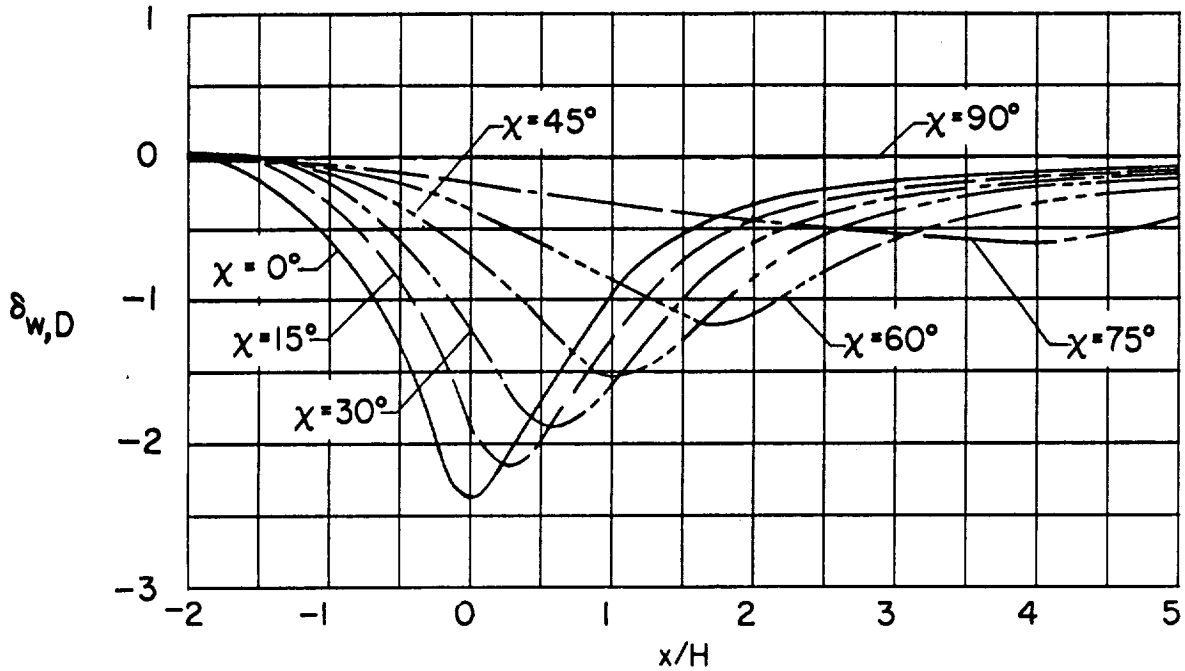


(a) $\gamma = 2.0$.

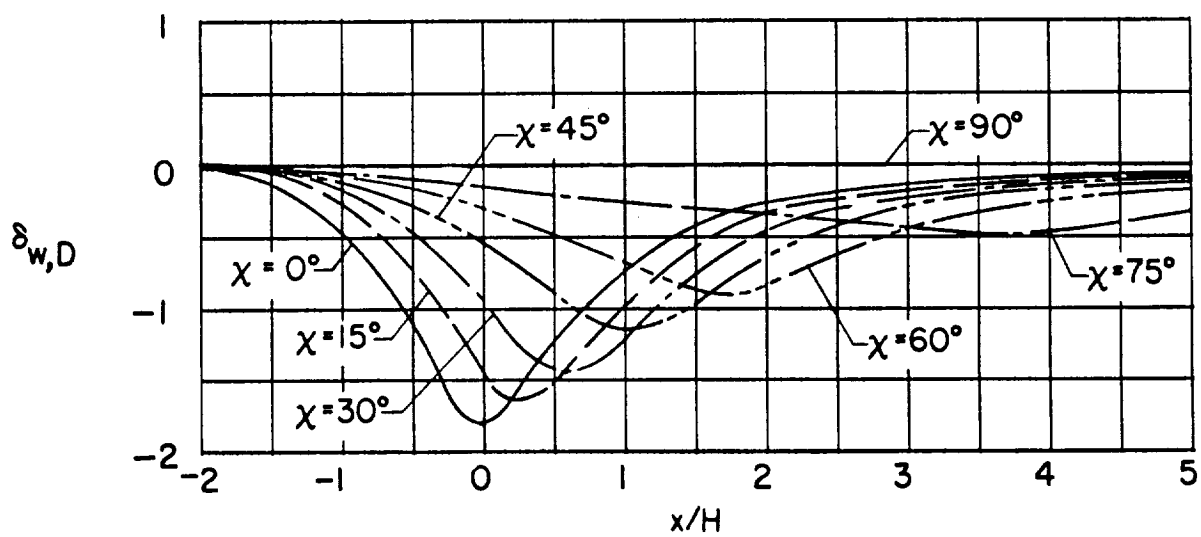


(b) $\gamma = 1.5$.

Figure 34.- Effect of wind-tunnel width-height ratio on the longitudinal distribution of vertical interference due to drag in a closed wind tunnel. $\zeta = 1.0$; $\eta = 1.0$.

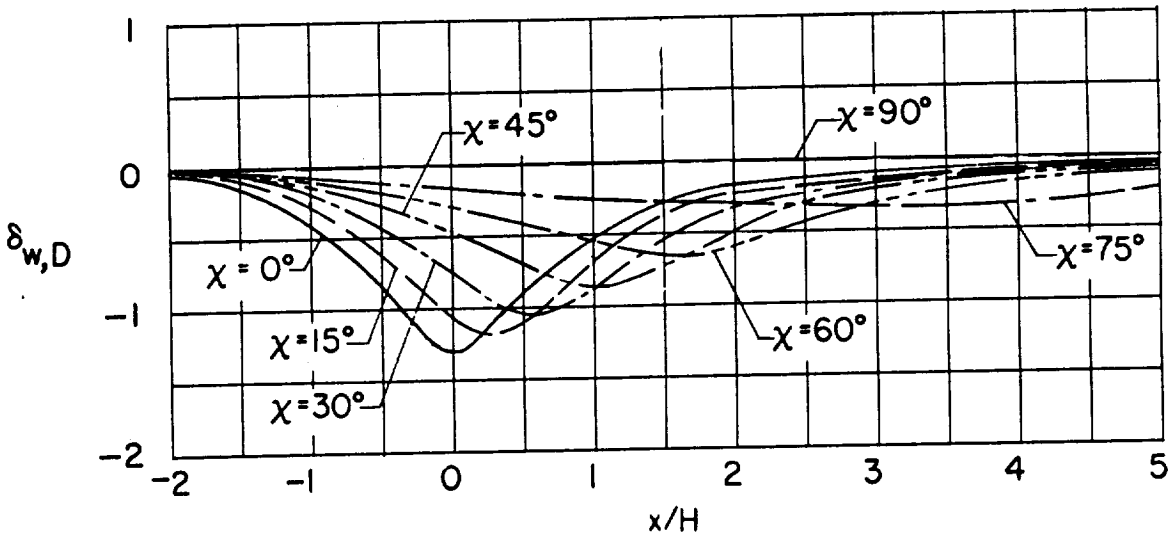


(c) $\gamma$ = 1.0.

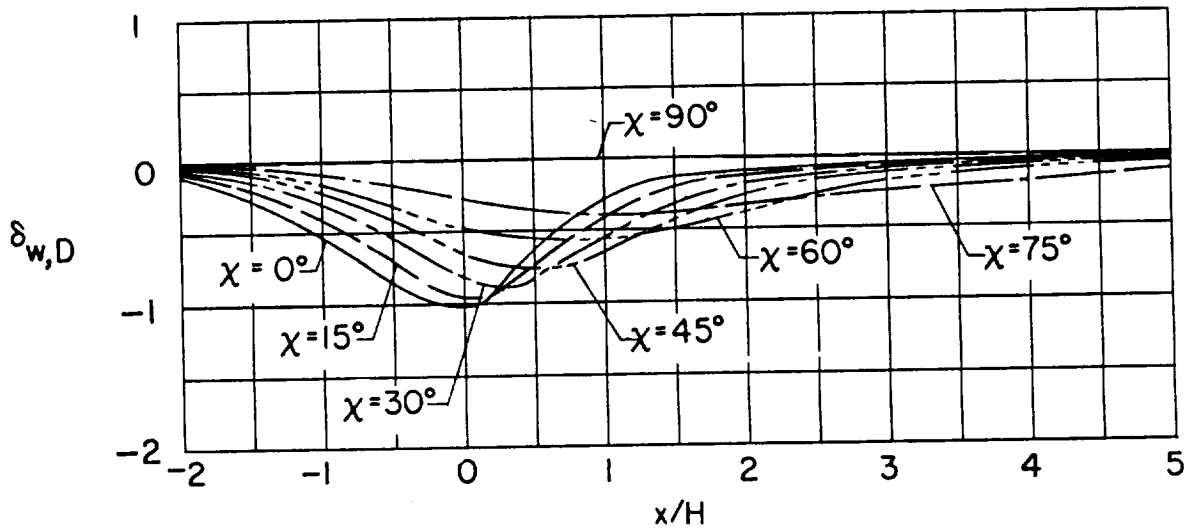


(d) $\gamma$ = 0.5.

Figure 34.- Concluded.

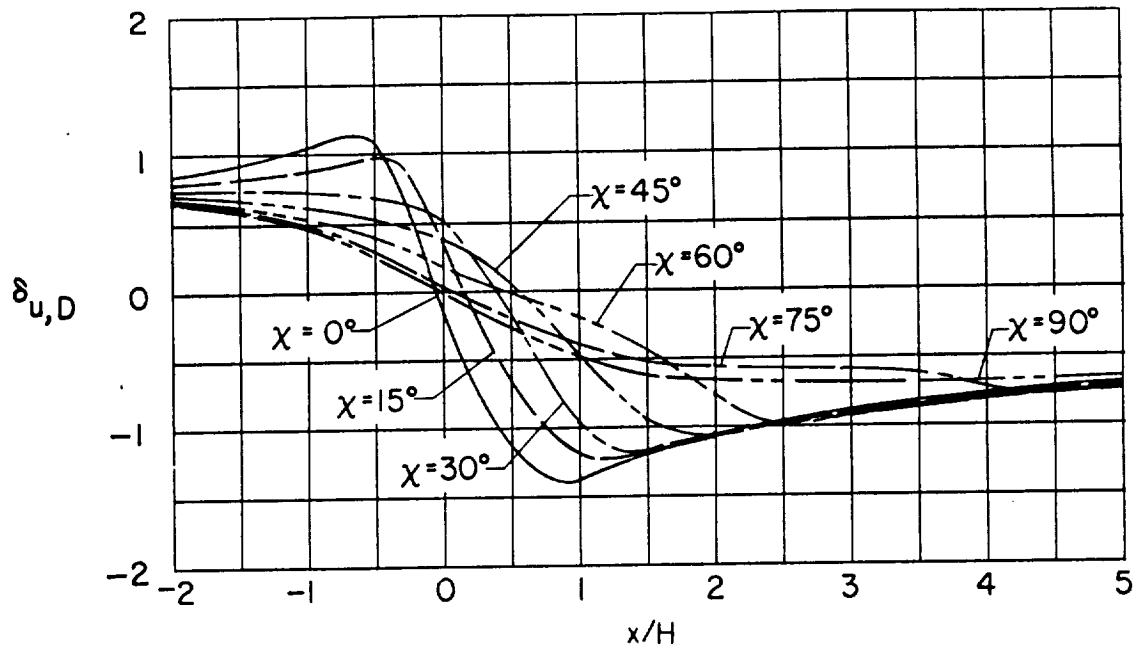


(a) $\gamma$ = 2.0.

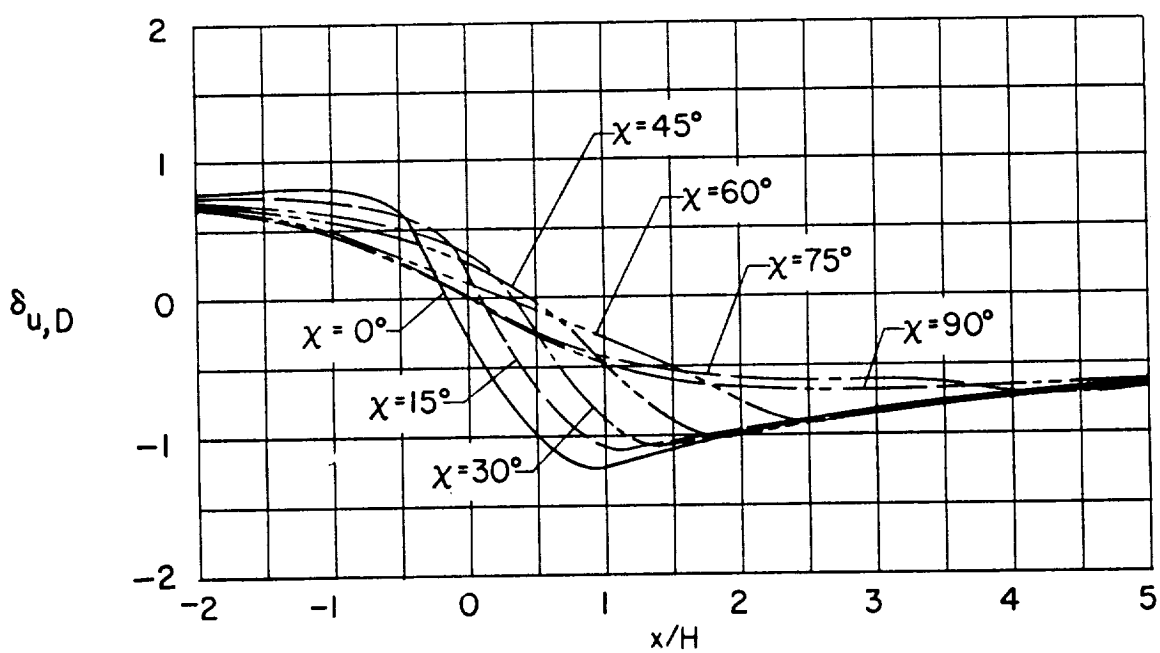


(b) $\gamma$ = 1.5.

Figure 35.- Effect of wind-tunnel width-height ratio on the longitudinal interference due to drag in a closed wind tunnel. $\zeta$ = 1.0; $\eta$ = 1.0.

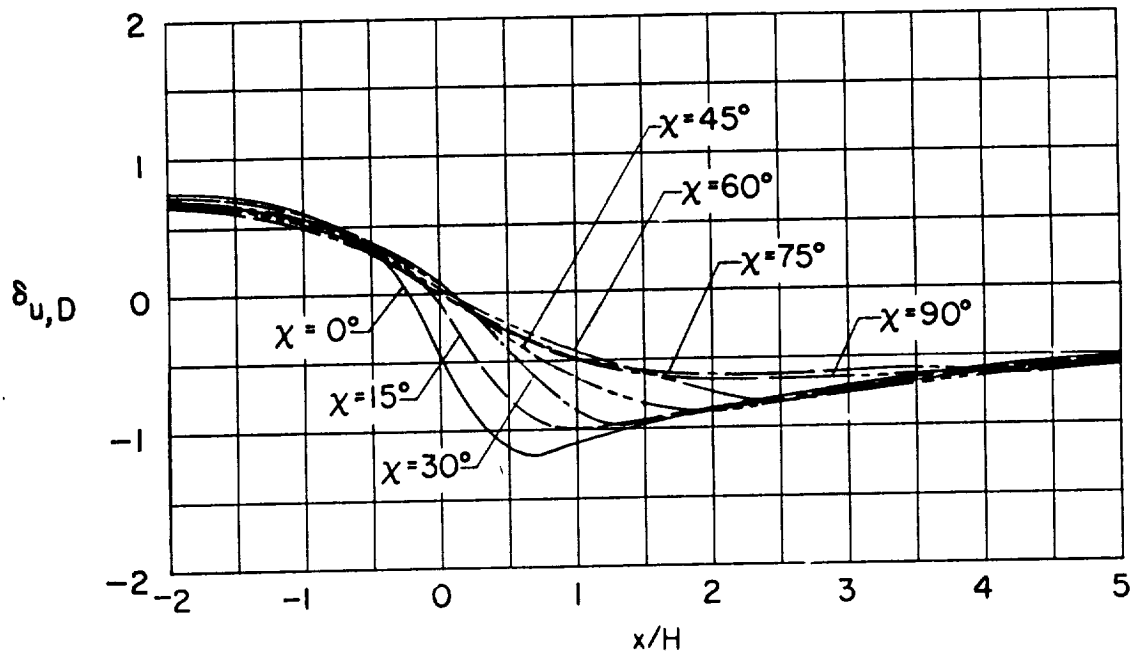


(c) $\gamma$ = 1.0.

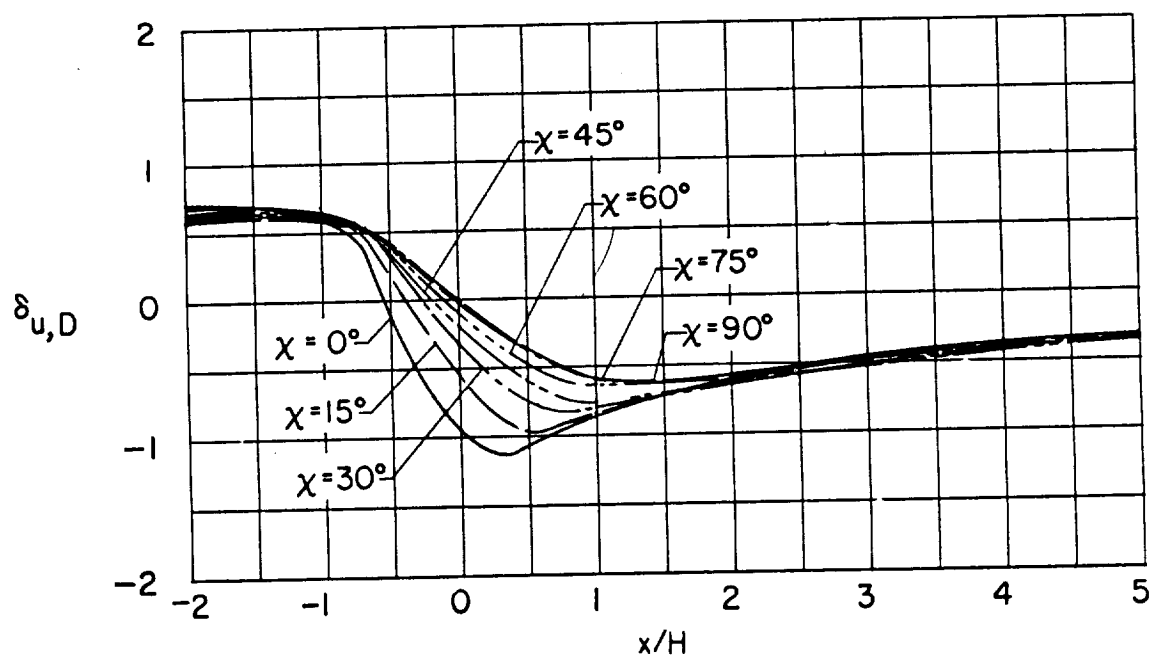


(d) $\gamma$ = 0.5.

Figure 35.- Concluded.

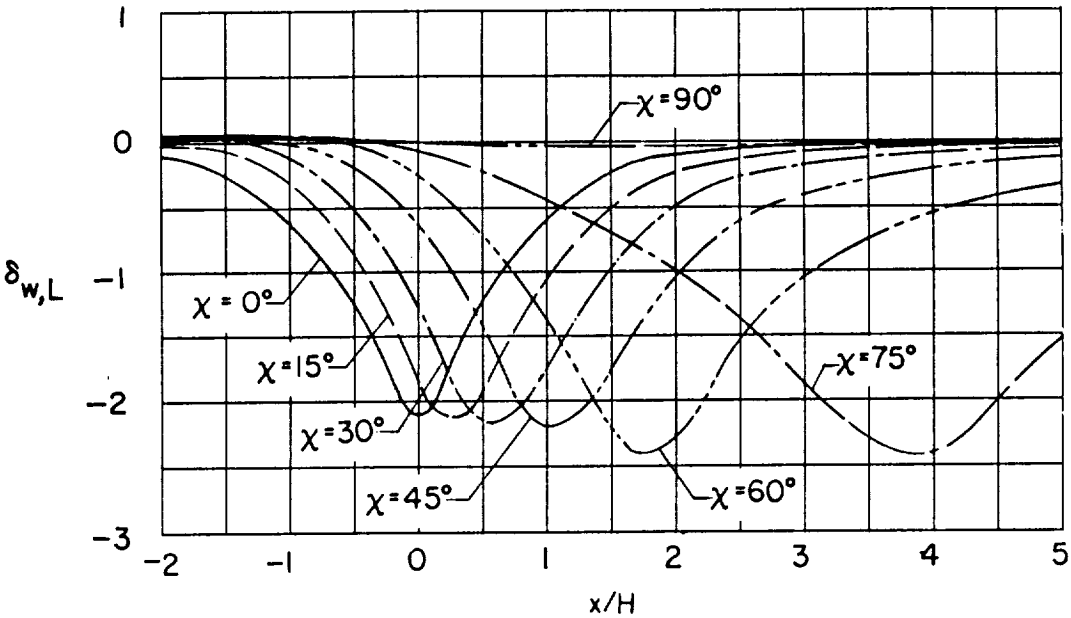


(a) $\gamma = 2.0$.

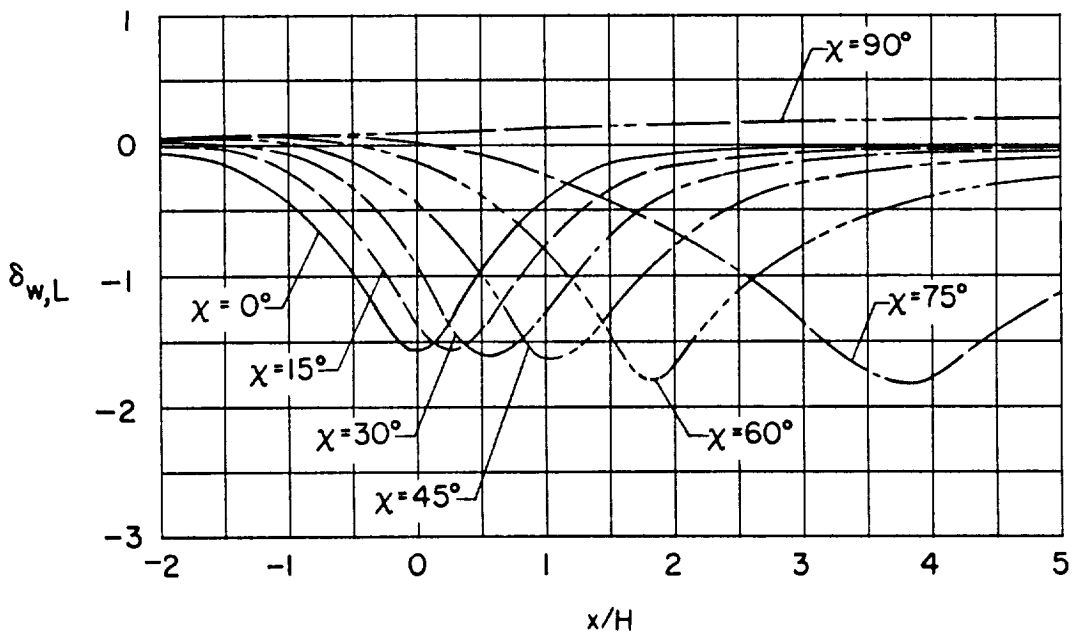


(b) $\gamma = 1.5$.

Figure 36.- Effect of wind-tunnel width-height ratio on the longitudinal distribution of vertical interference due to lift in wind tunnel closed on bottom only. $\zeta = 1.0$; $\eta = 1.0$.

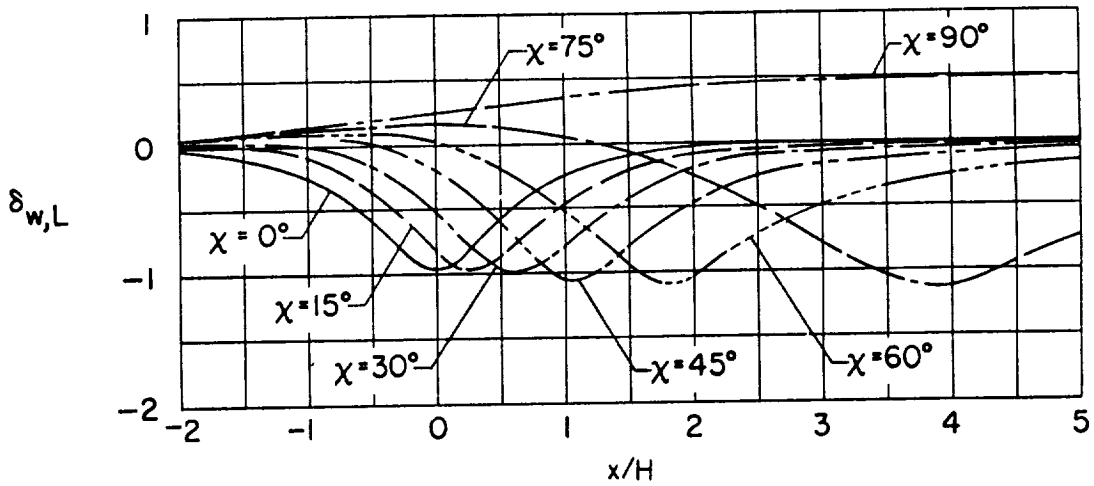


(c) $\gamma = 1.0$.

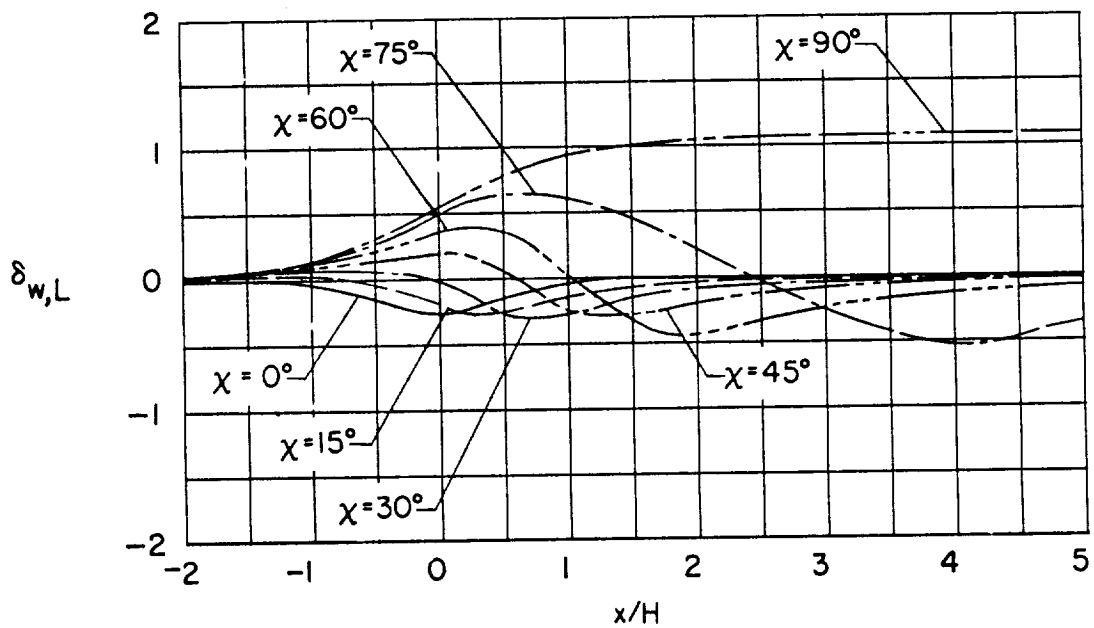


(d) $\gamma = 0.5$.

Figure 36.- Concluded.

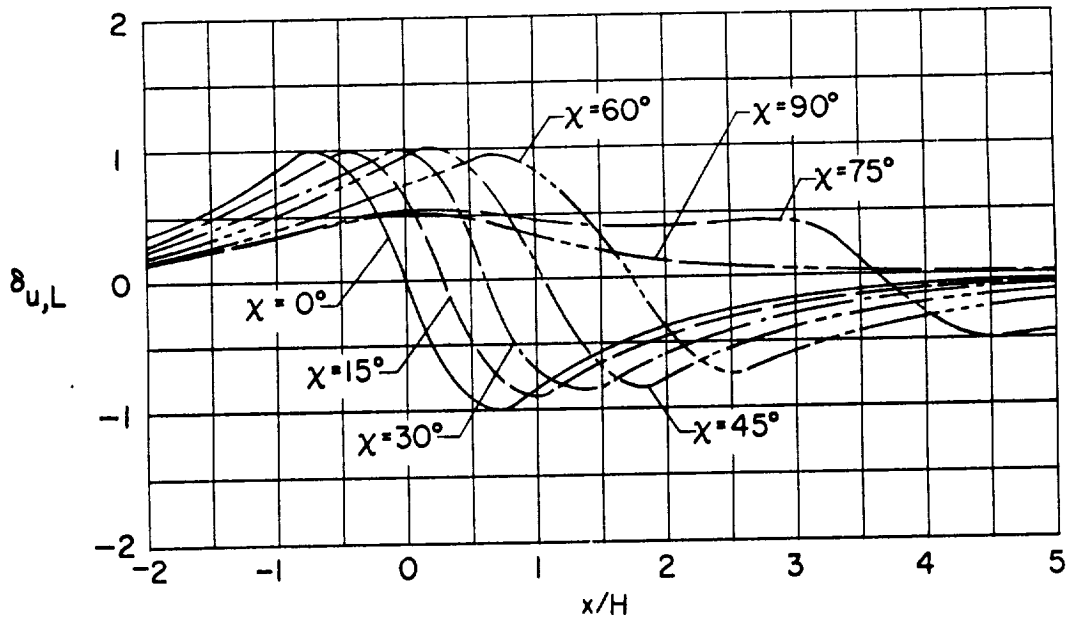


(a) $\gamma$ = 2.0.

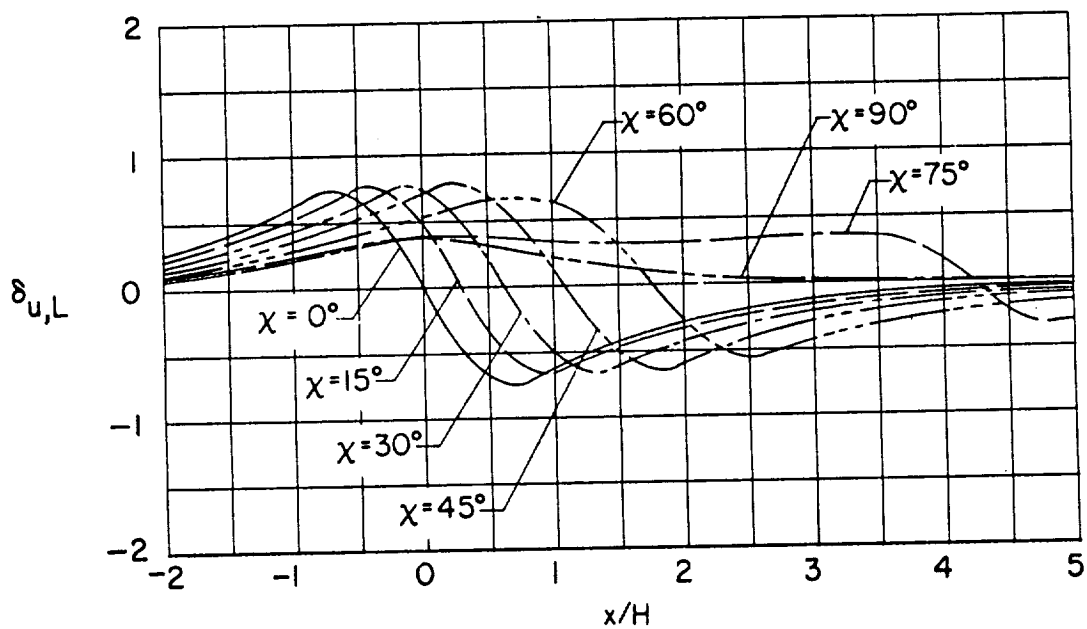


(b) $\gamma$ = 1.5.

Figure 37.- Effect of wind-tunnel width-height ratio on the longitudinal distribution of longitudinal interference due to lift in wind tunnel closed on bottom only. $\zeta$ = 1.0; $\eta$ = 1.0.

632643 O—62——9

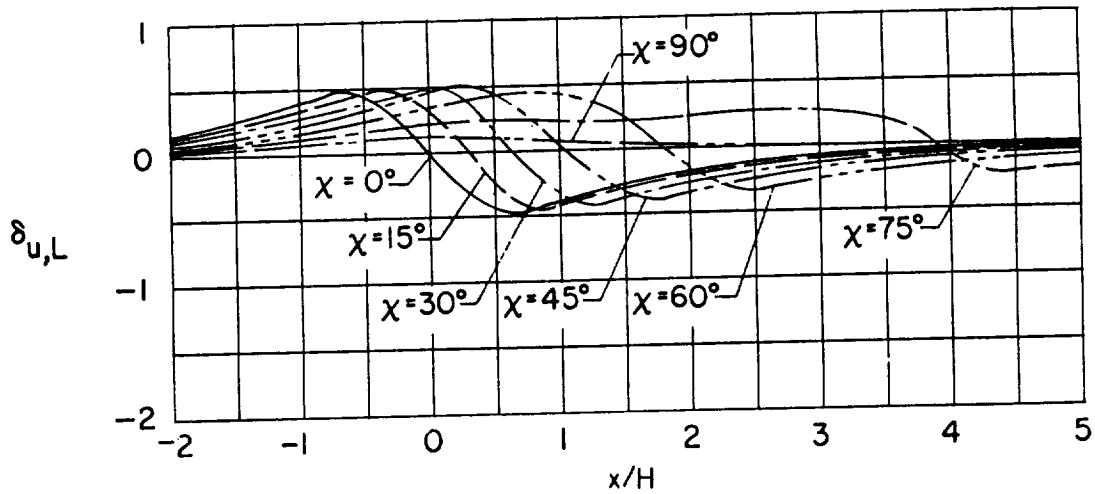


(c) $\gamma$ = 1.0.

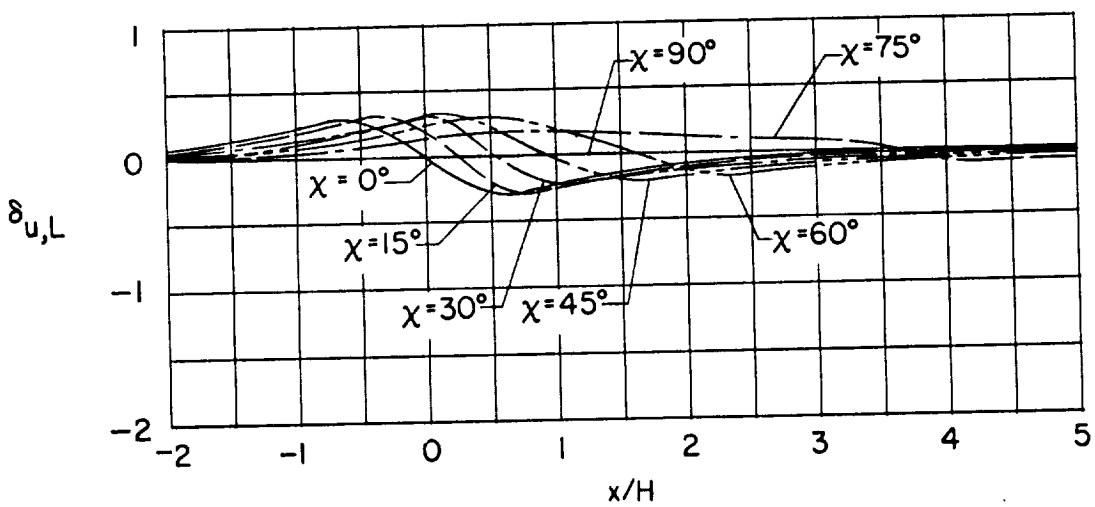


(d) $\gamma$ = 0.5.

Figure 37.- Concluded.

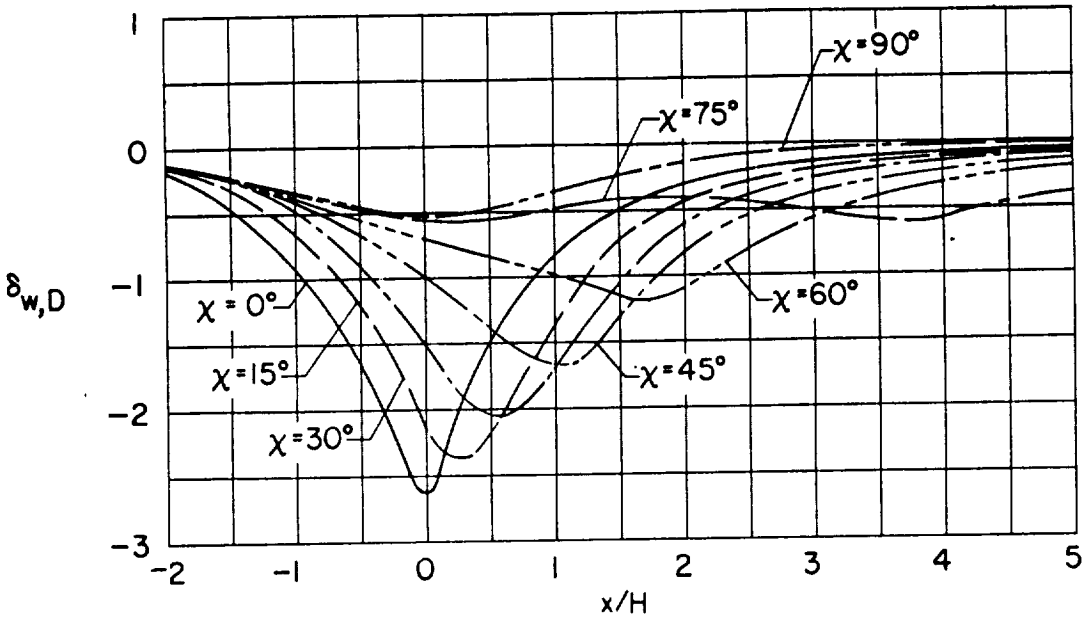


(a) $\gamma$ = 2.0.

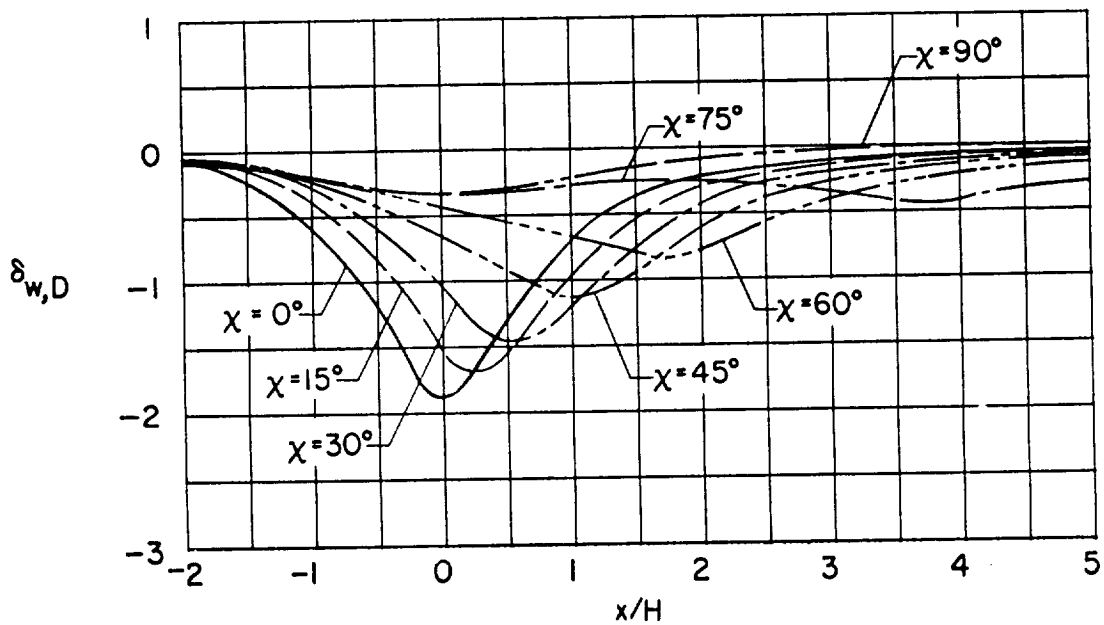


(b) $\gamma$ = 1.5.

Figure 38.- Effect of wind-tunnel width-height ratio on the longitudinal distribution of vertical interference due to drag in wind tunnel closed on bottom only. $\zeta$ = 1.0; $\eta$ = 1.0.

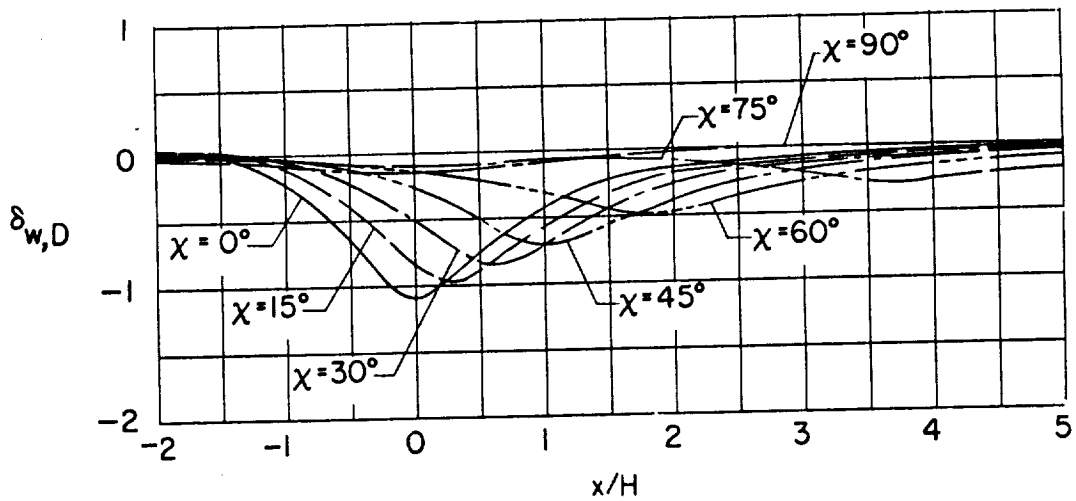


(c) $\gamma$ = 1.0.

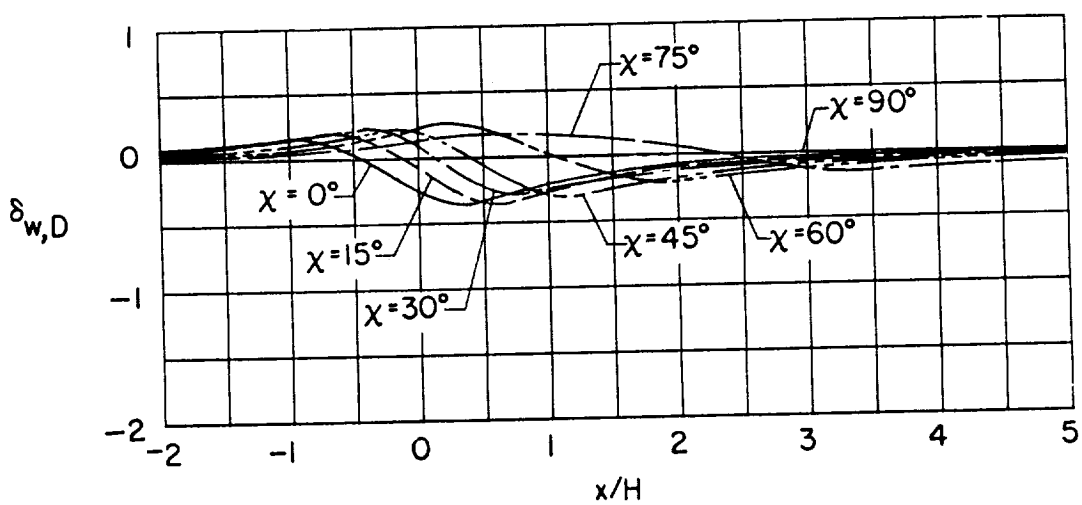


(d) $\gamma$ = 0.5.

Figure 38.- Concluded.

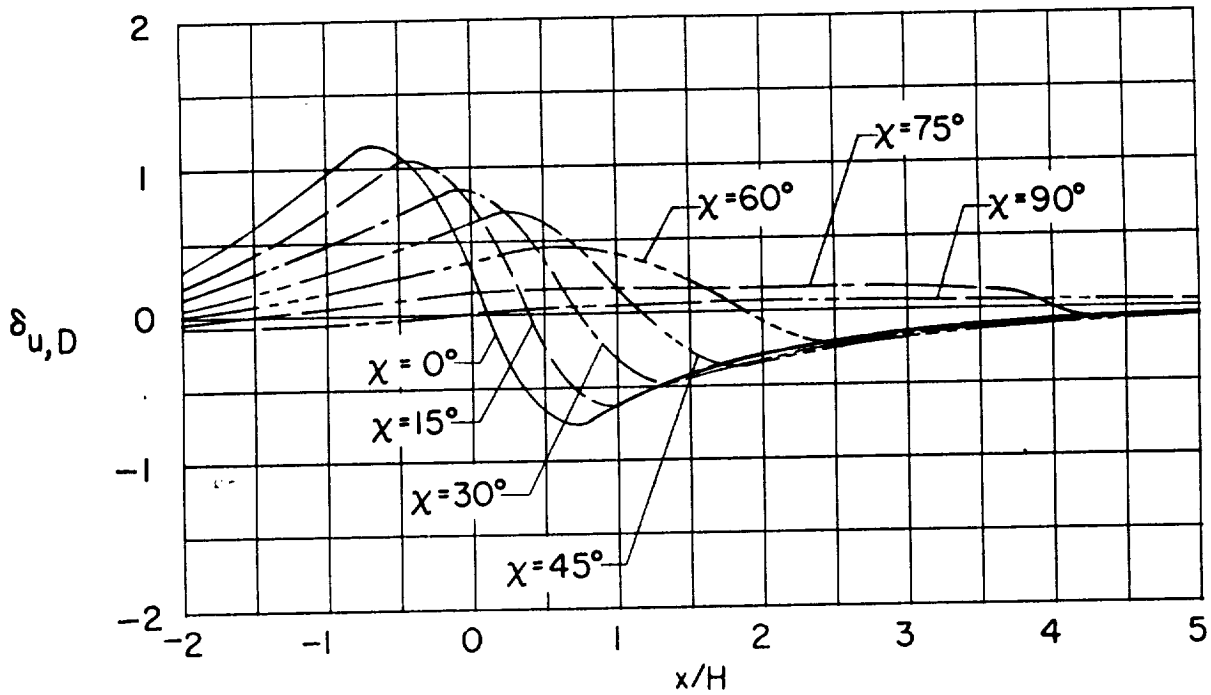


(a) $\gamma$ = 2.0.

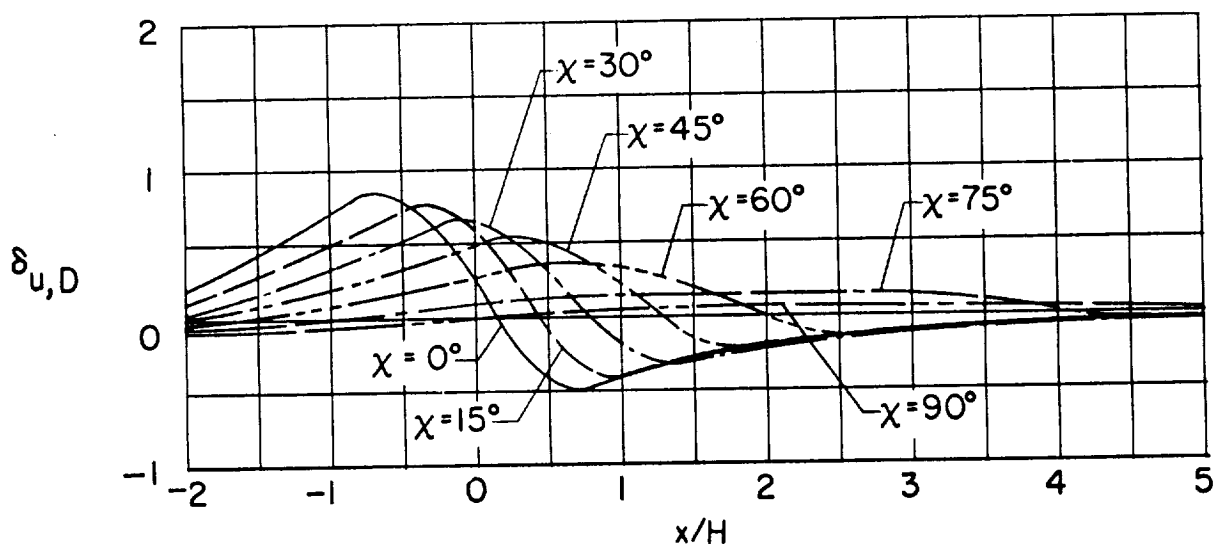


(b) $\gamma$ = 1.5.

Figure 39.- Effect of wind-tunnel width-height ratio on the longitudinal distribution of longitudinal interference due to drag in wind tunnel closed on bottom only. $\zeta$ = 1.0; $\eta$ = 1.0.

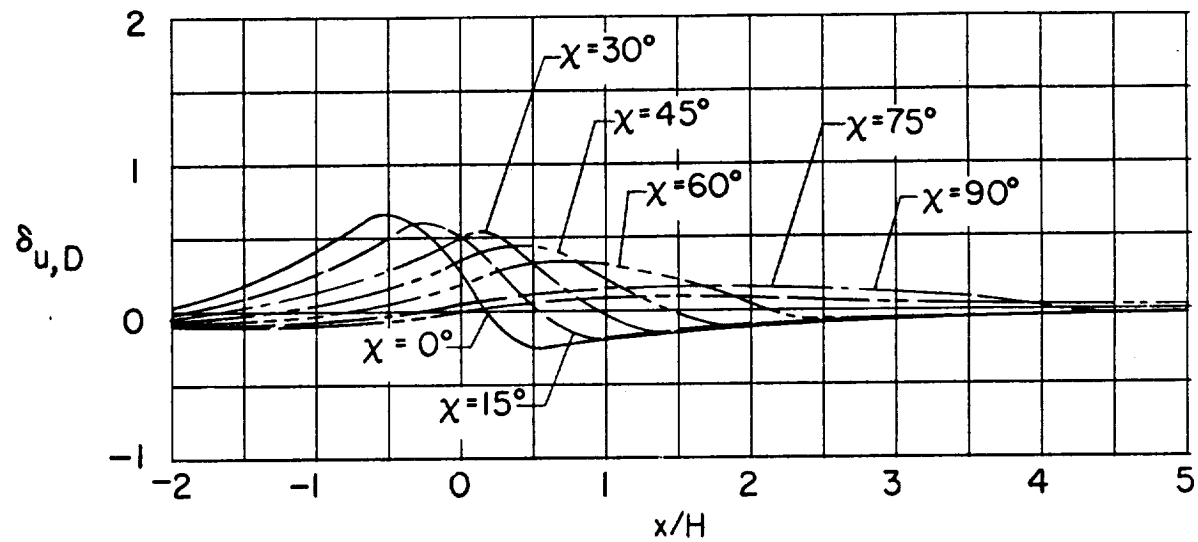


(c) $\gamma$ = 1.0.

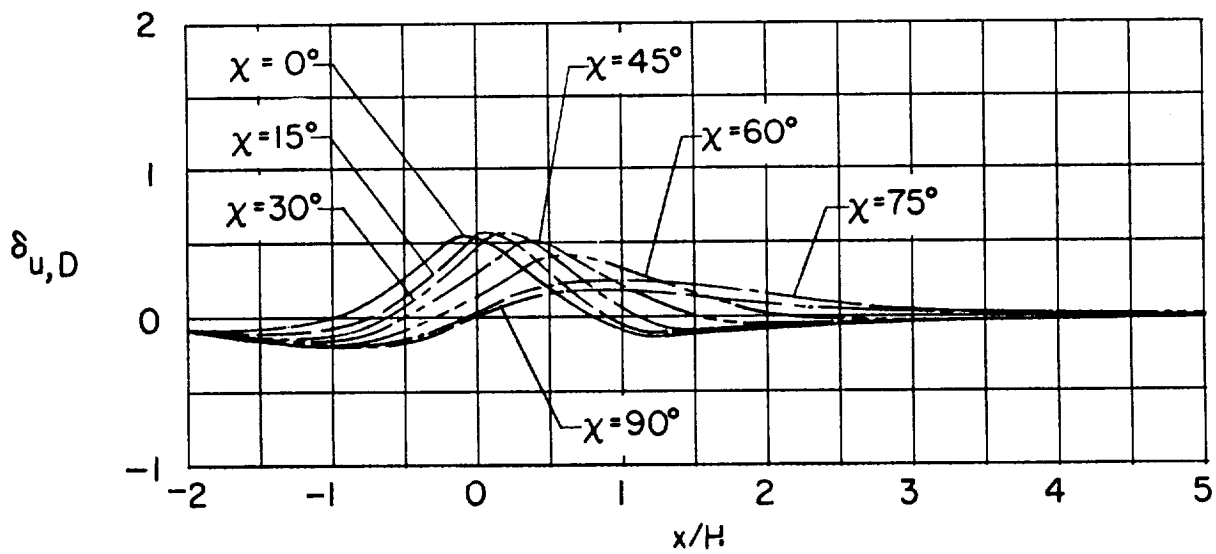


(d) $\gamma$ = 0.5.

Figure 39.- Concluded.

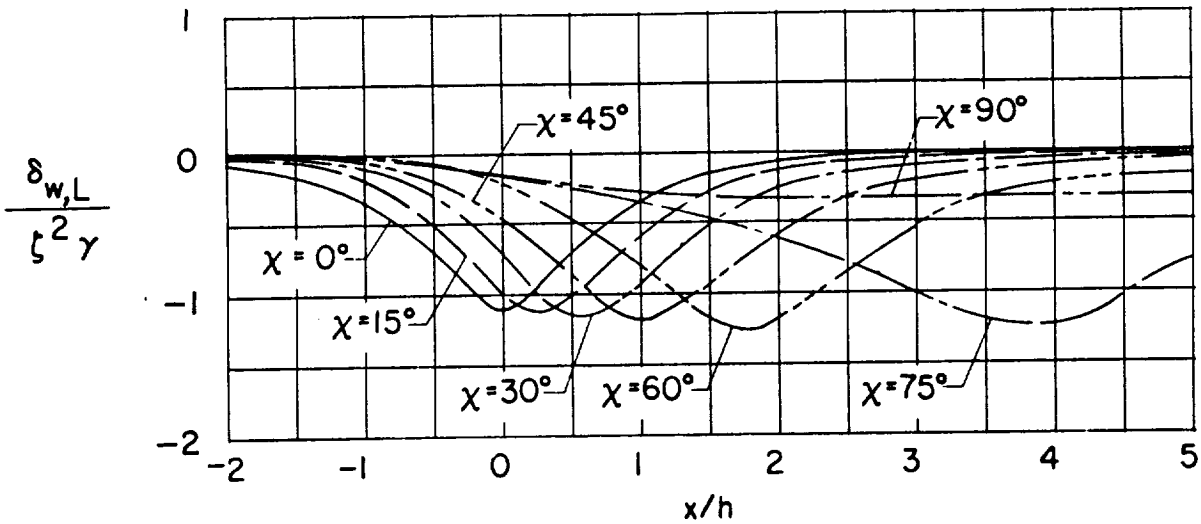


(a) Vertical interference due to lift.

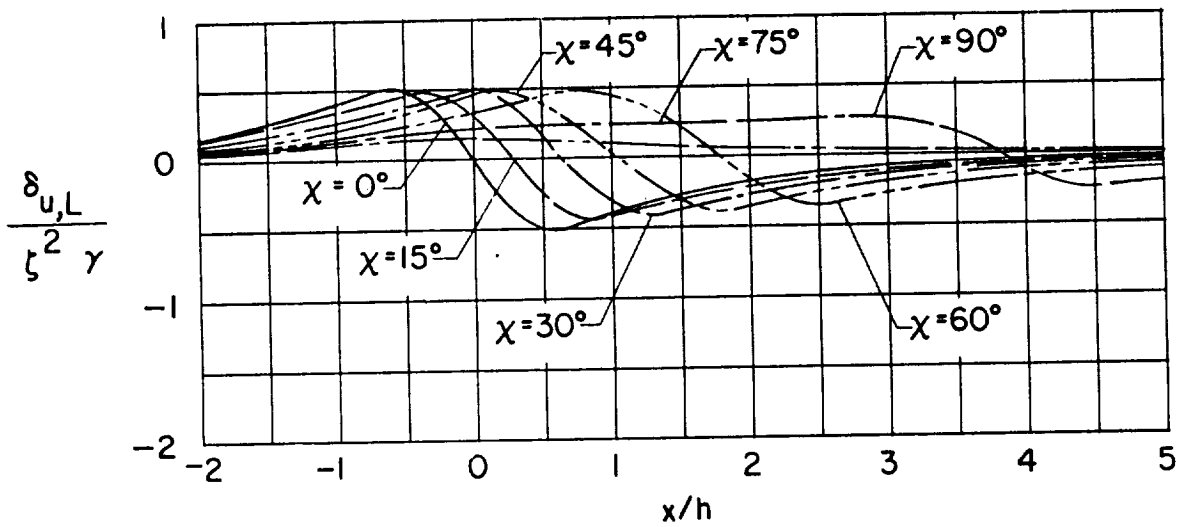


(b) Longitudinal interference due to lift.

Figure 40.- Distribution of interference factors along longitudinal axis for only the closed floor of a wind tunnel (ground effect).

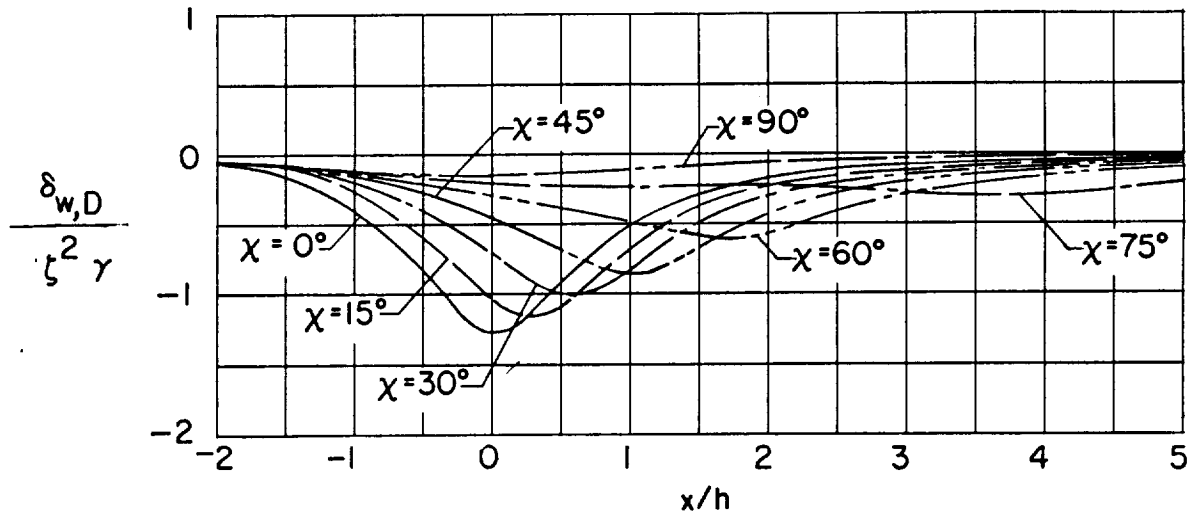


(c) Vertical interference due to drag.

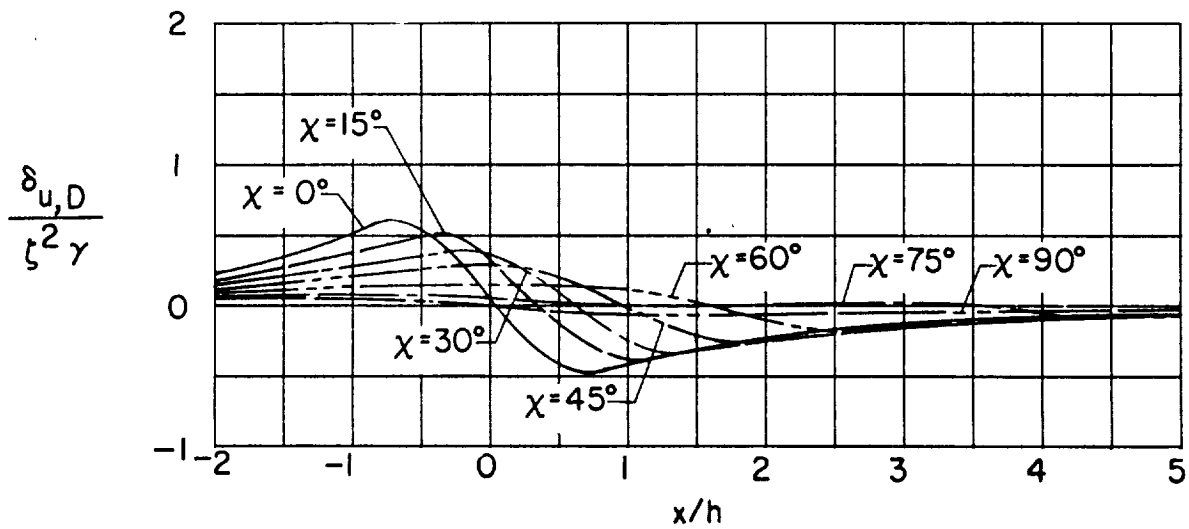


(d) Longitudinal interference due to drag.

Figure 40.- Concluded.

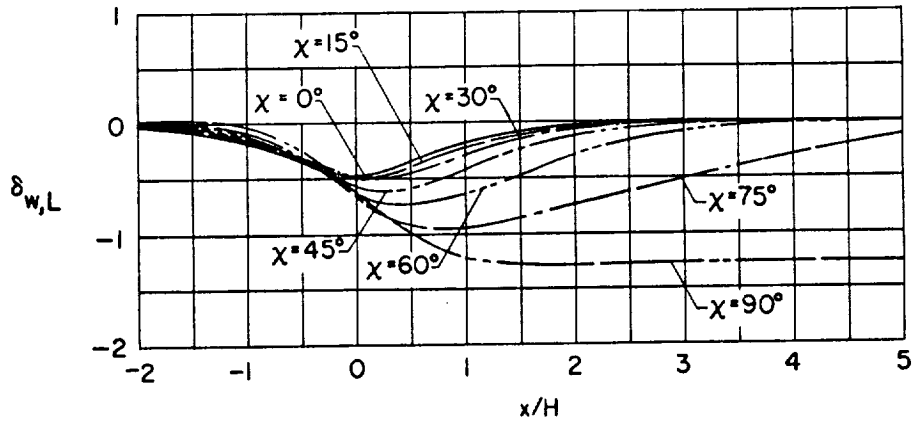


(a) $\zeta$ = 0.7.

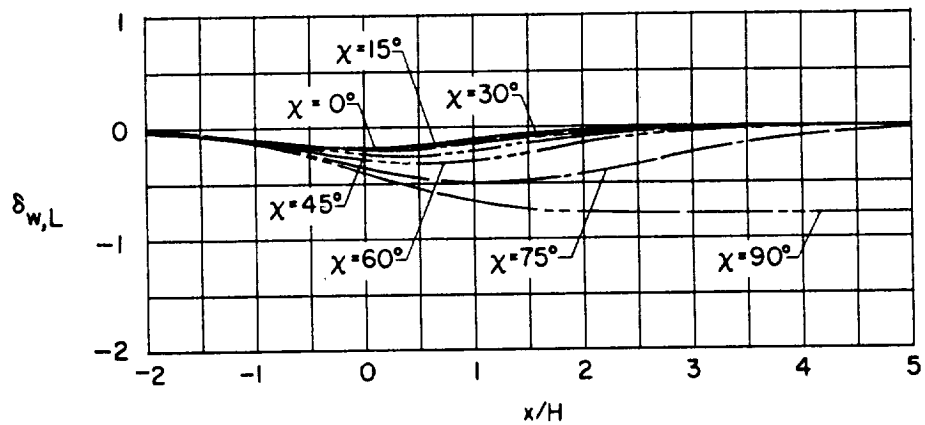


(b) $\zeta$ = 1.0.

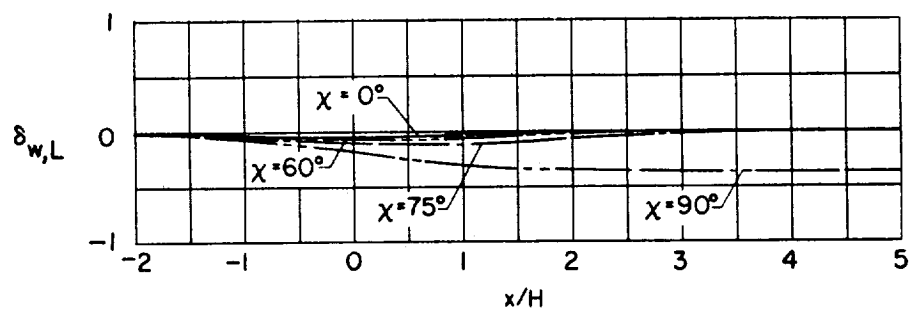


(c) $\zeta$ = 2.0.

Figure 41.- Effect of vertical location of model on the longitudinal distribution of vertical interference due to lift for correcting from a closed wind tunnel to ground effect. $\gamma$ = 1.0; $\eta$ = 1.0.

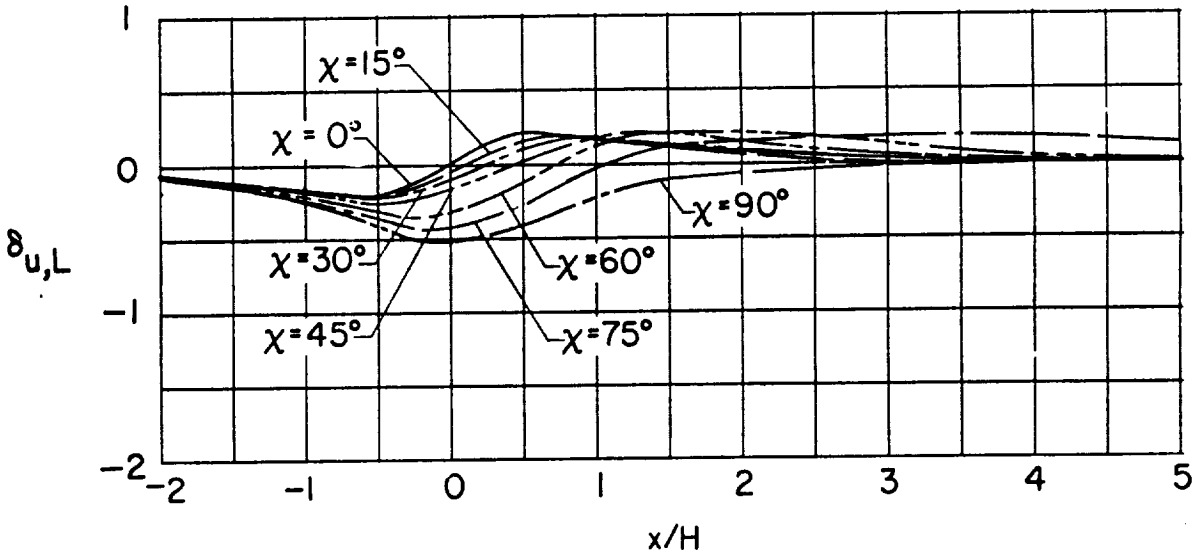


(a) $\zeta$ = 0.7.

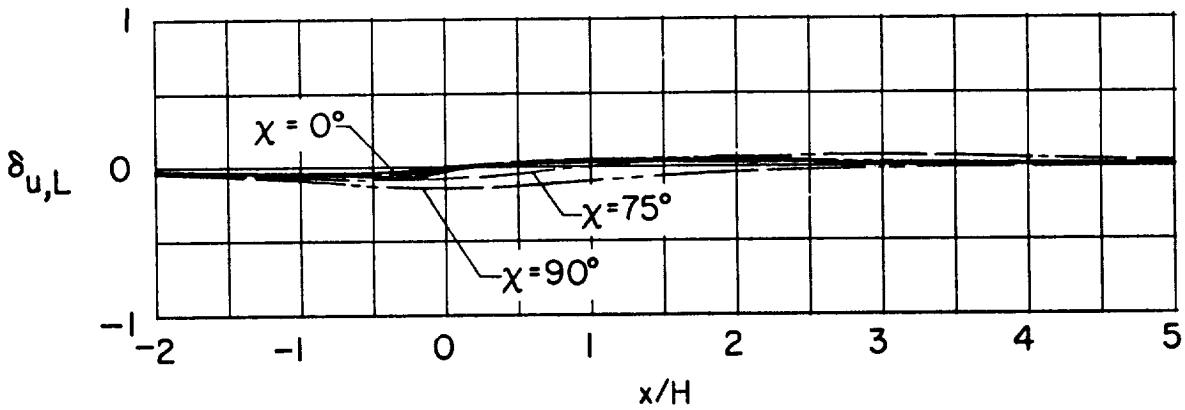


(b) $\zeta$ = 1.0.

Figure 42.- Effect of vertical location of model on the longitudinal distribution of longitudinal interference due to lift for correcting from a closed wind tunnel to ground effect. $\gamma$ = 1.0; $\eta$ = 1.0.

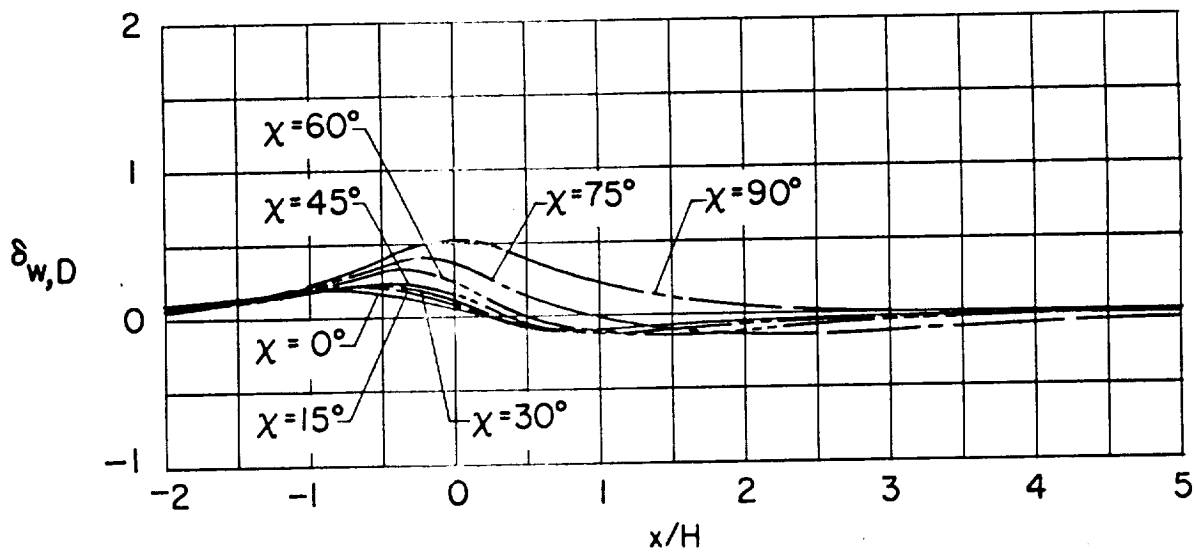


(a) $\zeta = 0.7$.

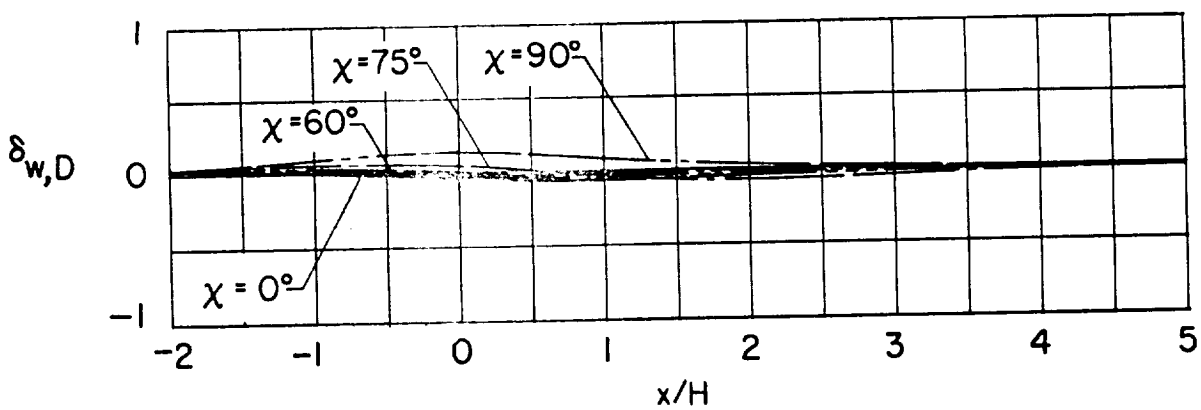


(b) $\zeta = 1.0$.

Figure 43.- Effect of vertical location of model on the longitudinal distribution of vertical interference due to drag for correcting from a closed wind tunnel to ground effect. $\gamma = 1.0$; $\eta = 1.0$.

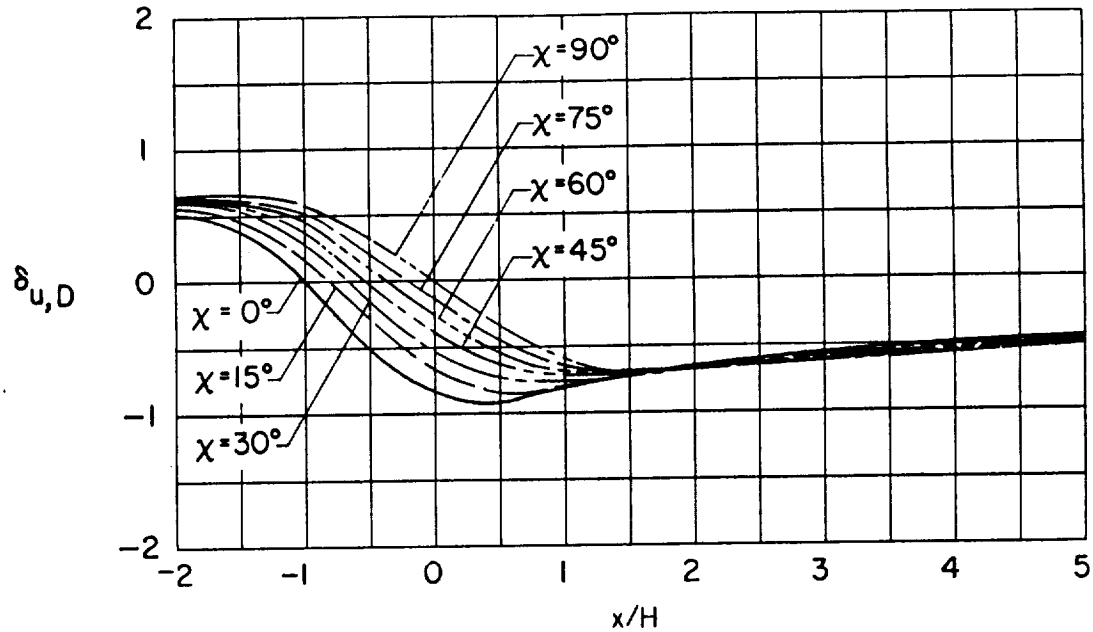


(a) $\zeta = 0.7$.

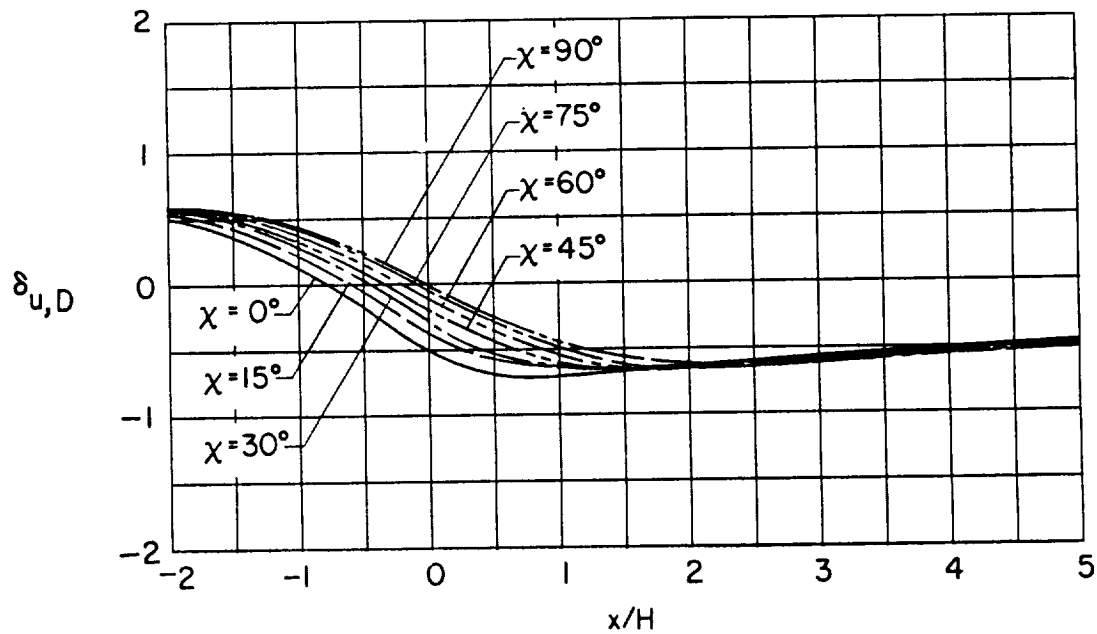


(b) $\zeta = 1.0$.

Figure 44.- Effect of vertical location of model on the longitudinal distribution of longitudinal interference due to drag for correcting from a closed wind tunnel to ground effect. $\gamma = 1.0$; $\eta = 1.0$.

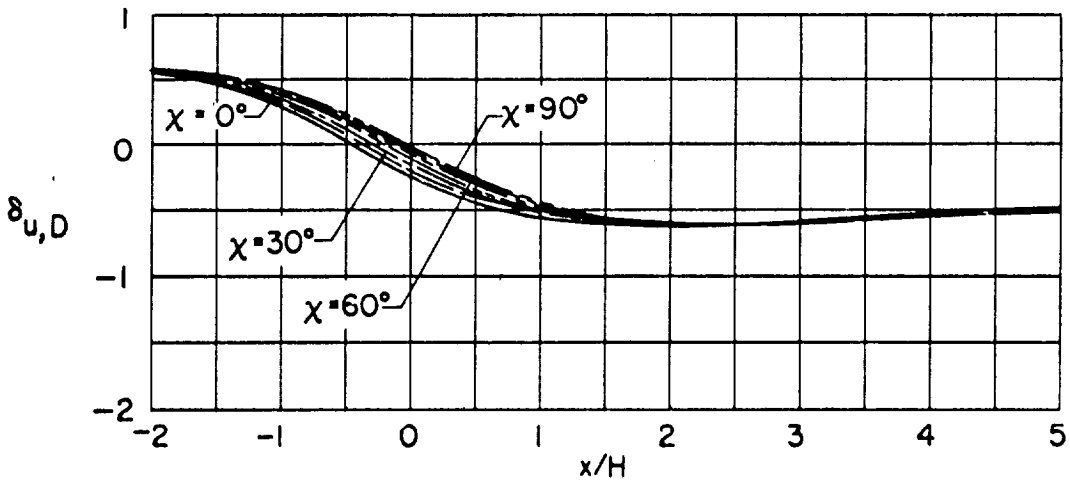


(c) $\zeta = 2.0$.

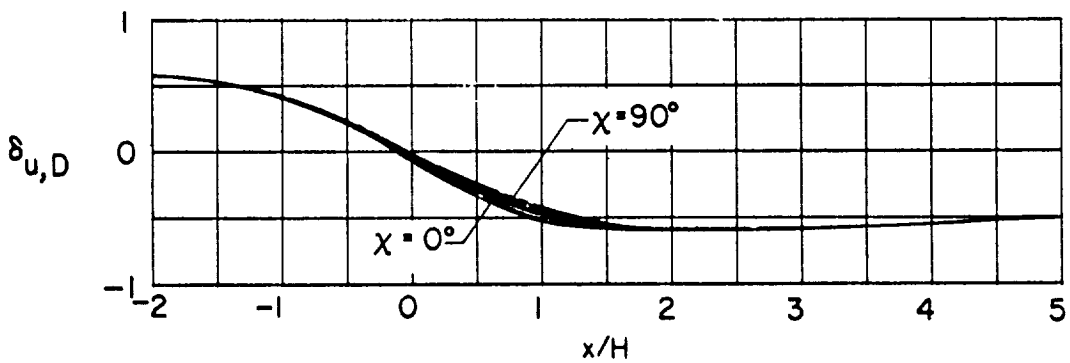


(d) $\zeta = 10.0$.

**Figure 44.- Concluded.**

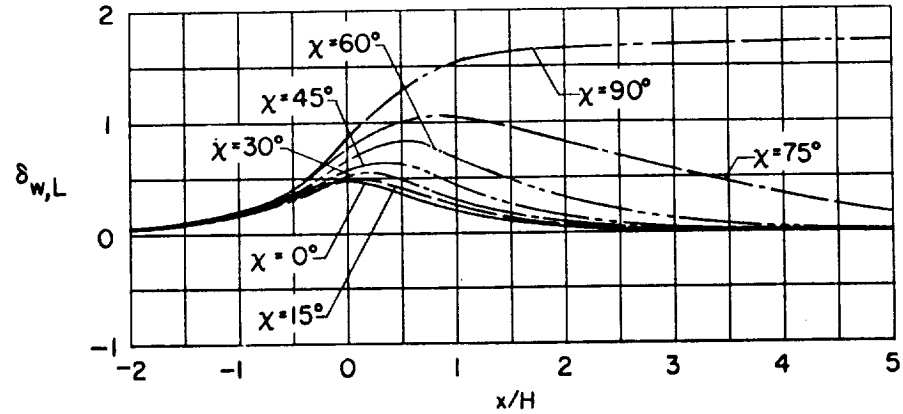


(a) $\zeta = 0.7$.

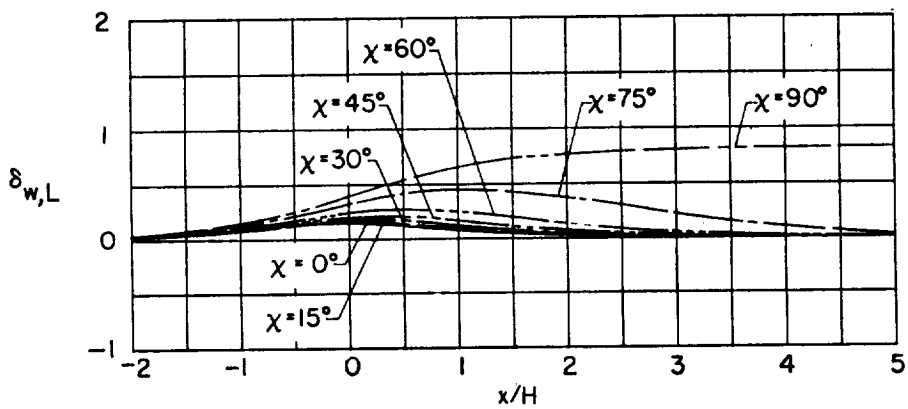


(b) $\zeta = 1.0$.

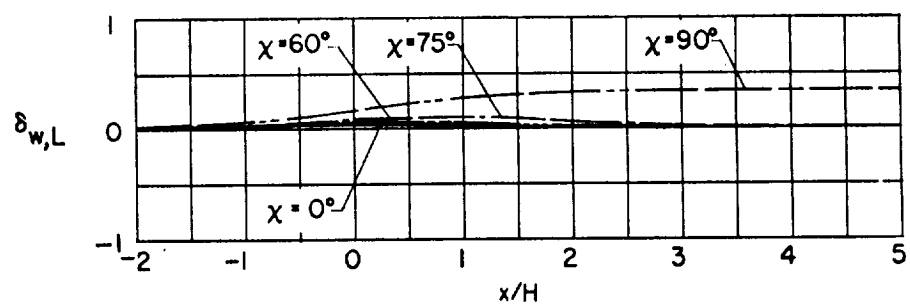


(c) $\zeta = 2.0$.

Figure 45.- Effect of vertical location of model on the longitudinal distribution of vertical interference due to lift for correcting from a wind tunnel closed on bottom only to ground effect. $\gamma = 1.0$; $\eta = 1.0$.

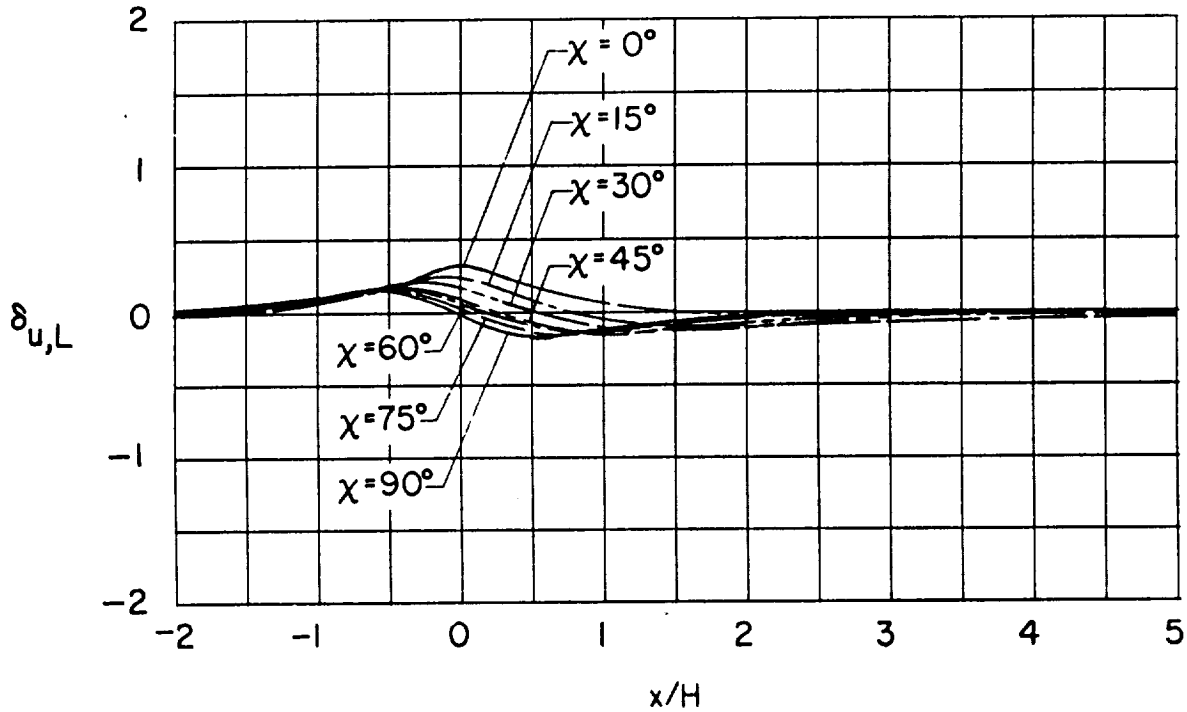


Figure 46.- Effect of vertical location of model on the longitudinal distribution of longitudinal interference due to lift for correcting from a wind tunnel closed on the bottom only to ground effect. $\gamma = 1.0$; $\zeta = 0.7$; $\eta = 1.0$. (Plots for other values of $\zeta$ are omitted since $\delta_{u,L}$ for $\zeta \geqq 1.0$ is negligible when plotted to this scale.)

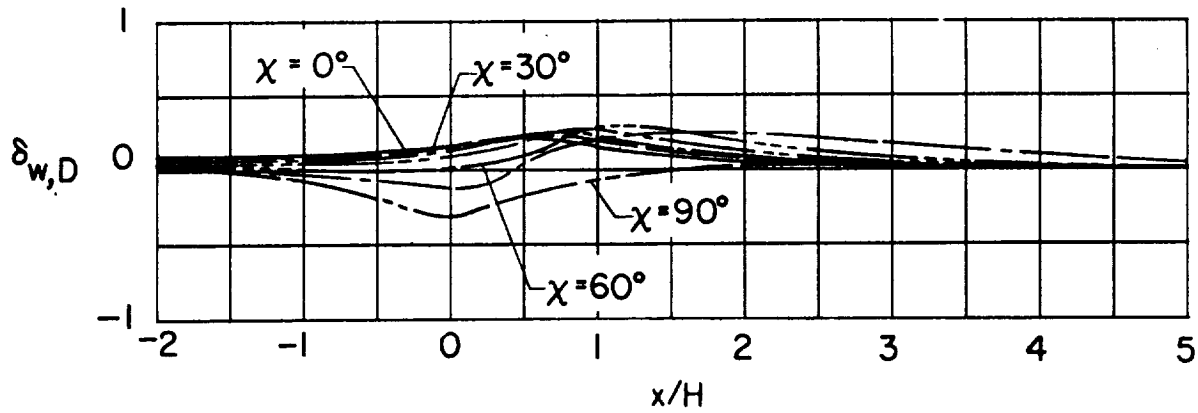


(a) $\zeta = 0.7$.

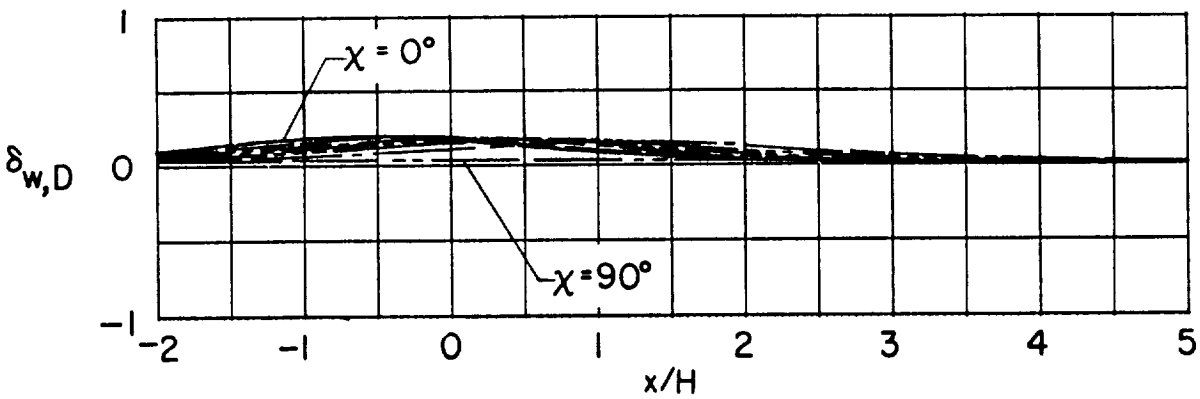


(b) $\zeta = 1.0$.

Figure 47.- Effect of vertical location of model on the longitudinal distribution of vertical interference due to drag for correcting from a wind tunnel closed on bottom only to ground effect. $\gamma = 1.0$; $\eta = 1.0$.

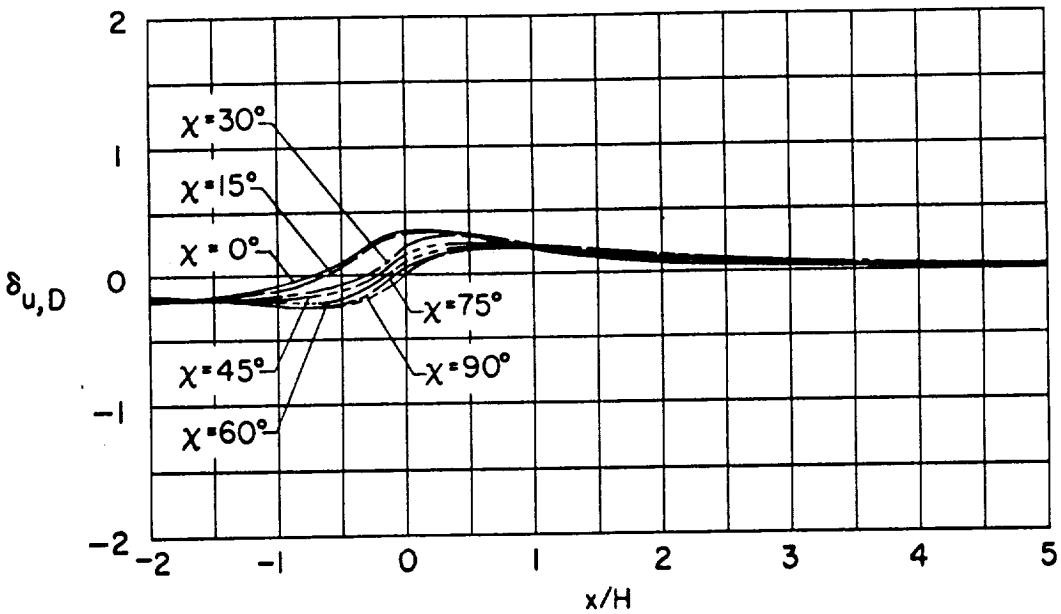


(a) $\zeta = 0.7$.

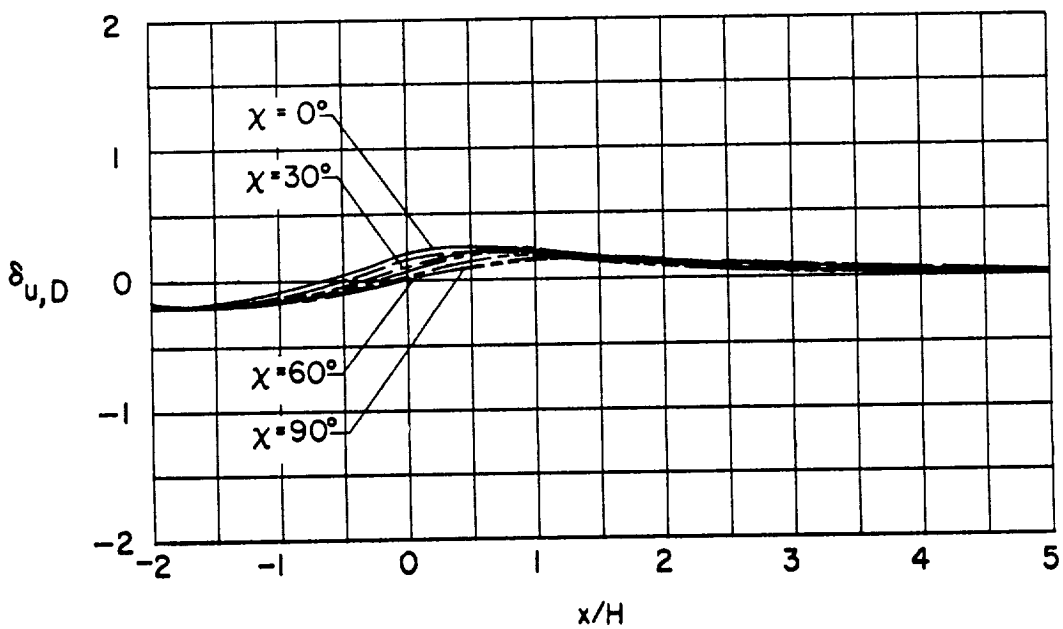


(b) $\zeta = 1.0$.

Figure 48.- Effect of vertical location of model on the longitudinal distribution of longitudinal interference due to drag for correcting from a wind tunnel closed on bottom only to ground effect. $\gamma = 1.0$; $\eta = 1.0$.

632643 O—62——10

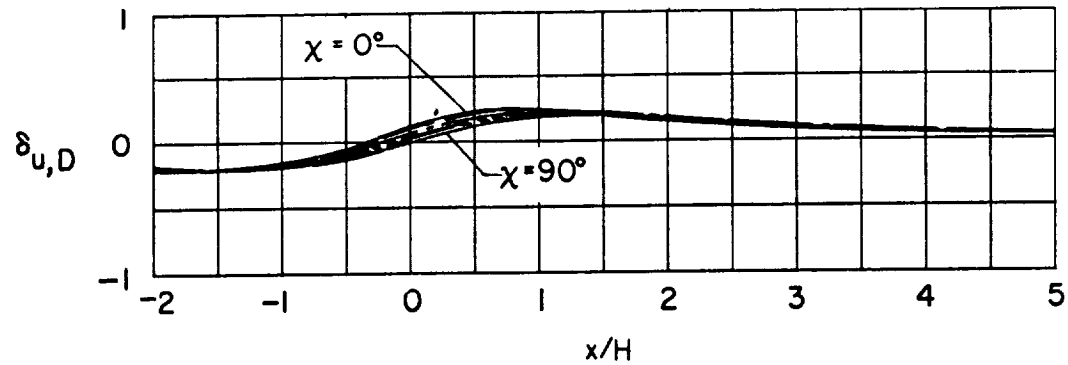


(c) $\zeta = 2.0$.

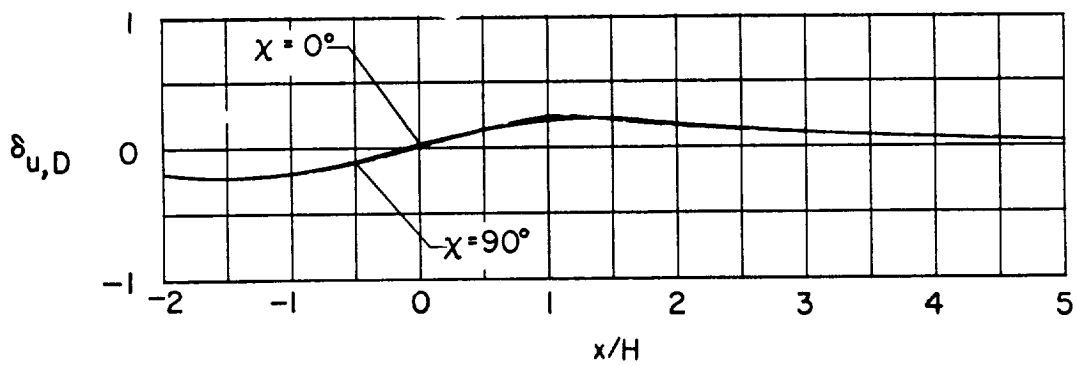


(d) $\zeta = 10.0$.

Figure 48.- Concluded.

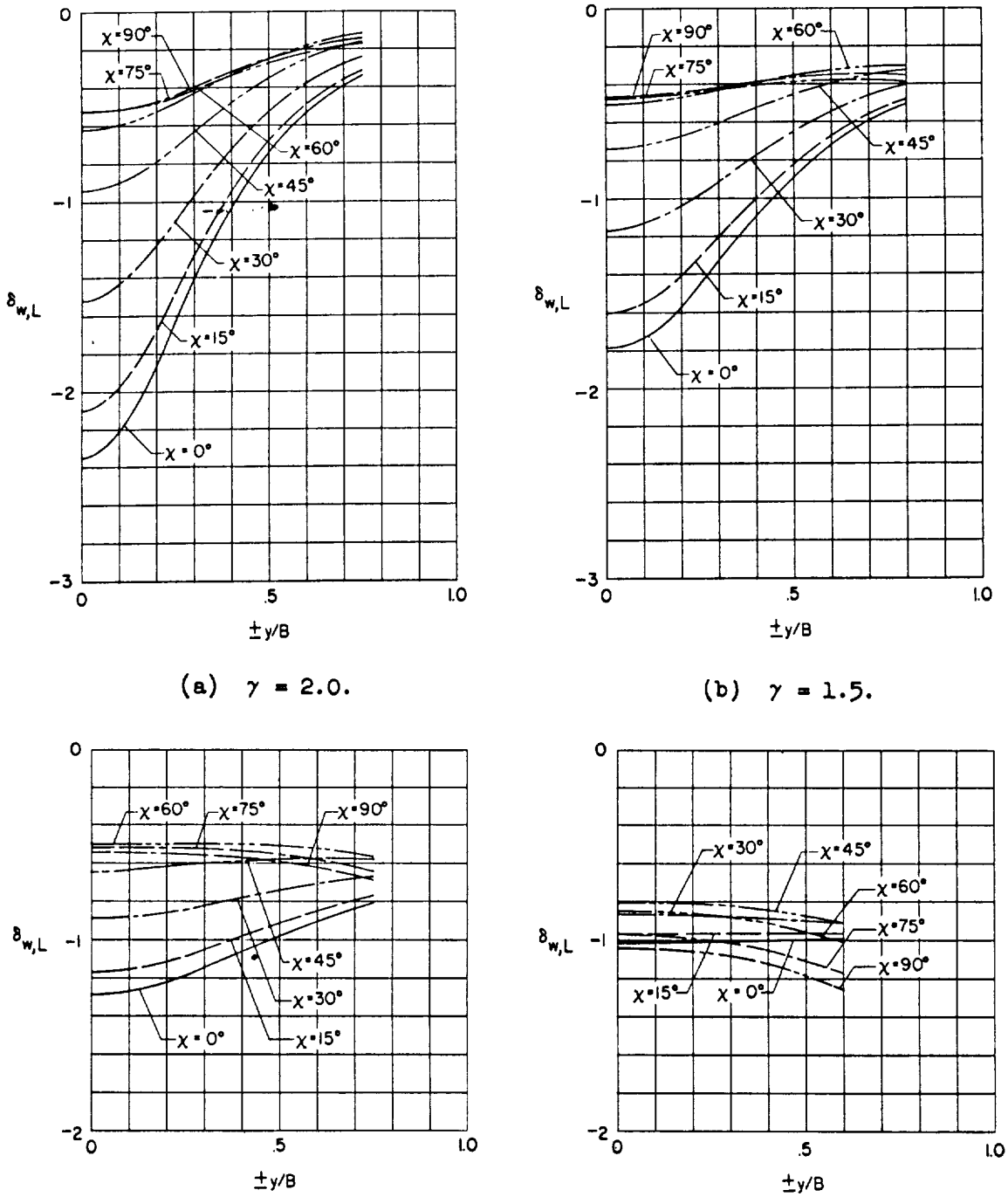


Figure 49.- Effect of wind-tunnel width-height ratio on the lateral distribution of vertical interference due to lift in a closed wind tunnel. $\zeta = 1.0$; $\eta = 1.0$.

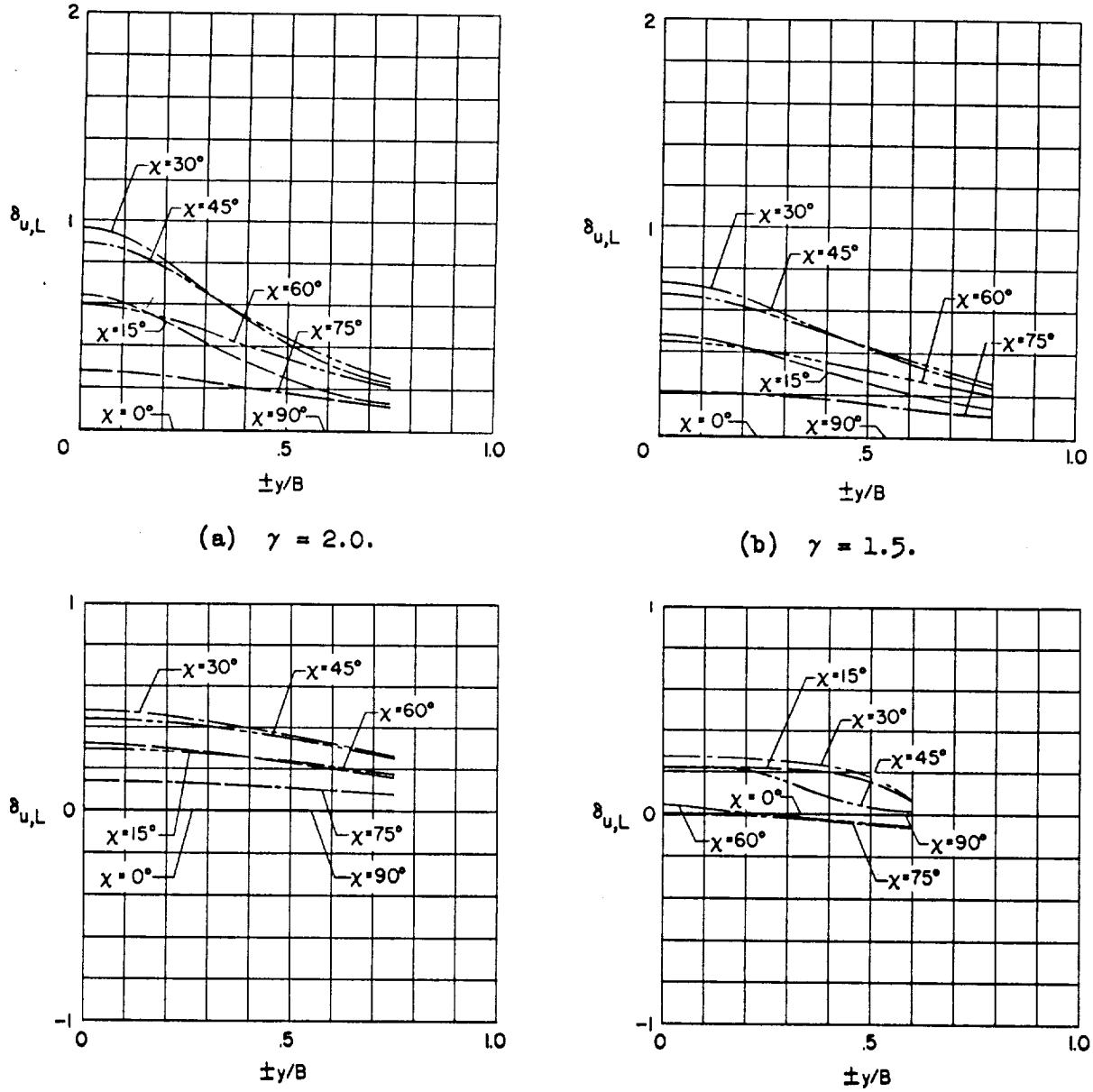


(a) $\gamma = 2.0$.

(b) $\gamma = 1.5$.

(c) $\gamma = 1.0$.

(d) $\gamma = 0.5$.

Figure 50.- Effect of wind-tunnel width-height ratio on the lateral distribution of longitudinal interference due to lift in a closed wind tunnel. $\zeta = 1.0$; $\eta = 1.0$.

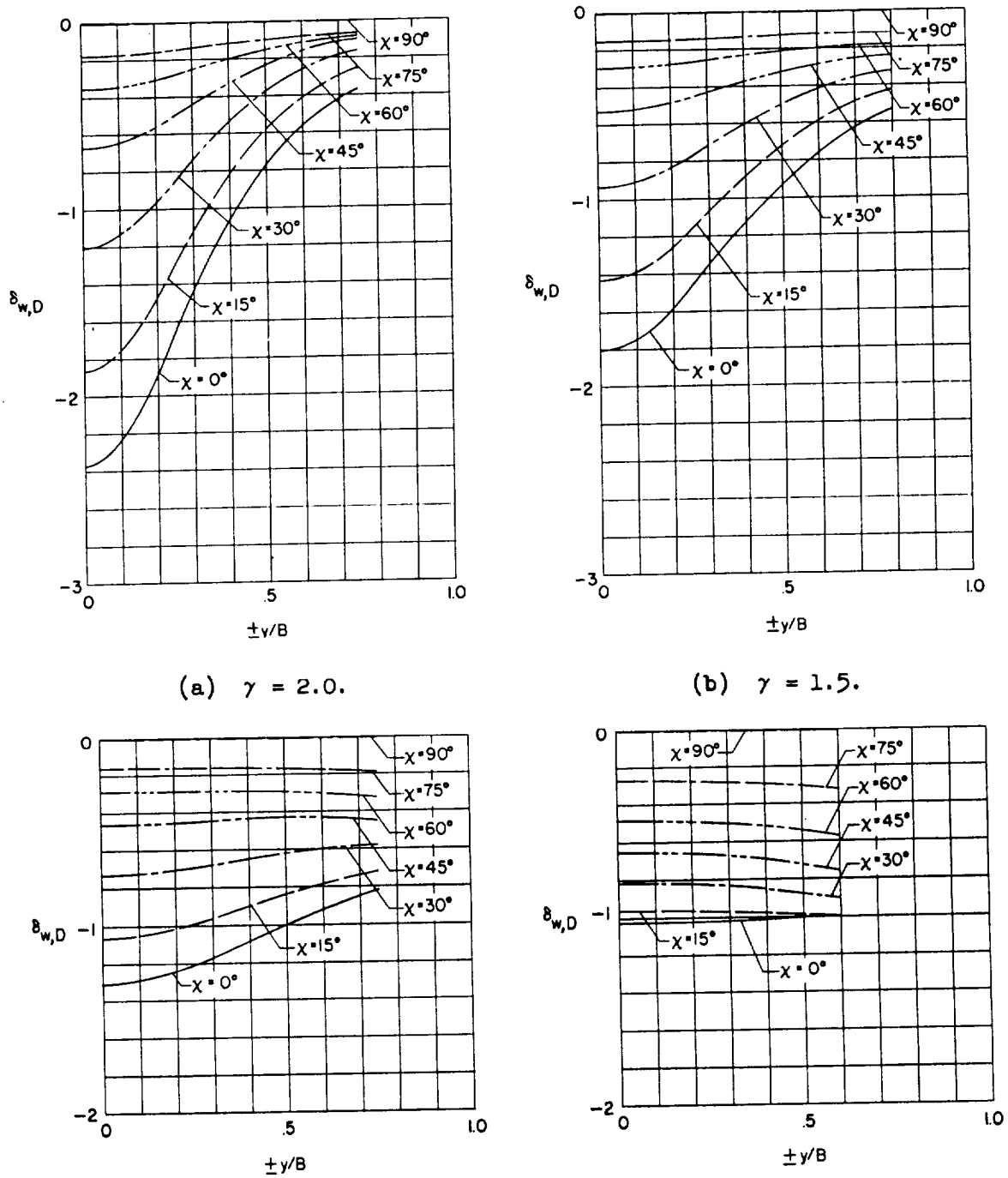


(a) $\gamma = 2.0$.

(b) $\gamma = 1.5$.

(c) $\gamma = 1.0$.

(d) $\gamma = 0.5$.

Figure 51.- Effect of wind-tunnel width-height ratio on the lateral distribution of vertical interference due to drag in a closed wind tunnel. $\zeta = 1.0$; $\eta = 1.0$.

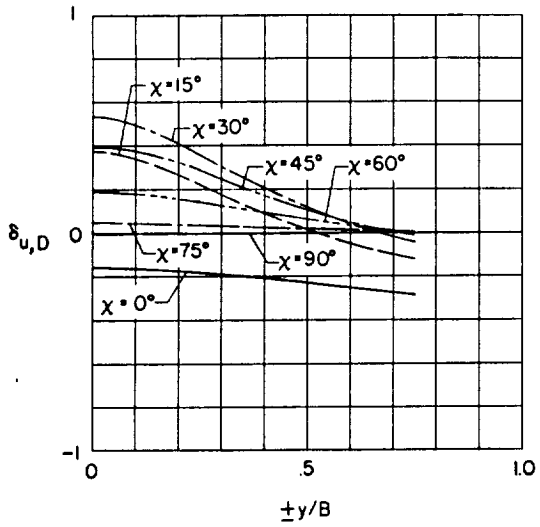


(a) $\gamma = 2.0$.

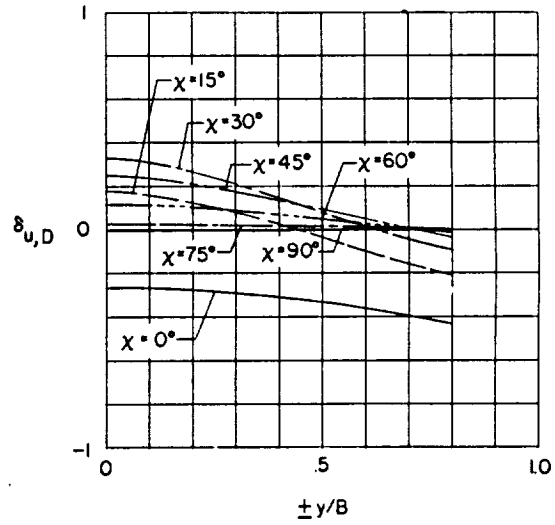


(b) $\gamma = 1.5$.

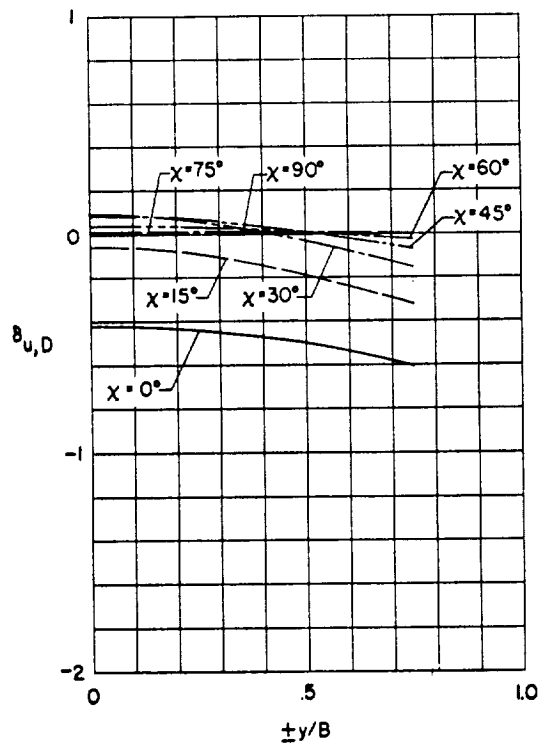


(c) $\gamma = 1.0$.

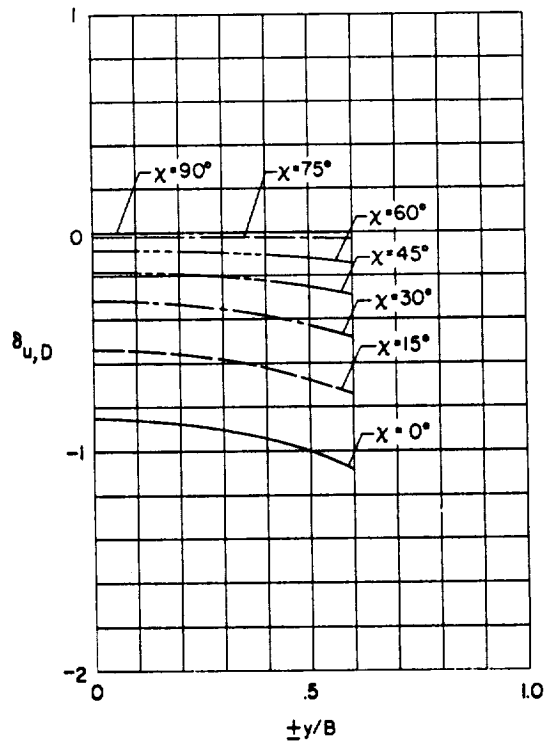


(d) $\gamma = 0.5$.

**Figure 52.- Effect of wind-tunnel width-height ratio on the lateral distribution of longitudinal interference due to drag in a closed wind tunnel. $\zeta = 1.0$; $\eta = 1.0$.**

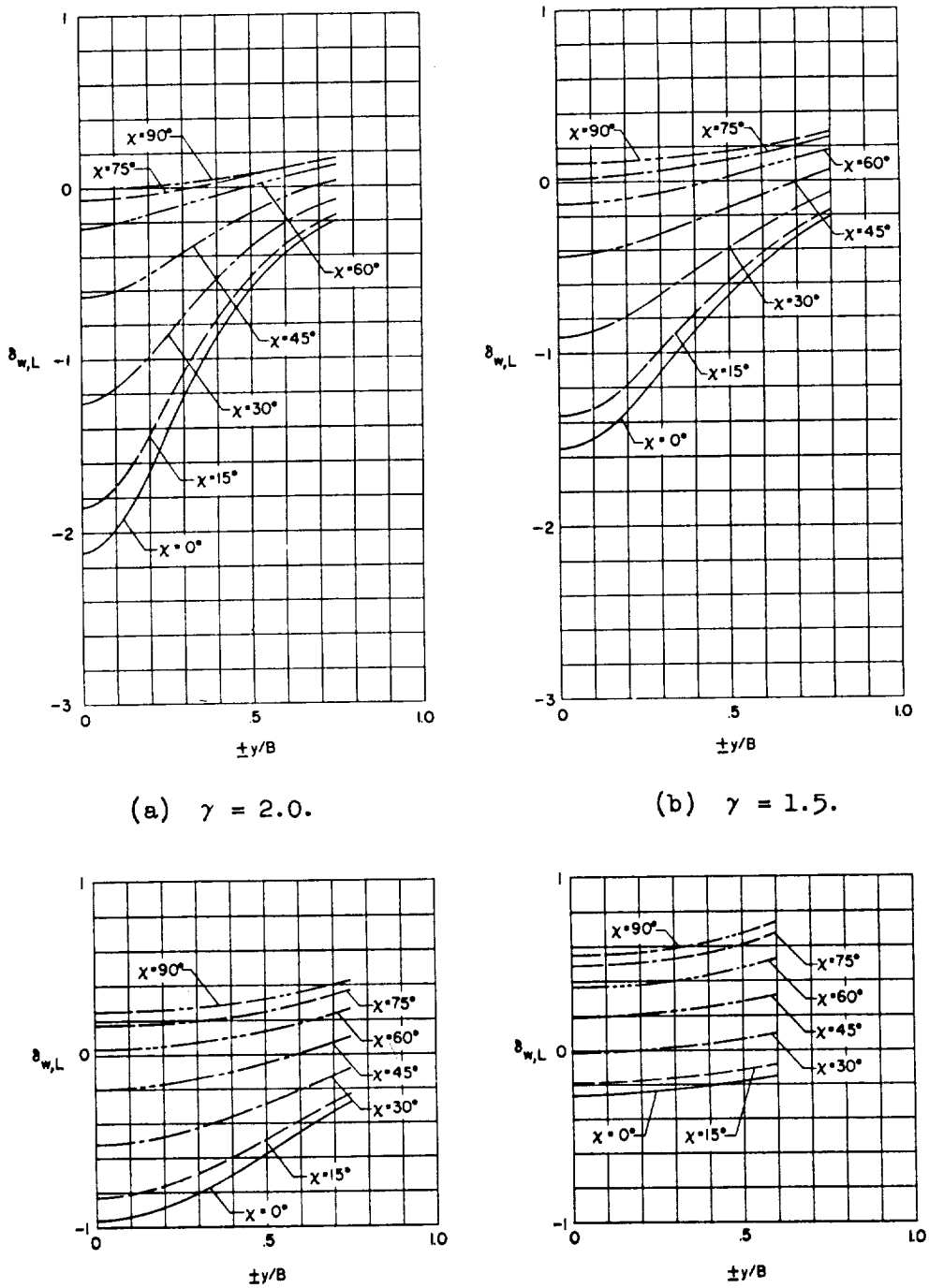


(a) $\gamma = 2.0$.

(b) $\gamma = 1.5$.

(c) $\gamma = 1.0$.

(d) $\gamma = 0.5$.

Figure 53.- Effect of wind-tunnel width-height ratio on the lateral distribution of vertical interference due to lift in a wind tunnel closed on the bottom only. $\zeta = 1.0$; $\eta = 1.0$.

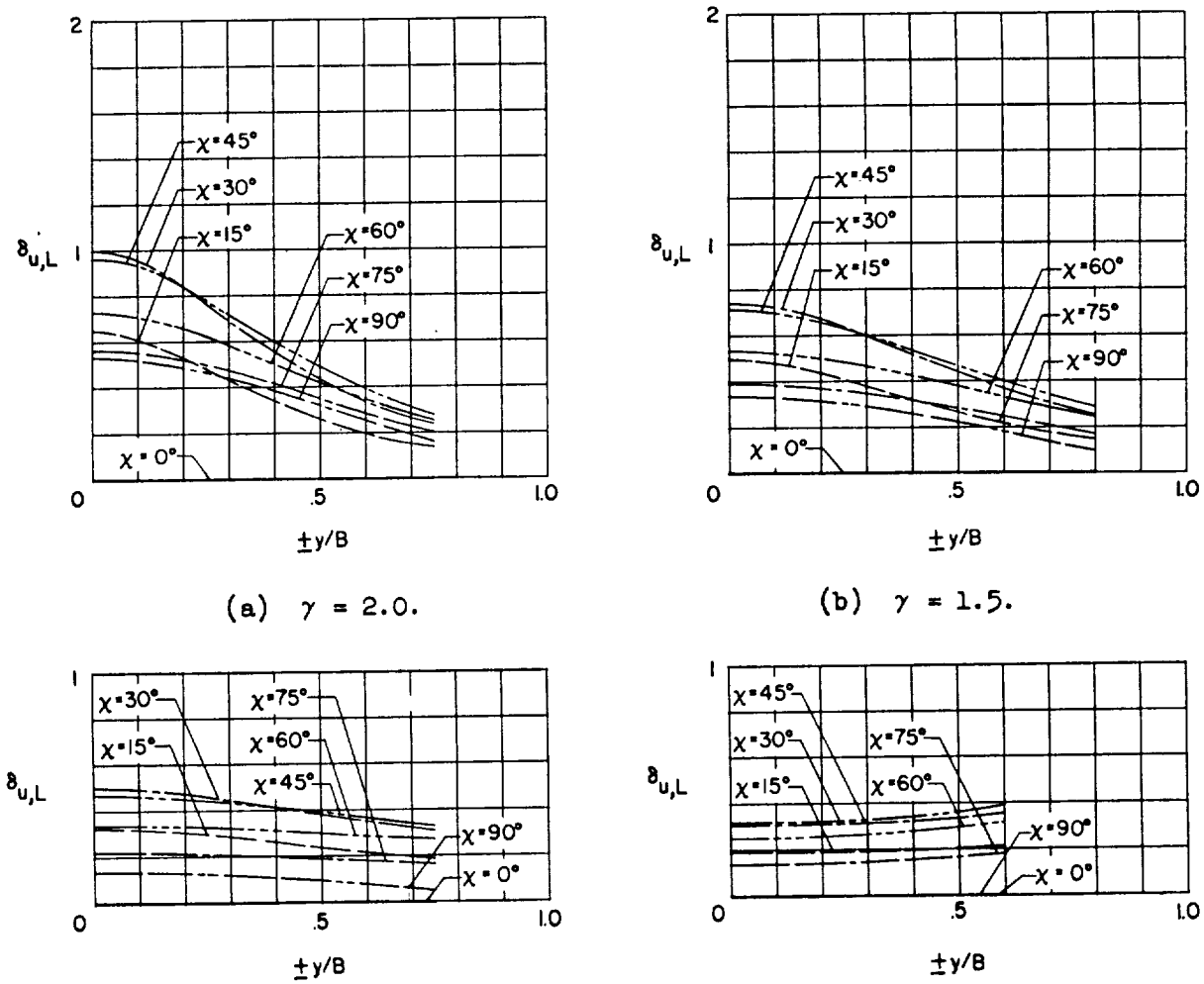


Figure 54.- Effect of wind-tunnel width-height ratio on the lateral distribution of longitudinal interference due to lift in a wind tunnel closed on the bottom only. $\zeta = 1.0$; $\eta = 1.0$.

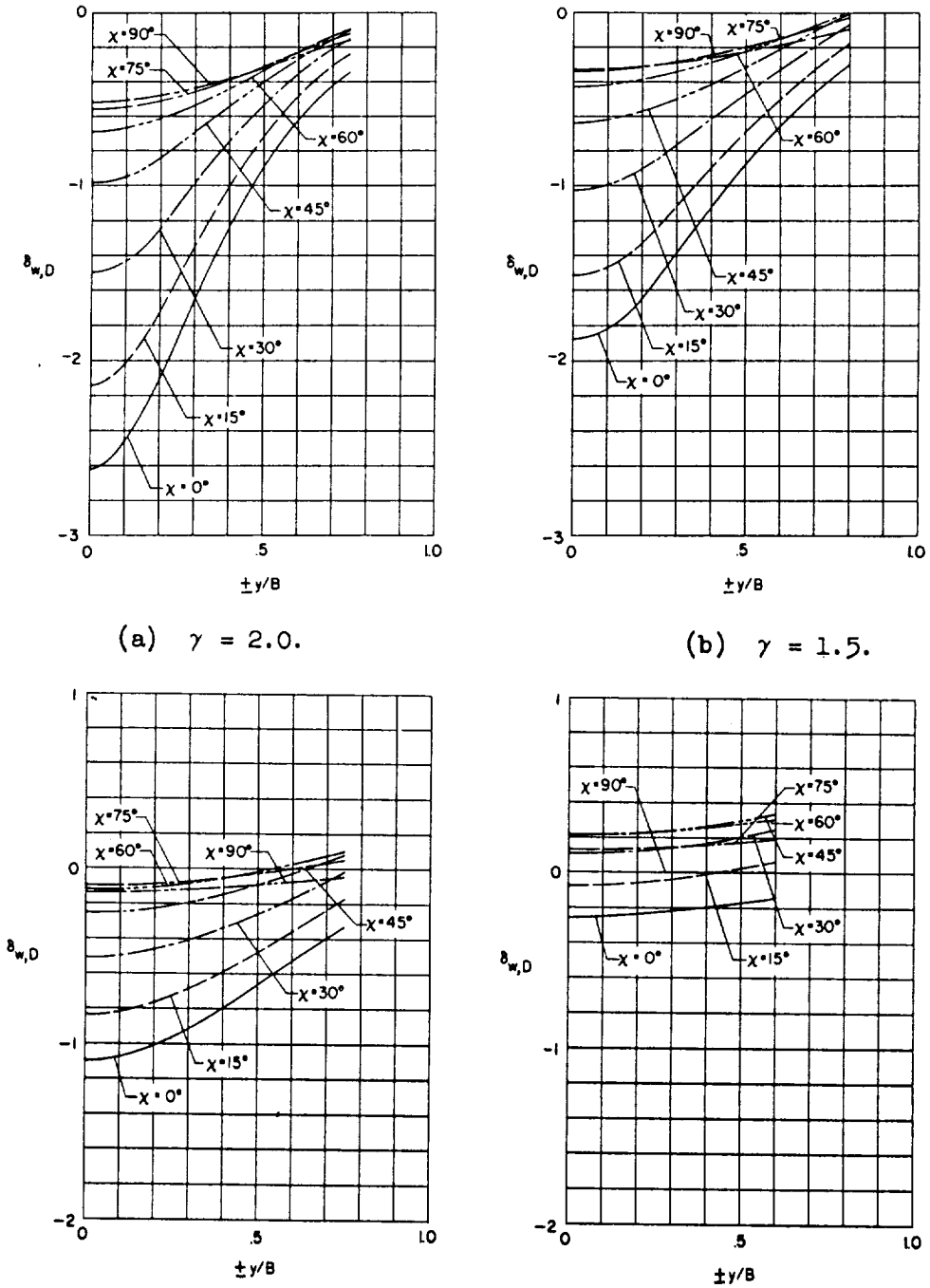


(a) $\gamma = 2.0$.

(b) $\gamma = 1.5$.

(c) $\gamma = 1.0$.

(d) $\gamma = 0.5$.

Figure 55.- Effect of wind-tunnel width-height ratio on the lateral distribution of vertical interference due to drag in a wind tunnel closed on the bottom only. $\zeta = 1.0$; $\eta = 1.0$.

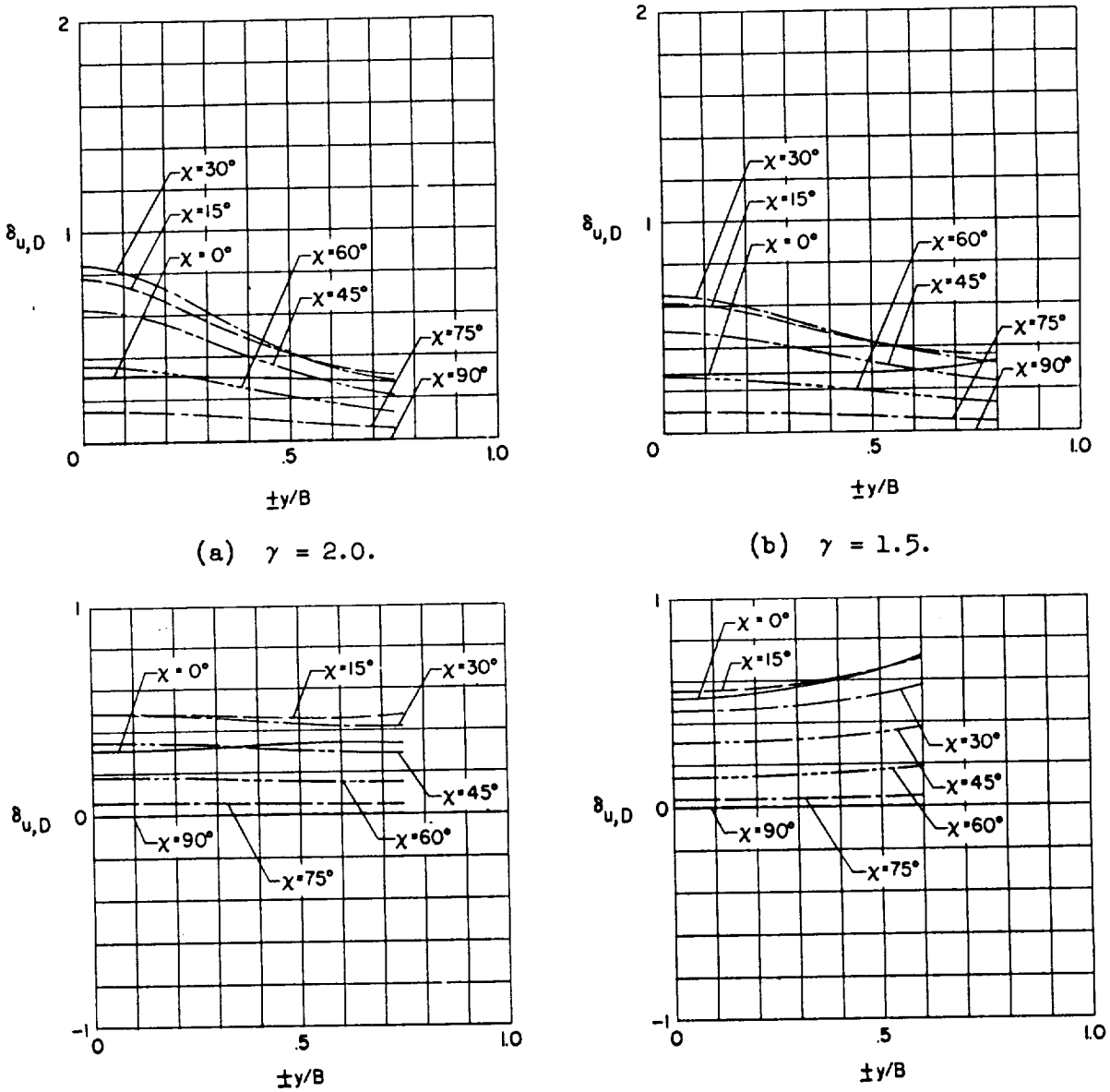


(a) $\gamma = 2.0$.

(b) $\gamma = 1.5$.

(c) $\gamma = 1.0$.

(d) $\gamma = 0.5$.

Figure 56.- Effect of wind-tunnel width-height ratio on the lateral distribution of longitudinal interference due to drag in a wind tunnel closed on the bottom only. $\zeta = 1.0$; $\eta = 1.0$.

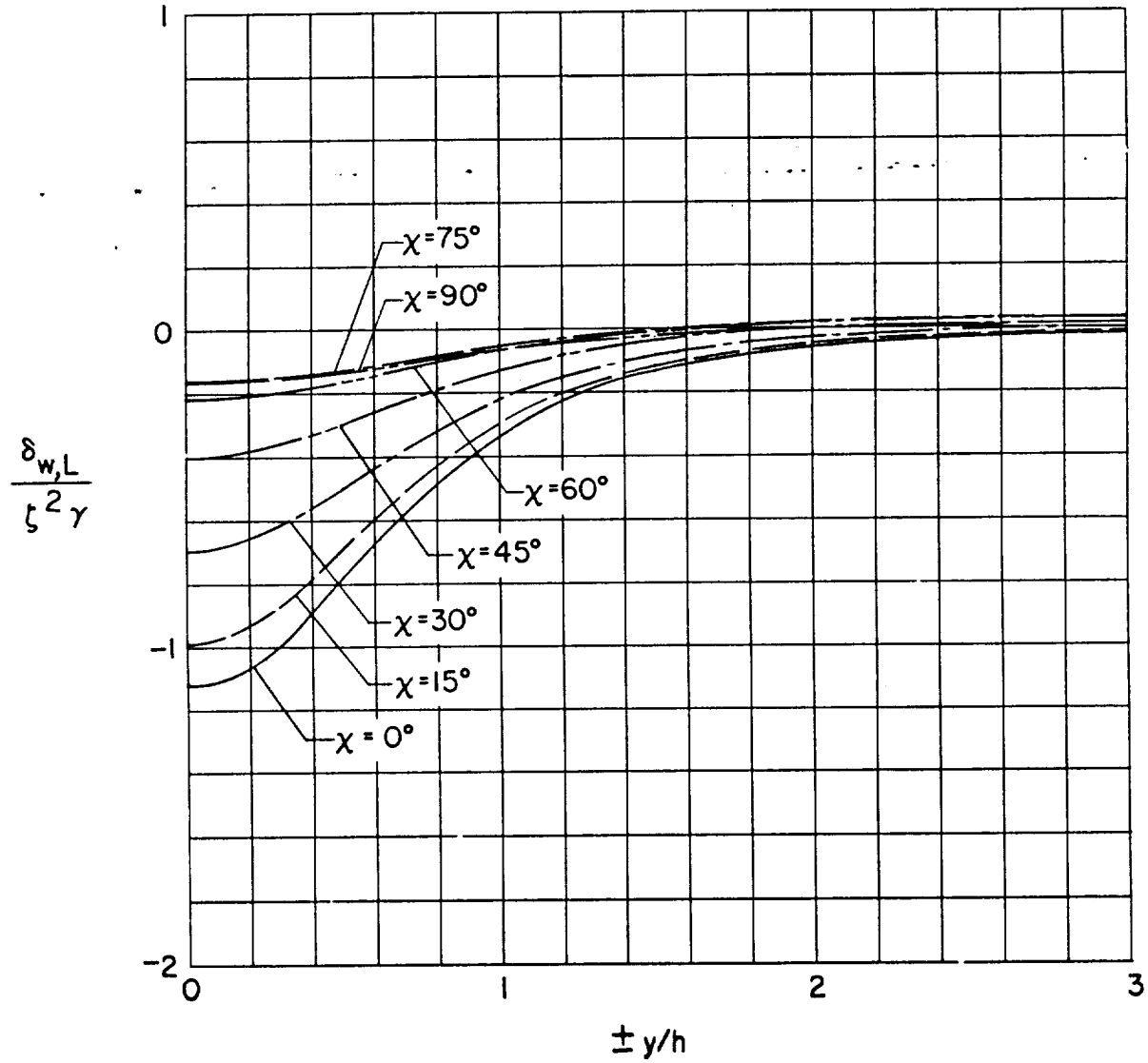


(a) Vertical interference due to lift.

Figure 57.- Lateral distribution of interference factors in ground effect.

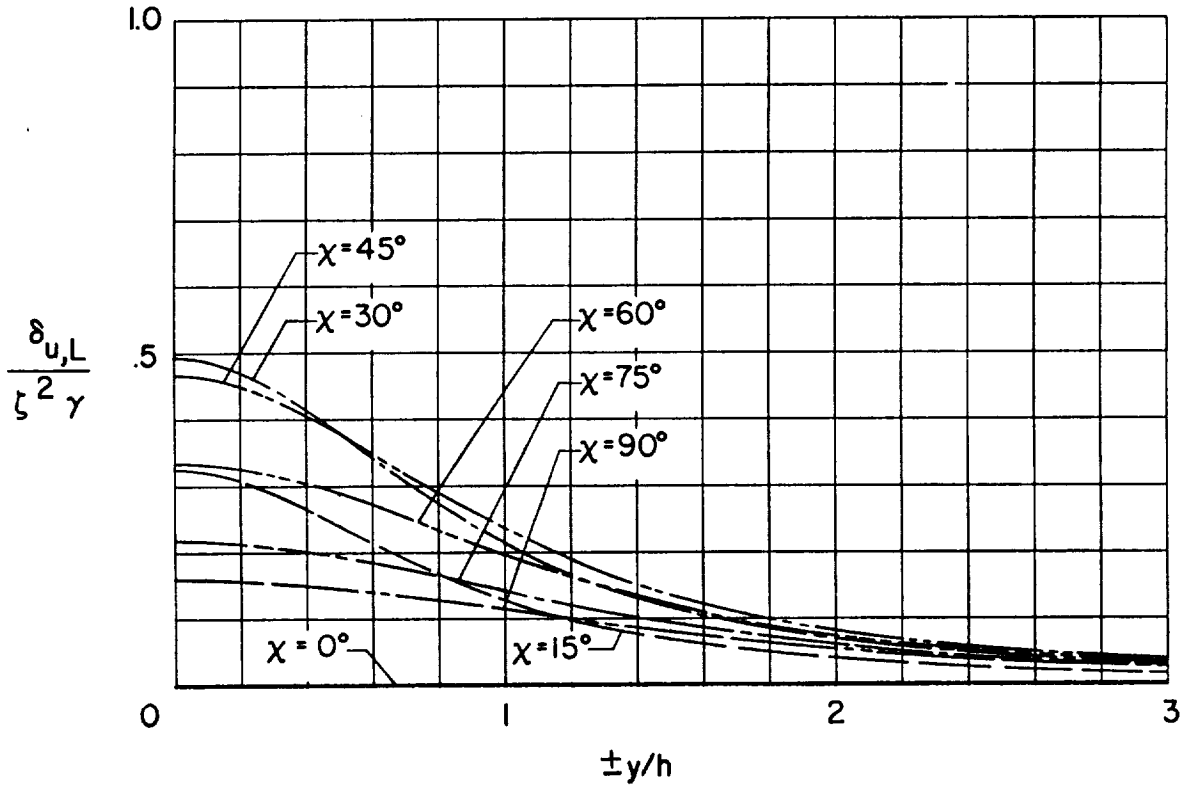


(b) Longitudinal interference due to lift.

Figure 57.- Continued.

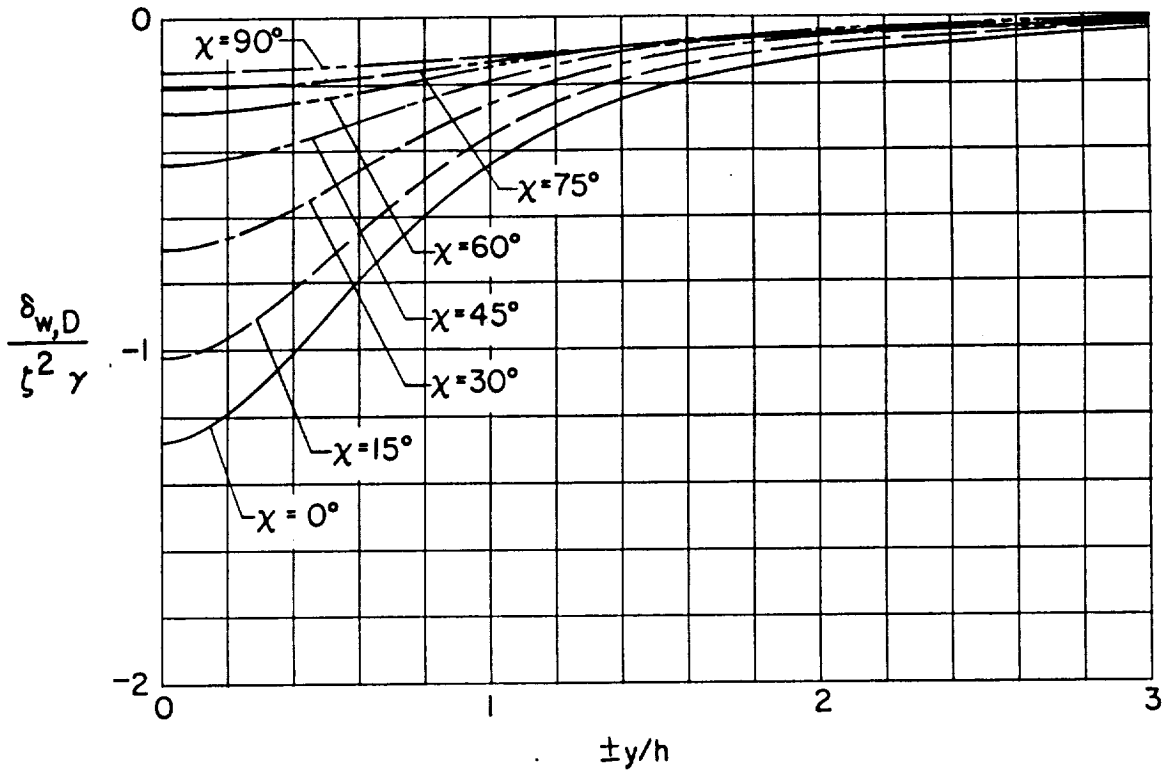


(c) Vertical interference due to drag.

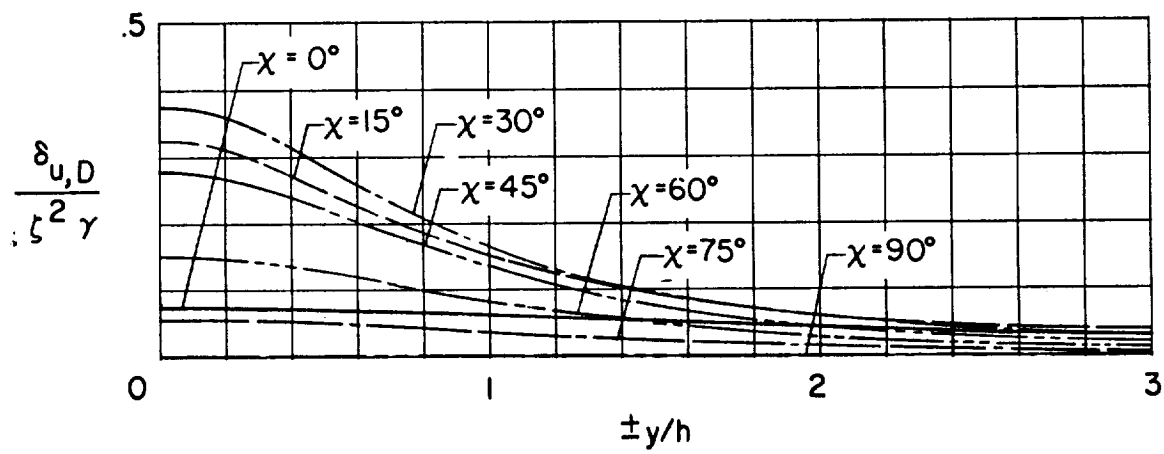


(d) Longitudinal interference due to drag.

Figure 57.- Concluded.

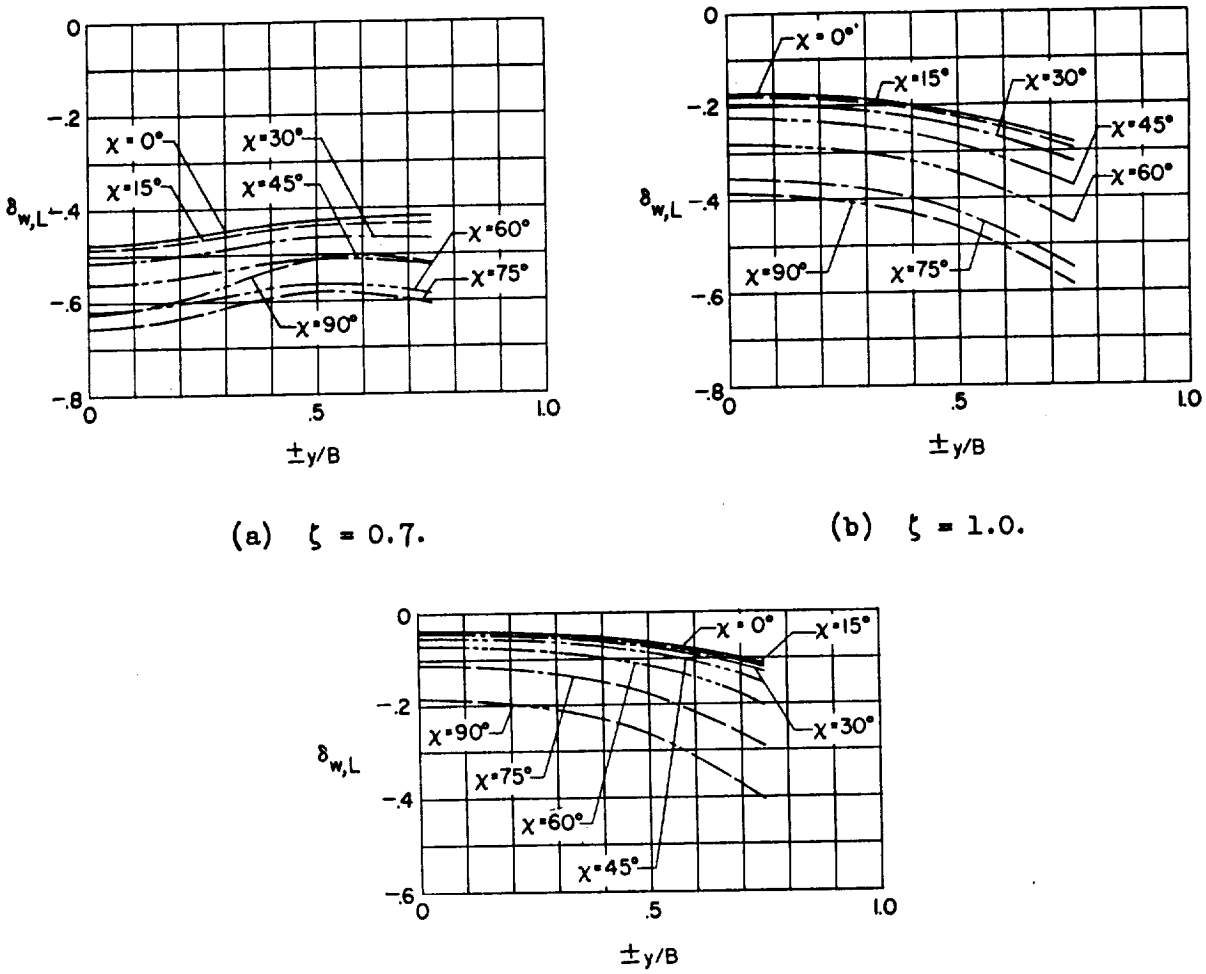


(a) $\zeta = 0.7$.

(b) $\zeta = 1.0$.

(c) $\zeta = 2.0$.

Figure 58.- Effect of vertical location of model on the lateral distribution of vertical interference due to lift for correcting from a closed wind tunnel to ground effect. $\gamma = 1.0$; $\eta = 1.0$.

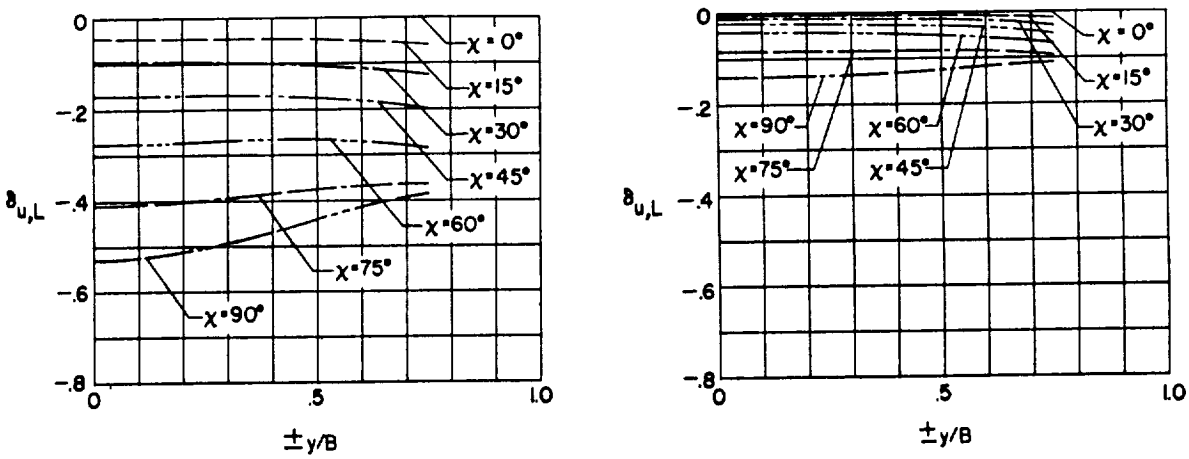


(a) $\zeta = 0.7$.

(b) $\zeta = 1.0$.

Figure 59.- Effect of vertical location of model on the lateral distribution of longitudinal interference due to lift for correcting from a closed wind tunnel to ground effect. $\gamma = 1.0$; $\eta = 1.0$.

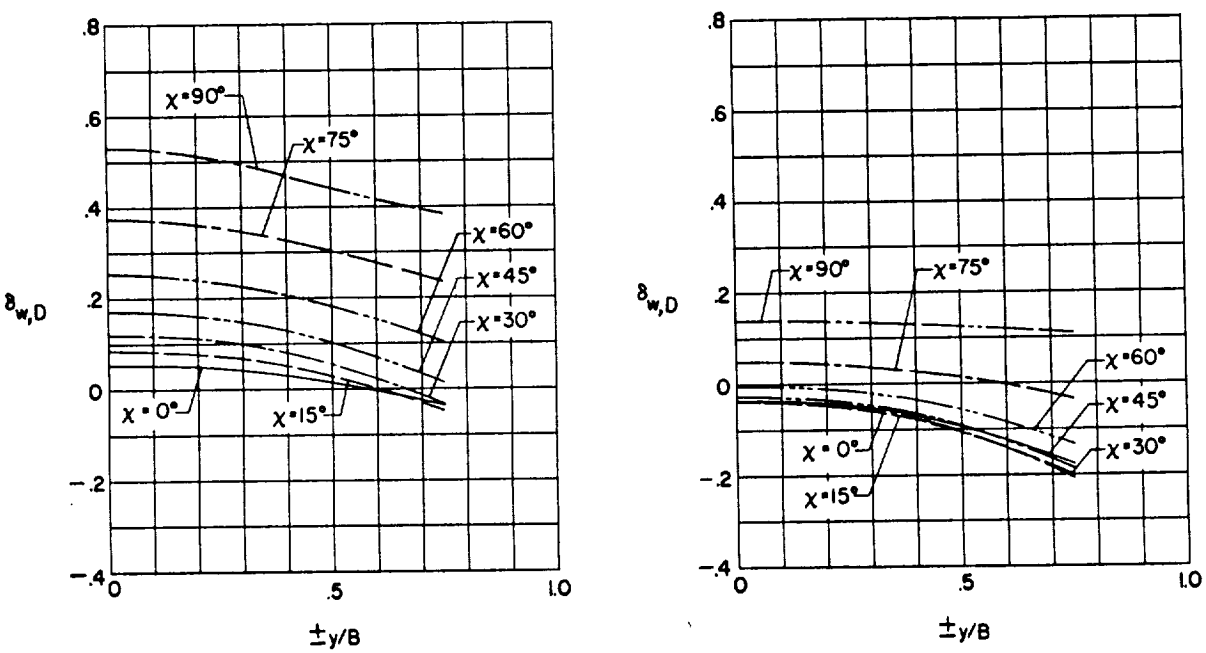


(a) $\zeta = 0.7$.

(b) $\zeta = 1.0$.

Figure 60.- Effect of vertical location of model on the lateral distribution of vertical interference due to drag for correcting from a closed wind tunnel to ground effect. $\gamma = 1.0$; $\eta = 1.0$.

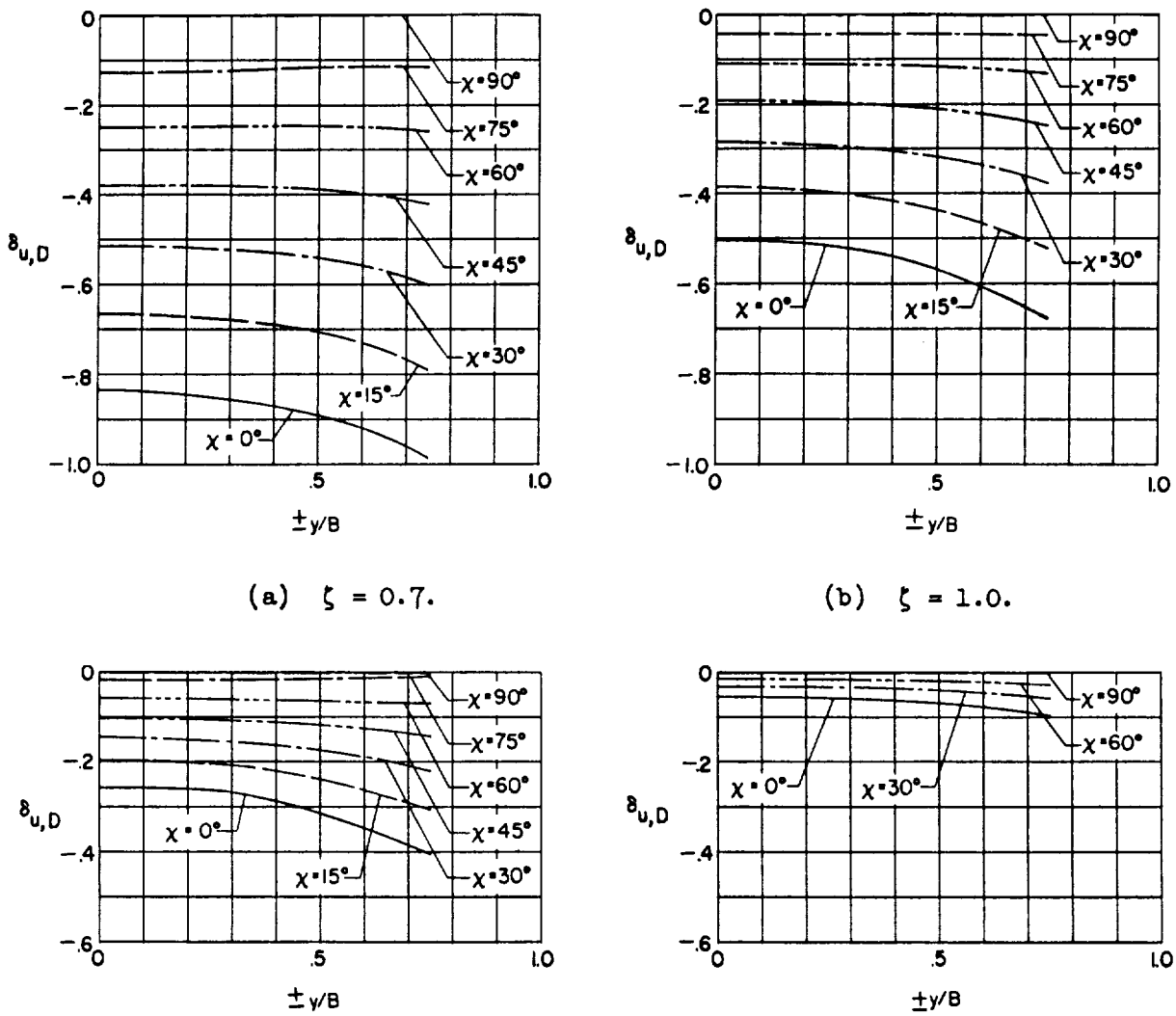


Figure 61.- Effect of vertical location of model on the lateral distribution of longitudinal interference due to drag for correcting from a closed wind tunnel to ground effect. $\gamma = 1.0$; $\eta = 1.0$.

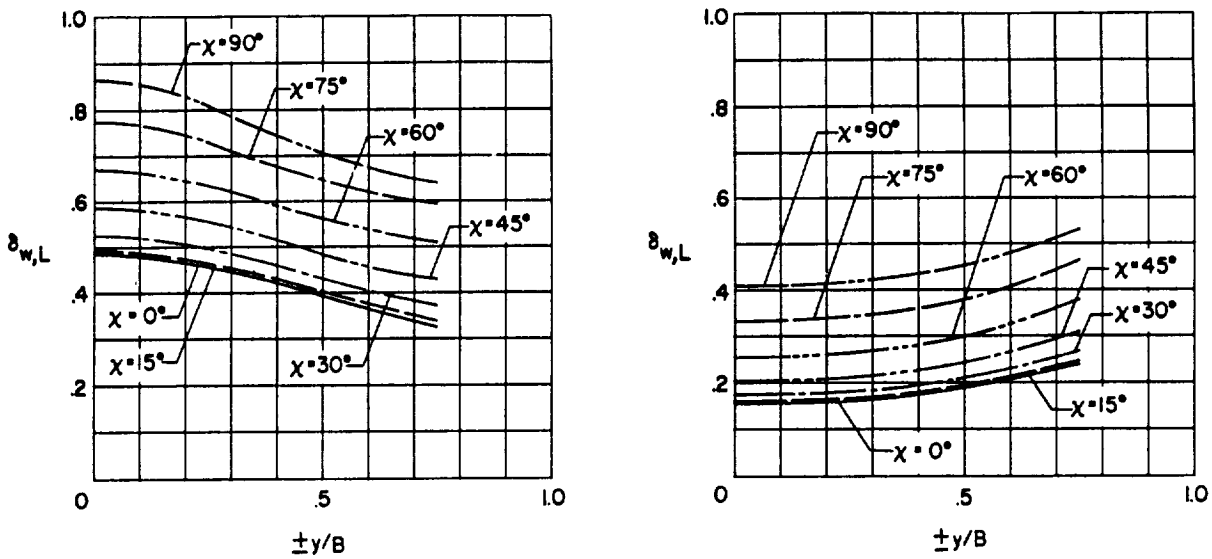


(a) $\zeta = 0.7$.

(b) $\zeta = 1.0$.

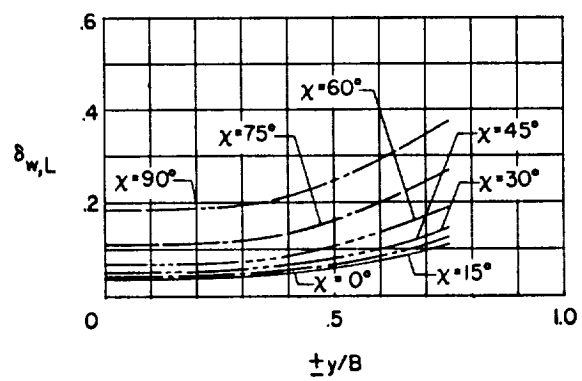


(c) $\zeta = 2.0$.

Figure 62.- Effect of vertical location of model on the lateral distribution of vertical interference due to lift for correcting from a wind tunnel closed on the bottom only to ground effect. $\gamma = 1.0$; $\eta = 1.0$.

632043 O—62——11

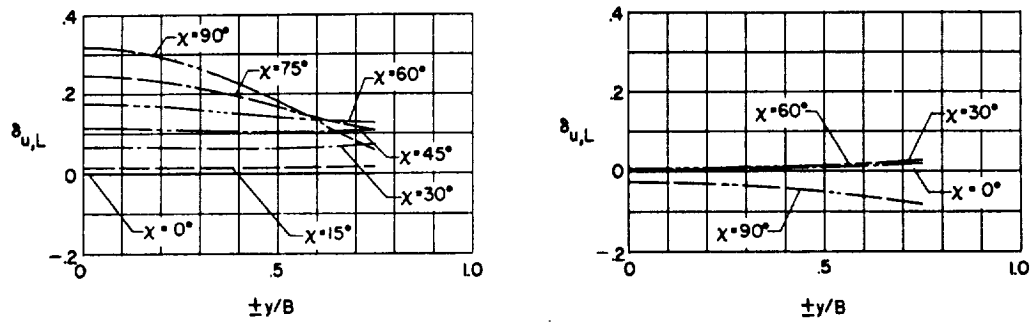


(a) $\zeta = 0.7$. (b) $\zeta = 1.0$.

Figure 63.- Effect of vertical location of model on the lateral distribution of longitudinal interference due to lift for correcting from a wind tunnel closed on the bottom only to ground effect. $\gamma = 1.0$; $\eta = 1.0$.

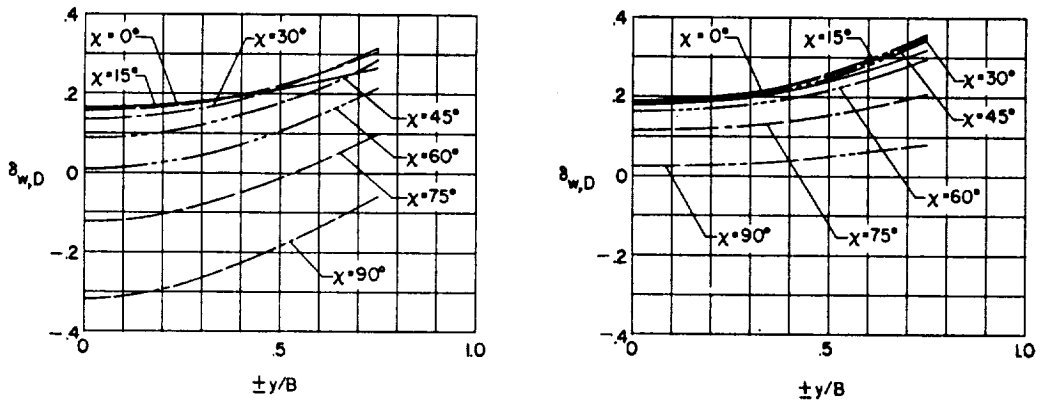


(a) $\zeta = 0.7$. (b) $\zeta = 1.0$.

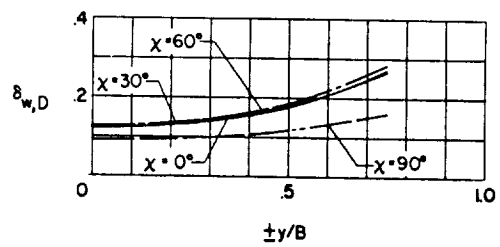


(c) $\zeta = 2.0$.

Figure 64.- Effect of vertical location of model on the lateral distribution of vertical interference due to drag for correcting from a wind tunnel closed on the bottom only to ground effect. $\gamma = 1.0$; $\eta = 1.0$.

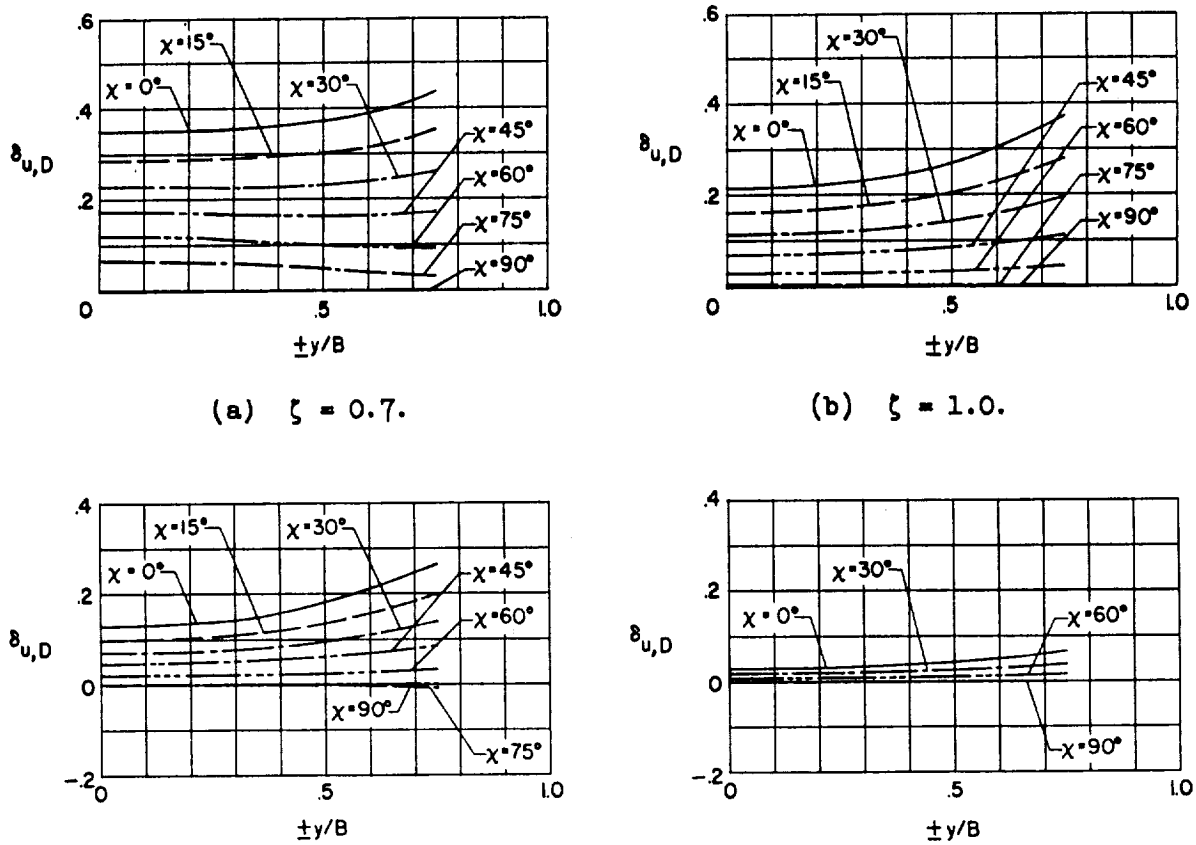


Figure 65.- Effect of vertical location of model on the lateral distribution of longitudinal interference due to drag for correcting from a wind tunnel closed on the bottom only to ground effect. $\gamma = 1.0$; $\eta = 1.0$.

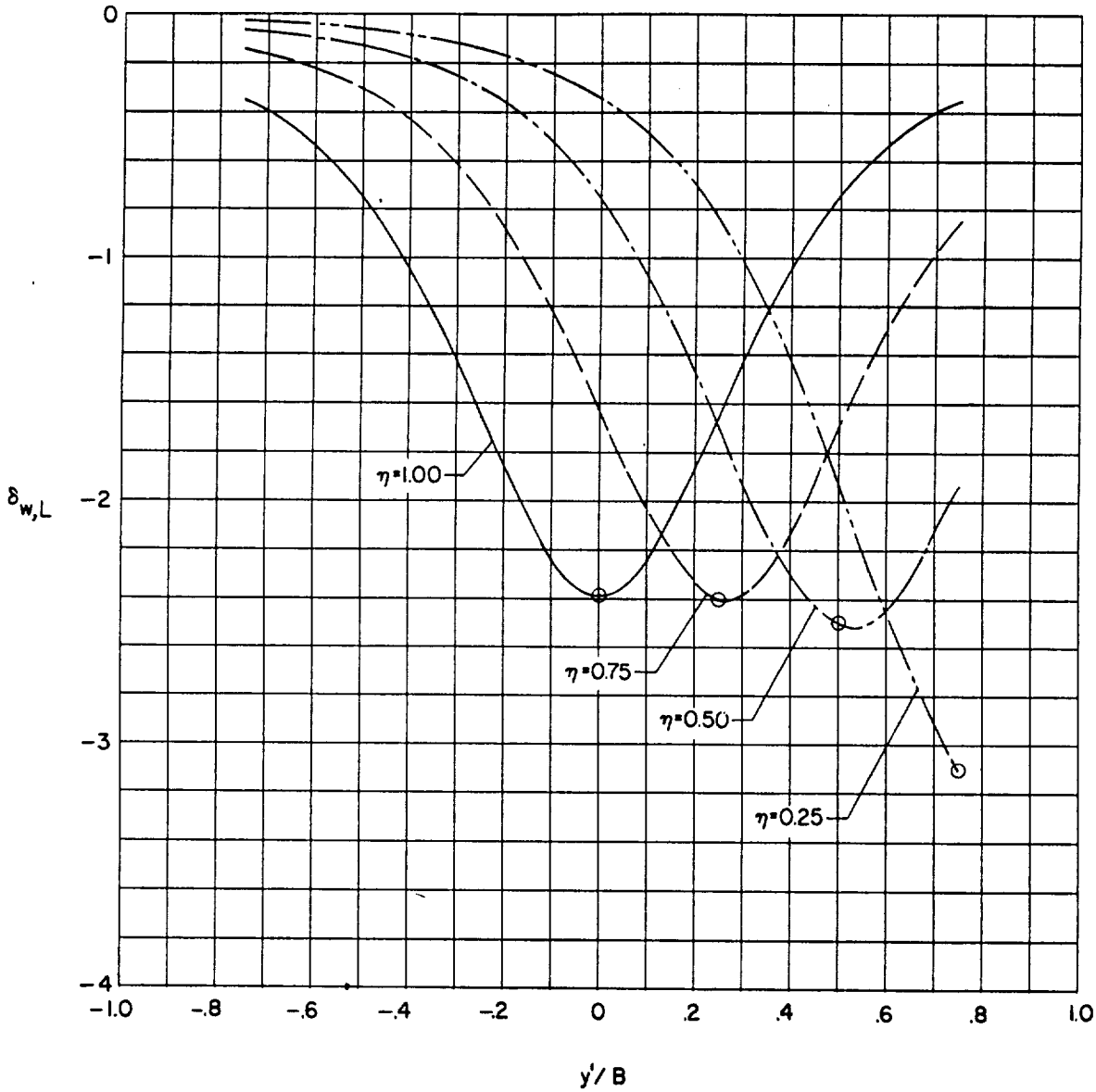


(a) $\chi = 0^{\circ}$.

Figure 66.- Lateral distribution of vertical interference due to lift for laterally offset small models in a closed wind tunnel. $\gamma = 2.0$; $\zeta = 1.0$; symbol denotes location of model.

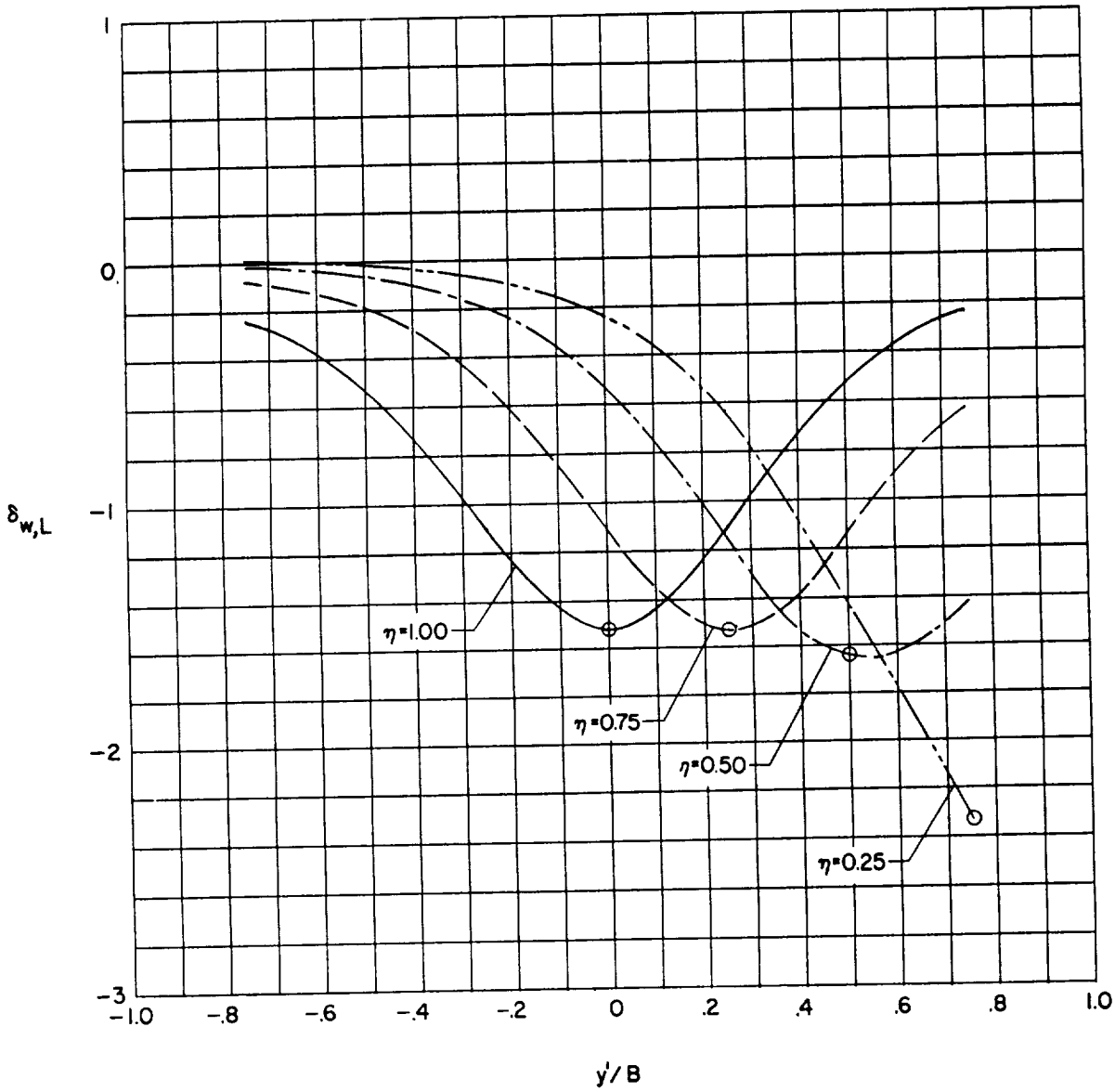


(b) $\chi = 30^{\circ}$.

Figure 66.- Continued.

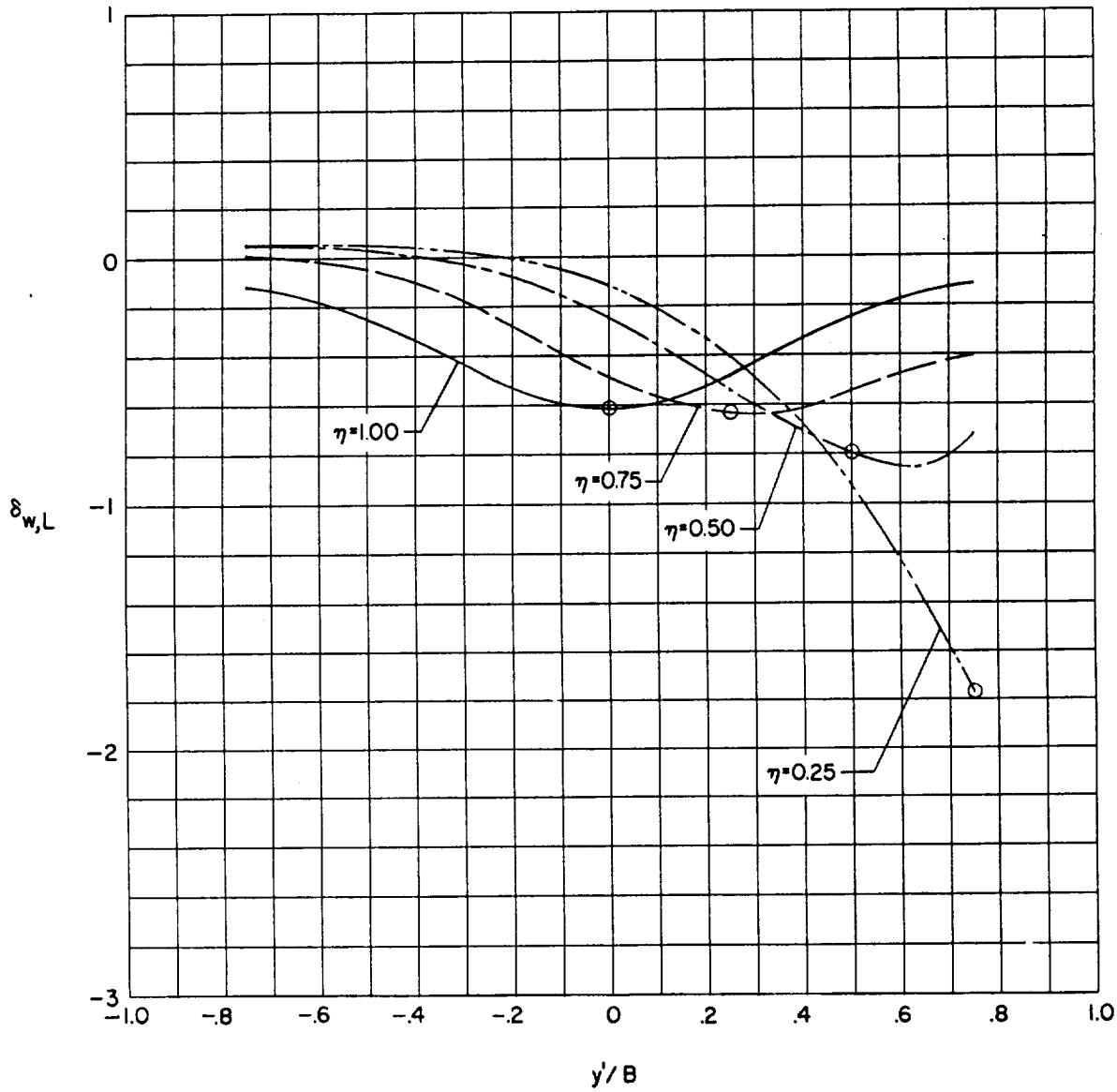


(c) $\chi = 60^{\circ}$.

Figure 66.- Continued.

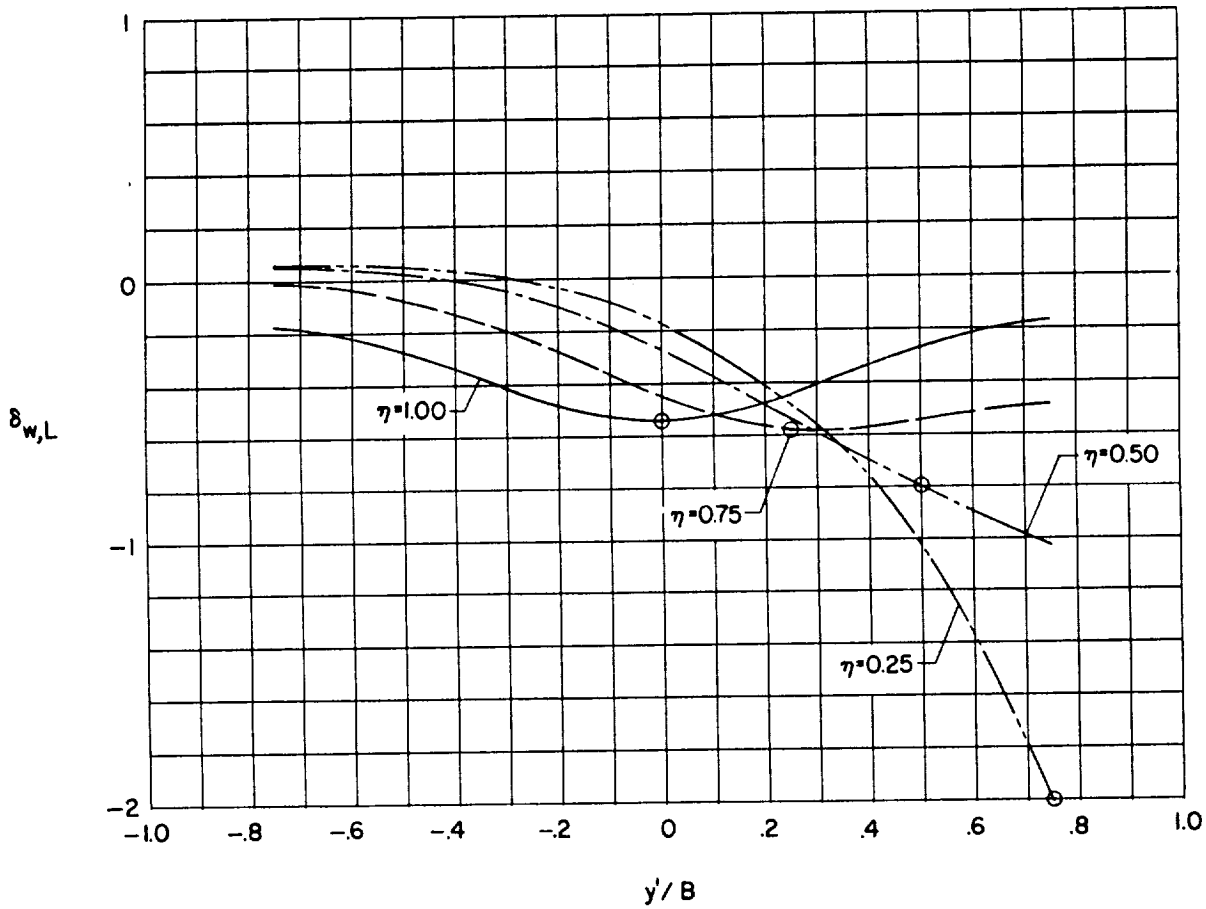


(d) $\chi = 90^{\circ}$.

Figure 66.- Concluded.

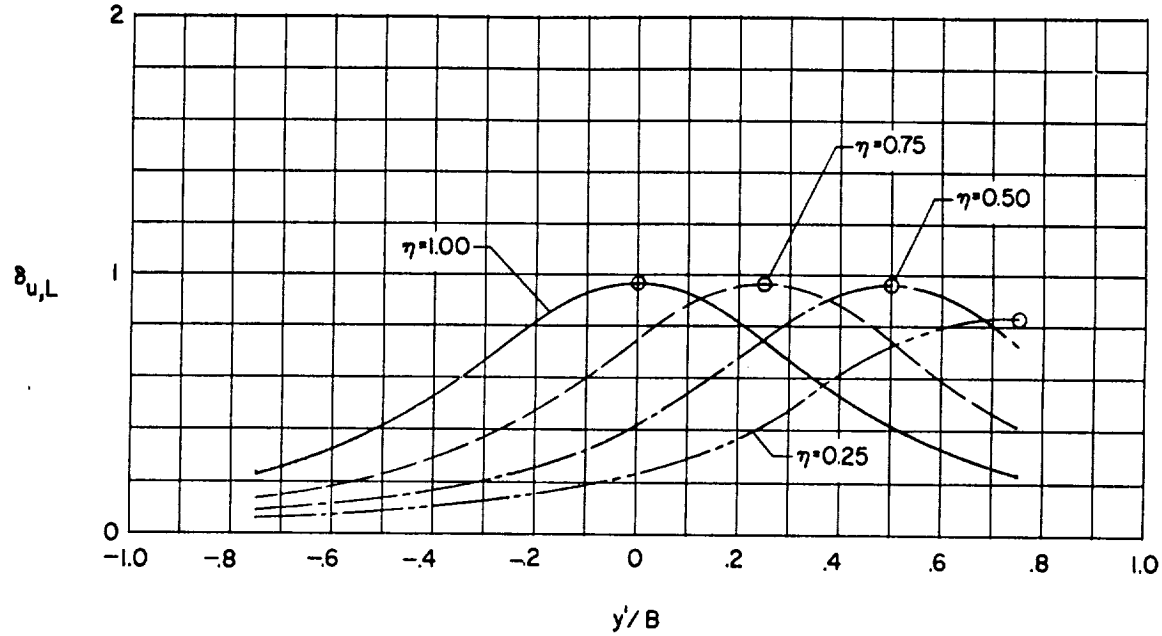


(a) $\chi = 30^{\circ}$.

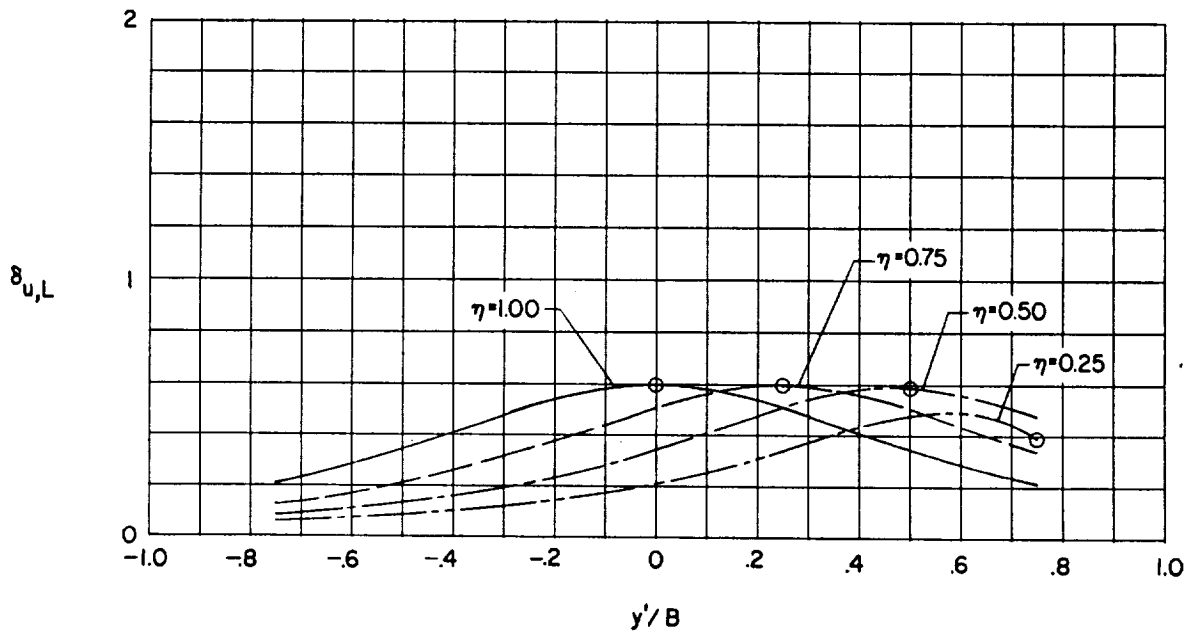


(b) $\chi = 60^{\circ}$.

Figure 67.- Lateral distribution of longitudinal interference due to lift for small models in a closed wind tunnel. $\gamma = 2.0$; $\zeta = 1.0$; symbol denotes location of model. (Plots for $\chi = 0^{\circ}$ and $\chi = 90^{\circ}$ are omitted since $\delta_{u,L}$ is uniformly zero.)

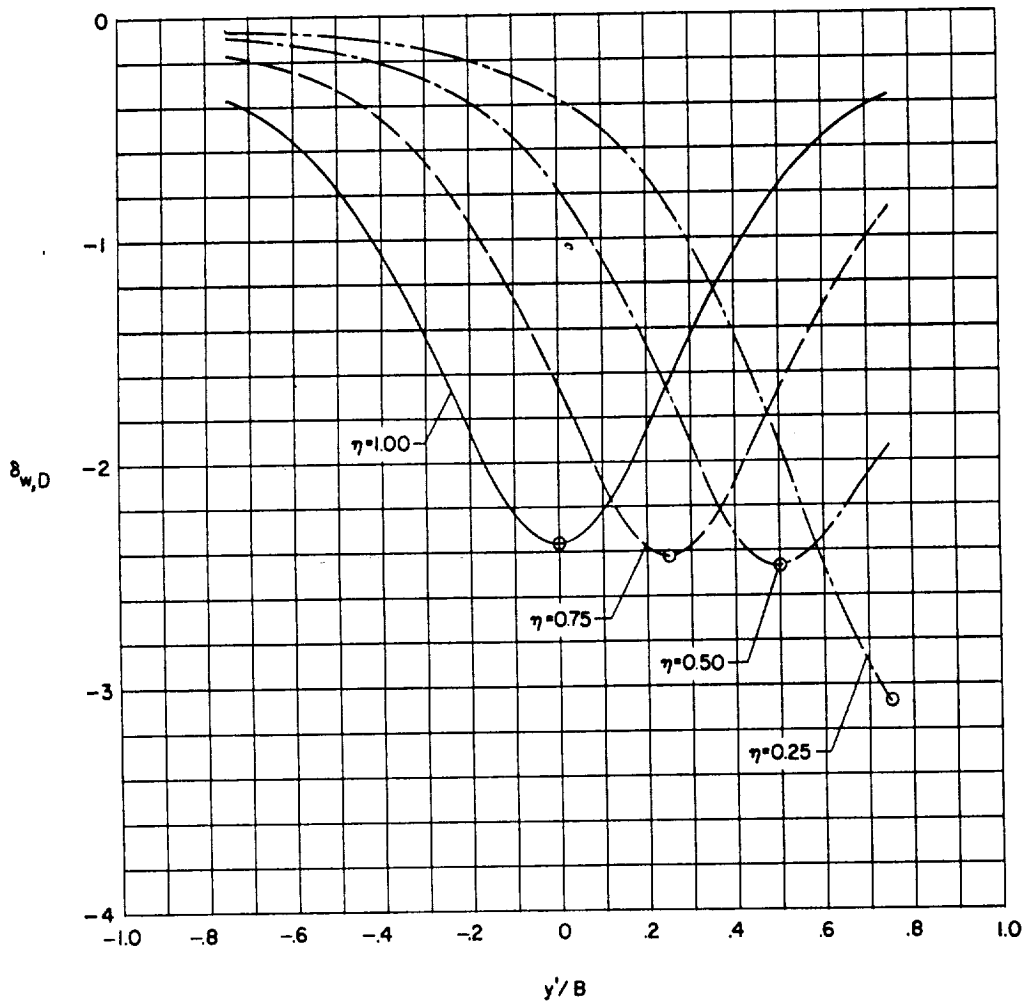


(a) $\chi = 0^{\circ}$.

Figure 68.- Lateral distribution of vertical interference due to drag for laterally offset small models in a closed wind tunnel. $\gamma = 2.0$; $\zeta = 1.0$; symbol denotes location of model. (Plot for $\chi = 90^{\circ}$ is omitted since $\delta_{w,D}$ is uniformly zero.)

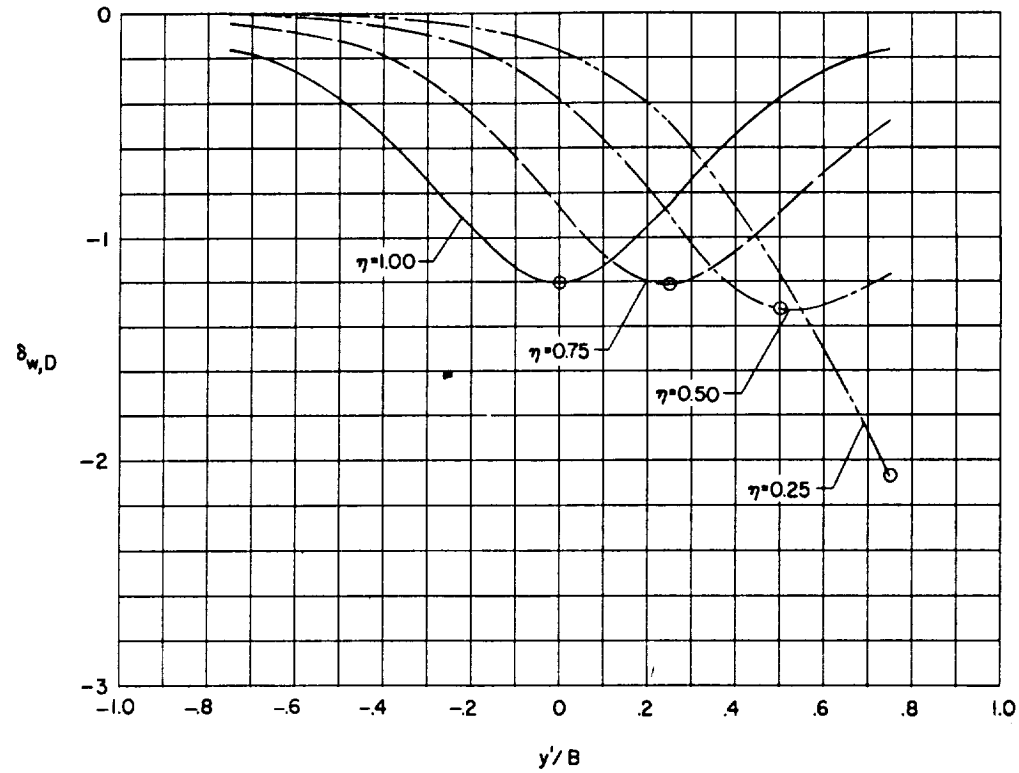


(b) $\chi = 30^{\circ}$.

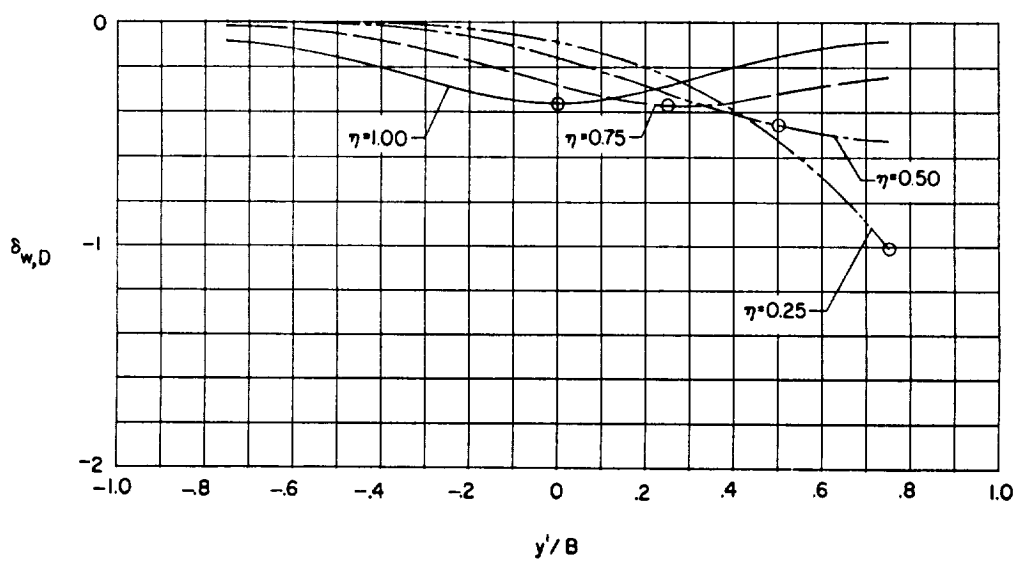


(c) $\chi = 60^{\circ}$.

Figure 68.- Concluded.

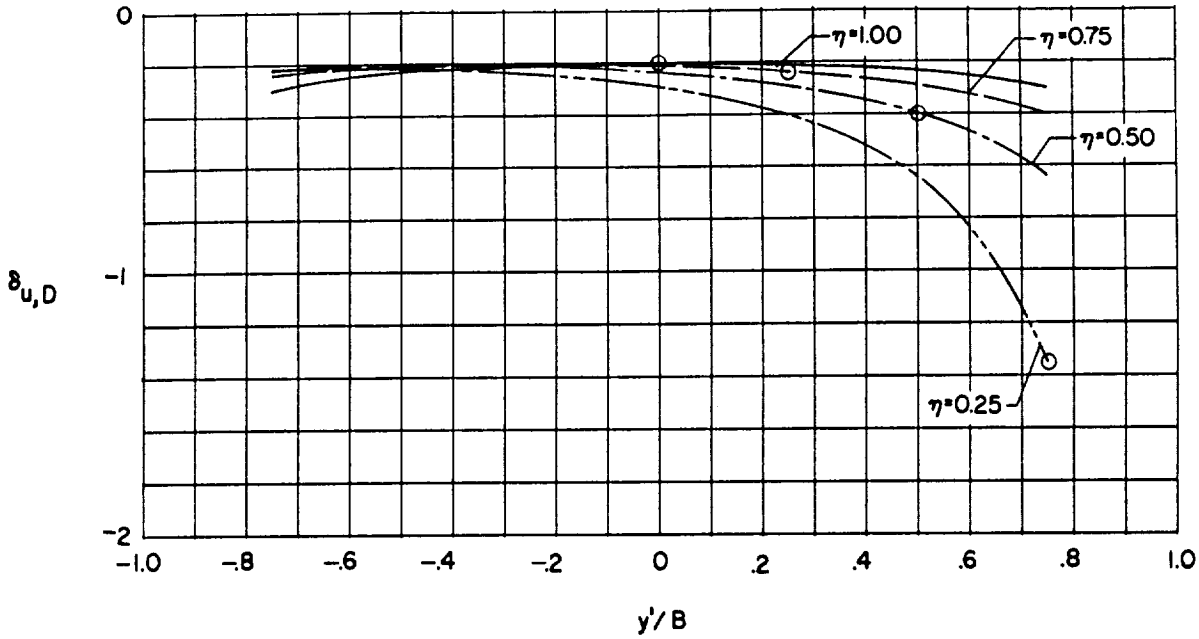


(a) $\chi = 0^{\circ}$.

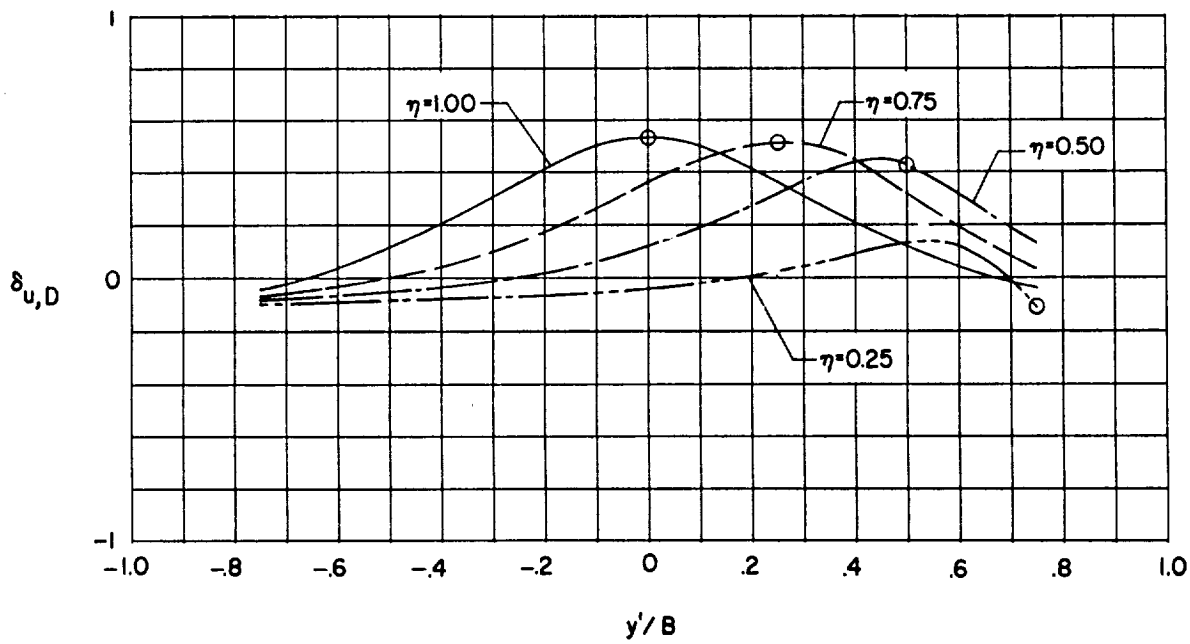


(b) $\chi = 30^{\circ}$.

Figure 69.- Lateral distribution of longitudinal interference due to drag for laterally offset small models in a closed wind tunnel. $\gamma = 2.0$; $\zeta = 1.0$; symbol denotes position of model. (Plot for $\chi = 90^{\circ}$ is omitted since $\delta_{u,D}$ is uniformly zero.)

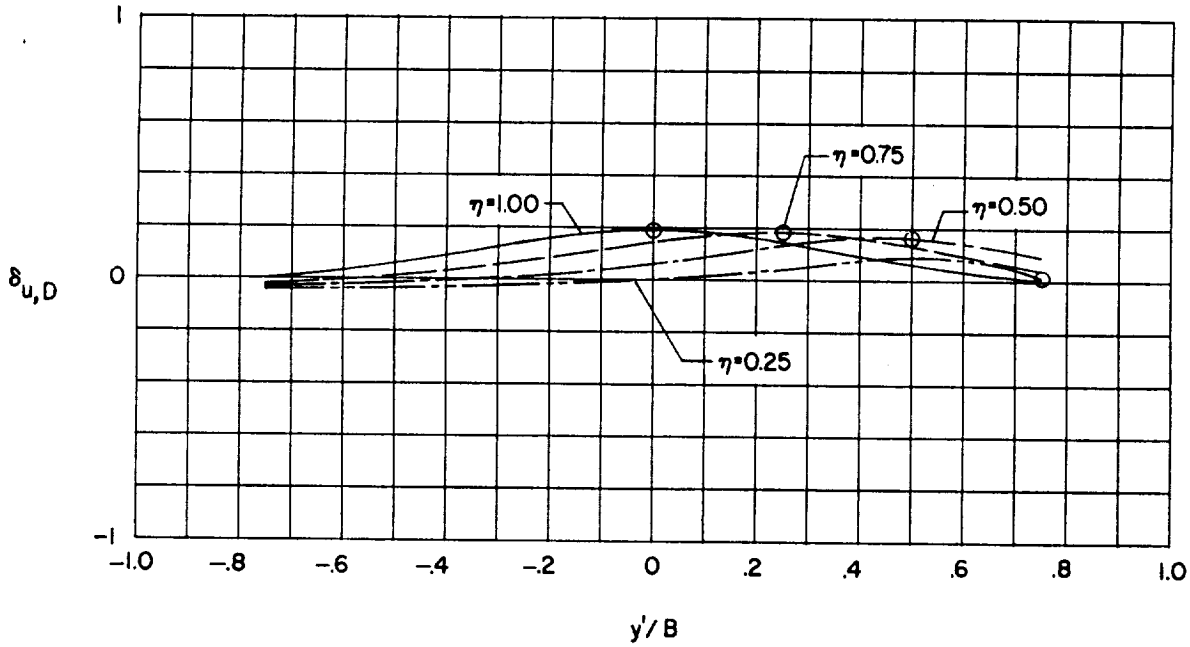


(c) $\chi = 60^{\circ}$.

Figure 69.- Concluded.

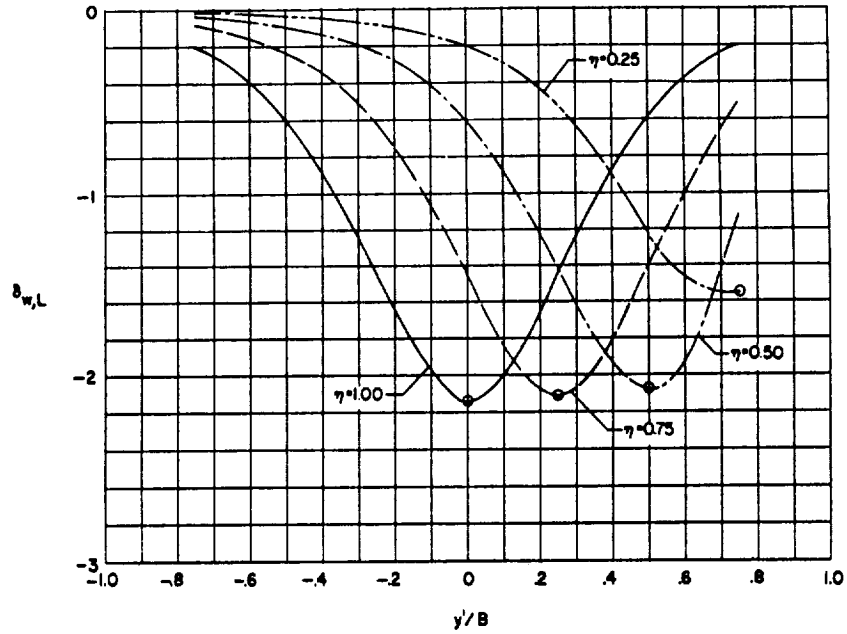


(a) $\chi = 0^{\circ}$.

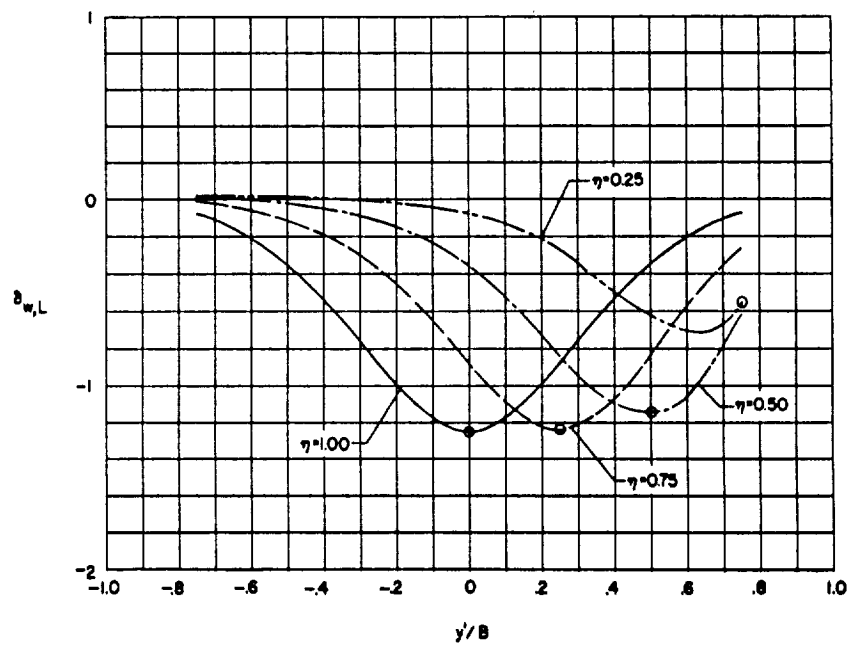


(b) $\chi = 30^{\circ}$.

Figure 70.- Lateral distribution of vertical interference due to lift for laterally offset small models in a wind tunnel which is closed on the bottom only. $\gamma = 2.0$; $\zeta = 1.0$; symbol denotes location of model.

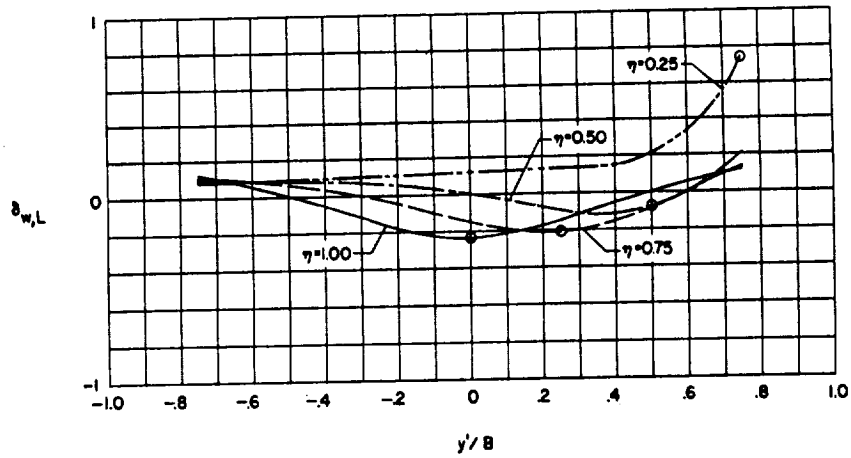


(c) $\chi = 60^{\circ}$.

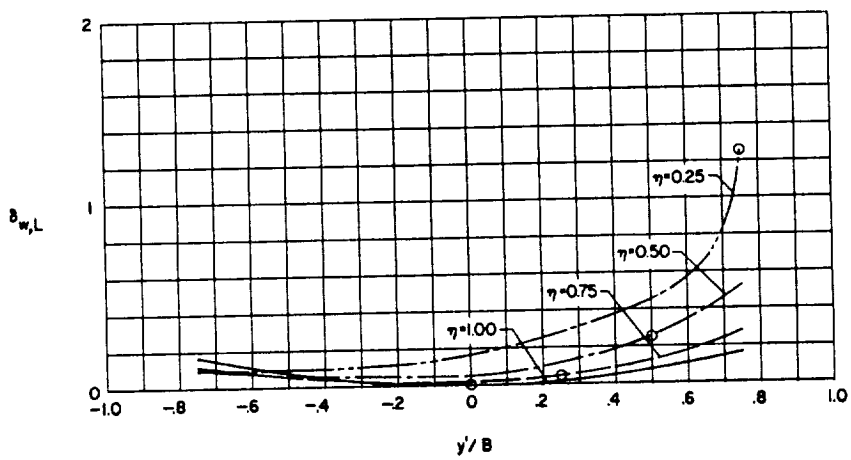


(d) $\chi = 90^{\circ}$.

**Figure 70.- Concluded.**

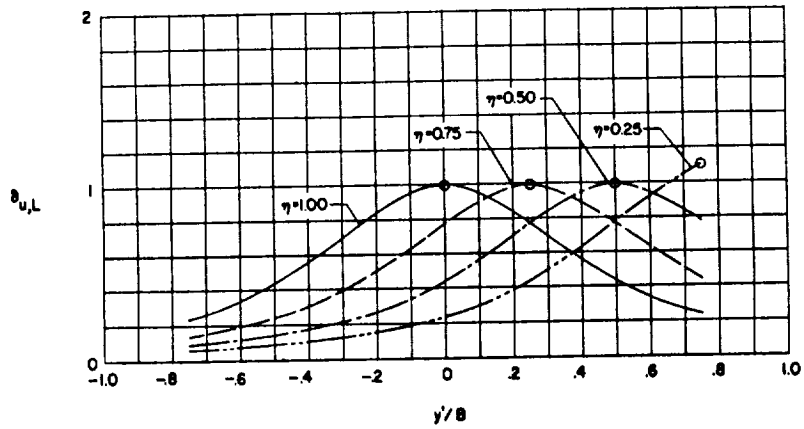


(a) $\chi = 30^{\circ}$.

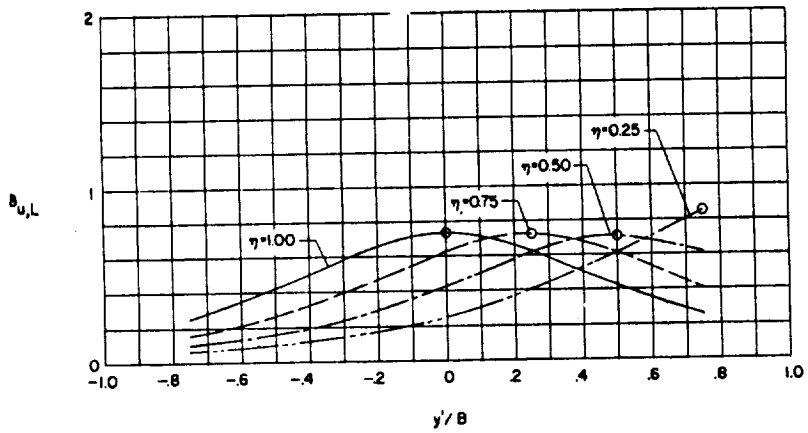


(b) $\chi = 60^{\circ}$.

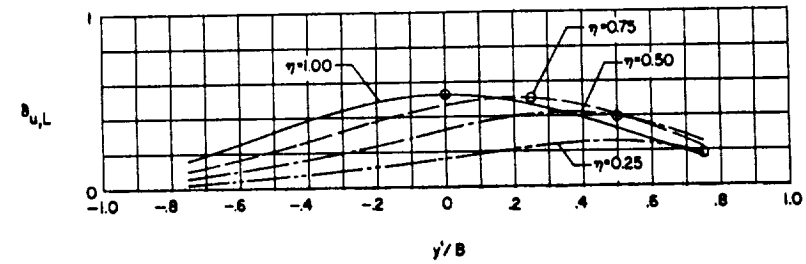


(c) $\chi = 90^{\circ}$.

Figure 71.- Lateral distribution of horizontal interference due to lift for laterally offset small models in a wind tunnel closed on the bottom only. $\gamma = 2.0$; $\zeta = 1.0$; symbol denotes position of model. Note that $\delta_{u,L}$ is uniformly zero for $\chi = 0^{\circ}$.

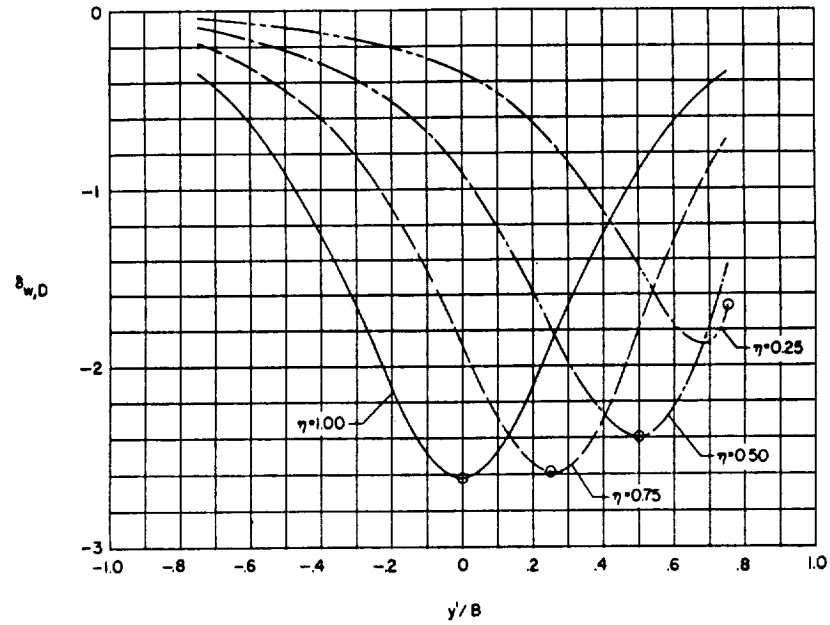


(a) $\chi = 0^{\circ}$.

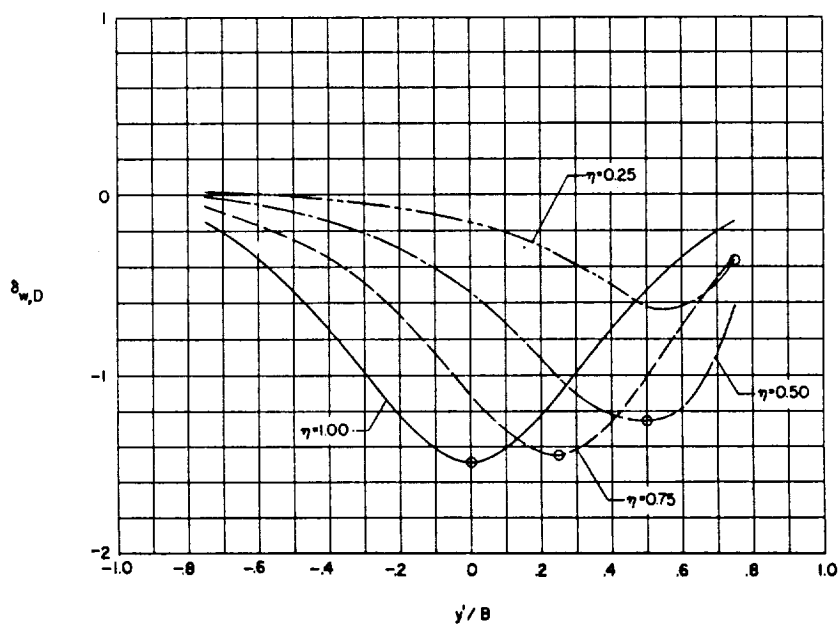


(b) $\chi = 30^{\circ}$.

Figure 72.- Lateral distribution of vertical interference due to drag for laterally offset small models in a wind tunnel which is closed on the bottom only. $\gamma = 2.0$; $\zeta = 1.0$; symbol denotes location of model.

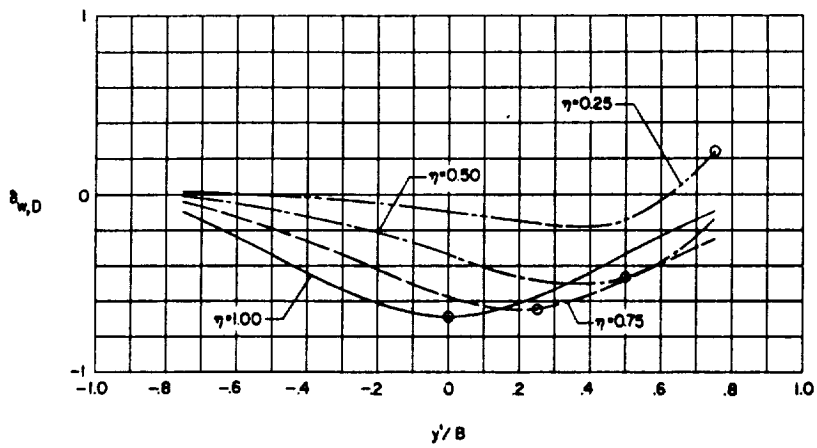


(c) $\chi = 60^{\circ}$.

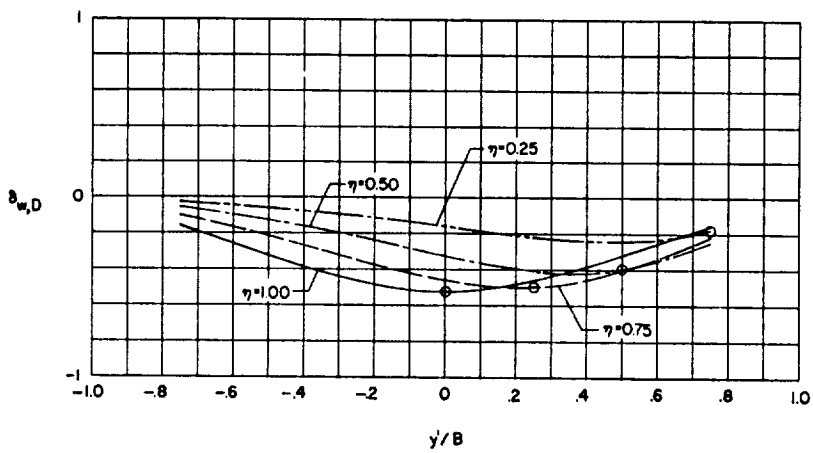


(d) $\chi = 90^{\circ}$.

Figure 72.- Concluded.

632643 O—62——12

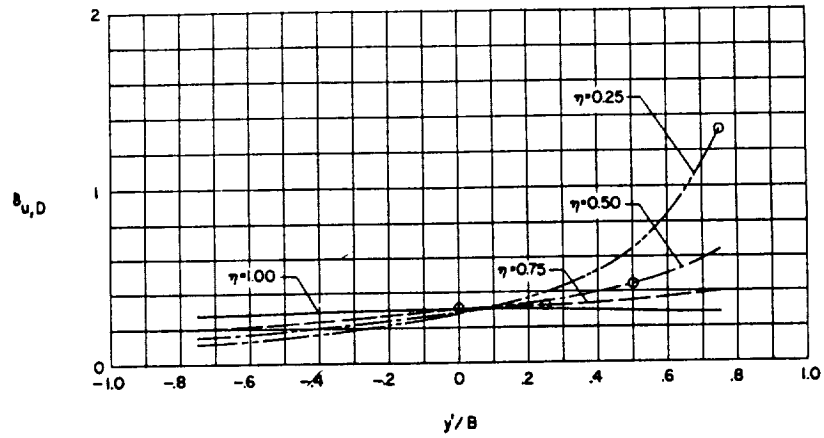


(a) $\chi = 0^{\circ}$.

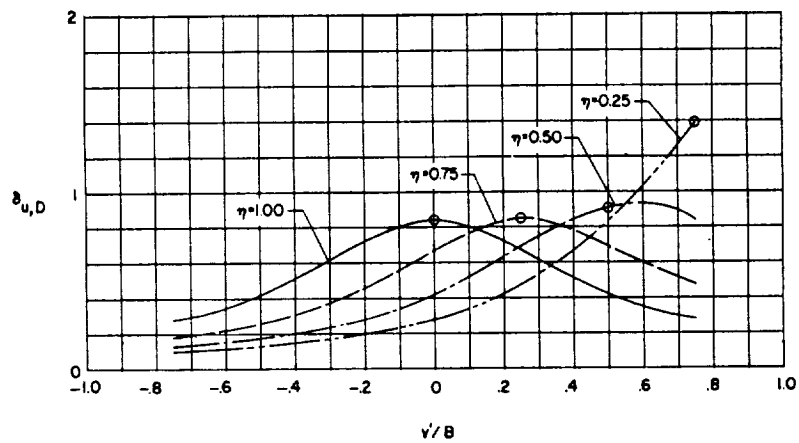


(b) $\chi = 30^{\circ}$.

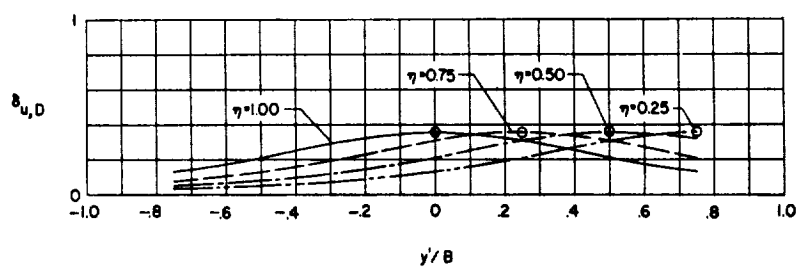


(c) $\chi = 60^{\circ}$.

Figure 73.- Lateral distribution of longitudinal interference due to drag for laterally offset small models in a wind tunnel which is closed on the bottom only. $\gamma = 2.0$; $\zeta = 1.0$; symbol denotes location of model. (Plot for $\chi = 90^{\circ}$ is omitted since $\delta_{u,D}$ is uniformly zero.)

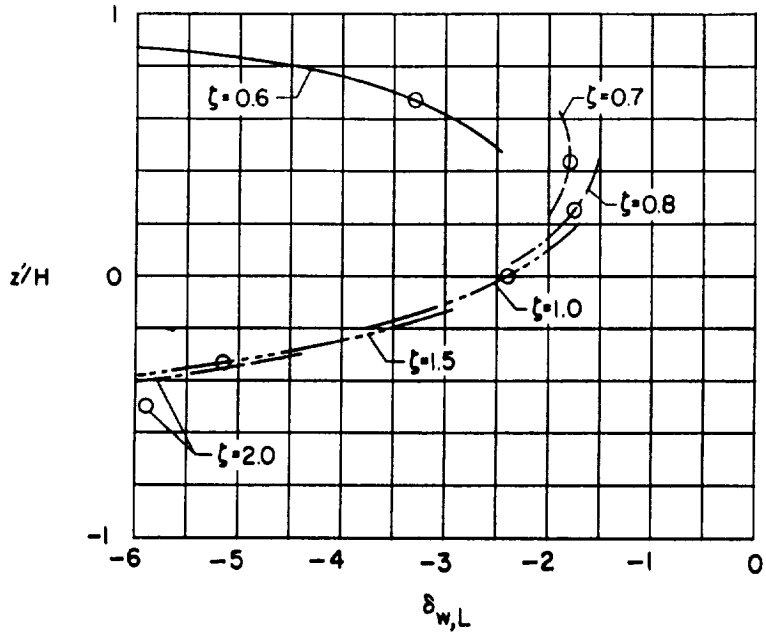


(a) $\chi = 0^{\circ}$.

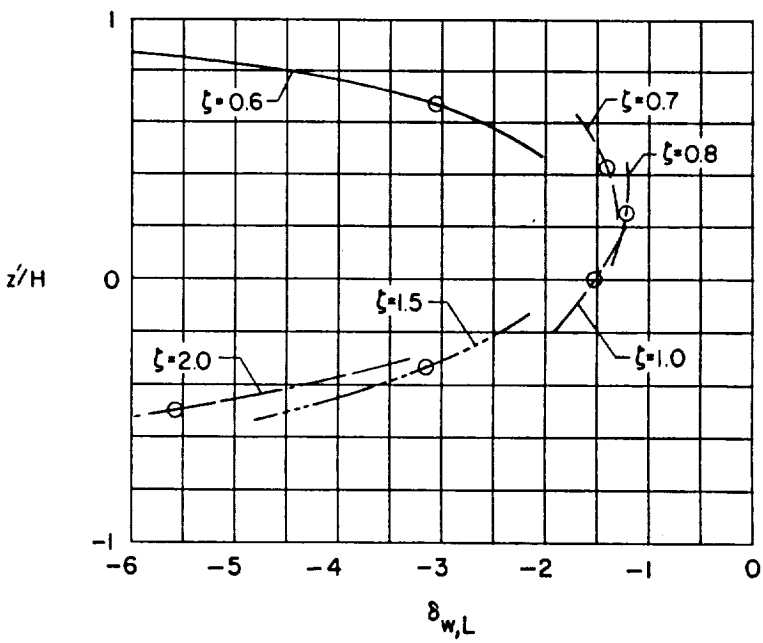


(b) $\chi = 30^{\circ}$.

Figure 74.- Vertical distribution of vertical interference due to lift for a small model in a closed wind tunnel. $\gamma = 2.0$; $\eta = 1.0$; symbol denotes location of model.

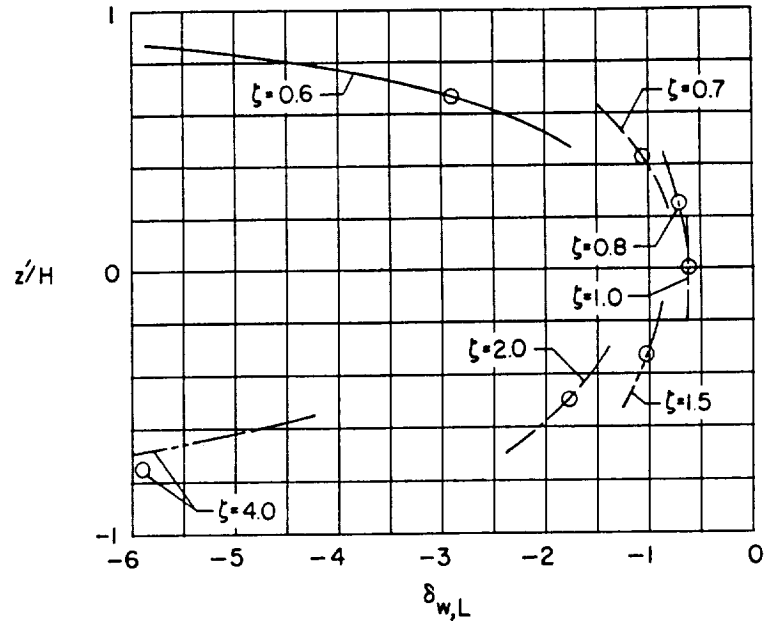


(c) $\chi = 60^{\circ}$.

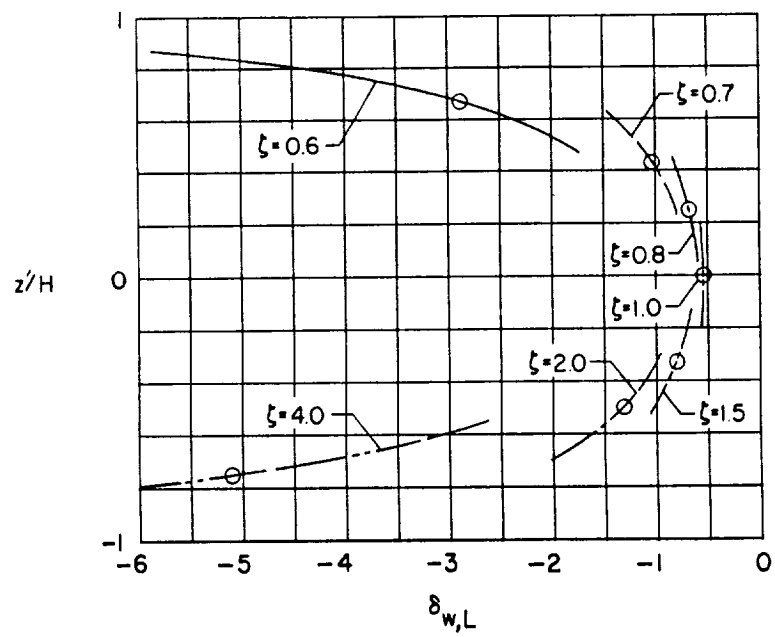


(d) $\chi = 90^{\circ}$.

Figure 74.- Concluded.

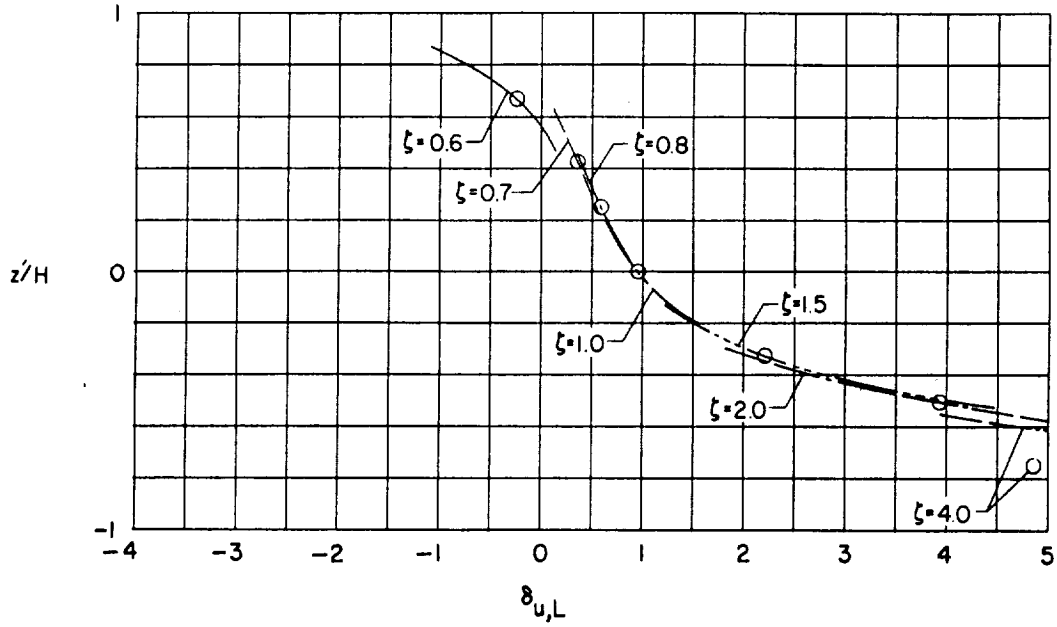


(a) $\chi = 30^{\circ}$.

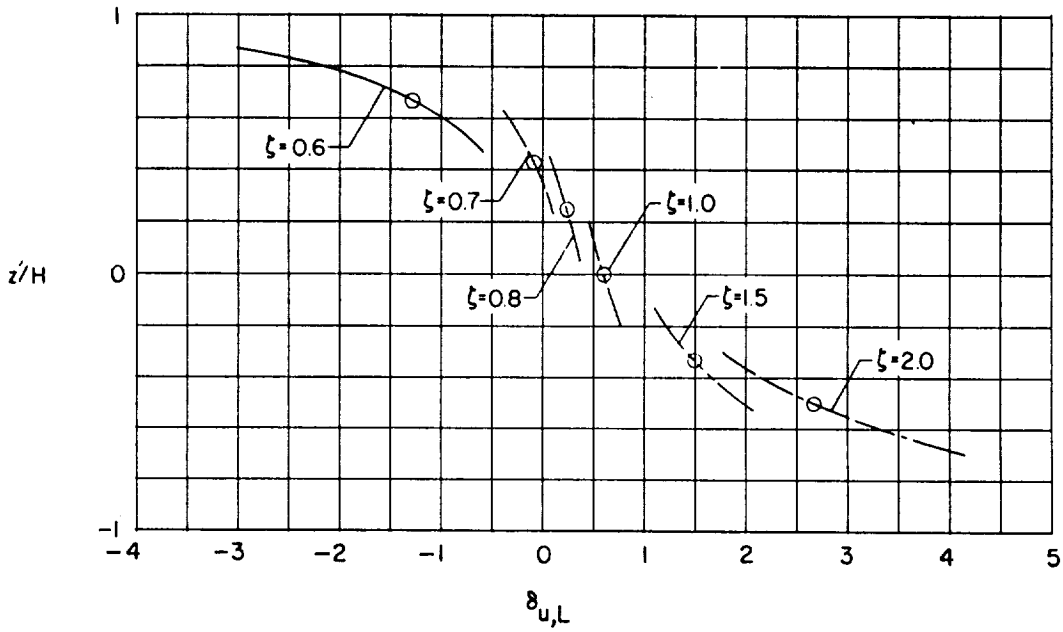


(b) $\chi = 60^{\circ}$.

Figure 75.- Vertical distribution of longitudinal interference due to lift for a small model in a closed wind tunnel. $\gamma = 2.0$; $\eta = 1.0$; symbol denotes location of model. (Plot for $\chi = 0^{\circ}$ is omitted since $\delta_{u,L}$ is zero for all values of $\zeta$.)

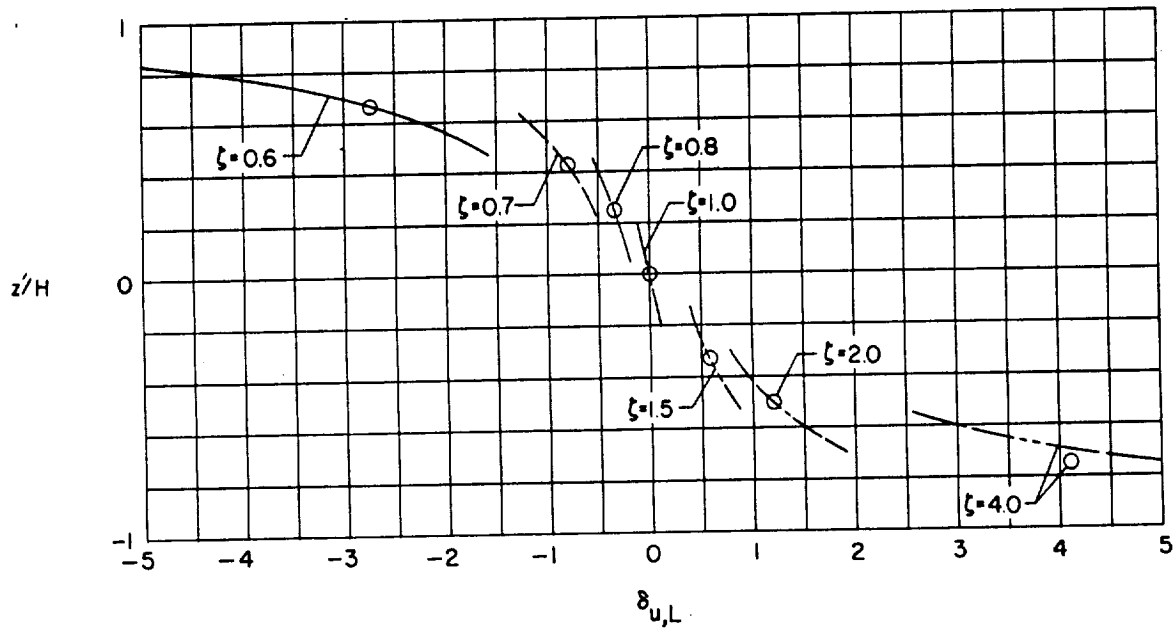


(c) $\chi = 90^{\circ}$.

Figure 75.- Concluded.

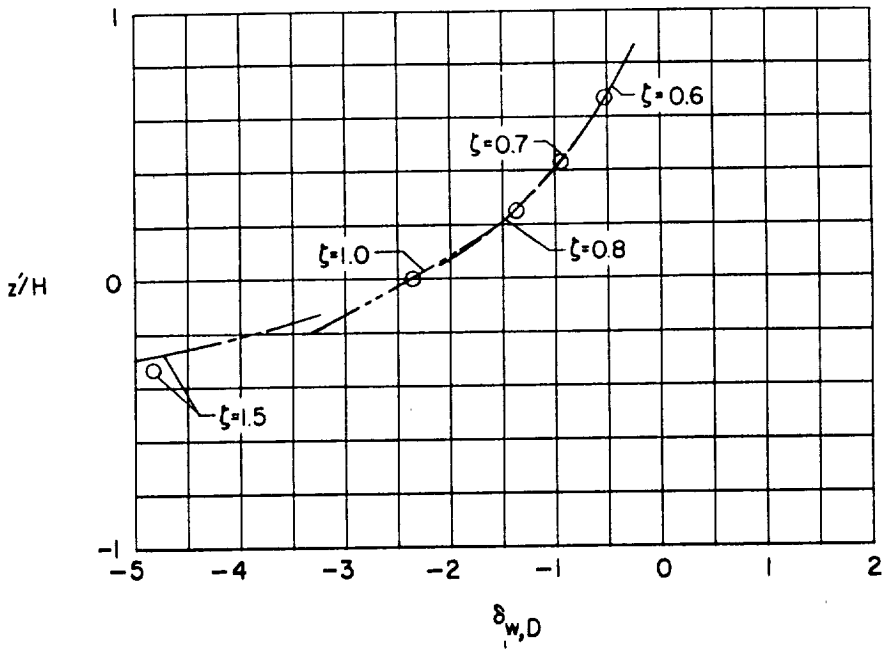


(a) $\chi = 0^{\circ}$.

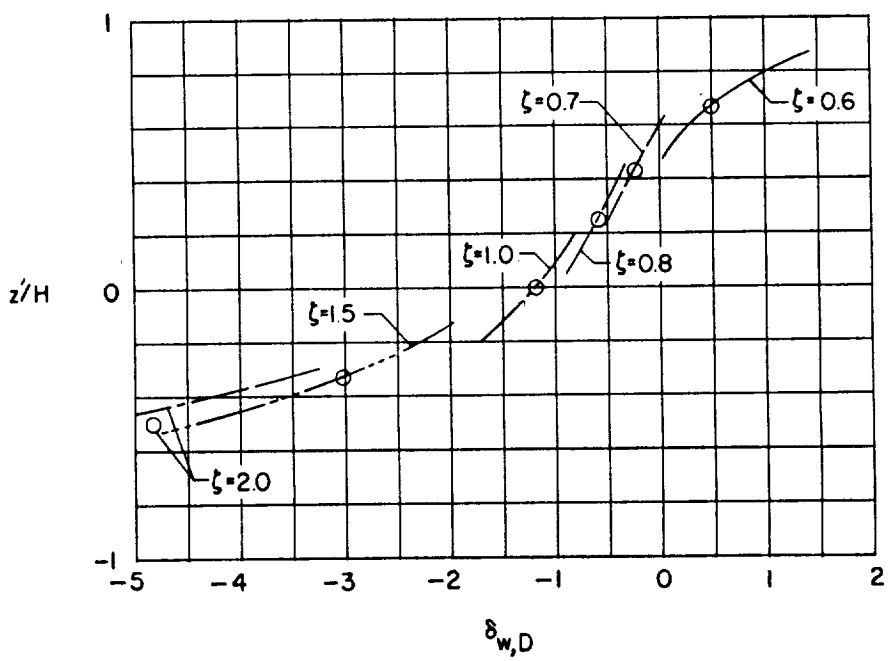


(b) $\chi = 30^{\circ}$.

Figure 76.- Vertical distribution of vertical interference due to drag for a small model in a closed wind tunnel. $\gamma = 2.0$; $\eta = 1.0$; symbol denotes location of model.

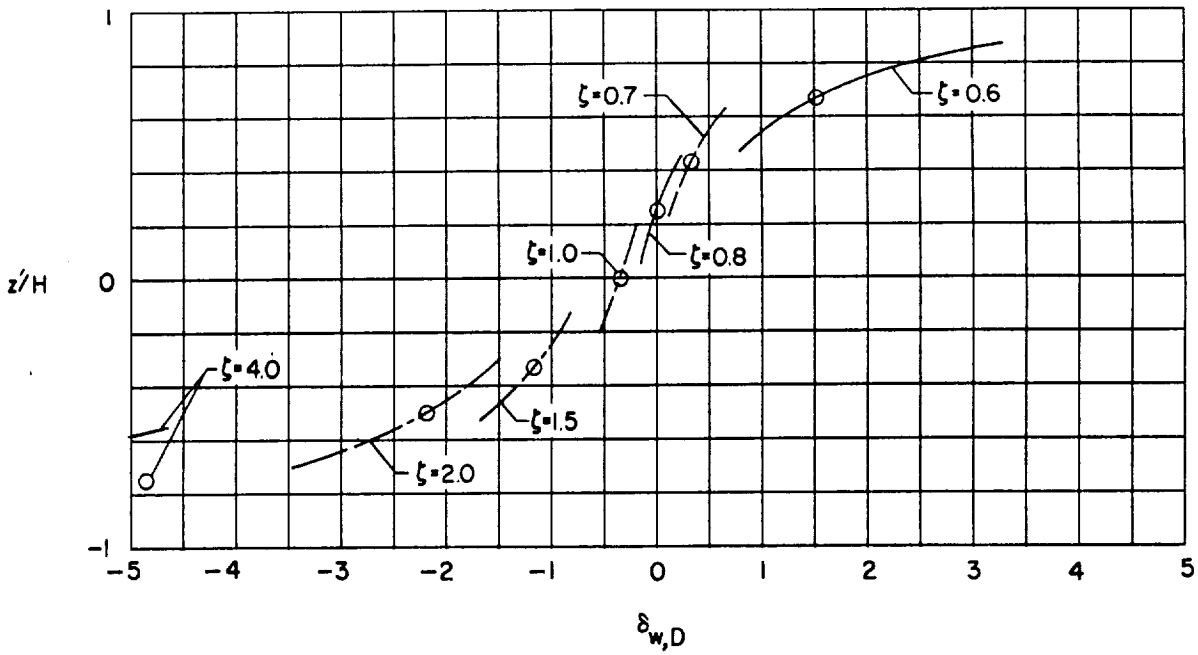


(c) $\chi = 60^{\circ}$.

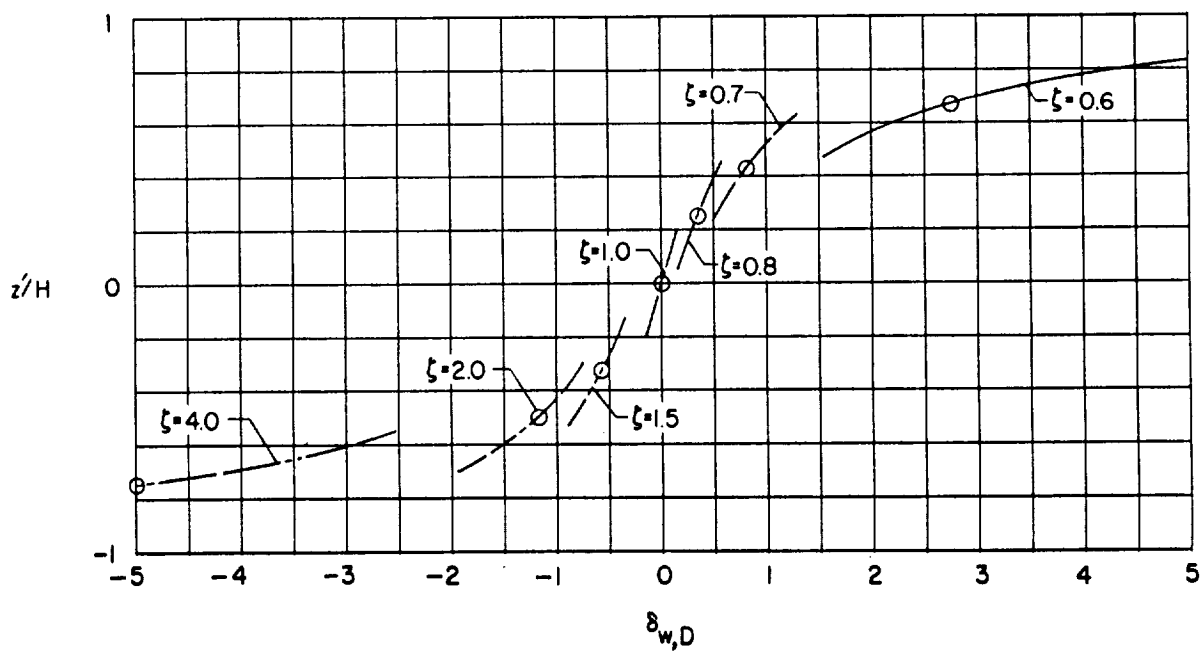


(d) $\chi = 90^{\circ}$.

Figure 76.- Concluded.

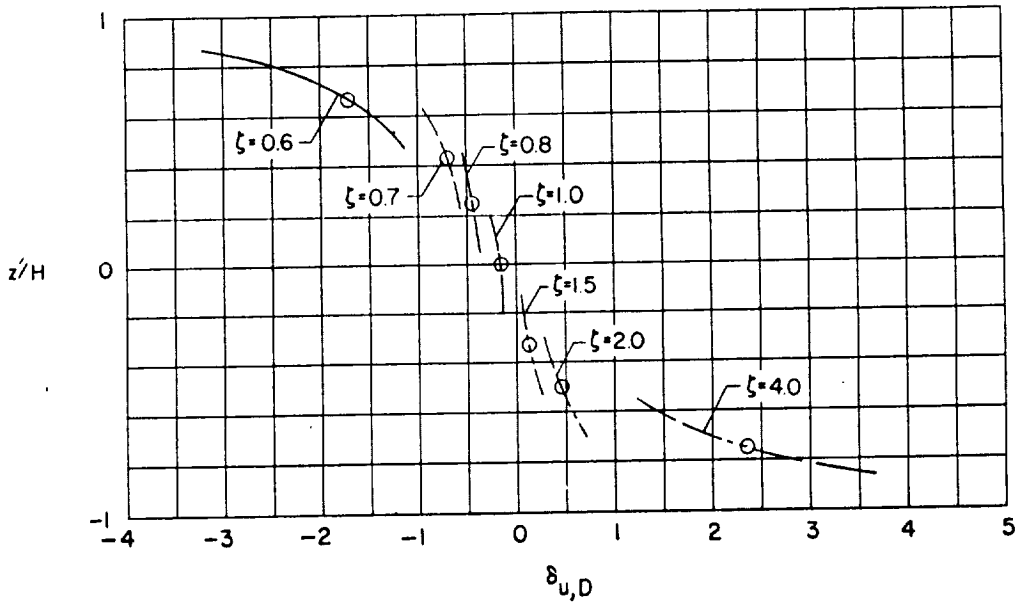


(a) $\chi = 0^{\circ}$.

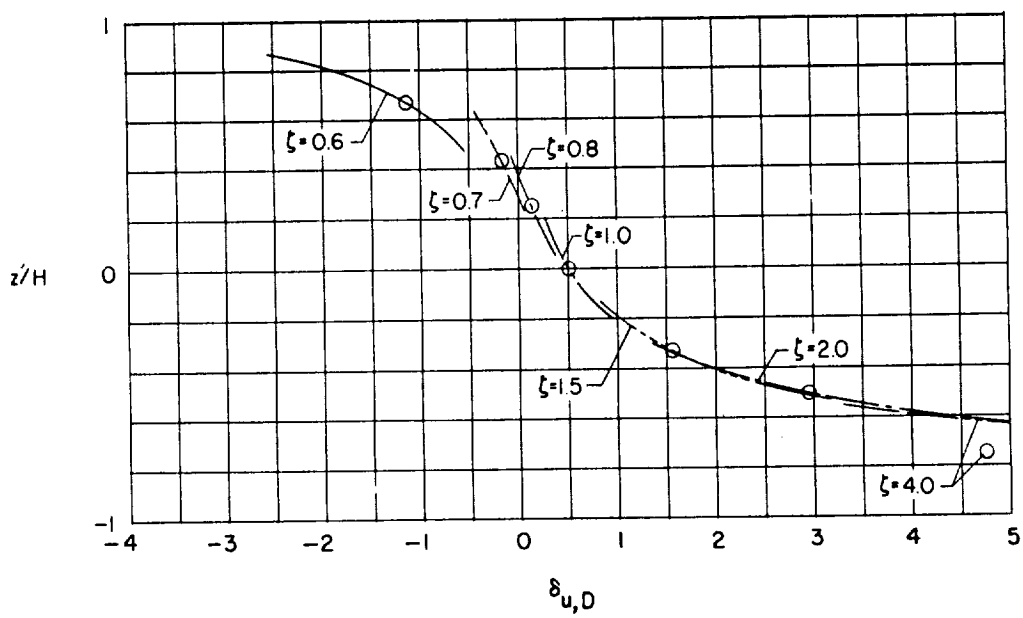


(b) $\chi = 30^{\circ}$.

Figure 77.- Vertical distribution of longitudinal interference due to drag for a small model in a closed wind tunnel. $\gamma = 2.0$; $\eta = 1.0$; symbol denotes location of model. (Plot for $\chi = 90^{\circ}$ is omitted since $\delta_{u,D}$ is zero for all values of $\zeta$.)

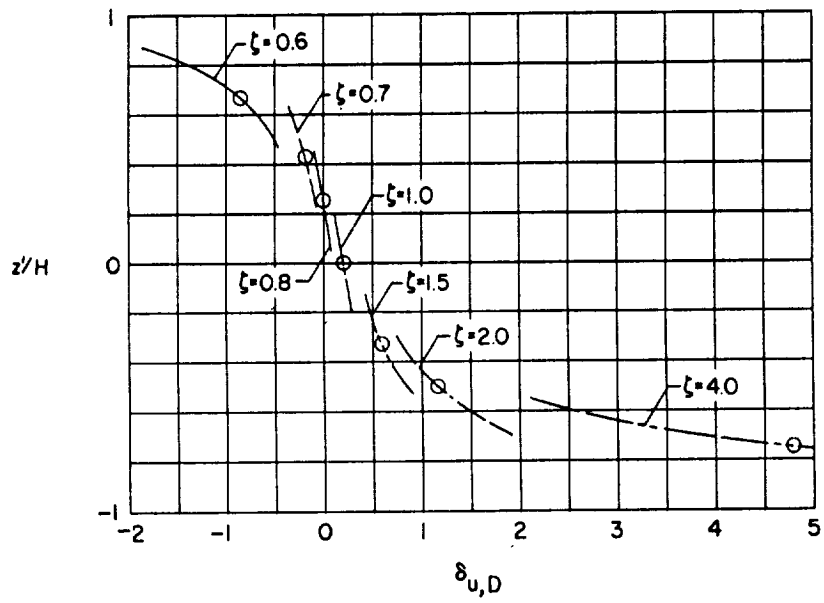


(c) $\chi = 60^{\circ}$.

Figure 77.- Concluded.

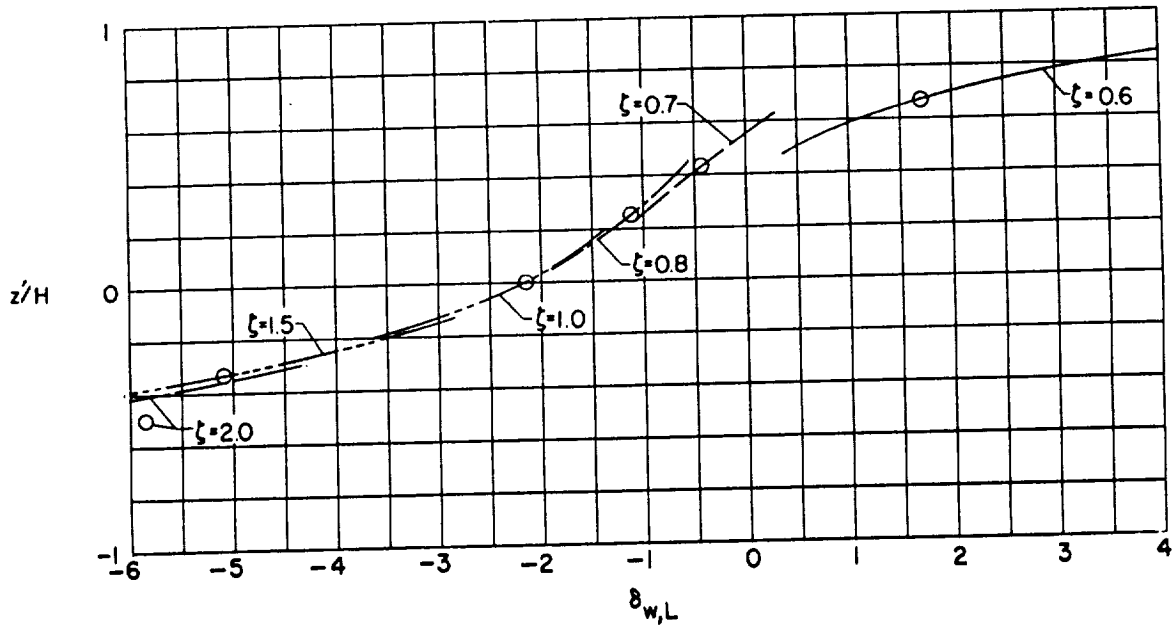


(a) $\chi = 0^{\circ}$.

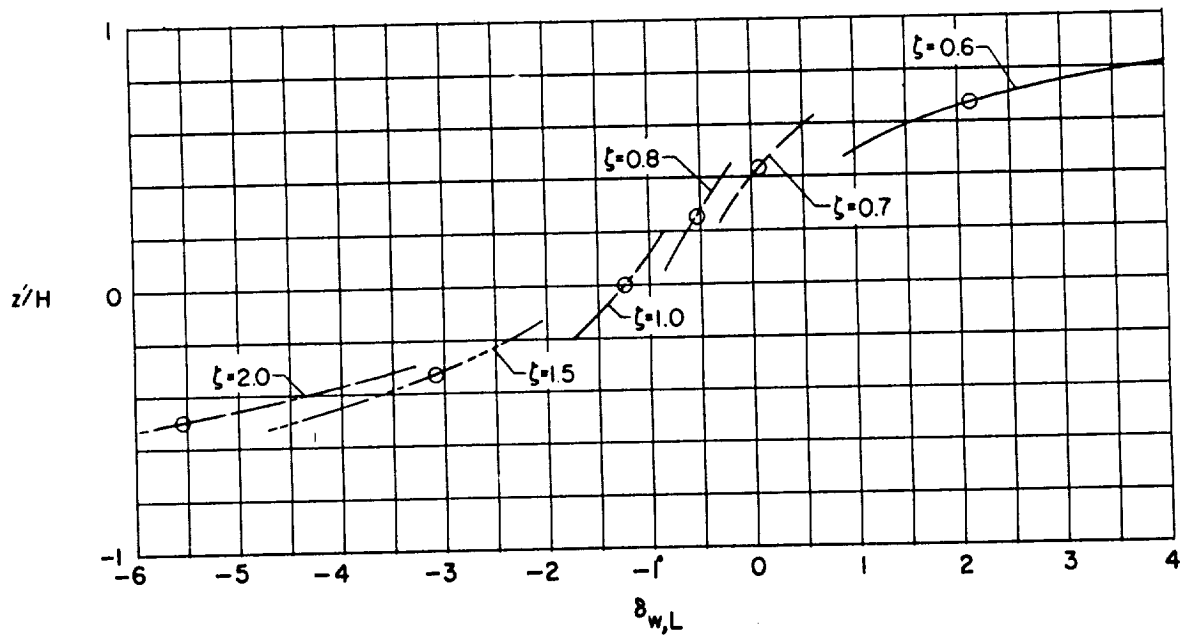


(b) $\chi = 30^{\circ}$.

Figure 78.- Vertical distribution of vertical interference due to lift for a small model in a wind tunnel which is closed on the bottom only. $\gamma = 2.0$; $\eta = 1.0$; symbol denotes location of model.

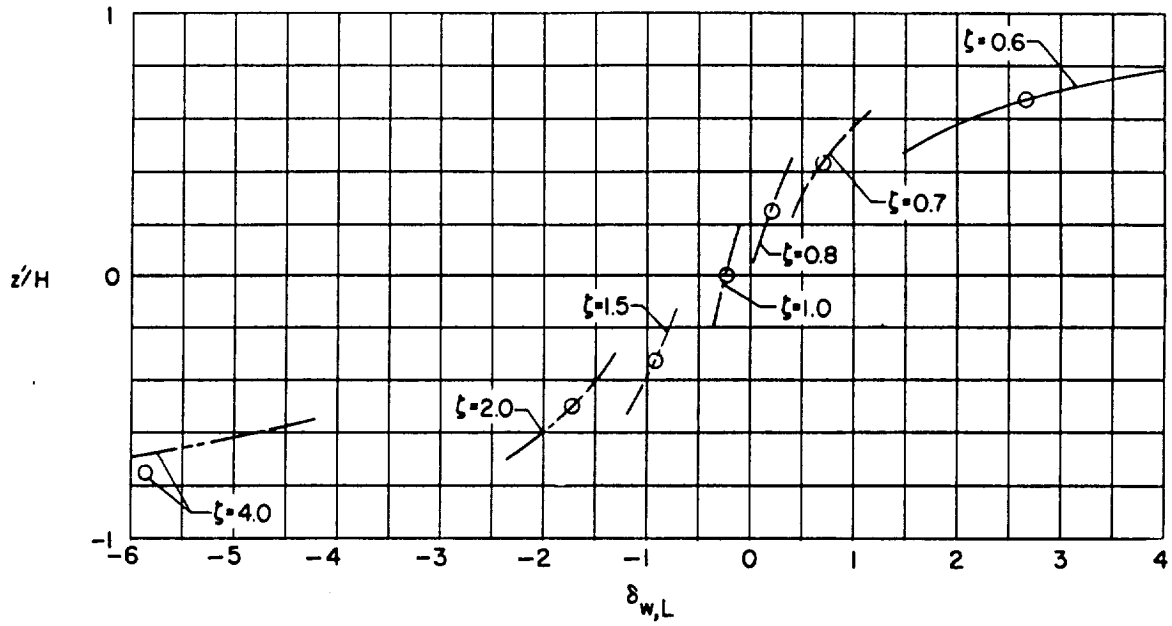


(c) X = 60°.

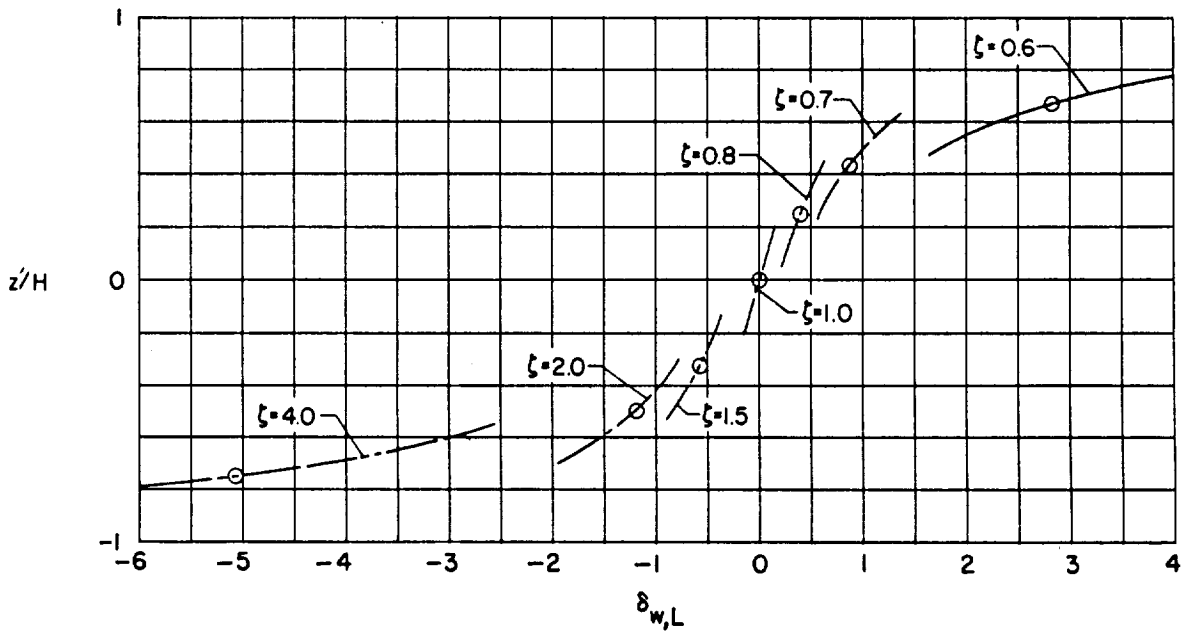


(d) X = 90°.

Figure 78.- Concluded.

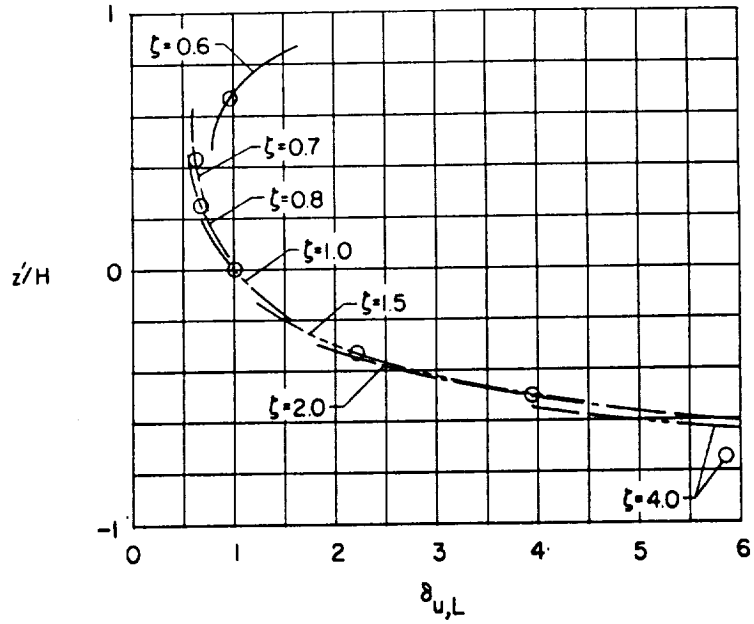


(a) $\chi = 30^{\circ}$.

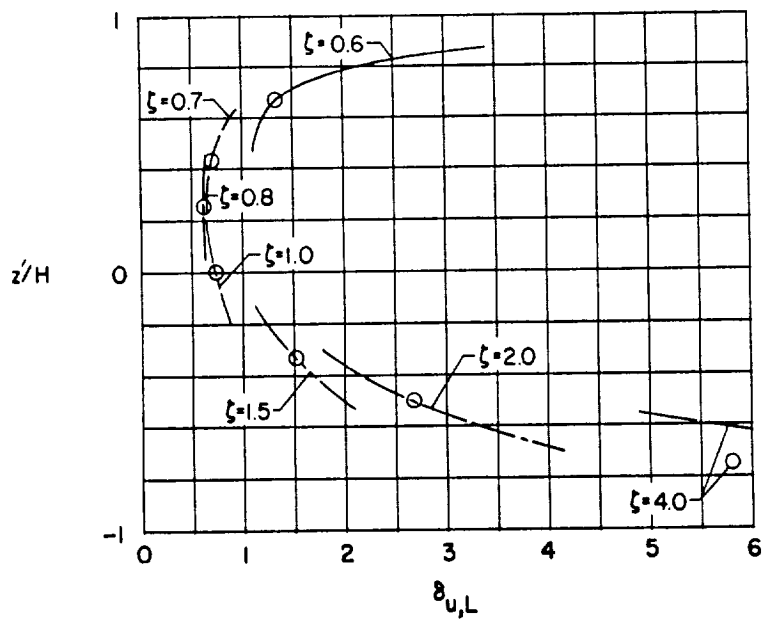


(b) $\chi = 60^{\circ}$

Figure 79.- Vertical distribution of longitudinal interference due to lift for a small model in a wind tunnel which is closed on the bottom only. $\gamma = 2.0$; $\eta = 1.0$; symbol denotes location of model. (Plot for $\chi = 0^{\circ}$ is omitted since $\delta_{u,L}$ is zero for all values of $\zeta$.)

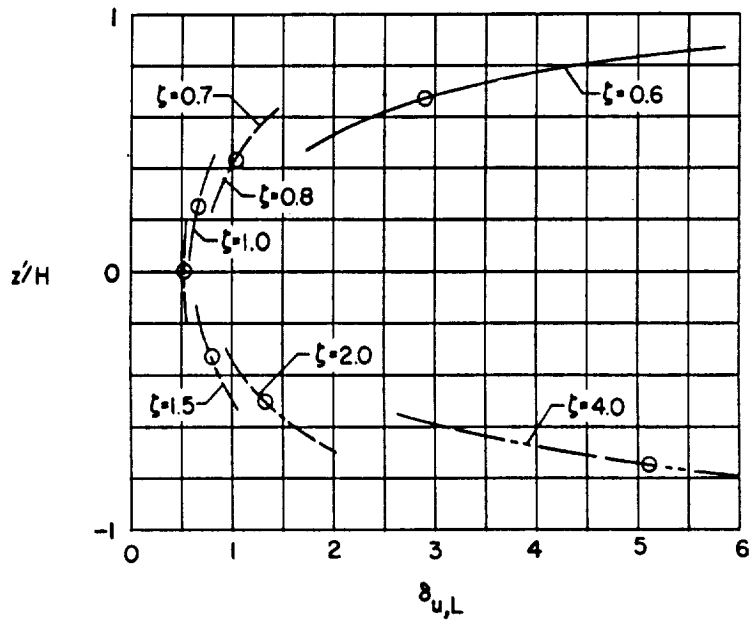


(c) $\chi = 90^{\circ}$.

Figure 79.- Concluded.

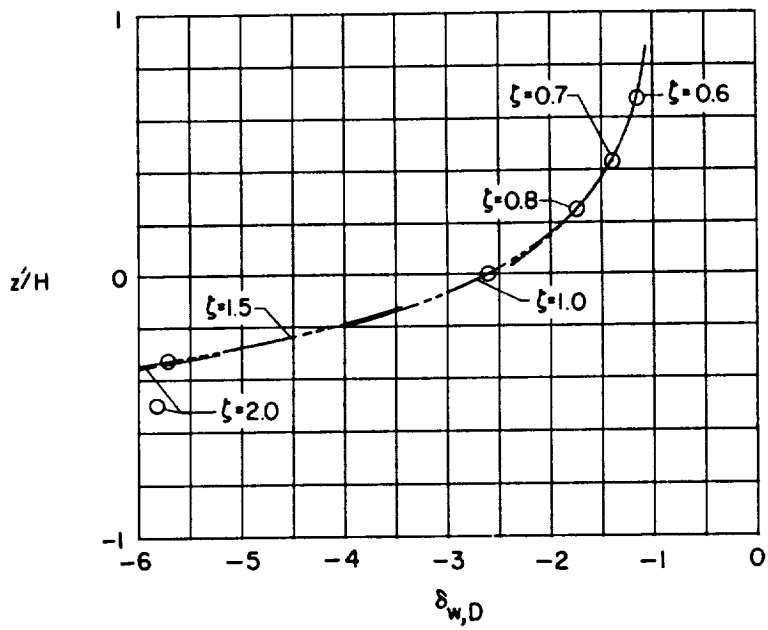


(a) $\chi = 0^{\circ}$.

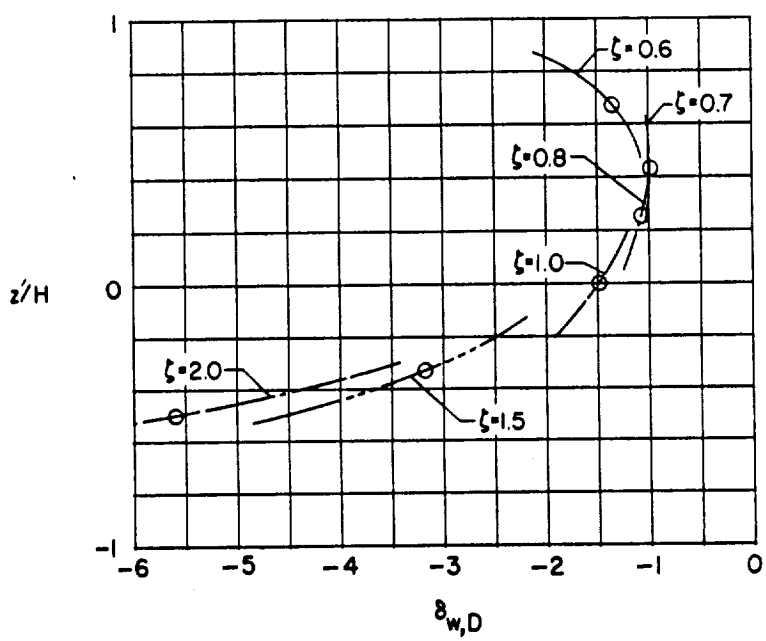


(b) $\chi = 30^{\circ}$.

Figure 80.- Vertical distribution of vertical interference due to drag for a small model in a wind tunnel which is closed on the bottom only. $\gamma = 2.0$; $\eta = 1.0$; symbol denotes location of model.

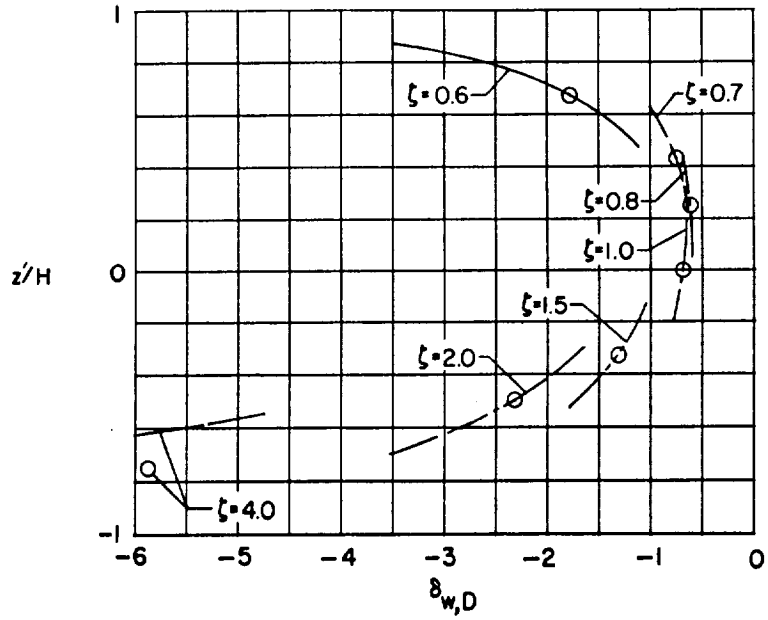


(c) $\chi = 60^{\circ}$.

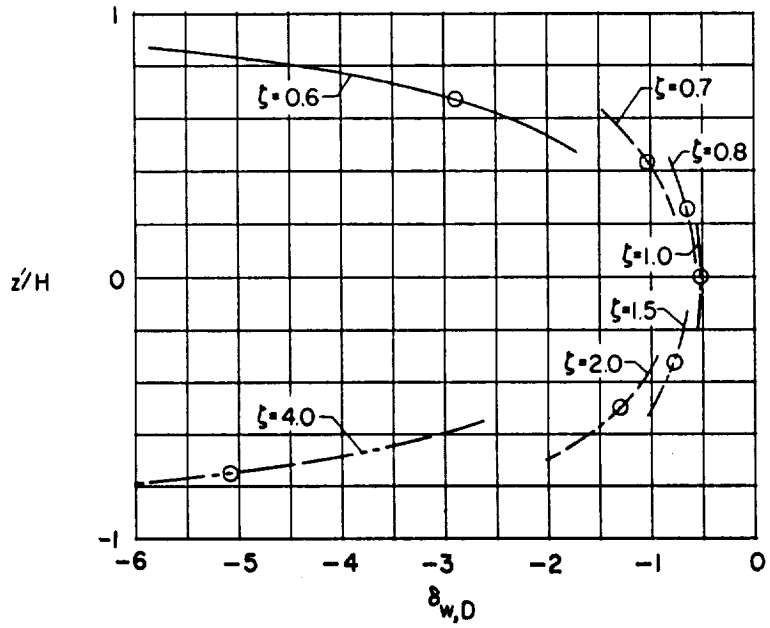


(d) $\chi = 90^{\circ}$.

Figure 80.- Concluded.

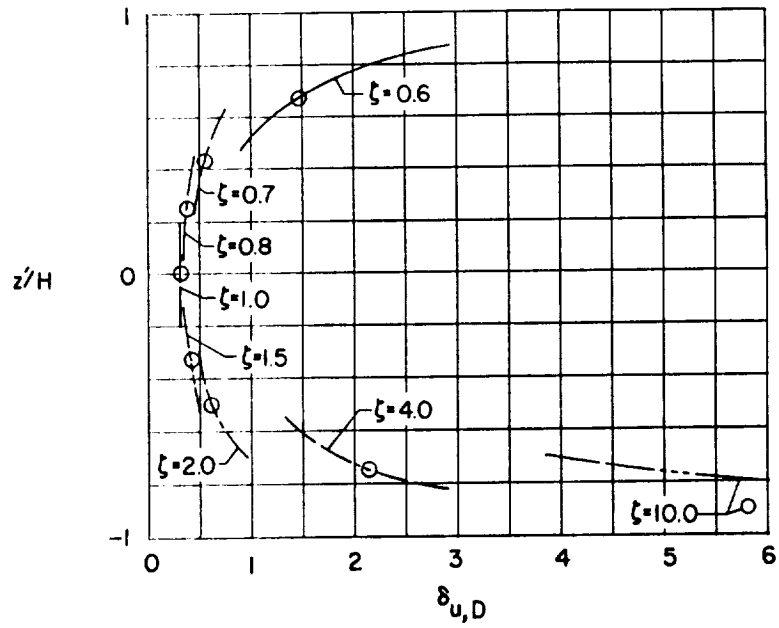


(a) $\chi = 0^{\circ}$.

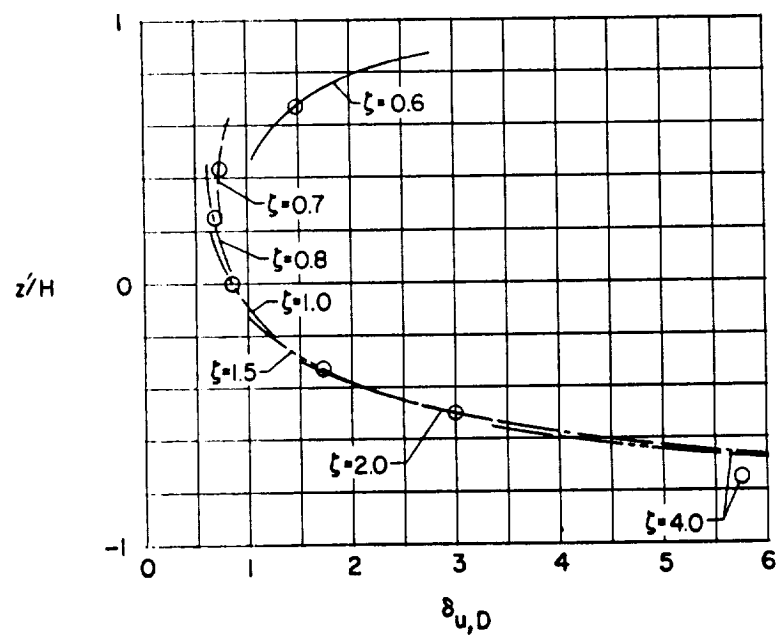


(b) $\chi = 30^{\circ}$.

Figure 81.- Vertical distribution of longitudinal interference due to drag for a small model in a wind tunnel which is closed on the bottom only. $\gamma = 2.0$; $\eta = 1.0$; symbol denotes location of model. (Plot for $\chi = 90^{\circ}$ is omitted since $\delta_{u,D}$ is zero for all values of $\zeta$.)

632043 O—62——13

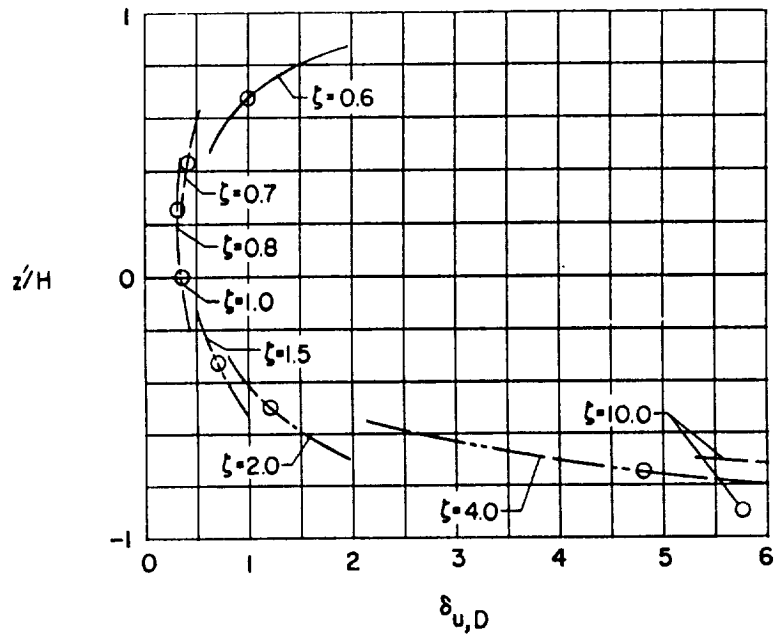


(c) $\chi = 60^{\circ}$.

Figure 81.- Concluded.

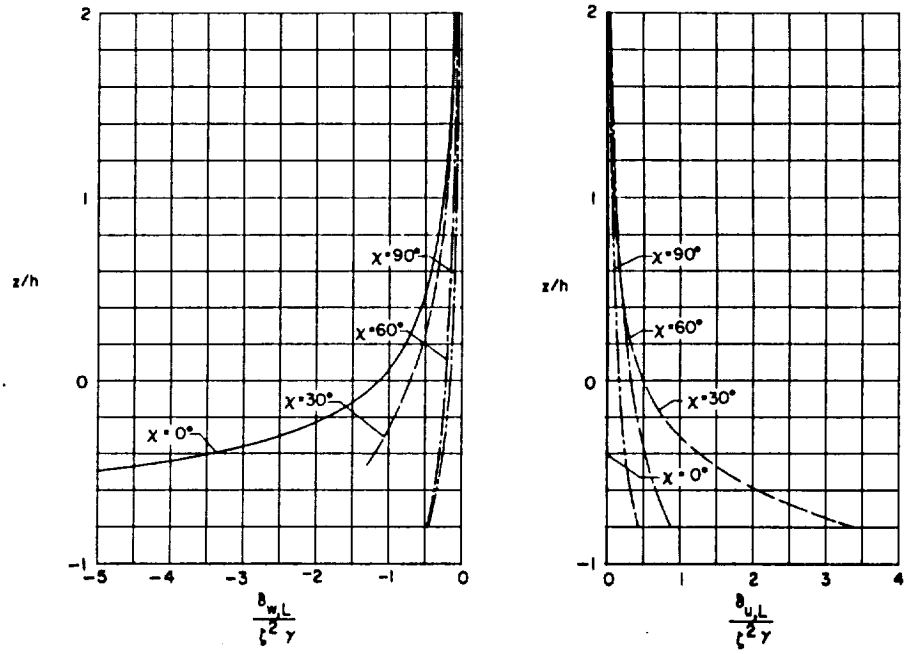


(a) Vertical interference due to lift.

(b) Longitudinal interference due to lift.

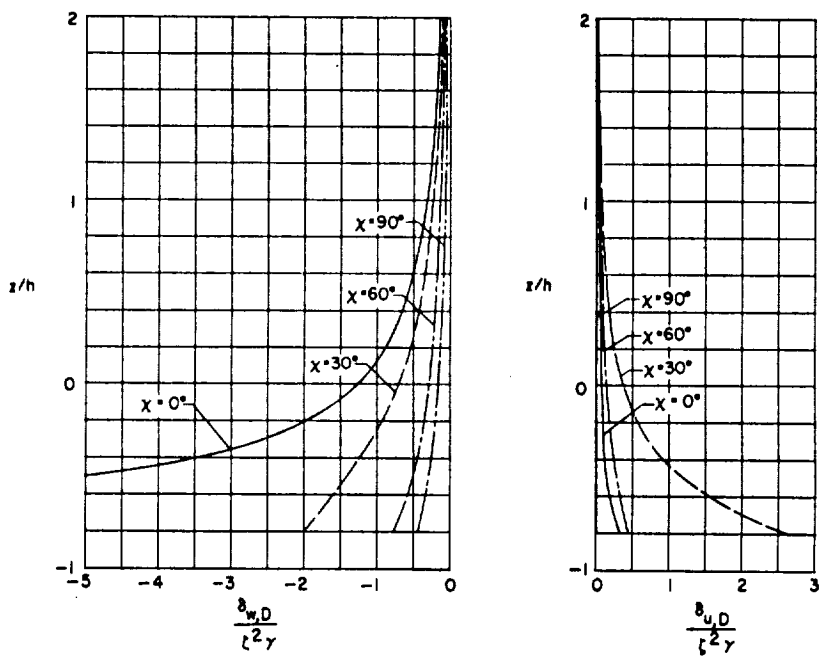


(c) Vertical interference due to drag.

(d) Longitudinal interference due to drag.

Figure 82.- Vertical distribution of interference factors in ground effect.

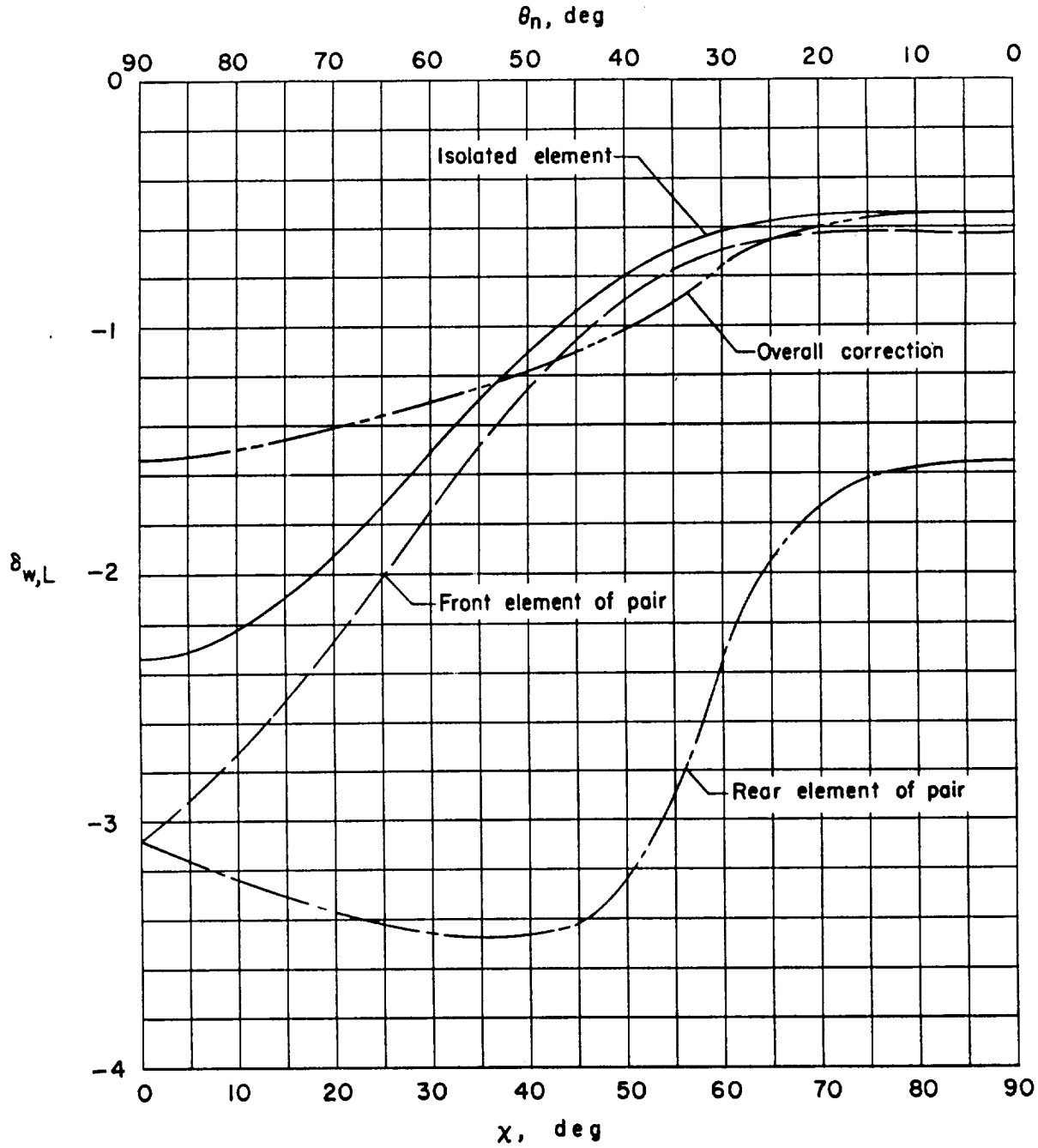


(a) Vertical interference due to lift.

Figure 83.- Correction factors for a two-element model centered in a closed wind tunnel with $\gamma = 2.0$. Elements are separated longitudinally by a distance equal to H. (Curve labeled "Overall correction" is based on $A_m$ of entire system.)

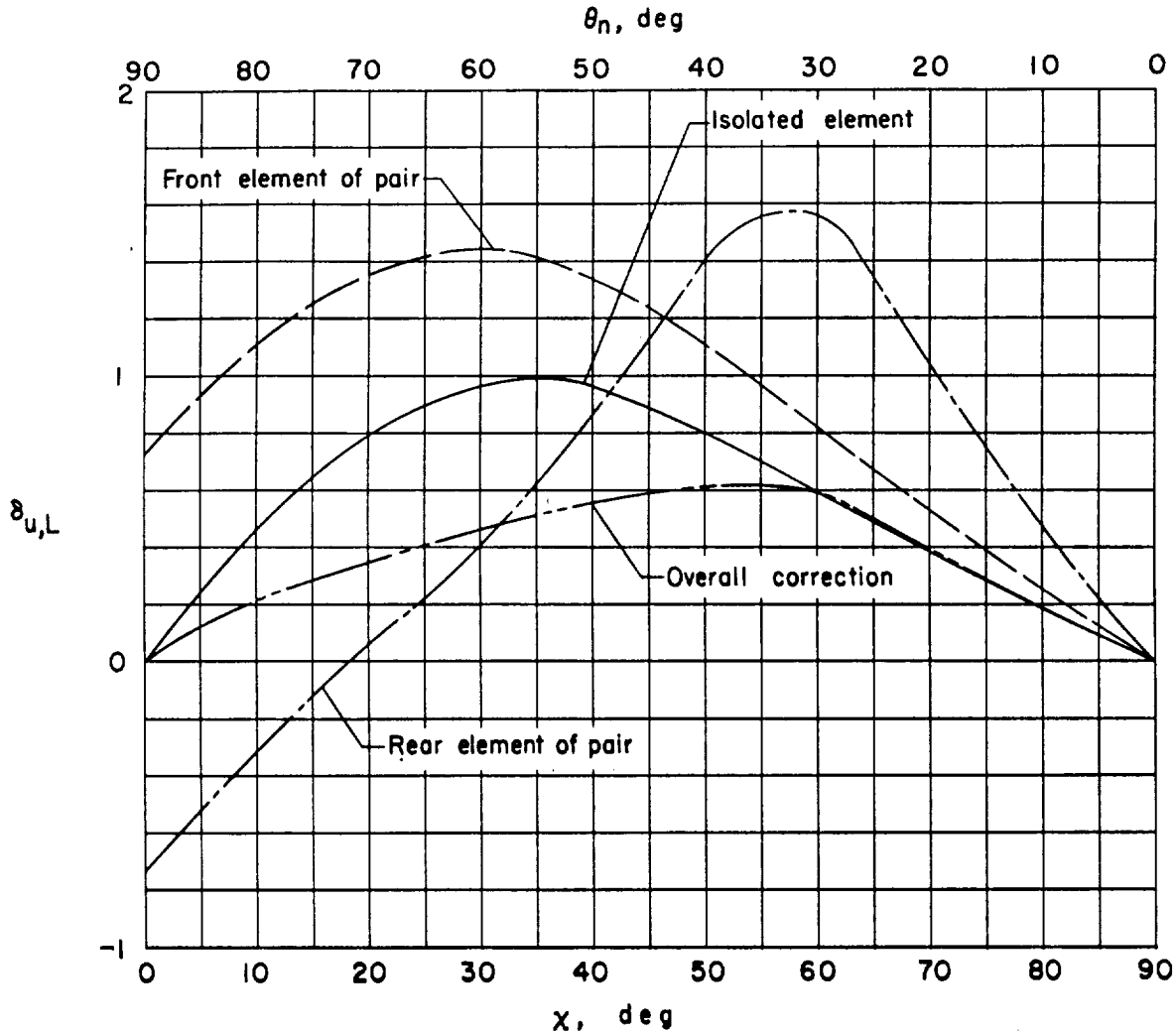


(b) Longitudinal interference due to lift.

Figure 83.- Continued.

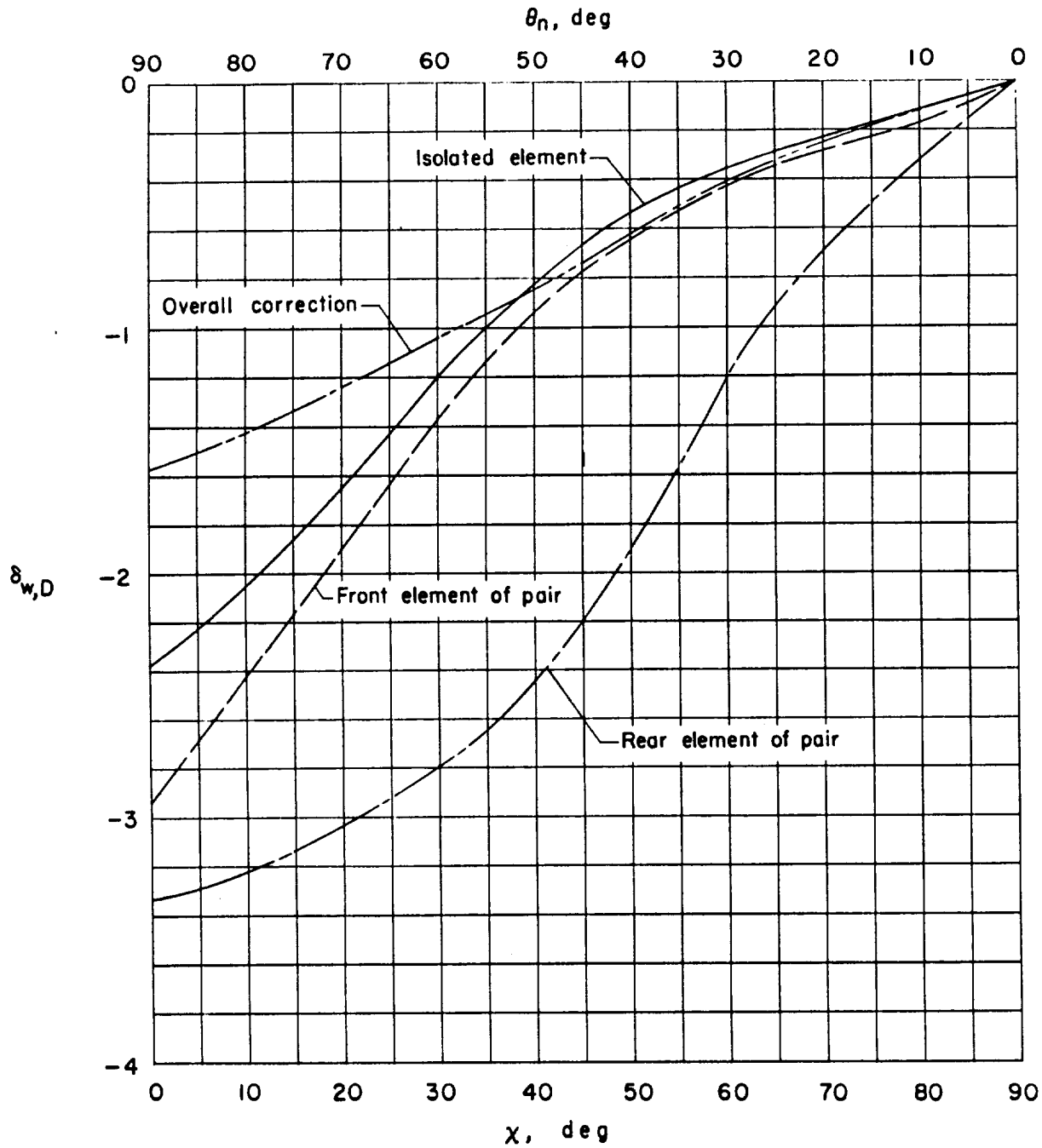


(c) Vertical interference due to drag.

Figure 83.- Continued.

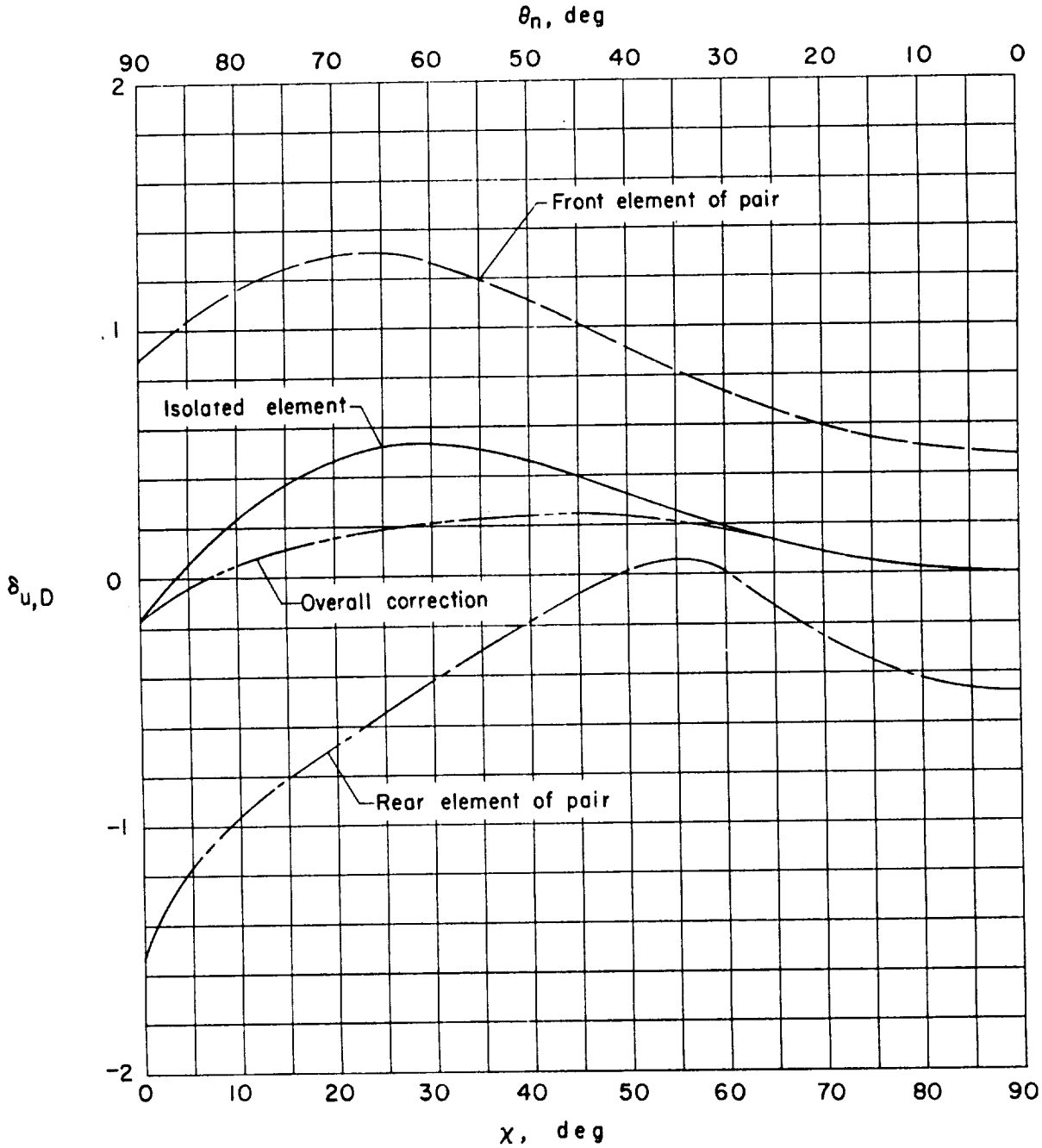


(d) Longitudinal interference due to drag.

Figure 83.- Concluded.

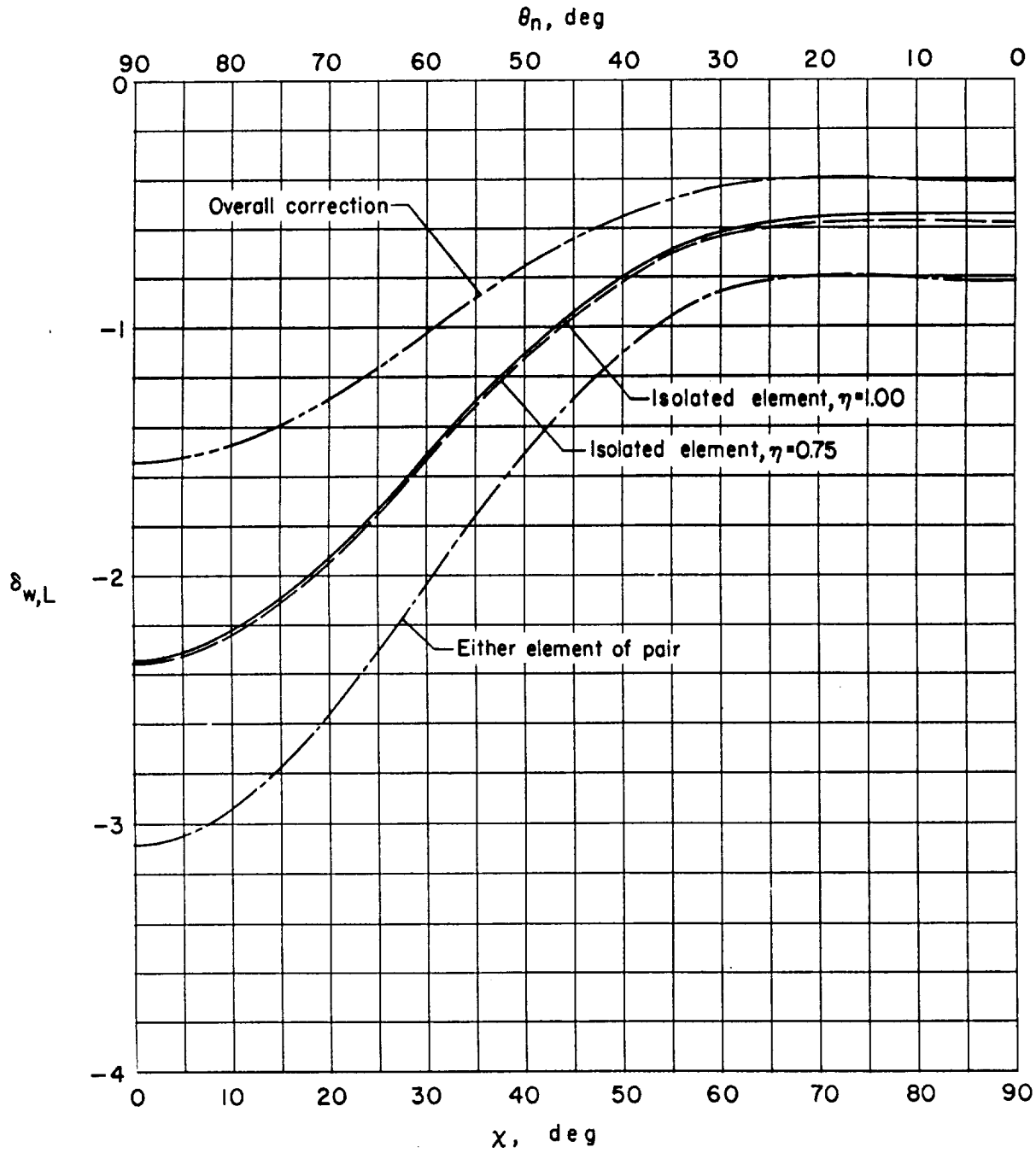


(a) Vertical interference due to lift.

Figure 84.- Correction factors for a two-element model centered in a closed wind tunnel with $\gamma = 2.0$. Elements are separated laterally by a distance equal to H. (Curve labeled "Overall correction" is based on $A_m$ of entire system.)

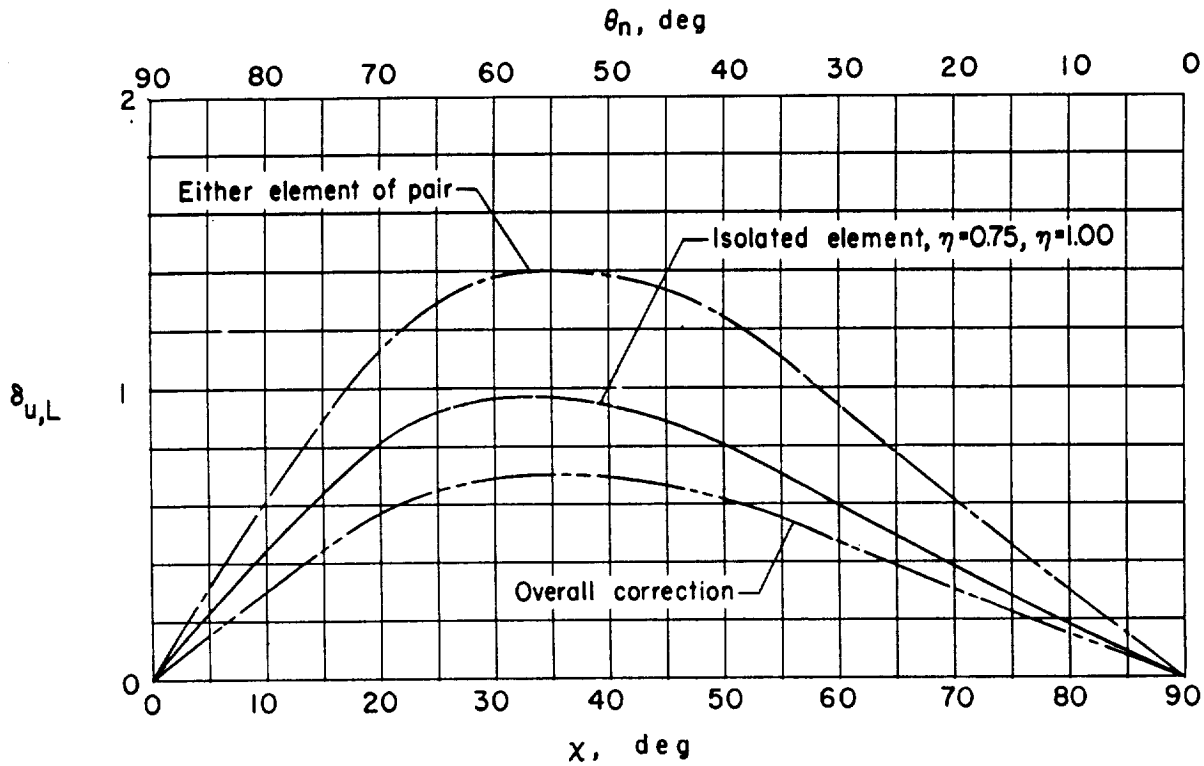


(b) Longitudinal interference due to lift.

Figure 84.- Continued.

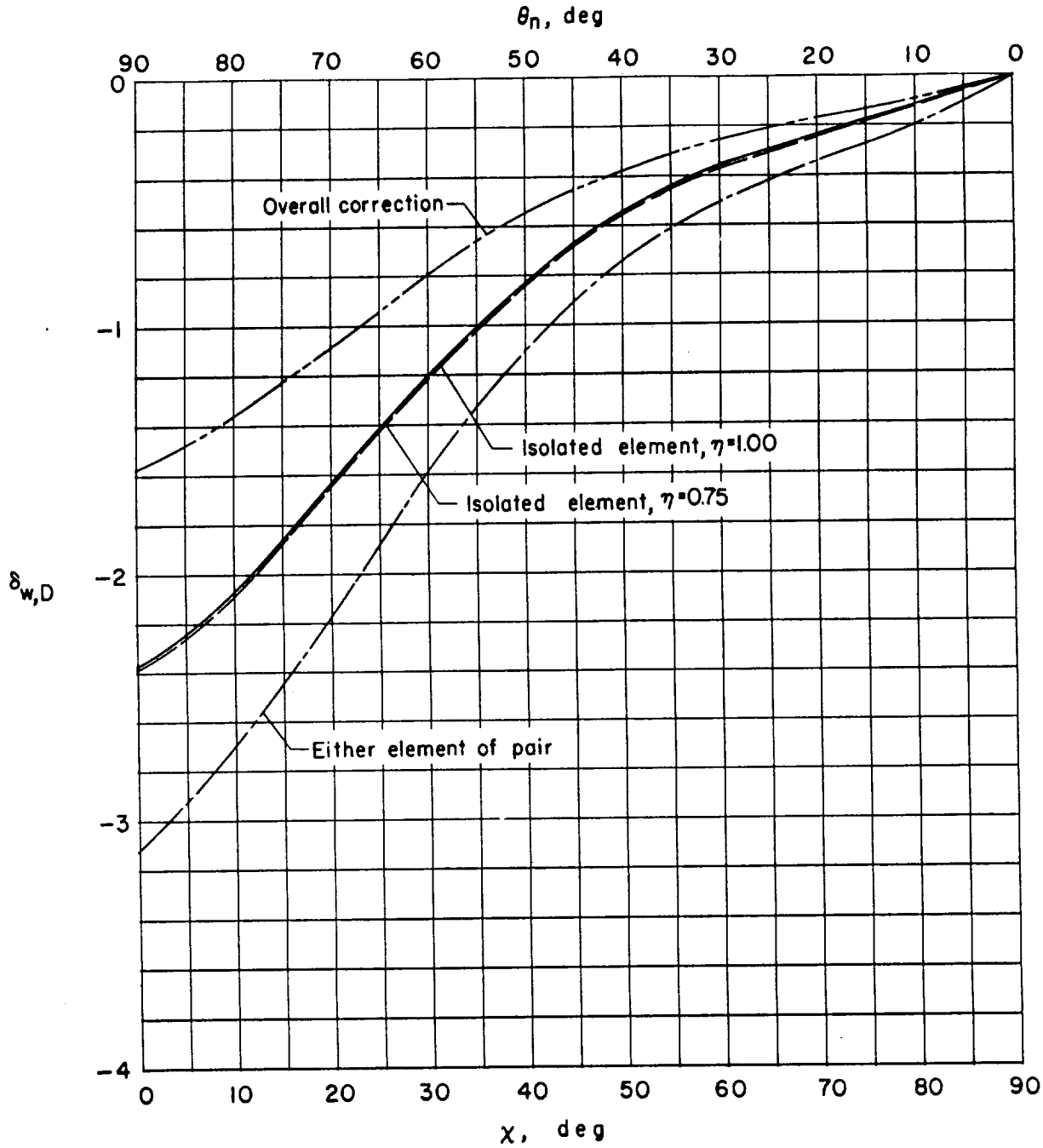


(c) Vertical interference due to drag.

Figure 84.- Continued.

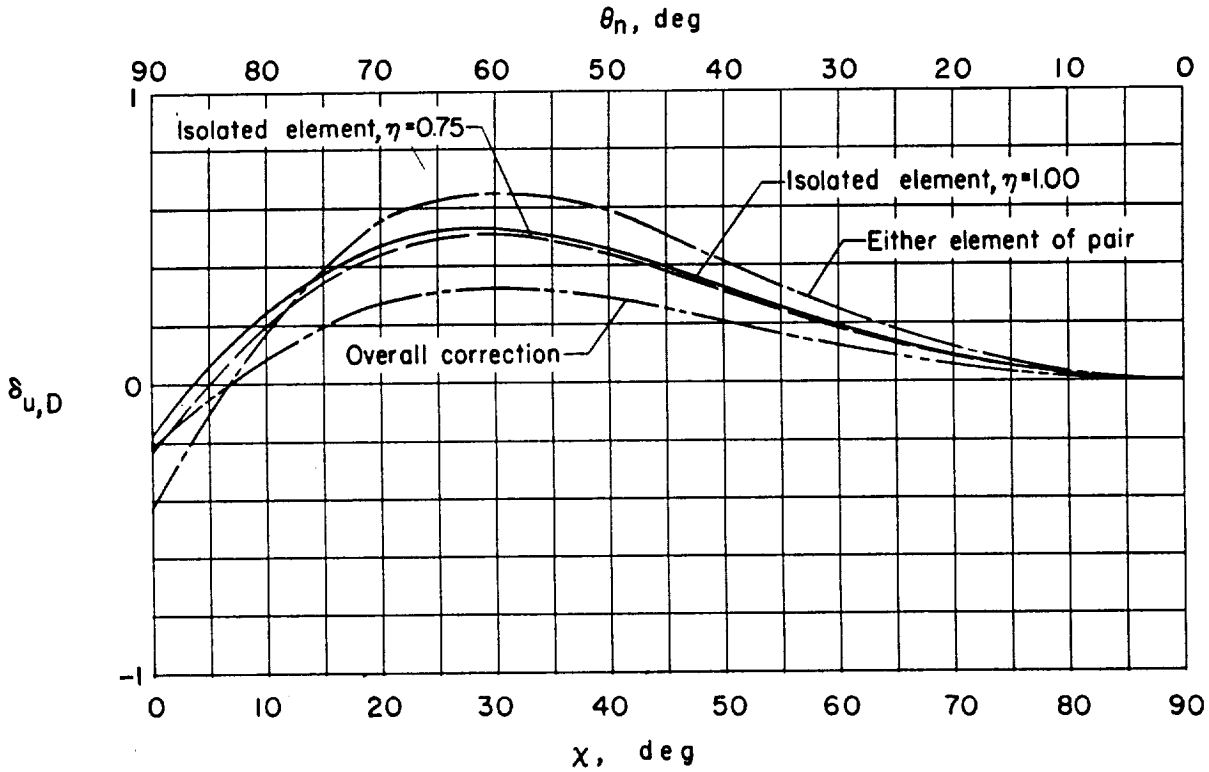


(d) Longitudinal interference due to drag.

Figure 84.- Concluded.

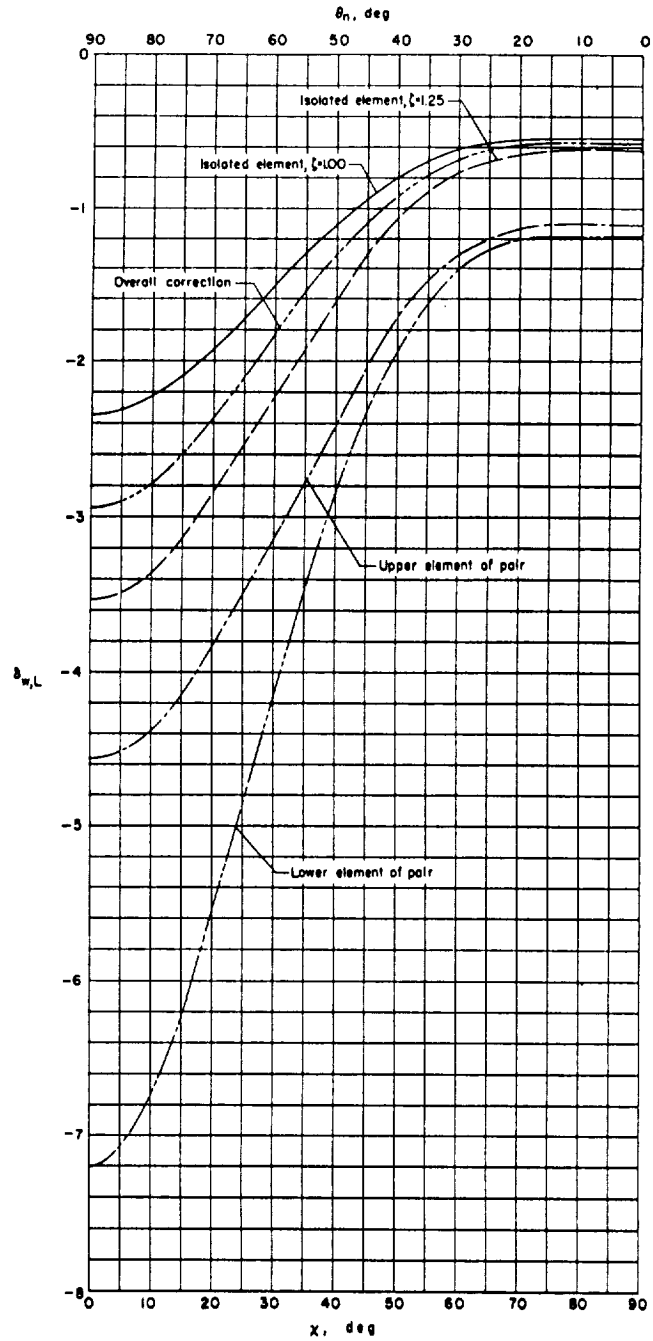


(a) Vertical interference due to lift.

Figure 85.- Correction factors for a two-element model in a closed wind tunnel with $\gamma = 2.0$. Elements are separated vertically by a distance of 0.2H with the upper element centered in wind tunnel. (Curve labeled "Overall correction" is based on $A_m$ of entire system.)

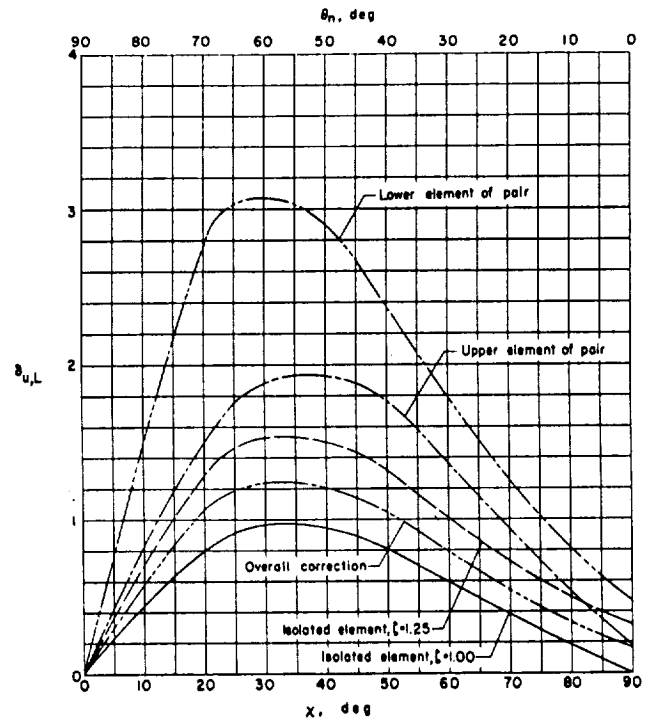


(b) Longitudinal interference due to lift.

Figure 85.- Continued.

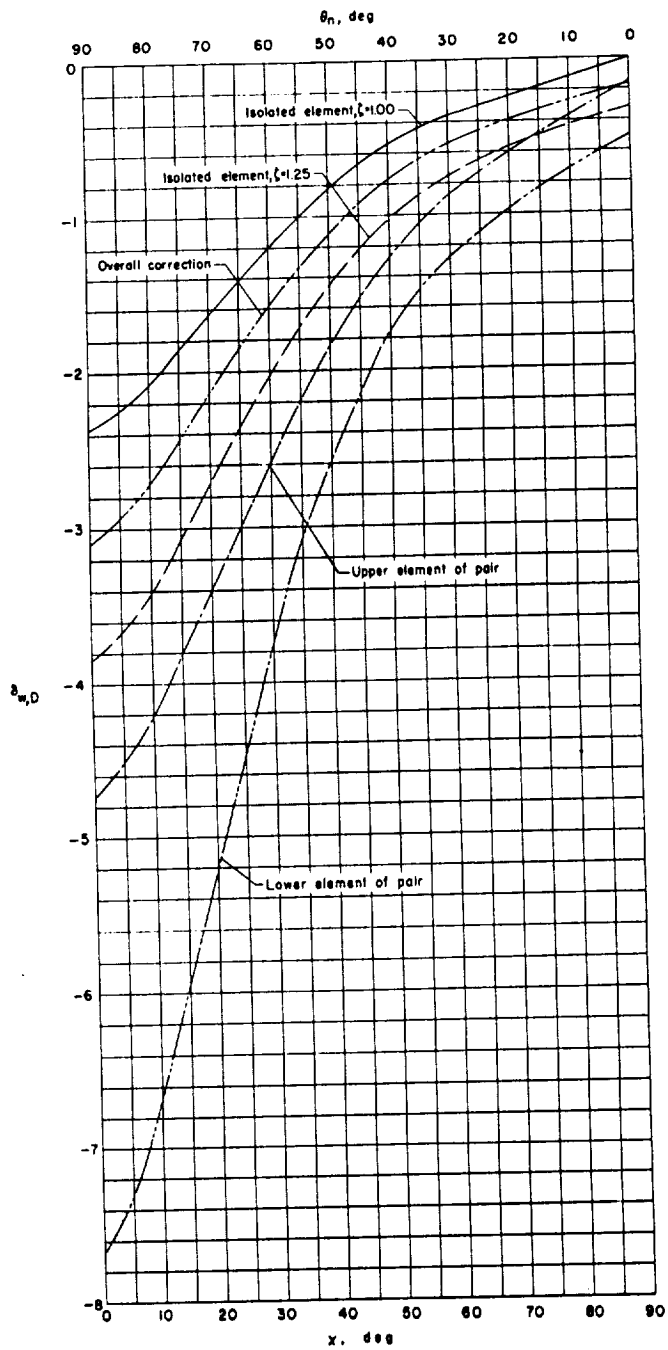


(c) Vertical interference due to drag.

Figure 85.- Continued.

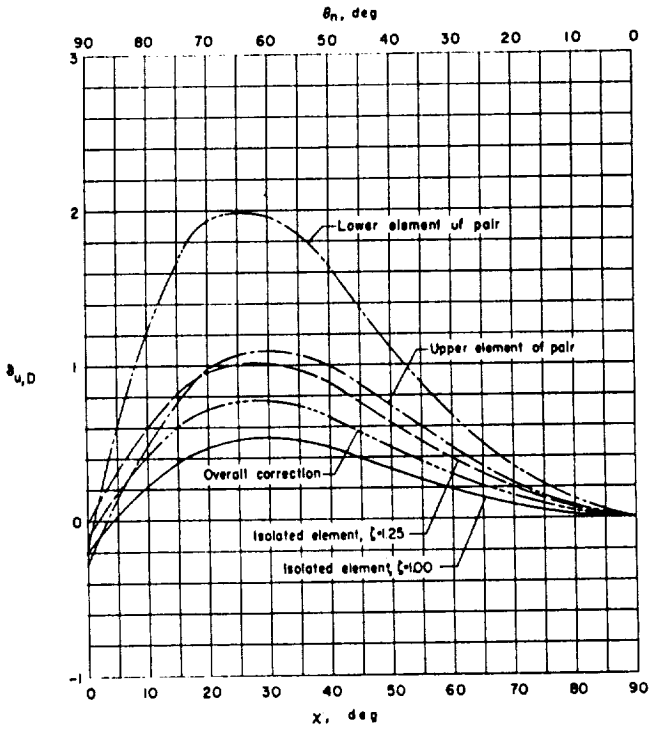


(d) Longitudinal interference due to drag.

Figure 85.- Concluded.

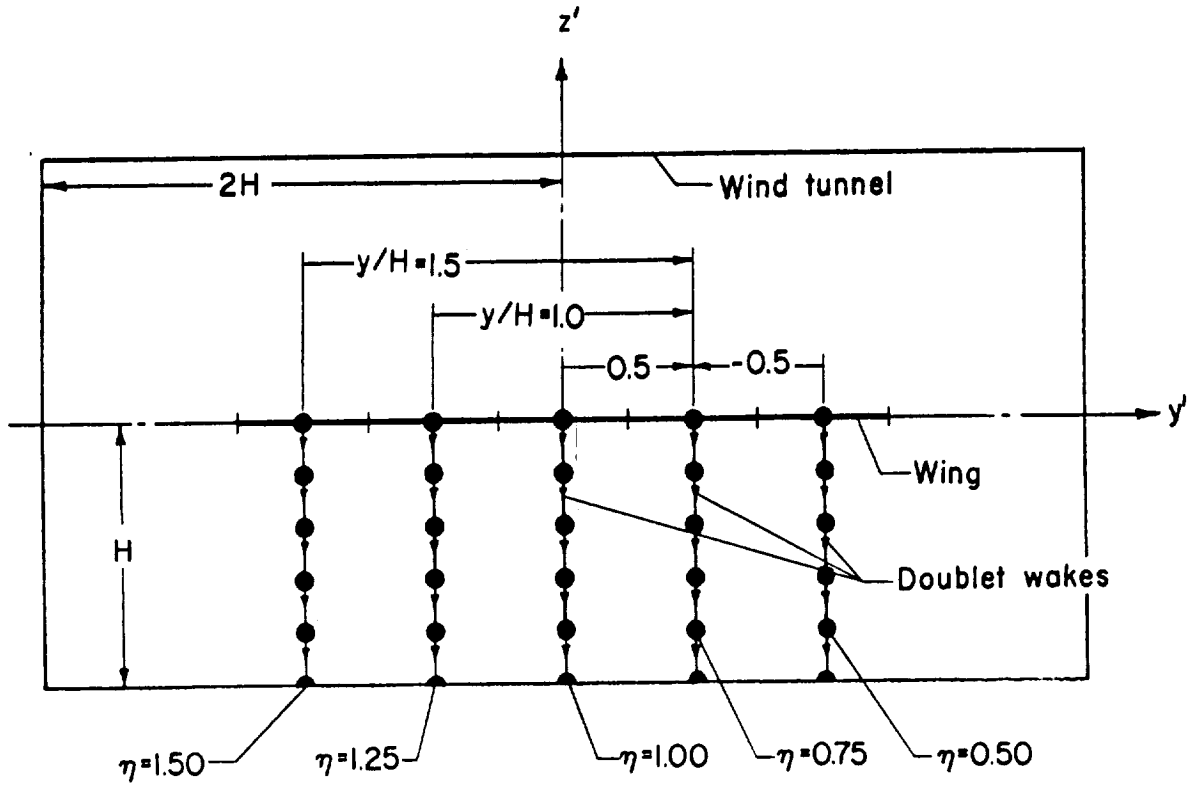


Figure 86.- Sketch illustrating calculation of interference factors at $y'/H = 0.5$ for a finite-span wing with $\sigma = 0.625$ in a closed rectangular wind tunnel with $\gamma = 2.0$.

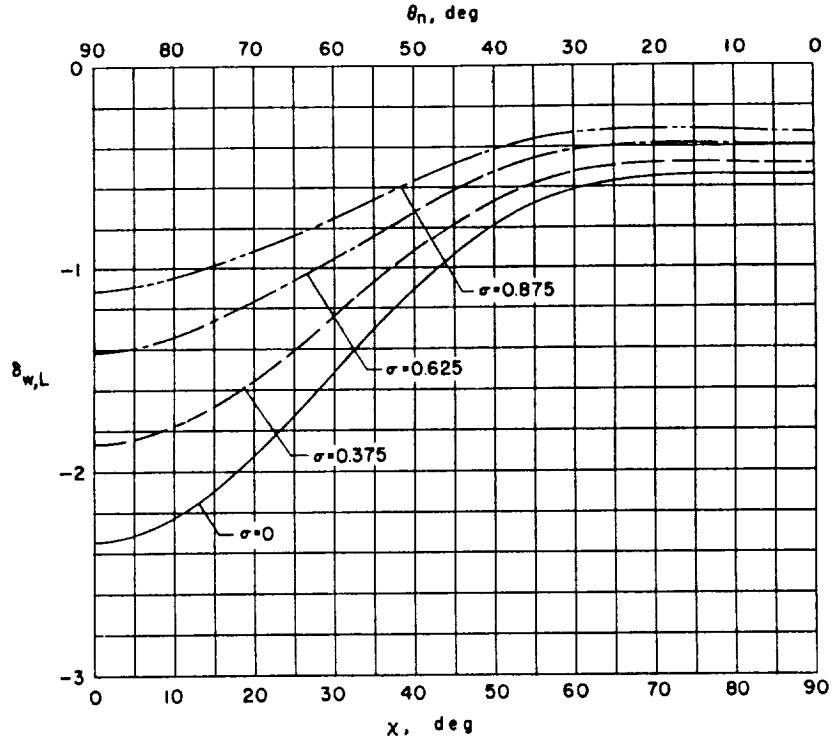


(a) Vertical interference due to lift.

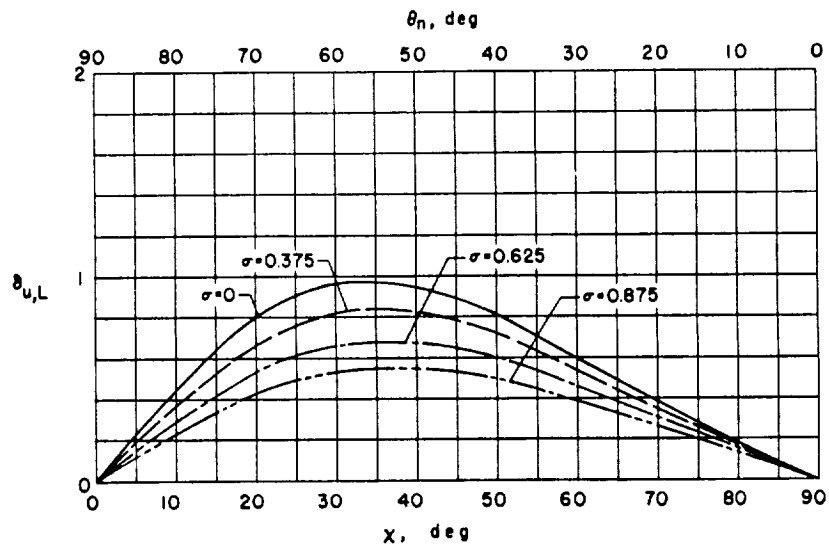


(b) Longitudinal interference due to lift.

Figure 87.- Interference factors at the center of a series of finite-span wings centrally located in a closed wind tunnel with $\gamma = 2.0$. Wings are assumed to be uniformly loaded.

632643 O—62— —14

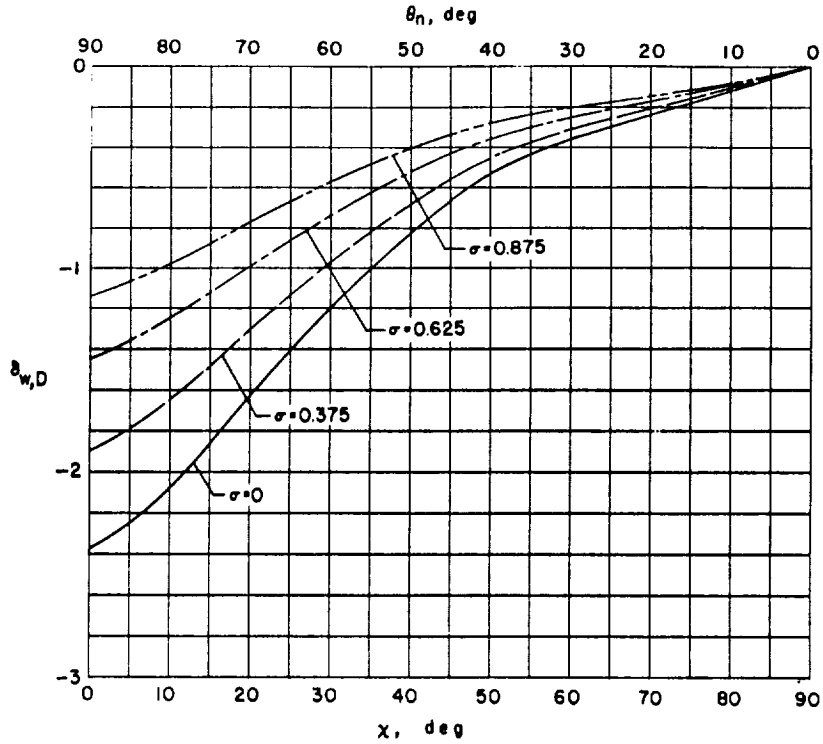


(c) Vertical interference due to drag.

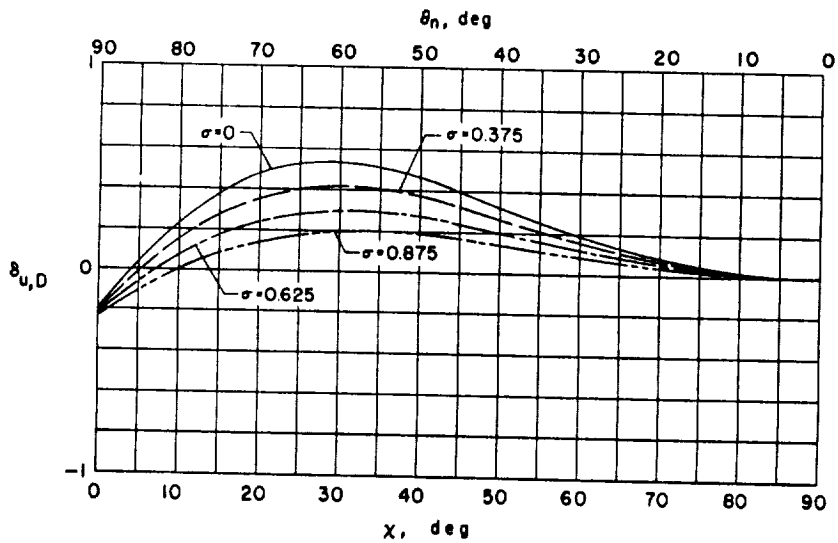


(d) Longitudinal interference due to drag.

Figure 87.- Concluded.

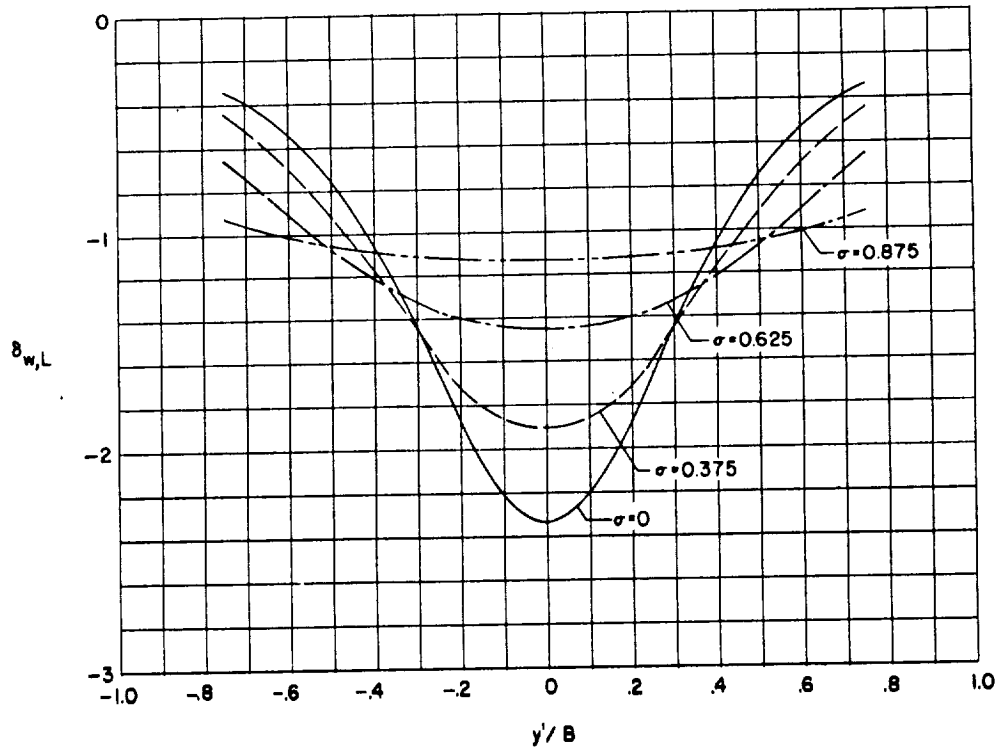


(a) $\chi = 0^{\circ}$.

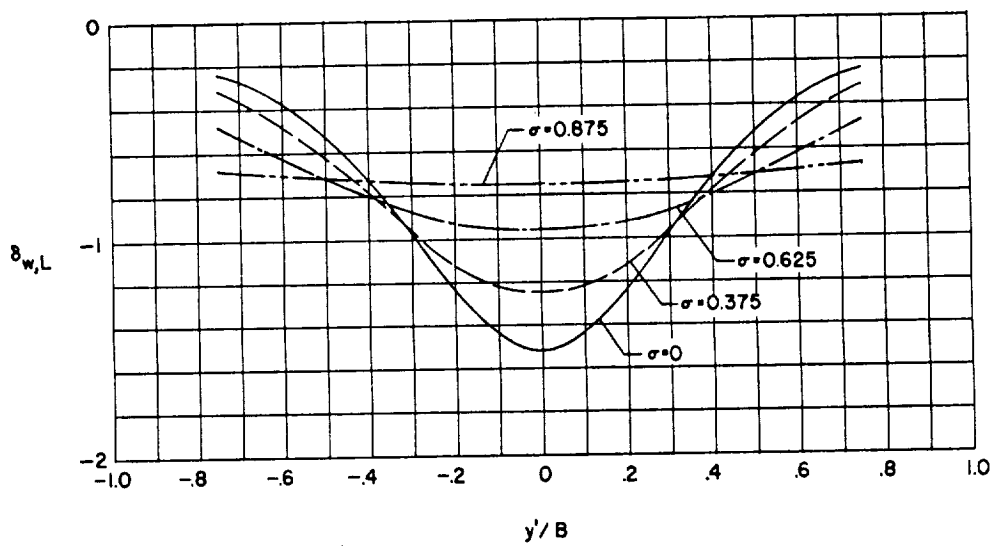


(b) $\chi = 30^{\circ}$.

Figure 88.- Lateral distribution of vertical interference due to lift for a series of finite-span uniformly loaded wings centered in a closed wind tunnel with $\gamma = 2.0$.

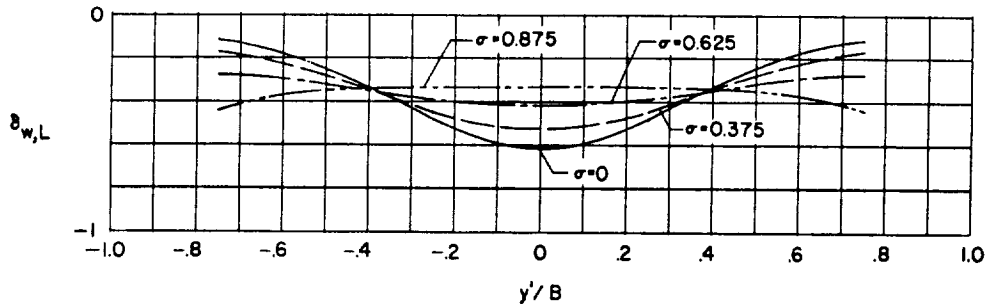


(c) $\chi = 60^{\circ}$.

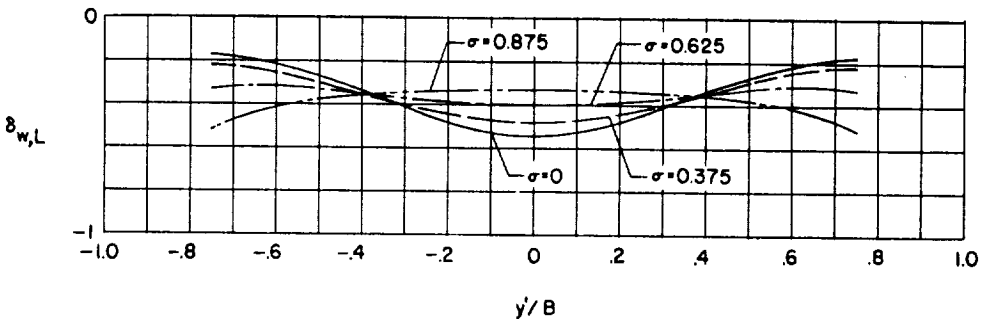


(d) $\chi = 90^{\circ}$.

Figure 88.- Concluded.

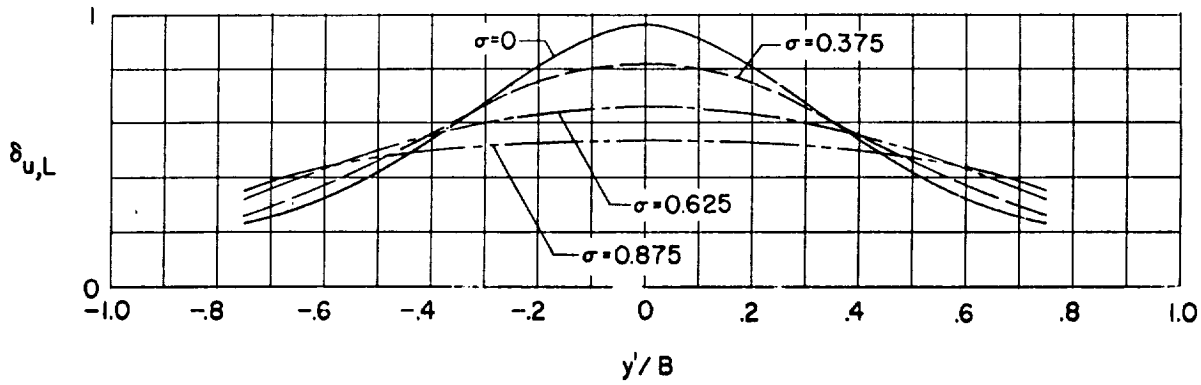


(a) $X = 30^{\circ}$

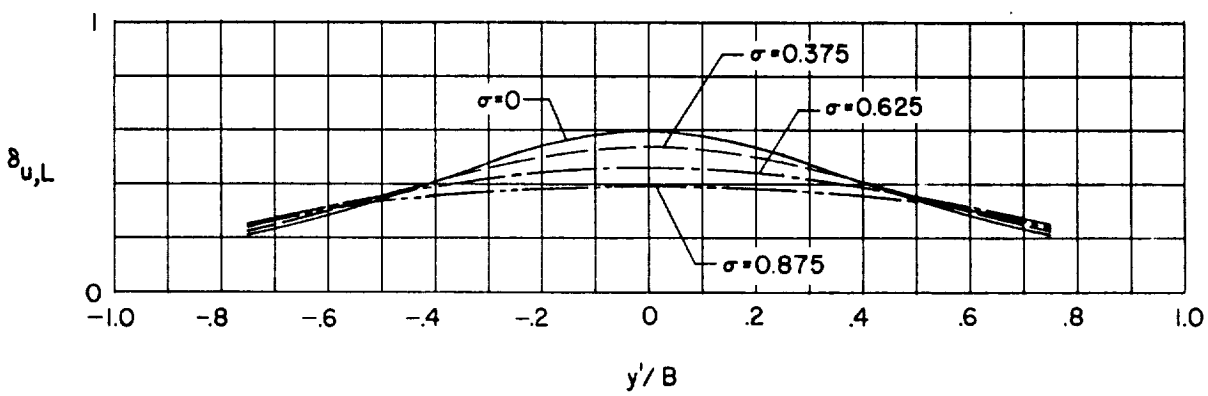


(b) $X = 60^{\circ}$.

Figure 89.- Lateral distribution of longitudinal interference due to lift for a series of finite-span uniformly loaded wings centered in a closed wind tunnel with $\gamma = 2.0$. (Plots for $X = 0^{\circ}$ and $X = 90^{\circ}$ are omitted since $\delta_{u,L}$ is uniformly zero.)

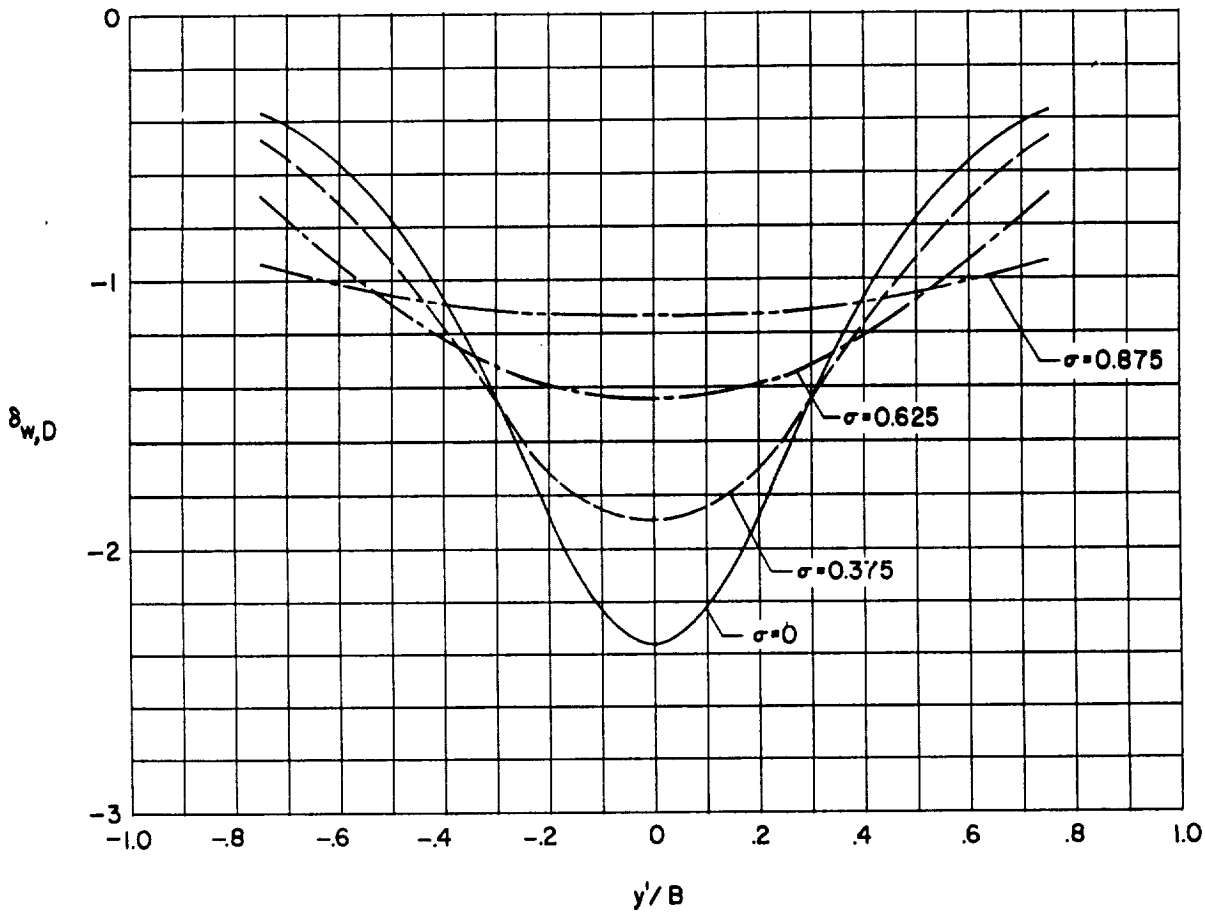


(a) $\chi = 0^{\circ}$.

Figure 90.- Lateral distribution of vertical interference due to drag for a series of finite-span uniformly loaded wings centered in a closed wind tunnel with $\gamma = 2.0$. (Plot for $\chi = 90^{\circ}$ is omitted since $\delta_{w,D}$ is uniformly zero.)

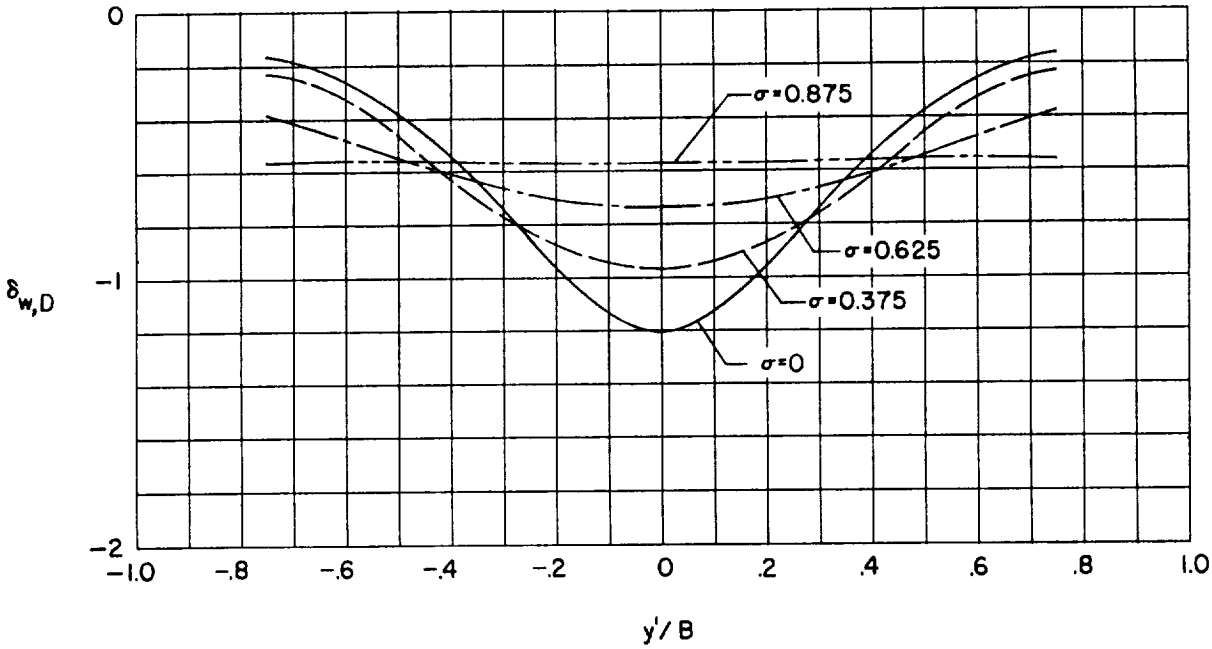


(b) $\chi = 30^{\circ}$.

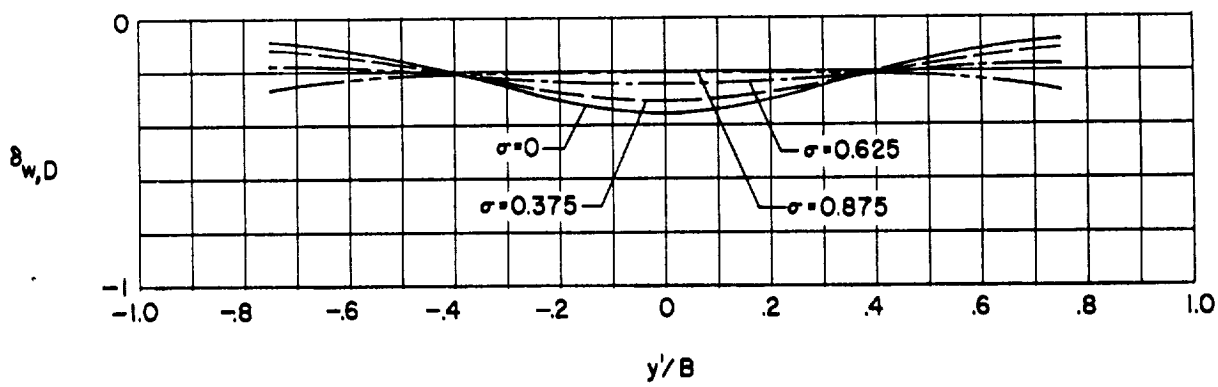


(c) $\chi = 60^{\circ}$.

Figure 90.- Concluded.

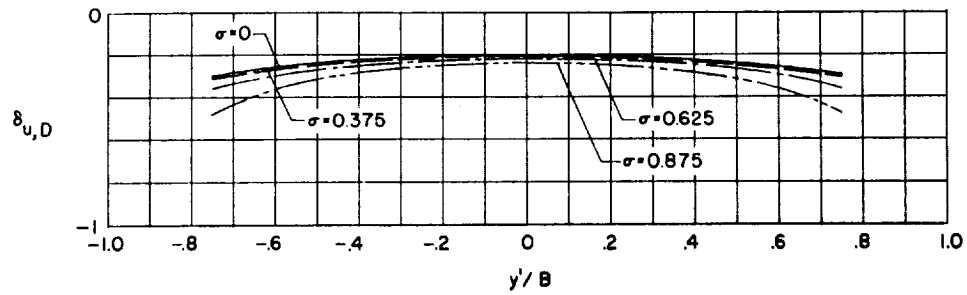


(a) X = 0°.

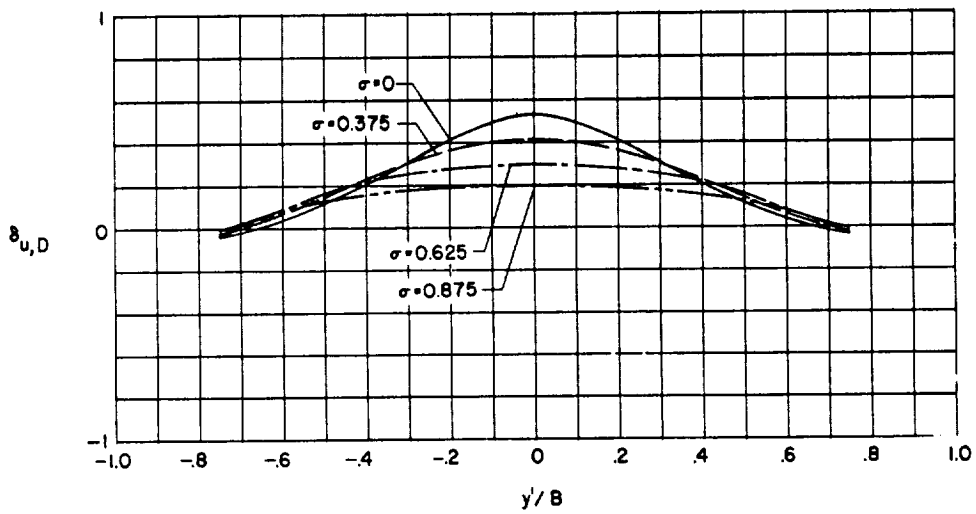


(b) X = 30°.

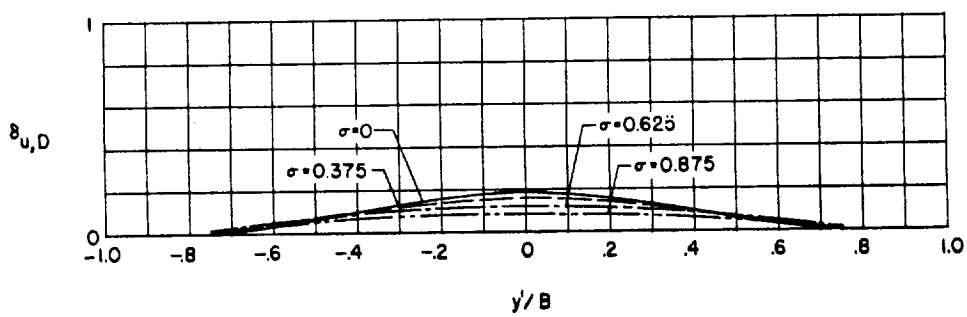


(c) X = 60°.

Figure 91.- Lateral distribution of longitudinal interference due to drag for a series of finite-span uniformly loaded wings centered in a closed wind tunnel with $\gamma = 2.0$. (Plot for $X = 90°$ is omitted since $\delta_{u,D}$ is uniformly zero.)

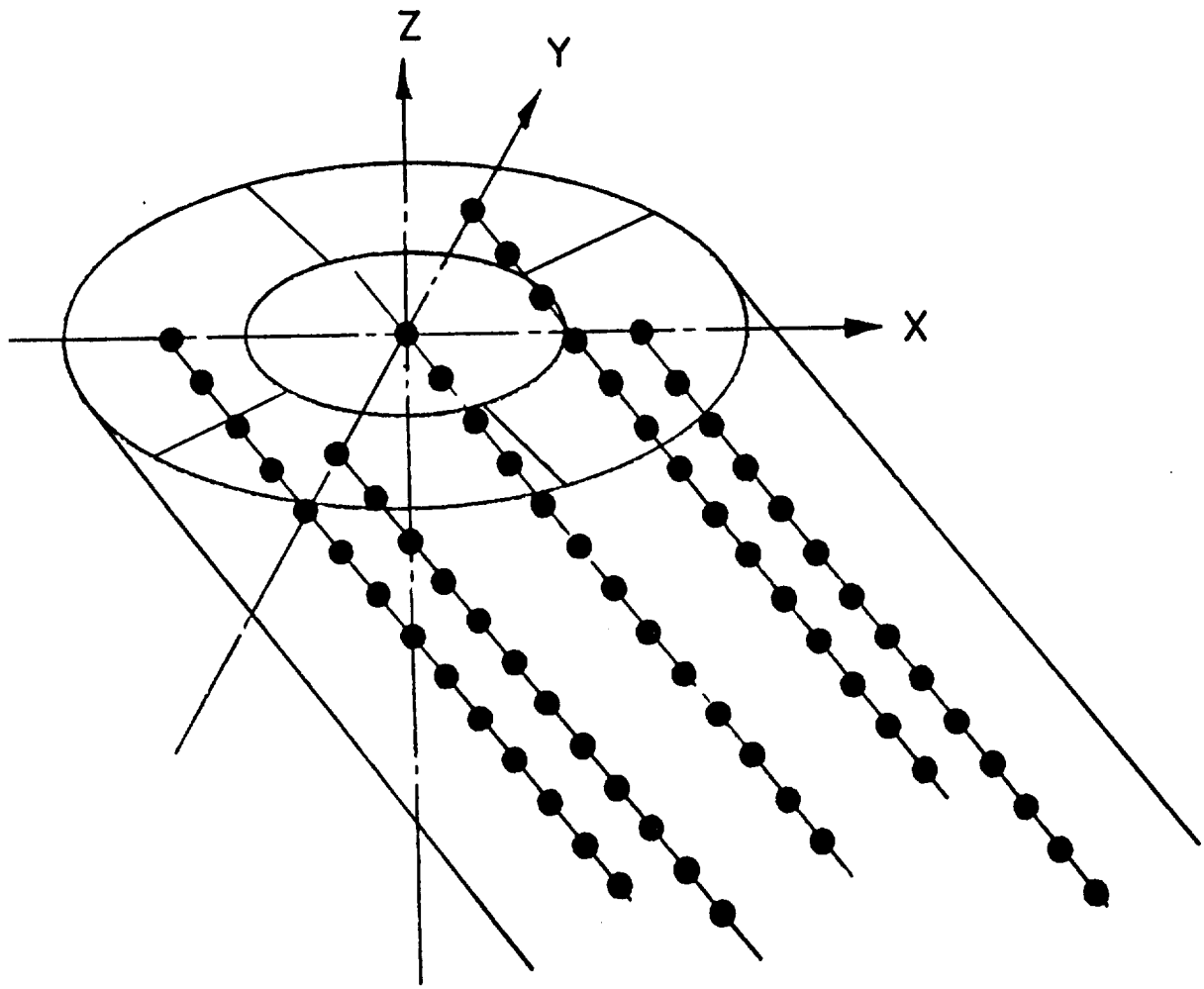


Figure 92.- Schematic view of doublet-wake representation of the wake of a helicopter rotor.

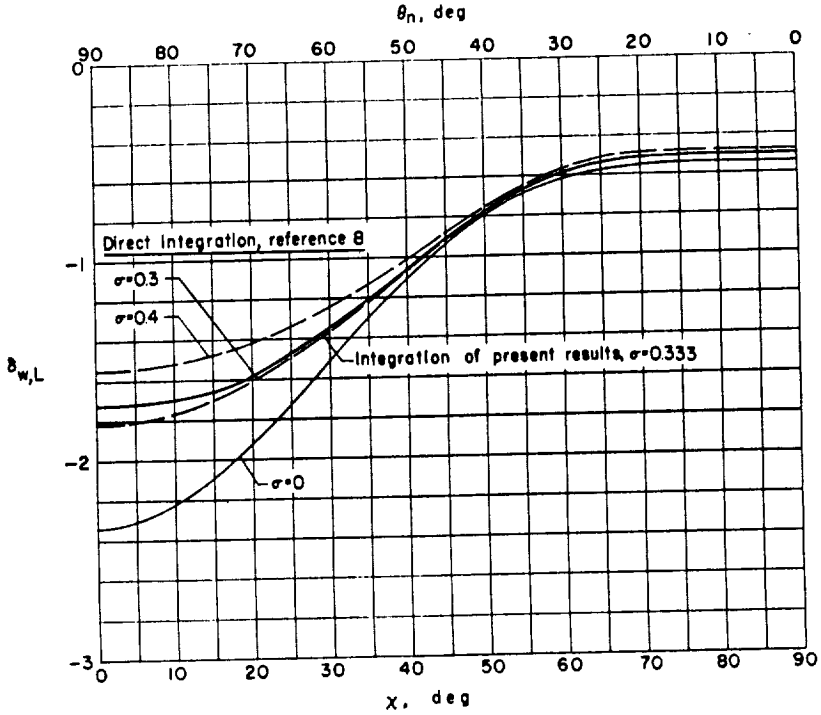


(a) Vertical interference due to lift.

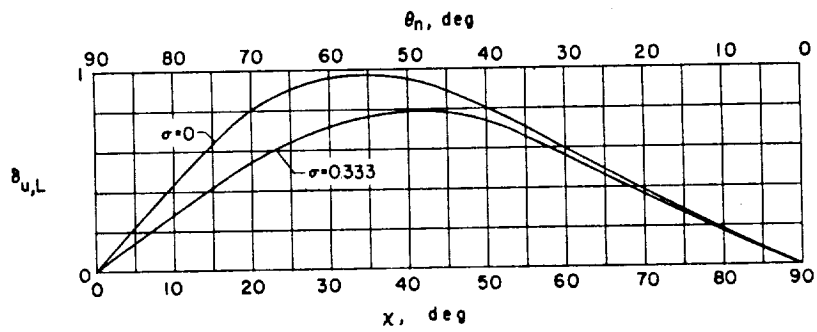


(b) Longitudinal interference due to lift.

Figure 93.- Interference factors at the center of a finite-size rotor ($\sigma$ = 0.333) for a closed wind tunnel ($\gamma$ = 2.0; $\zeta$ = 1.0; $\eta$ = 1.0), including a comparison with the results of reference 8.

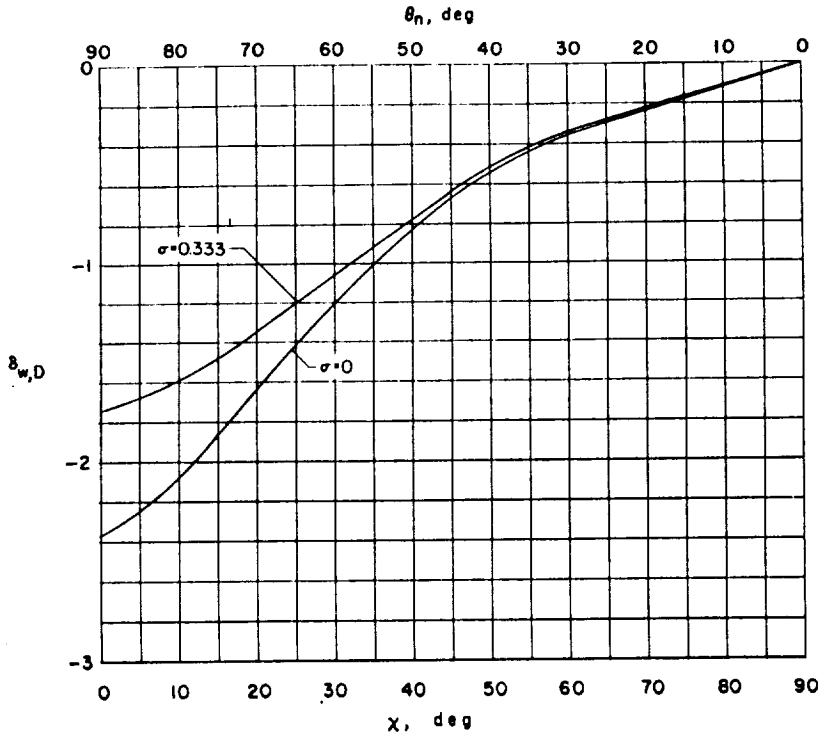


(c) Vertical interference due to drag.

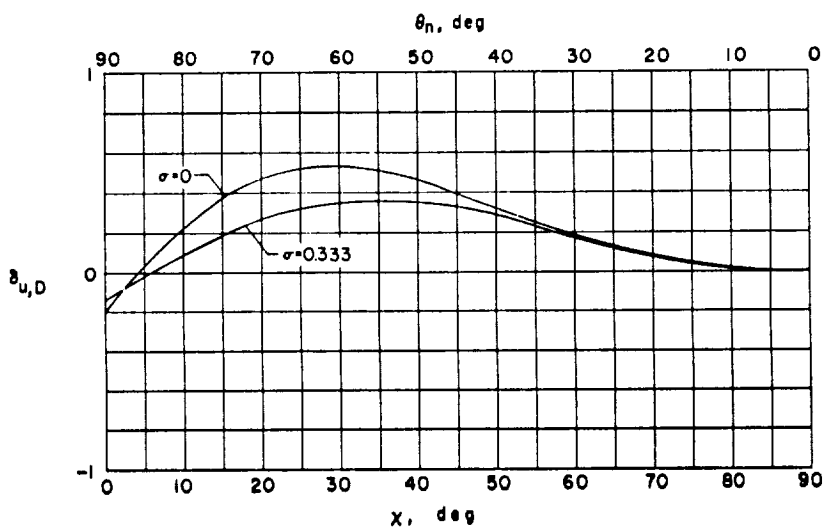


(d) Longitudinal interference due to drag.

Figure 93.- Concluded.

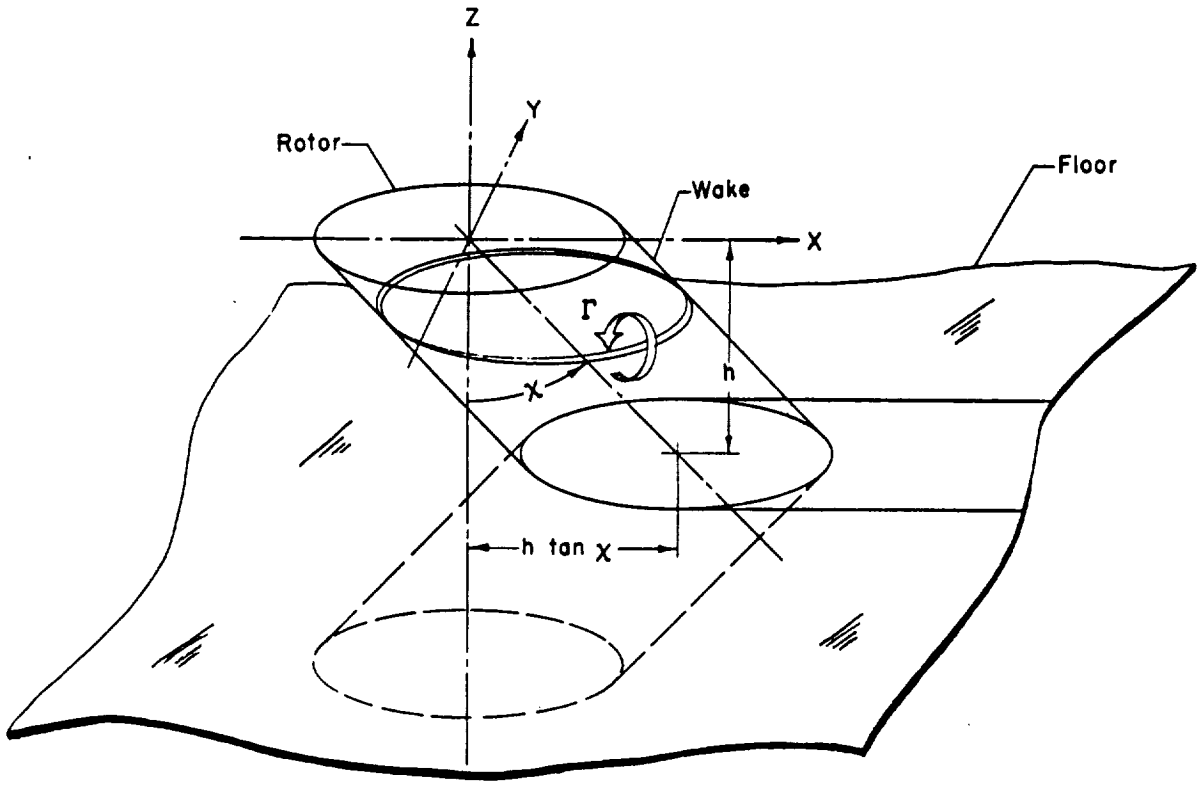


Figure 94.- Basic cylindrical wake and image system used to calculate corrections for a uniformly loaded rotor. Sample element of vorticity is shown.

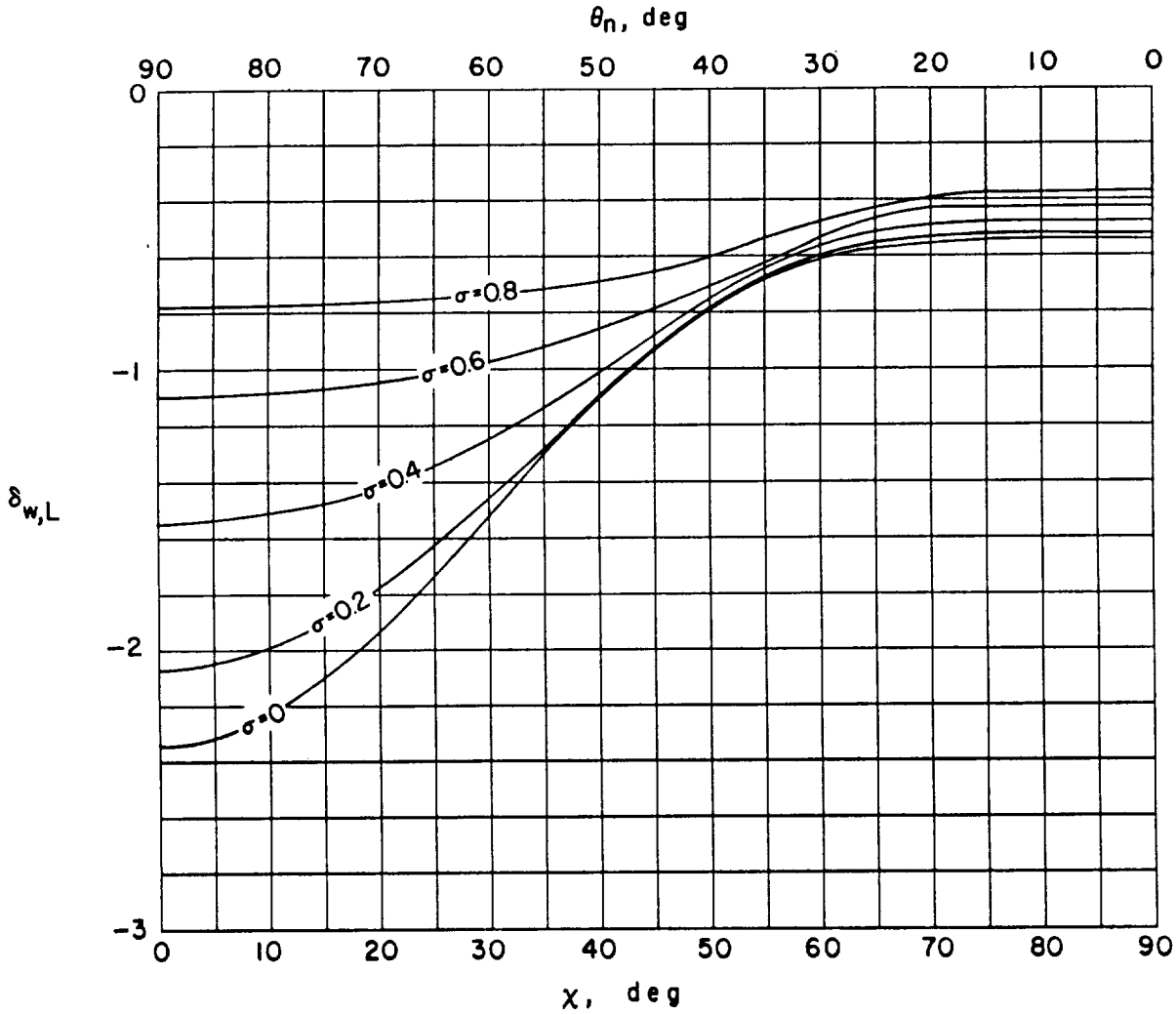


(a) Closed wind tunnel.

Figure 95.- Effect of finite rotor size on the vertical interference due to lift at the rotor center. $\gamma = 2.0$; $\zeta = 1.0$; $\eta = 1.0$.

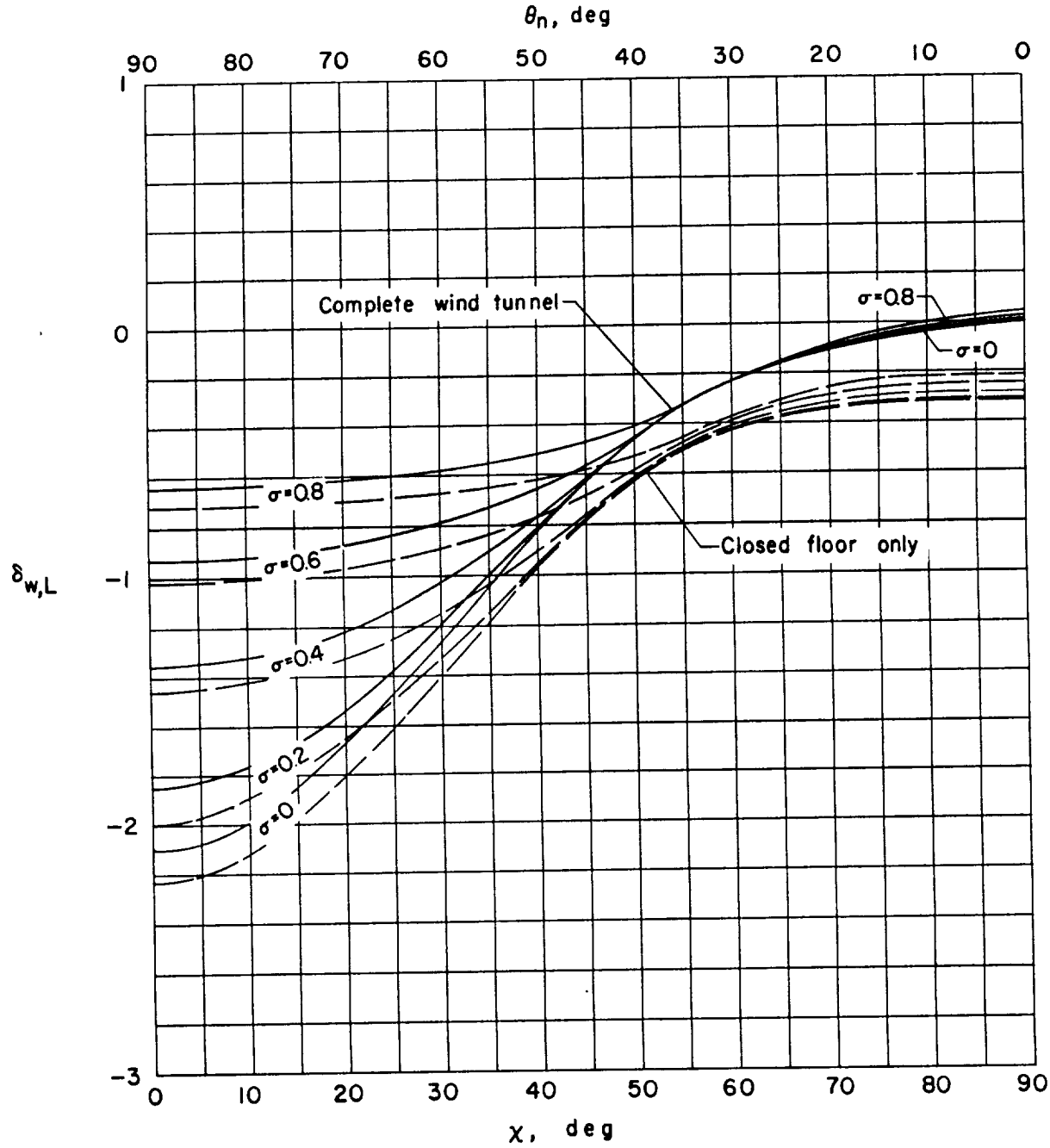


(b) Wind tunnel closed on the bottom only.

Figure 95.- Concluded.

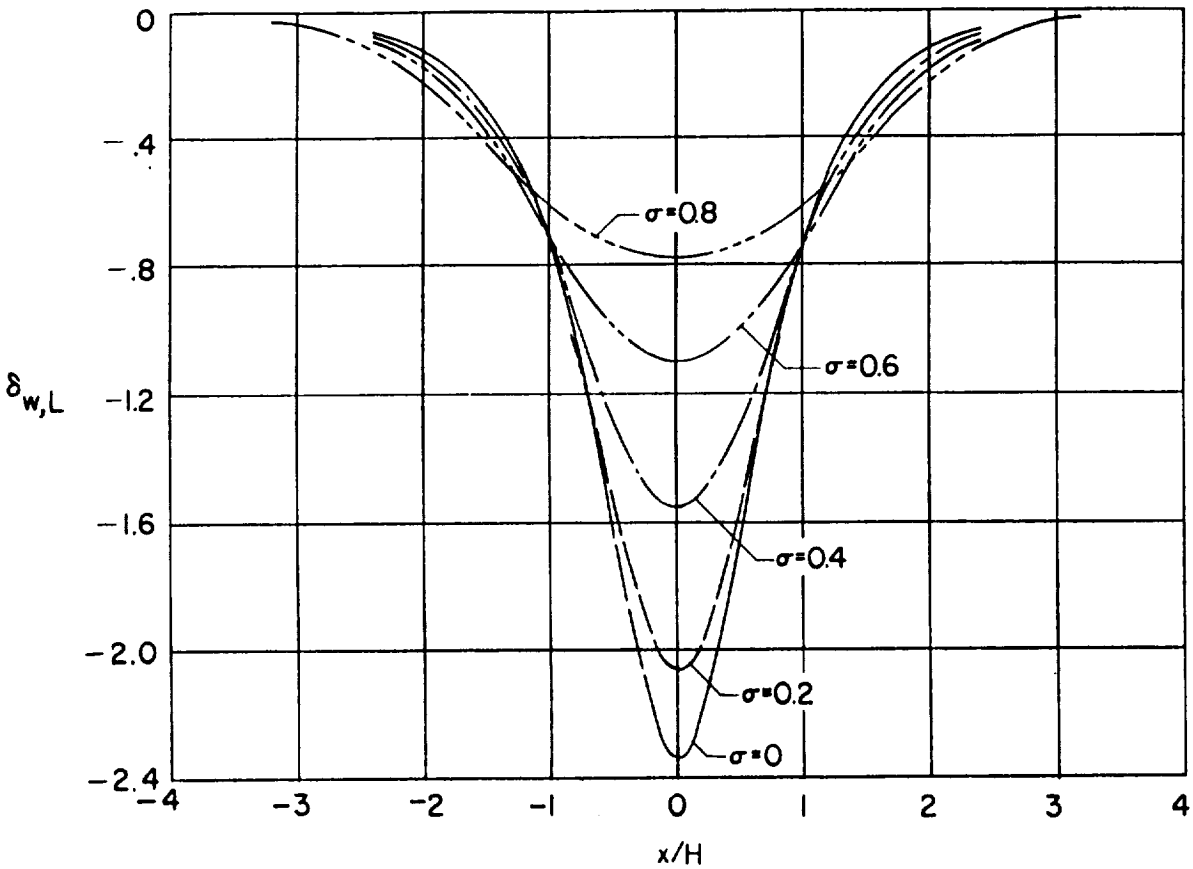


(a) $\chi = 0^{\circ}$.

Figure 96.- Effect of rotor size on the longitudinal distribution of vertical interference due to lift for closed wind tunnel. $\gamma = 2.0$; $\zeta = 1.0$.

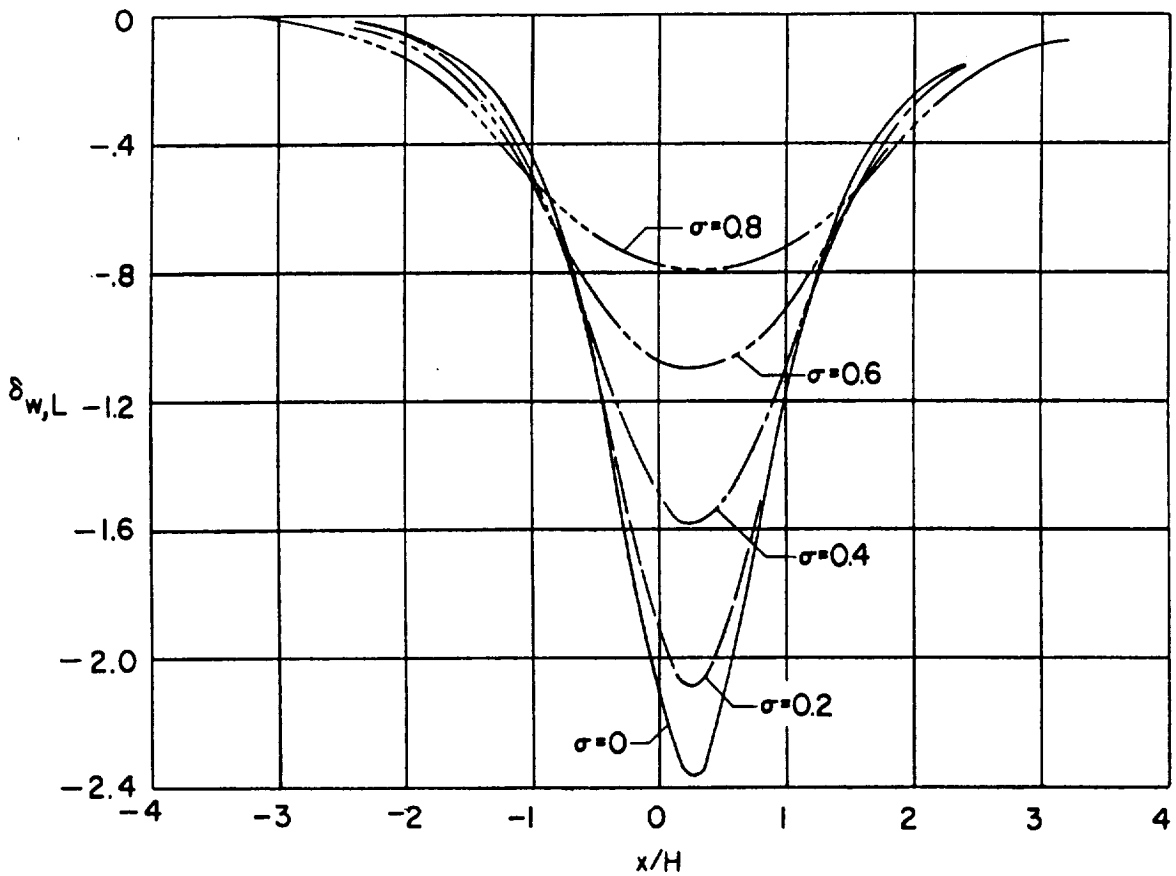


(b) $\chi = 14.04^{\circ}$.

Figure 96.- Continued.

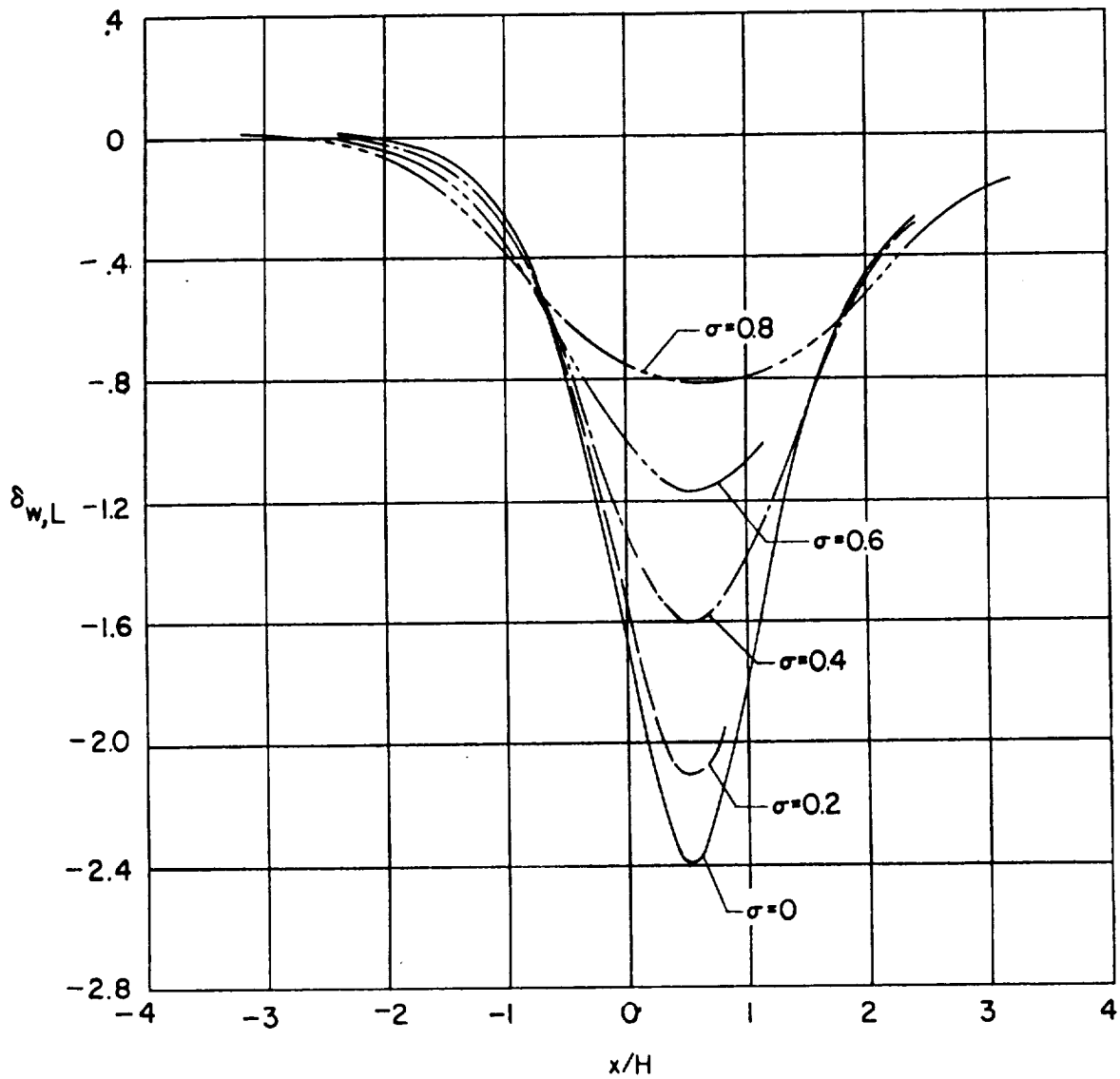


(c) $\chi = 26.56^{\circ}$.

Figure 96.- Continued.

632643 O—62——15

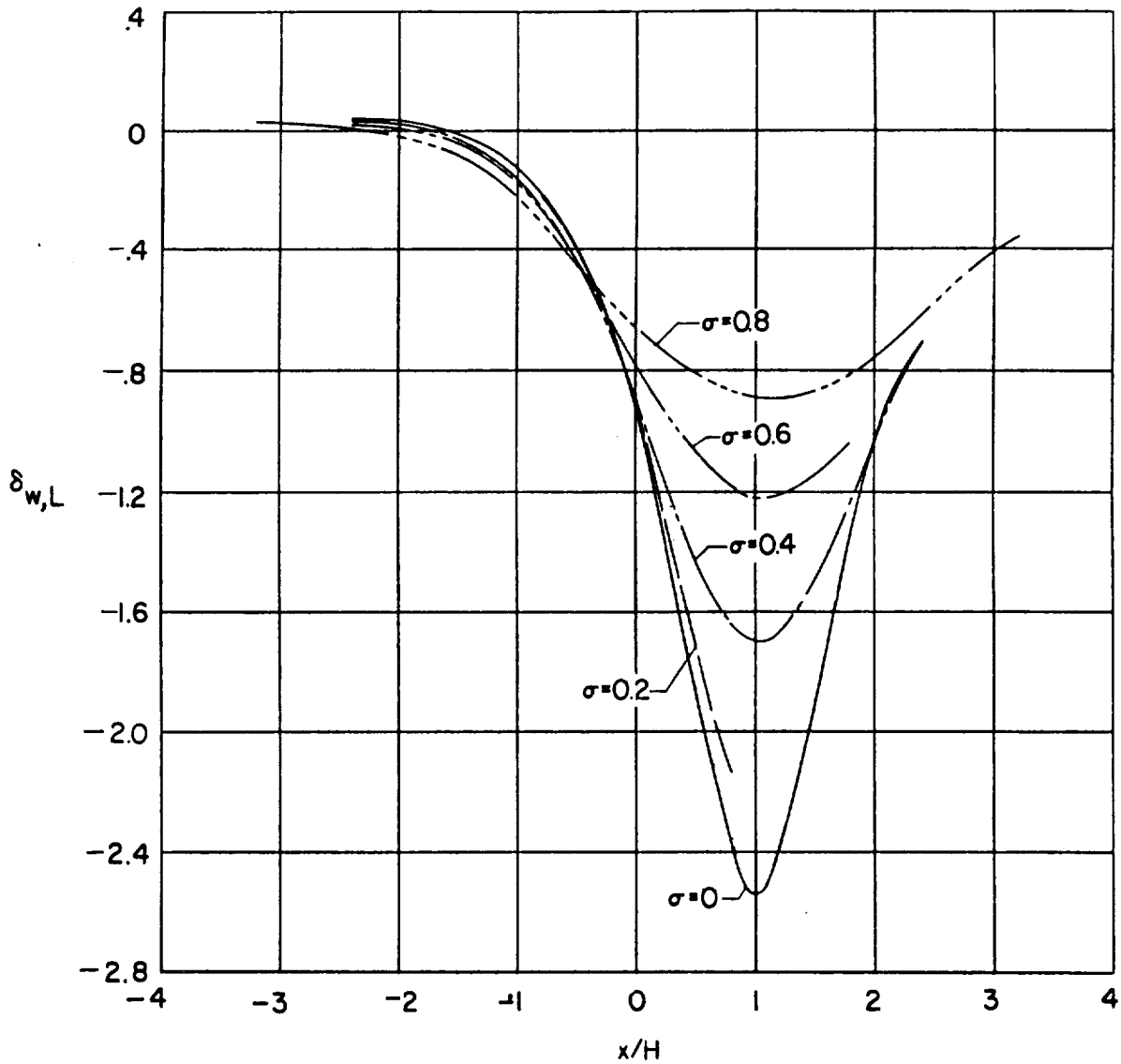


(d) $\chi = 45.00°$.

Figure 96.- Continued.

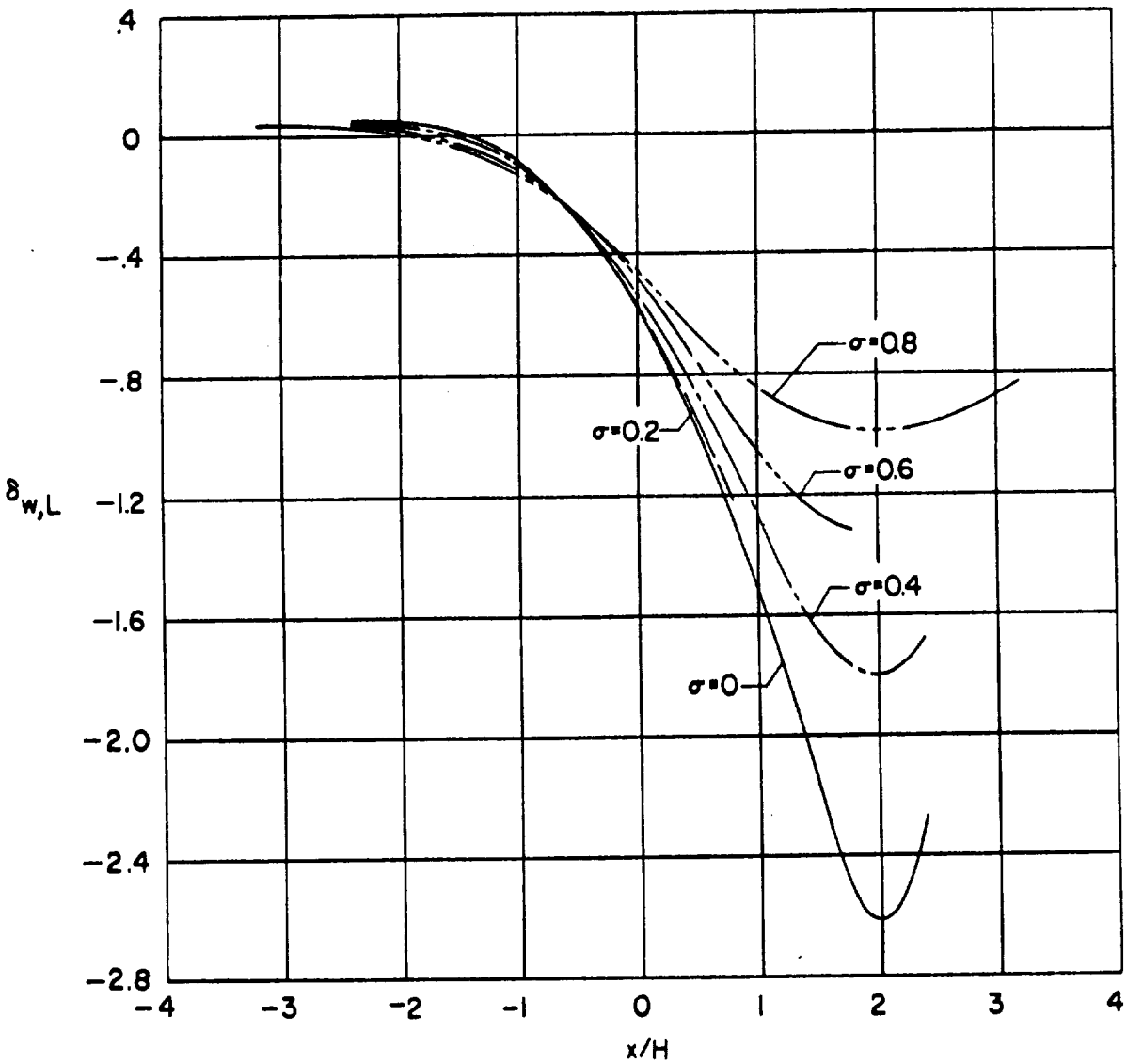


(e) $\chi = 63.43^{\circ}$.

Figure 96.- Continued.

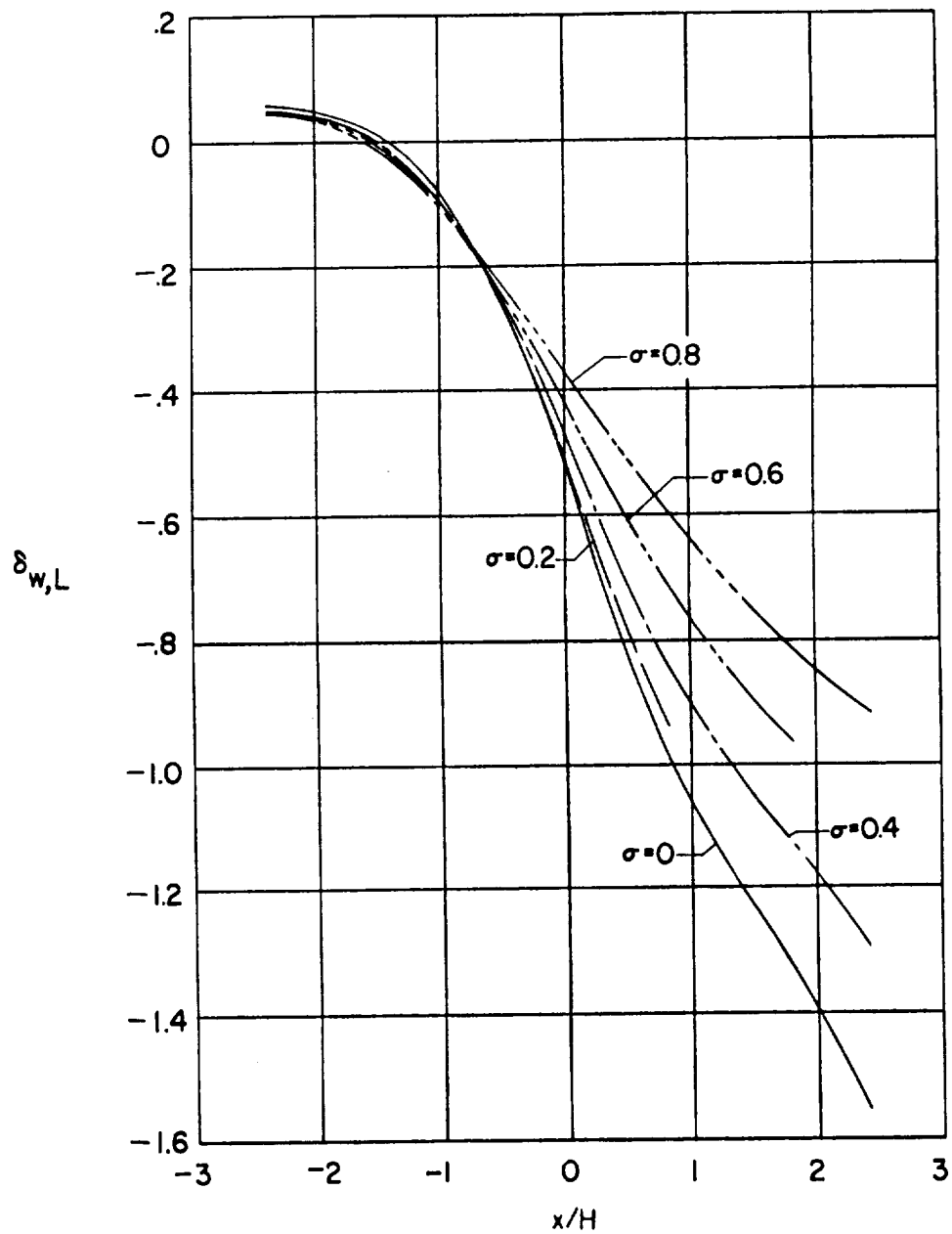


(f) $\chi = 75.97^{\circ}$.

Figure 96.- Continued.

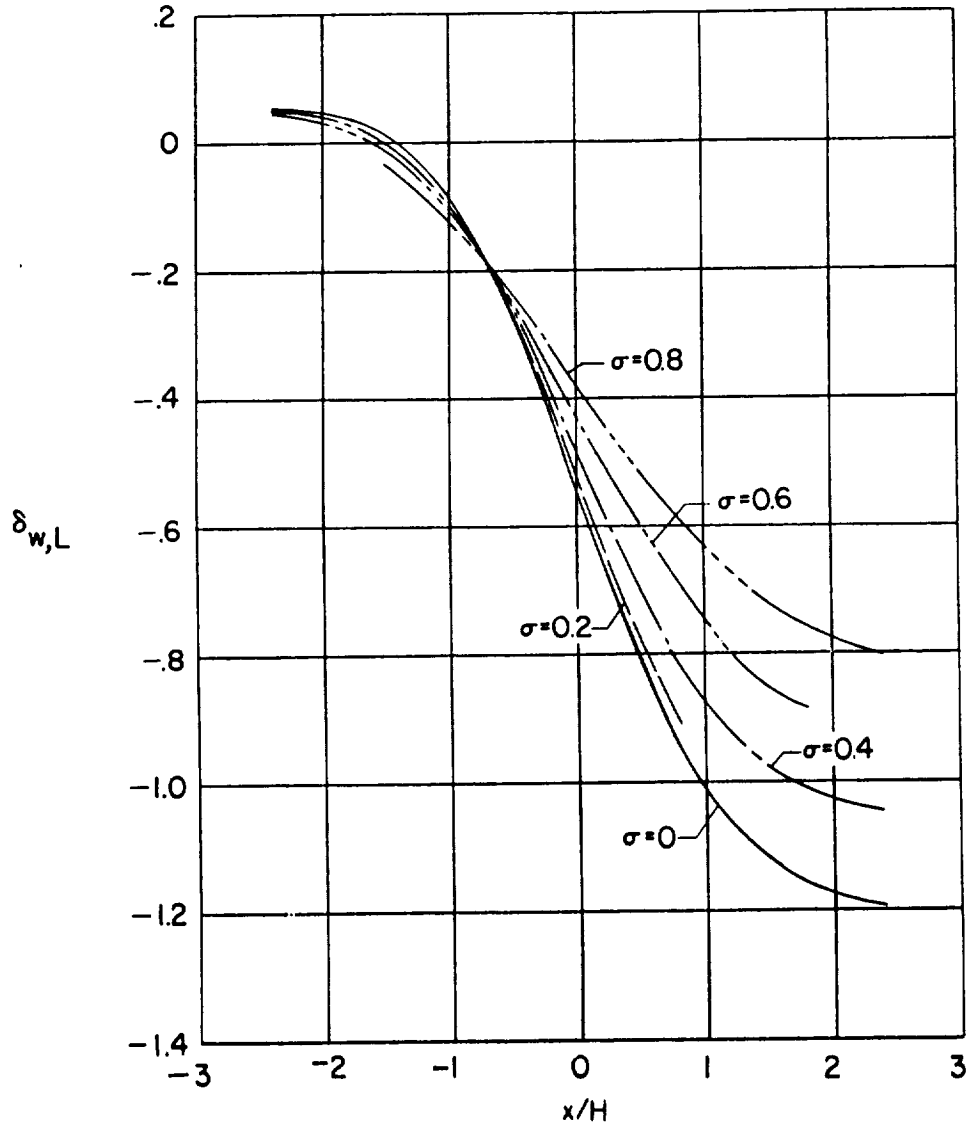


(g) $\chi = 84.29^{\circ}$.

Figure 96.- Continued.

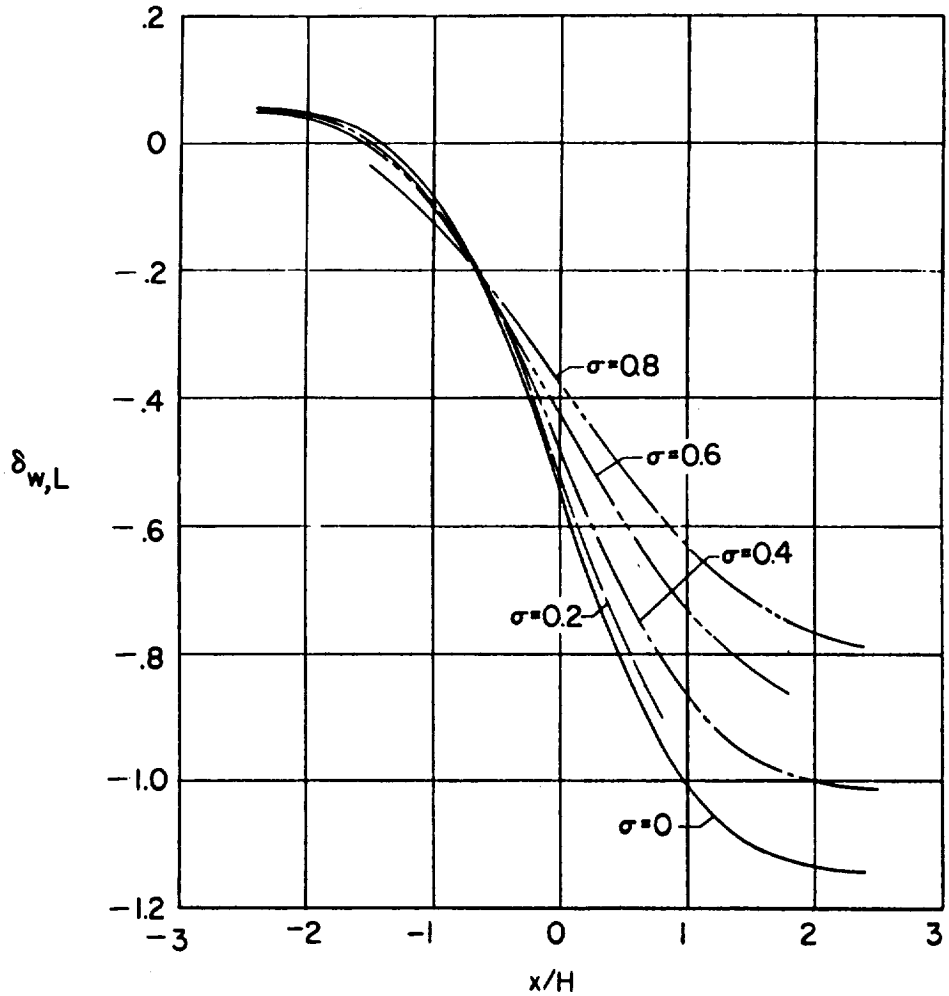


(h) $\chi = 90.00^{\circ}$.

Figure 96.- Concluded.

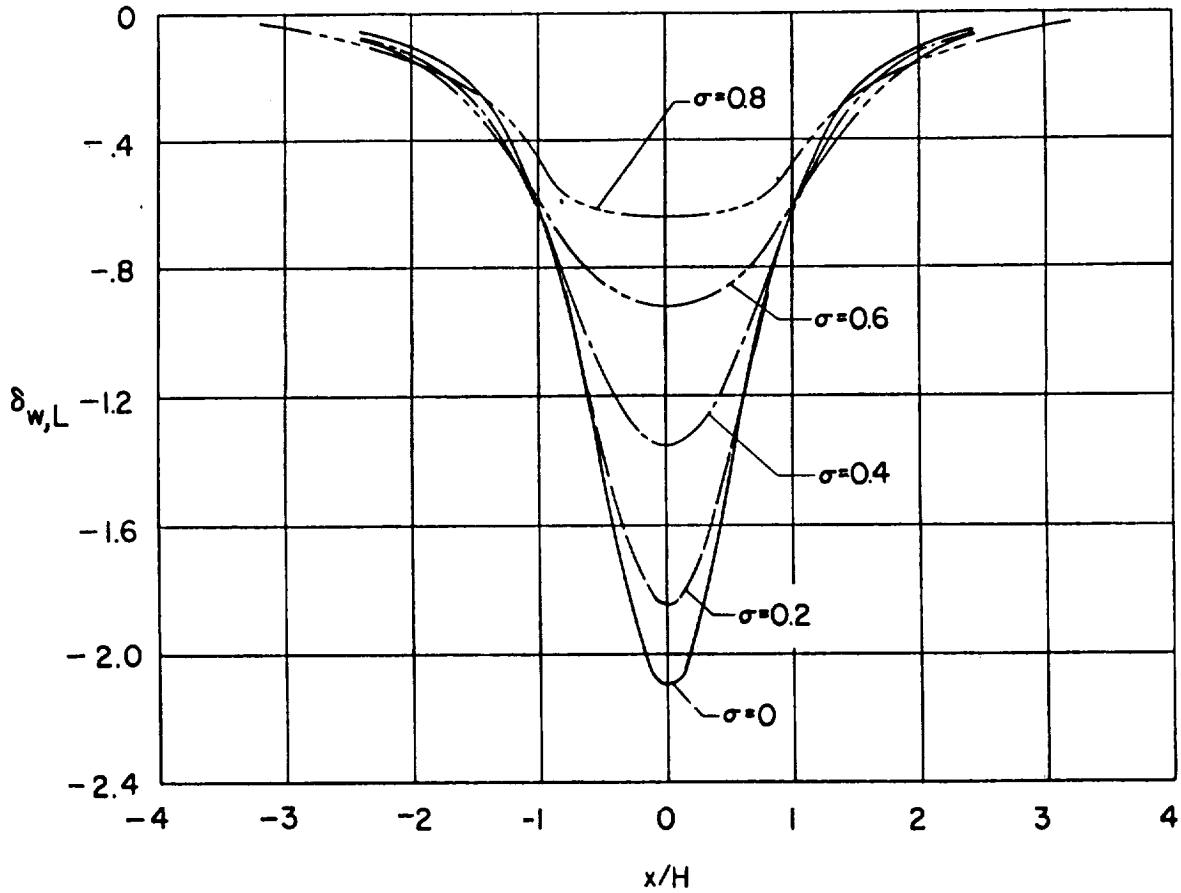


(a) $\chi = 0^{\circ}$.

Figure 97.- Effect of rotor size on the longitudinal distribution of vertical interference due to lift for wind tunnel closed on bottom only. $\gamma = 2.0$; $\zeta = 1.0$.

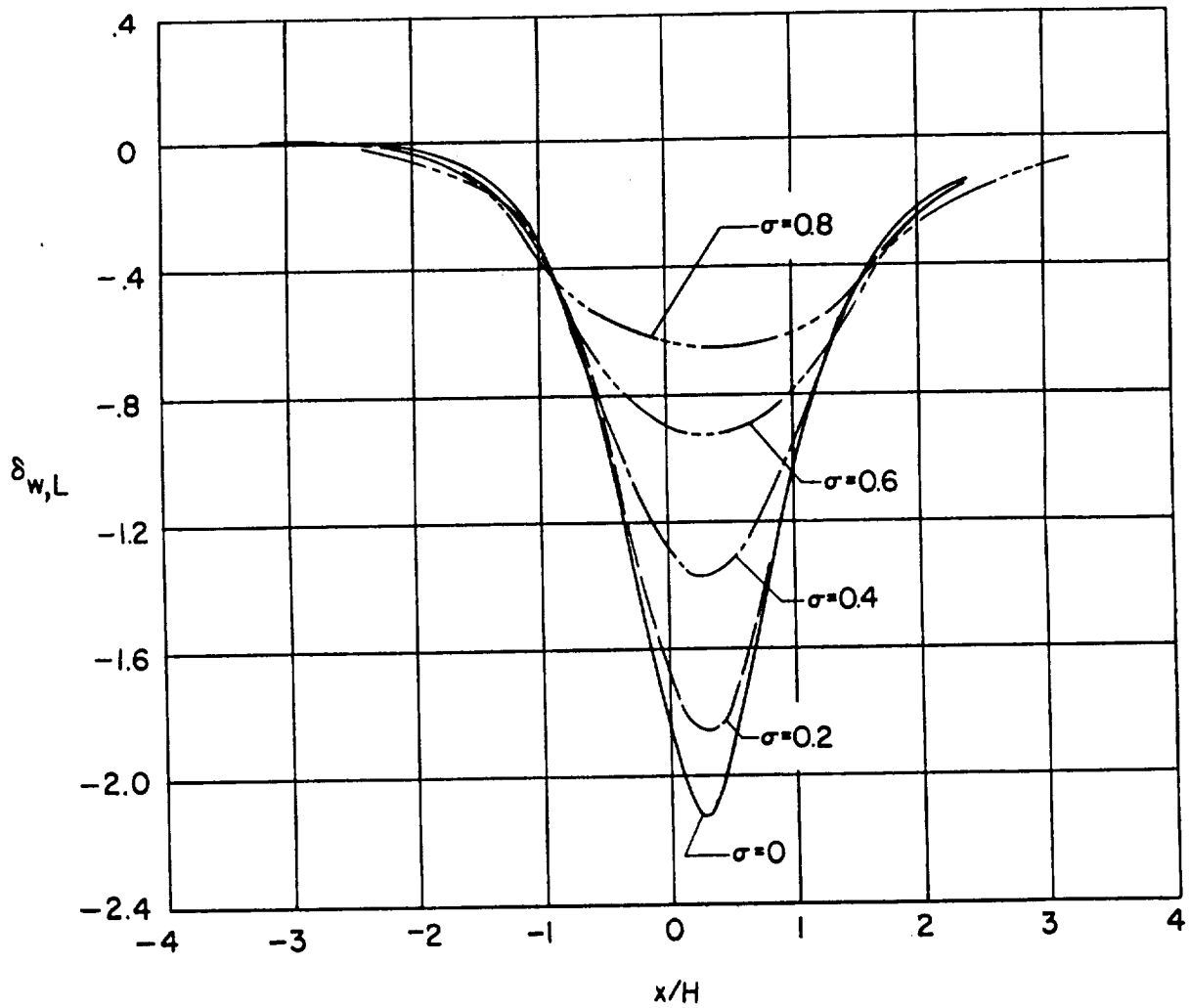


(b) $\chi = 14.04^{\circ}$.

Figure 97.- Continued.

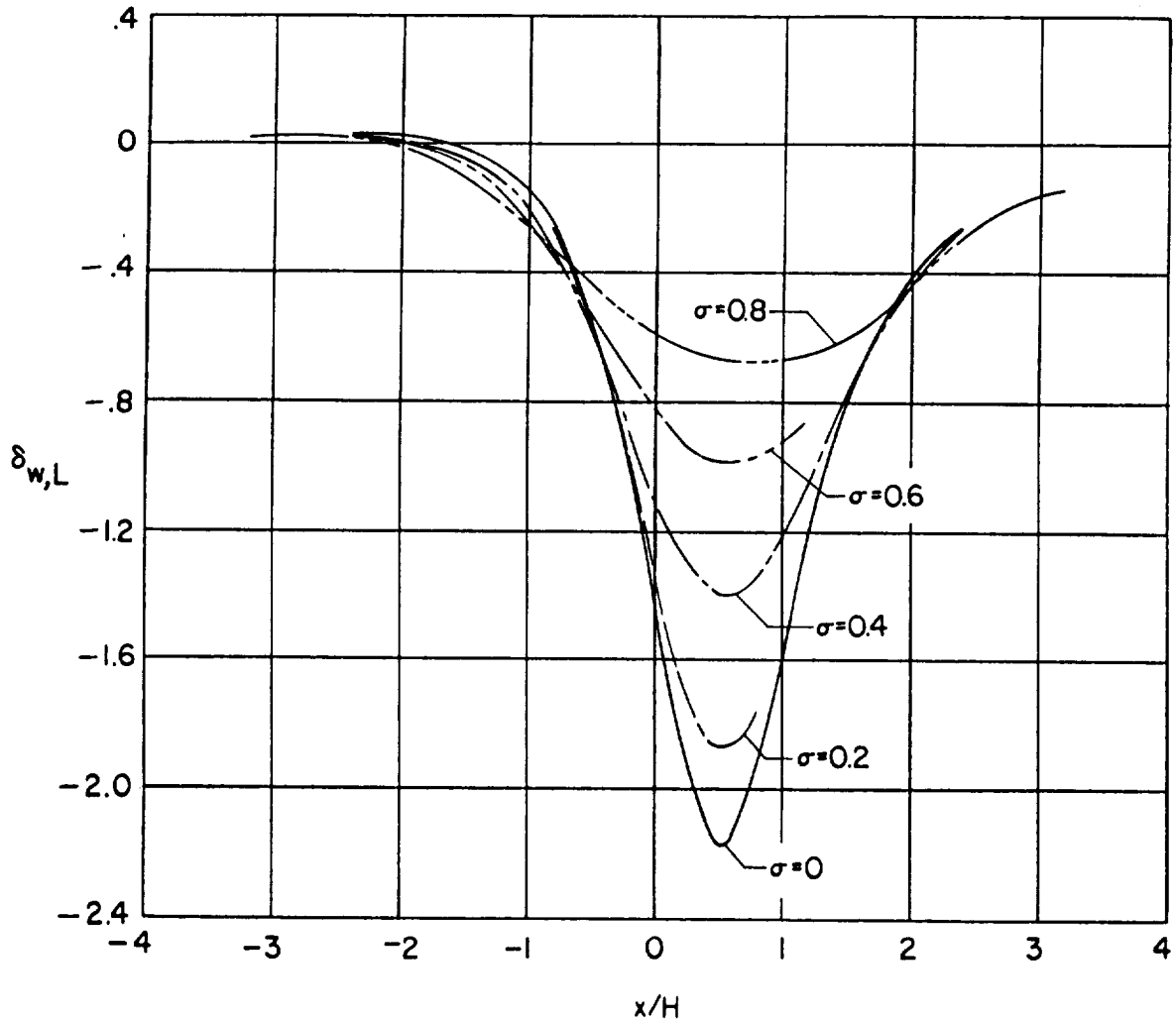


(c) $\chi = 26.56^{\circ}$.

Figure 97.- Continued.

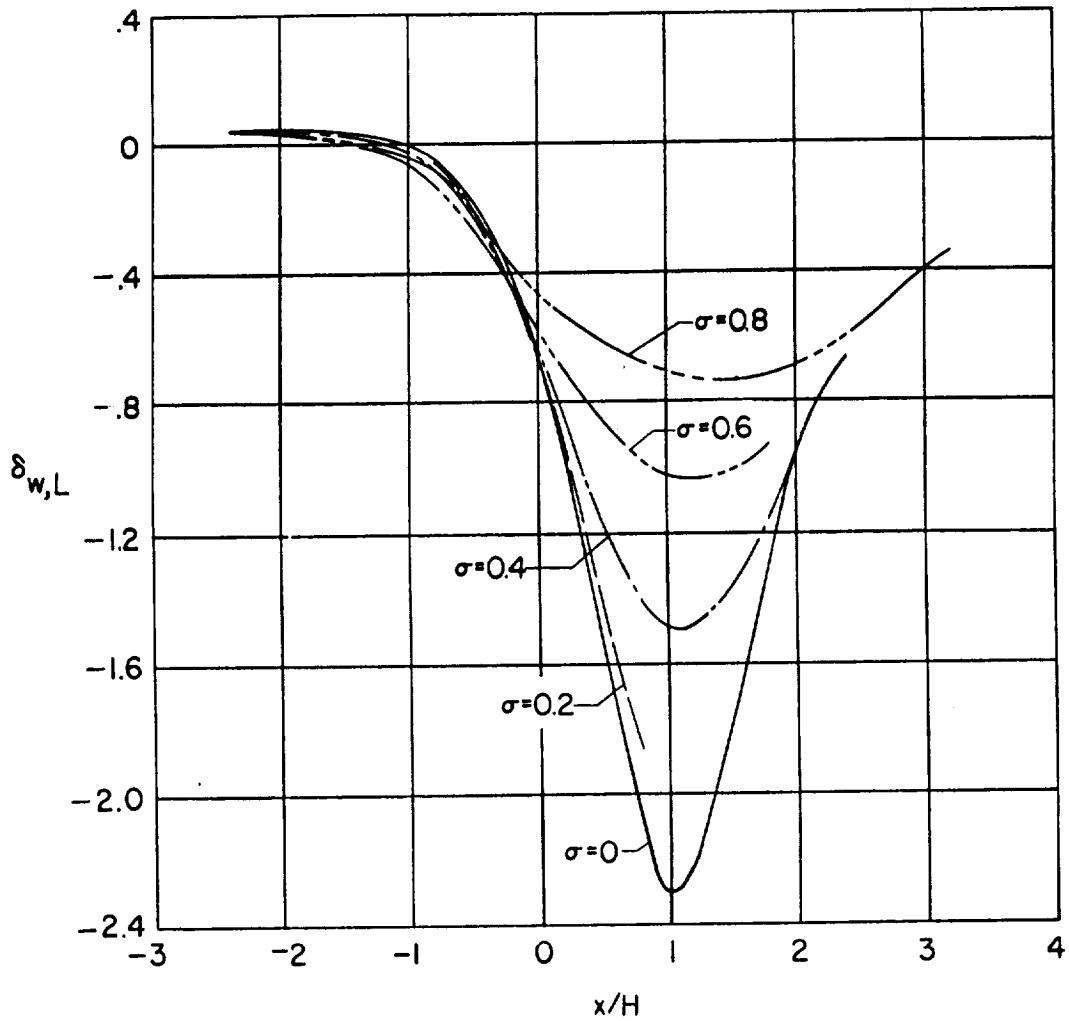


(d) $\chi = 45.00^{\circ}$.

Figure 97.- Continued.

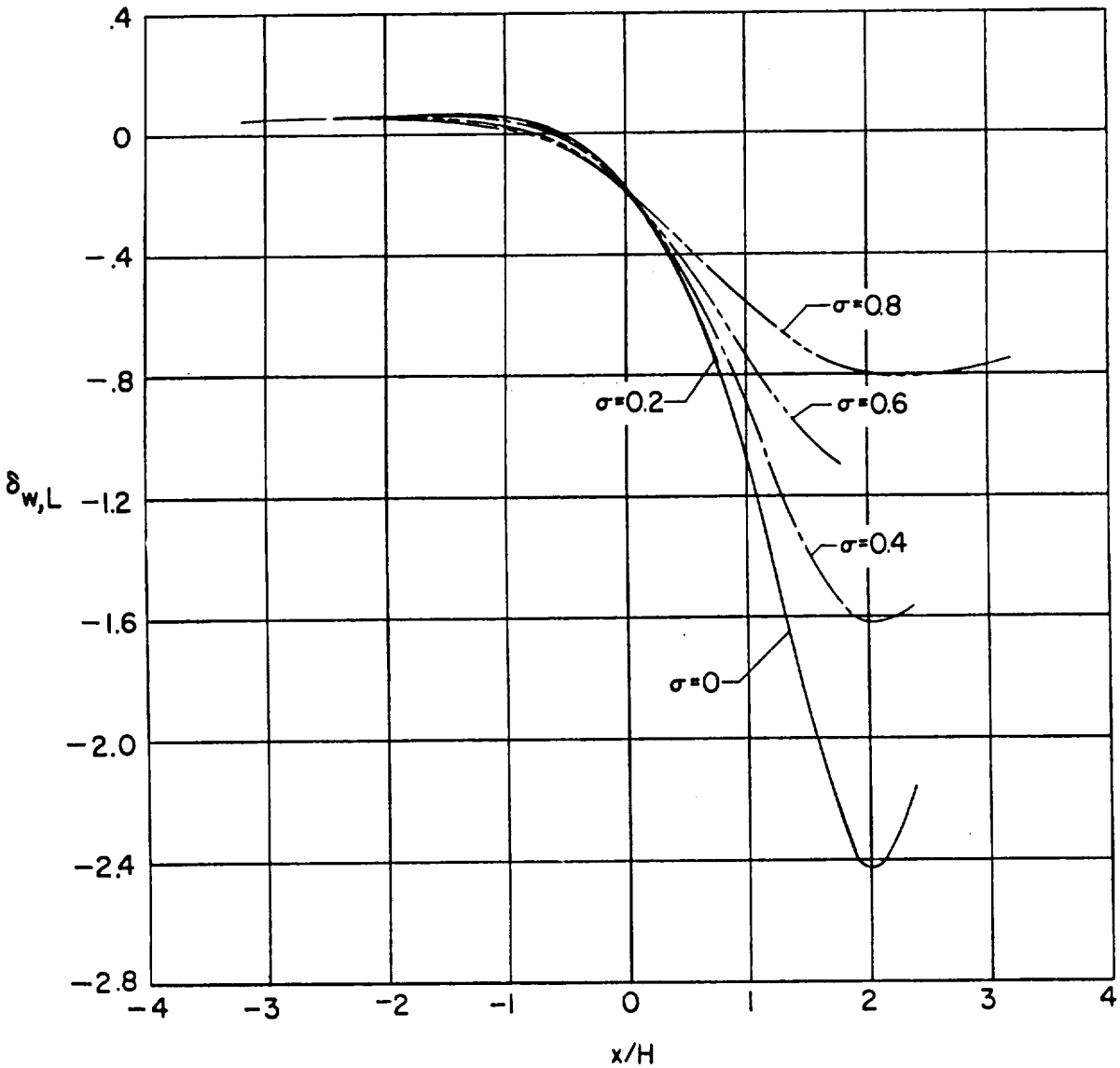


(e) $\chi = 63.43^{\circ}$.

Figure 97.- Continued.

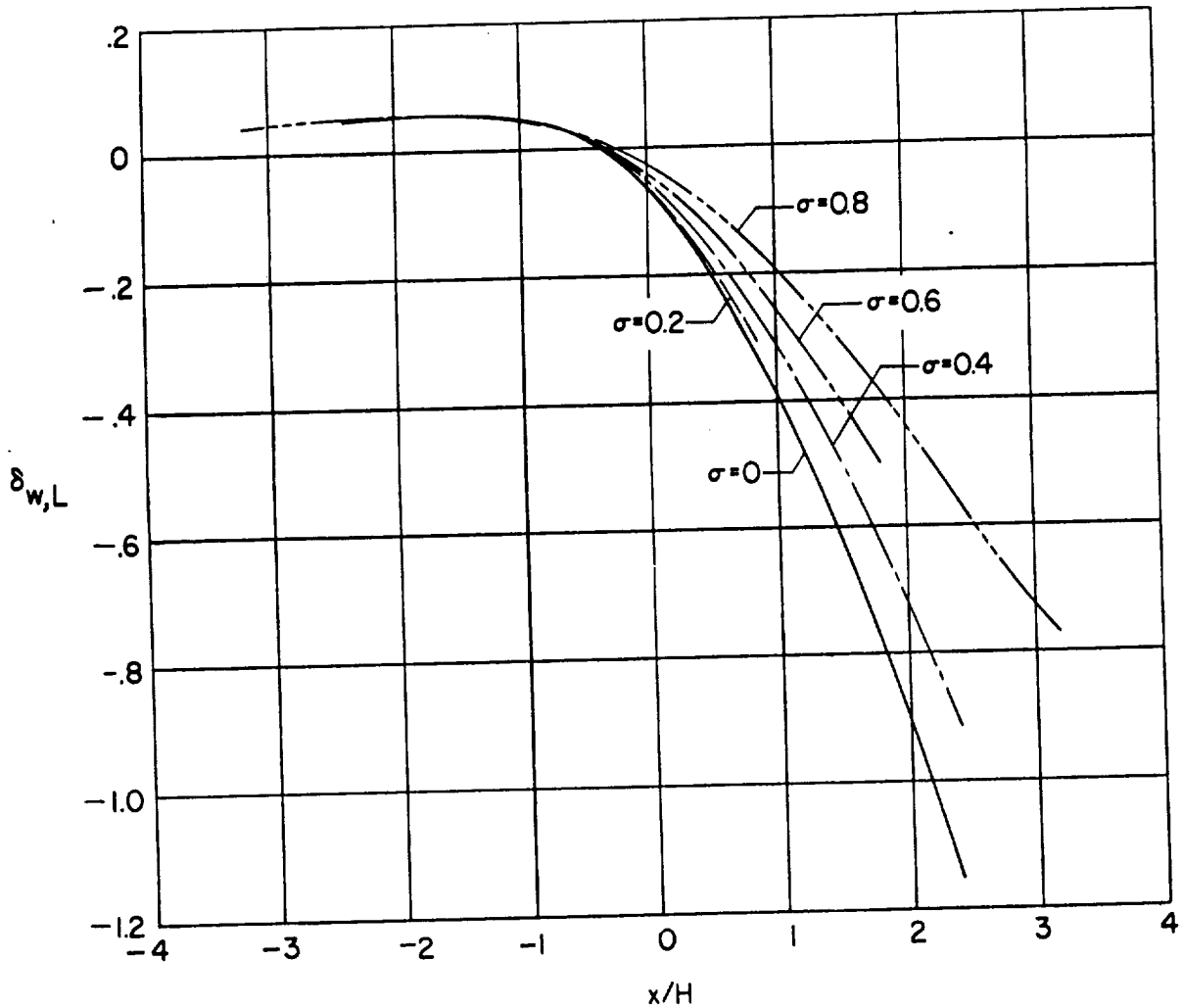


(f) $\chi = 75.97^{\circ}$.

Figure 97.- Continued.

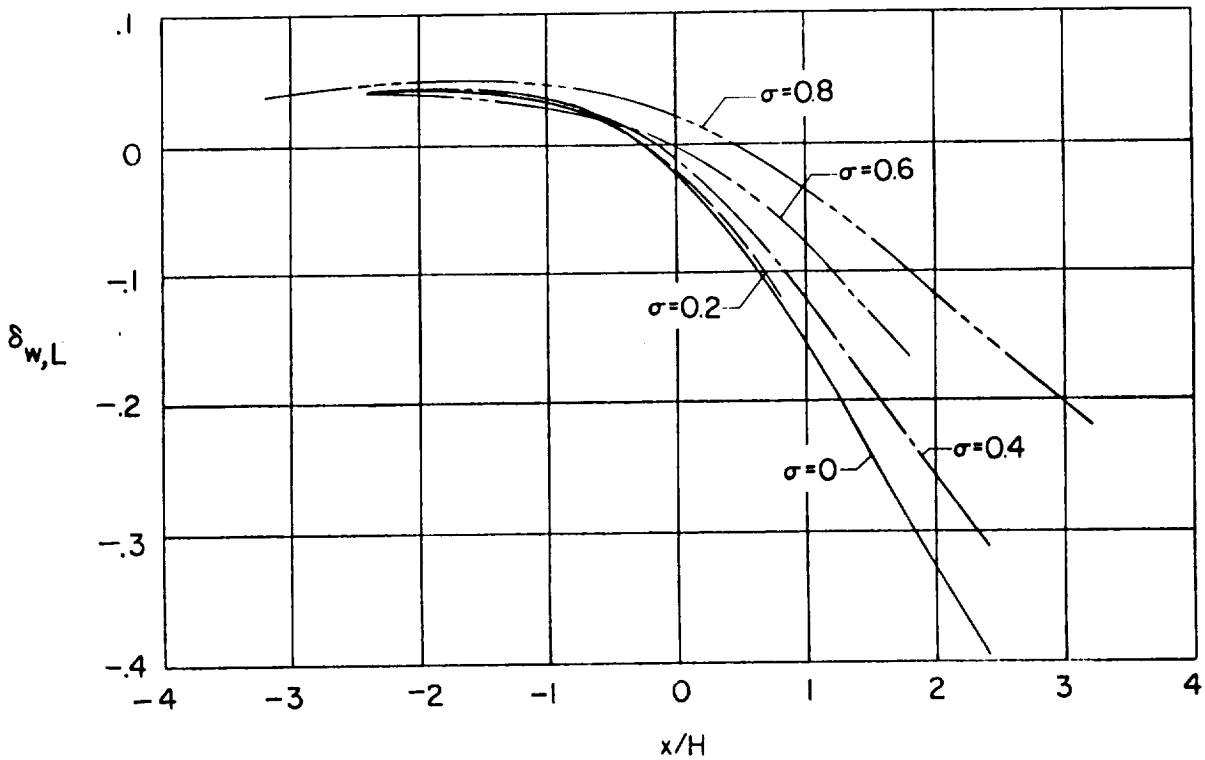


(g) $\chi = 84.29^{\circ}$.

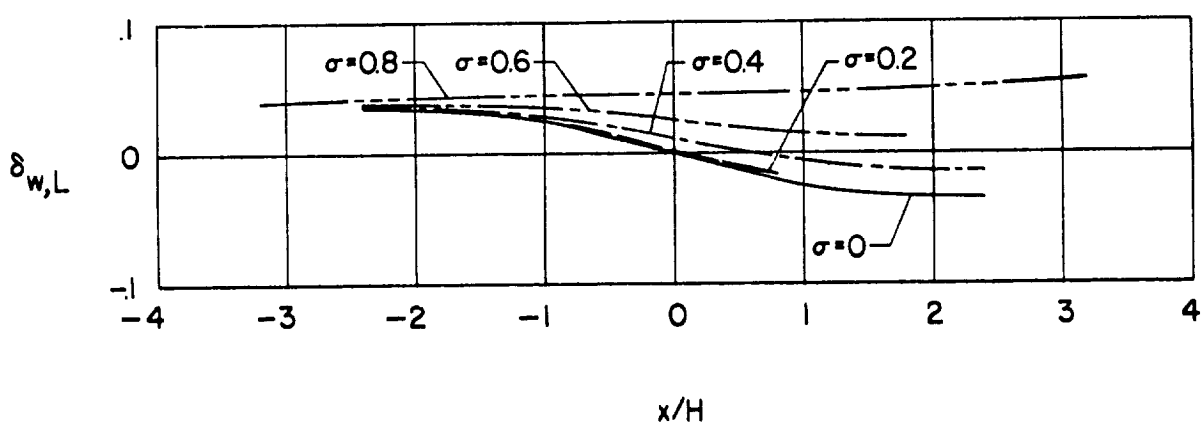


(h) $\chi = 90.00^{\circ}$.

Figure 97.- Concluded.

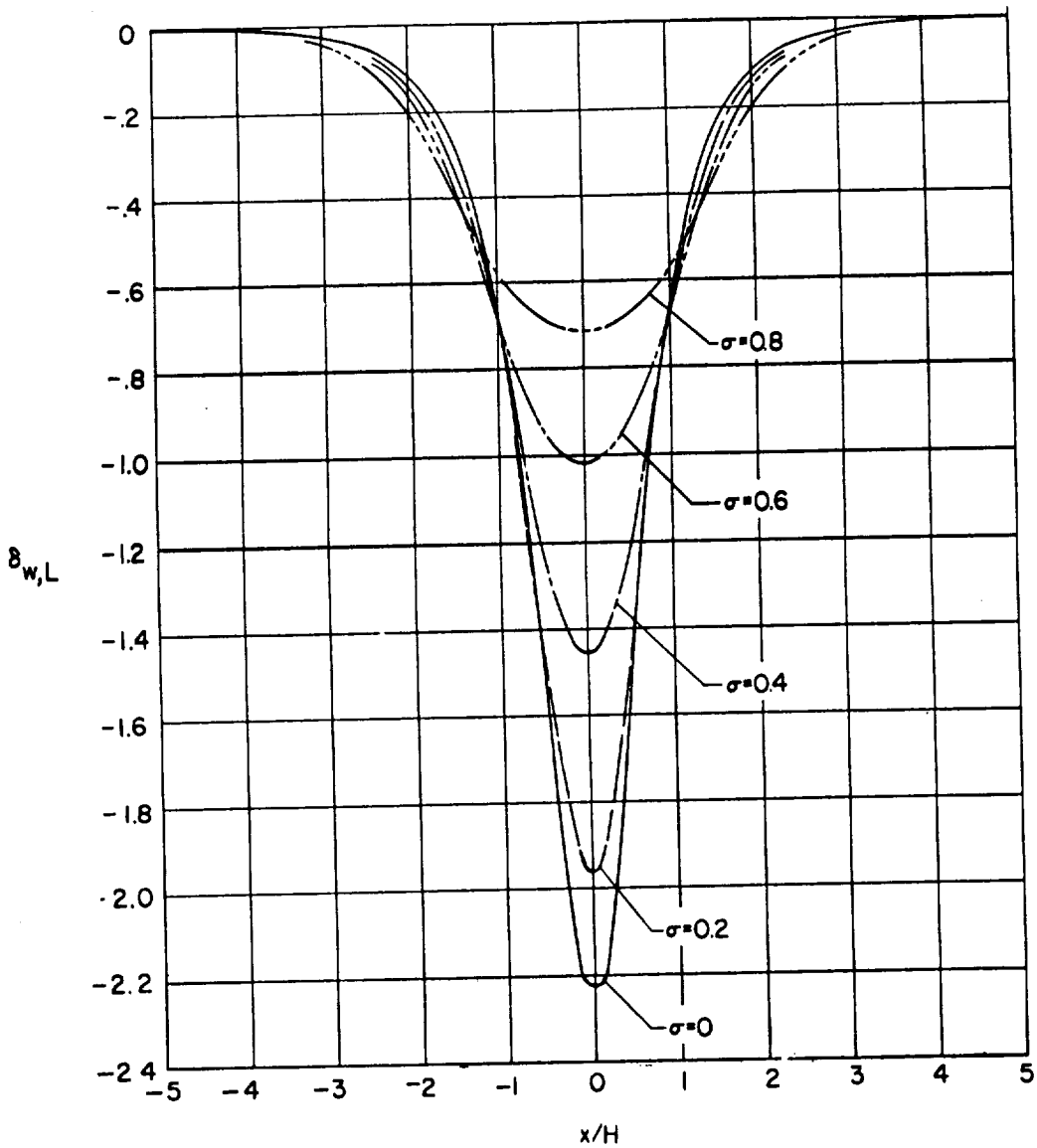


(a) $\chi = 0^{\circ}$.

Figure 98.- Effect of rotor size on the longitudinal distribution of vertical interference due to lift for closed floor only (ground effect). $\gamma = 2.0$; $\zeta = 1.0$.

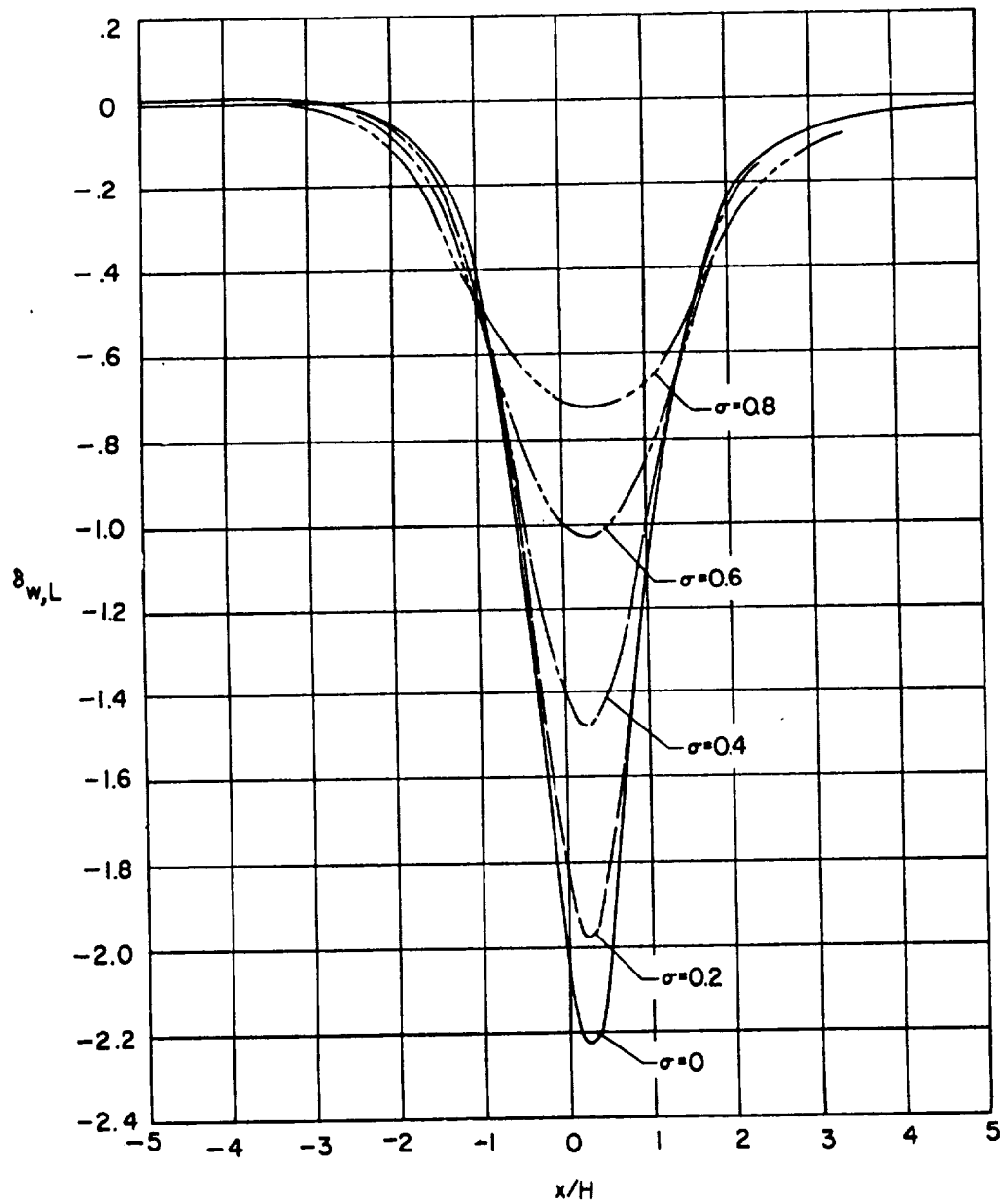


(b) $\chi = 14.04^{\circ}$.

Figure 98.- Continued.

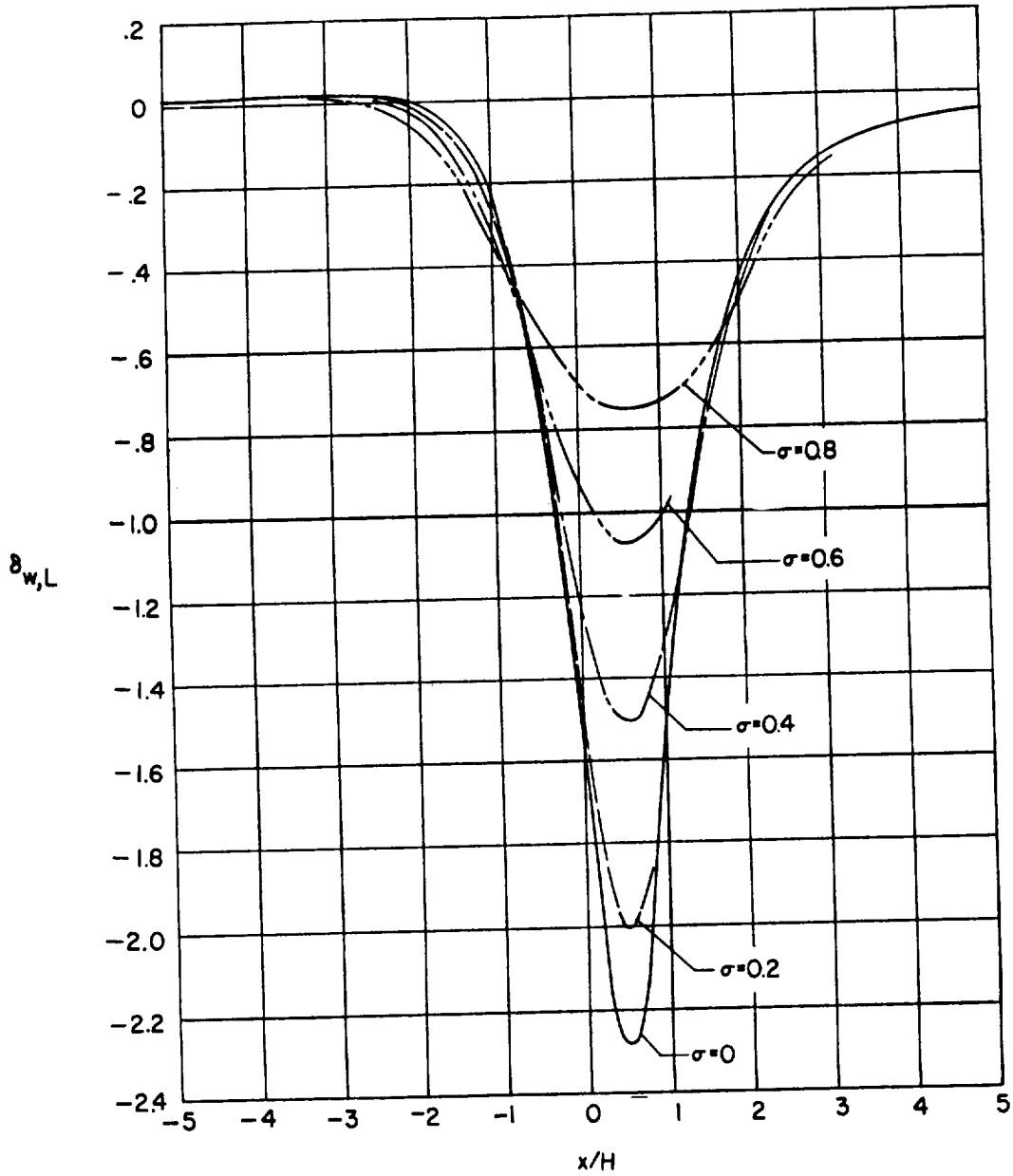


(c) $\chi = 26.56°$.

Figure 98.- Continued.

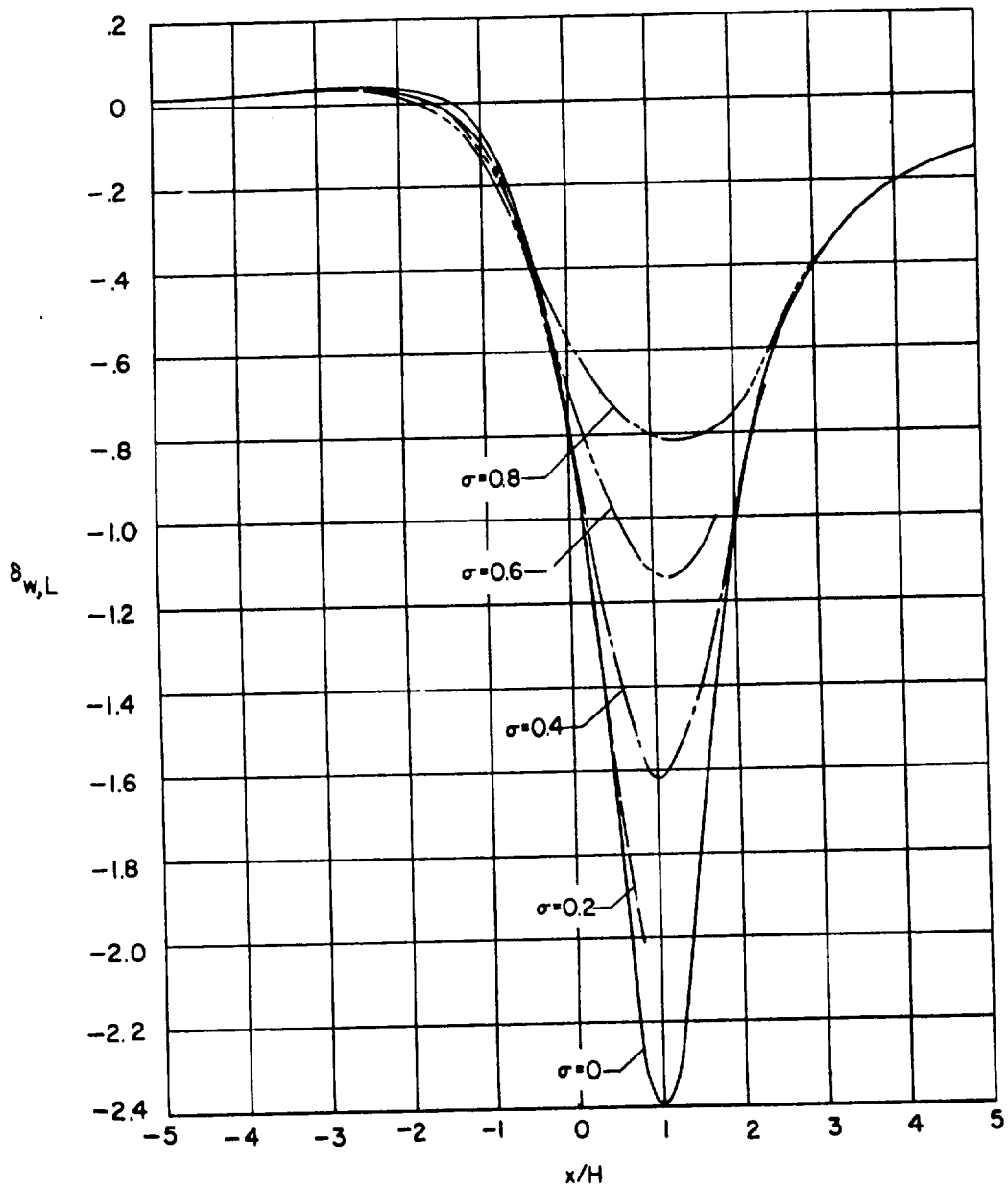


(d) $\chi = 45.00^{\circ}$.

Figure 98.- Continued.

632643 O—62——16

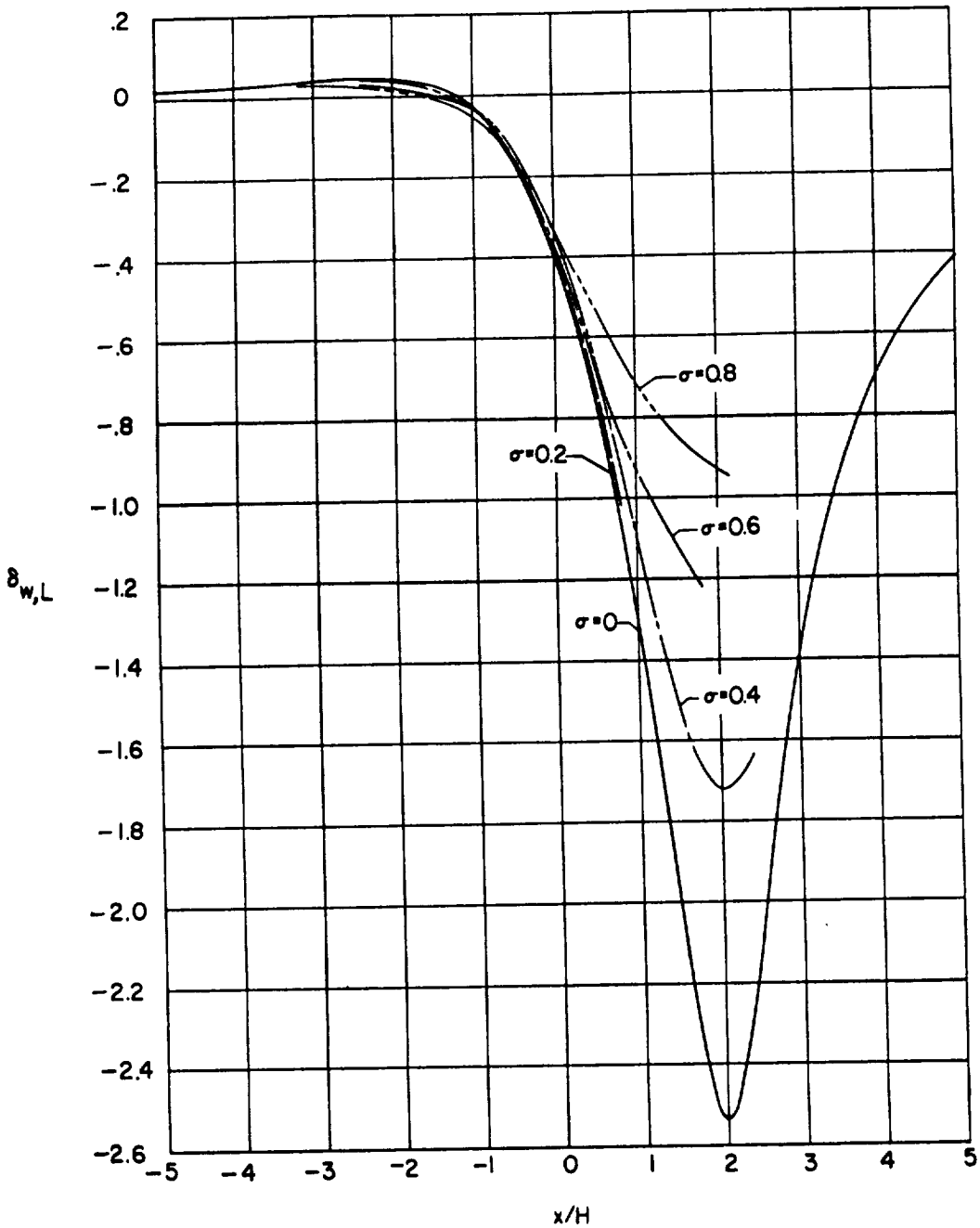


(e) $\chi = 63.43^{\circ}$.

Figure 98.- Continued.

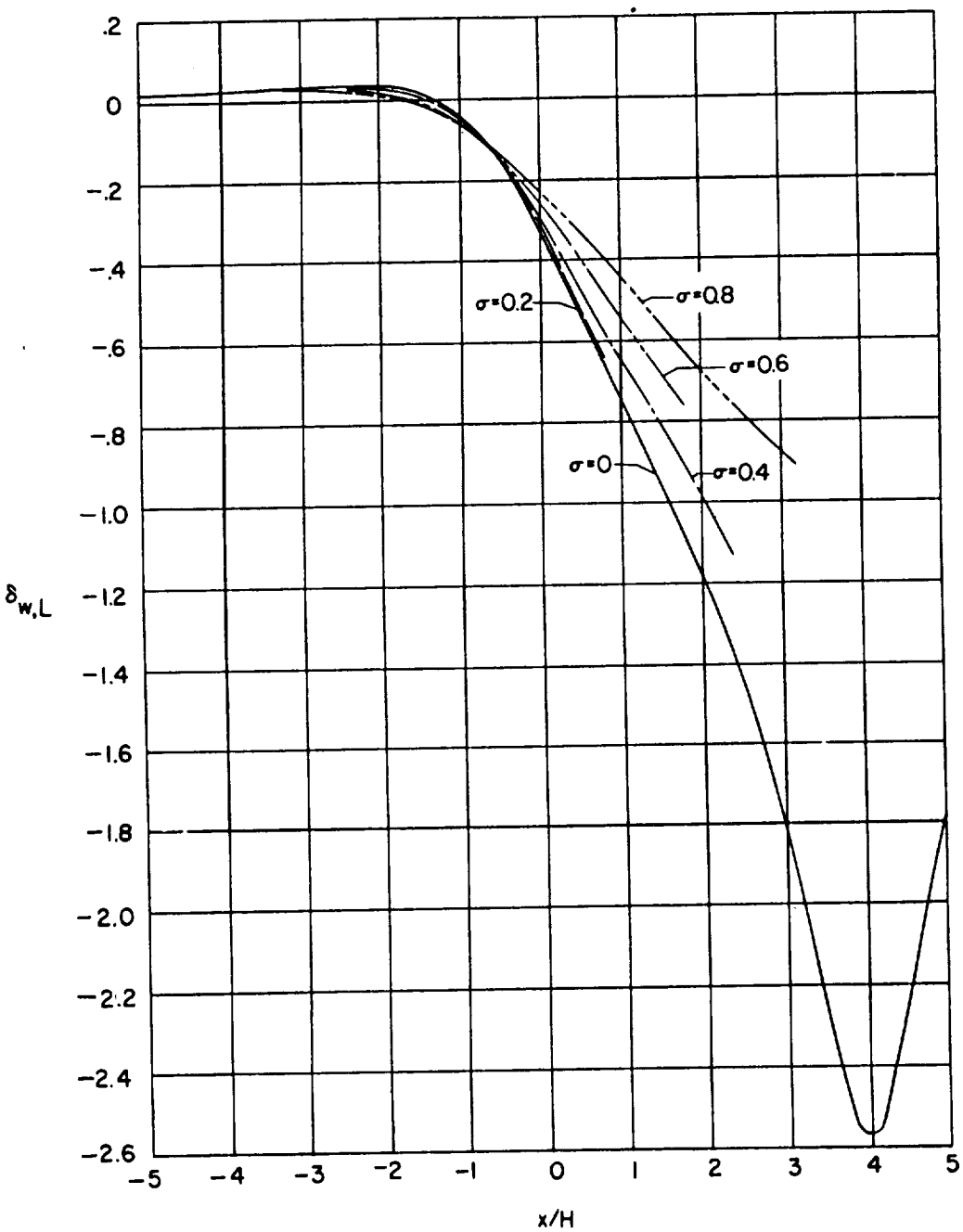


(f) $\chi = 75.97^{\circ}$.

Figure 98.- Continued.

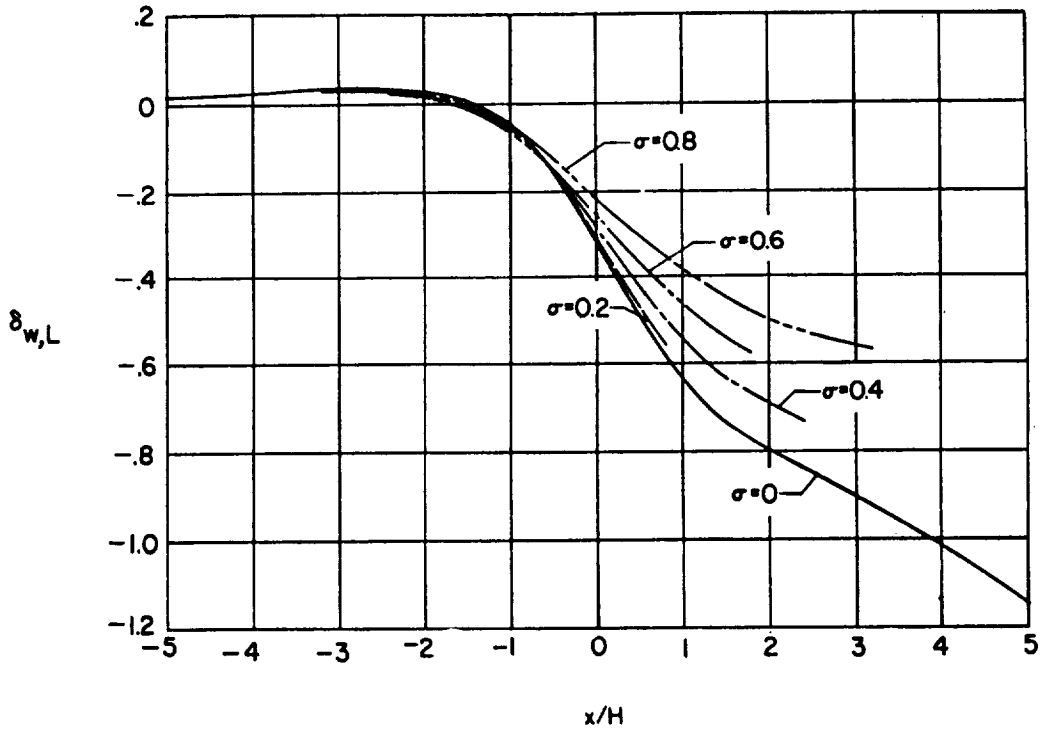


(g) X = 84.29°.

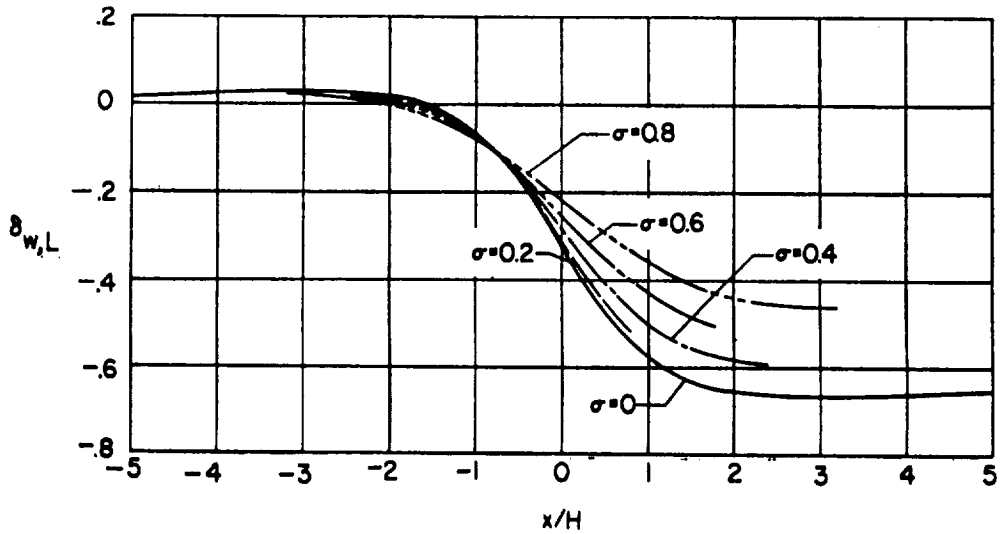


(h) X = 90.00°.

Figure 98.- Concluded.

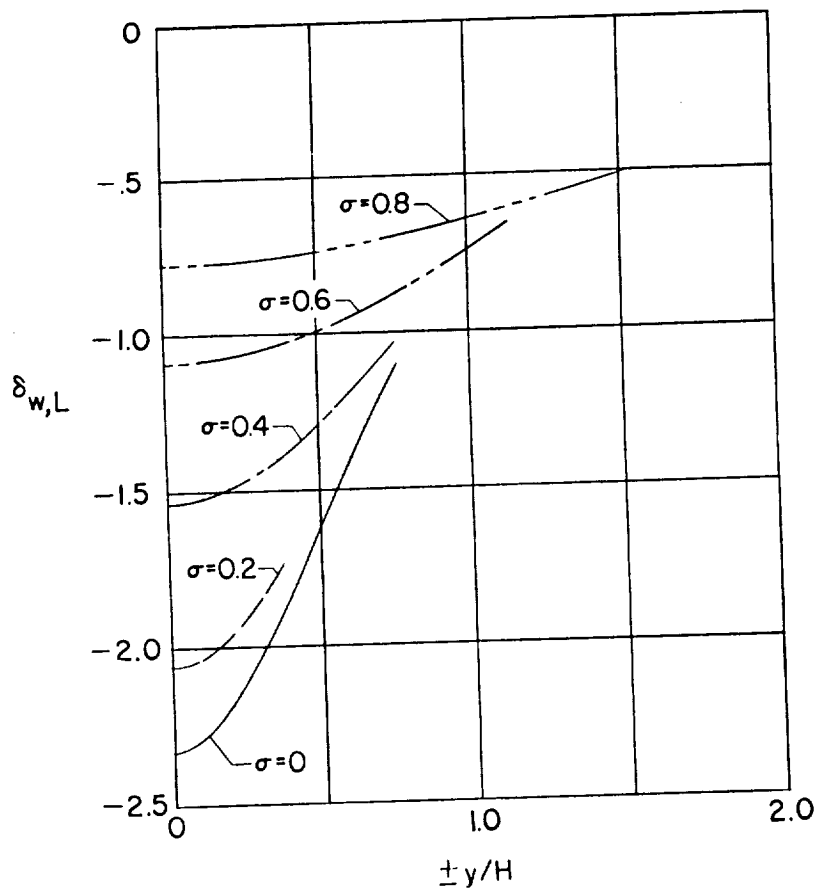


(a) $\chi = 0^{\circ}$.

Figure 99.- Effect of rotor size on the lateral distribution of vertical interference due to lift for closed wind tunnel. $\gamma = 2.0$; $\zeta = 1.0$.

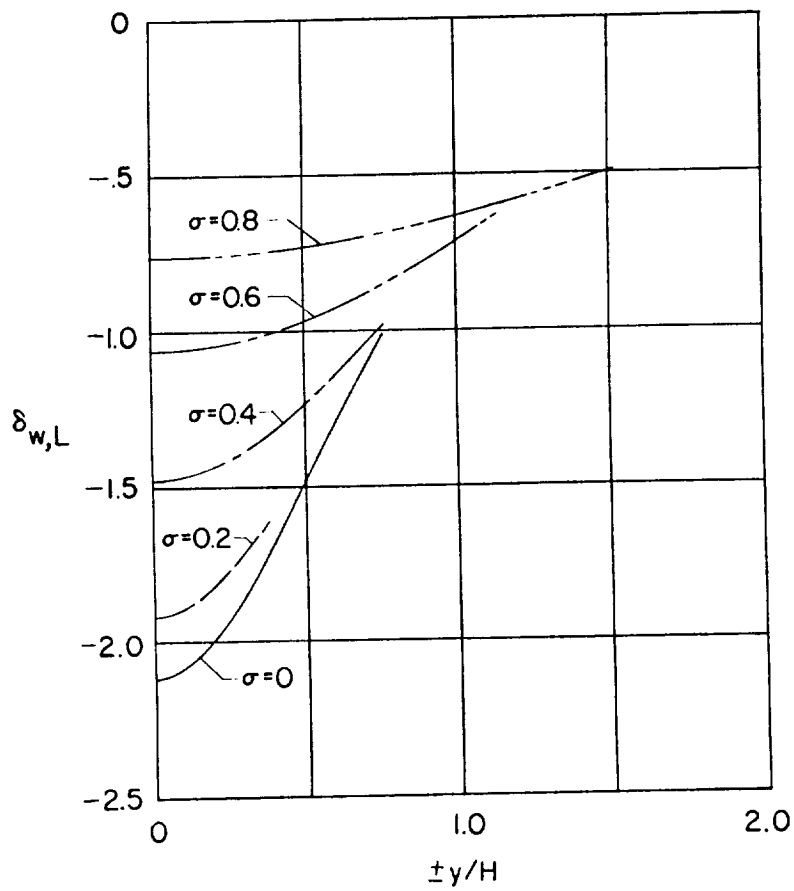


(b) $\chi = 14.04^{\circ}$.

Figure 99.- Continued.

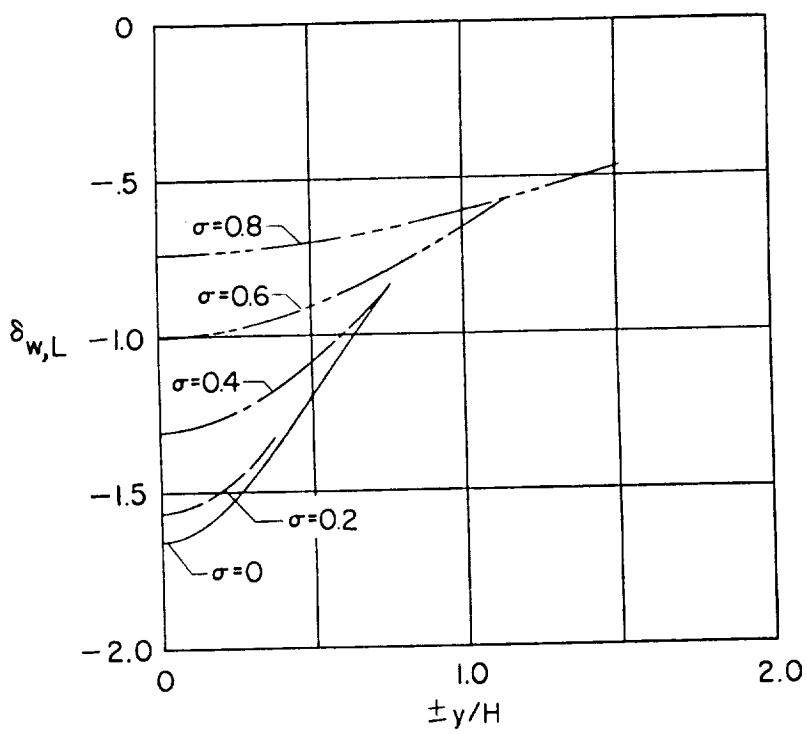


(c) $\chi = 26.56^{\circ}$.

Figure 99.- Continued.

632643 O—62——17

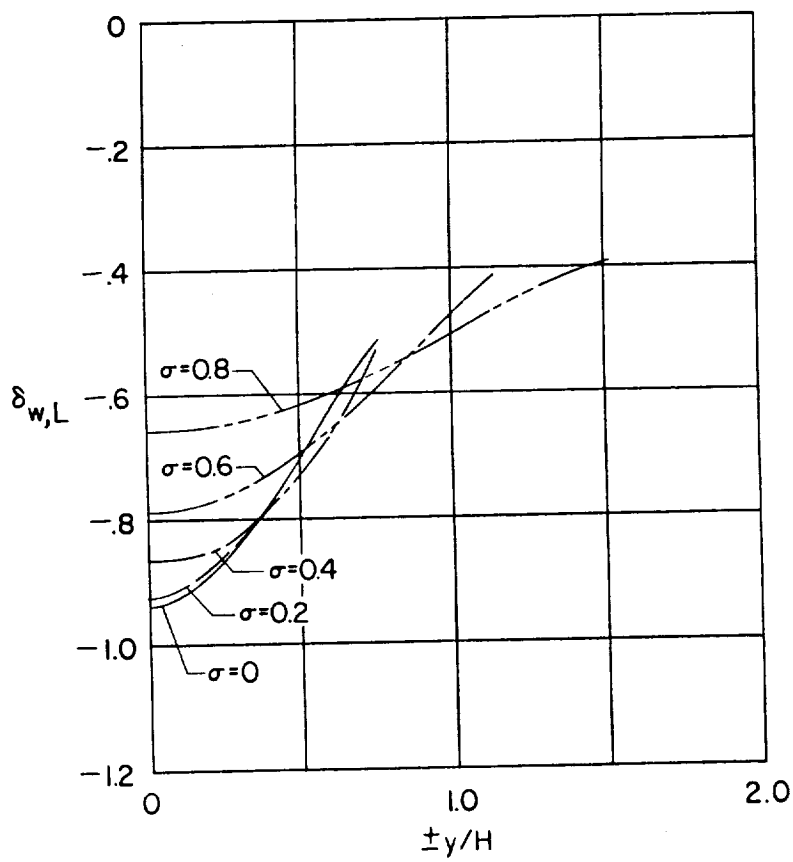


(d) $x = 45.00^{\circ}$.

Figure 99.- Continued.

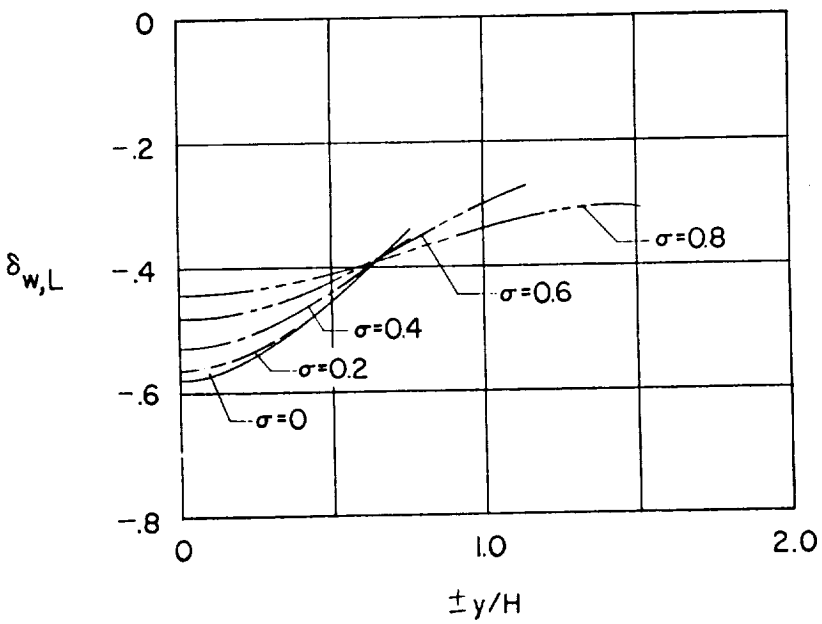


(e) $\chi = 63.43^{\circ}$.

Figure 99.- Continued.

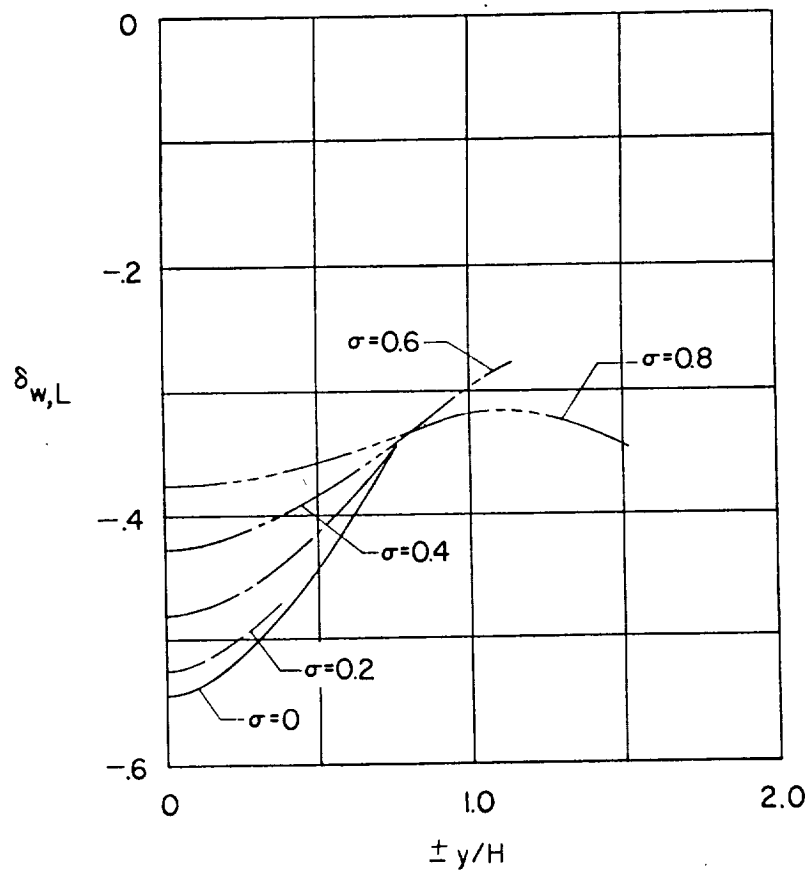


(f) $\chi = 75.97^{\circ}$.

Figure 99.- Continued.

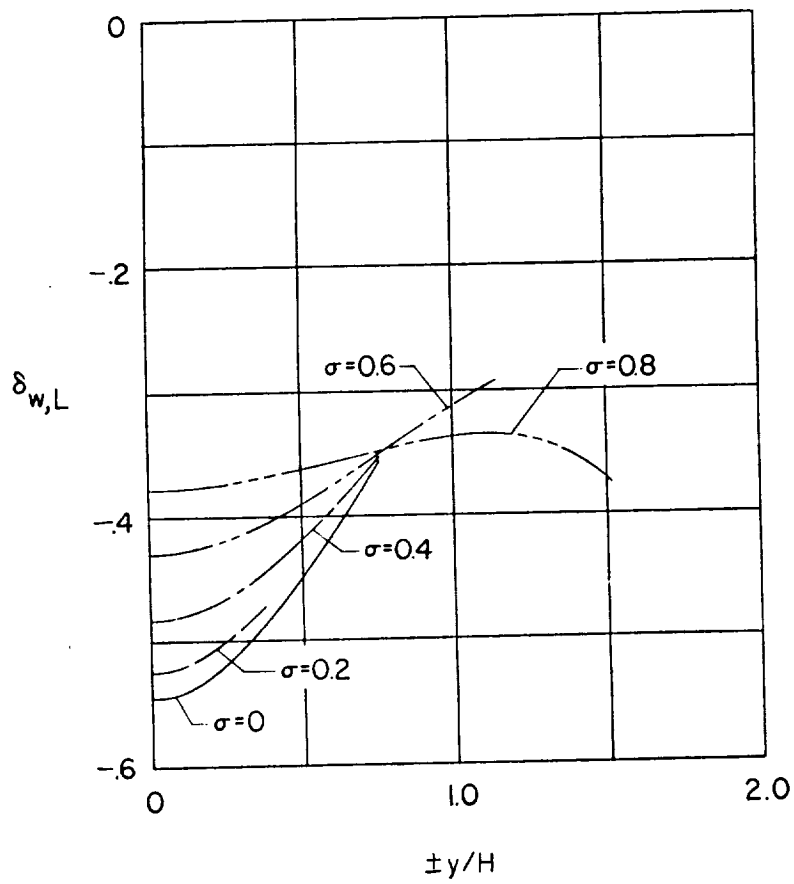


(g) $\chi = 84.29^{\circ}$.

Figure 99.- Continued.

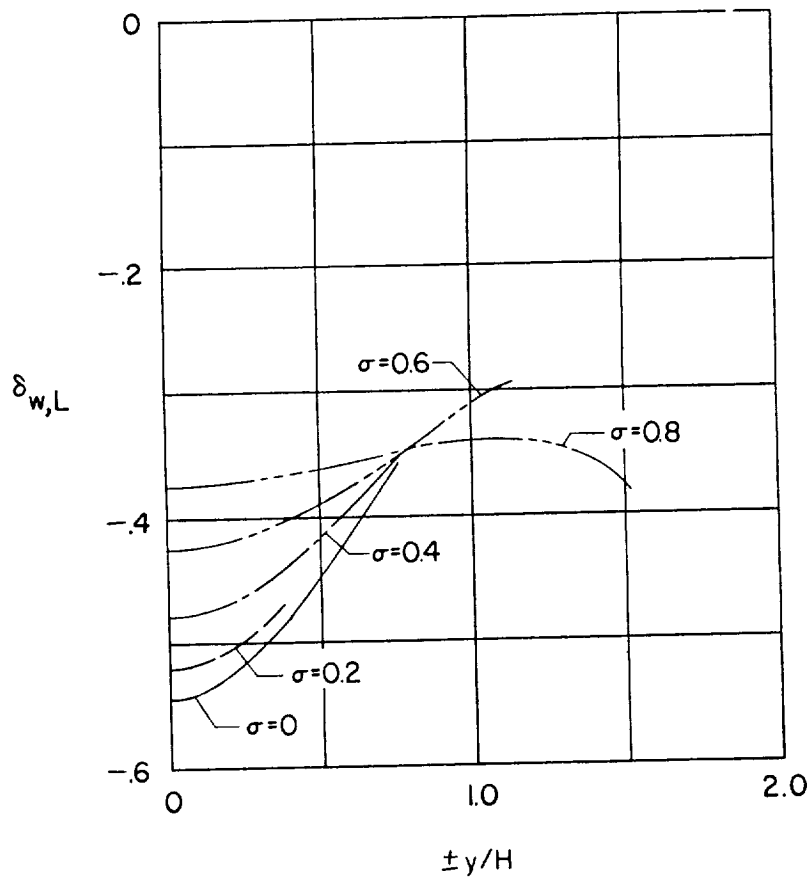


(h) $\chi = 90.00^{\circ}$.

Figure 99.- Concluded.

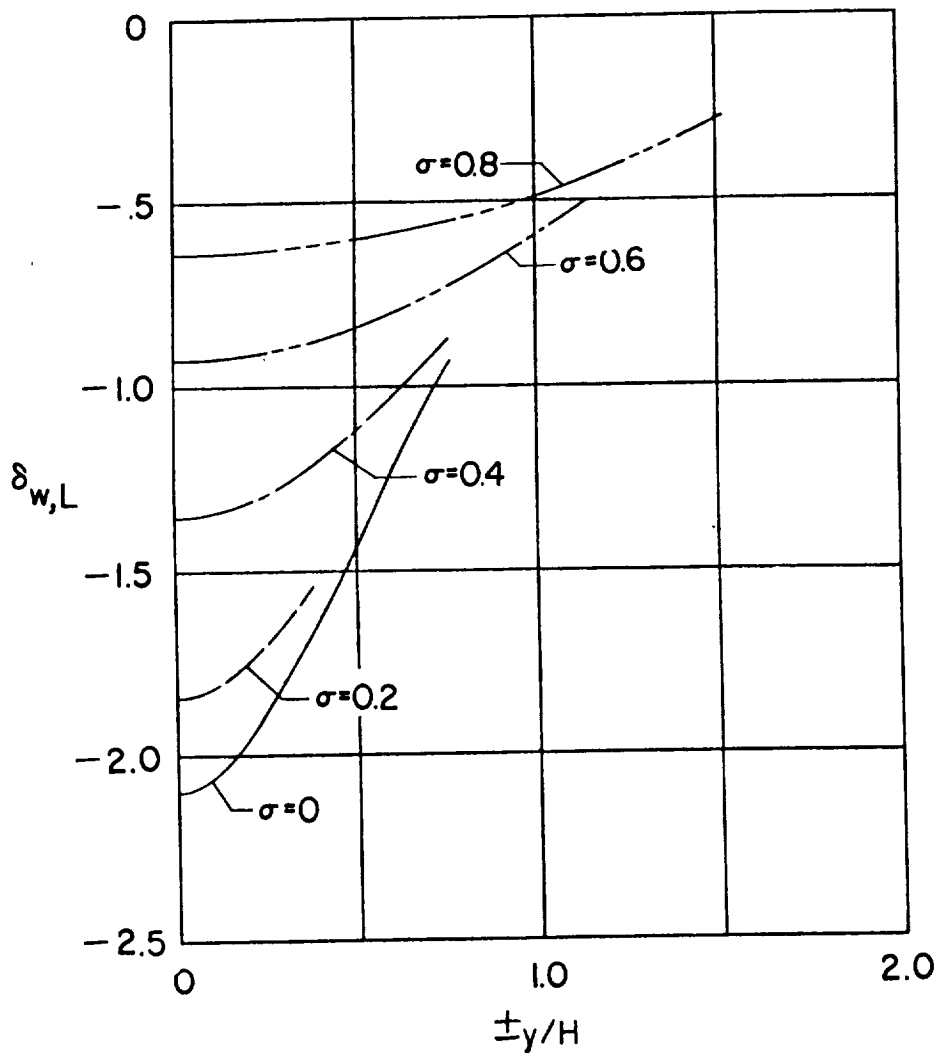


(a) $\chi = 0^{\circ}$.

Figure 100.- Effect of rotor size on the lateral distribution of vertical interference due to lift for wind tunnel closed on bottom only. $\gamma = 2.0$; $\zeta = 1.0$.

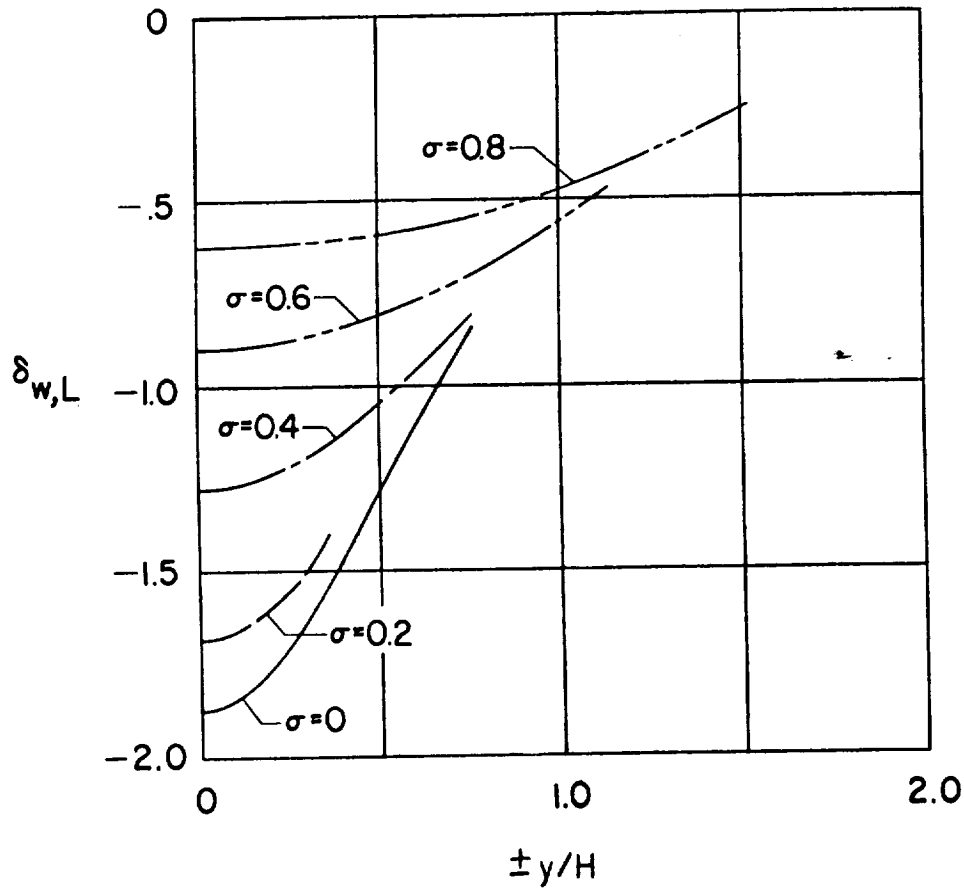


(b) $\chi = 14.04^{\circ}$.

Figure 100.- Continued.

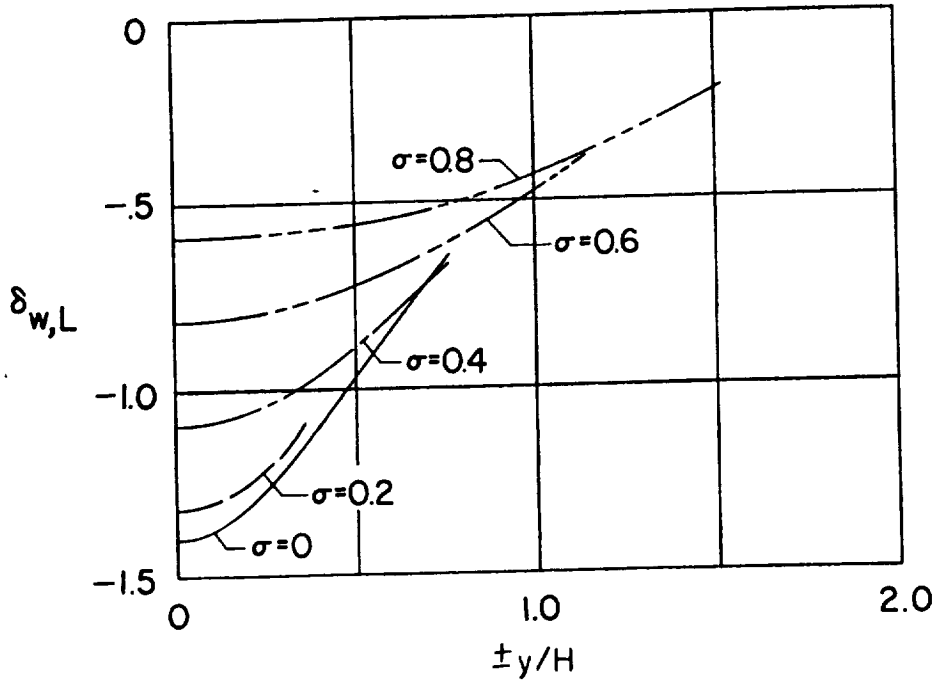


(c) x = 26.56°.

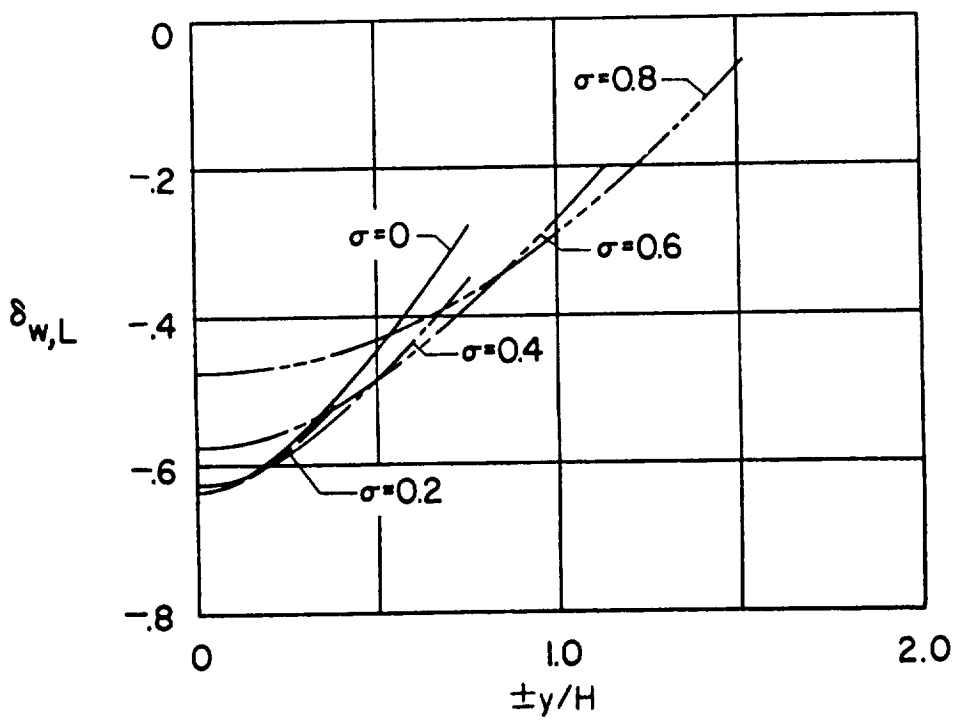


(d) x = 45.00°.

Figure 100.- Continued.

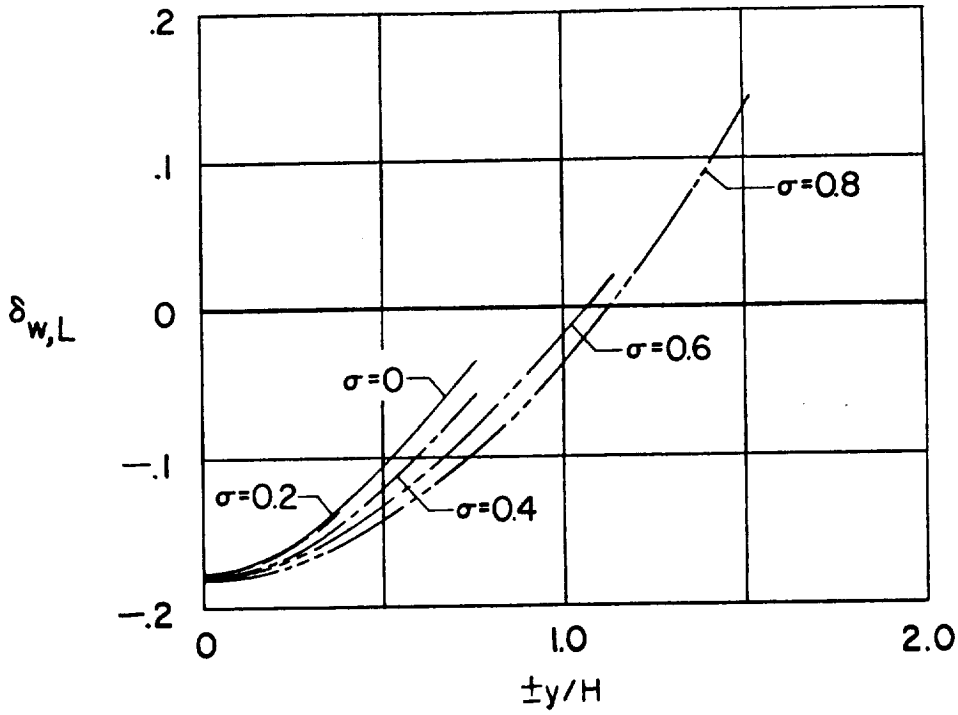


(e) x = 63.43°.

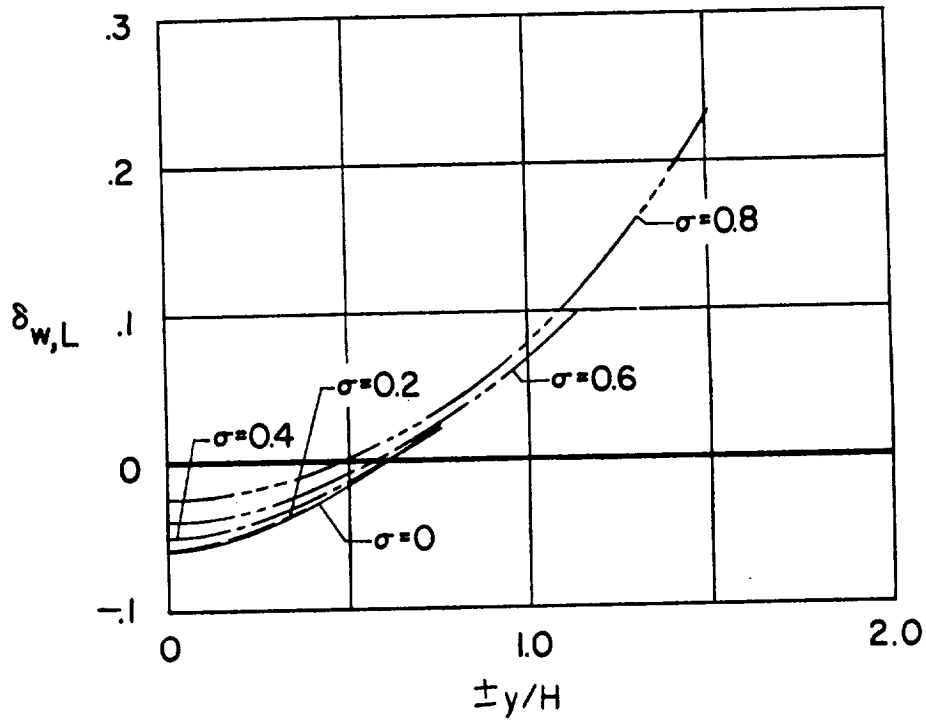


(f) x = 75.97°.

Figure 100.- Continued.

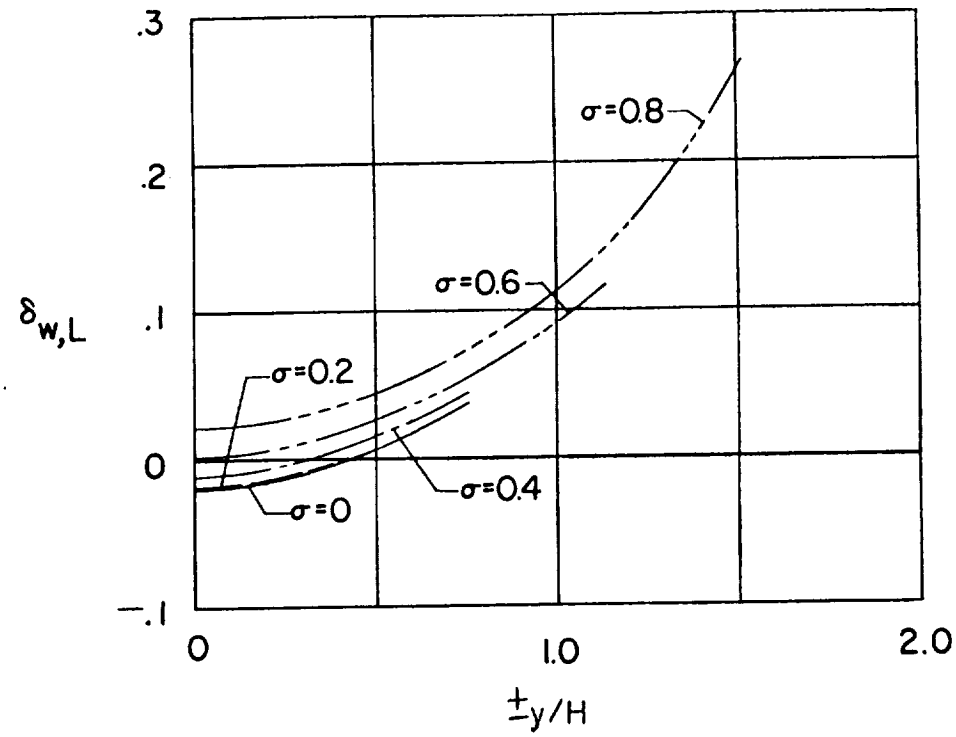


(g) x = 84.29°.

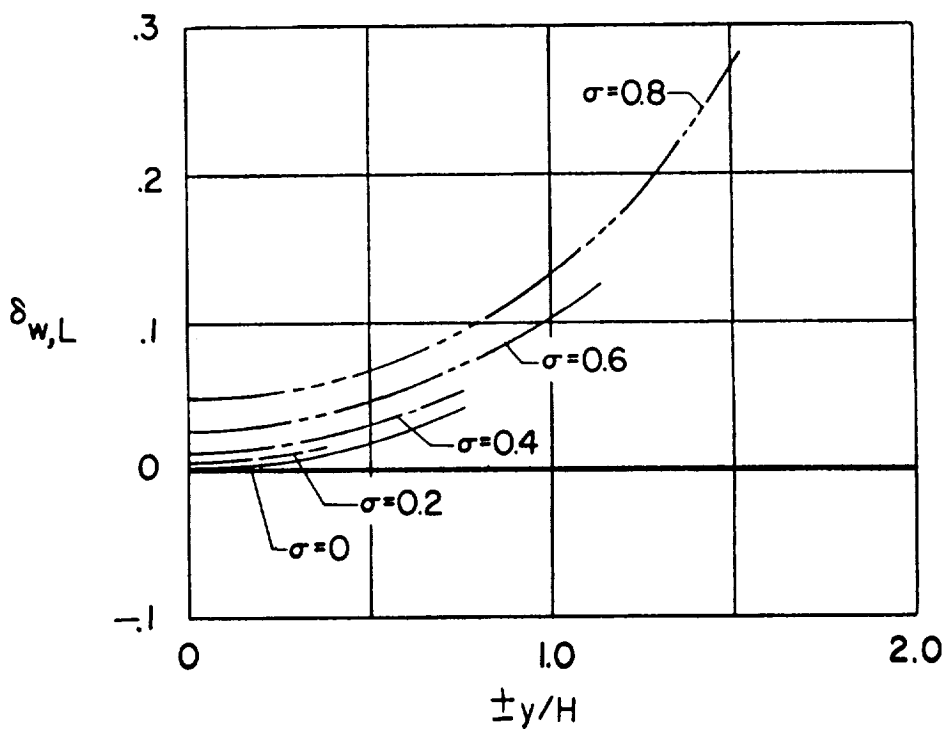


(h) x = 90.00°.

Figure 100.- Concluded.

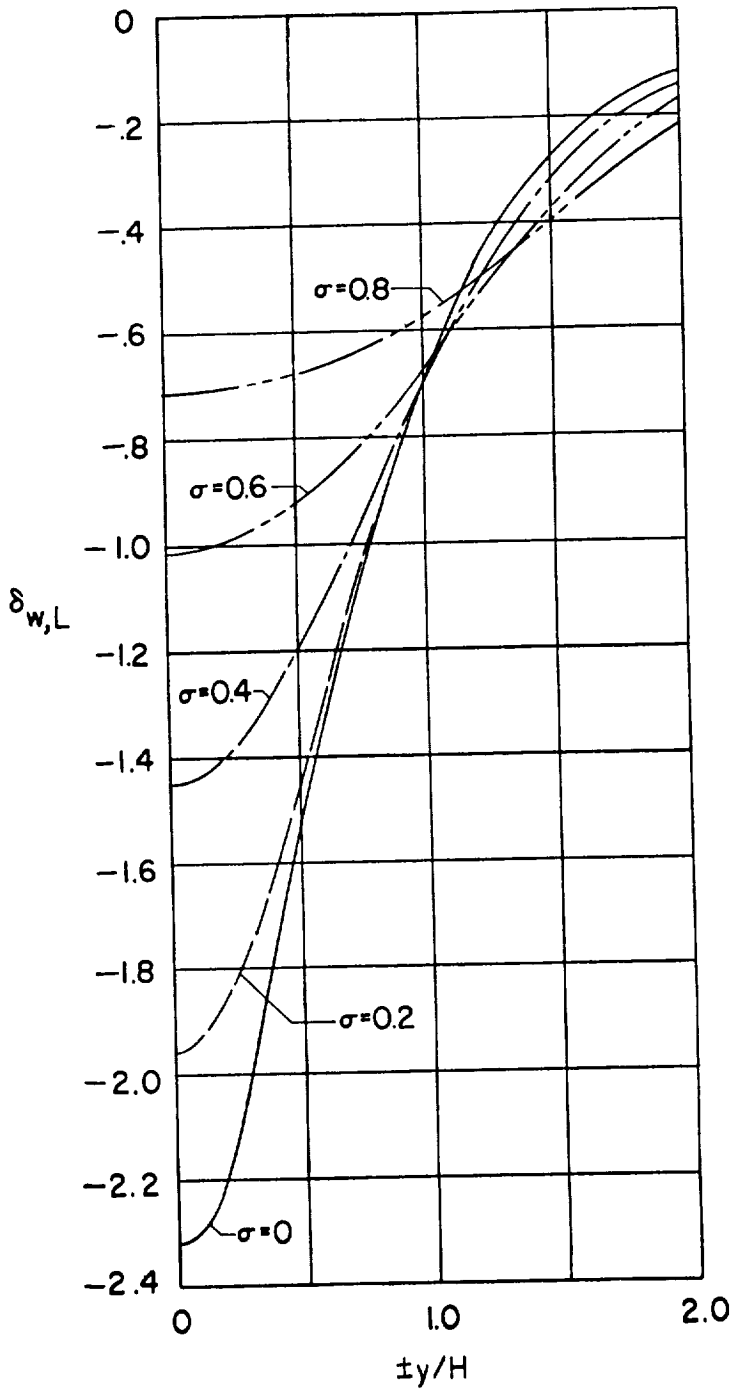


(a) $\chi = 0^{\circ}$.

Figure 101.- Effect of rotor size on the lateral distribution of vertical interference due to lift for closed floor only (ground effect). $\gamma = 2.0$.

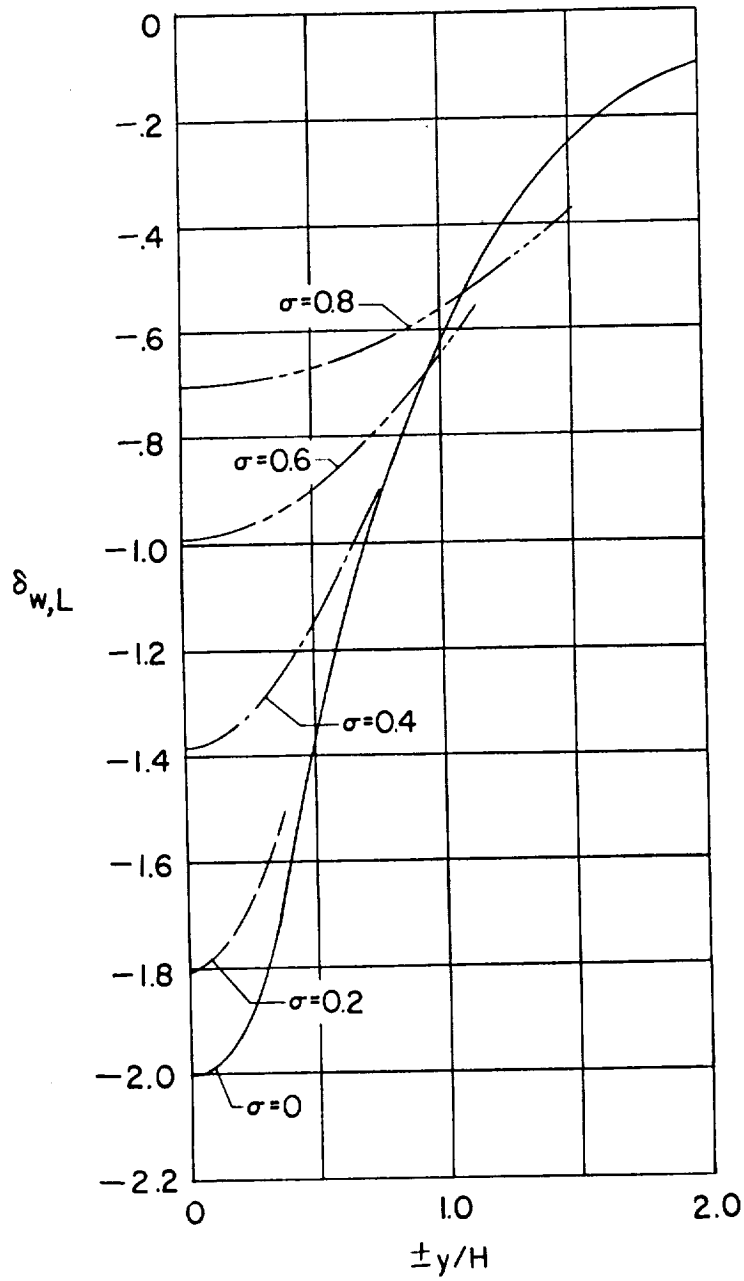


(b) $\chi = 14.04^{\circ}$.

Figure 101.- Continued.

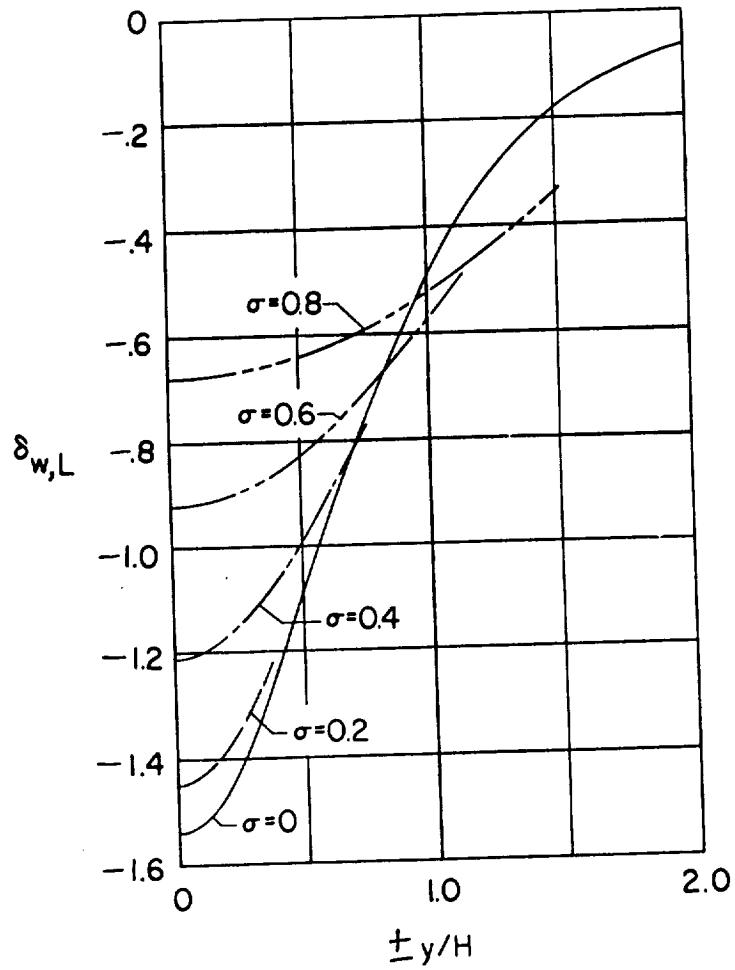


(c) $\chi = 26.56^{\circ}$.

Figure 101.- Continued.

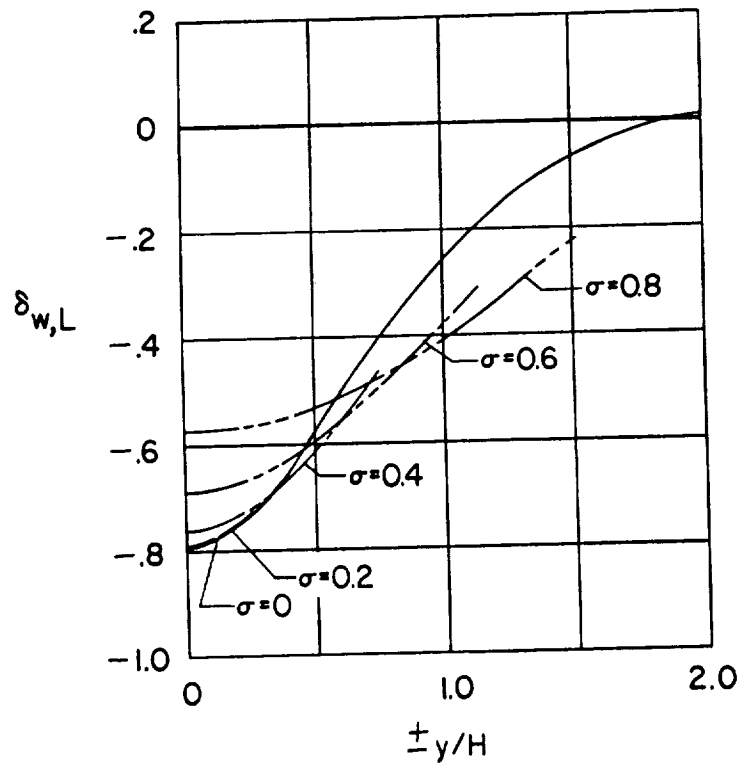


(d) $\chi = 45.00^{\circ}$.

Figure 101.- Continued.

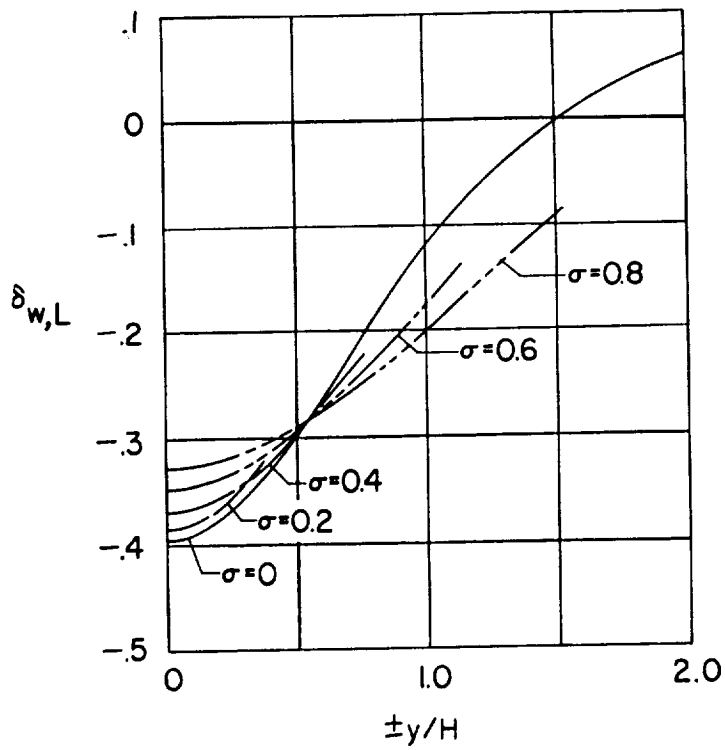


(e) $\chi = 63.43^{\circ}$.

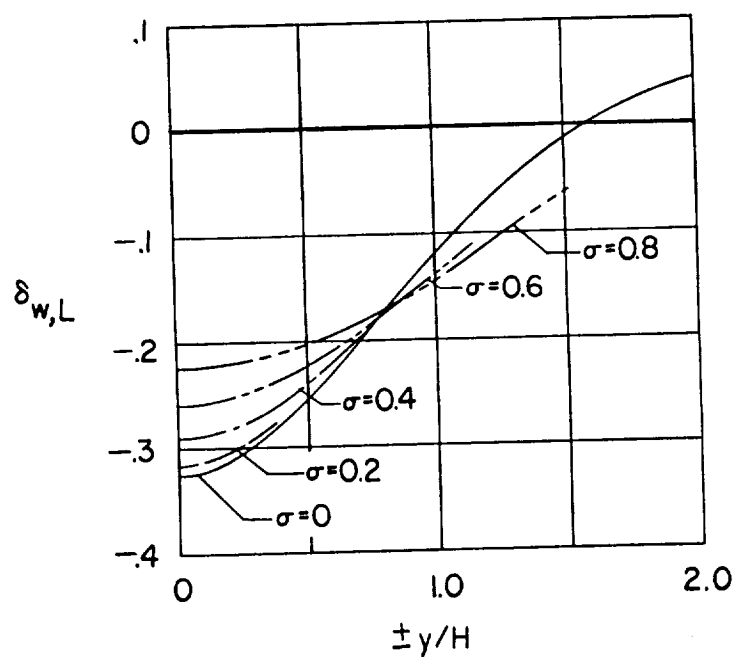


(f) $\chi = 75.97^{\circ}$.

Figure 101.- Continued.

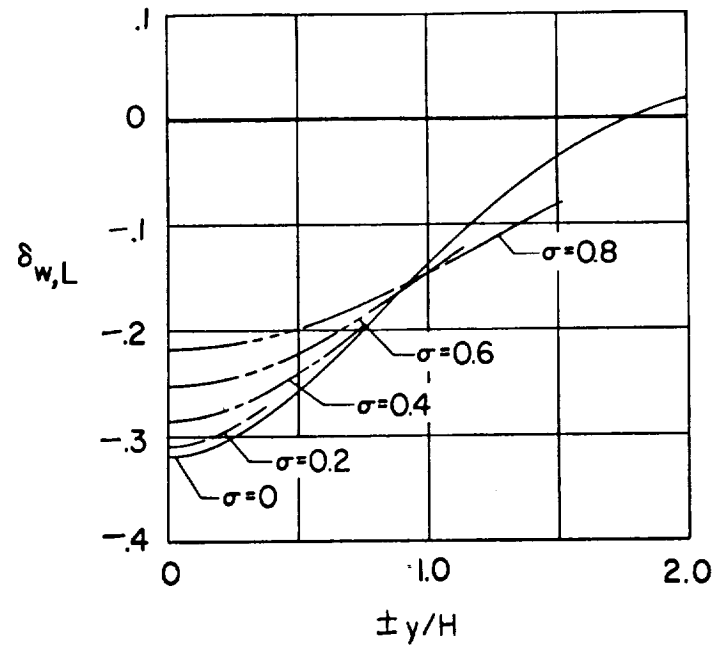


(g) $\chi = 84.29^{\circ}$.

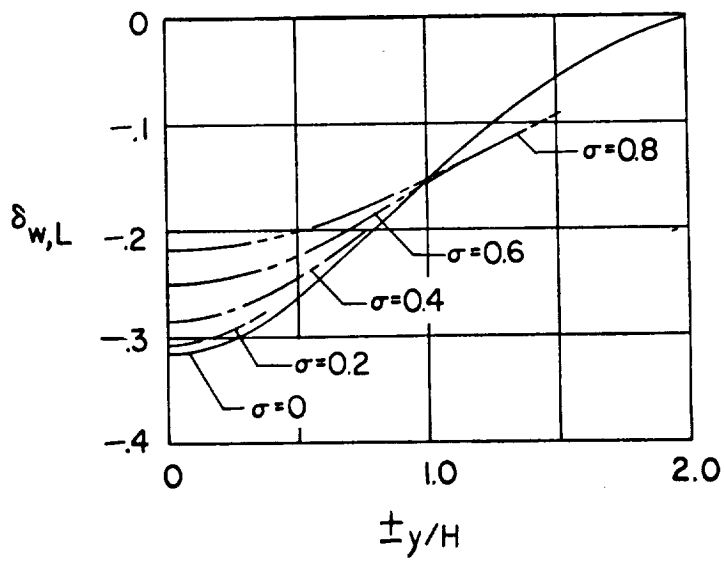


(h) $\chi = 90.00^{\circ}$.

Figure 101.- Concluded.

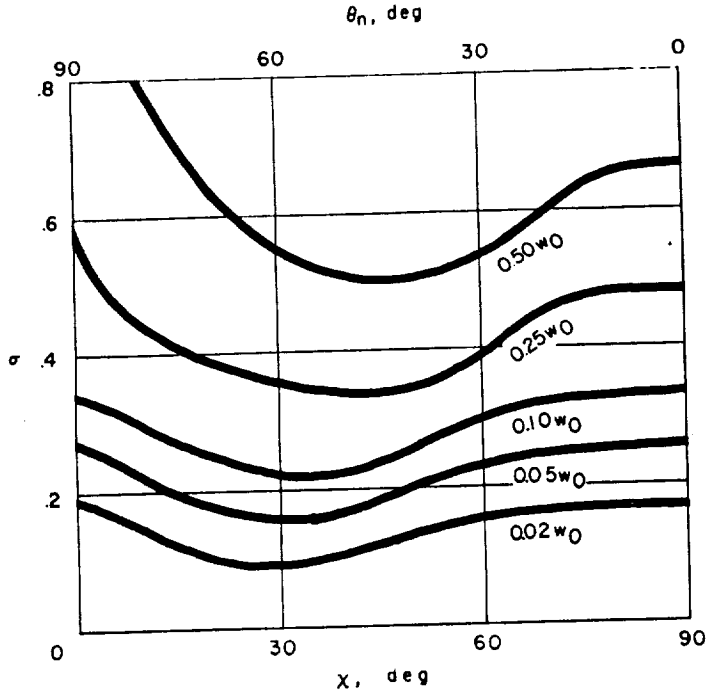


(a) Closed wind tunnel.

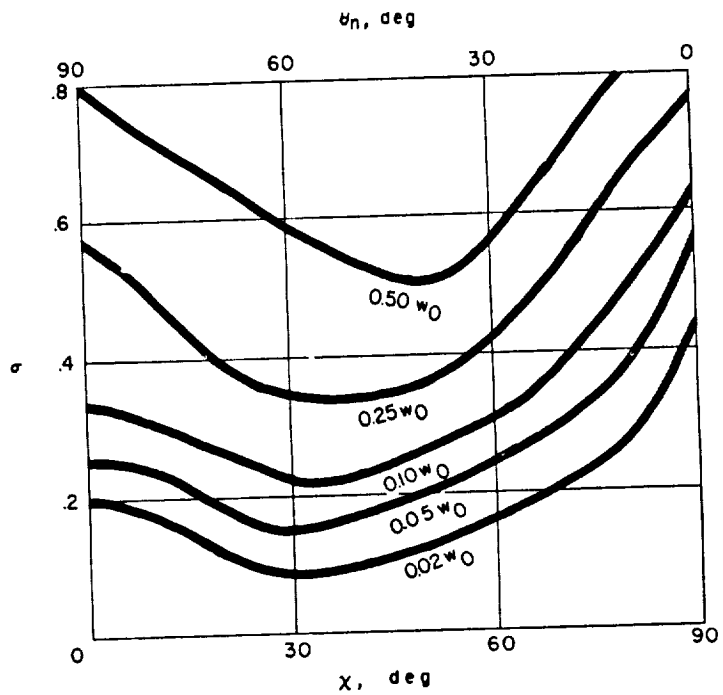


(b) Wind tunnel closed on the bottom only.

Figure 102.- Values of diameter-width ratio σ for given variations in vertical interference due to lift along the principal axes of rotors centered in a rectangular wind tunnel having a width-height ratio of 2.0.

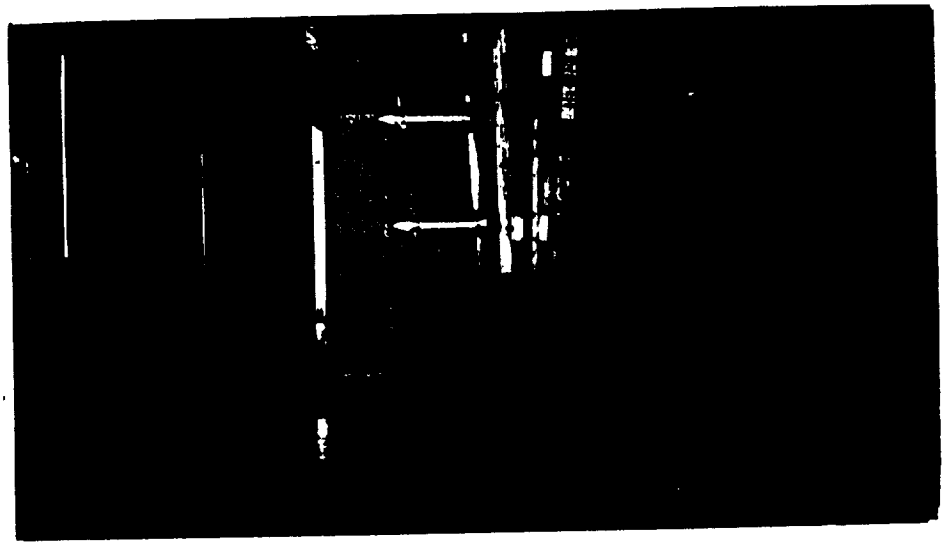

L-82208

Figure 103.- Typical semispan model installation in the Langley 300-MPH 7- by 10-foot tunnel.

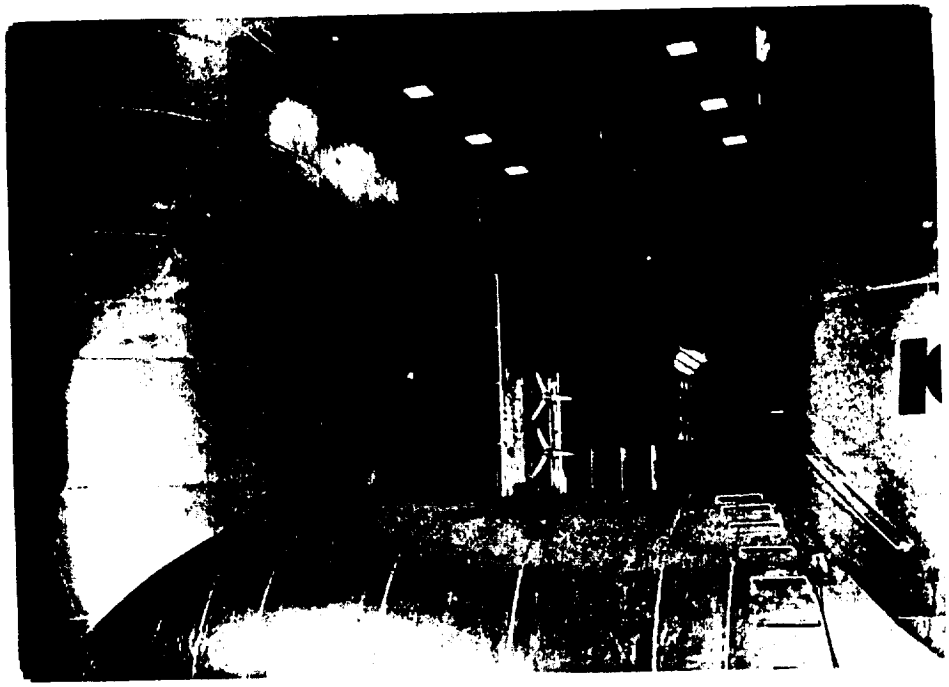

L-57-1192

Figure 104.- Typical installation of semispan model and ground board in 17-foot test section of Langley 300-MPH 7- by 10-foot tunnel.

632643 O—62——18

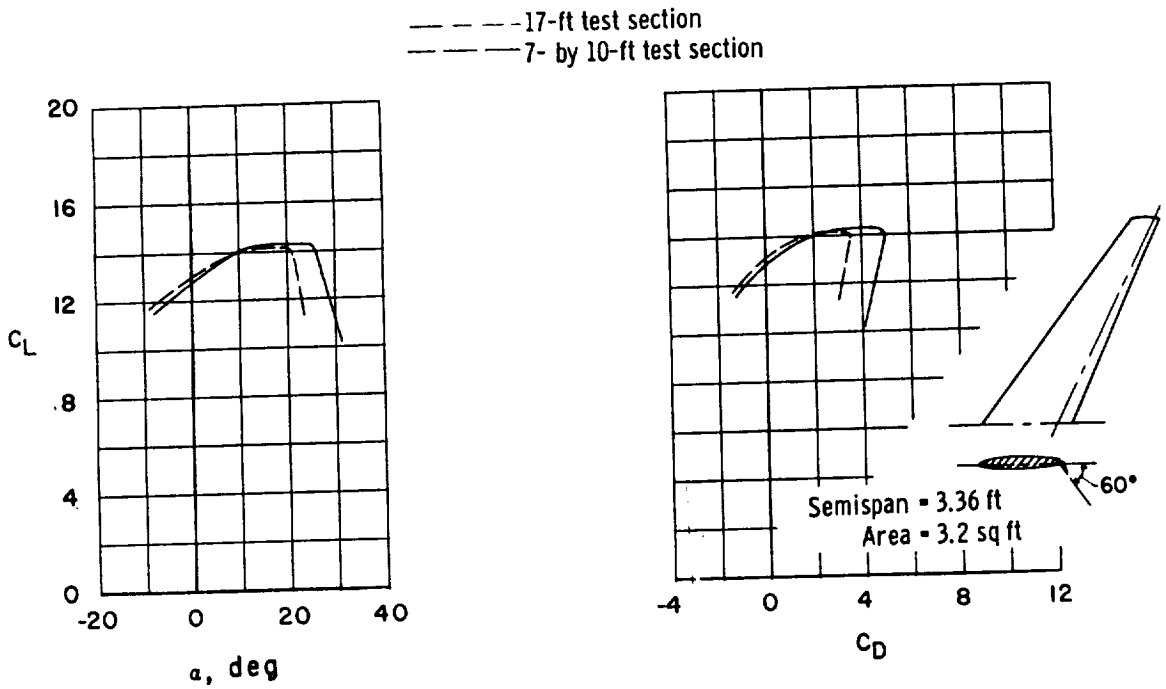


(a) As tested at $C_\mu$ = 6.20, with no jet-boundary corrections.

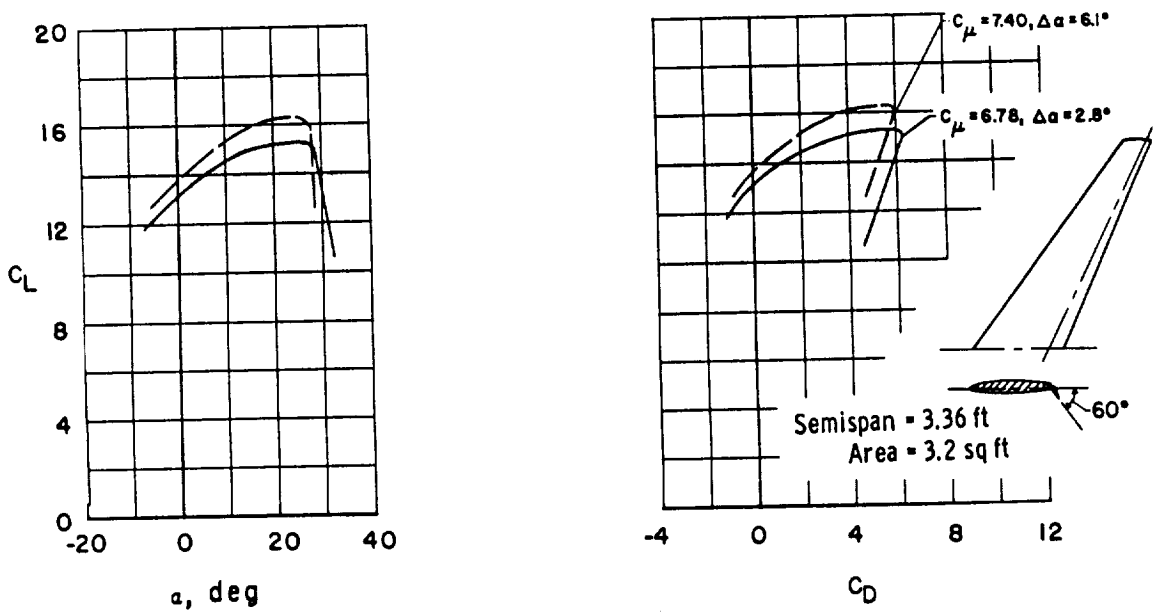


(b) With jet-boundary corrections.

Figure 105.- Tests of a swept-wing jet flap model in 17-foot test section compared with those in 7- by 10-foot test section. (Uncorrected data from fig. 9(a) of ref. 7.)

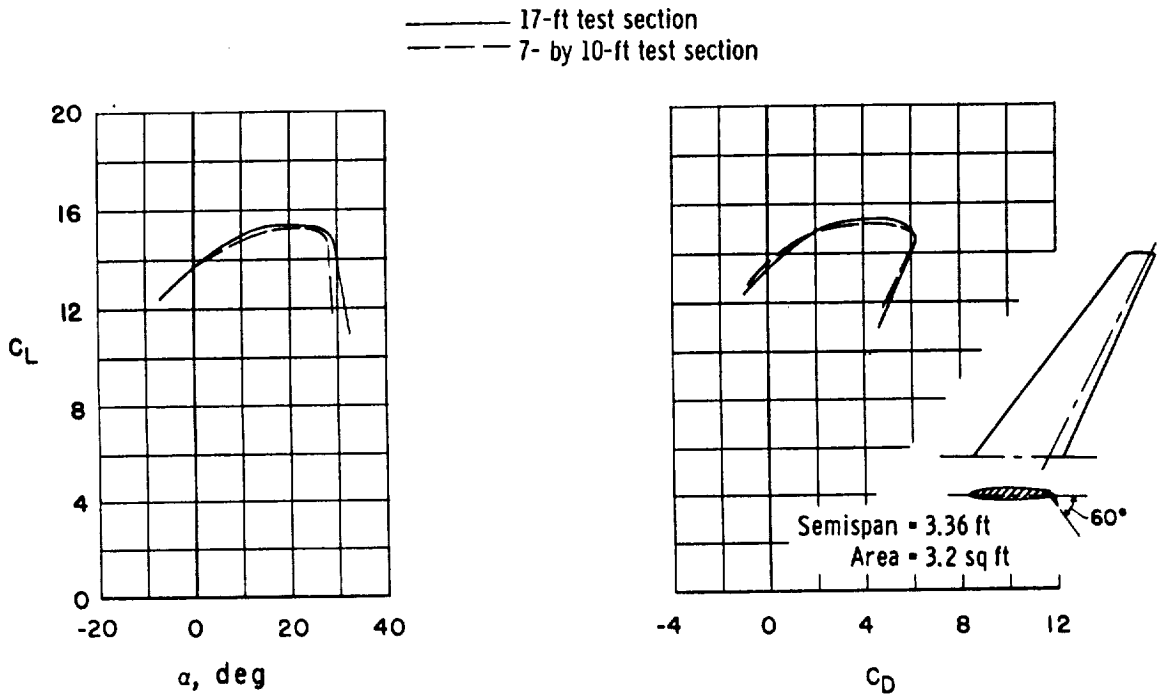


(c) With additional correction to $C_\mu = 6.75$.

Figure 105.- Concluded.

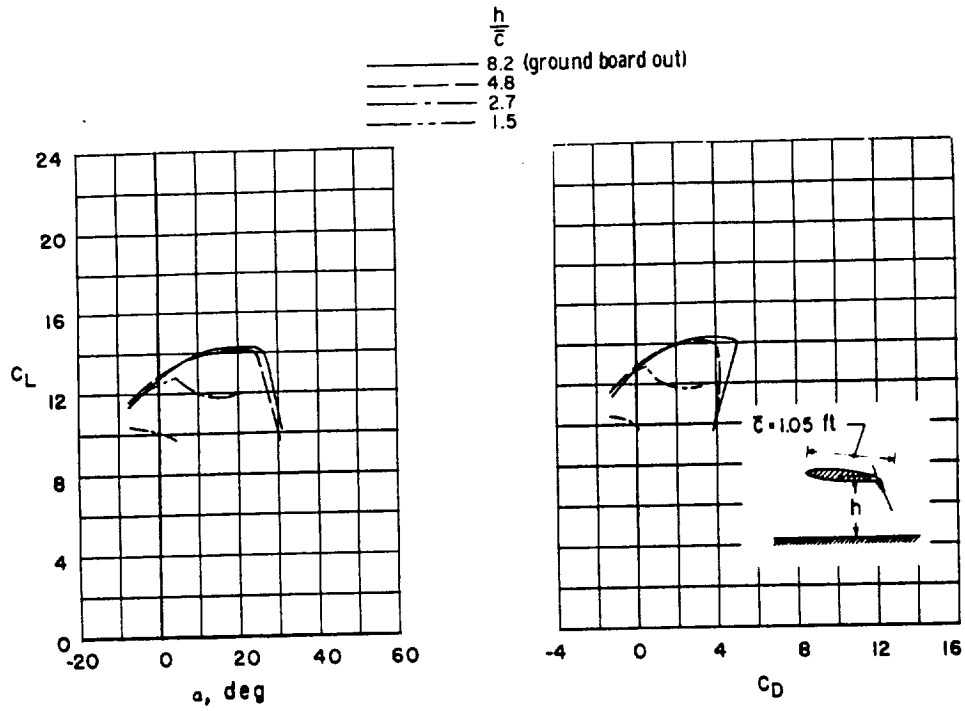


(a) As tested for ground effect at $C_\mu = 6.2$.

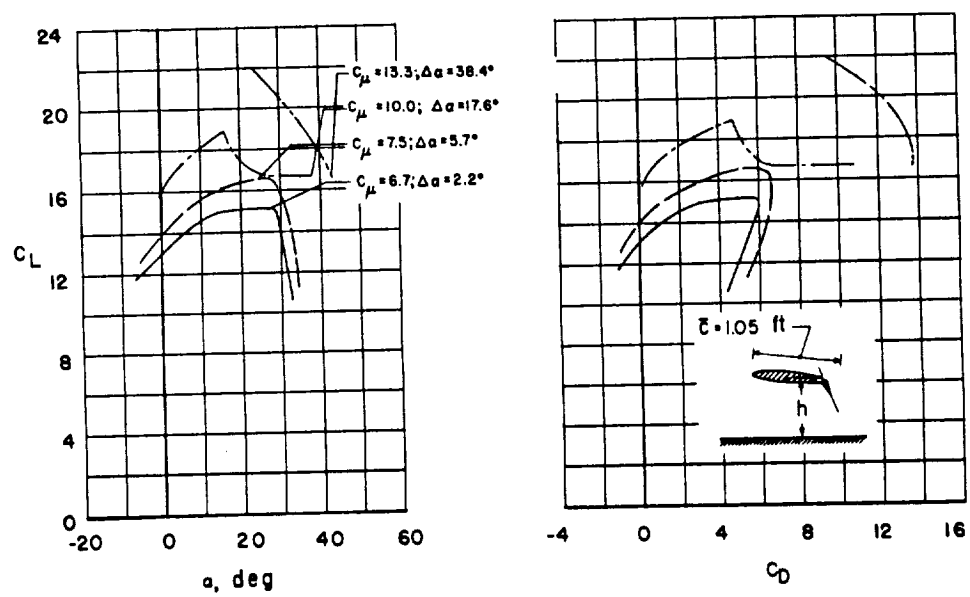


(b) Corrected to free air.

Figure 106.- Ground-effect tests of a swept-wing jet flap model using a ground board in the 17-foot test section. (Uncorrected data from fig. 10 of ref. 7.)

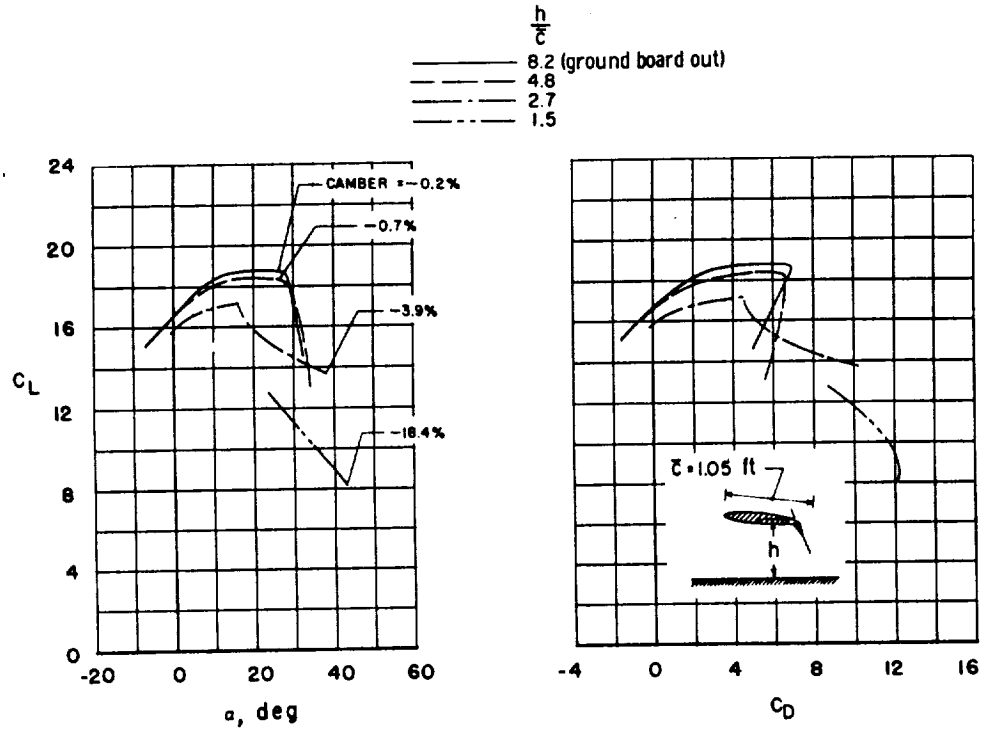


(c) With additional correction to $C_\mu = 8.4$.

Figure 106.- Concluded.

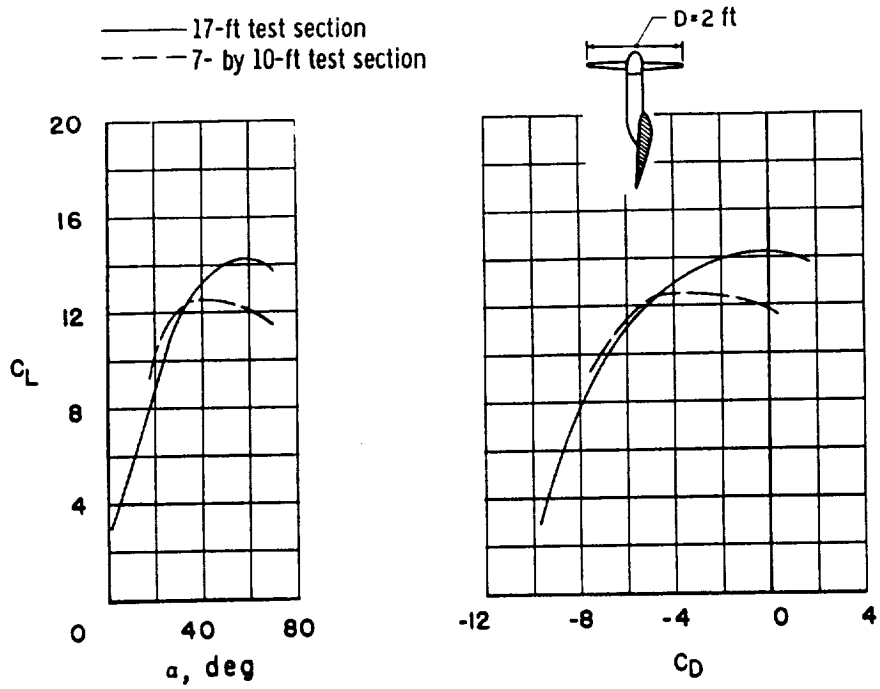


(a) As tested at $C_T$ = 10.3, with no jet-boundary corrections.

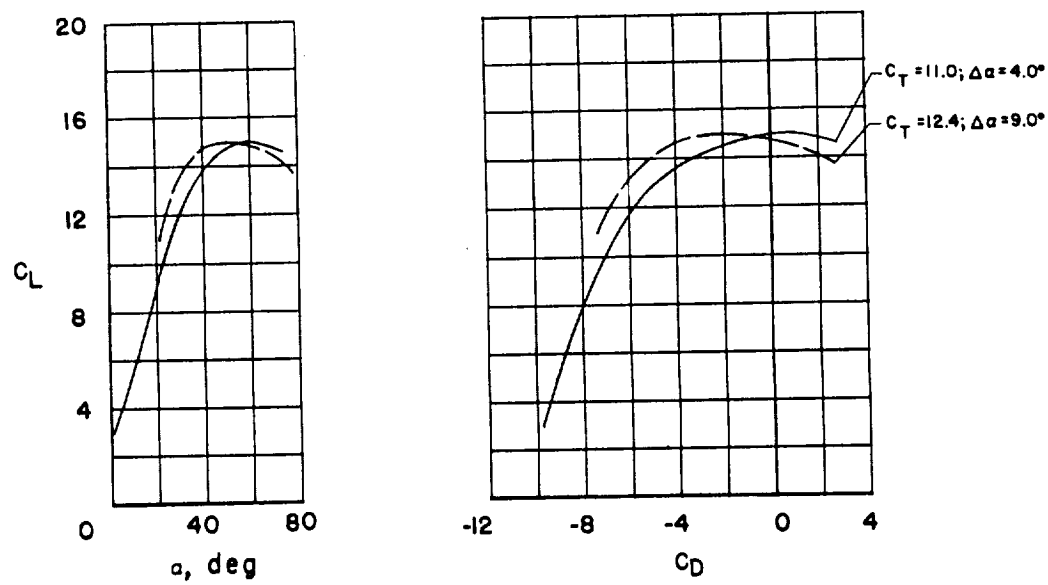


(b) With jet-boundary corrections.

Figure 107.- Tests of a tilt-wing VTOL configuration in 17-foot test section compared with those in 7- by 10-foot test section. (Uncorrected data from fig. 6(a) of ref. 7.)

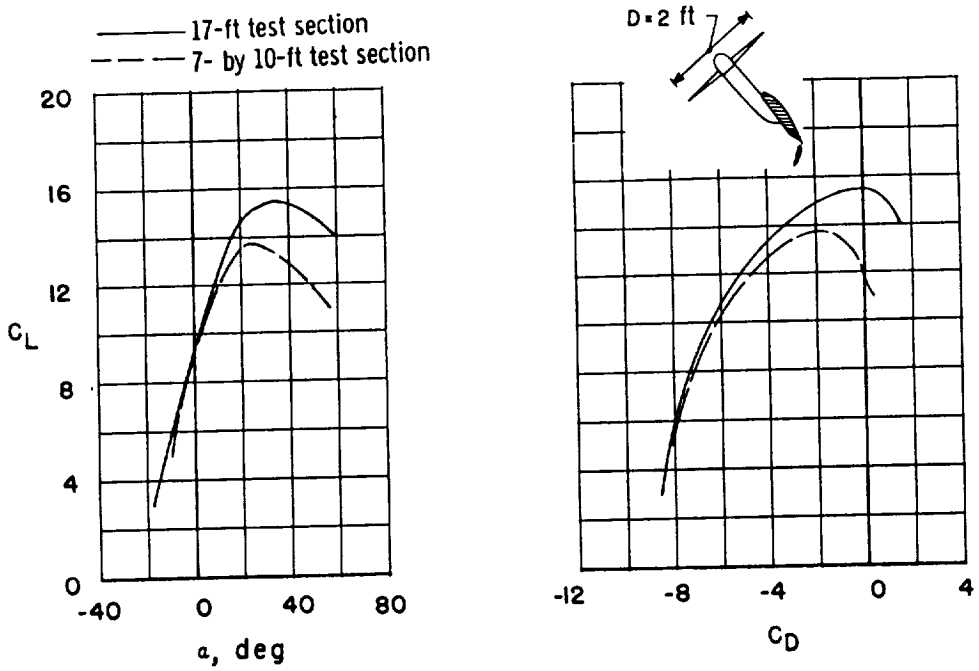


(a) As tested at $C_T = 9.2$, with no jet-boundary corrections.

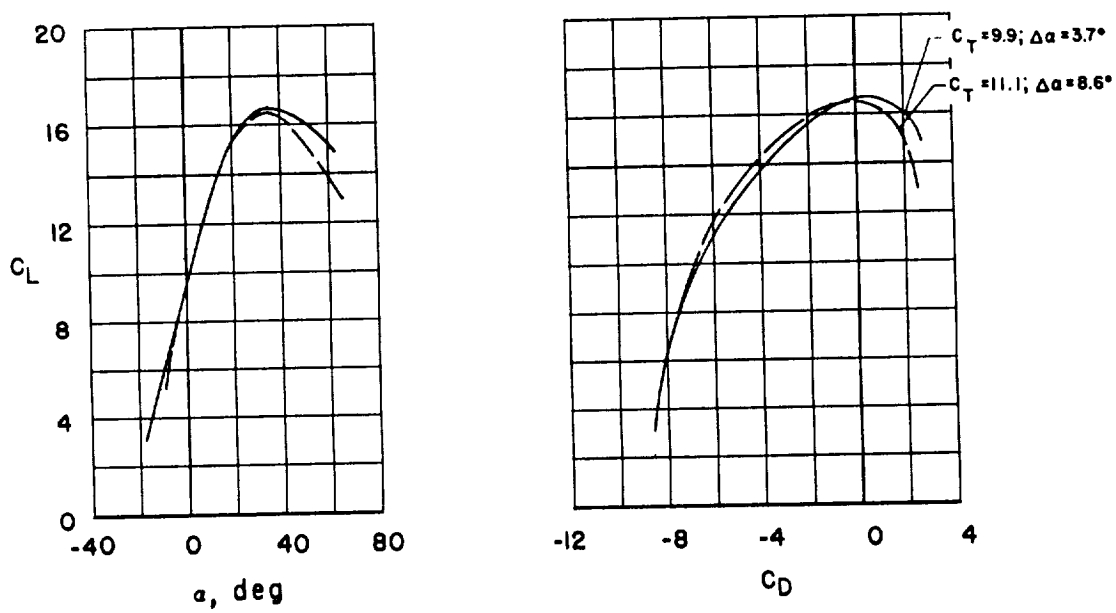


(b) With jet-boundary corrections.

Figure 108.- Tests of a tilt-wing-with-flap VTOL configuration in 17-foot test section compared with those in 7- by 10-foot test section. (Uncorrected data from fig. 6(b) of ref. 7.)

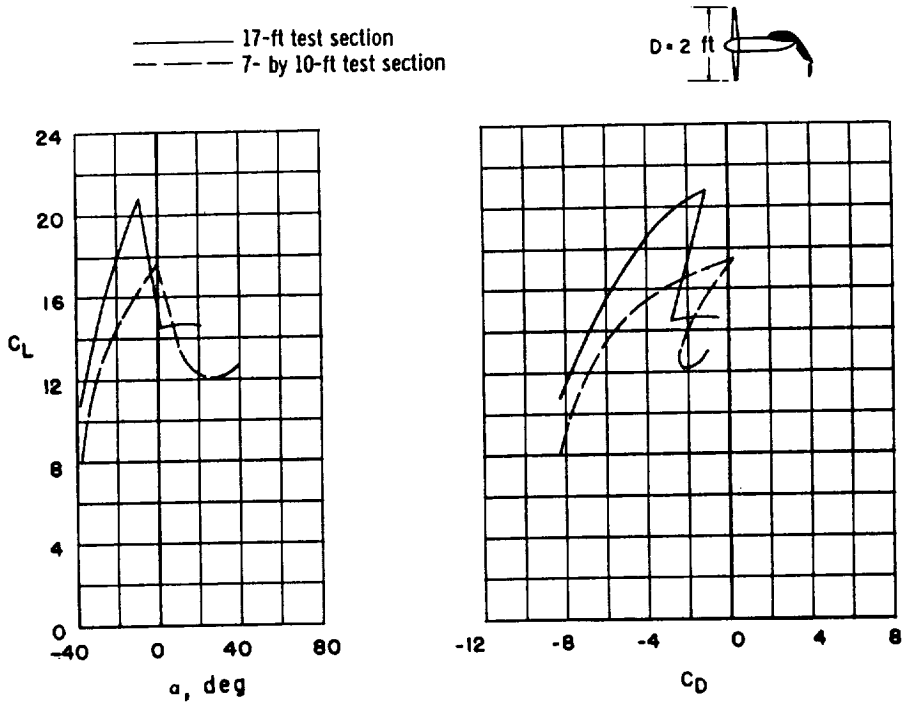


(a) As tested at $C_T = 14$, with no jet-boundary corrections.

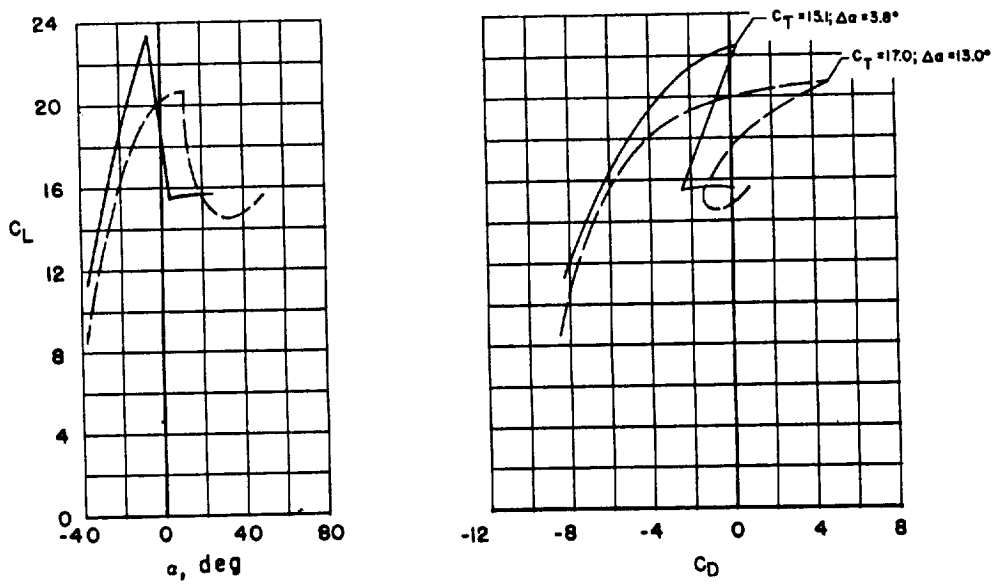


(b) With jet-boundary corrections.

Figure 109.- Tests of a deflected-slipstream VTOL configuration in 17-foot test section compared with those in 7- by 10-foot section. (Uncorrected data from fig. 6(c) of ref. 7.)

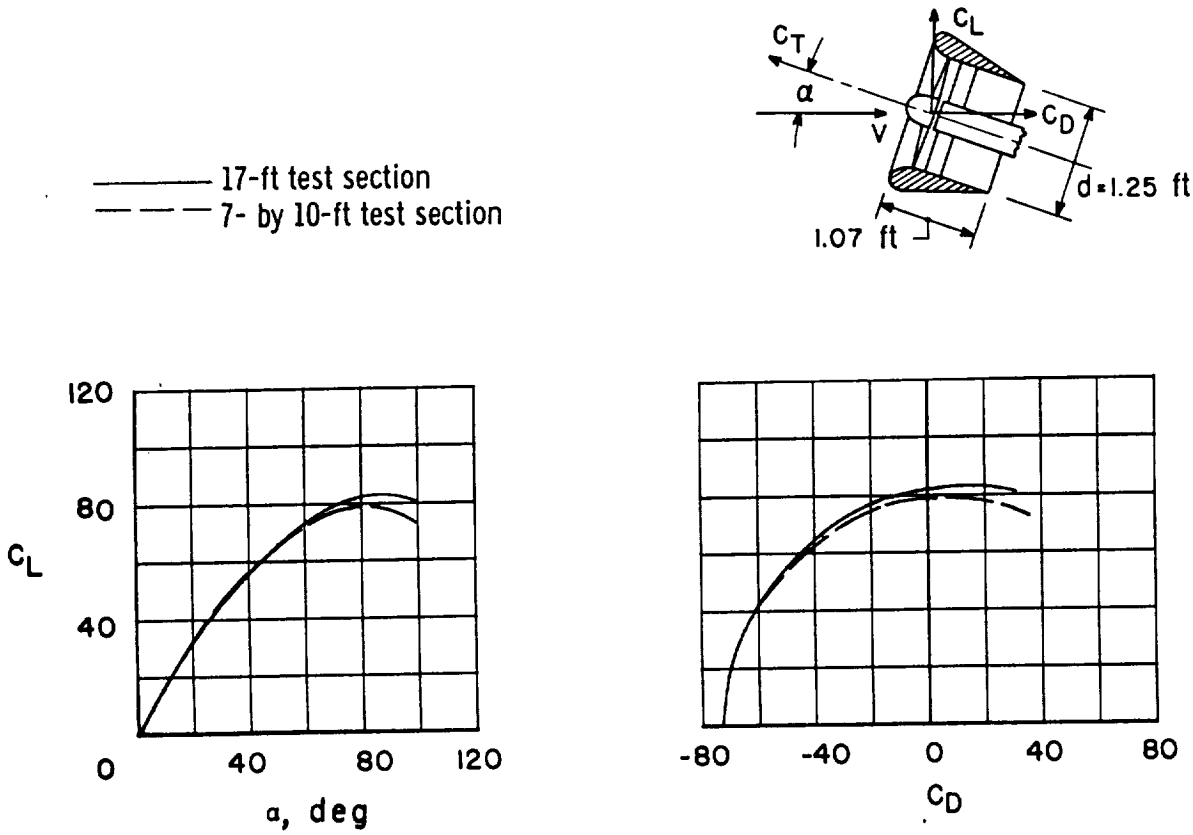


(a) As tested at $C_T$ = 73, with no jet-boundary corrections.

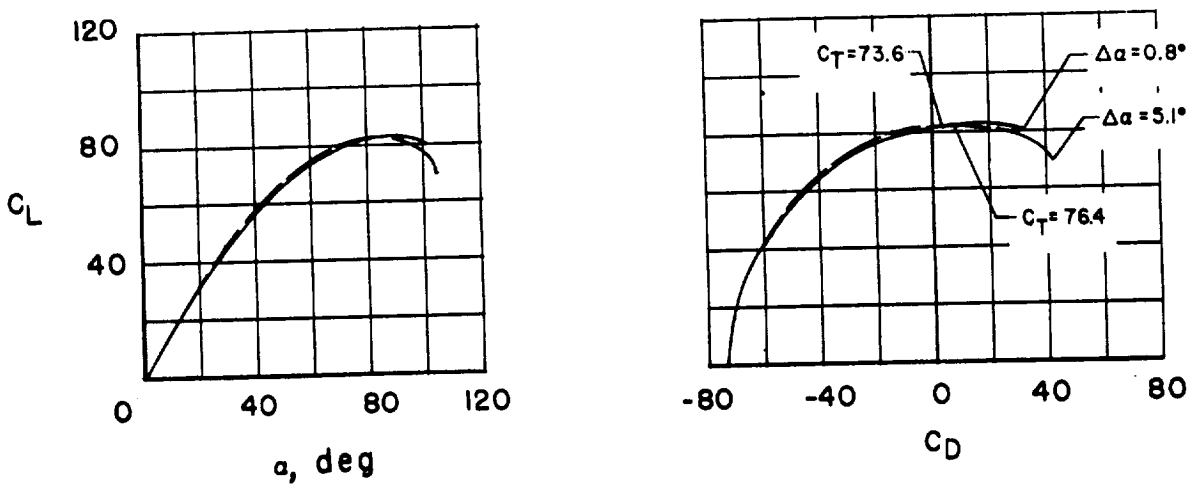


(b) With jet-boundary corrections.

Figure 110.- Tests of a ducted-fan configuration in 17-foot test section compared with those in 7- by 10-foot test section. (Uncorrected data from fig. 12 of ref. 7.)

U.S. GOVERNMENT PRINTING OFFICE: 1962 O—632643

NTIS does not permit return of items for credit or refund. A replacement will be provided if an error is made in filling your order, if the item was received in damaged condition, or if the item is defective.

*Reproduced by NTIS*
*National Technical Information Service*
*U.S. Department of Commerce*
*Springfield, VA 22161*

**This report was printed specifically for your order from our collection of more than 2 million technical reports.**

For economy and efficiency, NTIS does not maintain stock of its vast collection of technical reports. Rather, most documents are printed for each order. Your copy is the best possible reproduction available from our master archive. If you have any questions concerning this document or any order you placed with NTIS, please call our Customer Services Department at (703)487-4660.

Always think of NTIS when you want:
• Access to the technical, scientific, and engineering results generated by the ongoing multibillion dollar R&D program of the U.S. Government.
• R&D results from Japan, West Germany, Great Britain, and some 20 other countries, most of it reported in English.

NTIS also operates two centers that can provide you with valuable information:
• The Federal Computer Products Center - offers software and datafiles produced by Federal agencies.
• The Center for the Utilization of Federal Technology - gives you access to the best of Federal technologies and laboratory resources.

For more information about NTIS, send for our FREE *NTIS Products and Services Catalog* which describes how you can access this U.S. and foreign Government technology. Call (703)487-4650 or send this sheet to NTIS, U.S. Department of Commerce, Springfield, VA 22161. Ask for catalog, PR-827.

Name _____
Address _____
_____
_____
Telephone _____

*- Your Source to U.S. and Foreign Government Research and Technology.*

U.S. DEPARTMENT OF COMMERCE
Technology Administration
National Technical Information Service
Springfield, VA 22161 (703) 487-4650